3-23-2017

Investigation of Dynamic Store Separation out of a Weapons Bay Cavity Utilizing a Low Speed Wind Tunnel

Andrew D. Bower

INVESTIGATION OF DYNAMIC STORE SEPARATION OUT OF A WEAPONS BAY CAVITY UTILIZING A LOW SPEED WIND TUNNEL

THESIS

Andrew D. Bower, Civilian, USAF

AFIT-ENY-MS-17-M-244

DEPARTMENT OF THE AIR FORCE
AIR UNIVERSITY

AIR FORCE INSTITUTE OF TECHNOLOGY

Wright-Patterson Air Force Base, Ohio

AFIT-ENY-MS-17-M-244

INVESTIGATION OF DYNAMIC STORE SEPARATION OUT OF A WEAPONS BAY CAVITY UTILIZING A LOW SPEED WIND TUNNEL

THESIS

Presented to the Faculty

Department of Aeronautics and Astronautics

Graduate School of Engineering and Management

Air Force Institute of Technology

Air University

Air Education and Training Command

In Partial Fulfillment of the Requirements for the

Degree of Master of Science in Aeronautical Engineering

Andrew D. Bower, BSAE

Civilian, USAF

March 2017

AFIT-ENY-MS-17-M-244

INVESTIGATION OF DYNAMIC STORE SEPARATION OUT OF A CAVITY UTILIZING A LOW SPEED WIND TUNNEL

Andrew D. Bower, BSAE

Civilian, USAF

Committee Membership:

Dr. Mark Reeder
Chair

Dr. Bradley Liebst
Member

Dr. Donald Kunz
Member

AFIT-ENY-MS-17-M-244

Abstract

Characterizing mission store trajectories as they separate from a weapons bay cavity is highly relevant to the Air Force mission. The flow around a weapons bay is unsteady. The unsteady flow can cause a mission store separation trajectory to be unpredictable, and such is the case for what some have termed a pitch bifurcation. Traditional wind tunnel testing is incapable of detecting a bifurcation because traditional wind tunnel testing records time-averaged data. In this study, an experimental testing system was developed and refined in order to support the time-accurate characterization of dynamic mission store separation events. A Motion Test Apparatus integrated with a low-speed wind tunnel maneuvers a model within the wind tunnel test section along a prescribed trajectory. A dedicated data acquisition system, along with sensors, record time-accurate force-and-moment measurements as well as model attitude. Two mission store geometries fabricated of two different materials were studied as they performed a one-off store separation trajectory from a weapons bay cavity. The mission store models separated, alternatively, from forward and aft positions from the weapons bay. Data confirmed that variability in pitch moment experienced by the models was higher for store separation from the aft position. Force-and-moment data also suggests a bifurcation was present for certain test cases.

Acknowledgments

The following Warlords deserve special acknowledgment for their ultimate sacrifice for the USA in the Global War on Terrorism. Et etiam Lambda, Gamma, Delta, Kappa.

CPL Christopher Belchik	[22 AUG 2004]
CPL Benny Cockerham	[21 OCT 2005]
HM3 Christopher Thompson	[21 OCT 2005]
CPT Tyler Swisher	[21 OCT 2005]
SGT Michael Hodshire	[30 OCT 2005]
SGT Sean Miles	[24 JAN 2006]

Andrew D. Bower

Table of Contents

Page

List of Figures

Page

List of Tables

Page

TITLE

I. Introduction

1.1 Motivation

The United States Air Force (USAF) has been helping America win wars since 1947. In this endeavor, the two most familiar techniques the USAF employs are establishing air superiority and providing air support to friendly forces, in order to neutralize enemy forces. Establishing air superiority and providing air support both require the USAF to employ mission stores into the battlespace. Carrying mission stores into the battlespace requires the need to establish: safe and acceptable employment; safe and acceptable jettison. These requirements are outlined in Air Force Instruction (AFI) AFI 63-104, commonly referred to as the SEEK Eagle process.

Contemporary adversarial threats have driven the need for the USAF to adopt air vehicles with low radar cross section signatures. As a result, internal weapons bays are common on fifth-generation air vehicles [1]. When the bay doors open, a cavity flow forms, and mission stores are subject to strong acoustic loads and unsteady flows [2]. Weapons bay cavity flows are naturally and rather dramatically unsteady, due to a robust self-reinforced acoustic resonance phenomenon, coupled to and driven by an equally robust free shear layer instability [3]. Characterizing the aerodynamic interaction as a mission store departs a cavity is highly relevant to the USAF mission [1].

The importance of understanding mission store separation from an internal bay has risen in part, due to the development of “flexible” weapons systems that mitigate the costs and nuances associated with AFI 63-131 compliance. The goal of flexible weapon

systems is to acquire modular weapons that can be modified to meet specific mission requirements, as required by commanders within an area of operations. For example, mission needs may warrant various combinations of: warhead, tail kit, strap-on wing kit, EO/IR/radar seeker, rocket booster, etc. A second factor is that some of these flexible weapons are envisioned to be smaller and non-symmetric than traditional weapons. Modifying these ancillary components will certainly change mass properties and outer mold lines for any given mission store and could, in turn, influence sensitivity to acoustic loads and unsteady flow. Likewise, smaller weapons tend to have a higher surface-area-to-weight ratio, thus are more influenced by aerodynamic loading. As a result, wind tunnel testing would be utilized by the SEEK Eagle process in order to achieve safe and acceptable mission store separation [2].

The Air Force Institute of Technology (AFIT) has acquired a six degree-of-freedom (6-DOF) robotic arm, which will be referred to as the Motion Test Apparatus (MTA). The MTA was built by RE2, Inc. and has been combined with the AFIT low-speed wind tunnel and a National Instruments Data Acquisition (DAQ) system. The MTA has the capability to render motions on a mission store model within one to two cubic feet of the low-speed wind tunnel, as characterized by Lancaster [4]. The MTA can also be used in conjunction with sensors to gather force and moment data on a wind tunnel model as described by Sellers [5]. Furthermore, AFIT has the capability of conducting flight tests by utilizing the modified SUU-41 pod as developed by Probst [6]. The modified pod, designated as WASSP, can instrumented and attached as a store to an actual airframe. The weapons bay cavity used in this study, is geometrically similar to the WASSP [6].

Time-accurate mission store trajectory computational fluid dynamics (CFD) simulations have shown sensitivity to timing of the mission store release [7]. Typical wind tunnel data collected to support store separation analysis cannot detect this effect since data collected consists of time averaged store loads [7]. The goal of the current study is to use the MTA to support the dynamic characterization of mission store separation from a cavity and partly to support the flexible weapons system concept by acquiring time-accurate dynamic loads. Figure 1 shows the MTA in its configuration with the AFIT low speed wind tunnel.

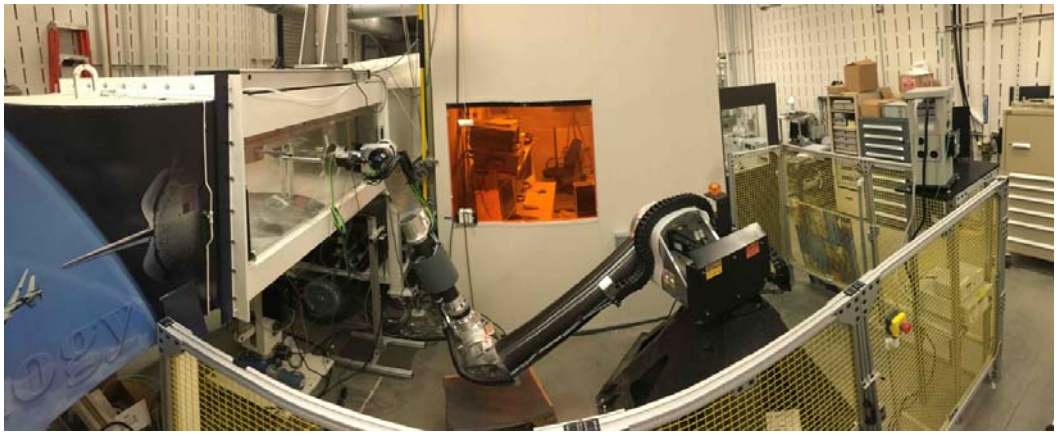

Figure 1. Motion Test Apparatus (MTA) combined with the AFIT low-speed wind tunnel.

1.2 Problem Statement

The goal of the current research is to utilize the MTA and DAQ system to carry out dynamic testing in the AFIT low speed wind tunnel in order to produce time-accurate force and moment measurements. While previous research focused on cyclic motion, the current study is devoted to a singular one-off motion. Mission store separation events were conducted on four models at speeds of 0, 60, 90 and 120 MPH. The DAQ captured:

time-accurate force measurements; and time-accurate moment measurements. Furthermore, dynamic pressure data was obtained within a cavity of a length-to-depth ratio of 4.465.

1.3 Methodology

Equipment setup includes the MTA positioned next to the AFIT low-speed wind tunnel. A sting, which is a rigid beam used to hold a model in the freestream of a wind tunnel, is attached to the MTA and protrudes into the wind tunnel through a circular access hole of nine inch diameter. The access hole is covered during wind tunnel operations by a light-weight corrugated fiberboard. The pressure inside the wind tunnel is less than the standard atmosphere, when the wind tunnel motor is on. The atmosphere outside the wind tunnel pushes the corrugated fiberboard snugly against the wind tunnel's side wall, which results in minimal pressure loss during wind tunnel operations. The mission store model is attached to the sting by dint of machine screw threads of an ATI Nano25 force balance. Analog voltage signals were produced by a recently-purchased ATI Nano25 6-DOF balance, as it experiences an aerodynamic load in the x-, y-, and z-directions as well as moments about these axis directions.

Figure 2. Aluminum missile model shown in proximity to the weapons bay.

The voltage signals corresponding to three orthogonal forces, and three orthogonal moments are collected from the Nano25 force balance using National Instruments (NI) DAQ. The collected signals are processed using LabVIEW software. Mission store model angle attitude data is produced by a LORD MicroStrain inertia measurement unit (IMU) attached to the MTA. The DAQ collects the IMU signals though an RS-22 connection. The DAQ system operates on a primary computer. MTA mission store trajectory commands are written as .txt files and sent to the MTA utilizing Linux operating software. The Linux operating system operates on a secondary computer.

Two trajectories were implemented. The first trajectory had the mission store exit a weapons bay cavity. Wind tunnel speeds were set to: 0, 30, 60, 90, and 120 MPH. The initial position of the mission store was one-half inch into the five and three-eighths inch deep weapons bay. The final position had the mission store nine inches above the weapons bay cavity and into the freestream. The second trajectory had the mission store perform a 0 to 41.5º increase of angle of attack (AoA) in the freestream. Wind tunnel speeds were set to: 0, 30, 60, 90, and 120 MPH as well.

Initial runs are gathered with the wind tunnel velocity set to zero, in order to capture inertial effects acting on the Nano 25 force balance. These initial inertial runs are used to tare subsequent runs, where the wind tunnel velocity is greater than zero. Post-processing of the data is performed by importing NI LabVIEW .lvm files into MATLAB. Post-processing yields time-accurate force and moment measurements for the four mission store models. The time-accurate results were verified by comparing the results for all models at the varying wind tunnel speeds.

1.4 Limitations

The joint layout of the MTA is similar to a human arm. There exists a yaw and pitch motion about the shoulder joint, as well as a yaw and pitch about the elbow joint. And finally, there is a yaw and pitch about the wrist joint. In this study, MTA commands are currently limited to only prescribing commands to the wrist pitch and wrist roll joints. MTA wrist pitch motions result in the mission store to rise away from the weapons bay cavity. MTA wrist roll motions result in mission store pitching up or down. As a result,

the mission store cannot be kept in a plane, as it travels out of the weapons bay cavity. In other words, the mission store traversed in an arc for the first trajectory.

Due to the constrained operating space that the MTA can prescribe trajectories through a nine-inch access hole, the current MTA configuration only permits the MTA to place a mission store one inch inside the weapons bay cavity. The weapons bay is five and three-eighths inches deep.

1.5 Overview of Subsequent Chapters

The remaining chapters are organized as follows. Chapter II addresses reference frames and coordinate transformations; kinematics; literature review of studies performed using dynamic wind tunnel testing, and experimental measurements. Chapter III addresses the experimental set up; MTA operating procedures; methodology for acquiring data. Chapter IV provides select experimental results for all trajectories a mission store model. Chapter V provides: conclusions on acquired time-accurate force and moment measurements and assessment of the MTA performance.

II. Literature Review

Chapter Overview

Literature on wind tunnel testing with mission stores and cavities was reviewed. The literature review shows the necessity to conduct experimental research with wind-tunnels. This chapter consists of seven sections: 1) reference frame definitions 2) coordinate transformation theory 3) Motion Test Apparatus (MTA) kinematics 4) approaches to characterizing store separation 5) experimental measurements 6) Dimensional references and aerodynamic coefficients and 7) chapter summary.

Section one describes the reference frames necessary to conduct dynamic motion wind-tunnel tests. Section two describes the coordinate transformations between the wind-tunnel reference frame and the mission store body reference frame, and vice-versa. Section three describes the mechanical relationship of the mission-store model motion without reference to the forces that cause the motion. Section four shows the need for dynamic wind-tunnel testing as well as describing the current capabilities of dynamic wind-tunnel testing. Section five describes the necessary equipment for acquiring force and moment measurements. Section six explains how aerodynamic data are post-processed to aerodynamic coefficients. And section seven summarized Chapter Two.

2.1 Reference Frames

In conducting mission store separation tests, multiple points of view are possible. Moreover, the reference frame of the MTA itself must be considered when executing tests. Thus, four reference frames were considered during dynamic testing [8]. These reference frames are: 1) the inertial reference frame of the MTA 2) the wind-tunnel

reference frame 3) the body-axes reference frame and 4) the model-axes reference frame. The reference frames are as shown in Figure 3 below. Every reference frame follows the right hand convention. Every reference frame is an orthogonal set of x-, y-, z- axes.

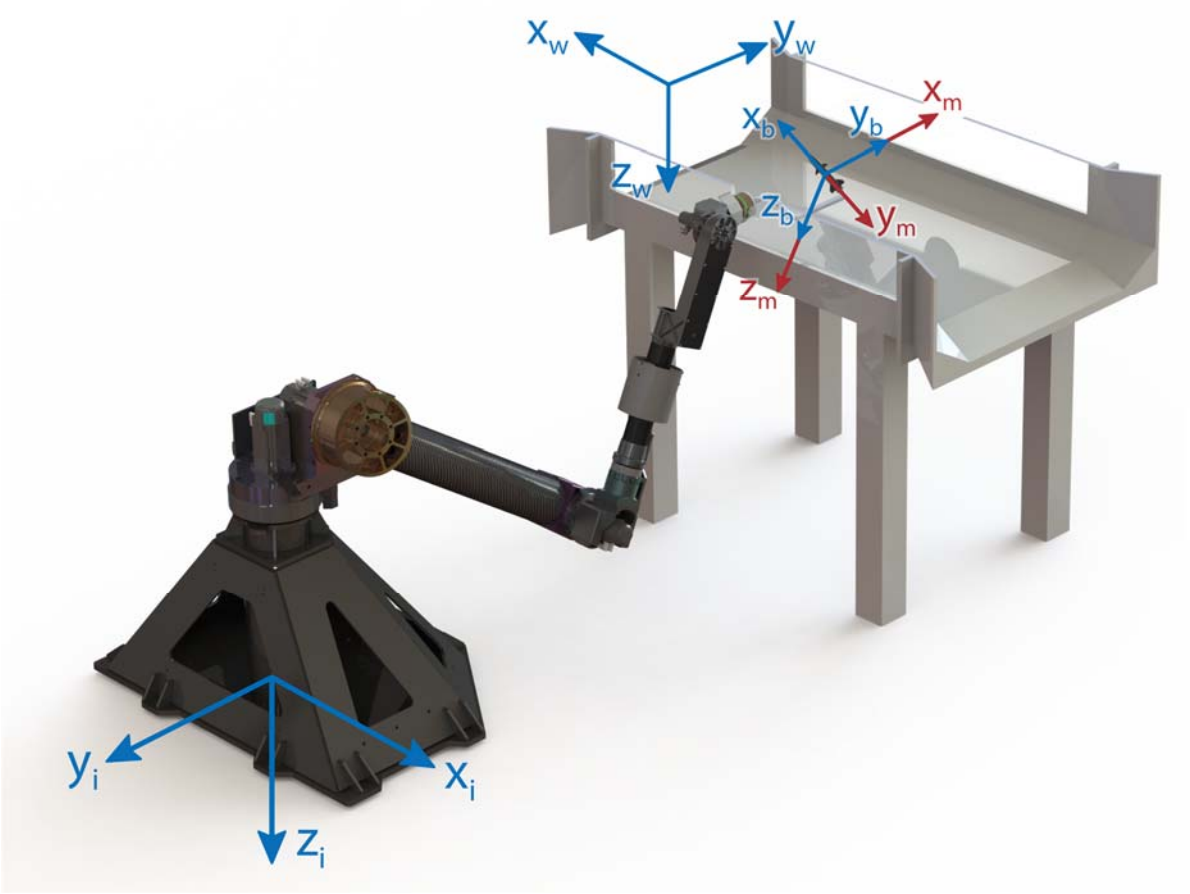

Figure 3. Wind Tunnel and MTA Reference Frames (CAD model from RE2, Inc.)

The first reference frame is the inertial reference frame located underneath the shoulder joint (at the base) of the MTA. The inertial reference frame is annotated with the subscript "i." The inertial reference frame is fixed for all time and does not accelerate.

The x_i axis is parallel to and in the same direction as the wind-tunnel flow. The y_i axis is perpendicular to the wind-tunnel flow. The z_i axis points down and into the laboratory floor.

The second reference frame is the wind-tunnel reference frame. The wind-tunnel reference frame is annotated with the subscript "w." The wind-tunnel reference frame is located in the center of the test section with the x_w pointing upwind towards the wind-tunnel intake, the y_w axis points to the test section side wall, and the z_w points downward towards the test section floor [9]. The wind-tunnel axis is non-accelerating and fixed for all time with the x_w in line, but opposing, the wind-tunnel freestream velocity.

The third reference frame is the body-axes reference frame and is annotated with the subscript "b." The body-axes reference frame is centered at a point on the mission store model and is initially the same as the wind-tunnel reference frame in that the -x,-y,-z axis align but the body-axes frame is fixed for all time to the mission store body i.e., the body-axes reference frame moves relative to the wind-axes reference frames [10]. Specifically, the body-axes reference frame has: the x_b pointing in out of the mission store ogive, the y_b pointing out of the mission store's right side, as the store faces upwind, and the z_b pointing downward and out of the mission store's belly [9].

The fourth reference frame is the model-axes reference frame. This reference frame is the point about which mission store model trajectories were executed [4]. The model-axes reference frame is coincident to the body-axes reference frame, except that the model-axes reference frame is rotated 90° about the z_b such that: the x_m axis points out of the mission store's right side as is faces upwind, the y_m points out of the mission store's rear, and the Z_m,b axis remain coincident. The model-axes reference

frame exists, because the original intended use for the MTA design was to have the MTA wrist pitch and wrist roll to be about the y_m and x_m respectively, with the x_m axis to be initially aligned with the wind-tunnel freestream velocity. The model-axes reference frame has its origin at the model control point - about which trajectories are executed [4]. The model-axes reference frame was only utilized herein, because the precursor research of Sellers [5] and Lancaster [4] called upon the model-axis reference frame in order to kinematically prescribe trajectories onto a wind-tunnel model.

In summary, traditional wind-tunnel testing uses a wind-tunnel reference frame and a body-axis reference frame. The MTA utilizes these but, due to the dynamic capabilities, it also requires an additional inertial reference frame. Together, these three reference frames are sufficient for conducting dynamic wind-tunnel experiments. However, the MTA also incorporates a model-axes reference frame due to its original design as describes above, and the model-axes reference frame is only necessary for kinematic purpose, which are describes in the work of Lancaster [4] and Sellers [5]. All forces and moments were measured in the balance-axes reference frame. Further details are described in section 2.4 below.

2.2 Motion Test Apparatus Kinematics

Mission store trajectories were originally meant to be created with respect to the MTA inertial-axes reference frame [8]. The trajectories in this thesis were created with respect to the model-axes reference frame. In order to successfully conduct dynamic wind-tunnel testing (by creating proper mission store trajectories), it becomes necessary to understand the relationship between the MTA inertial-axes reference frame and the

model-axes reference frame. The two forms of kinematics necessary to describe this relationship are forward and inverse kinematics. Forward kinematics use the six MTA joint angles plus the mission store offset (i.e. the distance between the wrist component of the MTA and the mission store model control point) to calculate the Cartesian positions. Inverse kinematics uses the mission store's Cartesian position to calculate MTA component angles. A detailed analysis of the mathematics specific to the MTA is laid out by Lancaster [4].

Figure 4 depicts all the reference frames necessary for MTA kinematics. The inertial reference frame is the same as the reference frame annotated with the subscript "0." which is centered along the shoulder yaw z-axis. In this study, only two of the MTA joints were used. The two MTA joints used were the MTA wrist joints i.e. joint five and joint six and they can be seen as the reference frames annotated with subscripts "5" and "6" in Figure 4 respectively.

The mission store model can be positioned to a desired location in the wind-tunnel test section by the six MTA joint angles [5]. These six angles are: torso yaw (θ_{tr}), shoulder pitch (θ_{sp}), elbow pitch (θ_{ep}), elbow roll (θ_{er}), wrist pitch (θ_{wp}), and wrist roll (θ_{wr}). Using the six calculated MTA joints to perform mission store trajectories is the preferred method for operation of the MTA [4]. However, due to: the confined area in the wind tunnel test section, the nine inch diameter access porthole, and with the intent to mitigate inertial noise introduced by MTA arm movement, only the MTA wrist pitch and MTA wrist roll movements were utilized. The wrist pitch and wrist roll correspond with joint "5" and joint "6" as shown in Figure 4.

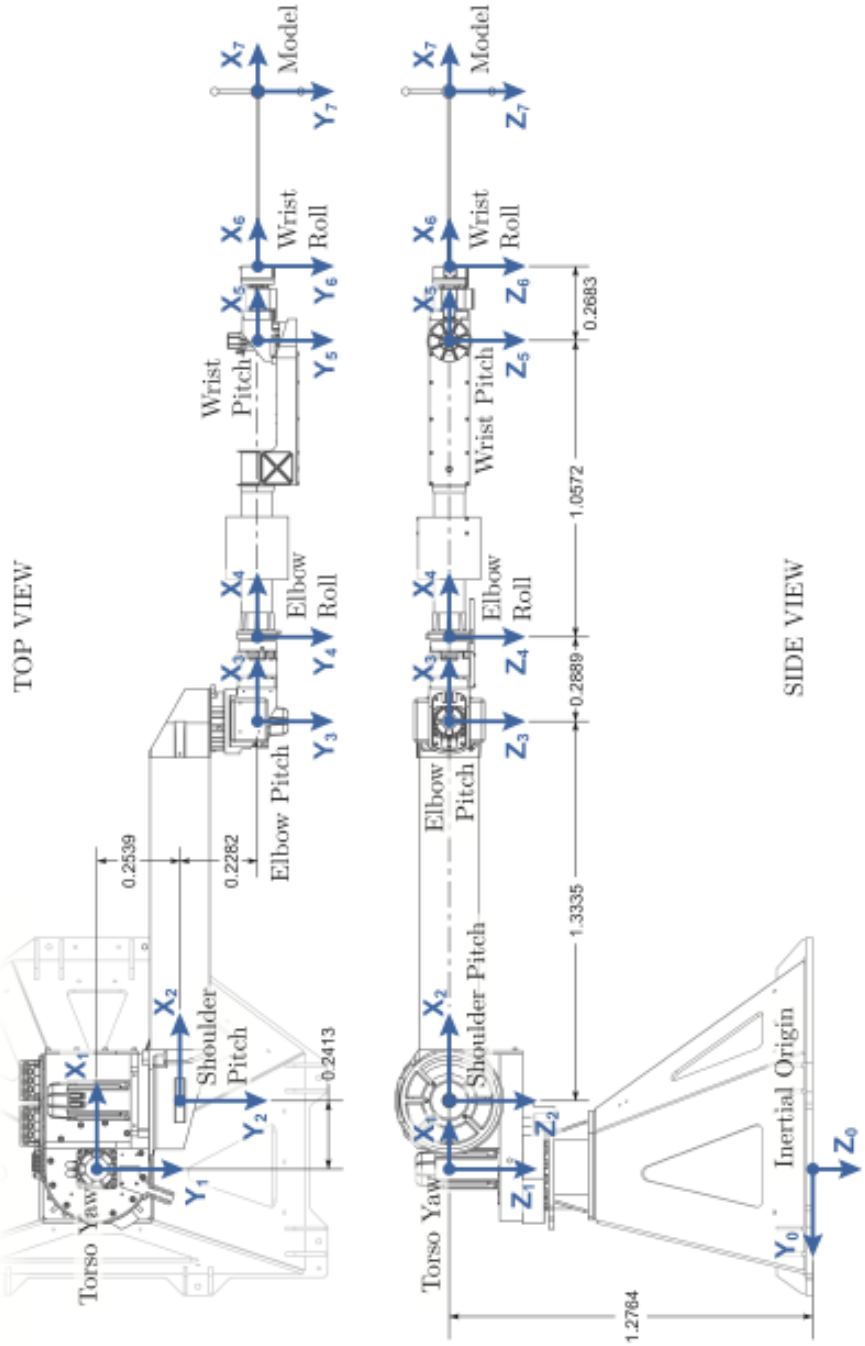

Figure 4. The reference frames labeled 0-7 necessary for MTA kinematics. The blue sphere represents the mission store's model control point. All angles are zero as shown in the diagram. Examples of distances between reference frames are shown (units in meters); adapted from [5]**.**

2.3 Approaches to Characterizing Mission Store Separation

Advances in computational fluid dynamics (CFD) models have led to improvements in the ability to analyze aerodynamic forces and moments for many configurations. Modeling of dynamic motion of store separation is quite challenging for CFD models as one object moves relative to another. To compute trajectories, the equations of motion for the fluid must be solved, typically utilizing a turbulence model for closure. Then, pressure and shear must be integrated over the model surface to determine the force acting on the aerodynamic body and the moment about the center of gravity of the body. The force and moment leads to a new location and orientation in the flow field. The reliance on a turbulence model and integration over the surface is difficult to overcome, but the benefit of reduced testing costs is strong if reliability of models are proven. Several CFD models have been developed to handle situations where one object moves relative to another. The BEGGAR code is one such model used by the US Air Force for analyses, as demonstrated by Prewitt, Belk, and Maple [11] and Babcock and Maple [12], among others.

With respect to internal store release, the level of difficulty is increased due primarily to the strong unsteady flow environment within the internal region (e.g., the weapons bay) and within the shear layer. As one example, Flora, Reeder, Lofthouse and Kraft [13] utilized OVERFLOW, an overset grid model developed by NASA for moving-body problems, to provide some insight into how well one computational model compared to drop test experiments from a specific cavity using a spherical model geometry and for limited flow conditions. However, other examples of computational

studies of more advanced geometries released from a cavity are difficult to find in the literature.

Whether for verification of computational models or for independent measurements, dynamic wind tunnel testing has potential to support store separation. Dynamic wind-tunnel testing measures: aerodynamic forces, aerodynamic moments about a specific location, dynamic pressure, and model attitude [4]. Dynamic wind-tunnel testing helps evaluate aircraft stability and control for air vehicle research [14]. For mission store deployment of new or upgraded stores on currently operational aircraft, wind-tunnel testing is important for determining safe and effective store release envelopes [2]. Many aircraft carry their weapons internally within bays [2]. Internal weapons carriage is being used to improve aircraft aerodynamic performance and low-observable characteristics [3]. Certain characteristics of flow over, into, and around weapons bays complicate store trajectory simulation and wind-tunnel testing for aircraft equipped with bays [2].

Typical wind-tunnel data collected to support mission store separation analysis cannot detect the unsteady aerodynamics since the data collected consists of time-averaged mission store loads [7]. The current wind tunnel testing system used by the USAF for mission store clearance is the Captive Trajectory System (CTS), located at Arnold AF Base. The CTS also gathers time-averaged results which has always worked well for stores carried externally, on pylons, where the flow is non-separated and relatively steady [3]. It may not be very conservative to use the CTS process to clear weapons released from within weapons bays [3]. As a result, dynamic testing with the

goal of acquiring time-accurate data is paramount in order to facilitate safe and acceptable mission store employment.

Dynamic test configurations come in three styles and are as follows: 1) free-flying wind-tunnel models, 2) free-motion rig, and 3) forced-motion rigs [15]. The MTA in this study is a force-motion rig. A forced-motion rig is one in which the mission store model undergoes a prescribed trajectory and the forces, movements, dynamic pressures, and attitude are measured. Force-motion rigs have been used in past studies to investigate aerodynamic characteristics of transport aircraft configurations undergoing different motions of roll, pitch, and yaw maneuvers [16].

Another example of a forced-motion rig is the captive trajectory system (CTS) utilized at the Arnold Engineering Development Center (AEDC). The AEDC maintains the Air Force's premier subscale store separation test and analysis capability [17]. The purpose of the captive trajectory analysis is to determine the maximum trajectory angles, as a function of the distance from carriage [17]. Captive trajectory simulations are generated in the wind-tunnel by a repetitive solution of the store Newtonian equations of motion (EOM). The process begins with predicted or measured forces and moments on the store at its installed position. Using the EOM and time-steps around 0.01 seconds, the store translational and rotational accelerations are integrated to compute linear and angular velocities, positions, and orientations. Forces and moments are measured at the new location, and the process is repeated, until the entire separation trajectory is defined [2]. In other words, CTS analysis records the trajectory envelope a mission store travels as it separates from the aircraft. However, mechanical limitation prevents full time accurate trajectory modeling with the CTS testing [7], due to the fact that it is acquiring

time averaged data. While the CTS method is valuable, its quasi-steady nature limits its usefulness in a highly unsteady flow environment. A weapons bay, with strong unsteady motion, is a keen example where additional approximation and engineering models are required to put the experiments into context [18].

Free-motion test rigs, which allow at least 1-DOF, allow researchers to characterize aerodynamic performance of a wind-tunnel model as it undergoes simple maneuvers such as pitching, rolling, or yawing. For example, high angle of attack and dynamic rate effects were characterized during rapid pitch-up maneuvers [15]. Higher-order DOF rigs do exist but are not as prevalent as 1-DOF rigs [19], [20]. An example of a higher-order DOF test rig would be a 5-DOF robotic arm that pitched a wing model about its aerodynamic center at constant rates. The experiment was used to examine the transition characteristics between forward flight and the near-hover in fixed-wing vertical-takeoff-and-landing (VTOL) micro air vehicles [21].

Free-flying wind-tunnel models would produce high fidelity models of flight characteristics, since there would be no sting or adjacent support structures interfering with the air flow over the test model. Current research utilizing free-flying rigs is limited by overcoming the difficulty in controlling a wind-tunnel model within a confined space [5]. This difficulty is further exacerbated when the model scale is decreased which, in turn, causes an increase in the rate of motion necessary to conduct maneuvers [15]. Nevertheless, there have been successful free-flight tests conducted, where one particular model performed spin and recovery maneuvers in a wind tunnel [22]. And another supersonic persistence fighter free-flying model was tested in a 30- by 60-foot wind-

tunnel in order to develop a gain schedule necessary for a fly-by-wire aircraft stability and control system [23].

2.4 Experimental Measurements

Force and moment measurements are some of the most important components of quantifying aircraft performance [24]. This is also true for quantifying the performance of mission stores as they separate from an aircraft. Furthermore, aerodynamic flow in and around weapons bays creates an unsteady flow regime where the unsteady aerodynamics have significant effects on the store separation trajectory [7]. The primary focus of this thesis it to develop a system capable of acquiring time-accurate force and moment measurements, in order to characterize mission store trajectories as they travel through unsteady flow regimes.

The acquisition of force and moment data require a 6-component transducer which uses a series of strain gauges attached to the sensor's internal structure [5]. As the force transducer is flexed or twisted, the resistance of the strain gauges changes, which results in a measurable difference in output voltages. A signal conditioner, such as a Wheatstone bridge or similar circuitry, leads to detectable values [4]. Additional measurements include dynamic pressure measurements as well as position, attitude, and acceleration of the model under test [5]. In this study, time-accurate measurements were sought.

The pressure measurements are used in order to characterize two major flow regimes: a low-dynamic pressure regime within the weapons bay that is separated from a high-dynamic-pressure flow outside the bay [2]. The shear layer is the region of unsteady

airflow regime that separates the low-dynamic-pressure and the high-dynamic-pressure regimes. Often, measuring the unsteady dynamic-pressure differences is useful for capturing the frequency associated with the shear-layer vortices shedding. Transducers with high frequency response are required to ensure that time-accurate pressure, forces, and moments are truly captured. Neglecting any phase shift between the vortex train and acoustic wave, an approximation for the vortex frequency for the first Rossiter mode is given by Equation (1) below [25].

$$f = \frac{V_\infty/2}{L} \tag{1}$$

Where:

V∞ = Freestream velocity (ft/s)
L = Weapons bay cavity length (ft)

Pressure coefficients are calculated by equation (2).

$$C_p = \frac{P - P_\infty}{\frac{1}{2}\rho V_\infty^2} \tag{2}$$

Where:

P = Local pressure as recorder by a pressure transducer, (psf)
P∞ = Free stream pressure, calculated from Bernoulli's equation (psf)
V∞ = Free stream velocity (ft/s)
ρ = Density of air, calculated from ideal gas law (slug/ft³)

Recording time-accurate force and moment measurement with the MTA forced-motion test rig requires a taring procedure in order to capture the true aerodynamics. When the balance undergoes a prescribed trajectory, it will record inertial effects

associated with its own mass. As a result, initial test record the inertial forces and moments associated with movement, where the wind-tunnel velocity is set to zero i.e. with the "wind-off." These final tare data are subtracted from subsequent "wind-on" test data, during the post-processing step of the analysis [26].

For the forced-motion test rig experiments herein, a prescribed motion is executed, and the Cartesian positions and angles are automatically recorded by the MTA DAQ system, as developed by Sellers [5]. These data should be verified in order to show the accuracy of the motion with respect to its commanded trajectory. Tracking this motion can be accomplished by an inertial measurement unit (IMU). An IMU consists of two primary components: 1) an accelerometer, for measuring triaxial linear accelerations and 2) a gyroscope, for measuring Euler angles and the associated angular rates [5]. Combining the trajectory data sets validates the experimental test and yields a baseline for future repeatability of experimental work.

2.5 Dimensional References and Aerodynamic Coefficients

Dimensional references are comprised of the model and tunnel reference lengths, areas, distances, and weights [27]. These dimensional references are used in conjunction with the measured forces and measured moments in order to calculate non-dimensional aerodynamic coefficient data. In practice, the mission store model reference area is typically derived from the cross-section area, based upon the mission store diameter [27]. The mission store diameter is annotated as "D" from here on out.

Traditional wind-tunnel testing has historically implemented force-balance mechanisms in order to capture forces exerted onto a wind-tunnel model [10]. As a result,

modern-day devices used to measure force data, such as the Nano25 force transducer, are commonly referred to as a "balance." The body-axes system used in the testing herein coincides with Nano25 force transducer axes system (balance axis system) components and is depicted in Figure 5.

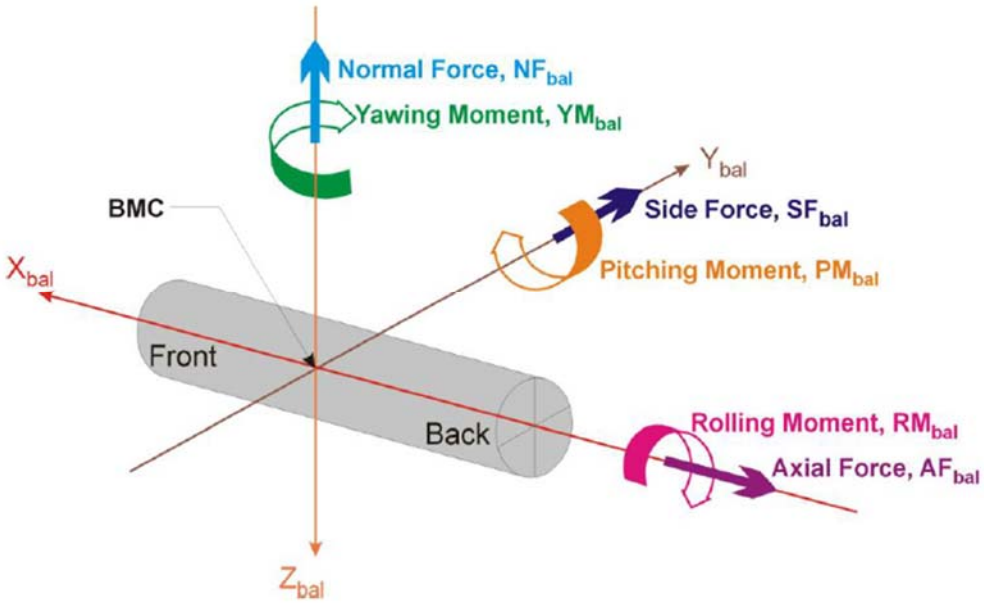

Figure 5. Balance axes system and forces and moments [27]**.**

With the balance-axes system introduced along with the associated forces and moments being measured: Normal, Side Force, Axial, Yaw Moment, Pitch Moment, and Roll Moment coefficient data can be calculated by Equations (3), (4), (5), (6), (7), and (8) respectively. Note that the convention for missile aerodynamic testing is to use the diameter as the reference length scale when computing coefficients [27].

$$C_N = \frac{F_x}{\frac{1}{2}\rho V_\infty^2 \left(\frac{\pi}{4} D^2\right)} \tag{3}$$

$$C_Y = \frac{F_y}{\frac{1}{2}\rho V_\infty^2 \left(\frac{\pi}{4} D^2\right)} \tag{4}$$

$$C_X = \frac{F_z}{\frac{1}{2}\rho V_\infty^2 \left(\frac{\pi}{4} D^2\right)} \tag{5}$$

$$C_n = \frac{T_x}{\frac{1}{2}\rho V_\infty^2 \left(\frac{\pi}{4} D^2\right) D} \tag{6}$$

$$C_m = \frac{T_y}{\frac{1}{2}\rho V_\infty^2 \left(\frac{\pi}{4} D^2\right) D} \tag{7}$$

$$C_l = \frac{T_z}{\frac{1}{2}\rho V_\infty^2 \left(\frac{\pi}{4} D^2\right) D} \tag{8}$$

Where:

D = Missile diameter reference length, (ft)
F_ = Force measured by Nano25, (lb)
T_ = Torque measured by Nano25, (ft*lb)
P∞ = Free stream pressure, calculated from Bernoulli's equation (psf)
V∞ = Free stream velocity (ft/s)
ρ = Density of air, calculated from ideal gas law (slug/ft³)

2.6 Chapter II Summary

This chapter outlines the need for acquiring time-accurate force-and-moment data by conducting dynamic wind-tunnel tests. All necessary reference frames were defined in detail and match the axis systems used world-wide as given by AIAA G-129-2012 [27]. Coordinate transformation theory was discussed in order to shed clarity on how MTA trajectory commands are translated to the mission store model attitude within the wind-tunnel test section. Three dynamic test rigs were discussed, outlining their strengths and weaknesses. The MTA at AFIT is a forced-motion test rig. And finally, an outline of necessary measurements and the appropriate equipment were discussed.

III. Methodology

3.1 Motion Test Apparatus Design

The Motion Test Apparatus (MTA) was built by RE2 Incorporated of Pittsburgh, Pennsylvania. The MTA was not originally designed for the AFIT low-speed wind tunnel. AFIT acquired the MTA from AFRL/RW. Partly because it was initially designed for a different wind tunnel, the MTA has a large footprint within the low-speed wind tunnel laboratory. The base covers an area of 46 x 60 inches. The MTA height is 33 inches tall. The total weight of the MTA is 1500 pounds [4]. Operational space is limited due to the MTA's size. Safety measures include: a safety fence circumscribing the MTA, emergency shutoff switches on each side of the safety fence, an emergency shutdown switch adjacent to the MTA controller computer, software limiters to prevent the MTA from moving beyond the safety fence, and mechanical stops are built within the MTA joints to prevent detrimental overextension of MTA limbs. Additionally, the MTA access

gate is equipped with an interlock that prevents operation of the MTA, if the gate is open [4].

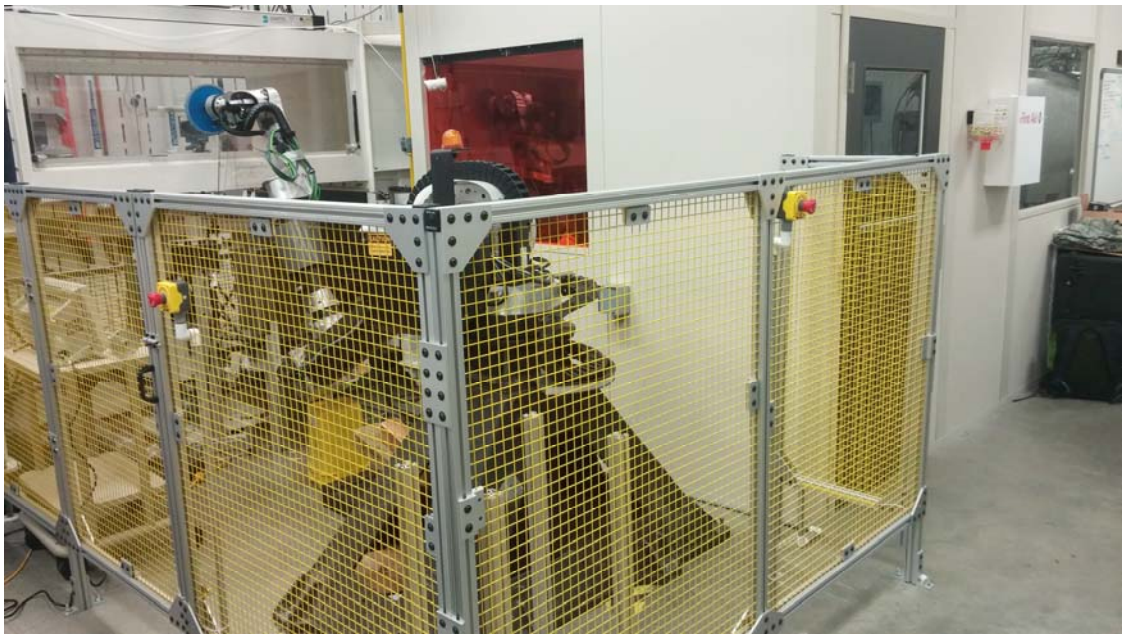

Figure 6. MTA circumscribed by safety fence.

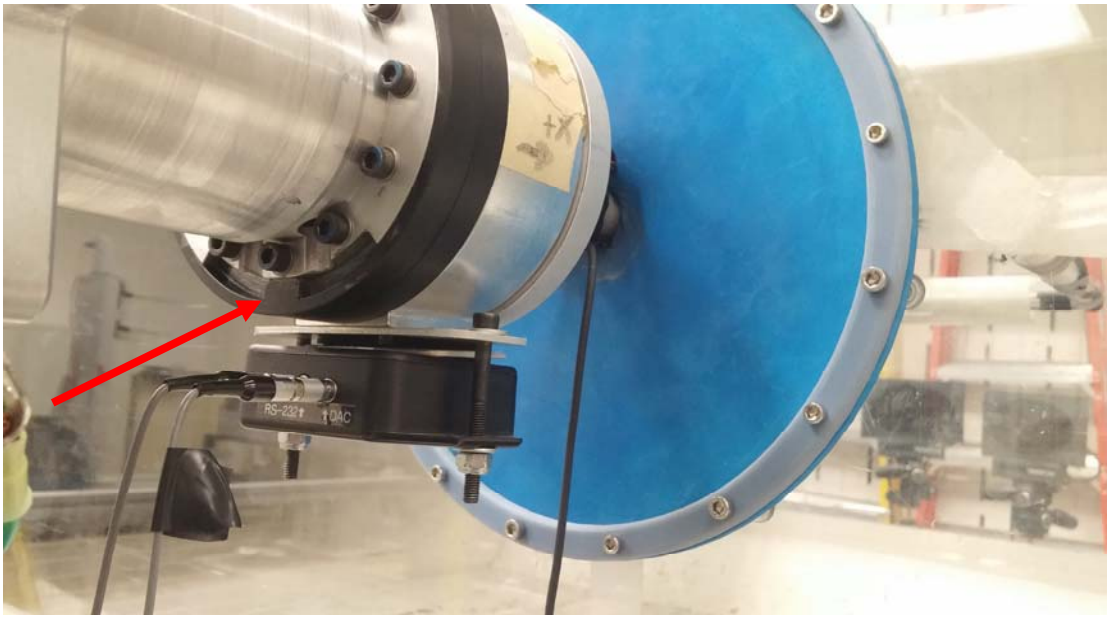

Figure 7. Physical hard stop mechanism to prevent over-rotation.

Recall from Chapter II that the MTA is a forced-motion test rig. The MTA is designed to move a wind tunnel model, within the test section, along a prescribed trajectory. The MTA moves wind tunnel models along prescribed trajectories through a nine inch diameter porthole. During wind-on tests, the porthole is covered by light weight corrugated fiberboard which allows for unimpeded movement of the MTA. The MTA has six operational joints and is similar to a human arm in that the MTA is capable of: torso yaw, shoulder pitch, elbow pitch, elbow roll, wrist pitch, and wrist roll. The joints can be seen in Figure 8. A major difference from the work of Lancaster [4] and Sellers [5] is that a different approach to moving the wind tunnel model was used thanks to the software purchased from Neya Systems. This new software is based on position-time scripts, and unlike prior work by Lancaster uses the motor encoder feedback. The research herein utilized only the wrist pitch and wrist roll motors to ensure correct positioning of the

wind tunnel model. Pertinent joint hardware component is given in Table 1. For more details, refer to reference [5].

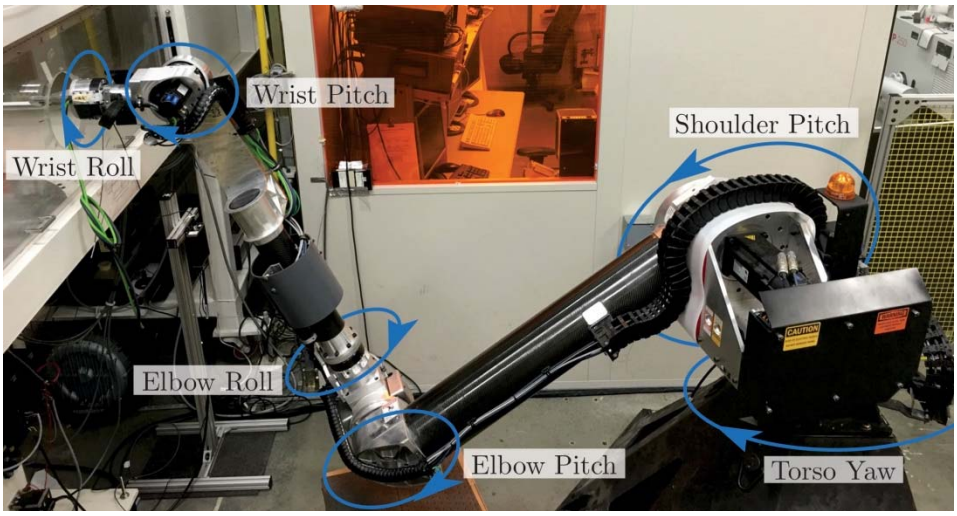

Figure 8. MTA Joint Rotation Axes.

Table 1. MTA Joint Hardware Components [8]

Joint	Motor	Controller	Gearbox
Manufacturer:	Kollmorgen[1]	Elmo	Onvio[2]
Wrist Pitch	AKM22E	Trombone (G-TRO6.1)	DN03055
Wrist Roll	AKM22E	Trombone (G-TRO6.1)	DM02015

[1]Each BLDC motor includes an EnDat Absolute Encoder [2]Zero Backlash

3.2 MTA Control System

The MTA is directly connected to a custom-built computer controller unit, referred to as the MTA computer [5]. The control unit, shown in Figure 9, sends angular velocity commands to each of the MTA joint controllers [5]. The digital encoders, built into the MTA joint motors, output orientation data for each joint [5] which can be saved for further post-processing. The orientation data were used to ensure that the MTA trajectory commands were properly executed.

Trajectory commands were uploaded into a Linux-powered laptop as .txt files. The MTA computer receives trajectory commands from the Linux-powered computer. Trajectory file formats, procedures for building, and procedures for uploading are outlined in section 3.3 MTA Operation.

Figure 9. MTA Computer Assembly Cabinet.

3.3 MTA Operation

Proper operation of the MTA system requires the researcher to be trained and to comply with specific instructions, as detailed in the MTA User Manual [8]. To begin, the MTA key must be inserted to unlock the power-on switch of the MTA computer assembly cabinet. Next, the power-on switch is toggled to the "Power On" position. A green light indicates that the computer assembly is powered on. Finally, the researcher must log into to the MTA computer using a secure shell (ssh) within the Linux-powered laptop. Once logged in, the MTA will be ready for operation and commands can be sent to the MTA through the Linux-powered laptop [5]. For convenience, log in commands are presented in Table 2 below.

Table 2. Linux log in commands

Linux Command	Result
ssh root@10.10.10.10	Logs-in to MTA computer. Password is "mtare2"
ls	Lists files in directory. Look for re2mta_rollpitch
cd re2mta_rollpitch/	Changes directory to where only the wrist-roll and wrist-pitch MTA joints are used.

Trajectory files come in two forms: a *home trajectory* and a *dynamic trajectory*. The home trajectory is the starting position of the wind tunnel model. The dynamic trajectory is the path the wind tunnel model follows as commanded. Further details are given in reference [8].

Trajectory home commands are formatted into seven columns:

(1) TIME, (2) X, (3) Y, (4) Z, (5) WRR, (6) WRP, and (7) YAW.

Column (1) includes time steps associated for the trajectory, and the units are in seconds. Using the current approach, time step increments are always 0.008 seconds. Columns (2)-(4) are Cartesian coordinate positions, with respect to the MTA base reference frames, and the units are in meters. Columns (5)-(7) are MTA roll, pitch, yaw, angles, and the units are in radians. Yaw is rotated about the z-axis of the MTA base reference frame. Roll is about MTA joint six: Wrist Roll Roll (WRR). Pitch is about MTA joint five: Wrist Roll Pitch (WRP). Figure 10 shows an example of a home trajectory file. All values, except for TIME, are constant for home trajectory files, since it is only a reference to the model starting position.

Time	*x*	*y*	*z*	*WRR*	*WRP*	*YAW*
0	-0.051	-2.492	-1.622	0.00000	-0.282	-1.654
0.008	-0.051	-2.492	-1.622	0.00000	-0.282	-1.654
0.016	-0.051	-2.492	-1.622	0.00000	-0.282	-1.654
0.024	-0.051	-2.492	-1.622	0.00000	-0.282	-1.654
0.032	-0.051	-2.492	-1.622	0.00000	-0.282	-1.654
0.04	-0.051	-2.492	-1.622	0.00000	-0.282	-1.654
0.048	-0.051	-2.492	-1.622	0.00000	-0.282	-1.654
0.056	-0.051	-2.492	-1.622	0.00000	-0.282	-1.654
0.064	-0.051	-2.492	-1.622	0.00000	-0.282	-1.654
0.072	-0.051	-2.492	-1.622	0.00000	-0.282	-1.654
0.08	-0.051	-2.492	-1.622	0.00000	-0.282	-1.654

Figure 10. Sample section of a home trajectory file. Column headers are for reference only.

Dynamic trajectory commands are formatted into three columns:

(1) TIME, (2) WRP, and (3) WRR.

Column (1) is time, and the units are in seconds. Time step increments are always 0.008 seconds. Column (2) is rotation about MTA joint five: WRP and units are in radians. Column (3) is rotation about MTA joint six: WRR. Figure 11 shows an example of a dynamic trajectory file. Only the TIME and WRP column varied for this particular trajectory.

Time	*WRP*	*WRR*
0	-0.282	0.06300
0.008	-0.27973	0.06300
0.016	-0.27746	0.06300
0.024	-0.27518	0.06300
0.032	-0.27291	0.06300
⋮	⋮	⋮
0.968	-0.00709	0.063
0.976	-0.00482	0.063
0.984	-0.00254	0.063
0.992	-0.00027	0.063
1	0.002	0.063

Figure 11. Sample section of a dynamic trajectory file that last one second. Column headers are for reference only.

3.3.1 MTA Trajectory Programming

Once the researcher is logged in to the MTA computer, the researcher can utilize two important Linux commands: 1) ./mtaAngles and 2) ./mtaMoveTo. The first command, ./mtaAngles, will display all the current angles in radians and degrees to which the MTA joints are currently set. The second command, ./mtaMoveTo, allows the researcher to move the MTA joints.

The first command, ./mtaAngles, is very useful for programing trajectory files. The MTA can be manually positioned to a desired starting location, and ./mtaAngles command will give the associated angles. Next, the MTA can be manually positioned to a desired final position, and ./mtaAngles will give those associated angles. The difference between the starting-position angle and final-position angle is the Sweep Angle (SA). This information is how the home trajectory files are built, as well as dynamic trajectories. Finally, the ./mtaMoveTo command allows the researcher to test moving from a start positon to final position, which assures that equipment moves unimpeded without great risk of damaging equipment. Figure 12 shows the process to create the home trajectory file shown in Figure 10 and the dynamic trajectory file, a sample of which is given in Figure 11.

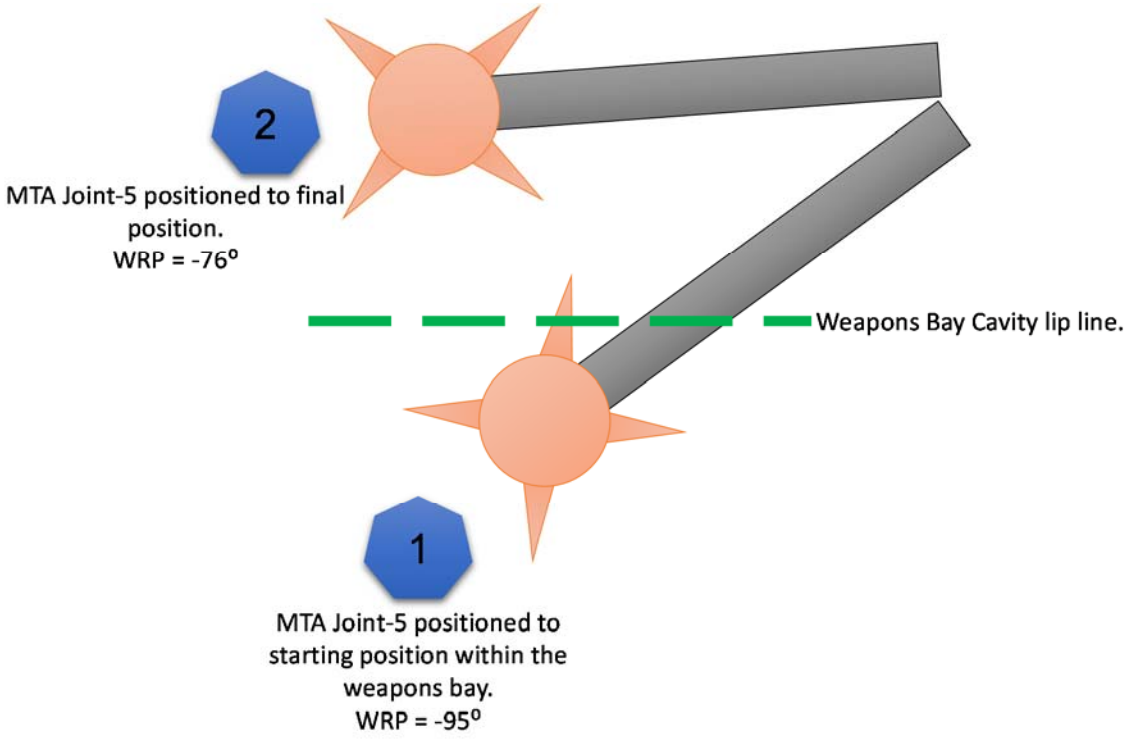

Figure 12. Building a set of trajectory files for use with the MTA. The Sweep Angle is 19°. The ./mtaAngle command yields starting and final WRP angles.

The dynamic trajectory angles are incremented by a small step beginning with the starting position angle. Each step is associated with a time starting at zero seconds. The angle step equation is given below by Equation (9).

$$h_{WRP} = \frac{SA}{TTD}\Delta t \tag{9}$$

Where:

SA = Sweep Angle, 0.3316 radians
TTD = Trajectory Time Duration, 1 second
Δt = 0.008

From Figure 12: starting position begins at -95^o and the final position is at -76^o. The Sweep Angle is thus 19^o or 0.3316 radians. YAW and WRP remain constant for this particular trajectory. The final position will be -76^o or -1.3265 radians. The h_{WRP} step increment is used with Equation (10) to build the WRP column of the dynamic trajectory shown in Figure 11.

$$WRP_{new} = WRP_{old} + h_{wrp} \tag{10}$$

Where:

WRP_{new} = The next WRP angle to be moved to at the next time step
WRP_{old} = The previous WRP angle

3.3.2 Executing MTA Trajectory Commands

Executing MTA trajectories is done with two lines of Linux commands. First, the MTA must be placed to its starting position with the ./mtaHome command. Next, the trajectory is executed with the ./mta command. The researcher must pay close attention to the movements and be prepared to press the emergency stop switch on the MTA Control Pendant, shown in Figure 13, if undesired motions occur, which might lead to equipment damage [5]. Once the trajectory is ready to be executed, one only has to press the green button and the mission store model will commence movement after a five second count-down.

Figure 13. MTA Control Pendant

./mtaHome *home_trajectory.txt*	Moves the WT model to the starting position of the trajectory.
./mta *home_trajectory.txt dynamic_trjectory.txt*	Upon pressing the green button on the control pendant, the trajectory executes.
./mtaMoveTo	A list of parameters are presented on the MTA laptop computer interface. Follow the que in order to mote MTA.
In Separate Terminal: cd Desktop	Changed directory to the desktop. Do this in a separate terminal in order to save MTA encoder data.
In Separate Terminal: scp root@10.10.10.10:/root/re2mta_rollpitch/*.csv . *Password is "mtare2"*	MtaCart.csv and MtaRawAngles.csv encoder data will be copied to the desktop. Subsequent runs will override these files.
scp *new_trajectory.txt* root@10.10.10.10:/root/re2mta_rollpitch/	Uploads a new trajectory into the re2mta_rollpitch directory.

Figure 14. Linux commands to execute MTA trajectories

3.4 Experimental Models

Four generic mission store models were implemented for the experimental analysis. The mission store models are: 1) a missile fabricated out of plastic 2) a missile fabricated out of aluminum 3) an ogive-cylinder fabricated out of plastic and 4) an ogive-cylinder fabricated out of aluminum. Plastic models were constructed with the AFIT Stratasys 3D printer. The aluminum models were constructed by the AFIT model shop. The mission store models are generic and do not represent any weapons currently used by the USAF. The design specifications and drawings are given in Appendix C. The length of each mission store model is 9.25 inches with an outside diameter of 1.29 inches.

3.4.1 Plastic Mission Store Models

The two plastic mission store models were created with an AFIT 3D printer and are shown in Figure 15. The first model is a traditional generic mission store in that it has canards and stability fins. This mission store is referred to as a missile. The second model is exactly the same, except that the second model has no canards nor fins. The second mission store model is described as an ogive-cylinder.

Each model was fabricated to enable mounting to an ATI Nano25 balance – at the x/L = ½ plane. In turn, the balance was attached to a sting which enters the aft region of the wind tunnel model. Great care was taken to ensure that the models were designed so they do not touch the sting in order to avoid erroneous measurements due to grounding of the model.

Alternating Current (A/C) noise was introduced by operation of the low-speed wind tunnel control box. The electrical noise was mitigated by electrically insulating the Nano25 from the sting. Figure 25 shows the insulation hardware. The bolts used to

attach the Nano25 to the sting were wrapped in Teflon tape. The use of plastic mission stores mitigated any inertial noise introduced since the plastic missile and ogive-cylinder weigh 0.200 lbs. and 0.185 lbs, compared to 0.525 lbs and 0.510 lbs, respectively, for the two aluminum models.

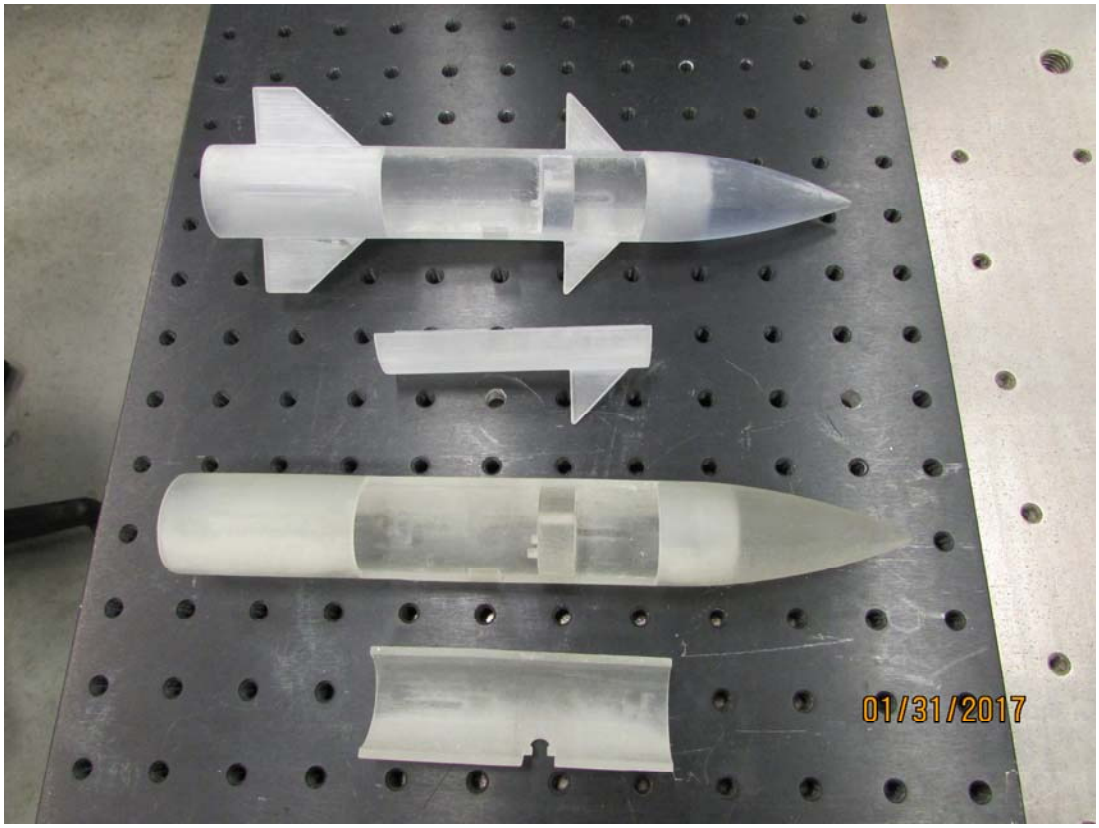

Figure 15. 3D printed: mission store missile model (top) and ogive-cylinder (bottom) with interface access plates removed.

3.4.2 Aluminum Mission Store Models

The AFIT Model Shop fabricated two aluminum mission store models. The first model is an aluminum missile. The second aluminum model is an ogive-cylinder. The aluminum mission store models are shown in Figure 16 below.

Similar to their plastic counterparts, each aluminum model was fabricated to enable mounting to an ATI Nano25 balance – at the x/L = ½ plane. In turn, the balance was attached to a sting which enters the aft region of the wind tunnel model. Great care was taken to ensure that the models were designed so they do not touch the sting in order to avoid erroneous measurements due to grounding of the model. The use of aluminum mission stores introduced an inertial noise, since the missile and ogive-cylinder weigh 0.525 lbs. and 0.510 lbs. respectively. An advantage of the aluminum models is that they resist mechanical and aerodynamic deformation.

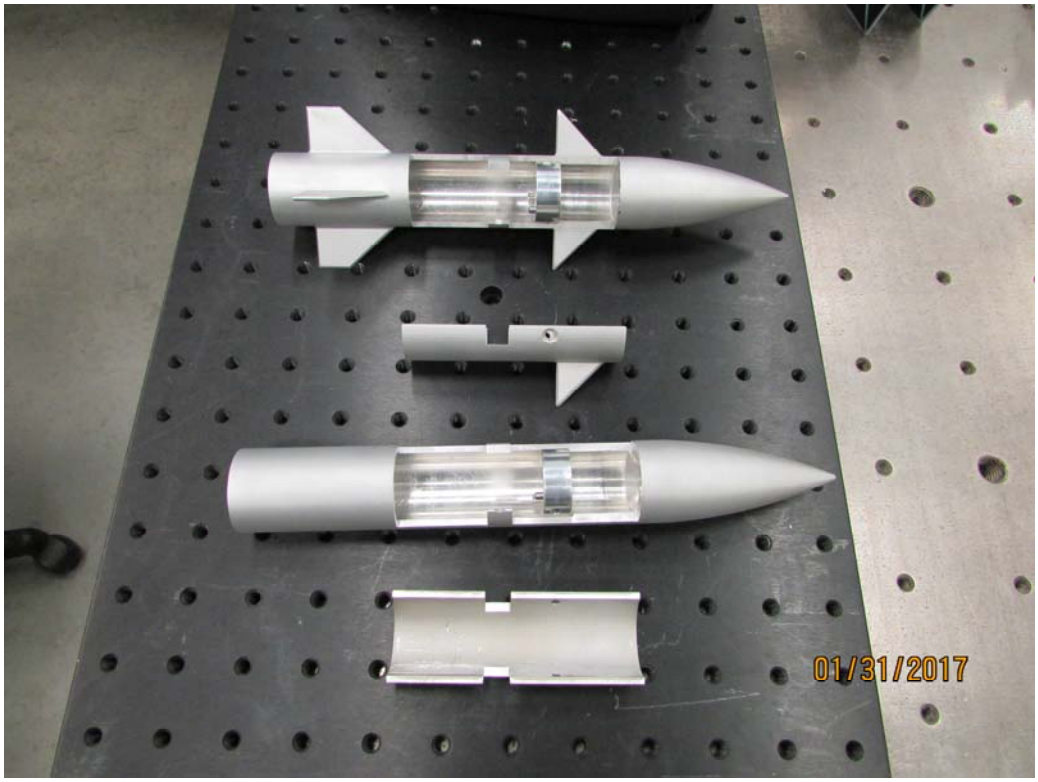

Figure 16. Aluminum mission store missile model (top) and ogive-cylinder (bottom) with interface access plates removed.

3.4.3 Weapons Bay Cavity

The weapons bay cavity is 24” long, 5⅜” wide, and 5⅜” in depth. Four pressure transducers were placed inside the weapons bay cavity. Three of the pressure transducers were placed along the floor of the weapons bay. The pressure transducer locations from the front end of the bay for pressure transducer 1, 2, 3 are: 6.5”, 12.5”, and 18.5” respectively. The fourth pressure transducer was placed 24” from the front end on the back wall of the weapons bay cavity and 3.75” above the floor. The weapons bay configuration is shown in Figure 17.

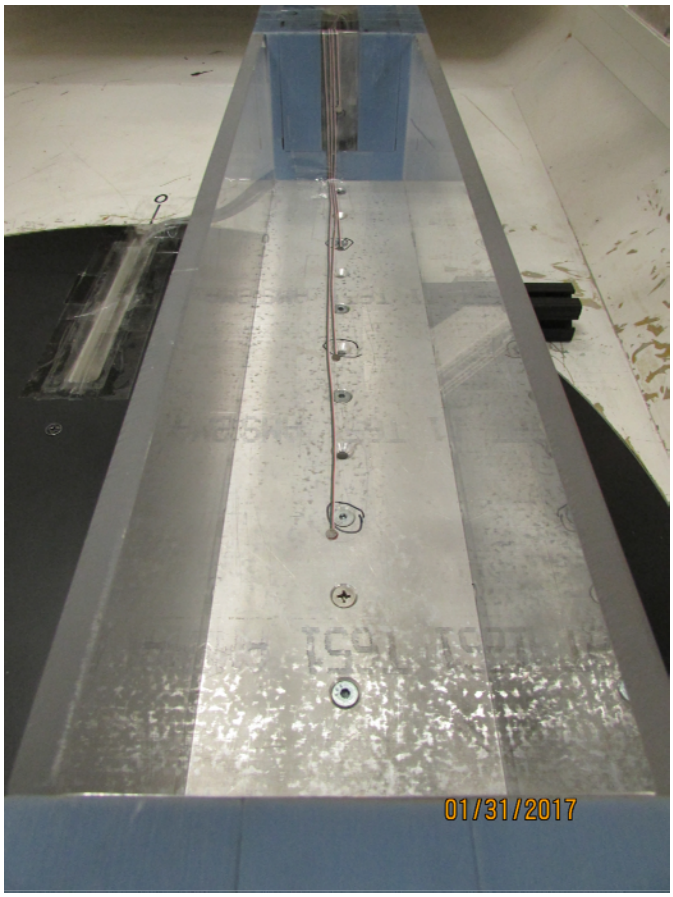

Figure 17. Weapons bay cavity (front-to-back view) with four pressure transducers installed.

Figure 18. MTA sting and aluminum missile model interface.

3.6 Sensors and Measurements

Two primary sensors were used for acquiring the time-accurate data during the motion emulating store release. The first sensor was the ATI Nano25 pressure transducer. This sensor was used to measure the aerodynamic forces and moments acting on the mission store model. The second sensor was a modified Lord MicroStrain 3DM GX1 IMU. This special-order sensor measured the orientation of the mission store model during a commanded trajectory and yielded an analog output. This differs from the work of Sellers and Lancaster in that each used an IMU with a separate digital output [5]. Herein, both the Nano25 and the IMU gave an analog voltage output to the same PXIe-6123 DAQ Card which samples eight channels simultaneously up to 100 kHz in order to ensure synchronized attitude and force data. This allowed for the force and moment data to be precisely aligned with position and velocity in the time domain. Finally, four

Endevco Model 8515C-15 pressure transducers were used to obtain pressure variations within the weapons bay cavity. These were input into a second PXIe-6123 card. The subsequent sections in this chapter give further detail on these sensors.

3.6.1 Nano25 Force/Torque Transducer

The Nano25 is a device used previously at AFIT for the purpose of obtaining force and moment data for oscillating wings [5]. A second Nano25 sensor was purchased with the signal output wire protruding out of the back. This permits the newer Nano25 to acquire aerodynamic loading with reduced wire interference with the airflow around the model.

Figure 19. Nano25 F/T sensor, with wire protruding in the negative z-axis direction.

Nano25 technical specifications are annotated in Table 3. The variables Fx, Fy, and Fz represent the forces acting in the x-, y-, and z- axes respectively. The variables Tx, Ty, and Tz represent the torques about the x-, y-, and z- axes respectively. The variable Fxy represents any combination of forces acting in the x- and y- axes. Similarly, the variable Txy represents any combination of torques acting about the x- and y- axes [5]. At the maximum wind tunnel speed of 120 MPH, all overload values are safe from being reached. Data output rates and measurement units are dependent on the specific data acquisition hardware setup [5]. Details for this information is given in section 3.7.

Table 3. Nano25 F/T Sensor Technical Specifications [5]

Calibration Specifications		
	Sensing Ranges	Resolution
Fx, Fy	25 lbf	1/224 lbf
Fz	100 lbf	3/224 lbf
Tx, Ty	25 lbf-in	1/160 lbf-in
Tz	25 lbf	1/320 lbf-in
Single-Axis Overload		
Fxy	± 520 lbf	
Fz	± 1600 lbf	
Txy	± 380 lbf-in	
Tz	± 560 lbf-in	
Physical Specifications		
Weight	0.14 lb	
Diameter	0.984 in	
Height	0.85 in	

The Nano25 senses forces and torques utilizing a right-hand rule coordinate reference frame system. The origin of the reference frame used for torque measurement is positioned front and center on the face of the Nano25 where it interfaces with the mission store model. Figure 20 shows the Nano25 sensing reference frame. A detailed drawing of the Nano25 from ATI is provide in Appendix C. All moment reference points for all

mission store models are at x/L = ½. Furthermore, all yaw reference points are also at x/L = ½.

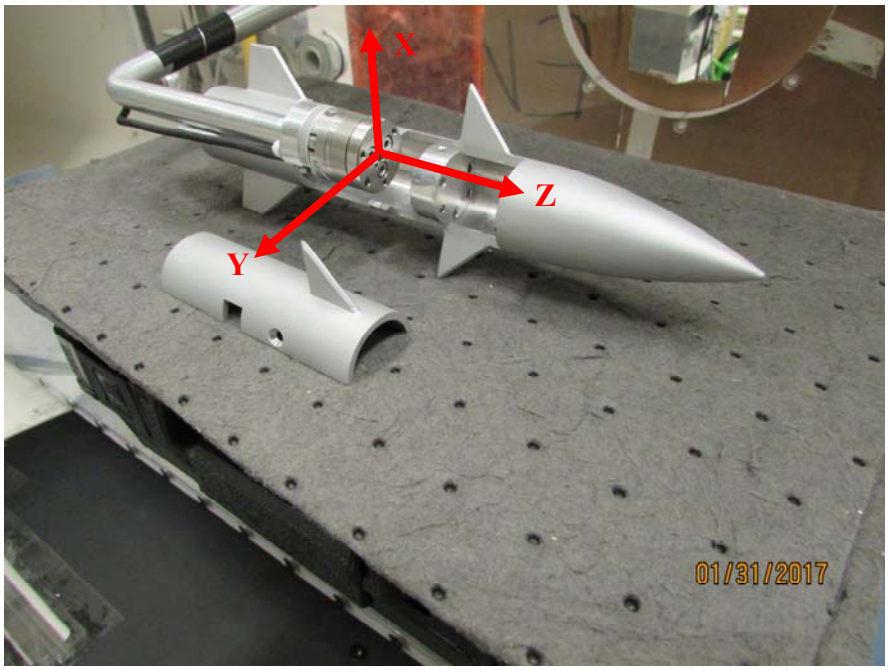

Figure 20. Nano25 Coordinate Reference Frame with origin on the face of the Nano25.

With the Nano25 coordinate reference frame system defined, great care was taken to ensure that measurements were obtained consistent with the coordinate system of Figure 5 as given by the AIAA Nomenclature and Axis Systems for Aerodynamic Wind Tunnel Testing Guide [27]. Specifically, the positive x-axis of the Nano25 aligns with positive normal forces. The y-axis of the Nano25 aligns with positive side forces. The negative z-axis of the Nano25 aligns with positive axial forces. If the load distribution would tend to cause the model to pitch up in the wind tunnel, that is – with the ogive

pointing up and away from the wind tunnel test section floor, a positive pitch moment is recorded.

Analog voltages were produced by the Nano25 as it was moved along prescribed trajectories. The voltages were recorded by LabVIEW as .lvm files, where they were post-processed and converted to forces and torques in MATLAB. Unique calibration matrices are provided by ATI, and the calibration matrix used during experiments is discussed in section 3.8 below.

3.6.2 3DM GX1 Inertial Measurement Unit

To obtain the mission store attitude as it undergoes its prescribed trajectories, an IMU was incorporated. A manufacturer-modified MicroStrain 3DM-GX1 was chosen because it offers an analog output that can be synchronized with the analog voltages produced by the Nano25. The data output rate for the 3DM-GX1 is 100 Hz.

The IMU was attached to the MTA joint-6 (Wrist Roll) so that it can record MTA wrist pitch and wrist roll maneuvers while not being in the free stream. The IMU x-axis is along the analog output wires as shown in Figure 21. The IMU y-axis points upstream when the arm is level. The IMU z-axis is down toward the laboratory floor.

The powered IMU produces a voltage signal as it undergoes a prescribed trajectory. Similar to the data obtained with the Nano25, LabVIEW saves the voltage data to .lvm files. The voltages were converted to angle data during post-processing with MATLAB.

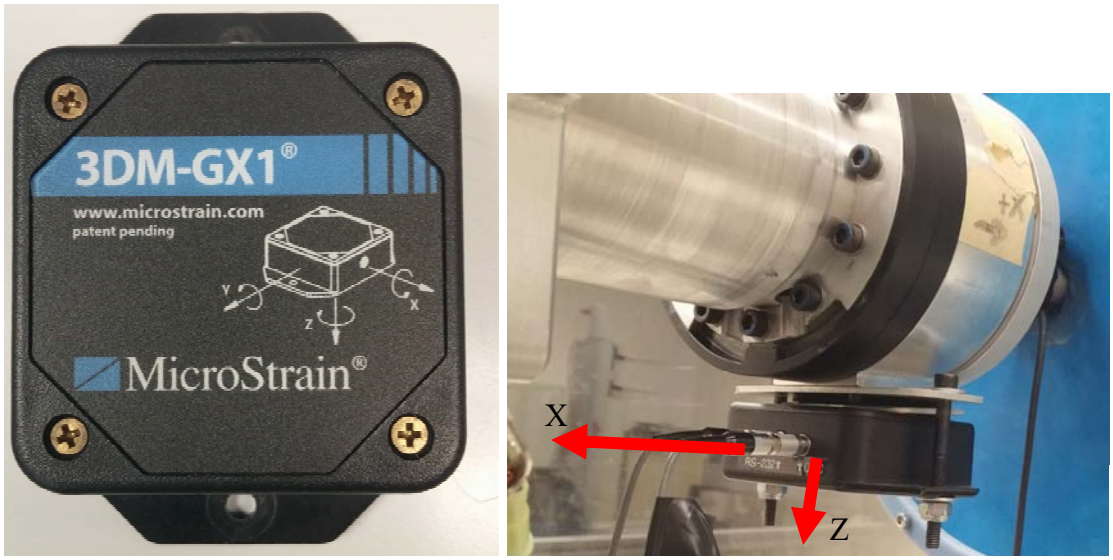

Figure 21. Special-Order LORD MicroStrain 3DM-GX1 IMU attached to MTA joint-6.

3.6.3 Endevco Model 8515C-15 Pressure Transducers

Four Endevco Model 8515C-15 piezoresistive pressure transducers were used to measure absolute pressure within the weapons bay cavity. The positions of each pressure transducer are shown in Figure 22. Each pressure transducer is 6.30mm in diameter, 0.76mm thick, can sample up to 180 kHz, and has a range of 0 to 15 psia.

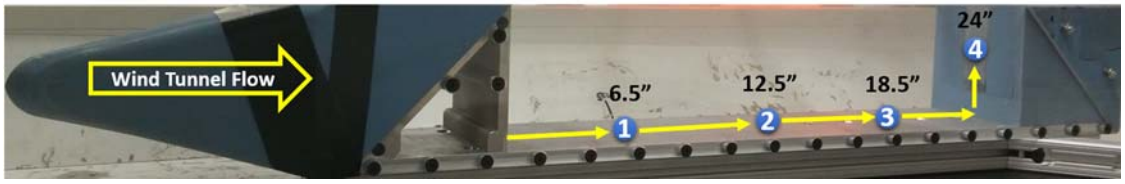

Figure 22. Endevco Model 8515C-15 pressure transducers installed in the weapons bay cavity.

Four wires protrude from each pressure transducer. Two of the wires are for excitation (+,-) and the other two are for output signals (+,-). The four wires connect to a custom RS-232 cable which interfaces with an Endevco Model 136 DC Differential Voltage amplifier [5]. The voltage amplifier supplies the pressure transducer with a 10V excitation signal, the output is filtered with a 10 kHz low-pass filter and the signal is amplified to a 200mV/psi analog output voltage signal [4].

Figure 23. Endevco Model 136 DC Differential Voltage Amplifiers.

The settings for the Endevco Model 136 voltage amplifier are given in Table 4. Each pressure transducer has a unique input sensitivity value provided by the supplier. This information can be found in data sheet stored in the pressure transducer storage box. As the user toggles through the menu items in the voltage amplifier box, one must set item number seven to “Vout” and record the value displayed by the voltage amplifier screen. The user must then toggle through the menu item again, but set item number

seven to “EU” which stands for Engineering Units and record that value. These two values are used to compute a unique gain for each pressure transducer. The gain is calculated by equation (11) as follows:

$$gain = \frac{EU}{V_{out}} \tag{11}$$

Where:

EU = From Voltage Amplifier box, menu item 7,1)
Vout = From Voltage Amplifier box, menu item 7,2)

Table 4. Endevco Model 136 Voltage Amplifier Settings with example gain calculation

	Menu Item on Voltage Amplifier Box	**User Input**
1	Voltage Excitation	10V
2	Pressure Transducer (PT) Sensitivity	See supplied data sheet unique to each pressure transducer
3	Output scaling	$\frac{maximum\ output\ voltage}{maximum\ PT\ range} = \frac{5V}{15psi}$
4	Set low-pass filter	10 kHz
5	Auto-zeroing	OFF
6	Shunt Calibration	OFF (N/A)
7	Monitoring State	1) Set to Vout and record the value e.g. ≈ 4.8 2) Set to EU and record the value e.g. ≈ 14.33 e.g. $gain = \frac{14.33}{4.3} = 2.98$

3.6.4 Electrical Noise

The wind tunnel control box introduced electrical noise to all sensor devices. The instant the wind tunnel was turned on, by its GUI on the wind tunnel control computer, electrical noise interference was observed with the aid of an oscilloscope. It was observed that metallic objects in the lab behave as antennas. The larger the antenna, the larger the noise signal. For example, Figure 24 shows the LabVIEW force and torque output with noise present in the signal. The goal to mitigate the electrical noise was to insulate the Nano25 in order to render it to be the smallest antenna as possible.

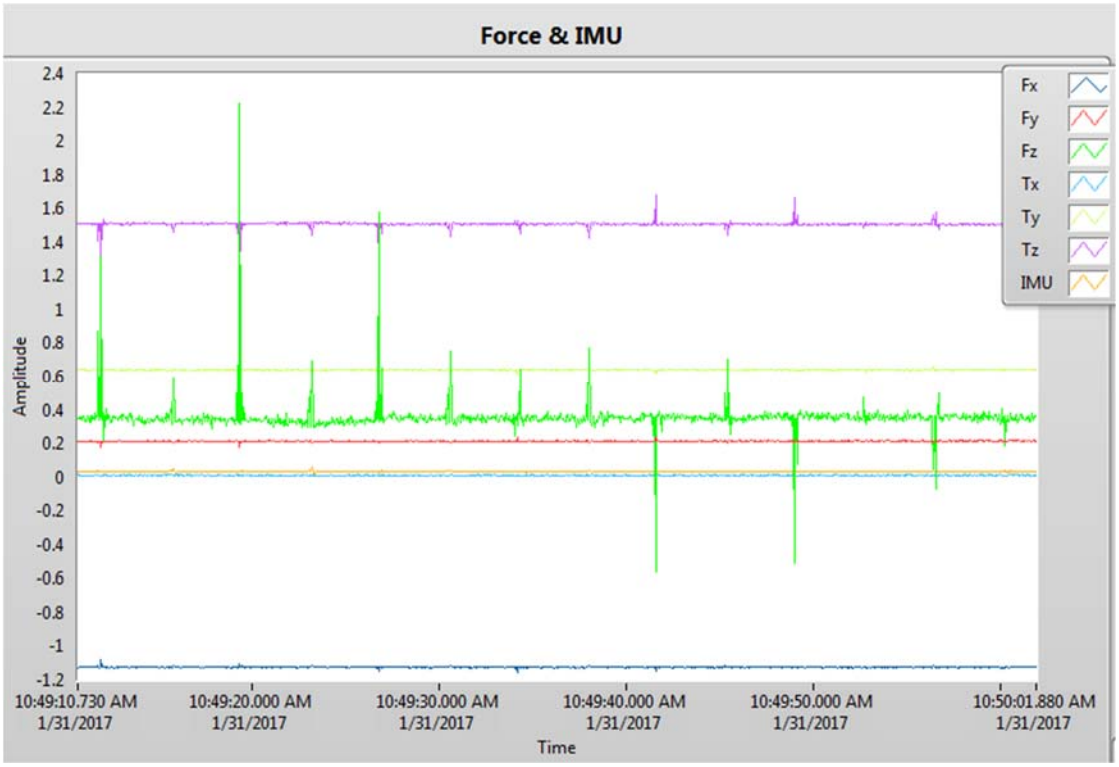

Figure 24. LabVIEW reading electrical noise emitted by wind tunnel control box for the Nano25 attached to the aluminum model. Amplitude reflects voltage.

In order to mitigate the electrical noise as much as possible, the Nano25 was electrically insulated from the sting. Insulation was achieved by placing a thin plastic disc between the Nano25 and the sting interface. The bolts attaching the Nano25 to the sting were wrapped in Teflon tape. Nylon washers insulated the bolt heads. Figure 25 shows the insulation mechanical setup. Once the Nano25 was insulated from the sting, the electrical noise introduced was less, as can be seen in Figure 26. Care was taken to ensure that the plastic disc and nylon washers did not touch the mission store model other than at the faces upon which they interface. Undesired physical contact points can yield erroneous force and moment measurements. Figure 27 shows the small amount of noise present on the 3DM GX1 IMU compared to a no-noise signal. Even under optimal conditions noise interference for the IMU up to ±6mV remained.

Figure 25. Nano25 insulation technique in order to mitigate electrical noise.

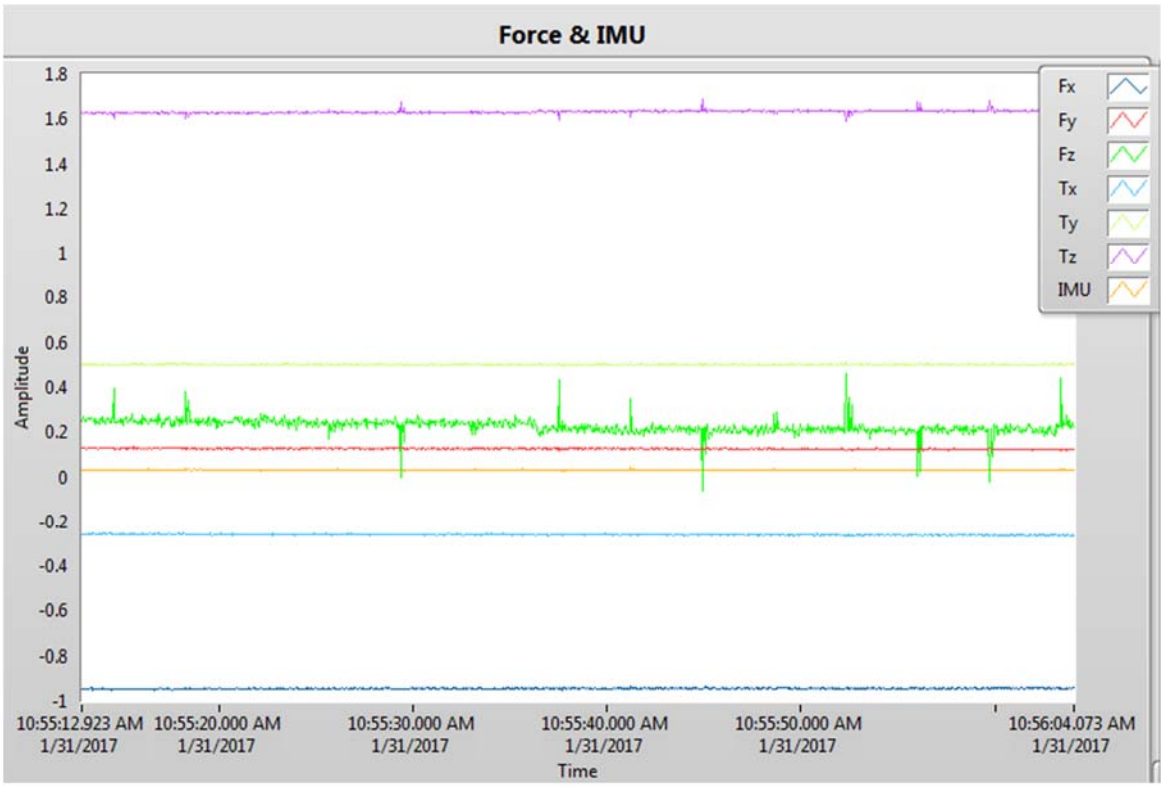

Figure 26. Mitigated electrical noise for the insulated Nano25 attached to the aluminum sting. Amplitude reflects voltage.

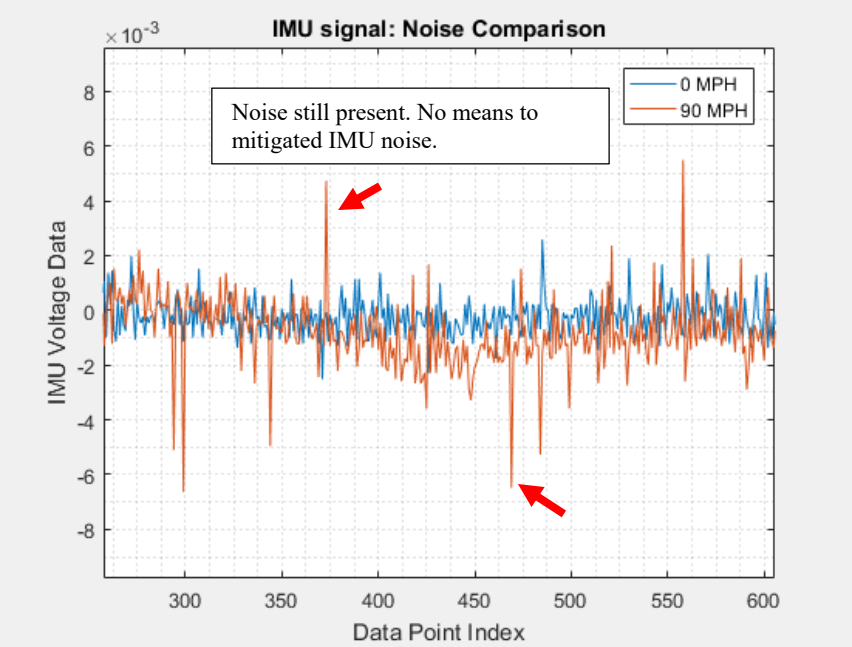

Figure 27. Example of noise peaks introduced by wind tunnel control box on the IMU. The 0 MPH data (blue line) has no control box noise on it. The 90 MPH data (orange line) has small amount to noise interference from the control box.

3.7 Real-Time Data Acquisition

The primary focus of this research is to obtain time-accurate force and moment measurements on a mission store model undergoing prescribed trajectories in the AFIT low-speed wind tunnel. National Instruments (NI) offers a data acquisition software package known as LabVIEW. LabVIEW is a graphical user interface (GUI) programing tool that easily facilitates the primary focus of research. The following two subsections describe the setup of the data acquisition (DAQ) system.

3.7.1 DAQ System Hardware

The primary component of hardware is the PXIe-8133 Embedded Controller. The PXIe-8133 connects to a computer by an Ethernet cable. The PXIe-8133 has a built-in hard drive and operating system which enables real-time data acquisition. Figure 28 shows the DAQ system control hardware.

The PXIe-8133 is embedded in a PXIe-1070 chassis. The PXIe-1078 chassis enables communication with other DAQ cards installed in the system. Two PXI-6123 DAQ card are installed within the chassis. The PXI-6123 DAQ cards provide connections to receive the analog (voltage) inputs produced by the sensors.

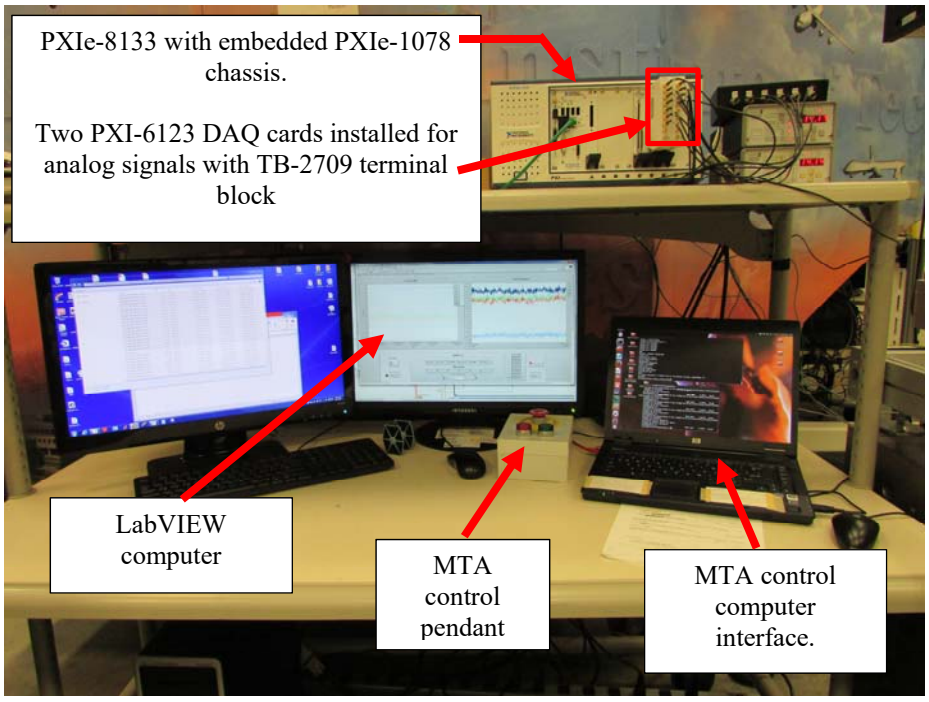

Figure 28. Complete DAQ system control hardware.

The Nano25 pressure transducer connects to a manufacturer supplied signal converter box. It is important to note that the signal converter box is unique to its respective Nano25 sensor. The signal converter box provides power to the internal sensor electronics. From the signal converter box, the six channels from the Nano25 are bundled in a single cable until they are met by a 6-Channel Output splitter. The splitter passes each of the six channels from the Nano25 into the TB-2709 terminal block where LabVIEW records the voltage data as an .lvm file. The six channels of the Nano25 are the voltages for the forces and torques: Fx, Fy, Fz, Tx, Ty, and Tz. Figure 29 shows the complete system hardware associated with the Nano25.

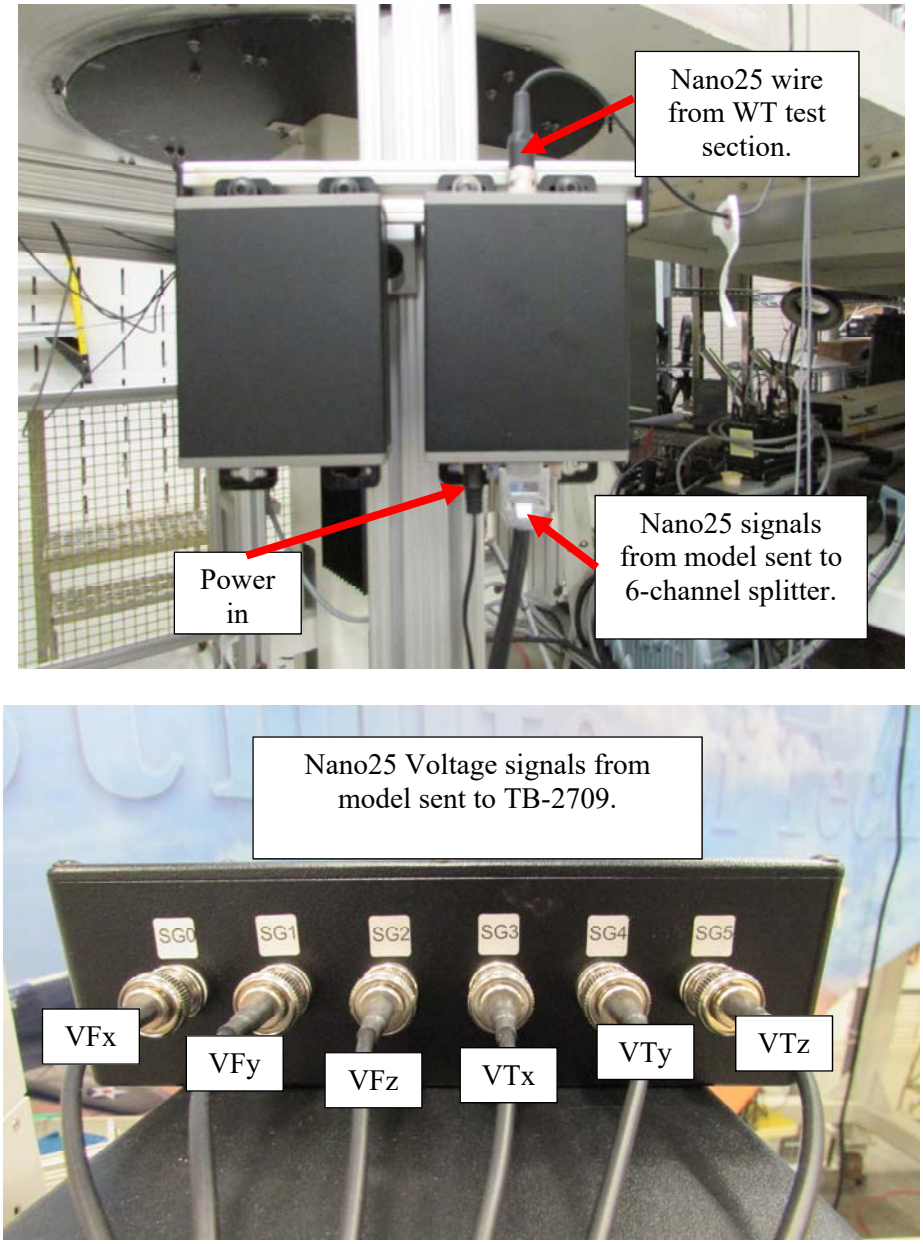

Figure 29. Nano25 hardware: signal converter box (above) and the 6-channel voltage output to PXI-6123 (below).

The 3DM-GX1 IMU has a power supply plug which wires directly into the IMU enclosure. One analog output wire runs from the IMU and connects directly to the TB-2709 terminal board for LabVIEW to record voltage data as the IMU attitude changes

about one axis. Thus, only one attitude angle can be recorded for any given trajectory. Depending on what IMU axis the trajectory is to rotate about, will drive the researcher to check for proper connection. While the model 3DM-GX1IMU is rated for 1000 Hz, in practice the signal proved faulty when sampling rate exceeded 100 Hz. Thus, using the IMU limited the sampling rate to 100 Hz for the LabVIEW program.

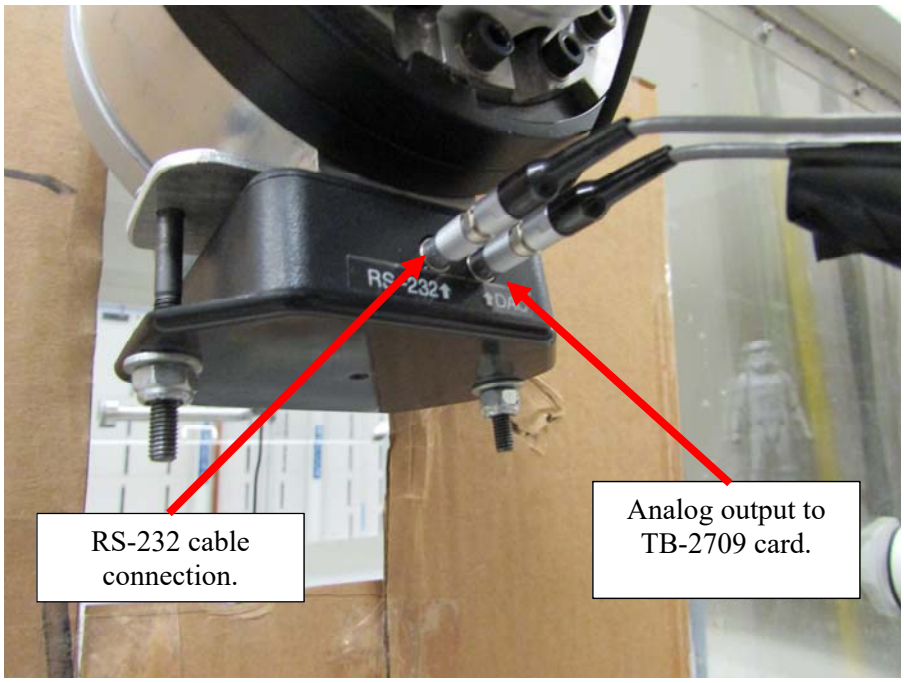

Figure 30. 3DM-GX1 IMU hardware.

Enevco Model 8515C-15 pressure transducers each have four wires. Two are for input signals and two are for output signals. The four wires of each pressure transducer connect to a RS-232 cable. The RS-232 cable connects to an Endevco Model 136 DC Differential Voltage amplifier which can receive up to three pressure transducer connections. Two Model 136 DC voltage amplifiers are required to permit the use of four

pressure transducers. Figure 31 shows the hardware set up associated with the pressure transducers.

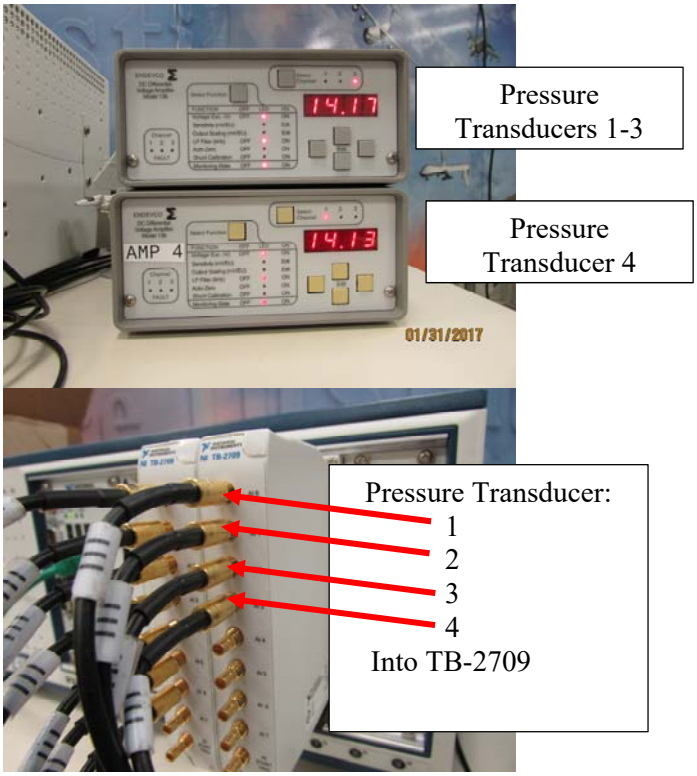

Figure 31. Endevco Model 8515C-15 hardware: Endevco Model 136 DC differential voltage amplifer (above) and PXI-6123 DAQ card (below).

3.7.2 NI LabVIEW Graphical Program

The LabVIEW program used in this study was identical to the code used by the research conducted by Sellers [5]. The only modifications made were: 1) the "while-loops" for acquiring Nano25 signals and the IMU 3DM-GX4-15 (digital output) signals respectively, was merged into one loop. And 2) the sampling rate was set to 100 Hz. The former was done so that the Nano25 signals and 3DM-GX1 (analog output) signals could

be synchronize during data acquisition. The latter was done because the limiting sampling rate was 100 Hz of the 3DM-GX1 IMU.

3.8 Setup of Wind Tunnel Experiments

Wind tunnel experiments consisted of two trajectories: Trajectory Number One and Trajectory Number Two (also referred to as the Pitch-Up Trajectory). Trajectory Number One pertained to mission store model separation from the weapons bay. It was created first but preliminary research led to the need of the development of a simpler trajectory in order to refine and better understand the data associated with the MTA acquisition system. Hence, Trajectory Number Two was created second, but studied and analyzed first. Trajectory Number Two was a simple pitch up maneuver where the model only pitched up while it was positioned in the freestream. No weapons bay cavity was used with the Pitch-Up Trajectory experiments.

Trajectory number one was for a mission store model initially positioned one-half inch deep into the weapons bay cavity. Over the course of one second, the mission store model was moved out of the cavity by MTA wrist pitch (joint-5) for a sweep angle of 19 degrees. The mission store model final position, for trajectory number one, is in the free stream of the wind tunnel, nine inches from the weapons bay cavity. The centerline of the mission store model is at the weapon bay lip line, the point at which the store crosses the threshold from being inside the bay and into the shear layer, when the sweep angle is at -18º. The purpose of trajectory number one is to obtain time-accurate force and moment coefficients as a store separates from a weapons bay cavity. A total of 192 experiments were conducted using this trajectory.

Trajectory number two was for a mission store centered in the wind tunnel test section at an angle of attack (AoA) of zero degrees. The mission store was rotated by the MTA wrist roll (joint-6) which caused the mission store model to be pitched up in the wind tunnel test section for 41.5 degrees. The purpose of trajectory number two was to verify IMU and Nano25 performance and timing alignment, which is the fundamental purpose of acquiring time-accurate force and moment data. Trajectory number two also was used to verify force and moment coefficient data since the simple maneuver distinctly represent the normal force acting on the mission store. A total of 12 experiments are documented herein for this trajectory. Trajectory Number Two data is presented first in Chapter IV.

3.8.1 Trajectory Number One: Store Separation

Mission store model separation tests utilized trajectory number one, described above. Mission store separation tests were conducted both with the mission store in the front of the weapons bay (nose at x/L=0.1) and with the mission store in the back of the weapons bay (x/L=0.6). Furthermore, mission store model separation tests were conducted with an initial AoA of: -10º, -5º, and 0º where the mission store was pitched by MTA joint-6 about at the moment reference of x/L = ½. The ability to perform positive AoA tests was prevented by the sting interfering with the side walls of the weapons bay. It is important to note that these model attitudes follow the convention given in Figure 5. A negative AoA in the wind tunnel is a positive AoA for operational purposes. Thus, the experiments corresponding to situations where the mission store models would be initially pitched up towards the airframe, which obviously reflects a worst-case scenario.

Figure 32 shows the store separation of the aluminum mission store model positioned in the aft of the weapons bay cavity and the final position in the wind tunnel test section freestream. All three initial AoAs are also shown in the figure. Figure 33 shows the frontal view of same store separation of the aluminum mission store model positioned in the back of the weapons bay cavity and the final position in the wind tunnel test section freestream. All three initial AoAs are also shown in the figure as well.

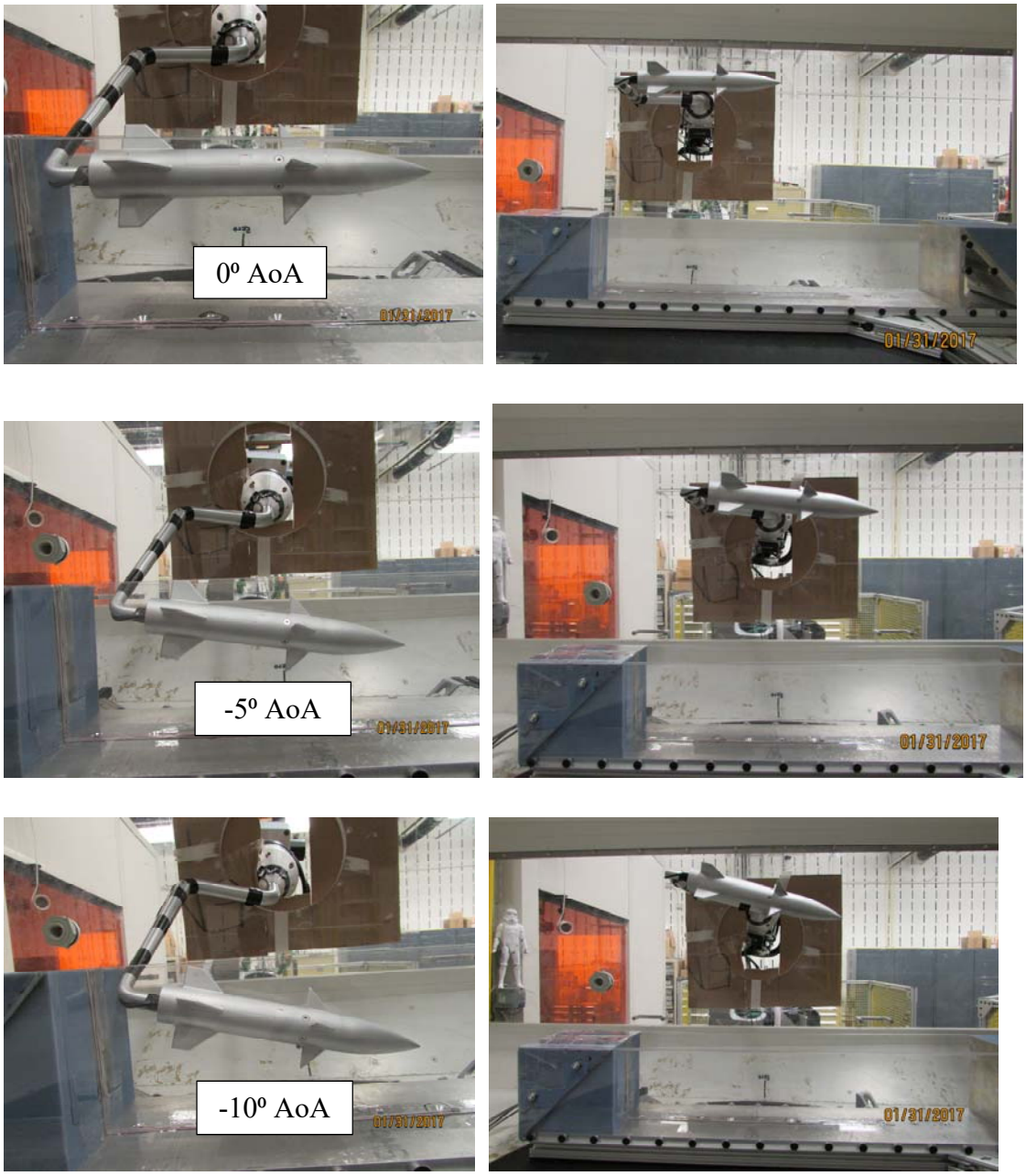

Figure 32. Side view of aluminum missile separation from back of weapons bay: positioned at the starting position (left column) with initial respective AoA of 0º, -5º, and -10º and then in the final position (right column).

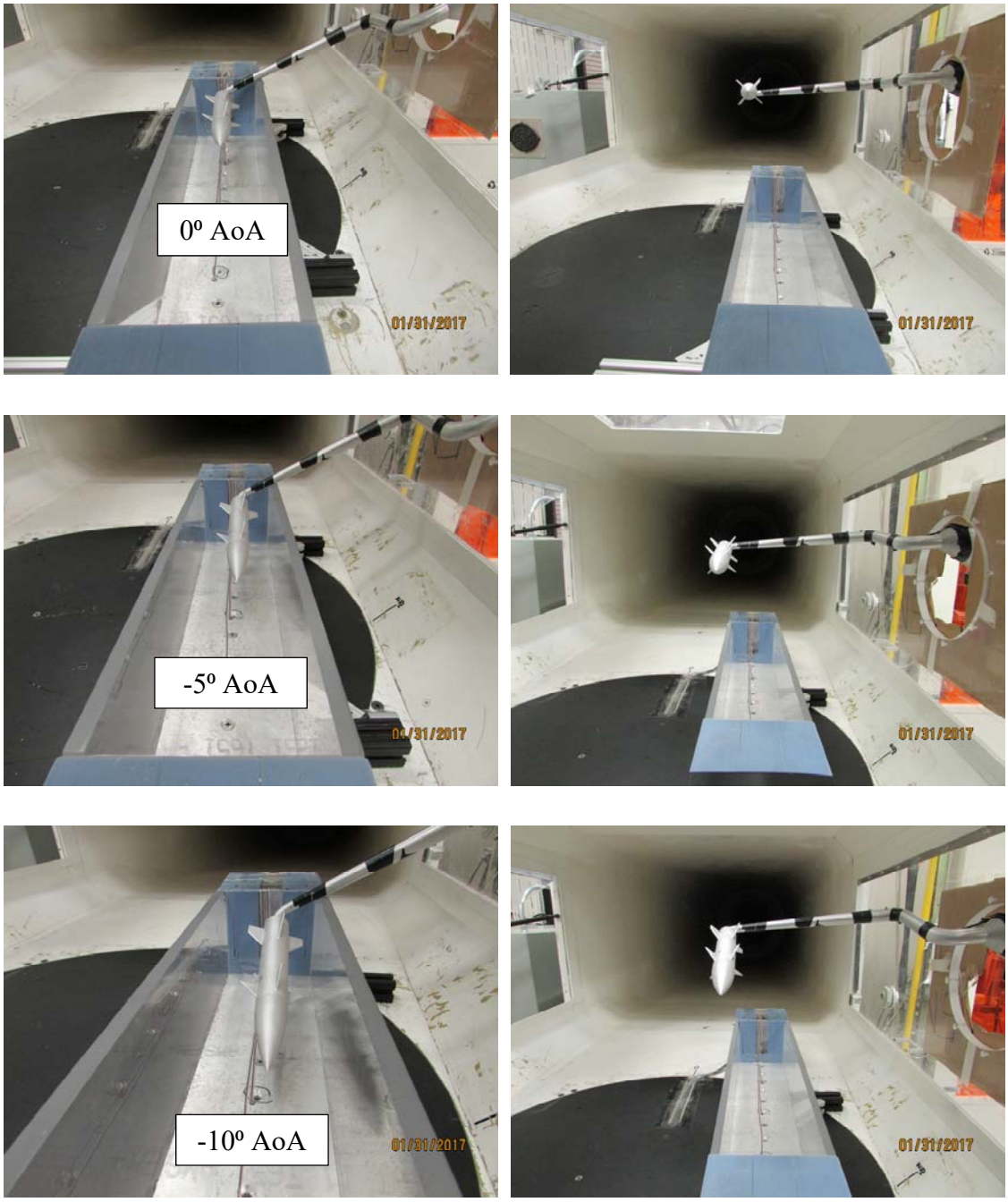

Figure 33. Frontal view of aluminum missile separation from back of weapons bay: positioned at the starting position (left column) with initial respective AoA of 0º, -5º, and -10º and then in the final position (right column).

Trajectories for mission store models separating from the front of the bay are identical to the trajectories where mission store model separated from the back of the bay. The weapons bay cavity, bolted to the wind tunnel test section floor, is positioned farther downstream within the test section in order to accommodate the mission store model. Figure 34 illustrates the difference in the two cavity positions with the top image corresponding to a “back-of-bay” separation while the lower image corresponds to a “front-of-bay” separation.

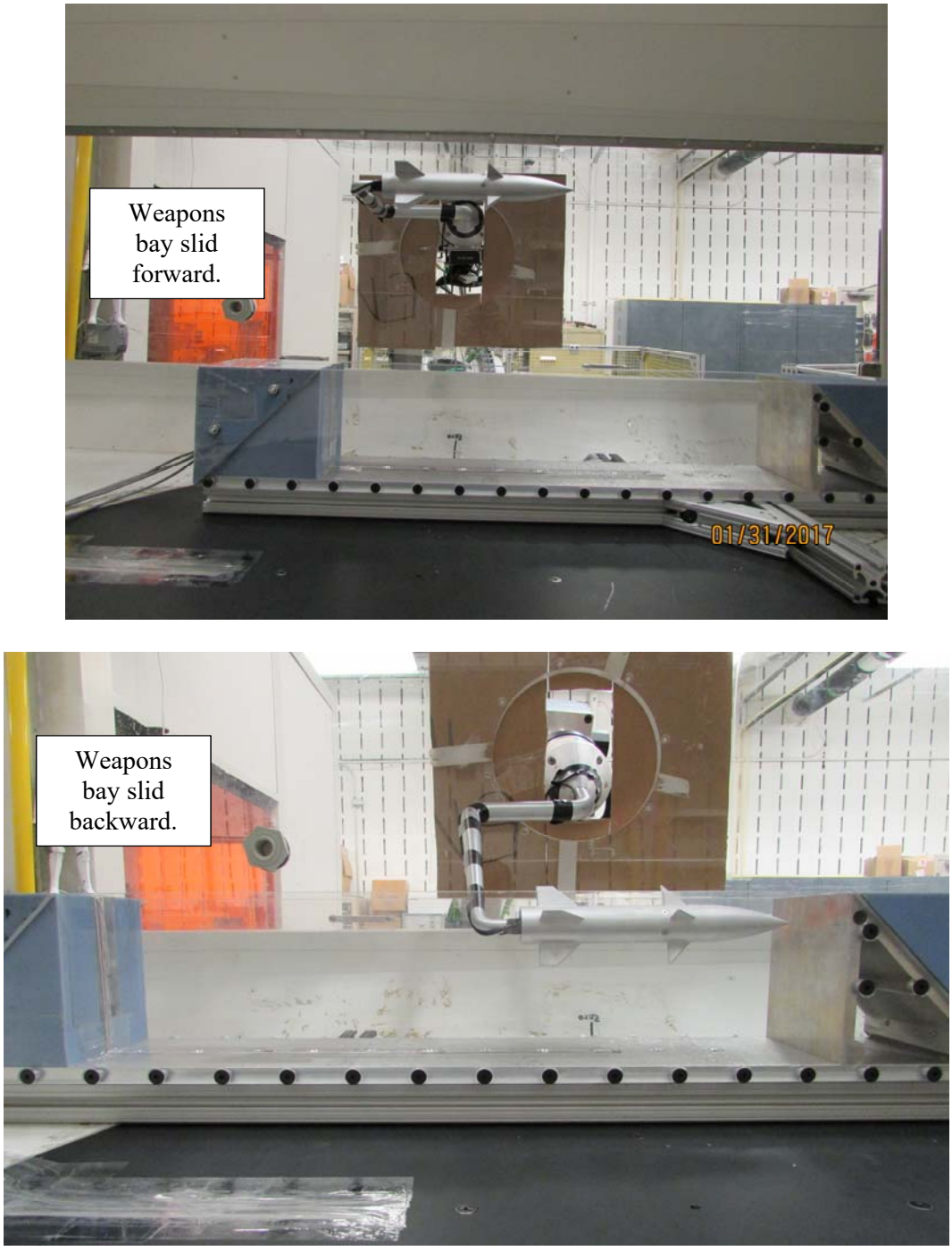

Figure 34. Weapons bay re-positioned to accommodate the aluminum missile for a "front of bay" store separation wind tunnel experiment. All trajectories are identical for “front-of-bay” and “back-of-bay” experimental test runs.

3.8.2 Pitch-Up Trajectory: Mission Store Model Positive Pitch

The Pitch-Up Trajectory consisted of using the wrist roll of the MTA to pitch the mission store from 0º upward to 41.5º about the moment reference of x/L = ½. The purpose of the trajectory was to acquire force and moment data at a high signal-to-noise ratio in order to objectively verify synchronized force-and-moment data with attitude positioning. This sequence of tests, performed prior to those of Trajectory Number One and any future one-off trajectories, provided confidence in the fidelity of the system. Specifically, the pitch rotation yielded distinct normal force and a distinct pitching moment. This trajectory also allowed baseline comparisons of the missile and ogive-cylinder, as well as illustrating differences between the plastic and aluminum models.

Figure 35. The aluminum missile mission store starting position of 0º AoA and final position of 41.5º AoA. Moment reference is x/L = ½.

3.9 Post Processing

The DAQ system recorded raw analog voltage data corresponding to all Nano25 and IMU signals. Converting the raw voltages to forces, torques, and attitude angles was achieved by post processing carried out by MATLAB. Furthermore, MATLAB was used to generate figures.

3.9.1 Converting Nano25 voltage signals

The Nano25 must be used with its unique signal conditioner box. A labeling system is provided by the manufacturer, ATI, in order to properly connect the Nano25 to its distinct signal conditioner box. The Nano25 used in this study has the label: FT18962. This label can be seen on top of the signal conditioner box. Furthermore, each Nano25 from ATI comes with a unique calibration matrix. The calibration matrix is used to convert the voltage, as recorded by LabVIEW, to forces and torques. Below is the Nano25 calibration matrix programed into MATLAB.

```
CalMat = ...
    [  0.15346  -0.01697  -0.01582   2.87077  -0.03571  -2.96696;
      -0.38481  -3.33084   0.09813   1.62079   0.07247   1.72610;
       5.71675   0.04764   5.47653   0.02115   5.63704  -0.18079;
      -0.13441  -1.10252   2.19394   0.53490  -2.12916   0.62782;
      -2.54867  -0.01872   1.20386  -0.96034   1.37114   0.95817;
      -0.05067  -1.04394  -0.13412  -1.01168   0.04208  -1.05521 ];
```

Figure 36. Nano25 calibration matrix used to convert voltage signals to force and torque measurements.

The 6x6 calibration matrix is multiplied by the 6x1 column vector of recorded voltage data, yielding forces and torques. Equation (12) below shows the matrix multiplication.

$$\begin{Bmatrix} Fx \\ Fy \\ Fz \\ Tx \\ Ty \\ Tz \end{Bmatrix} = \begin{bmatrix} 0.15346 & \cdots & -2.96696 \\ \vdots & \ddots & \vdots \\ -0.05067 & \cdots & -1.05521 \end{bmatrix} \begin{Bmatrix} V_{Fx} \\ V_{FY} \\ V_{Fz} \\ V_{TX} \\ V_{TY} \\ V_{TZ} \end{Bmatrix} \quad (12)$$

Where:

F_ = Computed Nano25 measured forces (lbf)
T_ = Computed Nano25 measured torques (inch*lbf)
V_ = Voltage signals recorded by LabVIEW

The matrix algebra was carried out by a "for loop" in MATLAB. Figure 37 below is an example of a "for loop" for a case where the wind tunnel speed was zero MPH. The full details of the MATLAB script are given in Appendix B. The results for this example were the tare data. The tare data were subtracted from three cases where the wind tunnel speed was either 60, 90, or 120 MPH. Force and torque data for these cases were produced in a similar manner.

```
for i = 1:length(time_0)

Voltages_0=[VFx_0(i);VFy_0(i);VFz_0(i);VTx_0(i);VTy_0(i);VTz_0(i)];

    Forces_0(:,i) = CalMat*Voltages_0;

end

%% Tare values
% Use these data to Tare
Tare_Fx = Forces_0(1,:);
Tare_Fy = Forces_0(2,:);
Tare_Fz = (-1)*Forces_0(3,:); % -1 is for AIAA convention

Tare_Tx = Forces_0(4,:)*(1/12); % converted to ft*lbs
Tare_Ty = Forces_0(5,:)*(1/12);%
Tare_Tz = Forces_0(6,:)*(1/12);%

Vimu_zero = Vimu_0;
```

Figure 37. "For loop" used in MATLAB to execute matrix multiplication.

3.9.2 Aligning Data for Taring

Once force and moment data are computed, the next procedure was to tare the data. This step is critical since the balance rotation leads to variation in the forces simply due to gravity. A proper tare isolates aerodynamic force and moments for further analysis. Taring requires that data sets are properly aligned. Figure 38 is an example of how misalignment of the tare in the time domain can contaminate data. The 90 MPH data (orange) leads the 0 MPH data (blue) by a few data points. The highest peak of the 0 MPH data was declared as “index_zero” in MATLAB. The highest peak of the 90 MPH data was declared as “index_mph” in MATLAB.

The initial peaks were caused by a sudden jolt when the MTA joint brakes release at the instant when the trajectory was commanded to execute by depressing the green

button on the MTA control pendant shown in Figure 13. The data from the initial jolt to where the trajectory begins to execute is known as the Incipient Data Set. The data from the point at which the mission store model finishes the trajectory to the end of the data is known as the Final Data Set. The date in between is the Trajectory Data Set. Aligning all data sets by these two peak indices aligned the remainder of the data entirely since the MTA always has a precise five second countdown following the time the control pendent was depressed to initiate the trajectory i.e. during the incipient phase. Furthermore; all force, torque, and IMU data become aligned by the same indices.

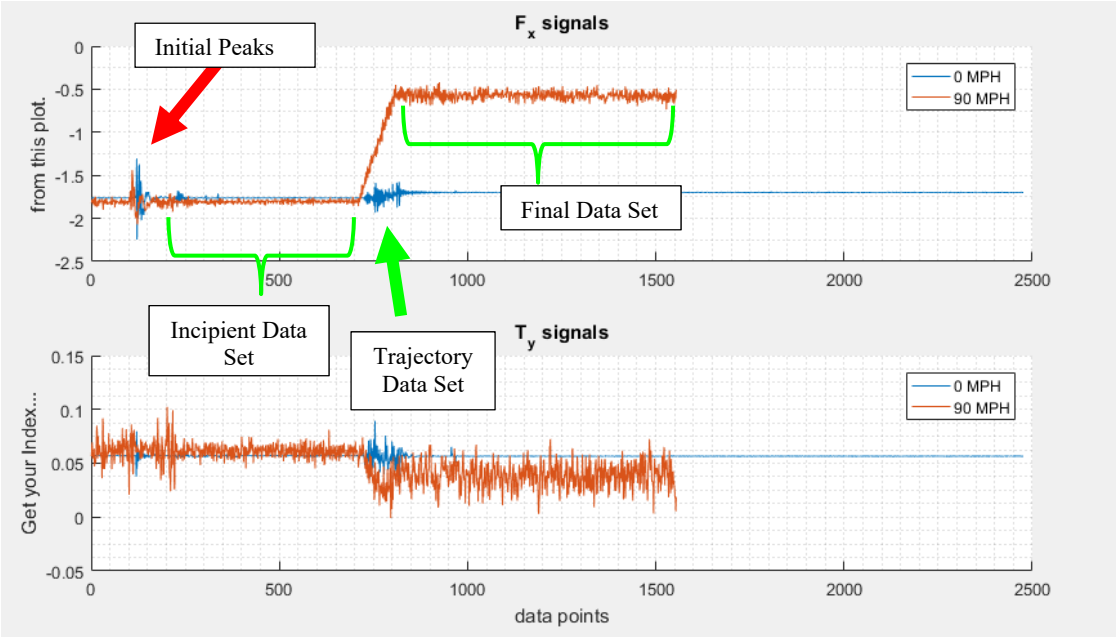

Figure 38. Force and torque data for the case of the plastic missile performing a 41.5° pitch-up trajectory with wind tunnel speed on 90 MPH. Data is aligned for taring based on the initial peaks. Here, the data is not aligned. The 90 MPH data leads the 0 MPH be several data points.

Once alignment indices were declared in MATLAB, an "if loop" was implemented in order to continue post processing as wind tunnel test speeds varied from 60, 90, and 120 MPH. Data acquired for the tare must always be the longest. This ensures that data sets are consistent in element size for easy matrix manipulation in MATALAB. Figure 39 shows the declared indices in an "if loop" to vary as wind tunnel test speeds vary from case-to-case. Furthermore, Figure 39 shows the indices being used for obtaining tared data of the force sensed in the x-axis direction of the Nano25.

```
%% Declare the indices
% These were chosen based on the Mk-1 eyeball

index_zero =   121;
                                    if   Test_Speed == 60
index_MPH = 141; %_____________________________________/
                                       elseif Test_Speed == 90
index_MPH = 104;%_____________________________________/
                                    elseif Test_Speed == 120
index_MPH = 116;%_____________________________________/
                                    end

%% Always run the TARE run goes the LONGEST when acquiring data!!!
% We cut the tail-end off of the 0 MPH data
o_MPH_end=...
length(Fx(index_MPH:end))+length(Tare_Fx(1:index_zero-1));

% % % Align the data sets
% % % Fx Tare

% Align the 0 MPH tare data
Tare_Fx_align = Tare_Fx(index_zero:o_MPH_end); % Tare data, 0 mph

% Align the Fx data for a Test Speed case #
Fx_align = Fx(index_MPH:end); % Normal Force data, # mph

% Once 0 mph data AND # mph data are aligned, TARE it!
TARED_Fx = (Fx_align) - (Tare_Fx_align);
```

Figure 39. Indices declared in MATLAB for the plastic missile as it undergoes trajectory number two and the taring process for Fx.

Once the data alignment and the tare were accomplished a visual inspection of the tare was performed. The visual inspection compares all: forces, torques, and IMU data. Figure 40 shows the successful data alignment and tare for the forces. One can see that the 0 MPH data correspond precisely with the 90 MPH data. Similarly, Figure 41 shows the successful alignment and tare of the torque data. Finally, Figure 42 shows the successful alignment and tare of the IMU data. It is important to note that these particular data are the IMU voltage output signals only. No conversion to angle data was necessary at this point since the primary goal of the post-processing step in to align data. The IMU tare is also unnecessary since IMU requires no physical tare. The subtraction is simply to verify that the IMU data (along with corresponding force and torque data) are truly temporally aligned.

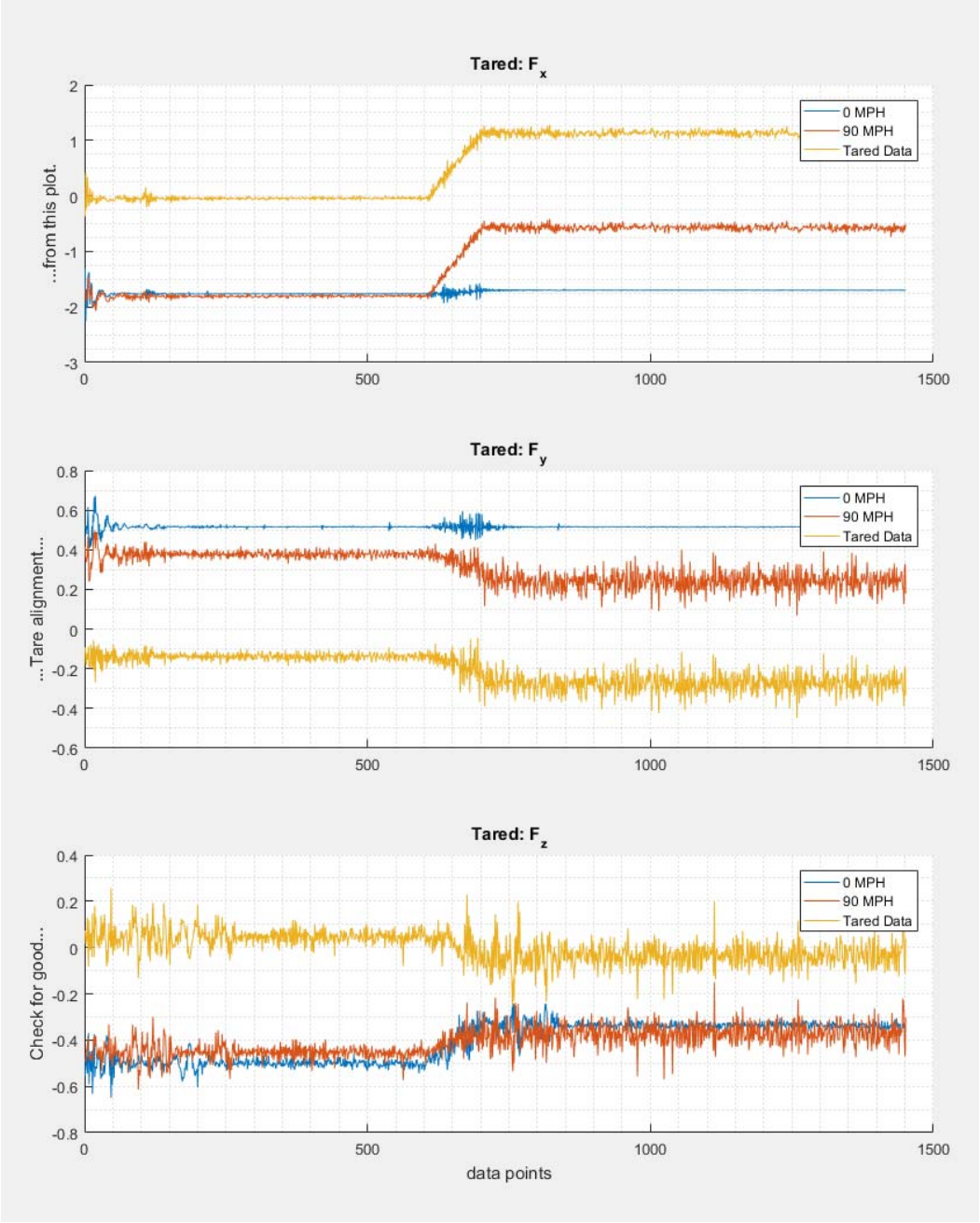

Figure 40. Aligned and tared results for Fx, Fy, and Fz.

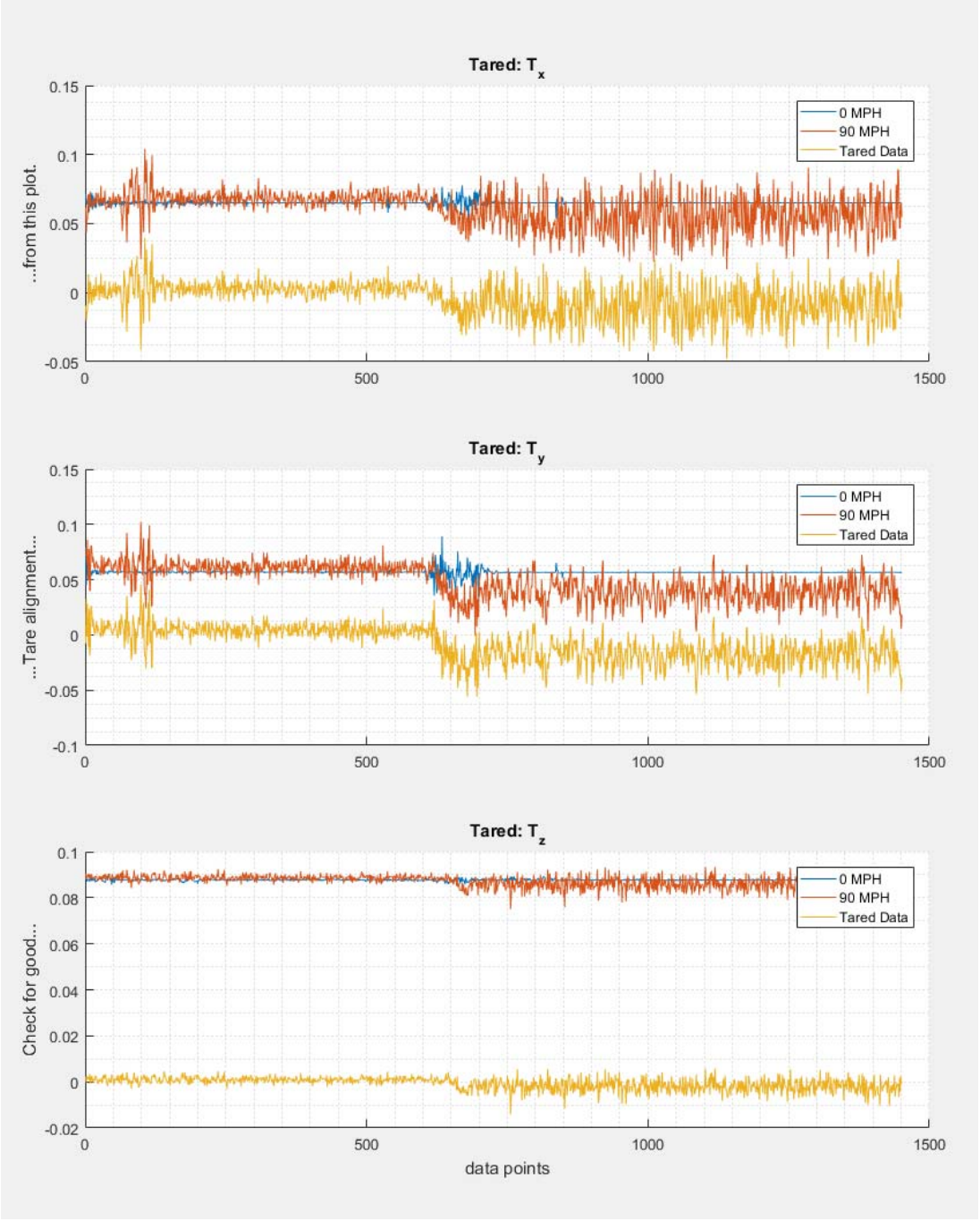

Figure 41. Aligned and tared results for Tx, Ty, and Tz.

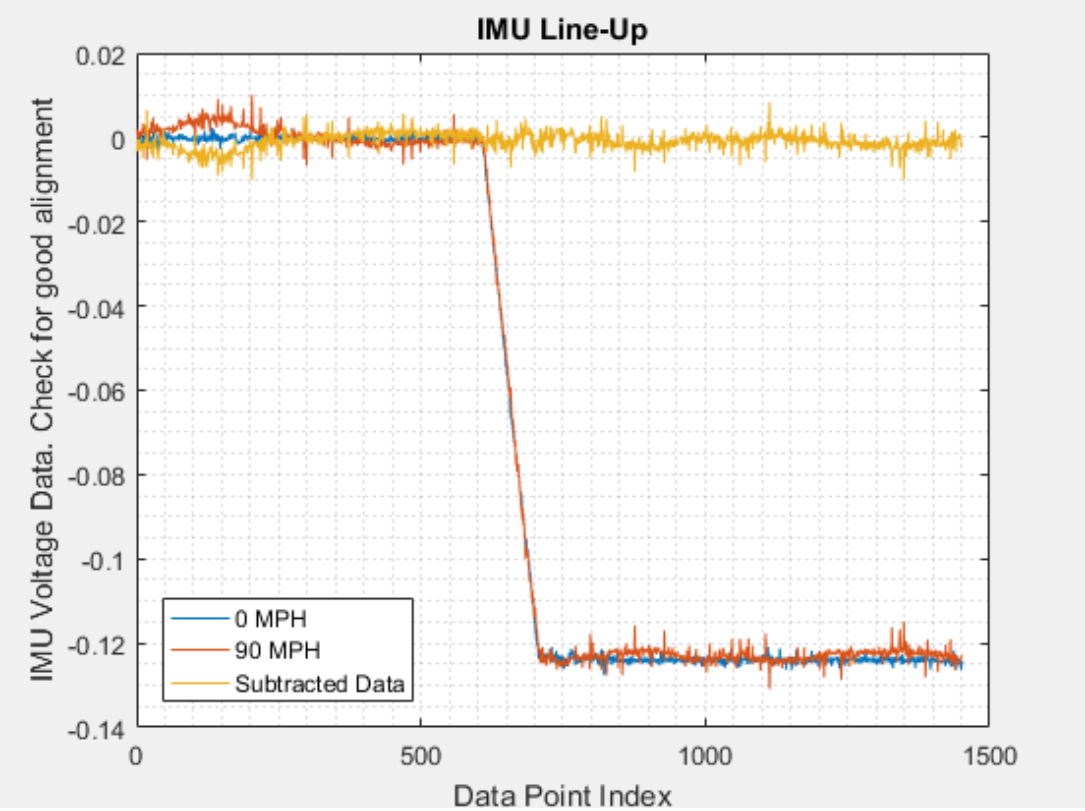

Figure 42. Aligned and tared results of the IMU voltage data. No taring was necessary for the IMU data. The subtraction is to verify that the data are indeed aligned.

3.9.3 Converting 3DM GX1 IMU voltage signals

LabVIEW recorded the voltage output from the IMU. The voltage signals were converted to mission store trajectory angles in MATLAB. Figure 43 shows how the IMU data was converted to pitch angle data for trajectory number two i.e. the pitching maneuver from 0º to 41.5º in the wind tunnel test section. Converting IMU data for trajectory number one was accomplished similarly. The results of the conversion are shown in Figure 44. Since the noise from the wind tunnel control box is still present on the IMU signal, a filter was employed in MATLAB primarily to improve data presentation. Figure 45 shows the MATLAB code used to filter the noisy angle data. The parameters for "cut-off frequency" and "order" were chosen base on best noisy data fit base on visual inspection as seen in Figure 45. In particular, it was paramount to ensure that the filter captures the transition of the data during the beginning and end of the Trajectory Data Set. A smoothing average would yield a fitted line that indicates the trajectory initiates forward in time as shown in Figure 47. It is important to note that some applications demanded that an unfiltered IMU signal be used, and that remained an option.

```
%% Convert Voltage for the IMU to Angles [deg]
% The pitch angle, MTA Wrist Pitch, from 0 to 41.5 degrees

    Vimu_start_avg = mean(Vimu(1:500)); % incipient
    Vimu_end_avg = mean(Vimu(1000:end));% final

PitchAngle = ...
(-1)*(Vimu-Vimu_start_avg)*(41.5)/(Vimu_start_avg-Vimu_end_avg);

PitchAngle = (PitchAngle(index_MPH:end))';
```

Figure 43. 3DM GX1 voltage signals converted to mission store model trajectory angles for trajectory number two.

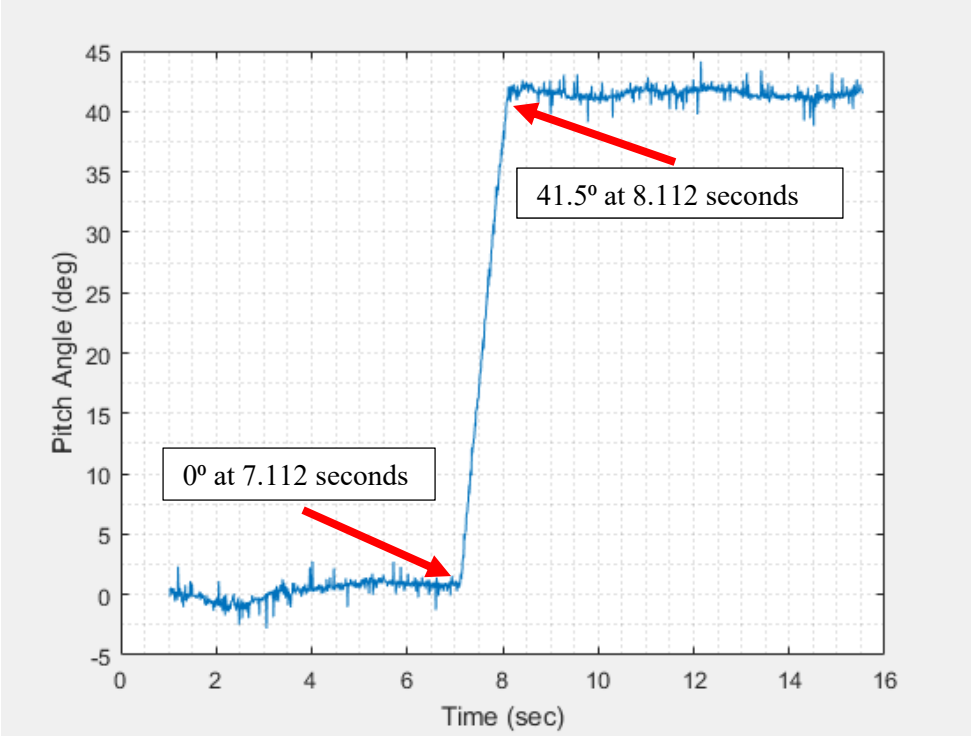

Figure 44. The IMU voltage signal converted to pitch angle for trajectory number two. The trajectory time duration is one second. The incipient data is averaged at 0º and the final angle data is averaged at 41.5º.

```
%% Filter Pitch Angle data [deg]
% This WRR trajectory starts at 0 deg and go up to 41.5 deg

Fs_imu = 100;          % sample rate in Hz
cof_imu = 1;         % cut-off frequency in Hz
order_imu = 20;        % 20th Order of low pass filter
Noisy_PitchAngle = PitchAngle';      % Noisy data
Fnorm_imu = cof_imu/(Fs_imu/2);      % Normalized frequency

df_imu = designfilt('lowpassfir','FilterOrder',order_imu,...
         'CutoffFrequency',Fnorm_imu);

% filter delay in samples
Delay_imu = mean(grpdelay(df_imu));

% Append Delay zeros to the input data
filtered_imu = filter(df_imu,[Noisy_PitchAngle; zeros(Delay_imu,1)]);

% Shift data to compensate for delay
FILTERED_PitchAngle = filtered_imu(Delay_imu+1:end);
```

Figure 45. Filter developed in MATLAB for the pitch angle data. The parameters for "cut-off frequency" and "order" were chosen based on best visual fit.

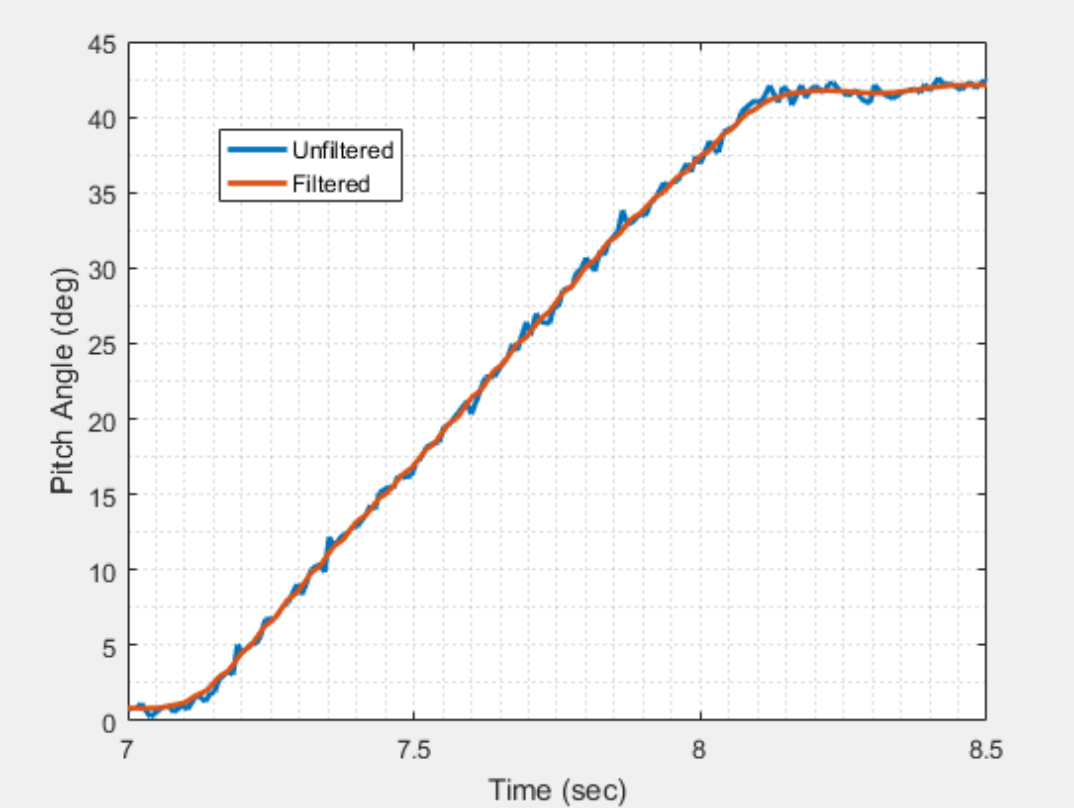

Figure 46. Filtered pitch angle data superimposed on unfiltered pitch angle data.

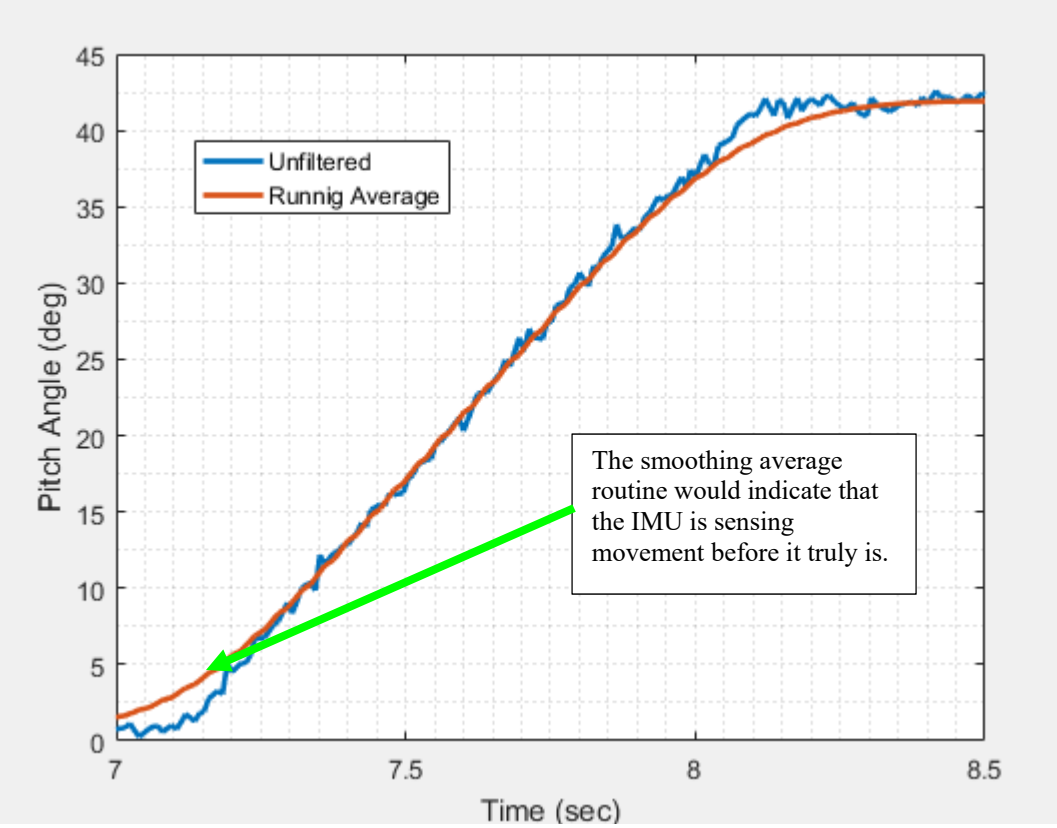

Figure 47. A running average routine leads the angle data to be moving before the IMU actually measures it.

3.9.4 Calculating Aerodynamic Coefficients

Aerodynamic coefficients were calculated. Equations (3) through (8) were from section 2.5 were used. The calculation were carried out utilizing MATLAB. Figure 48 depicts the MATLAB code used for perform the calculations. The tared data, as described in sub-section 3.9.2 above, was used.

```
%% Calculating Aerodynamic Coefficients

Dia = 1.29/12; % missile diameter converted to ft
Ref_Area = (pi/4)*Dia^2; % Model reference Area ft^3
P_psi = Inches_Hg*0.49115420057253 ;% Inches Hg converted to psi
P_psf = P_psi*12^2; % psi converted to psf
     T = Fahrenheit + 459.67;% temp deg F converted to Rankine
     R = 1716;  % (lb*ft)/(slug*R) Imperial Gas constant for Air
     rho = P_psf/(R*T); % density from ideal gas law [slug/ft^3]

V=Test_Speed*(1/60)*(1/60)*(5280/1);% velocity(# MPH) converted to ft/s
    q = (1/2)*rho*V^2; % dynamic pressure

    CN = ( TARED_Fx )/( q*Ref_Area );  % Normal force coeff
    CY = ( TARED_Fy )/( q*Ref_Area );  % Side force coeff
    CX = ( TARED_Fz )/( q*Ref_Area );  % Axial force coeff

    Cn = (TARED_Tx)/(q*Ref_Area*Dia);  % Yaw moment coeff
    Cm = (TARED_Ty)/(q*Ref_Area*Dia);  % Pitch moment coeff
    Cl = (TARED_Tz)/(q*Ref_Area*Dia);  % Roll moment coeff
```

Figure 48. Force and Moment coefficients calculated in MALTAB. Reference area was based on mission store diameter.

Once aerodynamic coefficients were calculated, a filter was develop for the data similarly to the way the filter was developed for the IMU angle data. Figure 49 below shows the MATLAB filter code. With the weapons bay in mind, and using equation (1) from reference [25], a vortex shedding frequency was calculated to be 40 Hz for the case of wind tunnel speed set to 120 MPH. The shedding frequency was calculated to be 33 Hz for the 90 MPH case. Observing that the vortex shedding frequencies decrease as wind tunnel speed decreases, initial "cut-off frequency" were set to 40 Hz as shown in Figure 50, (a) below. Only the "order" parameter of the filter could be varied. For different values of "order," similar filter lines were produced. As a result, the "cut-off frequency" and "order" parameters were both varied in order to produce a filter line that fits the noisy data best based on visual inspection. Figure 50, (b) shows how the

parameters could vary for the Normal Coefficient. Based on this graph, the parameters of "cut-off frequency" and "order" were chosen to be {1, 20} respectively. These parameters allow one to see the general trend of the Trajectory Data Set while mitigating the loss of time-accurate fidelity of data alignment since the same parameters were used for IMU angle data.

```
%% Filter Coefficient Data Sets
    Fs = 100;     % sample rate in Hz
cof = 1;      % cufoff frequency in Hz
order = 20;   % -th Order of lowpas filter
    CN = CN';      % noisy data
    CY = CY';
    CX = CX';
        Cn = Cn';
        Cm = Cm';
        Cl = Cl';
% Design a -th order lowpass FIR filter with cutoff frequency of (Hz)
Fnorm = cof/(Fs/2); % Normalized frequency

df =...
designfilt('lowpassfir','FilterOrder',order,'CutoffFrequency',Fnorm);
    Delay = mean(grpdelay(df)); % filter delay in samples

% Append Delay zeros to the input data
filtered_CN = filter(df,[CN; zeros(Delay,1)]);

% Shift data to compensate for delay
filtered_CN = filtered_CN(Delay+1:end);


 % Repeat steps above for remaining coeffs.
 filtered_CY = filter(df,[CY; zeros(Delay,1)]);
 filtered_CY = filtered_CY(Delay+1:end);
    filtered_CX = filter(df,[CX; zeros(Delay,1)]);
    filtered_CX = filtered_CX(Delay+1:end);

    filtered_Cn = filter(df,[Cn; zeros(Delay,1)]);
    filtered_Cn = filtered_Cn(Delay+1:end);
        filtered_Cm = filter(df,[Cm; zeros(Delay,1)]);
        filtered_Cm = filtered_Cm(Delay+1:end);
            filtered_Cl = filter(df,[Cl; zeros(Delay,1)]);
            filtered_Cl = filtered_Cl(Delay+1:end);
```

Figure 49. MATLAB code for filtering aerodynamic coefficients.

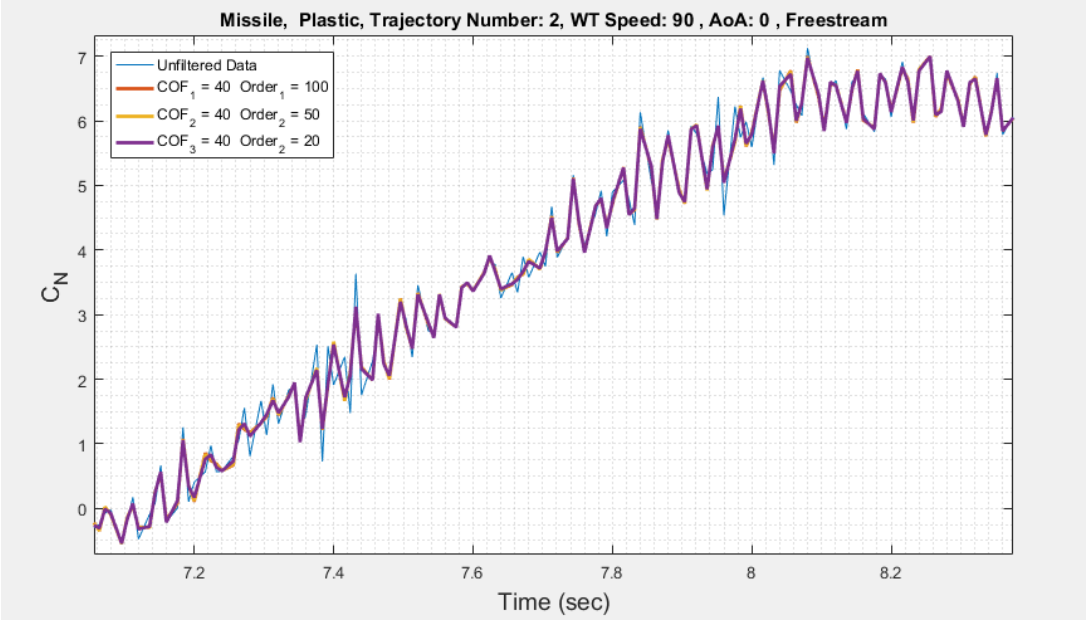

(a)

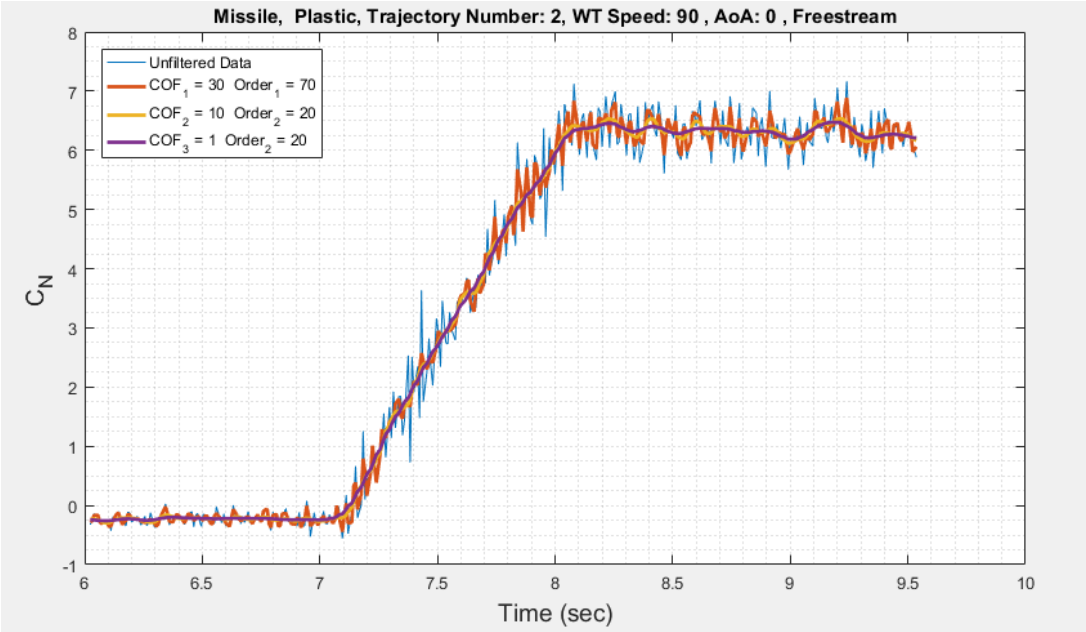

(b)

Figure 50. (a) Plot of Normal Force coefficient with "cut-off frequency" fixed at 40 Hz, zoomed in, to show that varying "order" resulted in similar filter lines. Part (b) varies "cut-off frequency" and "order."

3.10 Reynolds Number and Mach Number

Reynolds number was calculated in MATLAB and the code is given in Appendix B. The results are shown below in Table 5. Reynolds numbers remained relatively constant for all experimental test runs.

Table 5. The Reynolds Numbers

	Reynolds Number	
60 MPH	**90 MPH**	**120 MPH**
5.77e+04	8.67e+04	1.16e+05

Mach number was calculated in MATLAB and the code is given in Appendix B. The results are presented in Table 6 below. Mach numbers remained relatively constant for all experimental test runs.

Table 6. The Mach Numbers

	Mach Number	
60 MPH	**90 MPH**	**120 MPH**
0.078	0.117	0.157

3.11 Summary

Two mission store trajectories were created to perform dynamic wind tunnel tests. Four different mission store models were moved along the prescribed trajectories by the MTA. Wind tunnel speeds varied for experiments utilizing the Pitch-Up Trajectory. Wind tunnel speeds, mission store initial AoA, and streamwise store position within the weapons bay cavity varied for tests involving trajectory number one. Electrical noise from the wind tunnel control box was uncovered and mitigated through electrically insulating the balance. Key aspects of the taring and post processing procedures were explained. Examples of time-accurate force and moment measurements were presented. The scope of the experiments are summarized in Table 7 through Table 10. In Table 7, the experimental program for Trajectory 1 is laid out. In Table 8, a description of repeated store separation runs using a plastic missile model is given. Table 9 provides test conditions for repeated store separation experiments for the aluminum missile. Finally, Table 10 lays out test conditions for the Pitch-Up Trajectory.

Table 7. Summary of wind tunnel tests performed for all mission store models as they separated from weapons bay cavity to the freestream.

Weapons Bay: Aft Position			Weapons Bay: Forward Position		
Initial AoA: 0º 60 MPH 90 MPH 120 MPH	**Aluminum Missile** *Initial AoA: -5º* 60 MPH 90 MPH 120 MPH	*Initial AoA: -10º* 60 MPH 90 MPH 120 MPH	*Initial AoA: 0º* 60 MPH 90 MPH 120 MPH	**Aluminum Missile** *Initial AoA: -5º* 60 MPH 90 MPH 120 MPH	*Initial AoA: -10º* 60 MPH 90 MPH 120 MPH
Initial AoA: 0º 60 MPH 90 MPH 120 MPH	**Aluminum Ogive-cylinder** *Initial AoA: -5º* 60 MPH 90 MPH 120 MPH	*Initial AoA: -10º* 60 MPH 90 MPH 120 MPH	*Initial AoA: 0º* 60 MPH 90 MPH 120 MPH	**Aluminum Ogive-cylinder** *Initial AoA: -5º* 60 MPH 90 MPH 120 MPH	*Initial AoA: -10º* 60 MPH 90 MPH 120 MPH
Initial AoA: 0º 60 MPH 90 MPH 120 MPH	**Plastic Missile** *Initial AoA: -5º* 60 MPH 90 MPH 120 MPH	*Initial AoA: -10º* 60 MPH 90 MPH 120 MPH	*Initial AoA: 0º* 60 MPH 90 MPH 120 MPH	**Plastic Missile** *Initial AoA: -5º* 60 MPH 90 MPH 120 MPH	*Initial AoA: -10º* 60 MPH 90 MPH 120 MPH
Initial AoA: 0º 60 MPH 90 MPH 120 MPH	**Plastic Ogive-cylinder** *Initial AoA: -5º* 60 MPH 90 MPH 120 MPH	*Initial AoA: -10º* 60 MPH 90 MPH 120 MPH	*Initial AoA: 0º* 60 MPH 90 MPH 120 MPH	**Plastic Ogive-cylinder** *Initial AoA: -5º* 60 MPH 90 MPH 120 MPH	*Initial AoA: -10º* 60 MPH 90 MPH 120 MPH

Table 8. Summary of wind tunnel tests performed for plastic missile mission store model as it separated from the weapons bay cavity to the freestream.

Weapons Bay: Aft Position	Weapons Bay: Forward Position
Plastic Missile *Initial AoA:* *0^o* 90 MPH *Repeated 20 times*	**Plastic Missile** *Initial AoA:* *0^o* 90 MPH *Repeated 20 times*
Plastic Missile *Initial AoA:* *-10^o* 90 MPH *Repeated 20 times*	**Plastic Missile** *Initial AoA:* *-10^o* 90 MPH *Repeated 20 times*

Table 9. Summary of wind tunnel tests performed for aluminum missile mission store model as it separated from the weapons bay cavity to the freestream.

Weapons Bay: Aft Position	Weapons Bay: Forward Position
Aluminum Missile *Initial AoA:* *0^o* 120 MPH *Repeated 20 times*	**Aluminum Missile** *Initial AoA:* *0^o* 120 MPH *Repeated 20 times*

Table 10. Summary of wind tunnel test performed which utilized the Pitch-Up Trajectory (Pitched from 0^o to 41.5^o).

Aluminum Missile *Initial AoA: 0º* 60 MPH 90 MPH 120 MPH
Aluminum Ogive-cylinder *Initial AoA: 0º* 60 MPH 90 MPH 120 MPH
Plastic Missile *Initial AoA: 0º* 60 MPH 90 MPH 120 MPH
Plastic Ogive-cylinder *Initial AoA: 0º* 60 MPH 90 MPH 120 MPH

IV. Analysis and Results

Chapter Overview

Experimental tests were conducted using the two trajectories described in Chapter 3. Trajectory number one was a -19º to 0º sweep angle of MTA "wrist pitch" that maneuvered a mission store model inside of a weapons bay cavity to the freestream of the wind tunnel. Trajectory number two was the Pitch-Up Trajectory, a 0º to 41.5º pitch up MTA "wrist roll" maneuver of a mission store model while it was centered in the wind tunnel test section.

Trajectory number two results are presented first due to its simplicity and because it was used to verify the performance of the hardware and sensors. Specifically, the case where the plastic missile store was used at the wind tunnel speed of 90 MPH is shown. All six aerodynamic coefficients were calculated and are presented with the filtered IMU pitch angle data. Coefficient data are presented in unfiltered form and filtered form in order to document time-dependent behavior but also to present the results in a fashion that can be well-understood.

Trajectory number one results are presented next. For consistency, results are presented in the body of this work for the plastic missile store that was used at the wind tunnel speed of 90 MPH. Again, all six aerodynamic coefficients were calculated and presented with the corresponding filtered IMU sweep angle data. Coefficient data are also presented in unfiltered form and filtered form.

Finally, CN and Cm coefficient data for all mission store models are given in a series of tables in order to compare results based on mission store model geometries for

incipient and final phase data sets. Plot titles describe: the mission store model used, the trajectory number used, the wind tunnel (WT) speed, the initial AoA, and the position of the mission store model within the weapons bay. Remaining aerodynamic coefficient results for all test are given in Appendix A.

4.1 Pitch-Up Trajectory: Plastic Missile, WT 90 MPH

The plastic missile mission store initial and final attitude are shown in Figure 35 of Section 3.8. Figure 51 below shows the results of the normal force coefficient along with the filtered pitch angle data. The left y-axis, depicted in green, is the pitch angle. It holds at an angle of zero degrees for the incipient phase of the MTA maneuver. There is a small fluctuation in the pitch angle do to wind impinging on the MTA. At the time near seven seconds, the MTA executed the trajectory. One second later, the trajectory ended and the final phase of 41.5º pitch angle is held for three seconds. The incipient CN data set was averaged along with the final data set and the results are annotated in Table 11. This process was repeated for all mission store models as wind tunnel speed were set to 60, 90, and 120 MPH. As expected, the normal force coefficient increases as the missile model was pitched up. The average value of CN during the incipient phase was found to be about 6.5.

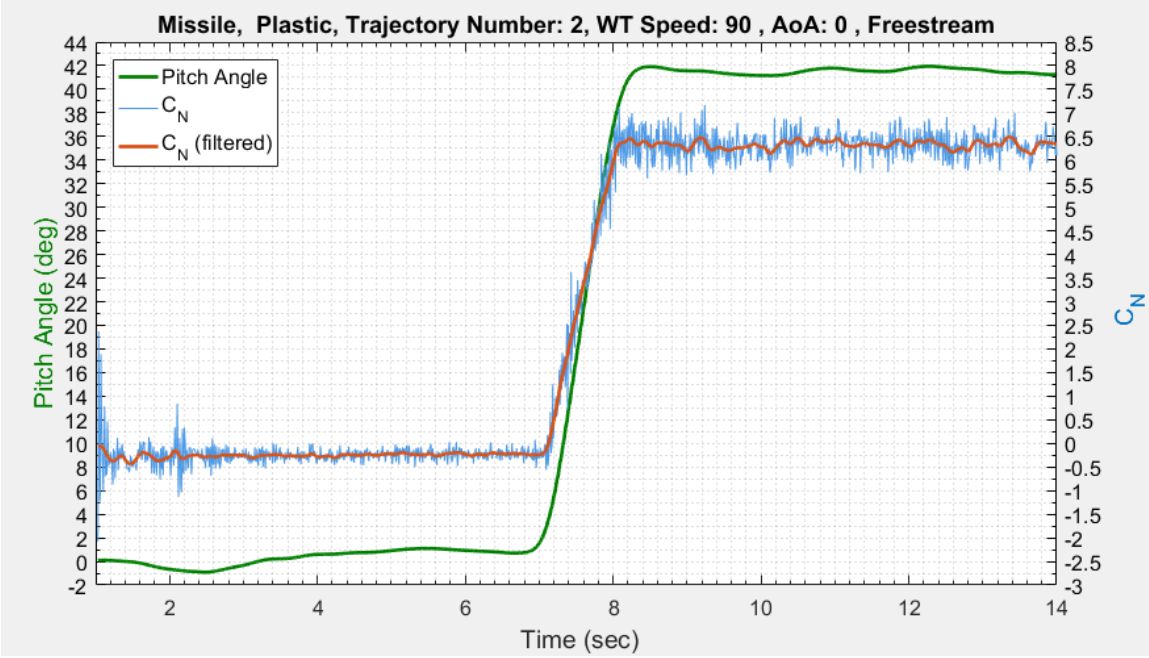

Figure 51. Plastic missile Normal Force coefficient results.

The mission store model was measured with a level as it was in its starting position in order to ensure that the mission store model was precisely in line with wind tunnel flow. Even though the model was set to 0º yaw throughout the trajectory, an identifiable side force was measured with a variation observed as shown in Figure 52. At 0º AoA there is a small amount of negative side force present, yielding a side force coefficient of -0.75. This is indicative of a force acting on the missile model tending to push the missile model towards the MTA. The presence of the sting causes a disruption in the wind tunnel flow, and may be the root cause of the side force. However, one might expect the direction to be opposite. As the model was pitched to 41.5º, the magnitude of the value of CY increased to 1.5, or about 20-25% of the value for CN.

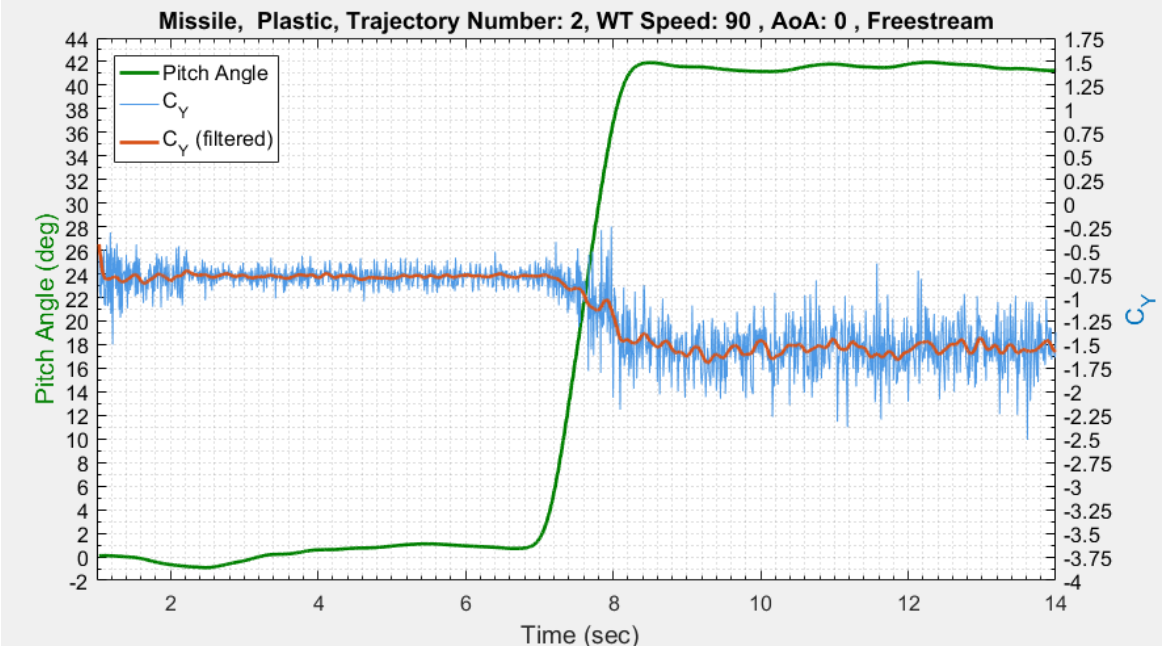

Figure 52. Plastic missile Side Force coefficient results.

The Nano25 is least sensitive in its z-axis direction as given in Table 3. Here the sensitivity range is 100 lbf with a resolution of 3/224 lbf. Nevertheless, axial forces were recorded and are shown in Figure 53 below. During the incipient phase, the axial force coefficient is a positive value of 0.25 which agrees with the convention given in Figure 5. As the missile was pitched up, the values of axial force coefficient decreased to a value of -0.25. Leading-edge suction can result in negative axial forces for some circumstances, so this outcome was considered reasonable.

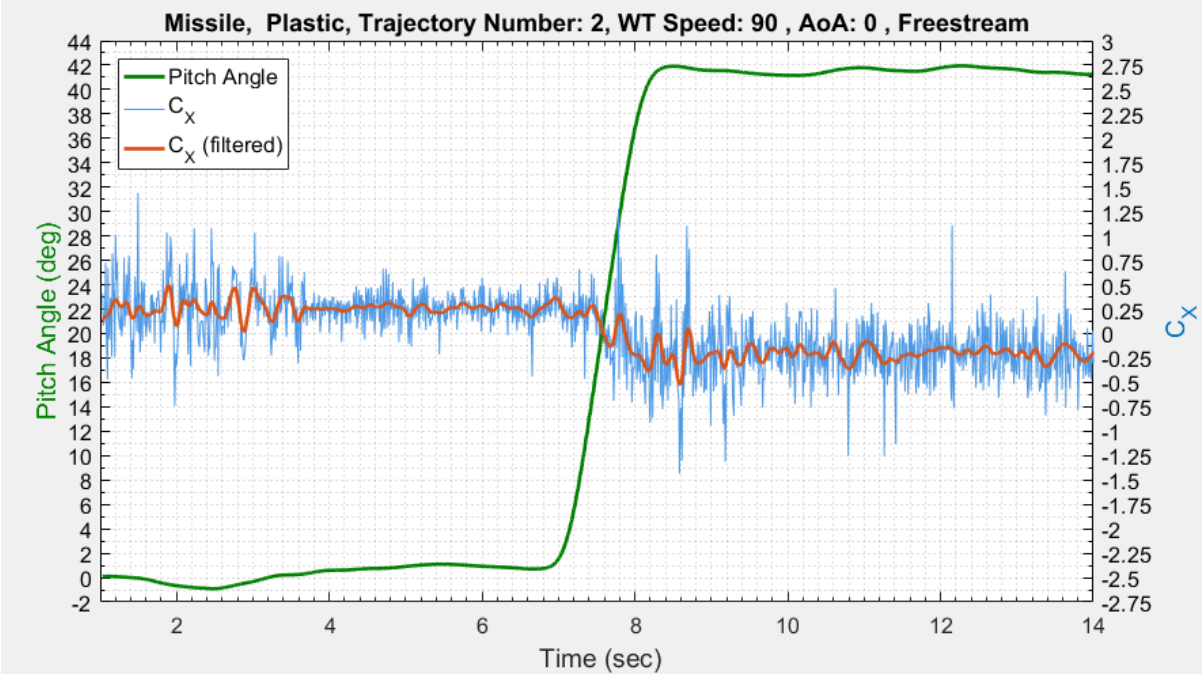

Figure 53. Plastic missile Axial Force coefficient results.

Pitch moment coefficient results are shown in Figure 54. Initial values are close to zero, and as the missile model was pitched up by a positive rotation, the pitching poment coefficient decreased. This indicates that the missile experiences a restoring moment of its pitch-attitude toward an AoA of 0º, as expected, since the missile geometry has more surface area aft of the x/L=½ due to the tail fins. Values of Cm changed from approximately 0.2 at 0º to -0.9 by 41.5º pitch.

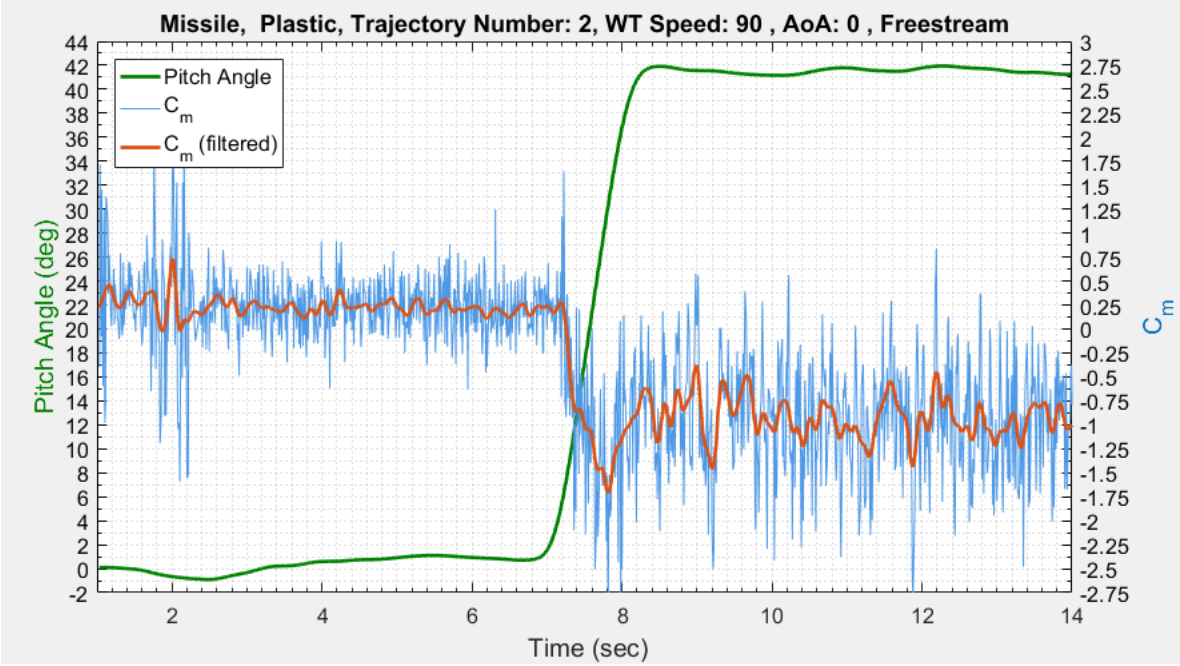

Figure 54. Plastic missile Pitching Moment coefficient results.

Yaw moment was present even though no yaw motion was deliberately executed by the MTA. Figure 55 shows the results of the yaw moment coefficient where a small variation in yaw was detected. Values of Cn decreased from 0.3 at 0º to -0.4 at 41.5º. The yaw moment variation may be to be due to the sting present causing a disruption in the flow field around the missile store model. Furthermore, some slender-body shapes do experience both side forces and a yaw moment. In the literature, this is sometimes described as "phantom yaw" because the geometry would imply that these values be zero [28].

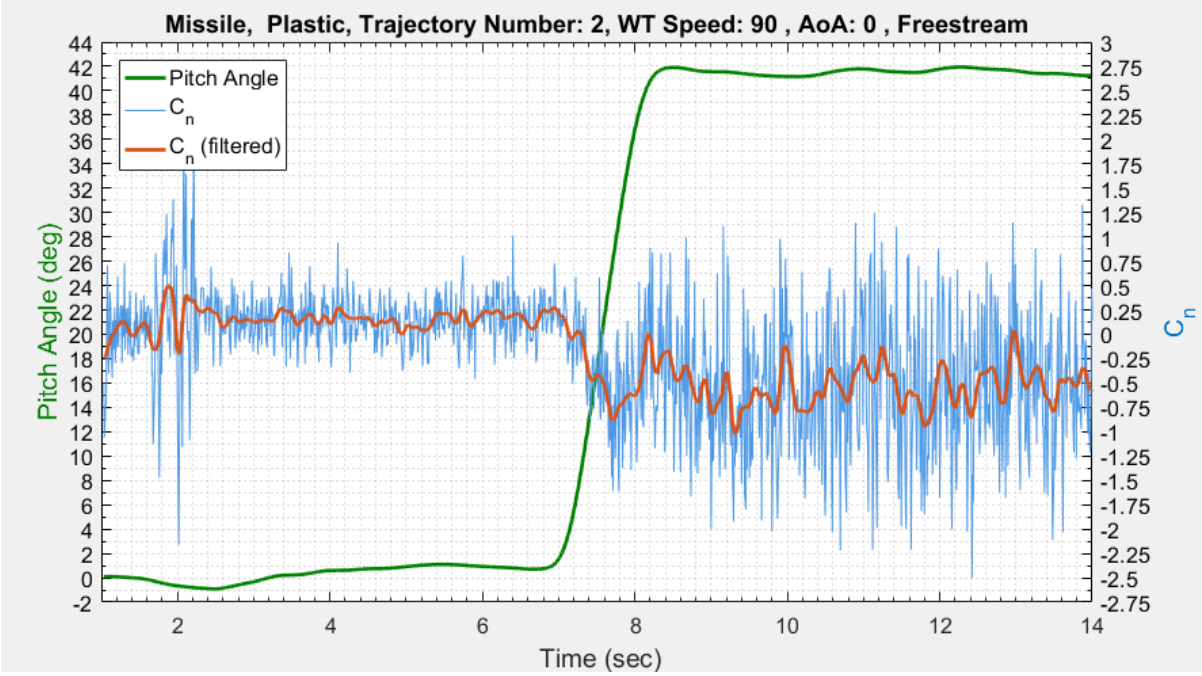

Figure 55. Plastic missile Yaw Moment coefficient results.

Roll moment coefficient results are shown below in Figure 56. The missile did not roll during trajectory number two maneuvers. Roll moment coefficient results indicate very little roll was sensed by the missile as expected. Magnitudes of Cl generally remained below 0.1 throughout the trajectory.

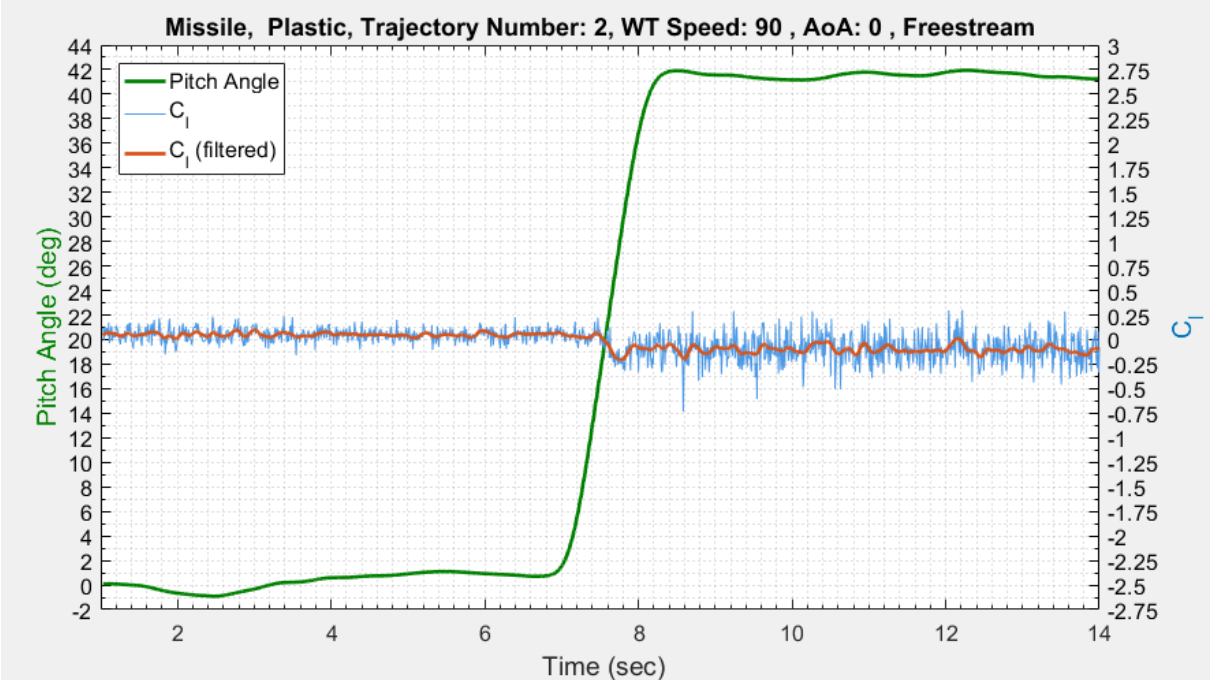

Figure 56. Plastic Missile Roll Moment coefficient results.

In order to clarify values of coefficients during rotation, unfiltered normal force coefficient data and unfiltered Pitch Moment coefficient data are plotted against pitch angle in Figure 57 (a) and (b) respectively. Normal Force grows more-or-less linearly as the missile was pitched up with some scatter in the data. Pitch Moment decreased as the missile was pitched up. These trends are consistent with expected trends. With the data associated with trajectory number two well understood, the data acquisition process was applied to the more complicated experiments of mission store separation. The next section explains the store separation experiments which utilized trajectory number one maneuvers.

In Table 11 the CN results agree well based upon mission store model geometries. Results are larger for missile geometries as compared to the ogive-cylinder results. The difference is due to the presence of canards and stability fins on the missile, where the ogive-cylinder does not have them. Furthermore, for ogive-cylinder models, the CN values decrease as wind tunnel speed increases. The same trend was observed for ogive-cylinders dynamically pitching in subsonic wind tunnel [29].

Table 11. Pitch-Up Trajectory: Incipient and Final Phase Averaged CN results.

Model	Incipient Phase			Final Phase		
	60 MPH	90 MPH	120 MPH	60 MPH	90 MPH	120 MPH
Al Missile	-0.25 0.21	-0.20 0.17	-0.18 0.40	6.32 0.49	6.36 0.40	6.53 0.47
Plastic Missile	-0.25 0.17	-0.24 0.10	-0.25 0.24	6.20 0.31	6.31 0.26	6.41 0.31
Al Ogive-cylinder	-0.03 0.24	-0.05 0.18	-0.07 0.37	4.77 0.29	4.56 0.32	4.47 0.33
Plastic Ogive-cylinder	-0.08 0.15	-0.06 0.12	-0.11 0.20	4.81 0.21	3.89 0.22	3.61 0.26

Table 12 reveals that the Cm results are less consistent for mission store models of the same geometry. Aluminum mission store models have standard deviations nearly 40% larger than their plastic counterparts. The variation in the data is from the mission store model material where inertial effects are introduce a ringing in the torsional data recorded by the Nano25.

Table 12. P itch-Up Trajectory: Incipient and Final Phase Averaged Cm Results.

Model	Incipient Phase			Final Phase		
	60 MPH	90 MPH	120 MPH	60 MPH	90 MPH	120 MPH
Al Missile	-0.02 1.11	-0.02 0.44	-0.04 1.34	-1.24 1.21	-1.40 0.86	-1.60 1.02
Plastic Missile	0.25 0.64	0.22 0.28	0.17 0.81	-0.84 0.66	-0.92 0.61	-1.16 0.62
Al Ogive-cylinder	-0.06 0.86	-0.13 0.47	-0.11 1.48	1.31 0.84	1.26 0.69	1.30 0.95
Plastic Ogive-cylinder	-0.24 0.56	-0.04 0.43	-0.07 0.87	1.99 0.45	1.78 0.50	2.10 0.60

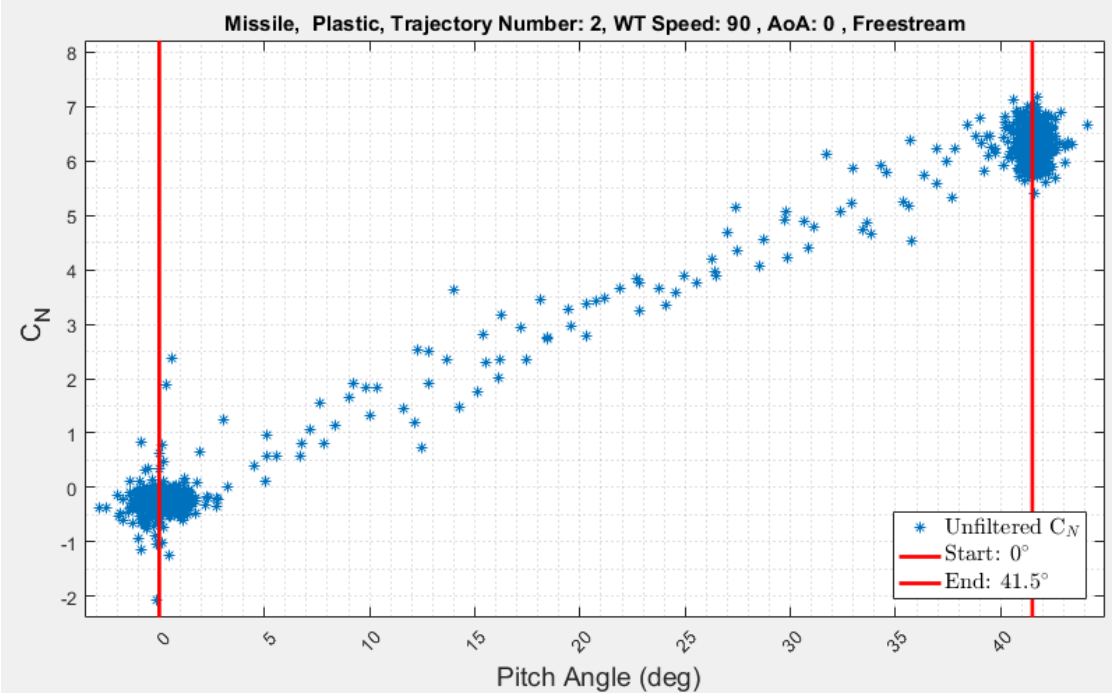

(a)

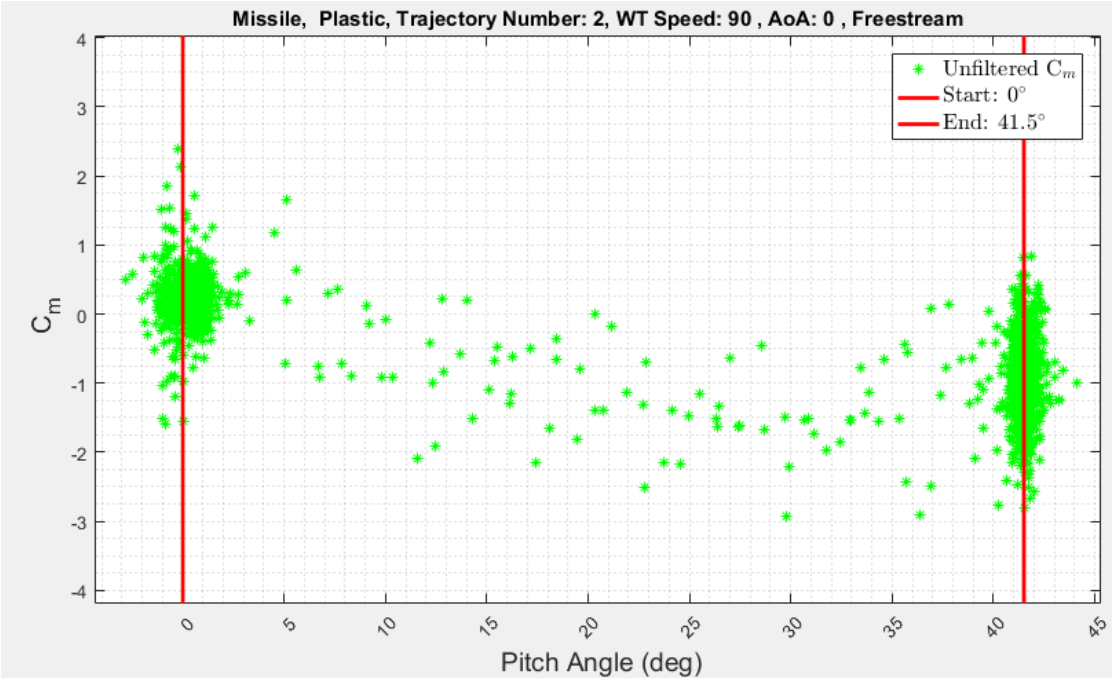

(b)

Figure 57. Normal force coefficient (a) and pitch moment coefficient (b) data plotted against pitch angle.

4.2 Trajectory Number One: Plastic missile, WT 90 MPH

Trajectory number one pertained to mission store models separating out of a weapons bay cavity, alternately from the back of the bay or the front of the bay. The starting and final position are depicted in Figure 32 and Figure 33 of Chapter III. The missile model (Nano25 reference axis origin) corresponds to the weapon bay cavity lip line when the Sweep Angle is -18º. Initial AoA were either 0º, -5º, or -10º for the experimental test runs. The plastic missile model results are presented in this section. Only 0º and -10º initial AoA attitudes are detailed in this chapter while remaining experimental results for the aluminum missile, the plastic ogive-cylinder, and the aluminum ogive-cylinder are given in Appendix A.

4.2.1 Front of Weapons Bay: Plastic Missile, WT 90 MPH, 0 Initial AoA

The experiment discussed in this section involved the plastic missile model where the initial AoA was held at 0º during its one-off store separation trajectory for the 90 MPH wind tunnel setting. From Figure 58, one can see that the CN coefficient experienced a higher magnitude of fluctuation during the incipient phase of the test in which the missile was within the weapon bay cavity. As the missile transitioned out of the bay, which corresponds to values of Sweep Angle just greater than above -18º, the CN fluctuated the strongest. At the end of the separation event, the CN fluctuations decreased in magnitude, but the normal force acting on the missile remained at near zero. The extra fluctuations during trajectory execution are believed to be due aerodynamic

forces acting on the missile during separation since any MTA joint 5 mechanical vibration measurements would have been subtracted out during the tare step of post-processing. Furthermore, there is a slight increase in CN near -8º. This indicates that the missile experiences a force pushing it away from the weapon bay, which is desired for safe and acceptable store separation.

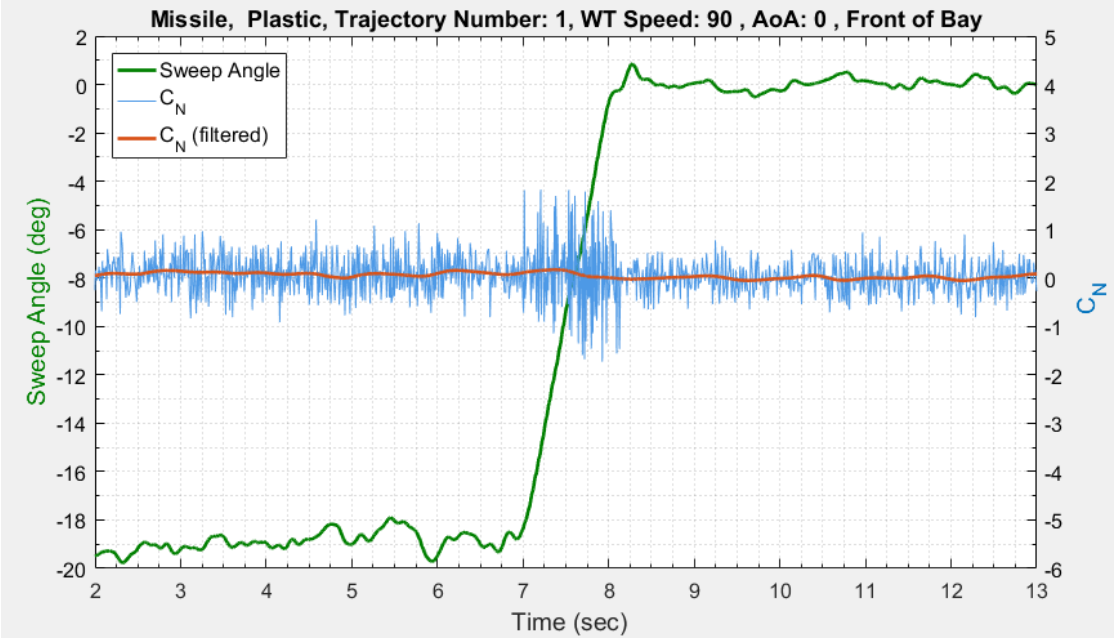

Figure 58. Normal force coefficient, CN, for the plastic missile separating from the front of the weapons bay.

Side force coefficients are negligible throughout the experiment as can be seen in Figure 59, though sting interference of the flow field causes a small disturbance. Similar to CN, the side forces fluctuate at a higher magnitude as the missile was in the weapons bay. The fluctuations dampened out as the missile transitioned into the freestream.

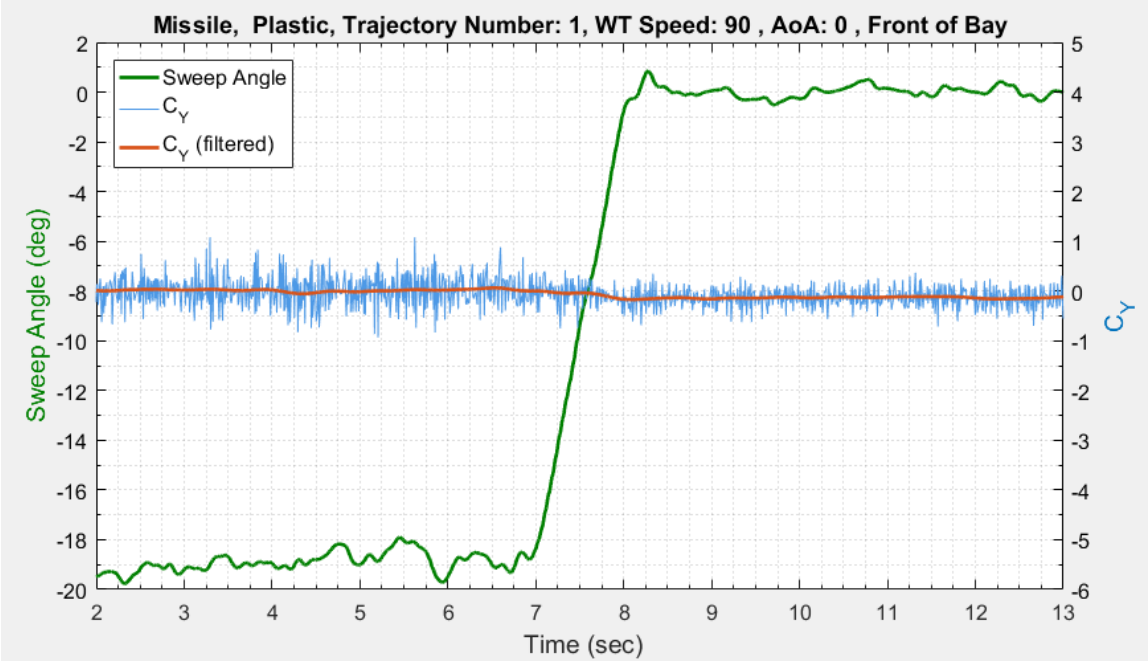

Figure 59. Side force coefficient, CY, for the plastic missile separating from the front of the weapons bay.

Axial forces were measured and the resulting CX are shown in Figure 60. The missile was subject to essentially zero average axial force acting on it while it was in the weapons bay. As the missile rose past the -18º lip line of the cavity, the axial force increased as expected and a small positive axial force was recorded. The positive CX values are consistent with drag for the balance axis system used in this study.

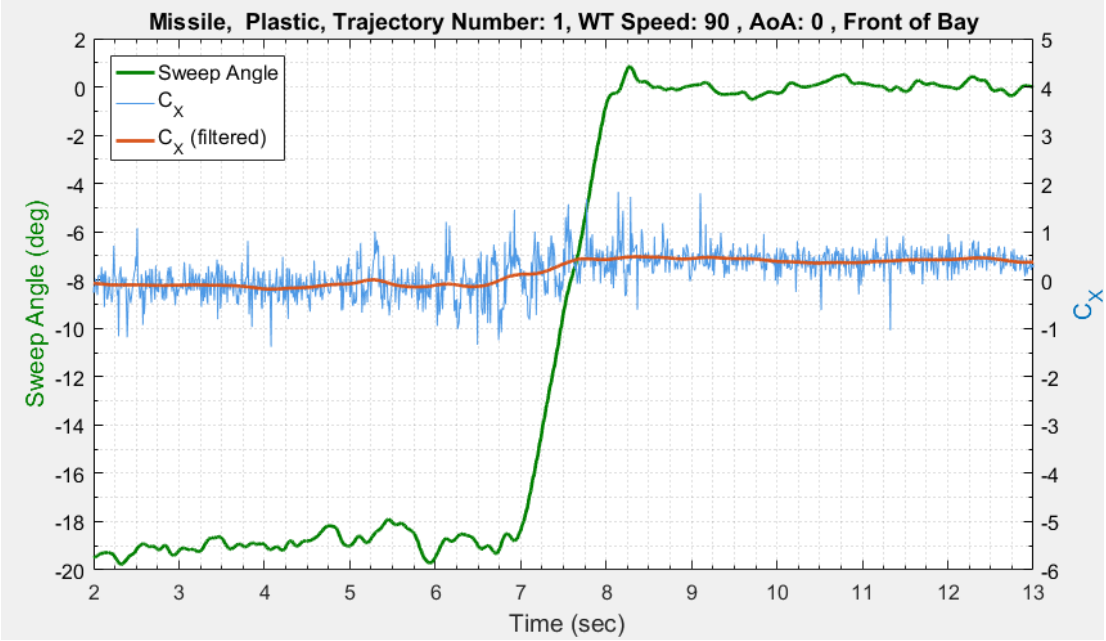

Figure 60. Axial force coefficient, CX, for the plastic missile separating from the front of the weapons bay.

Yaw moment remained essentially constant throughout the experiment. A similar fluctuation pattern to other coefficients was observed as the missile executed the one-off separation trajectory. Figure 61 shows the results for yaw moment coefficient, Cn. No yaw was expected for the missile for trajectory number one maneuvers.

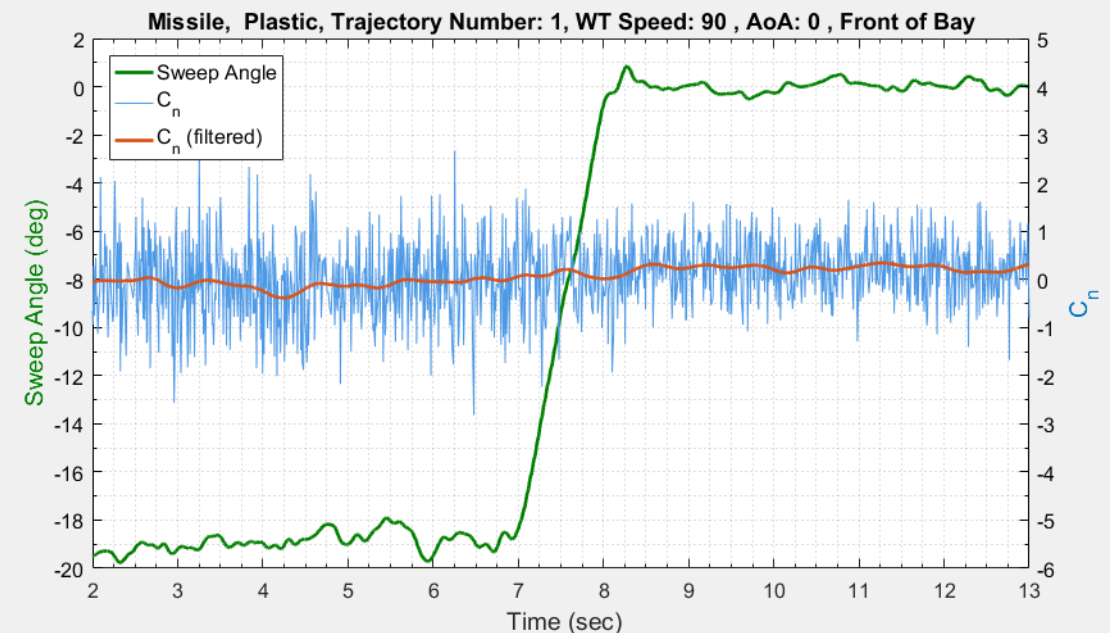

Figure 61. Yaw moment coefficient, Cn, for the plastic missile separating from the front of the weapons bay.

Pitch moment was recorded and the results for the pitch moment coefficient, Cm are shown in Figure 62. During the incipient phase of the test, the average moment acting on the missile was close to zero. As the missile passed the -18º lip line, the missile experienced a positive moment acting on it which would result in the missile pitching up and away from the weapons bay. Notably, mission store attitude such that it points away from the weapons bay is desired for safe and acceptable store separation. Once the missile entered the freestream, during the final phase of the experimental test run, the Cm values returned to zero since the missile was held at a 0º AoA attitude by the MTA joint-6.

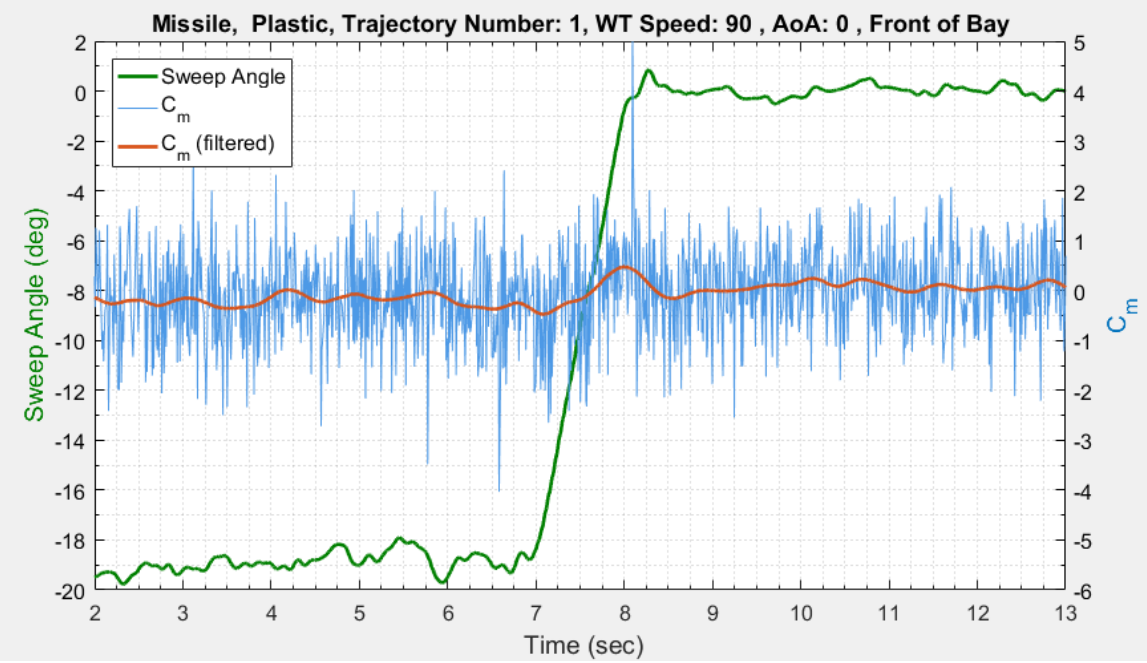

Figure 62. Pitch moment coefficient, Cm, for the plastic missile separating from the front of the weapons bay.

The missile experienced negligible roll moment during its one-off maneuver. Figure 63 shows that roll moment coefficient, Cl, remained essentially at zero throughout the entirety of the test. This is an expected result, since wind tunnel experiments incorporating missile-axis reference systems are known to be a “non-rolling body axis system” [27]

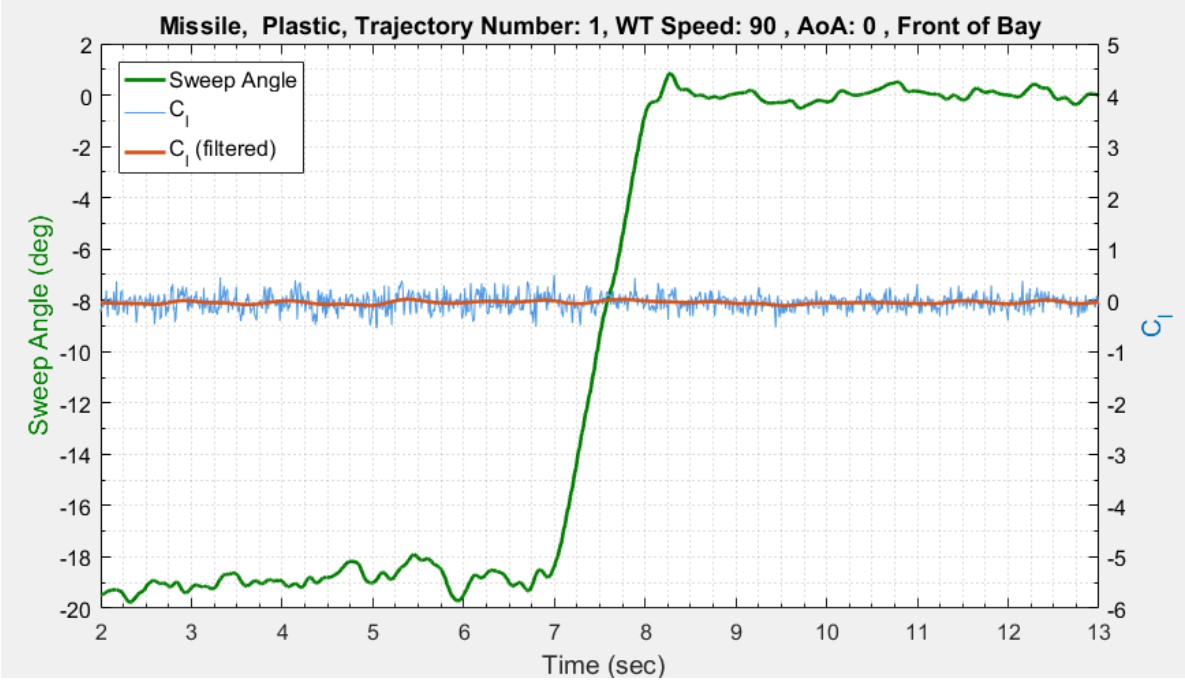

Figure 63. Roll moment coefficient, Cl, for the plastic missile separating from the front of the weapons bay.

Normal force coefficients (CN) and pitch moment coefficients (Cm) are plotted against the Sweep Angle associated with trajectory number one in Figure 64. Only these coefficient data were plotted since the CY, Cn, and Cl results are negligible for further analysis of this study of generic mission store separation. While axial force coefficient (CX) values are generally interesting, the signal-to-noise ratio is also low for this experiment. The plots show how the normal force and pitch moment are generally invariant as the missile separated from the weapons bay for cases corresponding to positions in the front of the bay. The experiment successfully emulates what is experienced in the operational environment. Stores separating from a cavity while they

are in the front of the bay usually have clean separation. One reason is that the shear layer thickness, which is related to the boundary-layer growth on the fore-body of an aircraft upstream of the bay, is typically thinner for mission stores carried in the front of a weapons bay [2] than the back of the bay.

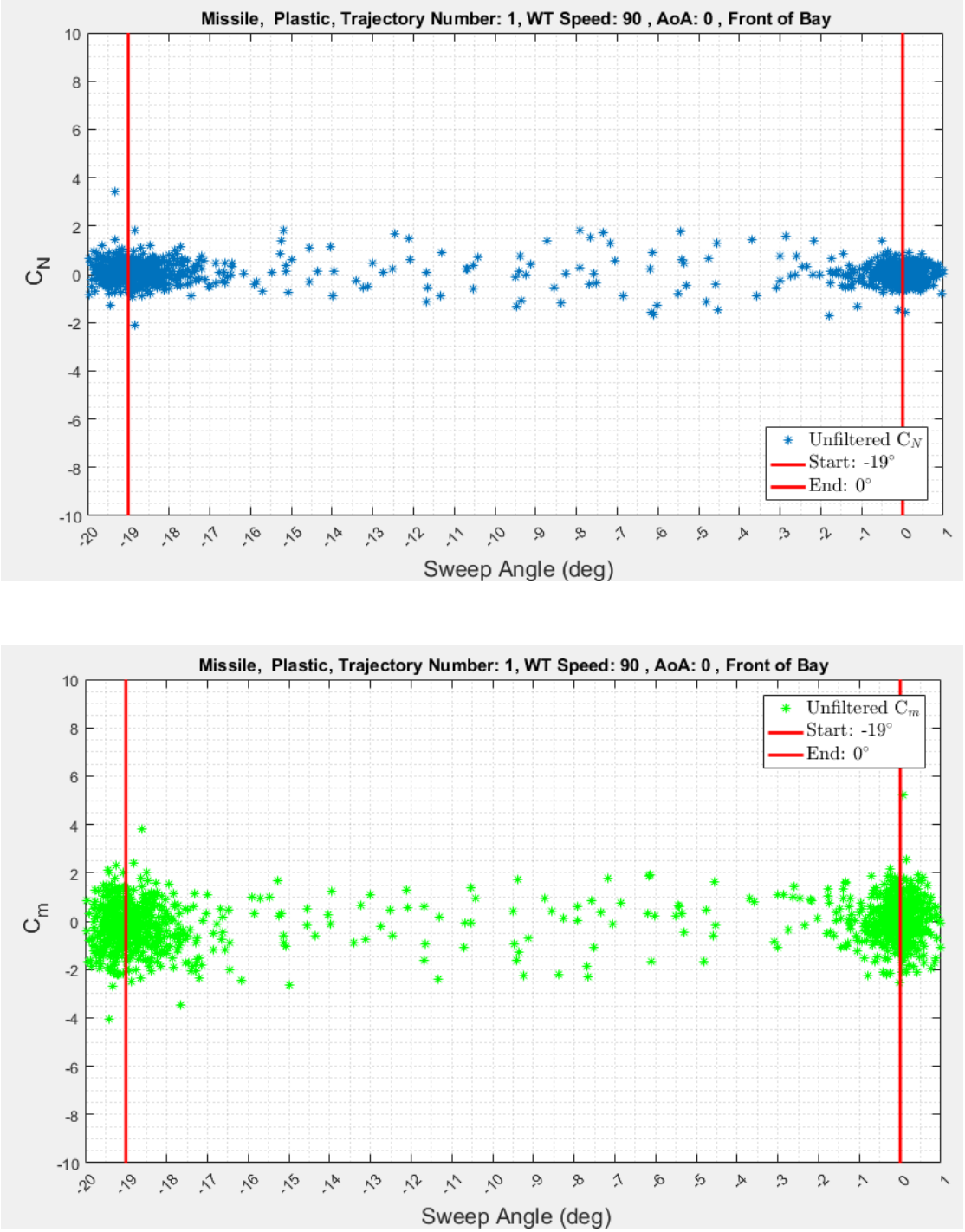

Figure 64. CN and Cm vs Sweep Angle as the plastic missile model separated from the front of the weapons bay.

4.2.2 Back of Weapons Bay: Plastic Missile, WT 90 MPH, 0 Initial AoA

The experiment discussed in this subsection involved the plastic missile model performing a one-off separation while it was initially stationed in the back of the weapons bay. The Missile maintained the initial AoA of 0º during the entirety of the experiment. Figure 65 shows the results for the CN as the missile performed its one-off maneuver for the 90 MPH wind tunnel setting.

The fluctuations are the highest while the missile was inside the weapons bay cavity. The level of fluctuation in CN is similar to, but slightly higher than, the level in the front of the bay, given in Figure 58. The initial normal force acting on the missile are negative, which would push the missile toward the bay. At the lip line of the cavity, -18º, the missile experienced a subtle negative Normal Force acting upon it. This Normal Force would push the missile towards the weapons bay which is undesirable for safe and acceptable store separation. As the missile transitioned to the freestream, nine inches above the weapons bay, the normal force increased and aerodynamic fluctuations dampened out.

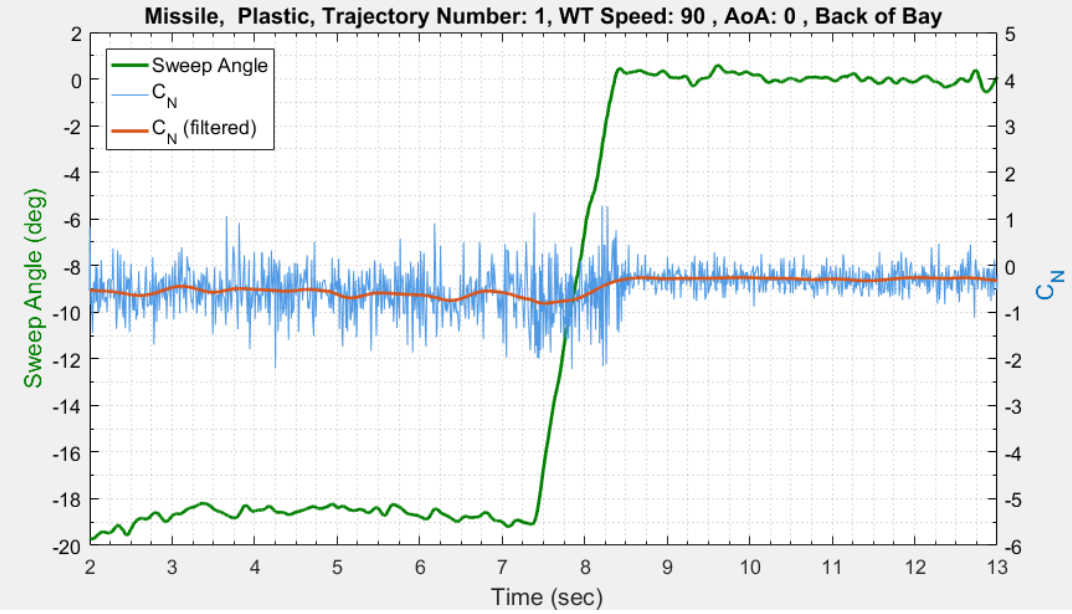

Figure 65. Normal force coefficient, CN, for the plastic missile separating from the back of the weapons bay.

Figure 66 is the side force coefficient, CY for the plastic missile. Trajectory number one was not expected to lead to a side force in the freestream. Nevertheless, a side force coefficient of -0.90 was recorded. Care was taken to ensure that the missile attitude was kept to have the Nano25 y-axis perpendicular to the weapons bay side walls, which were in line with wind tunnel flow, as shown in Figure 33. A possible reason for the side force is sting interference, similar to what was detected for trajectory number two maneuvers. However, such a side force was not seen for the same maneuver performed for the front-of-bay separation trajectory. Another possible reason for this side force could be related to the flow blockage caused by the cavity model in the wind tunnel and related streamline curvature. Interestingly, the level of fluctuation seen in CY is much higher when positioned in the back of the bay, compared to the front.

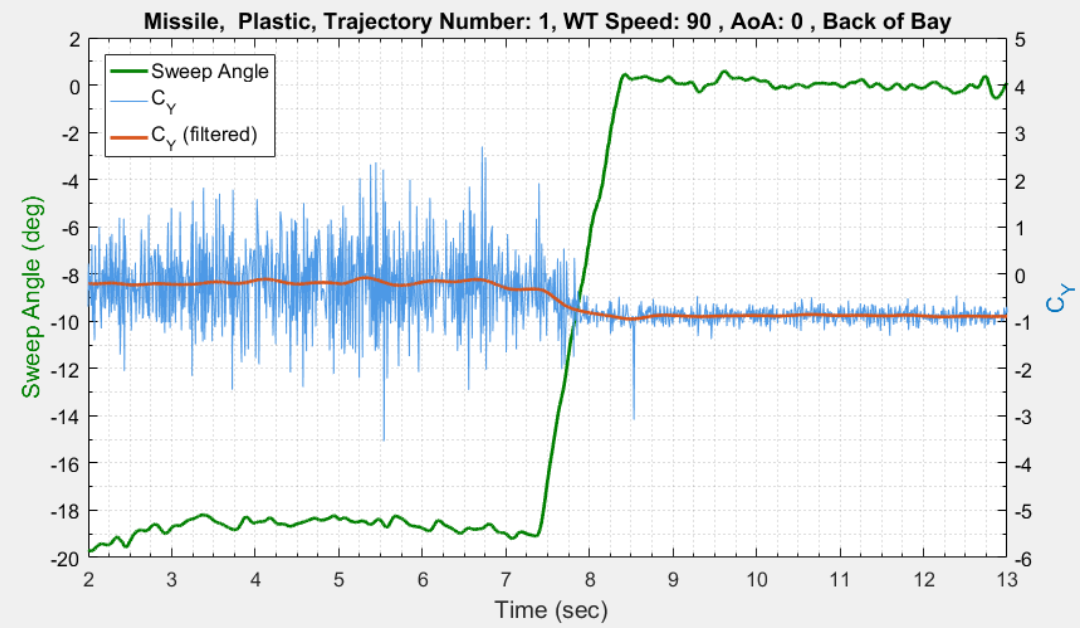

Figure 66. Side force coefficient, CY, for the plastic missile separating from the back of the weapons bay.

Figure 67 is the axial force coefficient, CX. While within the bay, a negative axial force was recorded, which would have resulted in the missile being pushed towards the front of the weapons bay cavity. If sufficiently high, a negative axial force would be undesirable for safe and acceptable store separation. The negative axial force is a distinct difference from the data presented in Figure 60 where negligible axial force was detected by the Nano25 for the front-of-bay carriage position. The negative axial force for the missile separating from the back of the weapons bay was suspected to be due to the recirculation from the shear layer impinging on the back wall of the weapons bay. Once the missile transitioned into the freestream, the axial forces went close to zero, which is similar to the case for the missile separating from the front of the weapons bay.

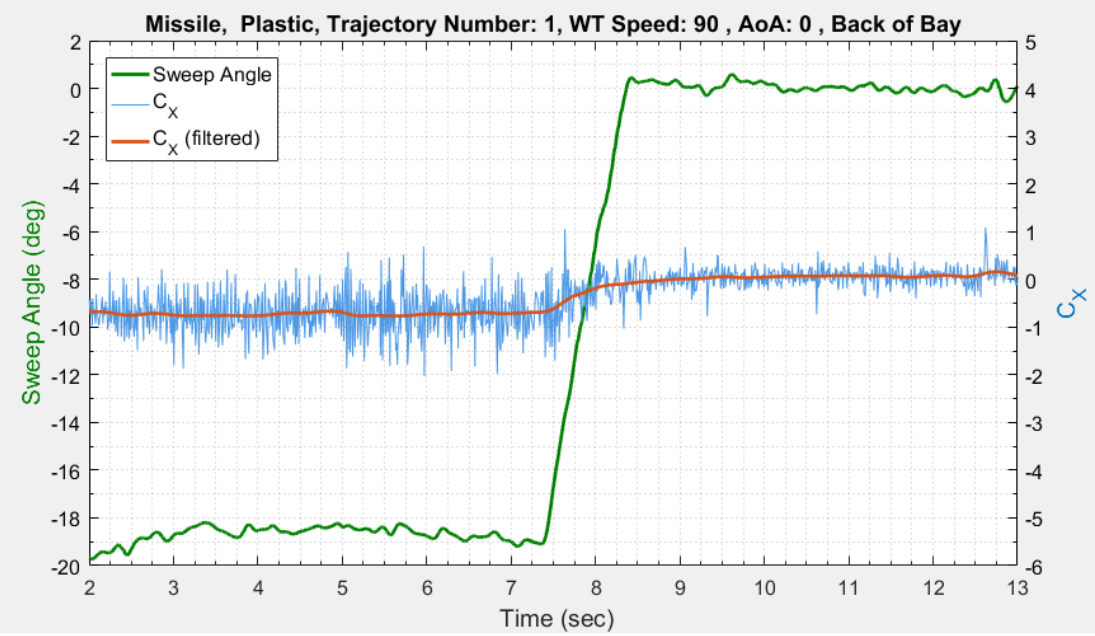

Figure 67. Axial force coefficient, CX, for the plastic missile separating from the back of the weapons bay.

Figure 68 presents the yaw moment coefficient, Cn. A subtle positive side yaw was suspected to occur due to the wind tunnel flow acting on the sting as it held the missile in the weapons bay similar to the case of the missile separating from the front of the weapons bay. Indeed a positive side force was recorded by the Nano25 during the incipient phase where the missile was positioned in the back of the weapons bay and then went to zero similar to the results shown in Figure 61. The larger fluctuations during the incipient phase as seen in Figure 68 are likely due to the larger fluctuation of the shear layer forming around the weapons bay cavity as compared to the smaller shear layer on the fore-body of the weapons bay.

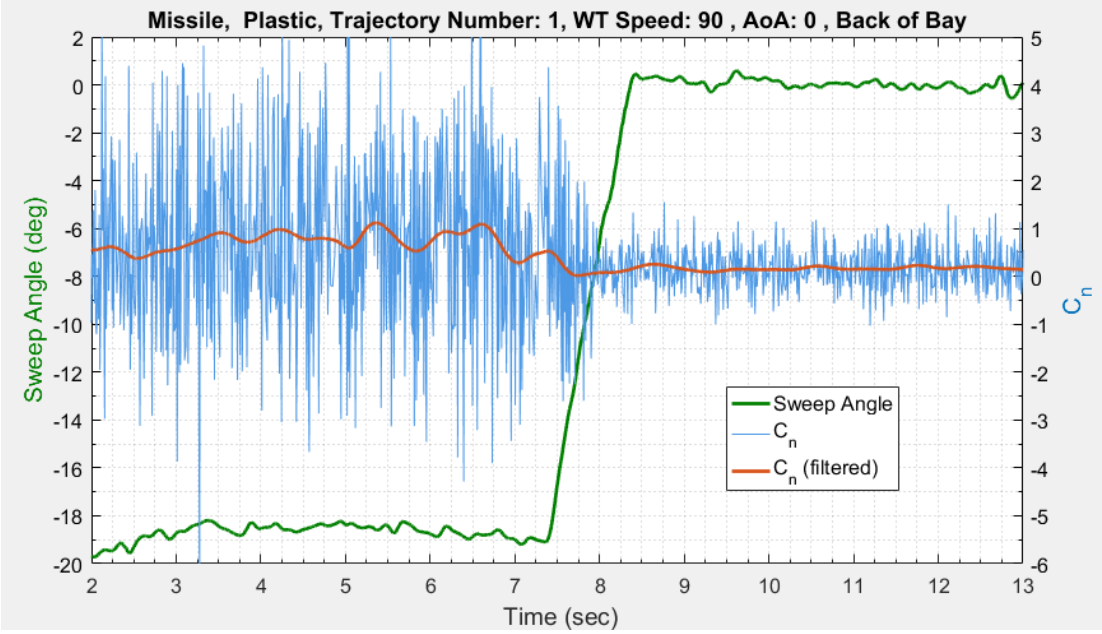

Figure 68. Yaw moment coefficient, Cn, for the plastic missile separating from the back of the weapons bay.

Figure 69 portrays the pitch moment coefficient, Cm. Here, the missile experienced a positive moment with Cm ≈ 2 during the incipient phase of the test run i.e. when the Sweep Angle was held at -19º. During the dynamic trajectory however, the pitch moment of the missile decreased from two towards zero as it moved toward the freestream. In this configuration a positive pitch moment would be desirable for safe and acceptable store separation. Once the missile reached the final portion of the test run, the Cm values were close to zero, as was the case for front-of-bay results presented in Figure 62 where the missile separated from the front of the weapons bay.

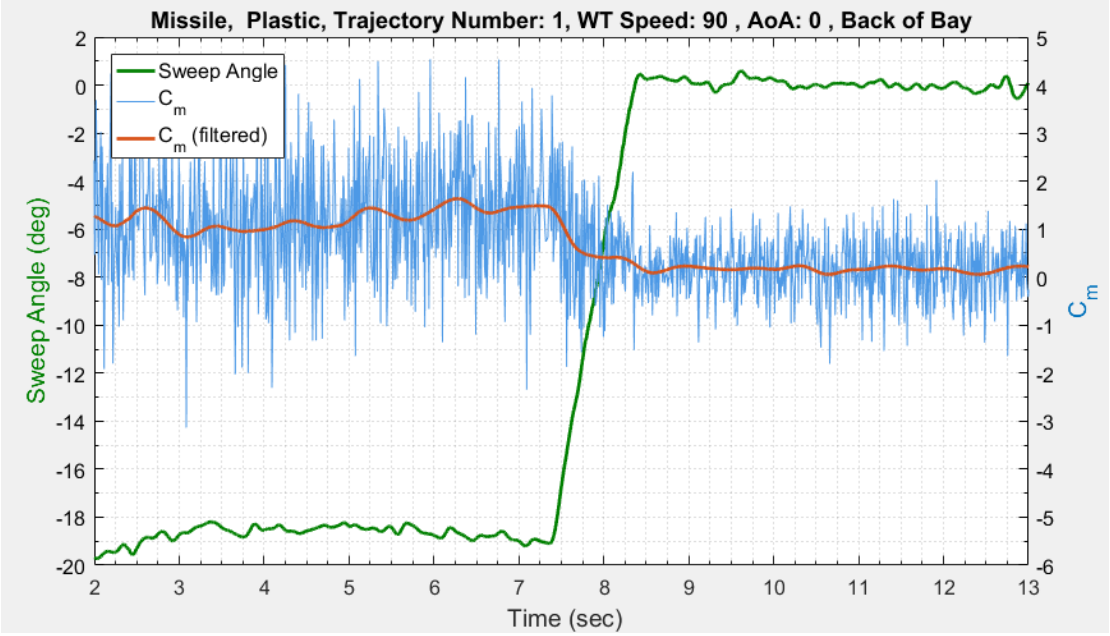

Figure 69. Pitch moment coefficient, Cm, for the plastic missile separating from the back of the weapons bay.

Figure 70 is the roll moment coefficient, Cl. As expected and as seen for the case shown in Figure 63, the roll moment is essentially zero for the entirety of the test run. Negligible Cl values are and were expected to be zero for the store separation trajectories.

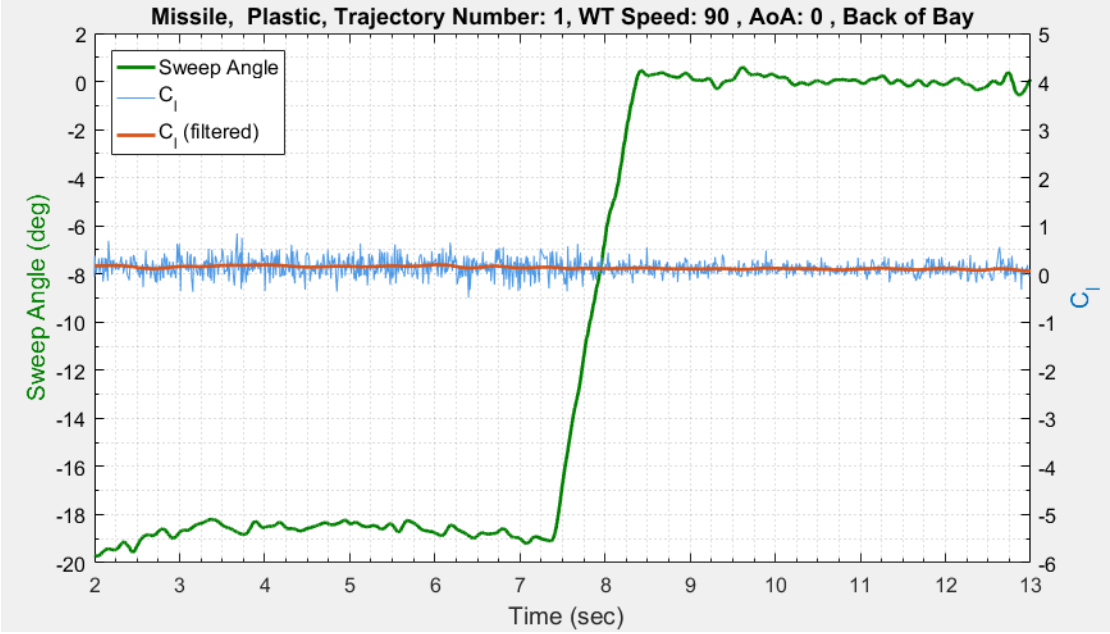

Figure 70. Roll moment coefficient, Cl, for the plastic missile separating from the back of the weapons bay.

Figure 71 shows the CN and Cm results for the missile model separating from the weapons bay cavity while it was initially stationed in the back of the weapons bay with the zero AoA attitude orientation. The results yields comparable trends as shown in Figure 64 where the missile separated from the front of the weapons bay. The noticeable differences are the magnitudes of the fluctuations. The fluctuations are greater for the case where the missile separated from the back of the weapons bay. Experiments where WT speeds varied, store models varied, store carriage position varied, and store attitude orientations (to either -5º of -10º) varied are presented in the following series of tables.

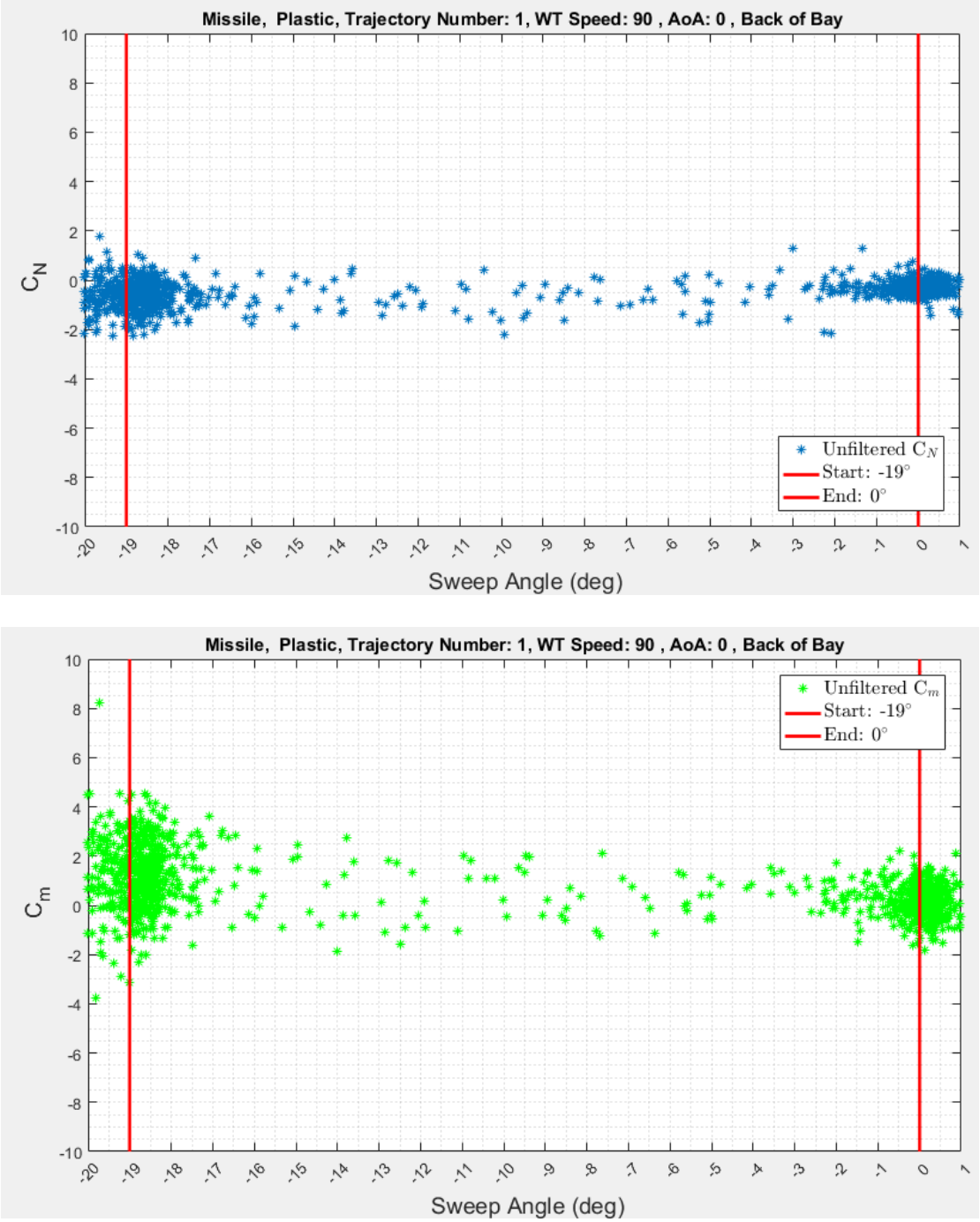

Figure 71. CN and Cm vs Sweep Angle as the plastic missile model separated from the back of the weapons bay.

The fluctuations, based on mission store carriage position, for CN and Cm are quantified in Table 13 and in Table 14 respectively. All test cases for CN and Cm are annotated in the tables with the averages on the top of a cell and the standard deviations below the averages (in the same cell). Stronger fluctuations for mission store carriage in the back of the weapons bay can be identified by Incipient Phase data having larger standard deviations for cases involving model carriage in the back of the weapons bay. All test cases, where model, WT speed, and attitude varied, are given in Appendix A.

Table 13. Trajectory number 1: incipient phase and final phase averaged CN results with mission store model AoA of 0º.

WT Speed	Model		Incipient Phase		Final Phase	
			Front of Bay	Back of Bay	Front of Bay	Back of Bay
60 MPH	Al Missile	Avg.	0.08	-0.72	-0.02	-0.37
		Std.	0.45	0.94	0.32	0.24
	Plastic Missile	Avg.	0.05	-0.59	-0.00	-0.26
		Std.	0.48	0.63	0.24	0.27
	Al Ogive-cylinder	Avg.	0.03	-0.37	-0.02	-0.08
		Std.	0.47	0.54	0.26	0.25
	Plastic Ogive-cylinder	Avg.	0.12	-0.19	0.12	0.06
		Std.	0.44	0.64	0.17	0.21
90 MPH	Al Missile	Avg.	0.09	-0.65	0.05	-0.30
		Std.	0.53	0.64	0.44	0.31
	Plastic Missile	Avg.	0.09	-0.58	0.01	-0.29
		Std.	0.39	0.46	0.31	0.24
	Al Ogive-cylinder	Avg.	0.07	-0.38	0.04	-0.07
		Std.	0.53	0.45	0.38	0.27
	Plastic Ogive-cylinder	Avg.	0.10	-0.28	0.08	-0.01
		Std.	0.29	0.43	0.23	0.22
120 MPH	Al Missile	Avg.	0.10	-0.61	0.03	-0.36
		Std.	0.44	0.64	0.48	0.51
	Plastic Missile	Avg.	0.06	-0.59	-0.01	-0.32
		Std.	0.34	0.46	0.20	0.25
	Al Ogive-cylinder	Avg.	0.09	-0.38	0.05	-0.09
		Std.	0.45	0.48	0.46	0.41
	Plastic Ogive-cylinder	Avg.	0.08	-0.29	0.02	-0.8
		Std.	0.27	0.42	0.22	0.23

Table 14. Trajectory number 1: incipient phase and final phase averaged Cm results with mission store model AoA of 0º.

WT Speed	Model		Incipient Phase		Final Phase	
			Front of Bay	Back of Bay	Front of Bay	Back of Bay
60 MPH	Al Missile	Avg.	-0.27	1.06	-0.10	0.03
		Std.	1.44	1.56	1.44	1.17
	Plastic Missile	Avg.	-0.20	1.30	0.10	0.20
		Std.	1.04	1.53	0.96	1.09
	Al Ogive-cylinder	Avg.	-0.20	0.56	-0.06	-0.07
		Std.	1.10	1.48	1.05	1.32
	Plastic Ogive-cylinder	Avg.	-0.08	0.38	-0.03	-0.32
		Std.	0.68	0.92	0.43	0.71
90 MPH	Al Missile	Avg.	-0.30	1.13	-0.03	-0.01
		Std.	1.49	1.62	1.81	1.10
	Plastic Missile	Avg.	-0.21	1.20	0.08	0.18
		Std.	0.92	1.29	0.83	0.67
	Al Ogive-cylinder	Avg.	-0.15	0.61	-0.18	-0.19
		Std.	1.06	1.23	1.48	1.26
	Plastic Ogive-cylinder	Avg.	-0.11	0.53	-0.04	-0.24
		Std.	0.61	0.90	0.74	0.67
120 MPH	Al Missile	Avg.	-0.26	1.06	-0.10	0.07
		Std.	1.34	1.67	1.57	1.51
	Plastic Missile	Avg.	-0.21	1.24	0.10	0.17
		Std.	0.99	1.25	0.53	0.52
	Al Ogive-cylinder	Avg.	-0.14	0.65	-0.14	-0.16
		Std.	1.24	1.57	1.65	1.47
	Plastic Ogive-cylinder	Avg.	-0.15	0.48	-0.02	-0.12
		Std.	0.60	0.90	0.55	0.60

In Table 15 and Table 16 below the same experiment, utilizing trajectory number one as described above, was conducted with CN and Cm reported respectively. The experiment difference was that the models and WT speeds varied while their attitudes were held at -5º. Larger standard deviations for incipient data sets quantifiably show that stores carried in the back-of-bay position experienced higher fluctuations. Final phase

data set standard deviations are generally similar since the models were held in the freestream.

Table 15. Trajectory number 1: incipient phase and final phase averaged CN results with mission store model AoA of -5º.

WT Speed	Model		Incipient Phase		Final Phase	
			Front of Bay	Back of Bay	Front of Bay	Back of Bay
60 MPH	Al Missile	Avg.	-0.10	-0.66	-0.95	-1.32
		Std.	0.54	0.75	0.30	0.40
	Plastic Missile	Avg.	-0.07	-0.65	-0.99	-1.27
		Std.	0.53	0.67	0.19	0.23
	Al Ogive-cylinder	Avg.	0.01	-0.48	-0.26	-0.43
		Std.	0.58	0.59	0.29	0.25
	Plastic Ogive-cylinder	Avg.	0.07	-0.32	-0.16	-0.30
		Std.	0.46	0.58	0.25	0.19
90 MPH	Al Missile	Avg.	-0.10	-0.73	-0.95	-1.34
		Std.	0.54	0.63	0.36	0.33
	Plastic Missile	Avg.	-0.10	-0.67	-1.00	-1.30
		Std.	0.43	0.49	0.22	0.24
	Al Ogive-cylinder	Avg.	0.03	-0.45	-0.18	-0.37
		Std.	0.49	0.53	0.39	0.26
	Plastic Ogive-cylinder	Avg.	0.04	-0.31	-0.19	-0.28
		Std.	0.36	0.43	0.17	0.22
120 MPH	Al Missile	Avg.	-0.16	-0.72	-0.95	-1.34
		Std.	0.58	0.65	0.42	0.41
	Plastic Missile	Avg.	-0.11	-0.66	-1.01	-1.33
		Std.	0.36	0.48	0.19	0.18
	Al Ogive-cylinder	Avg.	0.03	-0.42	-0.23	-0.39
		Std.	0.52	0.60	0.46	0.55
	Plastic Ogive-cylinder	Avg.	0.03	-0.35	-0.22	-0.31
		Std.	0.29	0.39	0.20	0.20

Table 16. Trajectory number 1: incipient phase and final phase averaged Cm results with mission store model AoA of -5º.

WT Speed	Model		Incipient Phase		Final Phase	
			Front of Bay	Back of Bay	Front of Bay	Back of Bay
60 MPH	Al Missile	Avg.	0.04	1.43	0.20	0.51
		Std.	2.00	1.97	1.44	1.05
	Plastic Missile	Avg.	0.13	1.35	0.38	0.62
		Std.	1.33	1.68	0.68	0.91
	Al Ogive-cylinder	Avg.	-0.11	0.73	-0.52	-0.43
		Std.	2.05	1.98	1.31	1.24
	Plastic Ogive-cylinder	Avg.	-0.05	0.49	-0.45	-0.62
		Std.	1.09	1.02	0.73	0.65
90 MPH	Al Missile	Avg.	0.14	1.37	0.17	0.46
		Std.	1.80	2.03	1.43	1.02
	Plastic Missile	Avg.	0.16	1.35	0.36	0.47
		Std.	1.06	1.40	0.66	0.65
	Al Ogive-cylinder	Avg.	-0.06	0.77	-0.60	-0.53
		Std.	1.74	2.12	1.40	0.98
	Plastic Ogive-cylinder	Avg.	-0.03	0.46	-0.45	-0.68
		Std.	0.79	1.02	0.62	0.63
120 MPH	Al Missile	Avg.	0.26	1.44	0.10	0.49
		Std.	1.80	2.03	1.40	1.20
	Plastic Missile	Avg.	0.19	1.29	0.30	0.48
		Std.	0.92	1.45	0.53	0.53
	Al Ogive-cylinder	Avg.	-0.07	0.67	-0.48	-0.46
		Std.	1.70	2.06	1.58	1.97
	Plastic Ogive-cylinder	Avg.	-0.05	0.53	-0.43	-0.58
		Std.	0.72	0.94	0.52	0.67

In Table 17 and Table 18 the CN and Cm results are reported, respectively, for the same one-off separation trajectory. Again, the model geometries and WT speeds varied but model attitudes were held at -10º. Larger standard deviations for incipient data sets quantifiably show that stores carried in the back-of-bay position experienced higher

fluctuations. Final phase data set standard deviations are generally similar since the models were held in the freestream.

Table 17. Trajectory number 1: incipient phase and final phase averaged CN results with mission store model AoA of -10º.

WT Speed	Model		Incipient Phase		Final Phase	
			Front of Bay	Back of Bay	Front of Bay	Back of Bay
60 MPH	Al Missile	Avg.	-0.56	-0.89	-1.82	-2.39
		Std.	0.51	0.64	0.34	0.48
	Plastic Missile	Avg.	-0.57	-0.68	-1.87	-2.17
		Std.	0.44	0.65	0.19	0.22
	Al Ogive-cylinder	Avg.	-0.06	-0.53	-0.50	-0.70
		Std.	0.44	0.59	0.34	0.30
	Plastic Ogive-cylinder	Avg.	-0.02	-0.31	-0.41	-0.52
		Std.	0.40	0.58	0.22	0.18
90 MPH	Al Missile	Avg.	-0.53	-0.78	-1.85	-2.34
		Std.	0.59	0.78	0.34	0.38
	Plastic Missile	Avg.	-0.55	-0.76	-1.95	-2.30
		Std.	0.38	0.53	0.25	0.31
	Al Ogive-cylinder	Avg.	-0.06	-0.51	-0.44	-0.66
		Std.	0.48	0.61	0.33	0.37
	Plastic Ogive-cylinder	Avg.	-0.07	-0.35	-0.44	-0.53
		Std.	0.32	0.44	0.24	0.21
120 MPH	Al Missile	Avg.	-0.56	-0.75	-1.89	-2.31
		Std.	0.58	0.75	0.48	0.43
	Plastic Missile	Avg.	-0.53	-0.82	-1.95	-2.35
		Std.	0.37	0.56	0.28	0.27
	Al Ogive-cylinder	Avg.	-0.11	-0.40	-0.47	-0.64
		Std.	0.52	0.60	0.41	0.41
	Plastic Ogive-cylinder	Avg.	-0.07	-0.42	-0.45	-0.57
		Std.	0.30	0.42	0.19	0.20

Table 18. Trajectory number 1: incipient phase and final phase averaged Cm results with mission store model AoA of -10º.

WT Speed	Model		Incipient Phase		Final Phase	
			Front of Bay	Back of Bay	Front of Bay	Back of Bay
60 MPH	Al Missile	Avg.	1.16	1.73	0.66	1.06
		Std.	2.01	2.12	1.10	1.08
	Plastic Missile	Avg.	1.38	1.42	0.84	0.94
		Std.	1.32	1.72	0.57	0.59
	Al Ogive-cylinder	Avg.	0.05	0.78	-0.83	-0.68
		Std.	2.01	2.15	1.31	1.34
	Plastic Ogive-cylinder	Avg.	0.04	0.47	-0.83	-1.08
		Std.	1.03	1.21	0.59	0.55
90 MPH	Al Missile	Avg.	1.18	1.64	0.69	1.09
		Std.	2.08	2.22	1.04	0.94
	Plastic Missile	Avg.	1.23	1.51	0.88	1.05
		Std.	0.99	1.53	0.70	0.71
	Al Ogive-cylinder	Avg.	0.16	0.83	-0.89	-0.79
		Std.	1.85	2.23	1.19	1.20
	Plastic Ogive-cylinder	Avg.	0.13	0.48	-0.77	-0.97
		Std.	1.02	1.15	0.70	0.63
120 MPH	Al Missile	Avg.	1.23	1.48	0.73	1.05
		Std.	2.03	2.13	1.86	0.89
	Plastic Missile	Avg.	1.21	1.58	0.88	1.12
		Std.	0.98	1.73	0.56	0.63
	Al Ogive-cylinder	Avg.	0.21	0.63	-0.75	-0.75
		Std.	1.98	2.20	1.61	1.68
	Plastic Ogive-cylinder	Avg.	0.14	0.65	-0.74	-0.91
		Std.	0.91	1.11	0.59	0.72

4.2.3 Front of Bay and Back of Bay: Repeated Test Runs

In subsections 4.2.1 and 4.2.2, the plastic missile was moved by the MTA for a one-off store separation trajectory. By and large, the experiment captured what is observed in the operational environment. That is, the effects of the unsteady shear layer over a cavity has less influence on mission store attitude as it separates from the front of a cavity while the unsteady shear layer has a larger effect on mission store separation attitude as it separates from the rear of a cavity [2]. In this subsection, the same experiments were repeated 20 times in order to investigate the consistency of measured values during the motion of the model. The plastic missile model was used for these 20 experimental test runs. Only the normal force coefficient and pitch movement coefficients are discussed in this section. Remaining aerodynamic coefficient data is in Appendix A.

Figure 72 shows the filtered CN data sets for the plastic missile model as it performed its one-off trajectory: from the front of the bay and from the back of the bay. For convenience, the -18º weapons bay lip line is plotted as a solid green line. The y-axis on the plots range from -3º to 0.5º in order to conduct direct comparison for when the missile model AoA was pitched down by -10º. The zoomed in view has the majority of the incipient phase data excluded in order to clearly show trends near the lip line.

Some of the literature suggests that a store might experience a substantially different load distribution (e.g. with Cm of different sign) in the shear layer depending on the timing of large vortices which grow from the leading edge [3]. This phenomenon has

been termed “bifurcation” by some authors [7]. Upon inspection, all of the CN values are positive while the missile is within the weapons bay forward position, and the majority of the CN data remains positive during the trajectory. However, the Nano25 was able to detect the dynamic trend of the CN values as the missile separated from the weapons bay. Near the -18º lip line, about half of the CN data trend up while the second half trend down, indicating that a bifurcation maybe present during the separation test run. Similar filtered CN lines for the one-off trajectory indicate that the experimental set up has precision. The CN values dampen at the Sweep Angle of -5º, which corresponds to the point at which the missile is about 5.2” above the weapons bay cavity.

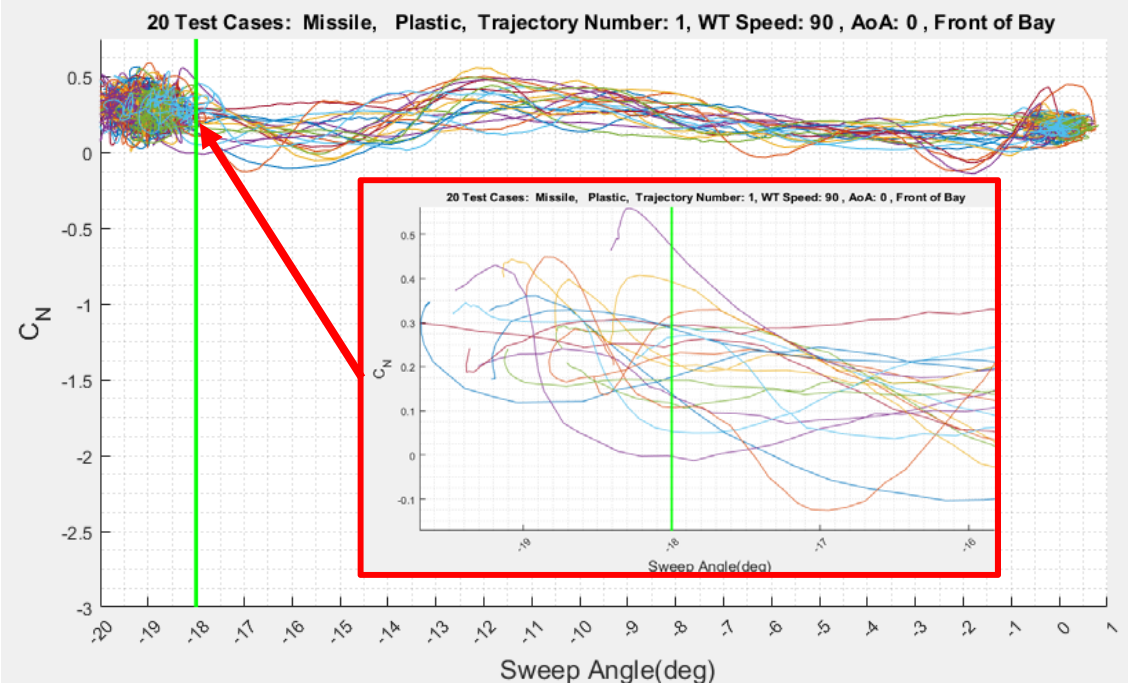

Figure 72. Twenty sets of filtered CN data for the front-of-bay missile model separation runs. Missile attitude held at 0º.

Figure 73 shows the filtered CN data for the plastic missile while it performed the one-off separation trajectory. From the plot, the majority of the CN values are negative while the missile was within the weapons bay, and remain negative for the duration of the trajectory. Again, the CN values dampen when the missile was at -5º (about 5.2" above the weapons bay) during the trajectory. The CN data also indicate a bifurcation is present for a store separating from the back of the weapons bay in that half of the 20 experimental runs tend downwards and the other half tend upwards for the data near the -18º lip line. Furthermore, the similar pattern of filtered CN lines for the one-off trajectory indicate that the experimental set up has precision for mission stores in the back of the cavity as well. The zoomed in view has the majority of the incipient phase data excluded in order to clearly show bifurcation trend near the lip line.

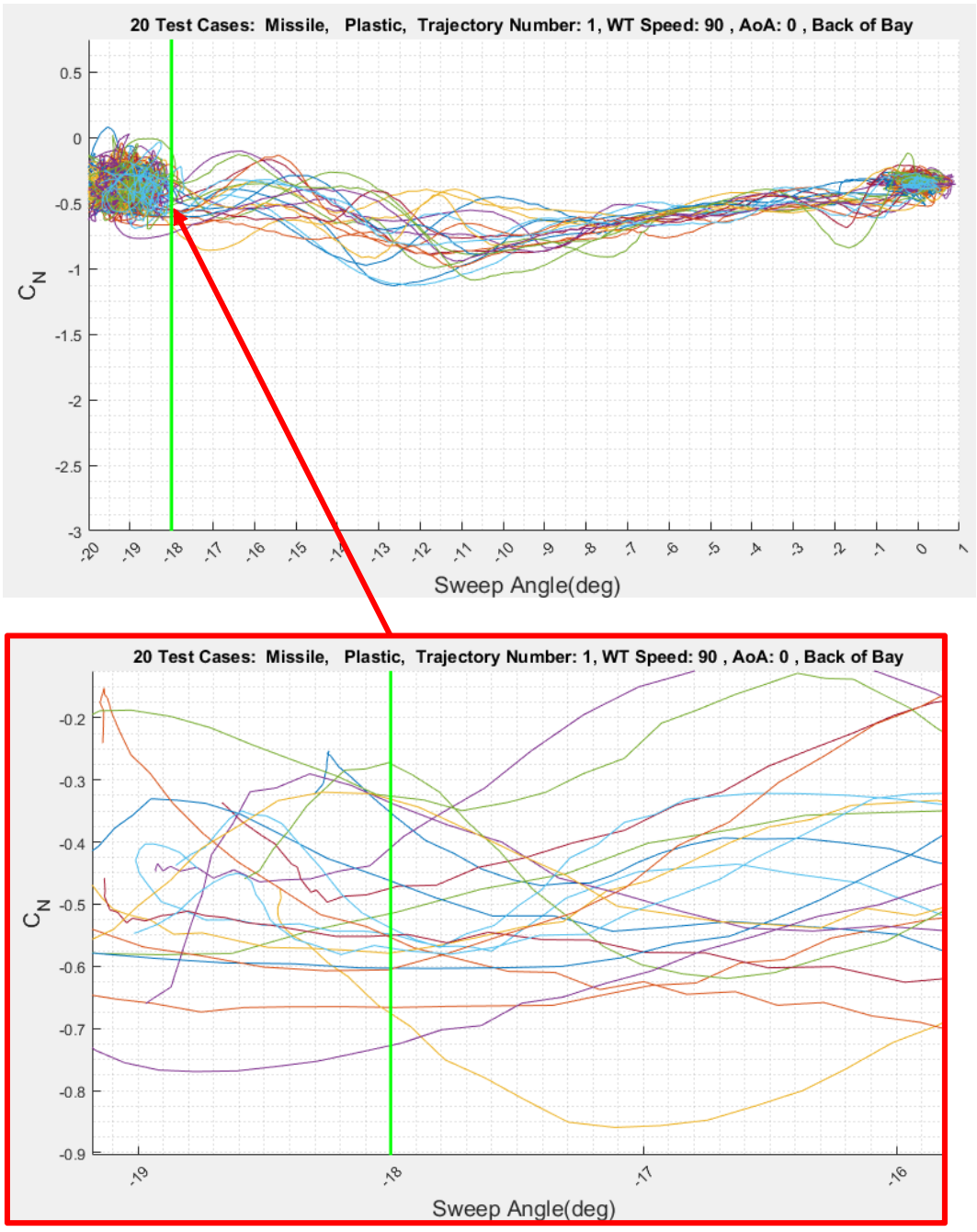

Figure 73. Twenty sets of filtered CN data for the back-of-bay missile model separation runs. Missile attitude held at 0º.

Comparing Figure 72 and Figure 73, there is a noticeable difference in CN fluctuation, particularly at the Sweep Angle of -18º to -5º. Furthermore, the two missile storage locations have different CN values for their initial locations within the weapons bay. In order to compare the magnitude of the fluctuations directly, the 20 filtered CN data sets were averaged from -18º to -1º. This range of Sweep Angle corresponds to the dynamic trajectory data set. The averaged filtered CN data were plotted with the corresponding two-standard deviations as can be seen in Figure 74 below. The results show how the unsteady shear layer influenced the missile based on the missile's position within the weapons bay. Interestingly, the CN trends are mirror images of each other and though they each trend towards zero, they do not converge entirely by Sweep Angle of -1º. This is suspected to be due to flow angularity resulting from the presence of the weapons bay cavity.

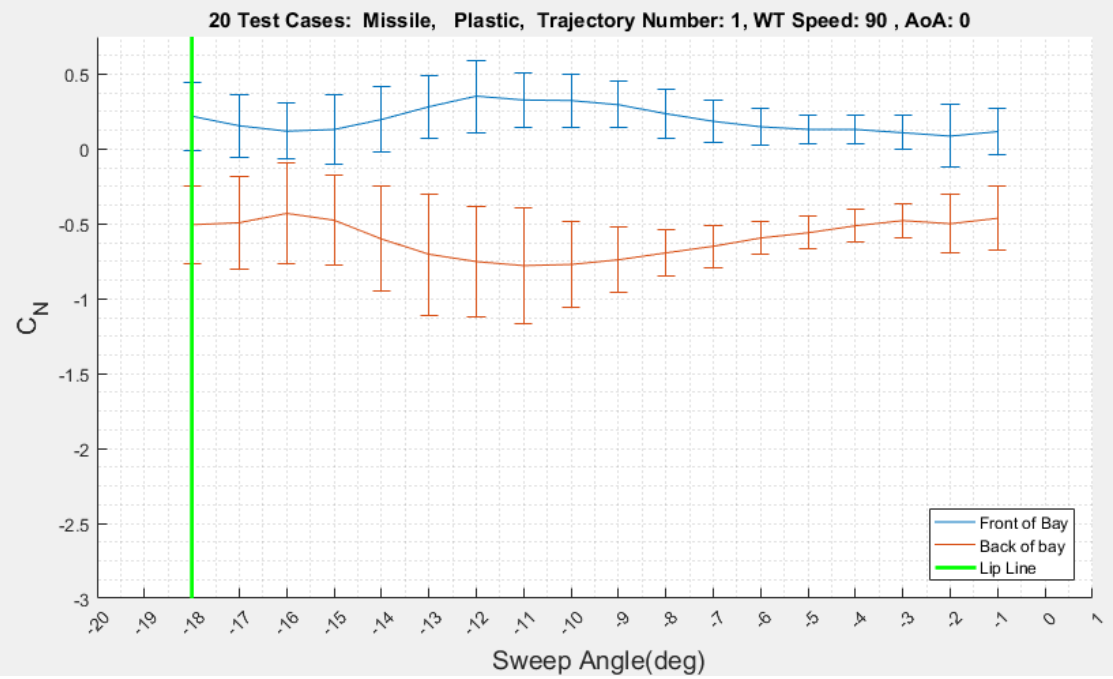

Figure 74. Averaged filtered CN data sets, plotted with 2-standard deviations, of the plastic missile performing store separation with 0º AoA attitude.

Figure 75 shows the pitch moment coefficient results for the plastic missile as it performed the one-off separation from the front of the weapons bay for the 20 repeated runs. Initial values of Cm are negative, which would cause the nose of the missile to pitch towards the weapons bay. As the missile transitioned into the freestream, the variation in Cm did not change much, but the Cm fluctuations did dampen out while it was at the -5º Sweep Angle (5.2" above the weapons bay). For values of Cm near the -18º lip line, a bifurcation is suspected since about half of the data trend downward and the other half trend upwards. For all of the 20 cases, the filtered Cm lines are generally consistent which implies the precision of the experimental set up for pitch moments. The zoomed in

box of Figure 75 excludes the majority of incipient data set in order to clearly show evidence of bifurcation.

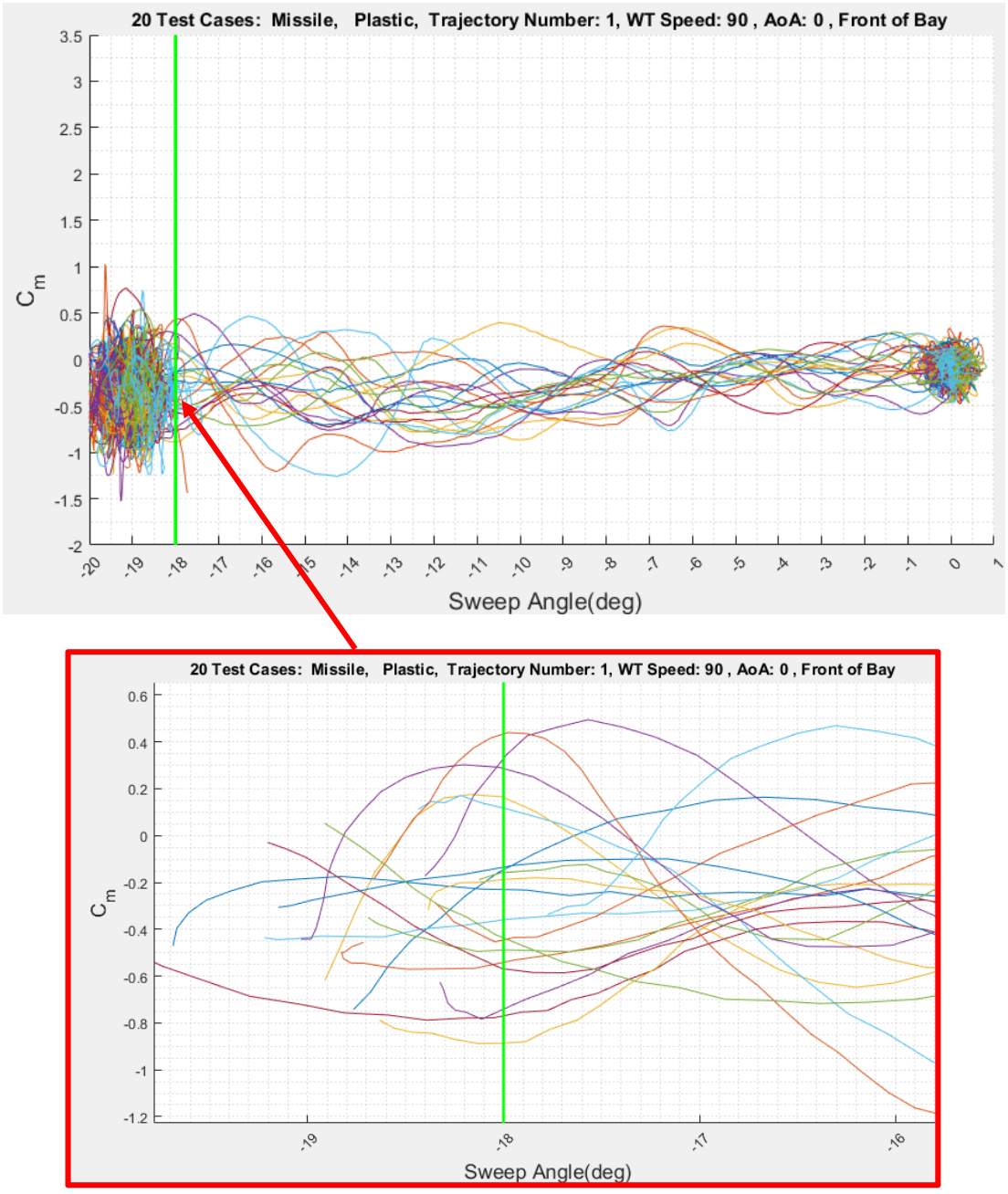

Figure 75. Twenty sets of filtered Cm data for the front-of-bay missile model separation runs. Missile attitude held at 0º.

Figure 76 shows the measured Cm results for the missile as it separated from the weapons bay while it was initially in the back of the bay. As seen from the graph, the values for Cm are mostly positive at -19º. This means that the missile would be pitched such that it would face away from the weapons bay. Fluctuations are dampen out when the missile was at a Sweep Angle of -5º, which is consistent with the rest of the data presented so far. Looking at the Cm values near the -18º lip line of Figure 76 below, about half of the test runs would correlate to the missile pitching away from the bay and the other half would correlate to the missile pitching towards the bay. The experiment seemingly captures the bifurcation that can occur as a mission store transitions through an unsteady shear layer. The zoomed in box of Figure 76 excludes the majority of the incipient data set in order to show the suspected bifurcation trends.

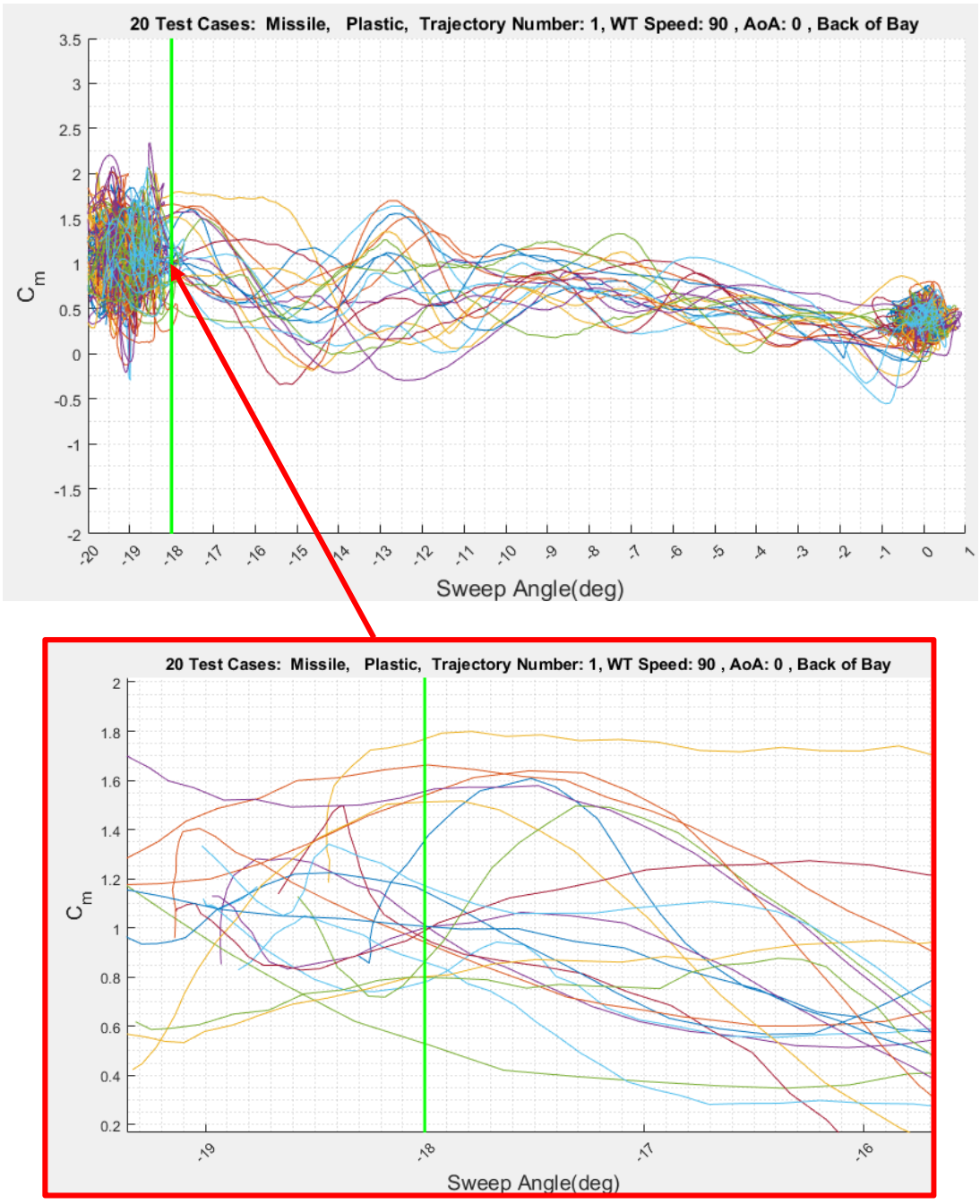

Figure 76. Twenty sets of filtered Cm data for the back-of-bay missile model separation runs. Missile attitude held at 0º.

Similarly to the CN values, the Cm data sets were averaged based on every Sweep Angle starting at the -18º and ending at -1º. The results are shown in Figure 77. Here, it is interesting to see that the magnitude of the fluctuation felt by the missile are greater while it was initial positioned in the back of the weapons bay. For example, by -13º values spanned about -0.5 to 1.5 whereas in the front-of-bay case values ranged from -1.1 to 0.3.

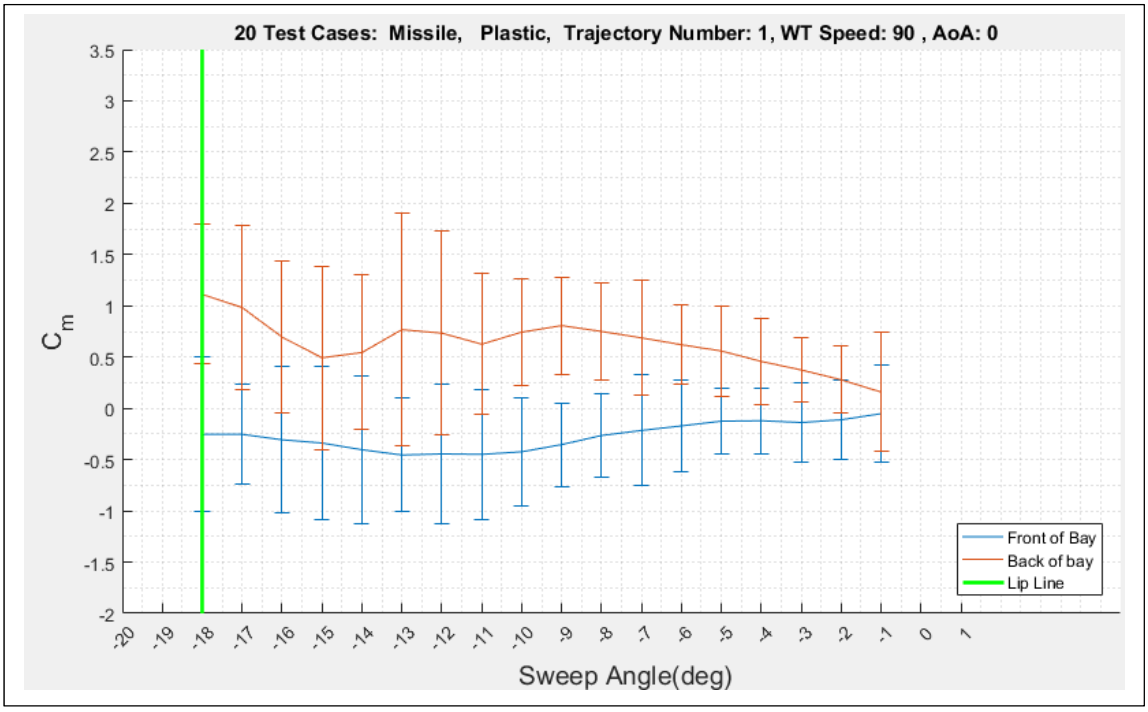

Figure 77. Averaged filtered Cm data sets, plotted with 2-standard deviations, of the plastic missile performing store separation with 0º AoA attitude

Next the experiments are considered for the plastic missile where the MTA joint-6 pitched the missile downward for an angle of -10º such that it was pitched towards the weapons bay. As before, this is representative of a worst case scenario. The initial and final positions of the store can be seen in Figure 32 and in Figure 33 of section 3.8. Only

the CN and Cm values are discussed. Zoomed in views of the data exclude the majority of the incipient data sets in order to clearly investigate trends near the lip line of the cavity.

Beginning with the front of the bay, Figure 78 shows the results of CN and Cm of the missile initially positioned in the front of the weapons bay. CN results reveal that the missile is subject to a downward force, which would push the missile towards the bay. This outcome is anticipated for the given arrangement. The values remain negative throughout the entirety of the one-off trajectory. No bifurcation evidence was detected for when the AoA is held at -10º.

Figure 79 shows the Cm coefficients are positive for all time which means that the missile would want to restore itself to an AoA of 0º as is separated from the cavity. Interestingly, about half of the Cm values near the -18º lip line are tending to increase and half tend to decrease (but never reach zero). The experiment also suggest that bifurcation occurs for the missile, similar to the Cm values of Figure 76 in which the missile was at 0º AoA as it separated from the back of the bay. The CN and Cm magnitudes in fluctuation dampened at -5º (5.2” above the weapons bay) just as the case for the missile at 0º AoA.

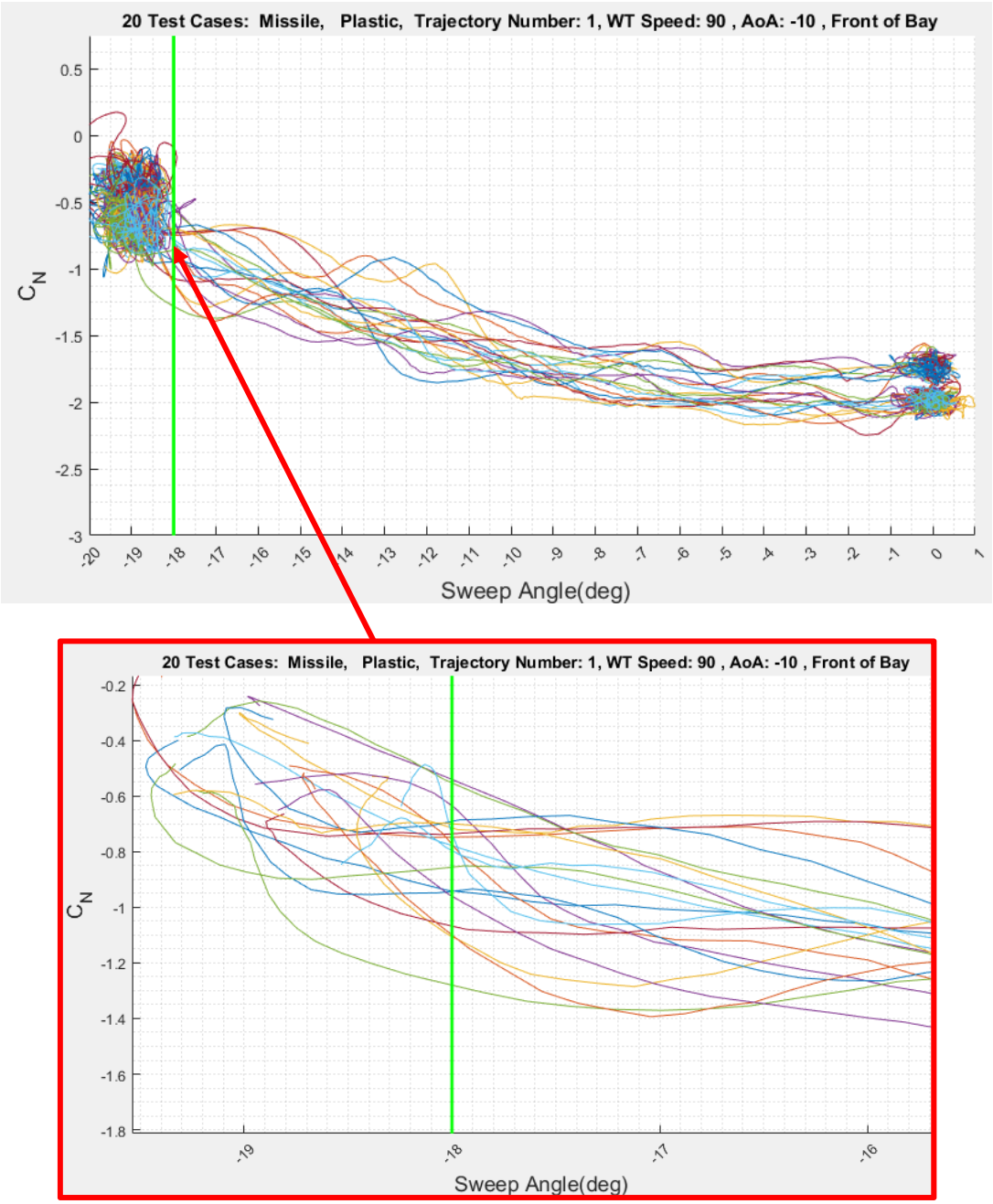

Figure 78. Twenty sets of filtered CN data for the front-of-bay missile model separation runs. Store attitude is -10º AoA.

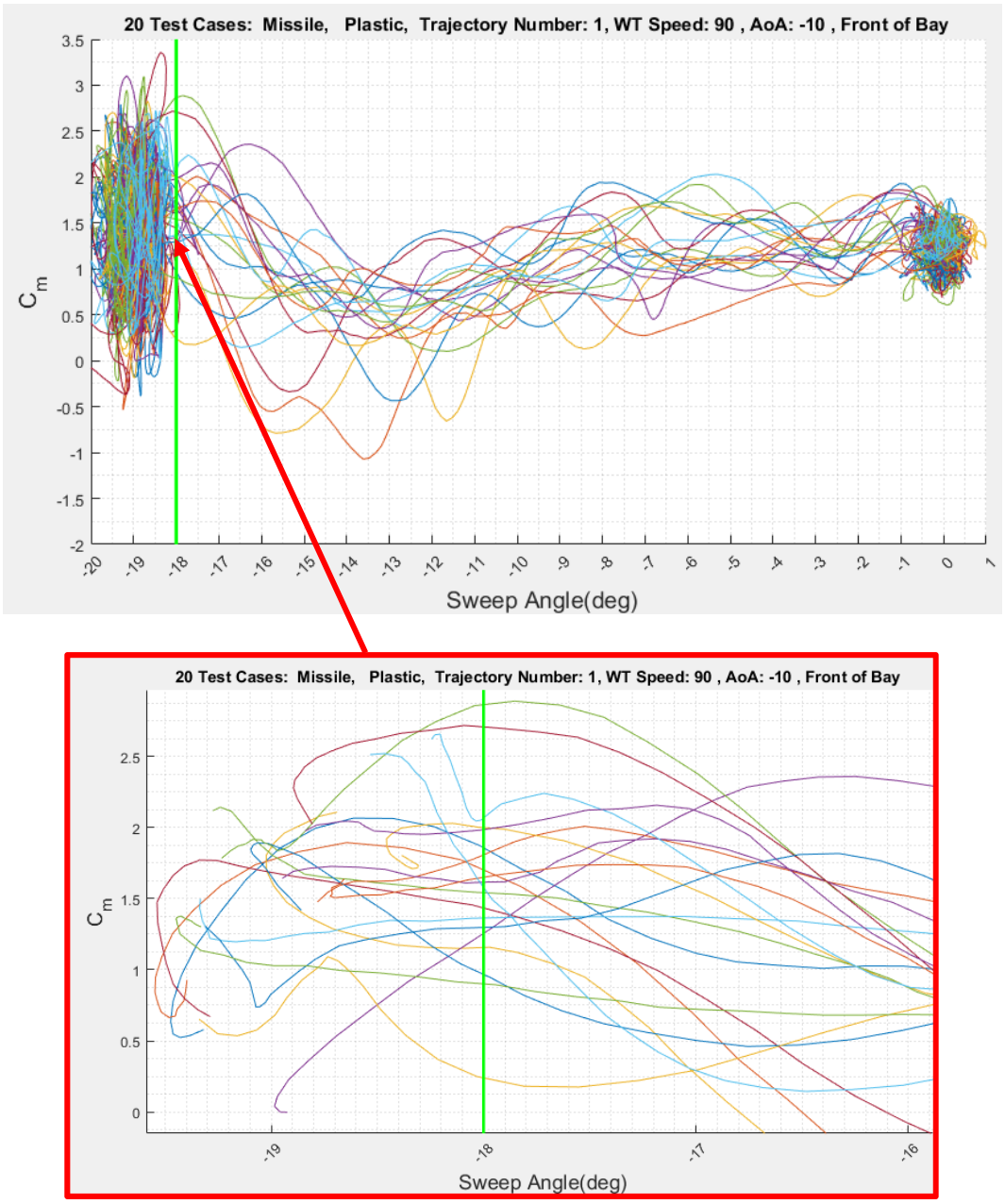

Figure 79. Twenty sets of filtered Cm data for the front-of-bay missile model separation runs. Store attitude is -10º AoA.

For contrast, Figure 80 shows the results for CN and Cm of the plastic missile with the -10º AoA attitude as it separated from the back of the weapons bay. CN values are negative for all Sweep Angles which means that the missile experienced an aerodynamic force acting on it such that the missile would tend to move towards the weapons bay as it separated. Interestingly there is no strong evidence of a bifurcation in this CN data.

Figure 81 shows that Cm values are positive for all Sweep Angles though some values tend to be decreasing (but never reach zero). The missile felt a pitch moment such that it would want to pitch up and restore itself to 0º pitch attitude. The variation in data for this case also indicates that a bifurcation may be present as the missile separated from the back of the weapons bay.

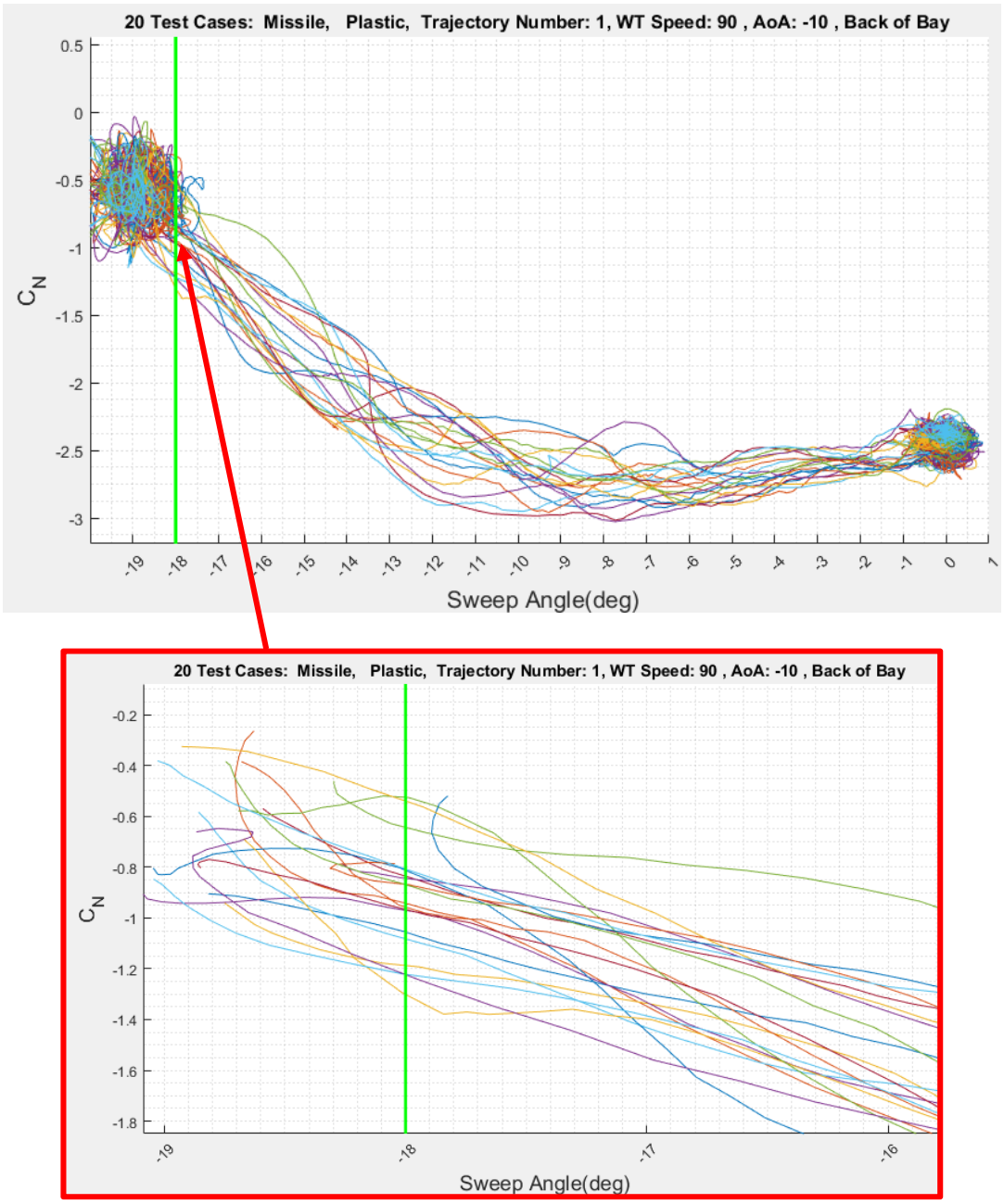

Figure 80. Twenty sets of filtered CN data for the back-of-bay missile model separation runs. Store attitude is -10º AoA.

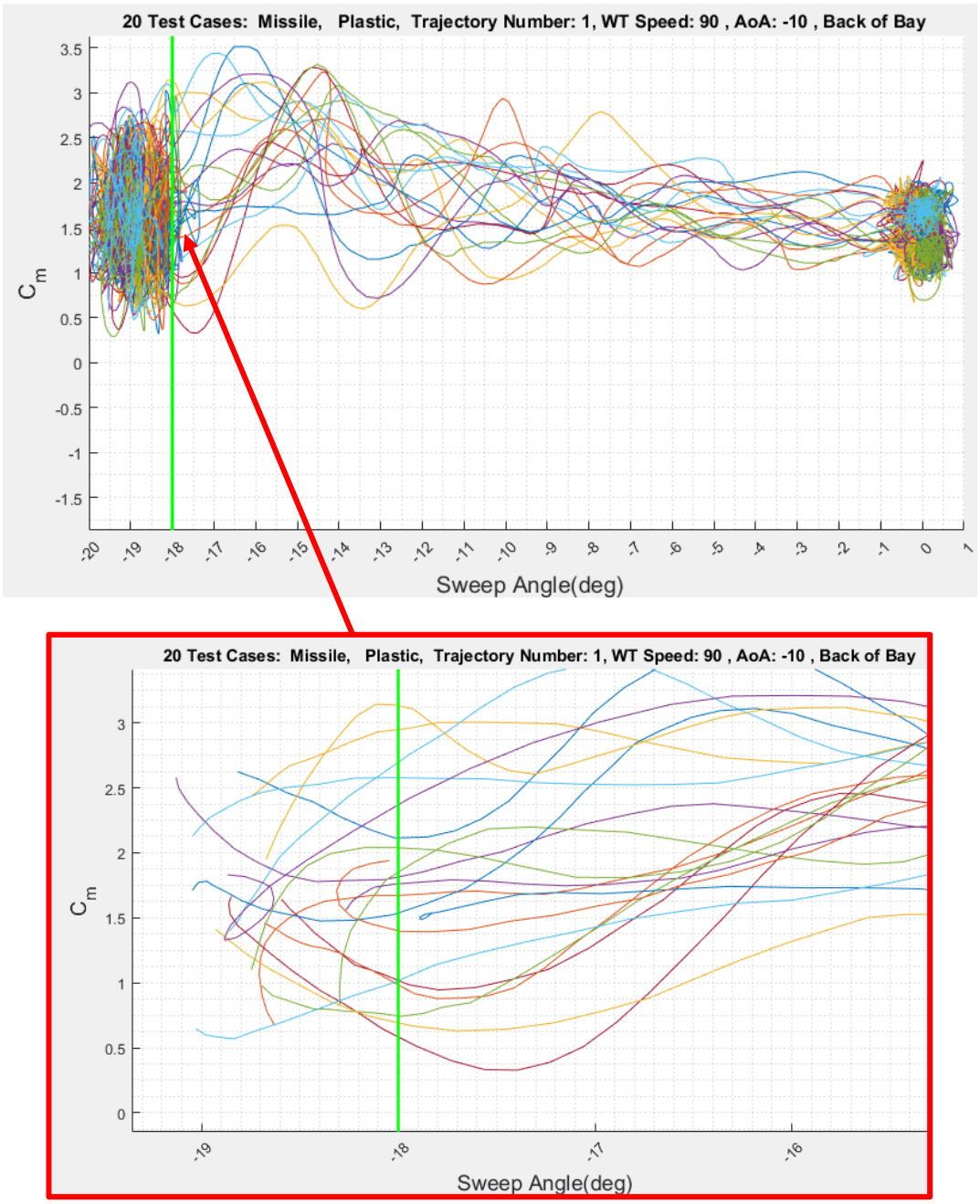

Figure 81. Twenty sets of filtered Cm data for the back-of-bay missile model separation runs. Store attitude is -10º AoA.

Figure 82 shows the filtered CN (a) and Cm (b) dynamic data results averaged starting at -18º and ranging to -1º of 1º Sweep Angle increments. The averaged results for both the front and back of the bay test cases where the initial AoA was held at -10º. The missile clearly experienced stronger fluctuations in magnitude while it was initially stationed in the back of the bay. CN data are near identical for both missile initial positions but vary throughout the test runs. As the Sweep Angle increases they are converging but the data suggests that the -1º position remains influenced by the flow around the cavity. Cm data have opposite trends of each other. The data shows that store carriage position can be drastically influenced by the unsteady shear layer. The averaged results however, fail to yield any evidence of bifurcation.

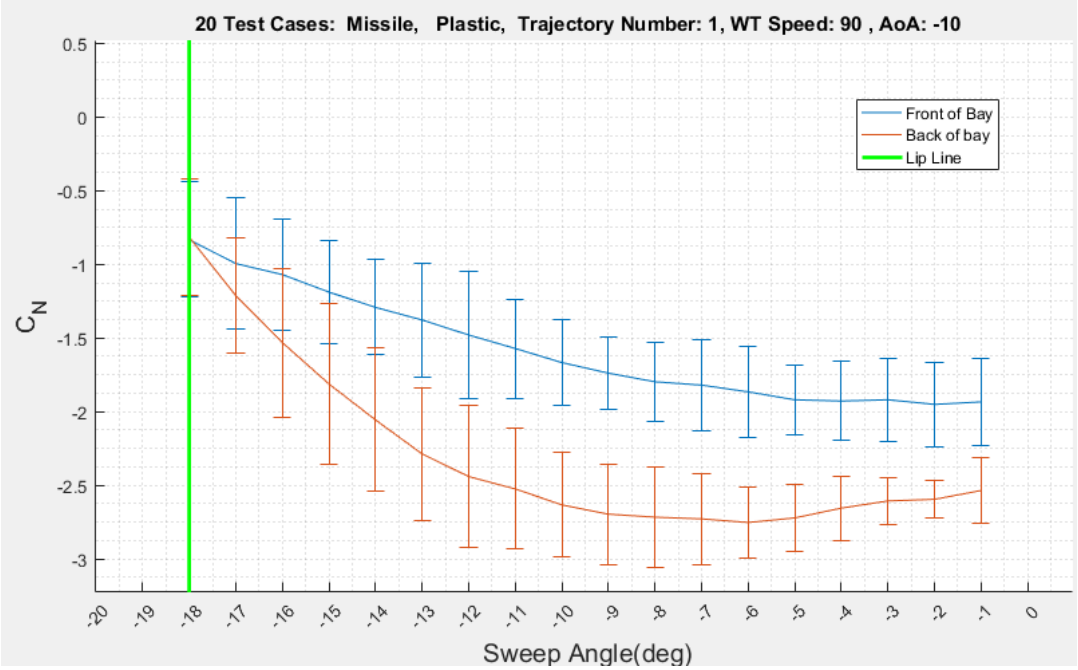

(a)

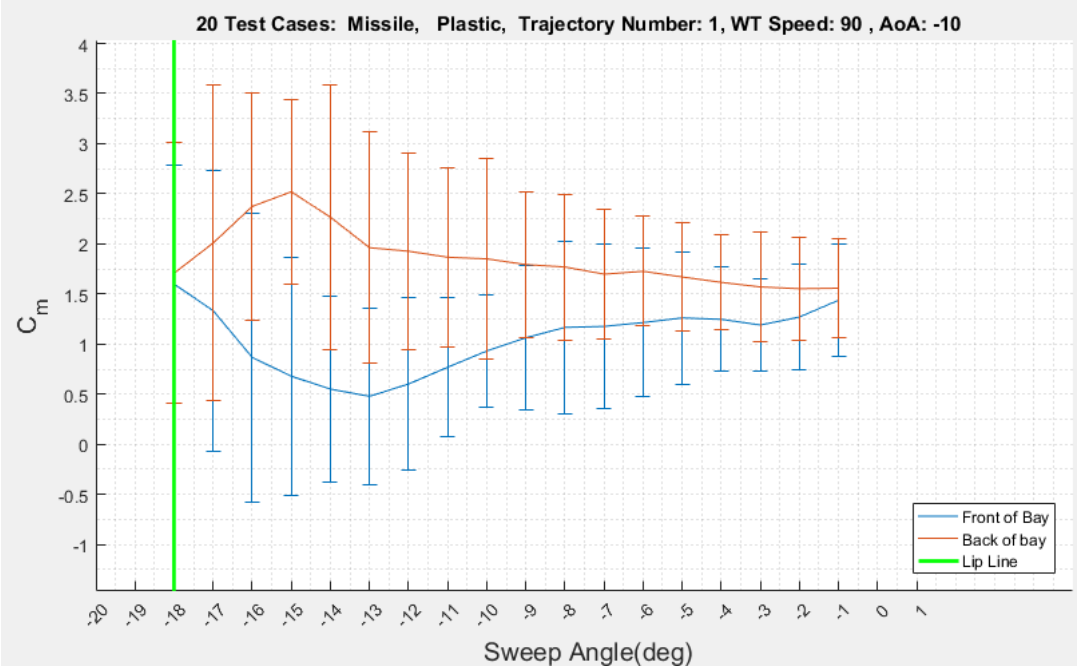

(b)

Figure 82. Averaged filtered CN (a) and Cm (b) data sets, plotted with 2-standard deviations, of the plastic missile performing store separation with -10º AoA attitude

Figure 83 provides a direct comparison of all the experiments discussed in this subsection for 0º and -10º pitch attitude based on averaged filtered data coefficients for the dynamic data sets. From the graph, it is clear how the missile can experience different effects as it traversed through the unsteady shear layer based on: its initial carriage position and attitude. In general, fluctuations are greater in magnitude for stores separating from the back of the weapons bay as compared to separations from the front.

The two cases where the missile model was held the attitude of -10º, have similar trend lines. These two cases yielded no evidence of a bifurcation based on the similar trends observed in Figure 78 and Figure 80 near the weapons bay cavity lip line. It follows that store attitude can be an approach to mitigate any undesirable bifurcation.

Observing bifurcation evidence based on averaged data, as is presented in Figure 83, is seemingly impossible. The averaged data does do well in describing store attitude as it is in proximity of the weapons bay cavity, as is the case for CTS experiments. The repeated test runs presented in this subsection clearly demonstrates the need to acquiring time-accurate force-and-moment data to identify bifurcation risks. Identifying risks with an experimental setup, such as the MTA, is always desirable before flight tests are conducted.

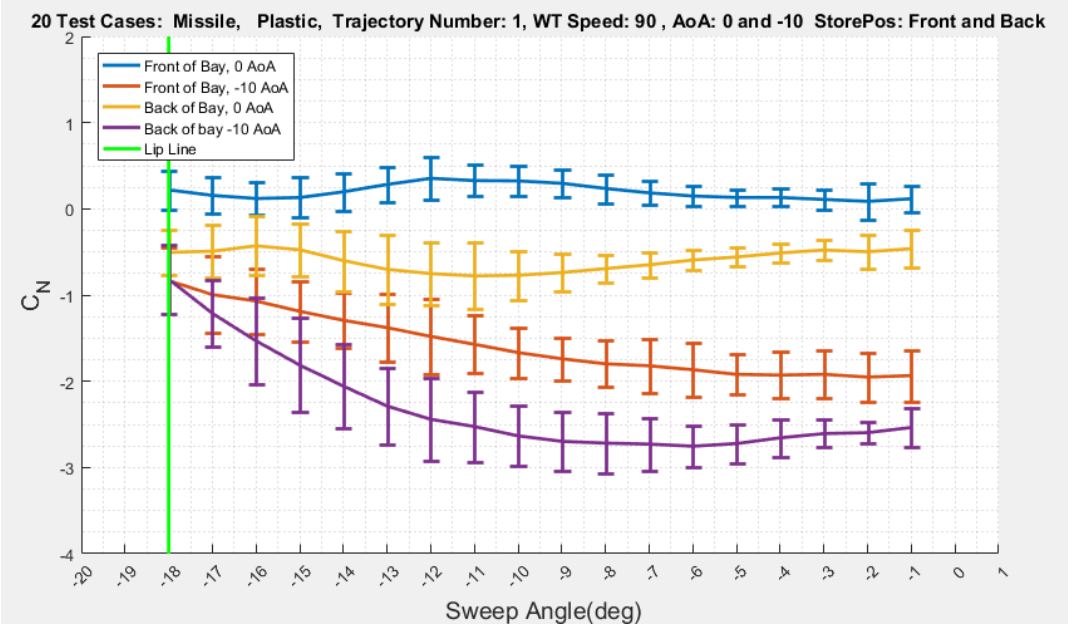

(a)

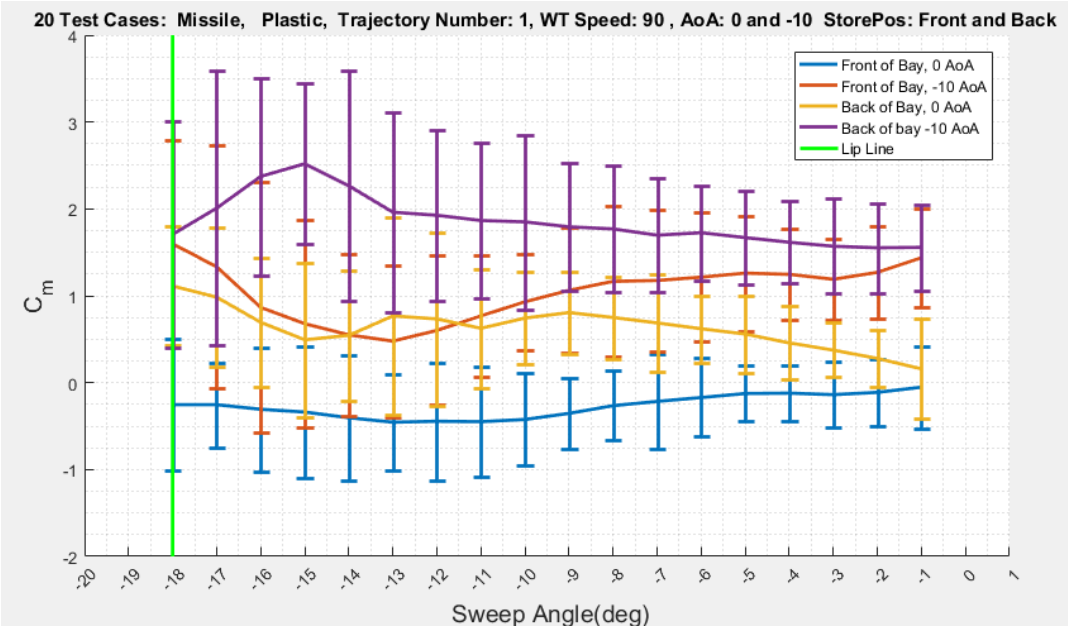

(b)

Figure 83. Averaged filtered CN (a) and Cm (b) data sets, plotted with 2-standard deviations, of the plastic missile performing store separation with 0º and -10º AoA attitudes.

4.4 Pressure Coefficients of Empty Weapons Bay

Dynamic pressure coefficients within the weapons bay cavity were calculated using equation (2). Calculations were carried out using MATLAB and the code is given in Appendix B. Figure 84 below gives the Cp values for the empty weapons bay. WT speeds varied from 60, 90, 120 MPH. The WT was set to 60 MPH and five Cp values were calculated. The WT speed was then set to 90 MPH and five Cp values were calculated. Finally, the WT was set to 120 MPH and five Cp were calculated. All Cp results, totaling 15 runs, were averaged and presented on the graph in Figure 84 along with their respective standard deviations. Values of Cp were generally consistent from run-to-run as tunnel speed was varied.

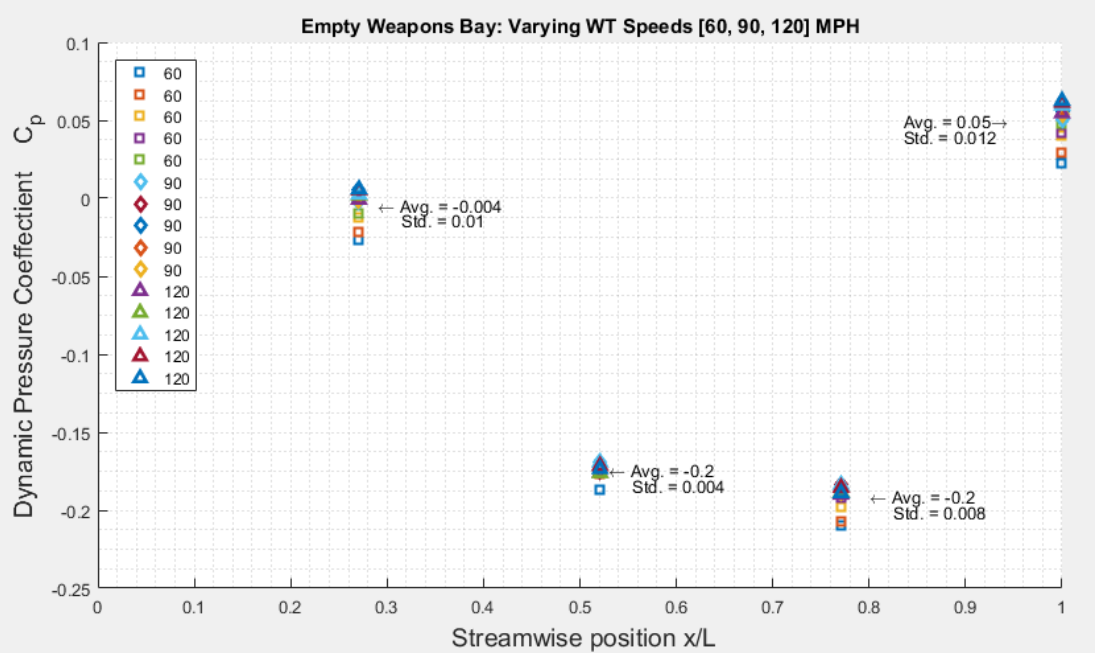

Figure 84. Dynamic pressure coefficients for the empty weapons bay cavity.

Summary

In this chapter the experimental tests involving the plastic missile at WT speed of 90 MPH were analyzed in detail. Plastic missile trajectory number two results were presented first. All six aerodynamic coefficients were calculated and were presented with the filtered IMU pitch angle data. Coefficient data were presented in unfiltered form and filtered form. Anomalies were explained.

Trajectory number one results for the plastic missile at WT speed of 90 MPH were presented next. Again, all six aerodynamic coefficients were calculated and presented with the corresponding filtered IMU sweep angle data. Coefficient data were presented in unfiltered form and filtered form. Anomalies were explained.

The CN and Cm coefficient data for all mission store models were given in a series of tables in order to compare results based on mission store model geometries for incipient and final phase data sets. In general, the CN and Cm data agree based on mission store model geometry as WT speeds, model attitude, and weapons bay carriage positions varied. Finally, the dynamic pressure coefficients for the empty weapons bay was presented for WT speeds at 60, 90, and 120 MPH.

V. Conclusions and Recommendations

5.1 MTA Utility for Mission Store Separation Testing

Characterizing the aerodynamic interaction as a mission store departs a weapons bay cavity is highly relevant to the USAF mission [1]. In order to characterizing mission store separation, CFD models and wind tunnel experiments are used [2]. Proper characterization, by predicting force-and-moment data, is then used in order to identify risks associated for the test flight envelope, in which the mission stores will be employed [3].

The AFIT MTA is a unique force-motion test rig system [15] that proved itself capable of acquiring time-accurate aerodynamic force-and-moment data. These data can be used in conjunction with flight tests, namely the SUU-41 WASSP [30] where the weapons bay cavity used in this study is geometrically the same as the WASSP, in order to accurately correlate wind tunnel data and flight test data. This correlation is highly desirable for those who study cavity flow in the scientific and engineering community [7], [2].

5.2 Summary of Results

While the ability to acquire force-and-moment measurements for a cyclic motion was verified by Sellers [5] by comparing aerodynamic lift measurements of the Nano25 to the AFIT low-speed wind tunnel force balance, tests performed for one-off motions are more demanding of time synchronization. The MTA and associate data acquisition system was enhanced by recording six Nano25 outputs and an IMU output simultaneously. The Nano25 was able to record all six forces-and-moments. By locating

the Nano25 to be coincident with the body-axis system the acquisition of associated forces and moments was straight forward. The Nano25 was susceptible to electrical noise, introduced by the wind tunnel control box, and a technique was discovered and employed to mitigate the noise.

A specially modified 3DM GXI IMU was purchased from LordMicrostrain. The IMU was a special order sensor that was key to acquiring mission store model attitude at the precise time the force-and-moment data was acquired. This was achievable because the 3DM GX1 output was analog, as is the Nano25. The research work of Sellers used the 3DM GX4-15 IMU sensor where the output was digital thus being incapable of time-synchronization with the analog Nano25. The 3DM GX1 was susceptible to wind tunnel control box noise, however no noise mitigation technique could have been employed to mitigate the noise save for filtering techniques during post-processing. Studies performed by Sellers [5] and Lancaster [4] had the 3DM GX4-15 attached to the sting and in the wind tunnel flow. The placement of the 3DM GX1 in this study was on the MTA joint-6 where it was not in the wind tunnel flow. The IMU still picked up MTA movements caused by the wind tunnel flow acting on the MTA.

Four Endevco Model 8515C-15 pressure transducers were placed within the empty weapons bay. Fifteen experimental test runs were conducted at wind tunnel speeds of 60, 90, and 120 MPH. Four pressure differentials were recorded and used to calculate four dynamic pressure coefficients. The results were all consistent, regardless of wind tunnel test speed, and the standard deviations for all four dynamic pressure values computed were small.

5.3 Significance of Research

One significance of this research is that the first step in acquiring time-accurate force-and-moment data was achieved. The MTA should play a complementary role with the CTS, which records time-averaged data. The latter is useful for mission store integration in which the mission stores are attached to a pylon where they are already in the freestream. For 5th generation air vehicles, weapons bay cavities will be utilized, and time-accurate data becomes a necessity. The unsteady shear layer flowing across the weapons bay, through which the mission store must traverse, can only be characterized by detecting subtle variations in aerodynamic forces as the mission store travels through the unsteady shear layer. Furthermore, since mission stores will be carried inside weapons bays, mission stores will become smaller. Smaller stores are more susceptible to turbulent and unsteady nature associated with the weapons bay flow field [31].

AFIT now has a wind tunnel system that acquires time-accurate force-and-moment data, where mission store model attitude and force-and-moment data are synchronized. The data collected in this study strongly suggests that a pitch bifurcation [7] is present as the mission store models separated the weapons bay. Bifurcation detection is important in order to mitigate the undesired dramatic effect unsteady flow can have on separation trajectories [7]. Wind tunnel experimental studies can now be conducted by routine operation. The system is primed. The wind tunnel experimental studies can be compared and correlated with actual flight test data generated by the WASSP test bed. AFIT is on the verge of leading a scientific breakthrough.

5.4 Recommendations for Future MTA Testing

The majority of the USAF fifth-generation air vehicles operate at higher Mach numbers than can be replicated by the AFIT low-speed wind tunnel. A linear motor exists in the wind tunnel lab equipment inventory. The linear motor should be installed into the weapons bay cavity and configured in a way such that it can manipulate the weapons bay flow field in order to replicate the vortex shedding that occurs, as air flows over cavities at higher these higher Mach numbers. Developing this capability should be the priority of work for the next researcher.

The first mode of the Rossiter tone, as given by equation (1) was calculated to be 33 Hz for the 90 MPH wind tunnel test speed and 44 Hz for when the wind tunnel was set to 120 MPH. The rate at which LabVIEW acquired data was set to 100 Hz. Nyquist theory was satisfied, but sampling faster would be desirable. The 3DM GX1 is the reason why the DAQ system sampled at 100 Hz. That is has fast as the 3DM GX1 can sample. The 3DM GX1 had to be in the same "while loop" as the Nano25 in order to obtained time-synced data. By ordering a newer IMU with the ability to render analog output at a faster rate, would permit faster data sampling. Furthermore, the 3DM GX1 is only capable of recording mission store model attitude about one axis at a time. The capability to record mission store attitude position and rates is paramount for proper analysis of store trajectories.

Appendix A. Additional Experimental Data

This Page Intentionally Left Blank

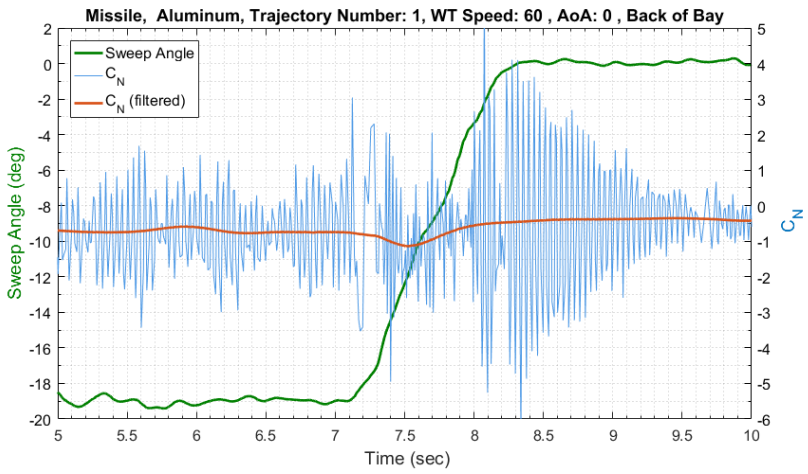
Missile, Aluminum, Trajectory Number: 1, WT Speed: 60 , AoA: 0 , Back of Bay
Sweep Angle
C_N
C_N (filtered)
Sweep Angle (deg)
C_N
Time (sec)

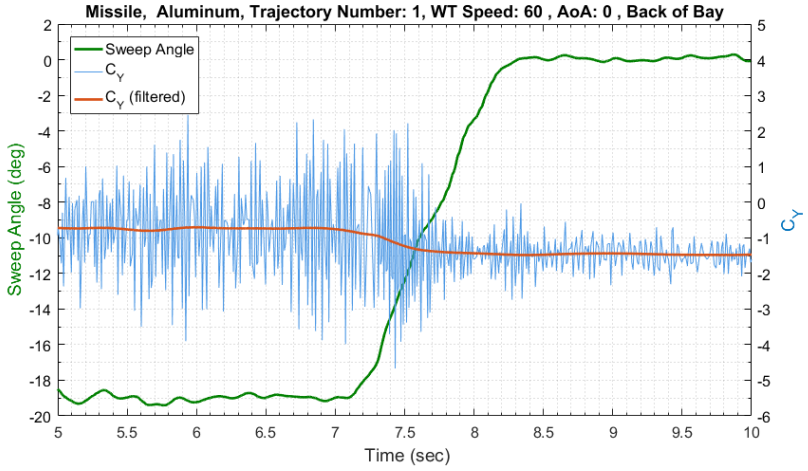
Missile, Aluminum, Trajectory Number: 1, WT Speed: 60 , AoA: 0 , Back of Bay
Sweep Angle
C_Y
C_Y (filtered)
Sweep Angle (deg)
C_Y
Time (sec)

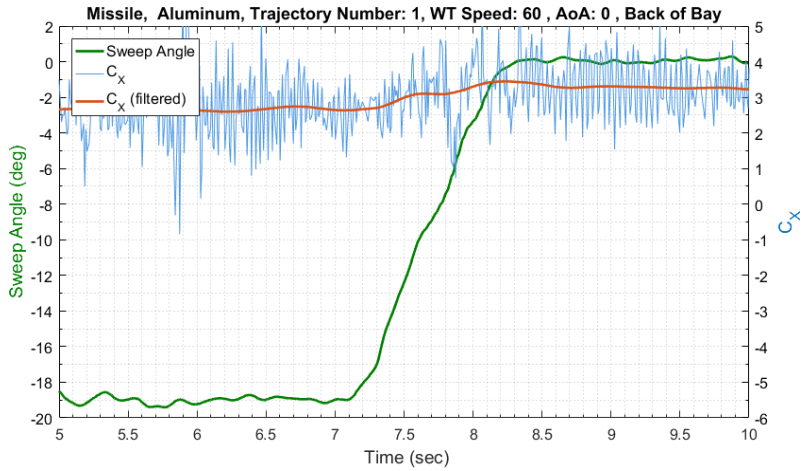
Missile, Aluminum, Trajectory Number: 1, WT Speed: 60 , AoA: 0 , Back of Bay
Sweep Angle
C_X
C_X (filtered)
Sweep Angle (deg)
C_X
Time (sec)

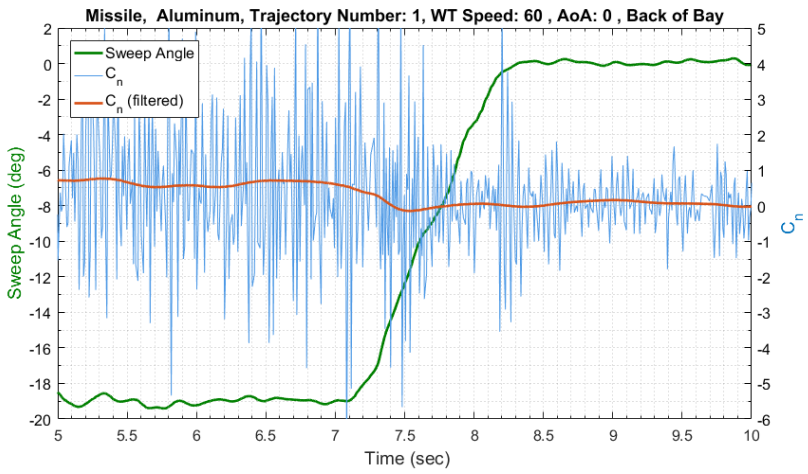
Missile, Aluminum, Trajectory Number: 1, WT Speed: 60 , AoA: 0 , Back of Bay
Sweep Angle
C_n
C_n (filtered)
Sweep Angle (deg)
C_n
Time (sec)

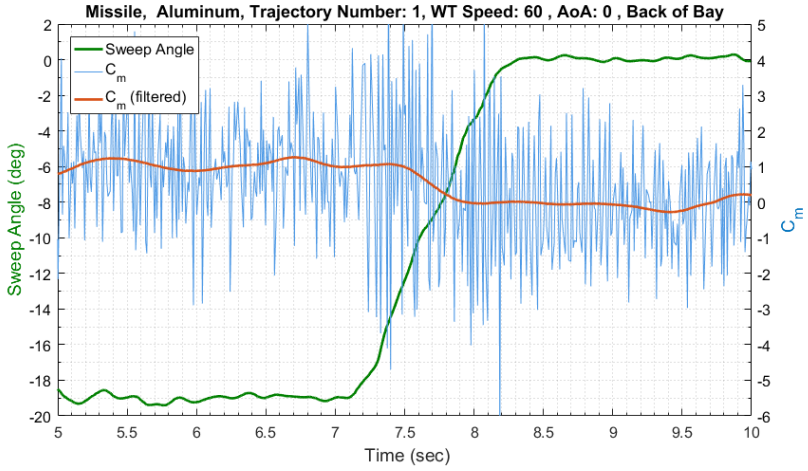
Missile, Aluminum, Trajectory Number: 1, WT Speed: 60 , AoA: 0 , Back of Bay
Sweep Angle
C_m
C_m (filtered)
Sweep Angle (deg)
C_m
Time (sec)

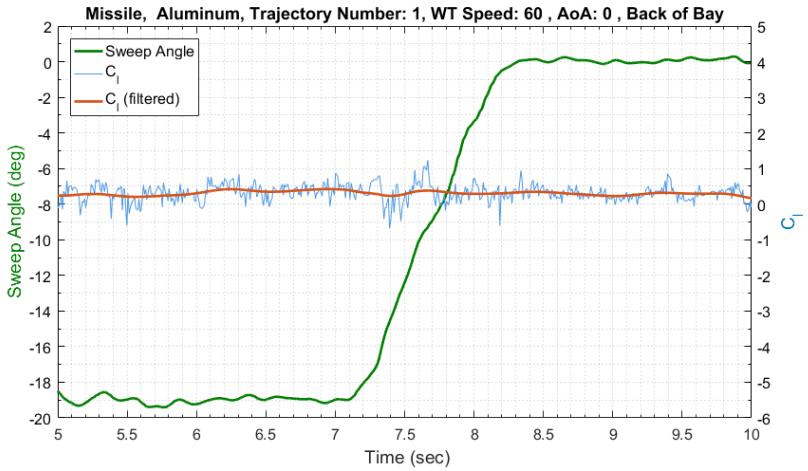
Missile, Aluminum, Trajectory Number: 1, WT Speed: 60 , AoA: 0 , Back of Bay
Sweep Angle
C_l
C_l (filtered)
Sweep Angle (deg)
C_l
Time (sec)

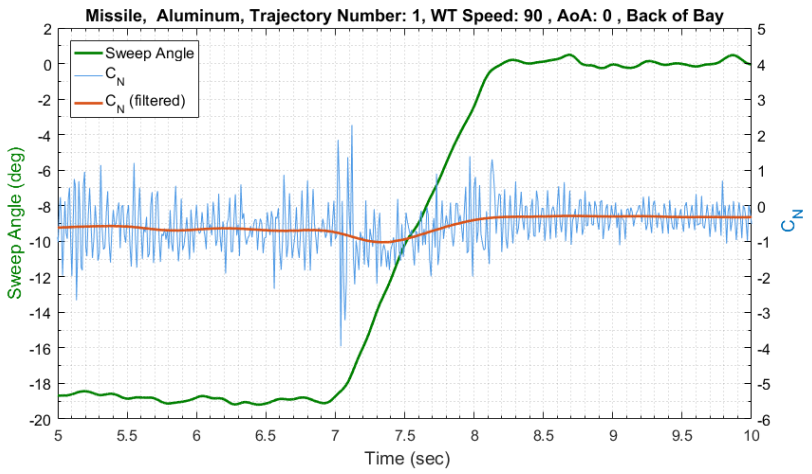
Missile, Aluminum, Trajectory Number: 1, WT Speed: 90 , AoA: 0 , Back of Bay
Sweep Angle
C_N
C_N (filtered)
Sweep Angle (deg)
C_N
Time (sec)

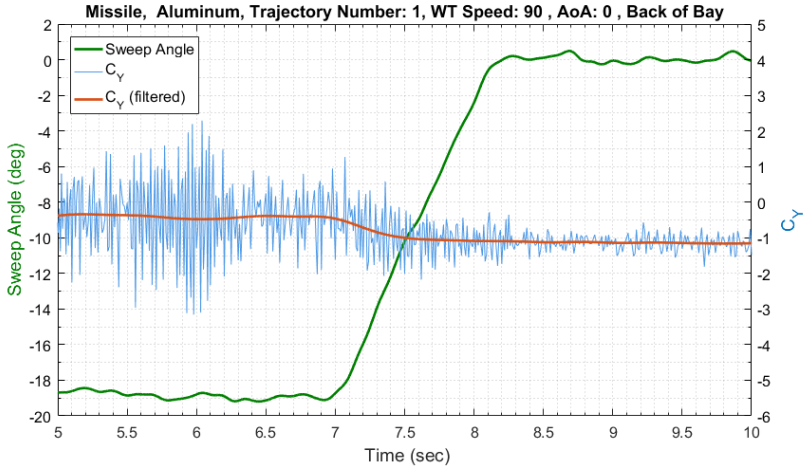
Missile, Aluminum, Trajectory Number: 1, WT Speed: 90 , AoA: 0 , Back of Bay
Sweep Angle
C_Y
C_Y (filtered)
Sweep Angle (deg)
C_Y
Time (sec)

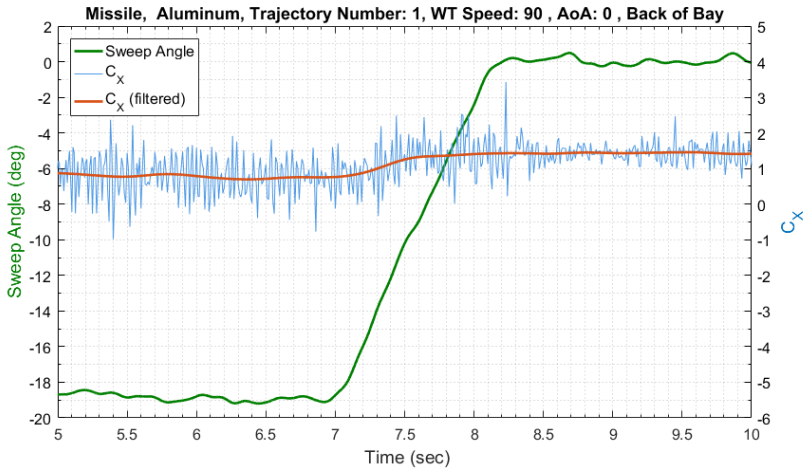
Missile, Aluminum, Trajectory Number: 1, WT Speed: 90 , AoA: 0 , Back of Bay
Sweep Angle
C_X
C_X (filtered)
Sweep Angle (deg)
C_X
Time (sec)

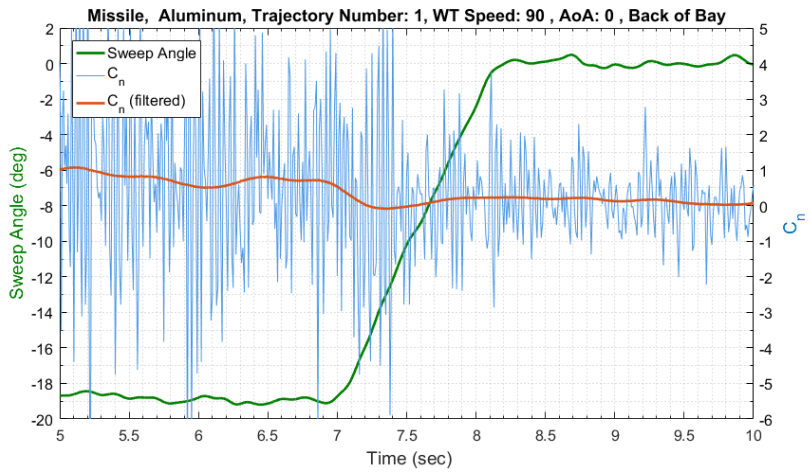
Missile, Aluminum, Trajectory Number: 1, WT Speed: 90 , AoA: 0 , Back of Bay
Sweep Angle
C_n
C_n (filtered)
Sweep Angle (deg)
C_n
Time (sec)

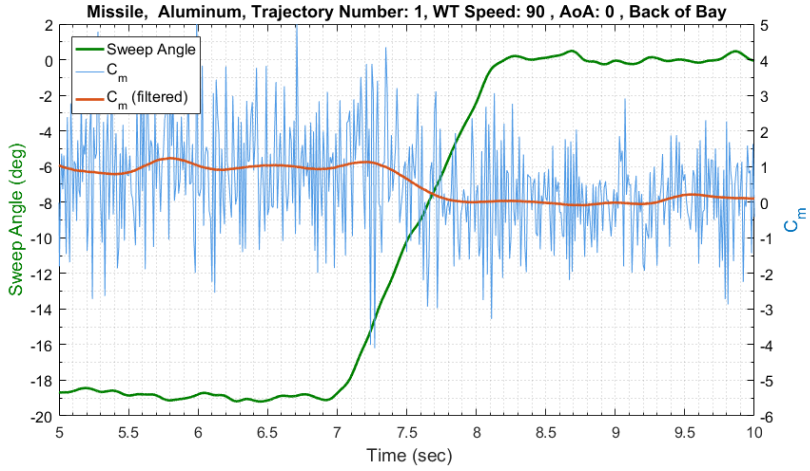
Missile, Aluminum, Trajectory Number: 1, WT Speed: 90 , AoA: 0 , Back of Bay
Sweep Angle
C_m
C_m (filtered)
Sweep Angle (deg)
C_m
Time (sec)

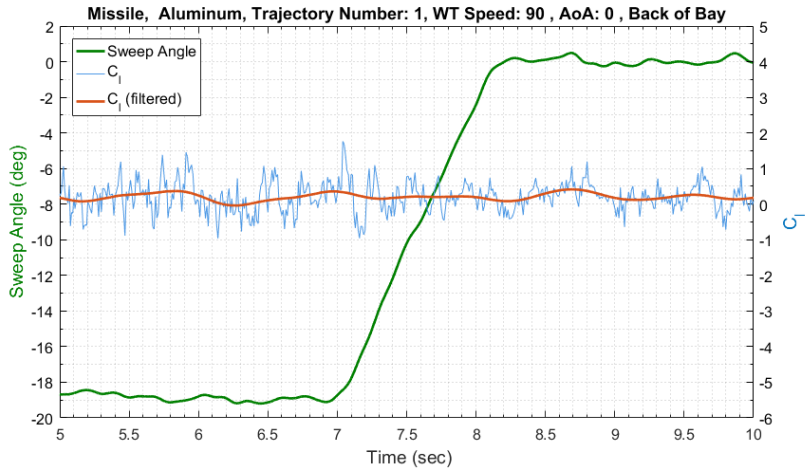
Missile, Aluminum, Trajectory Number: 1, WT Speed: 90 , AoA: 0 , Back of Bay
Sweep Angle
C_l
C_l (filtered)
Sweep Angle (deg)
C_l
Time (sec)

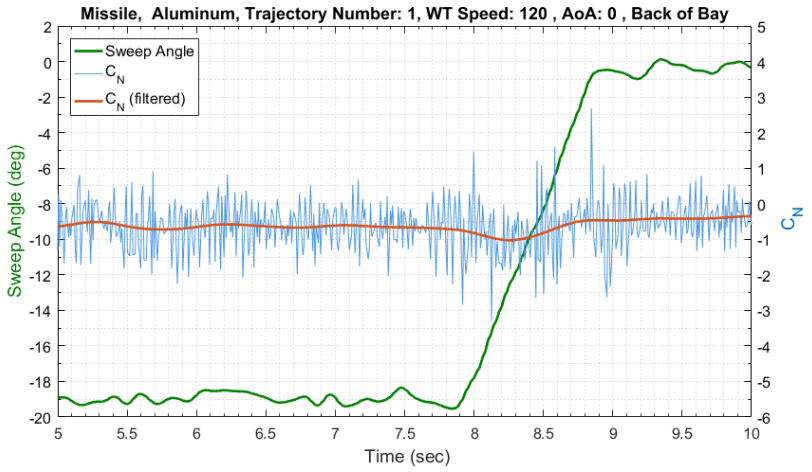
Missile, Aluminum, Trajectory Number: 1, WT Speed: 120 , AoA: 0 , Back of Bay
Sweep Angle
C_N
C_N (filtered)
Sweep Angle (deg)
C_N
Time (sec)

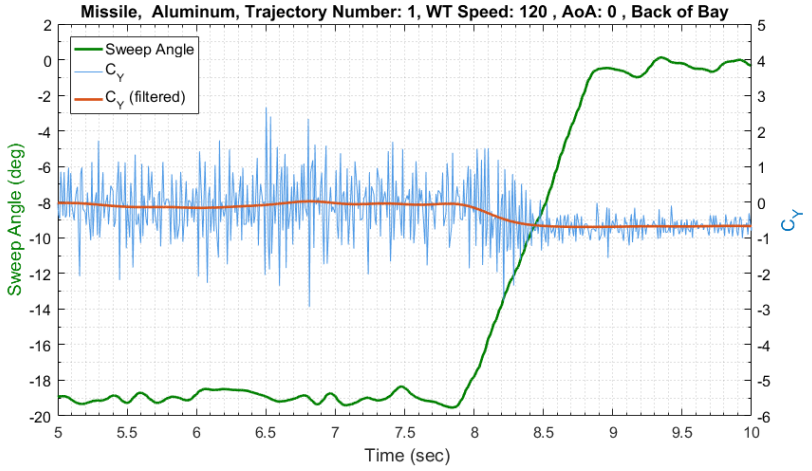
Missile, Aluminum, Trajectory Number: 1, WT Speed: 120 , AoA: 0 , Back of Bay
Sweep Angle
C_Y
C_Y (filtered)
Sweep Angle (deg)
C_Y
Time (sec)

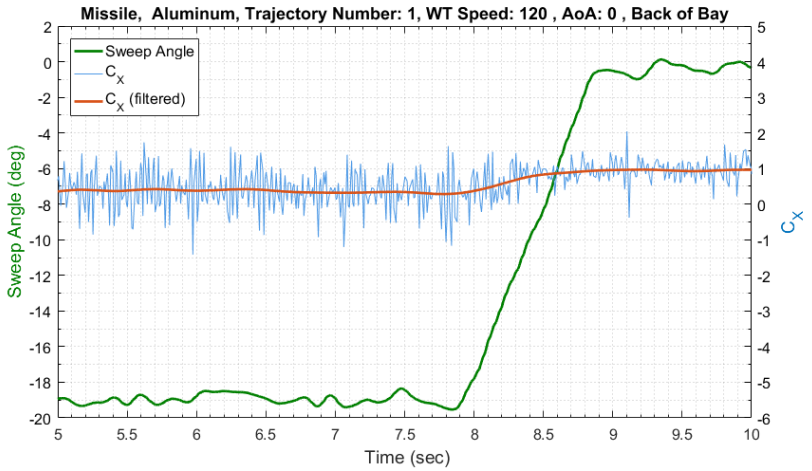
Missile, Aluminum, Trajectory Number: 1, WT Speed: 120 , AoA: 0 , Back of Bay
Sweep Angle
C_X
C_X (filtered)
Sweep Angle (deg)
C_X
Time (sec)

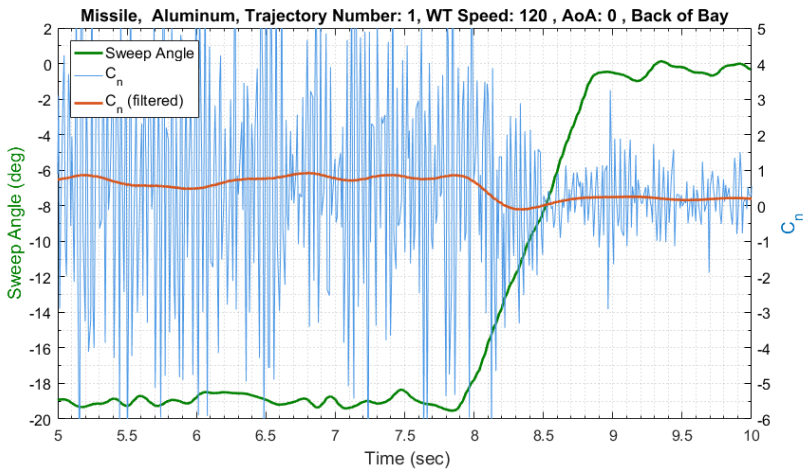
Missile, Aluminum, Trajectory Number: 1, WT Speed: 120 , AoA: 0 , Back of Bay
Sweep Angle
C_n
C_n (filtered)
Sweep Angle (deg)
C_n
Time (sec)

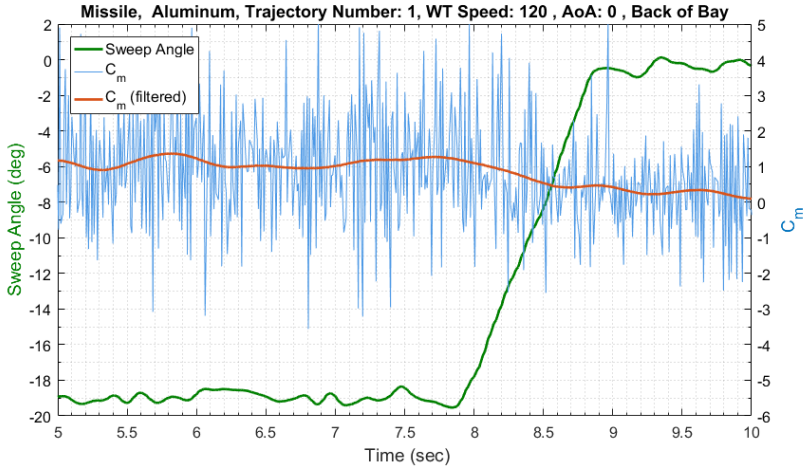
Missile, Aluminum, Trajectory Number: 1, WT Speed: 120 , AoA: 0 , Back of Bay
Sweep Angle
C_m
C_m (filtered)
Sweep Angle (deg)
C_m
Time (sec)

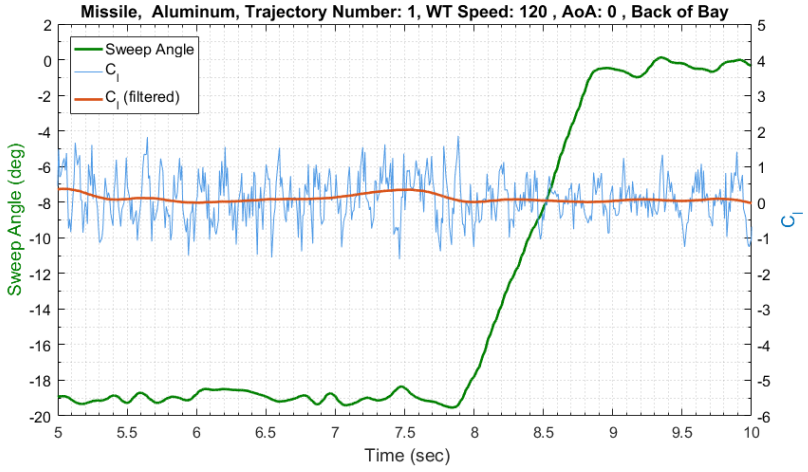
Missile, Aluminum, Trajectory Number: 1, WT Speed: 120 , AoA: 0 , Back of Bay
Sweep Angle
C_l
C_l (filtered)
Sweep Angle (deg)
C_l
Time (sec)

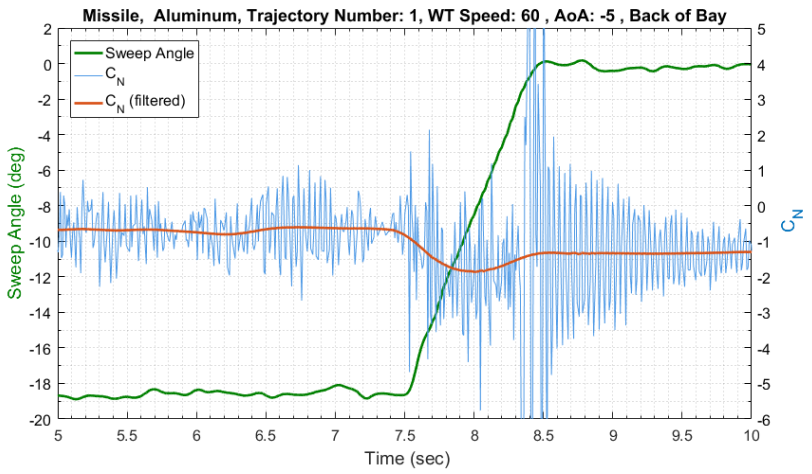
Missile, Aluminum, Trajectory Number: 1, WT Speed: 60 , AoA: -5 , Back of Bay
Sweep Angle
C_N
C_N (filtered)
Sweep Angle (deg)
C_N
Time (sec)

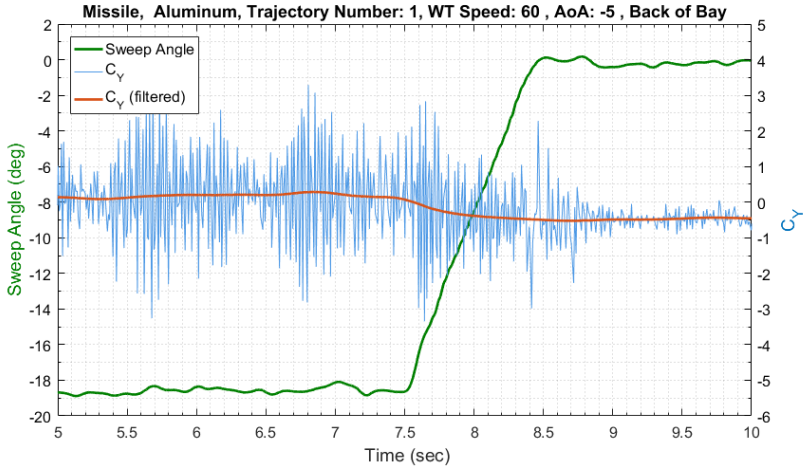
Missile, Aluminum, Trajectory Number: 1, WT Speed: 60 , AoA: -5 , Back of Bay
Sweep Angle
C_Y
C_Y (filtered)
Sweep Angle (deg)
C_Y
Time (sec)

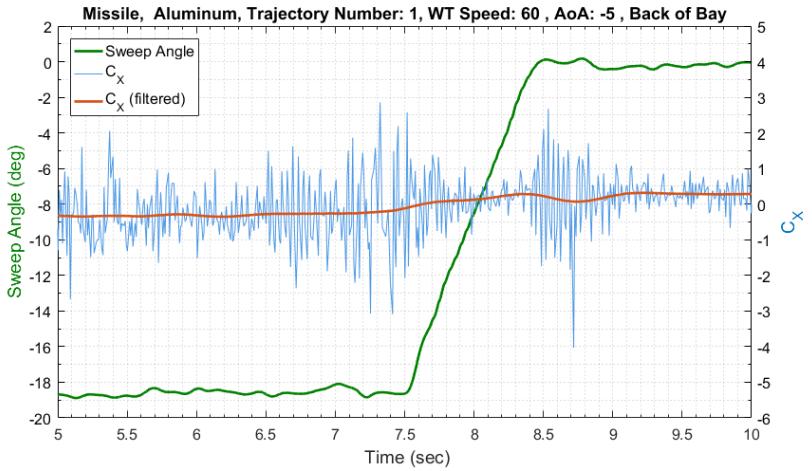
Missile, Aluminum, Trajectory Number: 1, WT Speed: 60 , AoA: -5 , Back of Bay
Sweep Angle
C_X
C_X (filtered)
Sweep Angle (deg)
C_X
Time (sec)

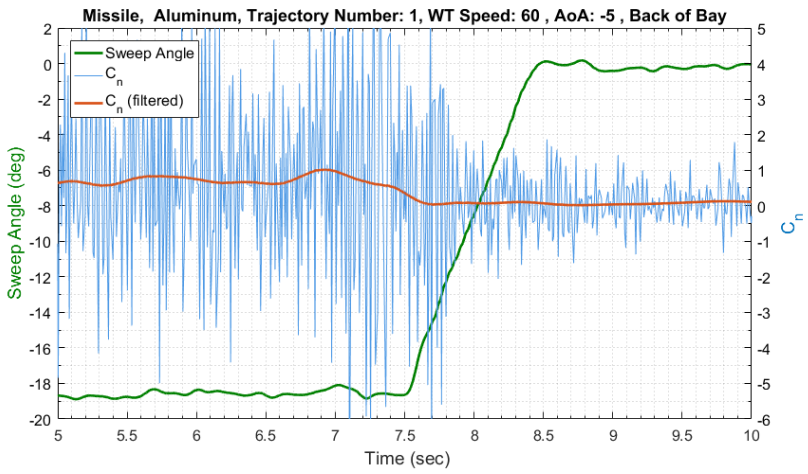
Missile, Aluminum, Trajectory Number: 1, WT Speed: 60 , AoA: -5 , Back of Bay
Sweep Angle
C_n
C_n (filtered)
Sweep Angle (deg)
C_n
Time (sec)

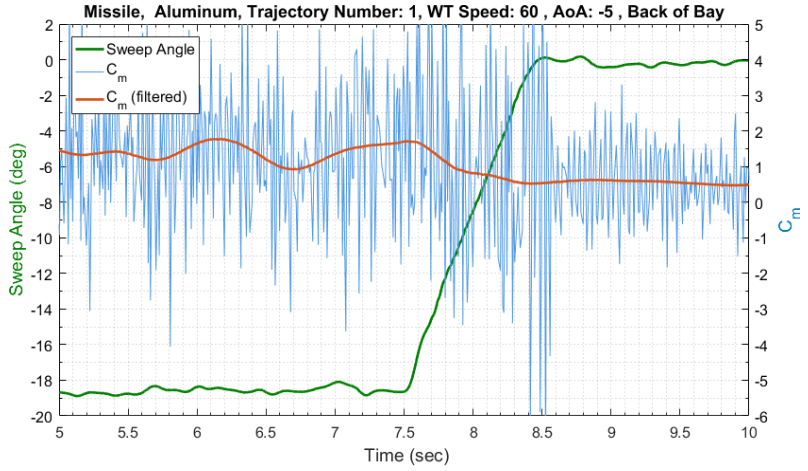
Missile, Aluminum, Trajectory Number: 1, WT Speed: 60 , AoA: -5 , Back of Bay
Sweep Angle
C_m
C_m (filtered)
Sweep Angle (deg)
C_m
Time (sec)

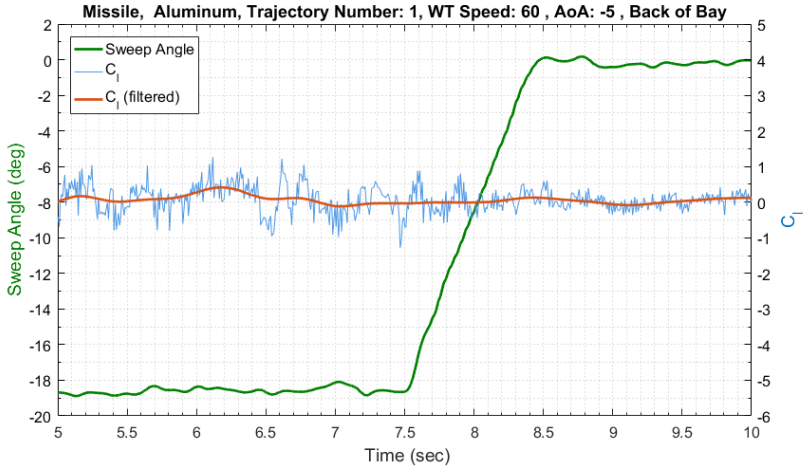
Missile, Aluminum, Trajectory Number: 1, WT Speed: 60 , AoA: -5 , Back of Bay
Sweep Angle
C_l
C_l (filtered)
Sweep Angle (deg)
C_l
Time (sec)

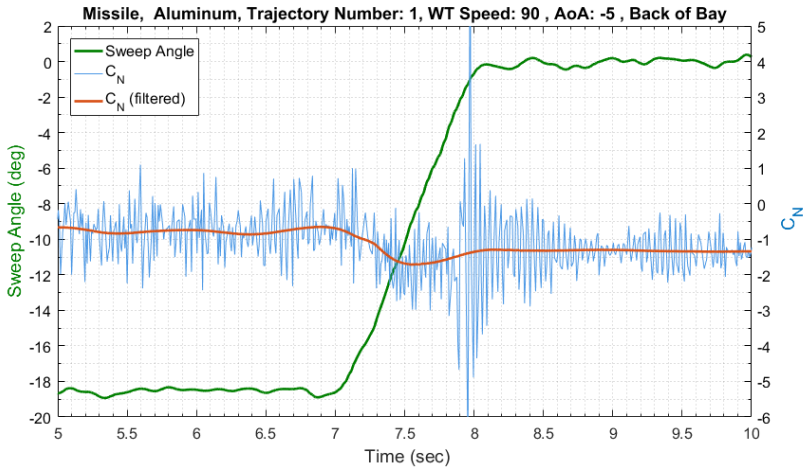
Missile, Aluminum, Trajectory Number: 1, WT Speed: 90 , AoA: -5 , Back of Bay
Sweep Angle
C_N
C_N (filtered)
Sweep Angle (deg)
C_N
Time (sec)

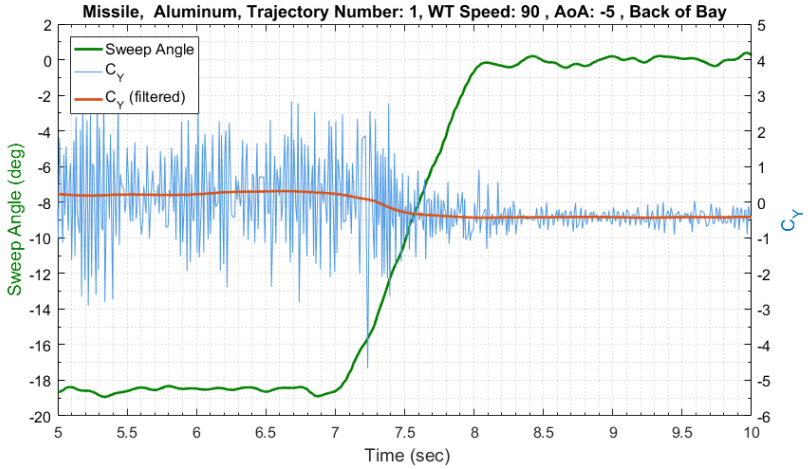
Missile, Aluminum, Trajectory Number: 1, WT Speed: 90 , AoA: -5 , Back of Bay
Sweep Angle
C_Y
C_Y (filtered)
Sweep Angle (deg)
C_Y
Time (sec)

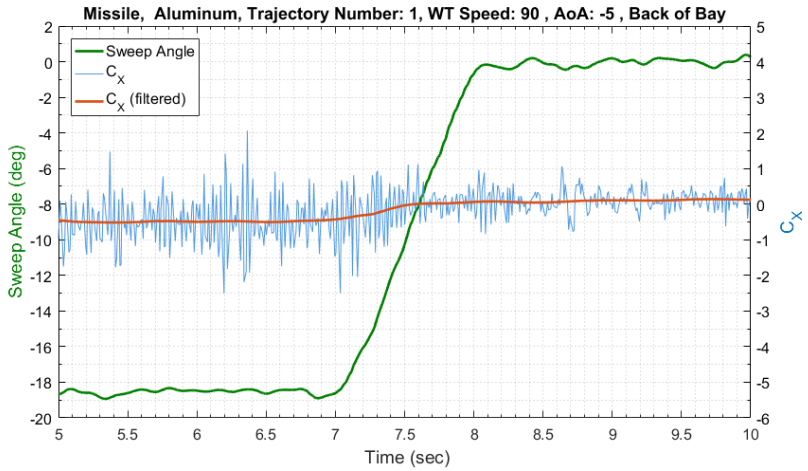
Missile, Aluminum, Trajectory Number: 1, WT Speed: 90 , AoA: -5 , Back of Bay
Sweep Angle
C_X
C_X (filtered)
Sweep Angle (deg)
C_X
Time (sec)

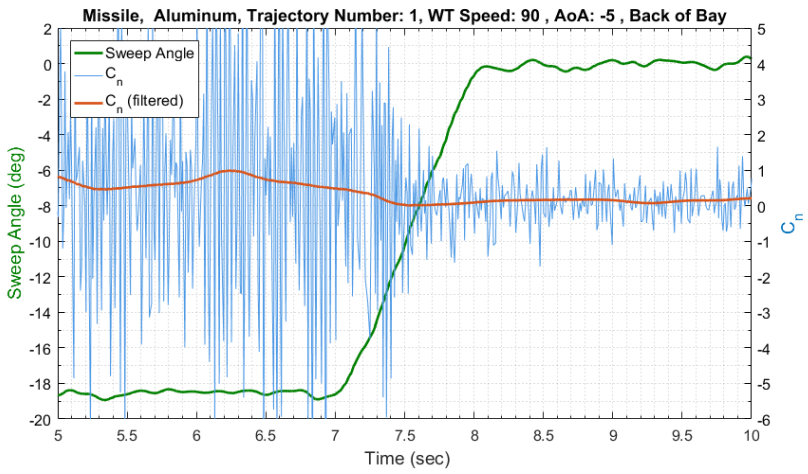
Missile, Aluminum, Trajectory Number: 1, WT Speed: 90 , AoA: -5 , Back of Bay
Sweep Angle
C_n
C_n (filtered)
Sweep Angle (deg)
C_n
Time (sec)

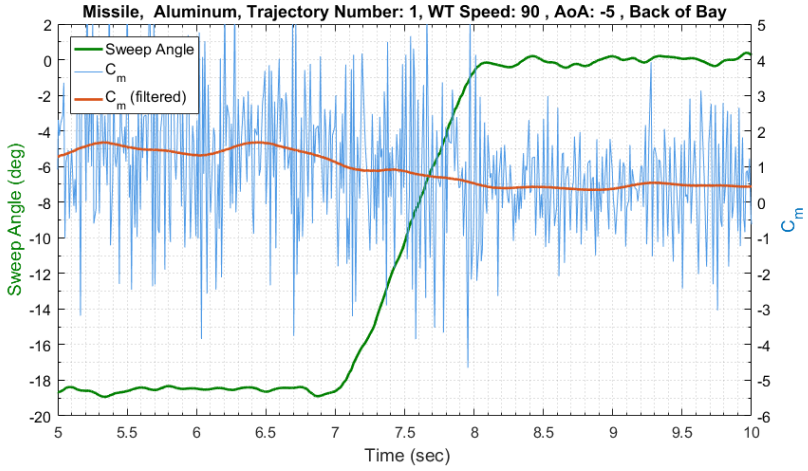
Missile, Aluminum, Trajectory Number: 1, WT Speed: 90 , AoA: -5 , Back of Bay
Sweep Angle
C_m
C_m (filtered)
Sweep Angle (deg)
C_m
Time (sec)

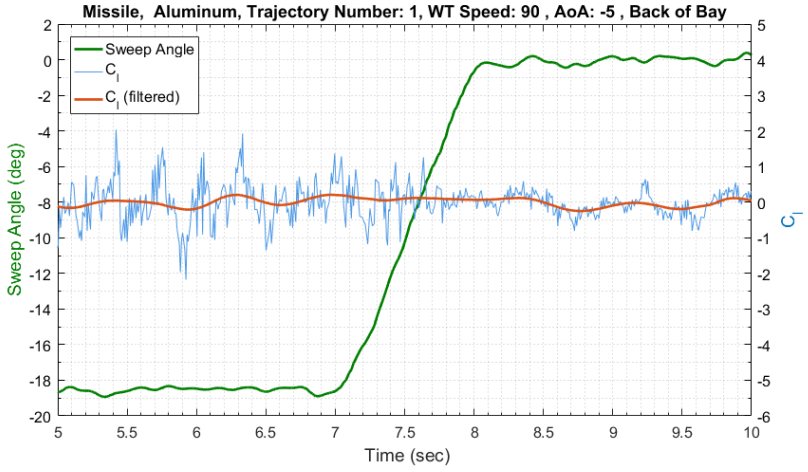
Missile, Aluminum, Trajectory Number: 1, WT Speed: 90 , AoA: -5 , Back of Bay
Sweep Angle
C_l
C_l (filtered)
Sweep Angle (deg)
C_l
Time (sec)

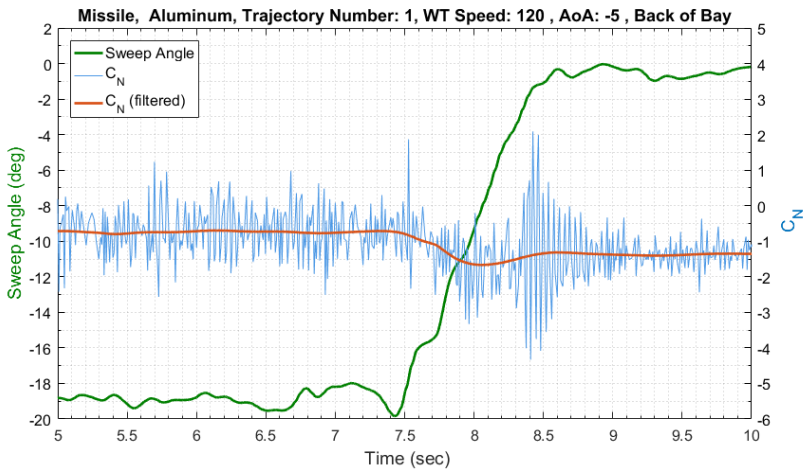
Missile, Aluminum, Trajectory Number: 1, WT Speed: 120 , AoA: -5 , Back of Bay
Sweep Angle
C_N
C_N (filtered)
Sweep Angle (deg)
C_N
Time (sec)

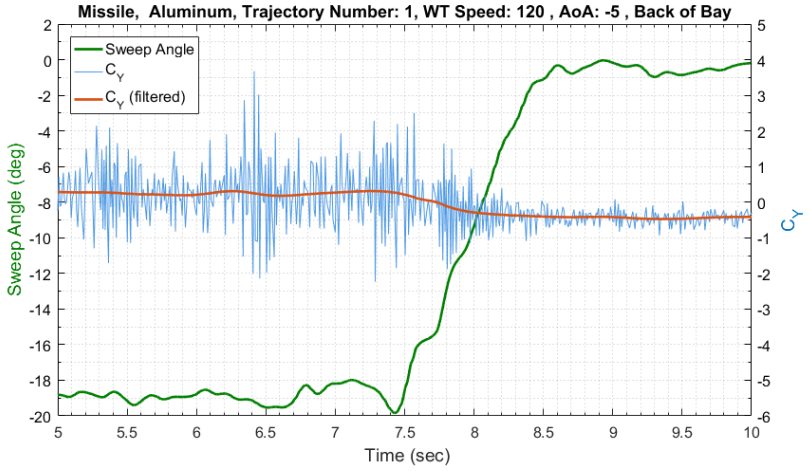
Missile, Aluminum, Trajectory Number: 1, WT Speed: 120 , AoA: -5 , Back of Bay
Sweep Angle
C_Y
C_Y (filtered)
Sweep Angle (deg)
C_Y
Time (sec)

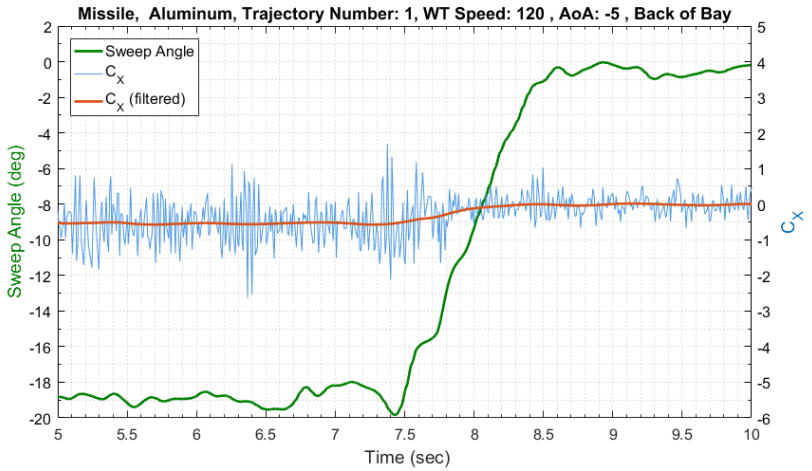
Missile, Aluminum, Trajectory Number: 1, WT Speed: 120 , AoA: -5 , Back of Bay
Sweep Angle
C_X
C_X (filtered)
Sweep Angle (deg)
C_X
Time (sec)

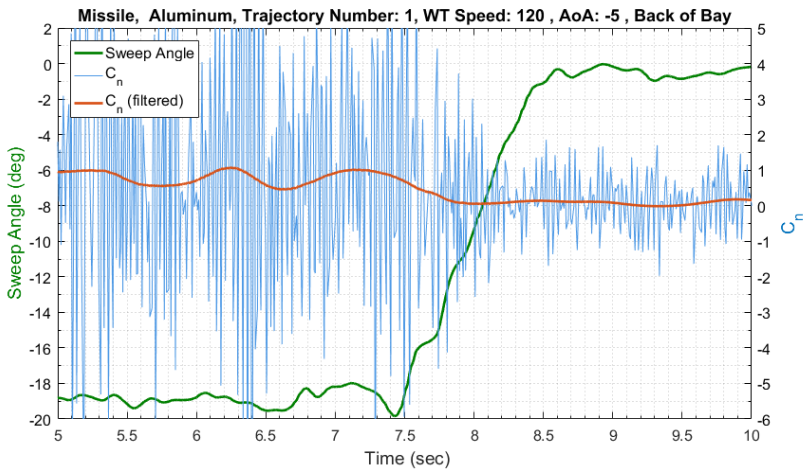
Missile, Aluminum, Trajectory Number: 1, WT Speed: 120 , AoA: -5 , Back of Bay
Sweep Angle
C_n
C_n (filtered)
Sweep Angle (deg)
C_n
Time (sec)

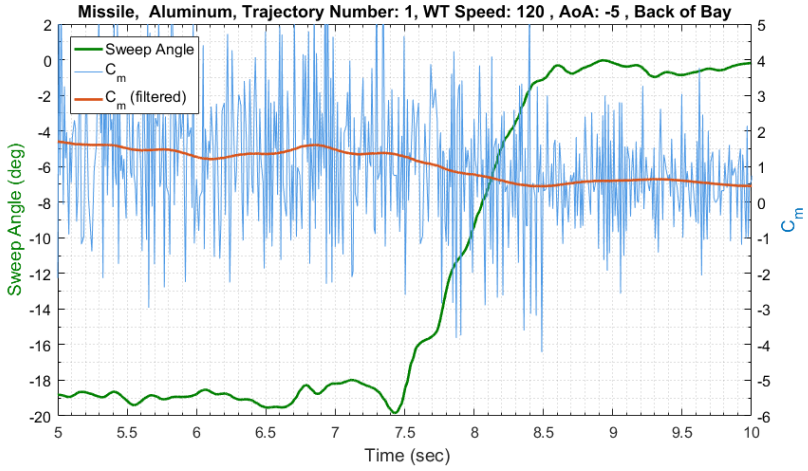
Missile, Aluminum, Trajectory Number: 1, WT Speed: 120 , AoA: -5 , Back of Bay
Sweep Angle
C_m
C_m (filtered)
Sweep Angle (deg)
C_m
Time (sec)

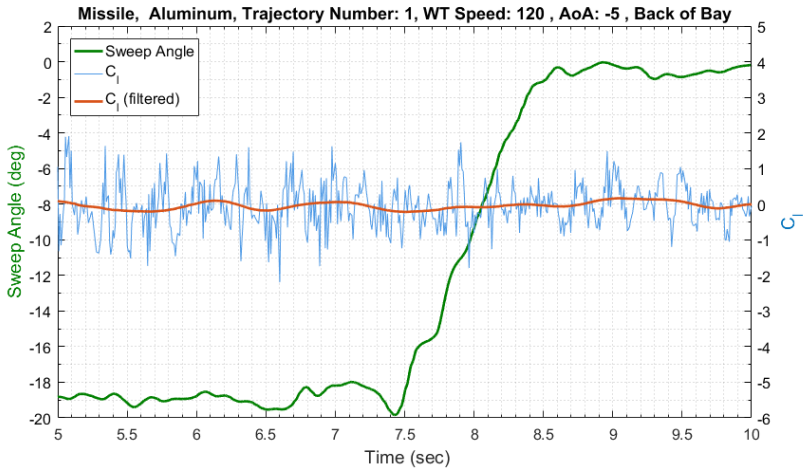
Missile, Aluminum, Trajectory Number: 1, WT Speed: 120 , AoA: -5 , Back of Bay
Sweep Angle
C_l
C_l (filtered)
Sweep Angle (deg)
C_l
Time (sec)

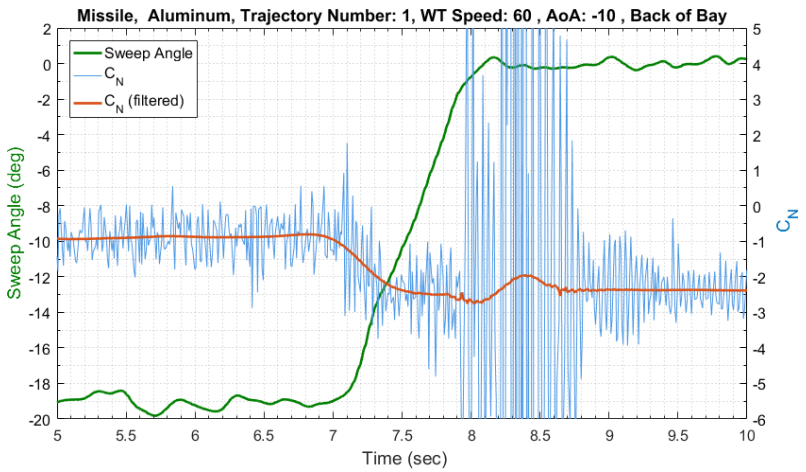
Missile, Aluminum, Trajectory Number: 1, WT Speed: 60 , AoA: -10 , Back of Bay
Sweep Angle
C_N
C_N (filtered)
Sweep Angle (deg)
C_N
Time (sec)

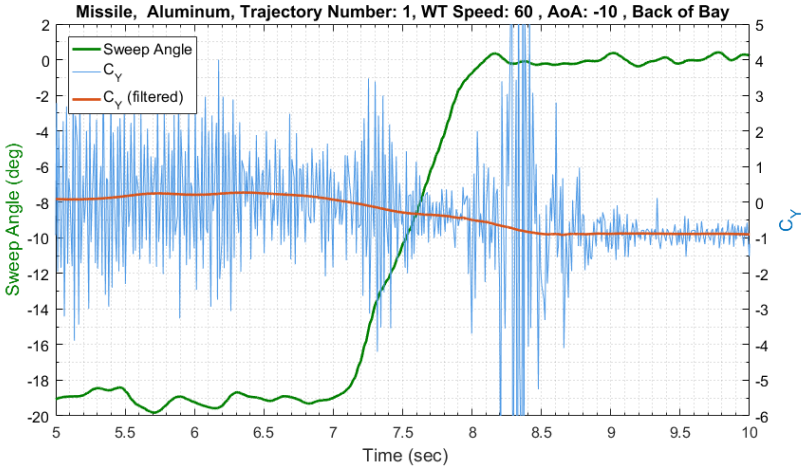
Missile, Aluminum, Trajectory Number: 1, WT Speed: 60 , AoA: -10 , Back of Bay
Sweep Angle
C_Y
C_Y (filtered)
Sweep Angle (deg)
C_Y
Time (sec)

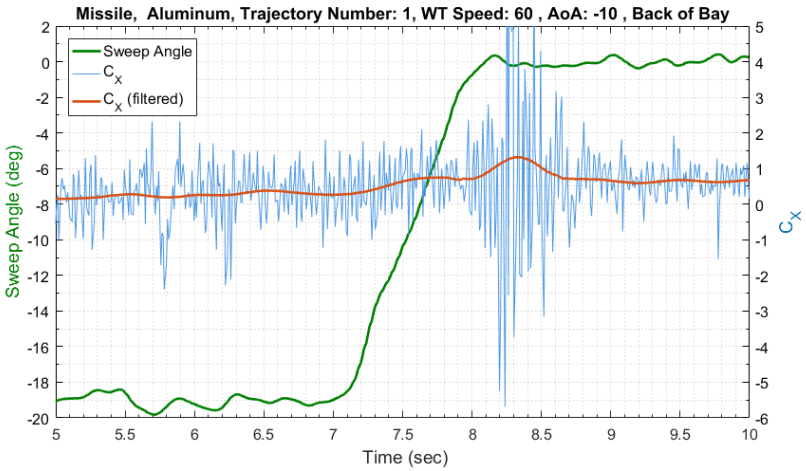
Missile, Aluminum, Trajectory Number: 1, WT Speed: 60 , AoA: -10 , Back of Bay
Sweep Angle
C_X
C_X (filtered)
Sweep Angle (deg)
C_X
Time (sec)

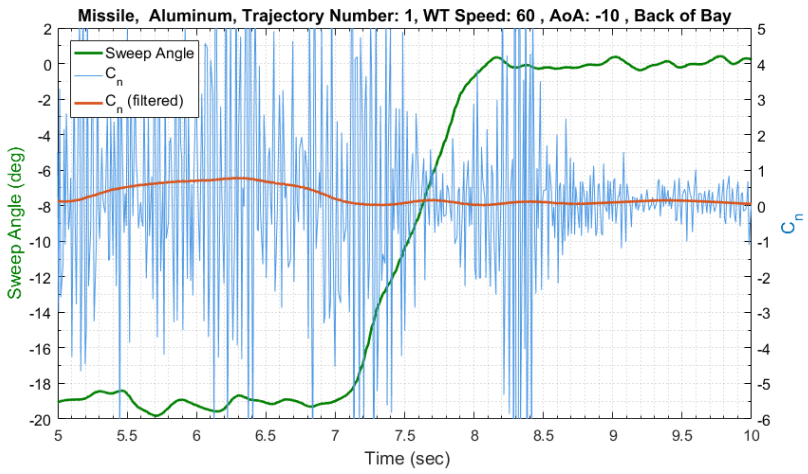
Missile, Aluminum, Trajectory Number: 1, WT Speed: 60 , AoA: -10 , Back of Bay
Sweep Angle
C_n
C_n (filtered)
Sweep Angle (deg)
C_n
Time (sec)

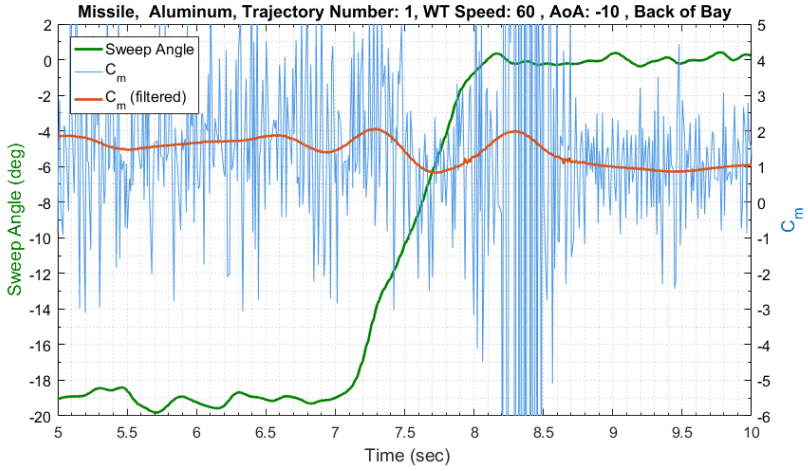
Missile, Aluminum, Trajectory Number: 1, WT Speed: 60 , AoA: -10 , Back of Bay
Sweep Angle
C_m
C_m (filtered)
Sweep Angle (deg)
C_m
Time (sec)

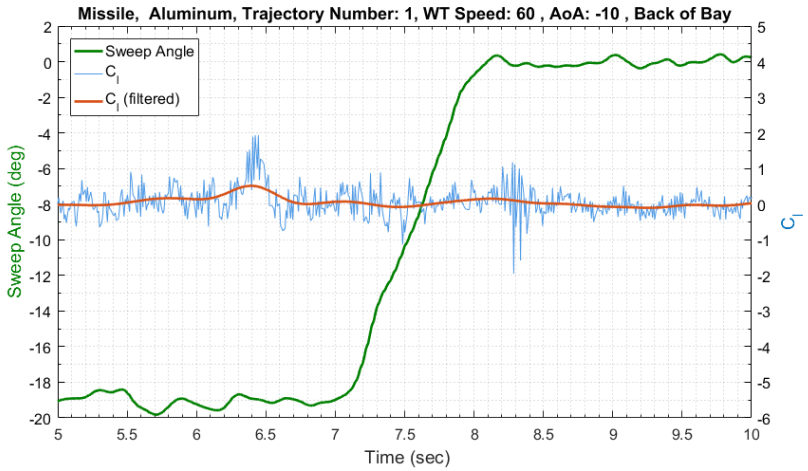
Missile, Aluminum, Trajectory Number: 1, WT Speed: 60 , AoA: -10 , Back of Bay
Sweep Angle
C_l
C_l (filtered)
Sweep Angle (deg)
C_l
Time (sec)

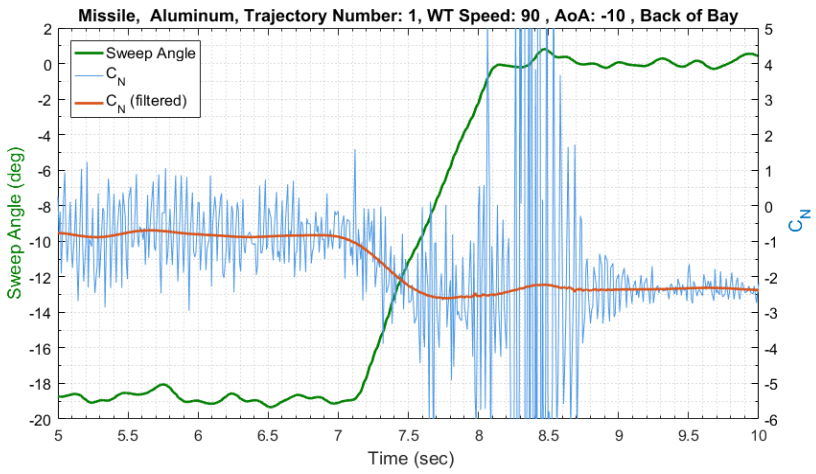
Missile, Aluminum, Trajectory Number: 1, WT Speed: 90 , AoA: -10 , Back of Bay
Sweep Angle
C_N
C_N (filtered)
Sweep Angle (deg)
C_N
Time (sec)

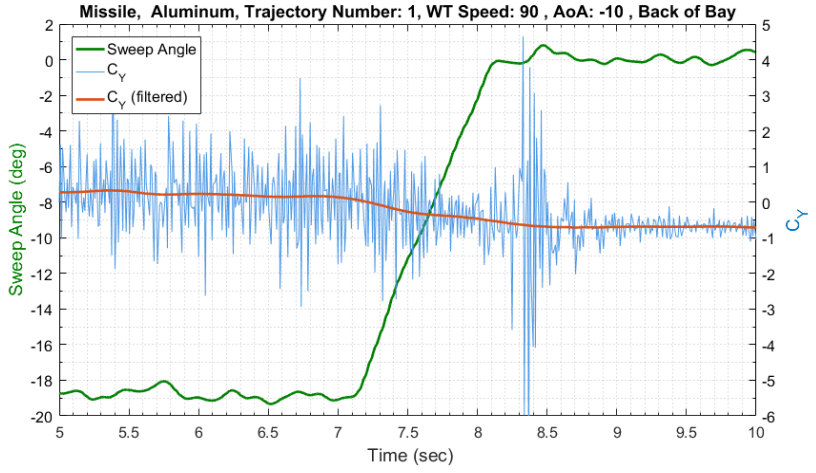
Missile, Aluminum, Trajectory Number: 1, WT Speed: 90 , AoA: -10 , Back of Bay
Sweep Angle
C_Y
C_Y (filtered)
Sweep Angle (deg)
C_Y
Time (sec)

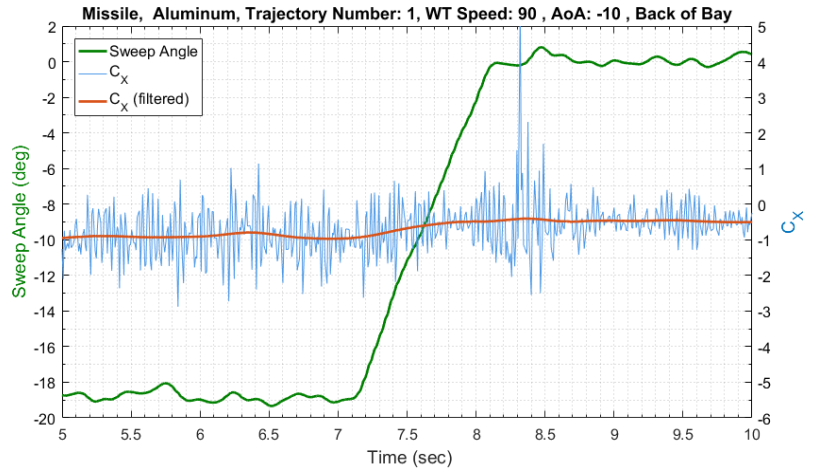
Missile, Aluminum, Trajectory Number: 1, WT Speed: 90 , AoA: -10 , Back of Bay
Sweep Angle
C_X
C_X (filtered)
Sweep Angle (deg)
C_X
Time (sec)

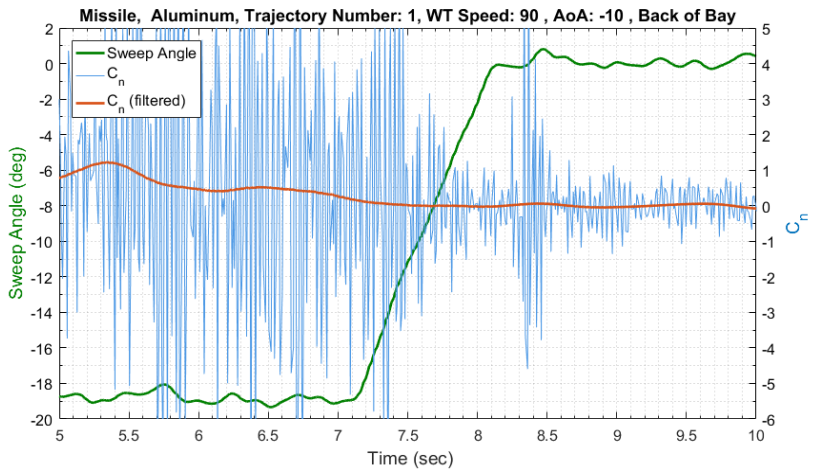
Missile, Aluminum, Trajectory Number: 1, WT Speed: 90 , AoA: -10 , Back of Bay
Sweep Angle
C_n
C_n (filtered)
Sweep Angle (deg)
C_n
Time (sec)

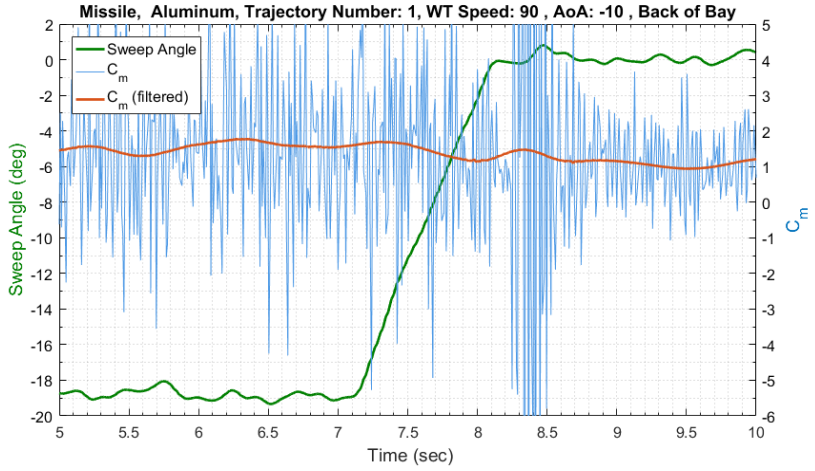
Missile, Aluminum, Trajectory Number: 1, WT Speed: 90 , AoA: -10 , Back of Bay
Sweep Angle
C_m
C_m (filtered)
Sweep Angle (deg)
C_m
Time (sec)

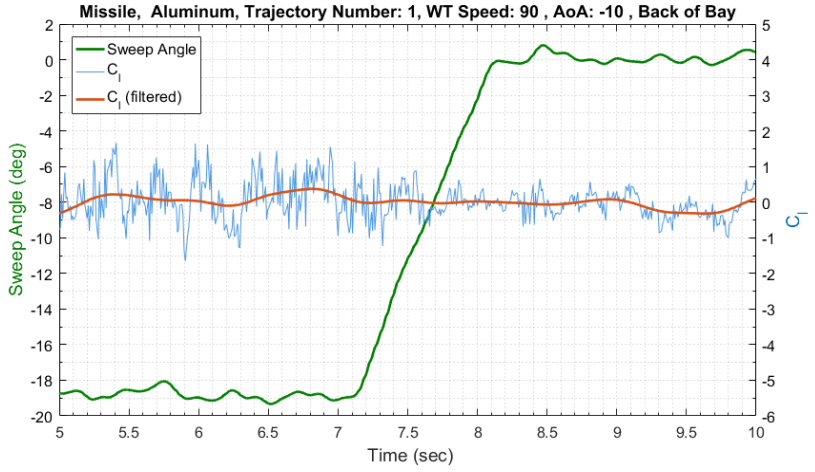
Missile, Aluminum, Trajectory Number: 1, WT Speed: 90 , AoA: -10 , Back of Bay
Sweep Angle
C_l
C_l (filtered)
Sweep Angle (deg)
C_l
Time (sec)

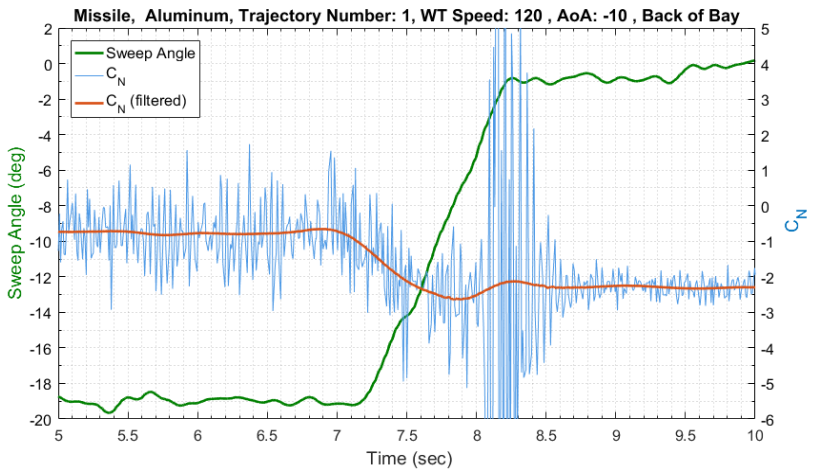
Missile, Aluminum, Trajectory Number: 1, WT Speed: 120 , AoA: -10 , Back of Bay
Sweep Angle
C_N
C_N (filtered)
Sweep Angle (deg)
C_N
Time (sec)

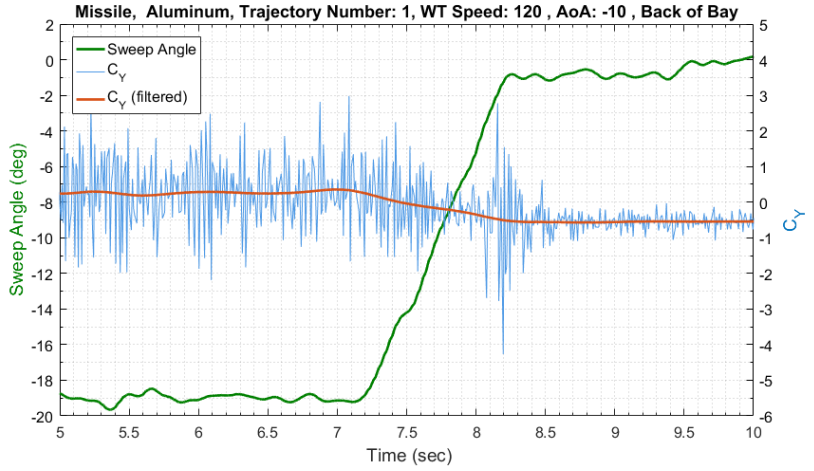
Missile, Aluminum, Trajectory Number: 1, WT Speed: 120 , AoA: -10 , Back of Bay
Sweep Angle
C_Y
C_Y (filtered)
Sweep Angle (deg)
C_Y
Time (sec)

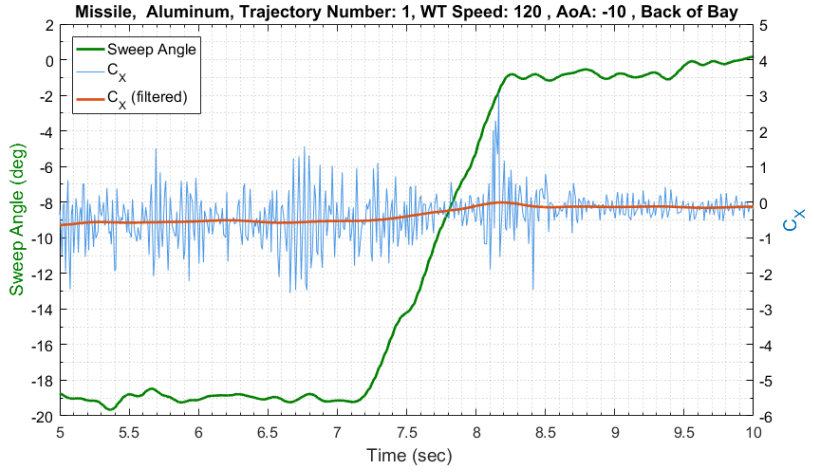
Missile, Aluminum, Trajectory Number: 1, WT Speed: 120 , AoA: -10 , Back of Bay
Sweep Angle
C_X
C_X (filtered)
Sweep Angle (deg)
C_X
Time (sec)

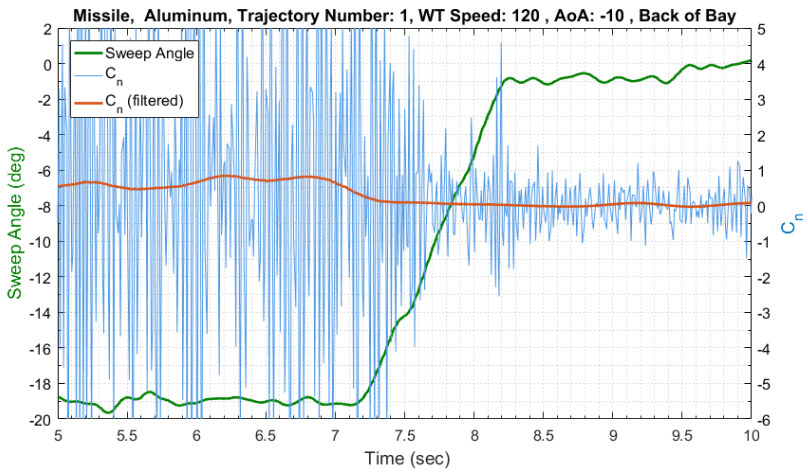
Missile, Aluminum, Trajectory Number: 1, WT Speed: 120 , AoA: -10 , Back of Bay
Sweep Angle
C_n
C_n (filtered)
Sweep Angle (deg)
C_n
Time (sec)

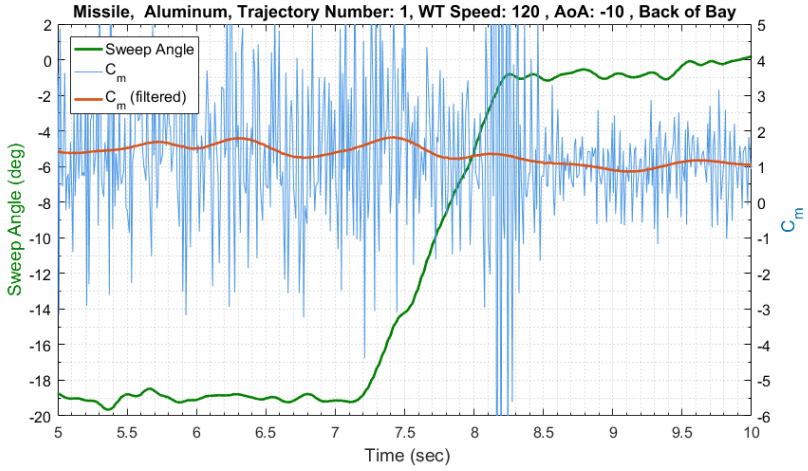
Missile, Aluminum, Trajectory Number: 1, WT Speed: 120 , AoA: -10 , Back of Bay
Sweep Angle
C_m
C_m (filtered)
Sweep Angle (deg)
C_m
Time (sec)

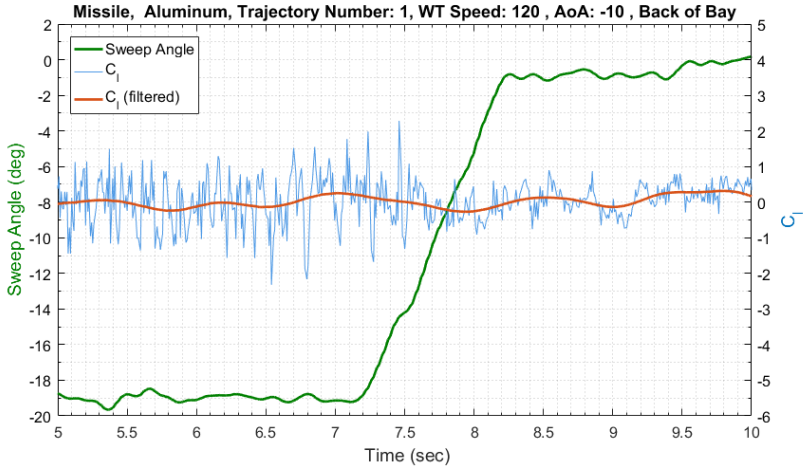
Missile, Aluminum, Trajectory Number: 1, WT Speed: 120 , AoA: -10 , Back of Bay
Sweep Angle
C_l
C_l (filtered)
Sweep Angle (deg)
C_l
Time (sec)

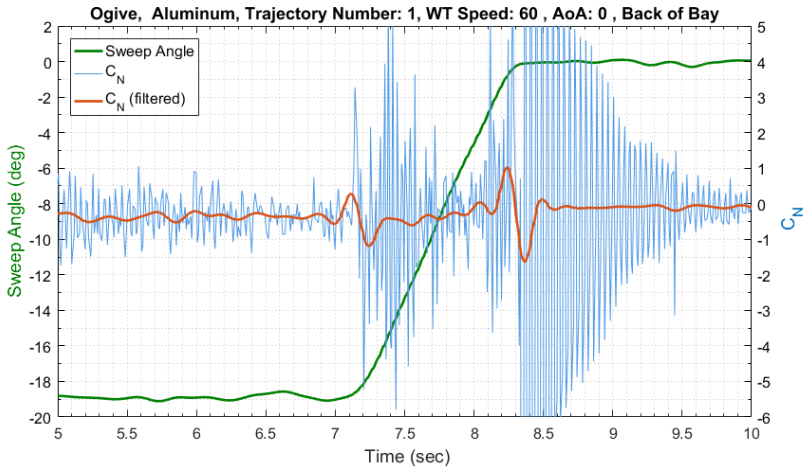
Ogive, Aluminum, Trajectory Number: 1, WT Speed: 60 , AoA: 0 , Back of Bay
Sweep Angle
C_N
C_N (filtered)
Sweep Angle (deg)
C_N
Time (sec)

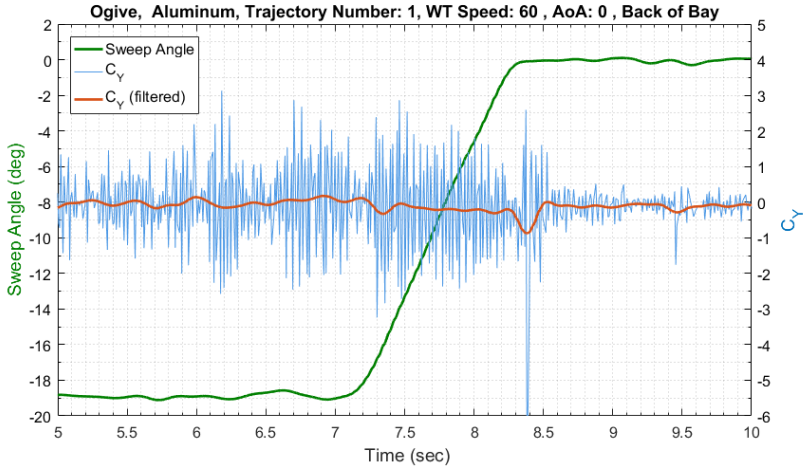
Ogive, Aluminum, Trajectory Number: 1, WT Speed: 60 , AoA: 0 , Back of Bay
Sweep Angle
C_Y
C_Y (filtered)
Sweep Angle (deg)
C_Y
Time (sec)

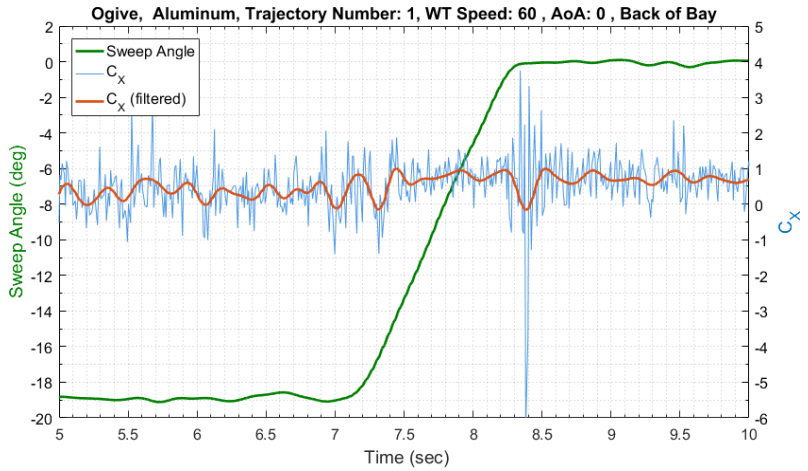
Ogive, Aluminum, Trajectory Number: 1, WT Speed: 60 , AoA: 0 , Back of Bay
Sweep Angle
C_X
C_X (filtered)
Sweep Angle (deg)
C_X
Time (sec)

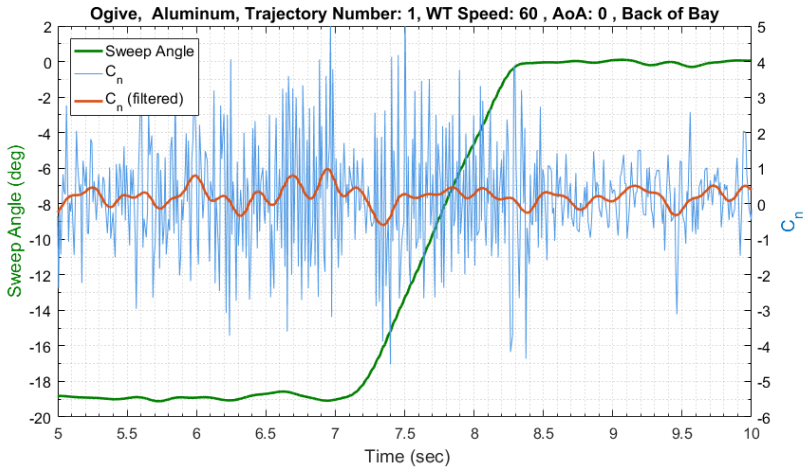
Ogive, Aluminum, Trajectory Number: 1, WT Speed: 60 , AoA: 0 , Back of Bay
Sweep Angle
C_n
C_n (filtered)
Sweep Angle (deg)
C_n
Time (sec)

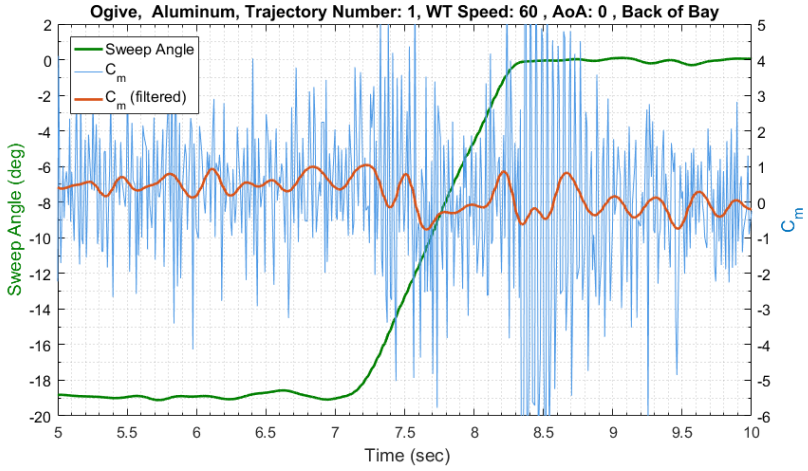
Ogive, Aluminum, Trajectory Number: 1, WT Speed: 60 , AoA: 0 , Back of Bay
Sweep Angle
C_m
C_m (filtered)
Sweep Angle (deg)
C_m
Time (sec)

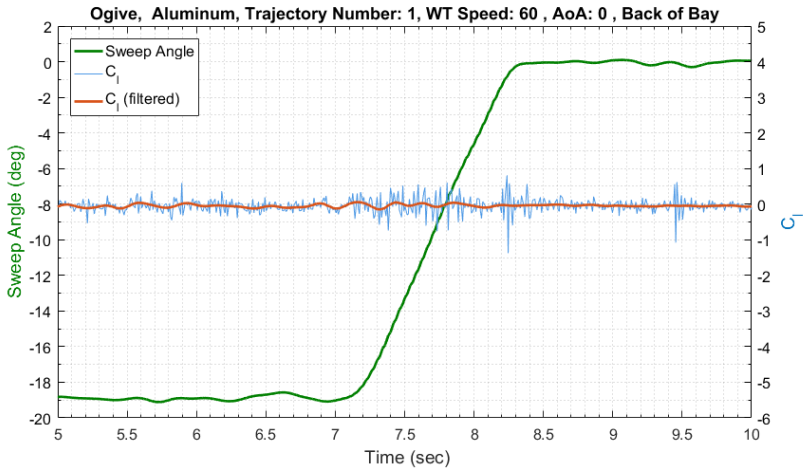
Ogive, Aluminum, Trajectory Number: 1, WT Speed: 60 , AoA: 0 , Back of Bay
Sweep Angle
C_l
C_l (filtered)
Sweep Angle (deg)
C_l
Time (sec)

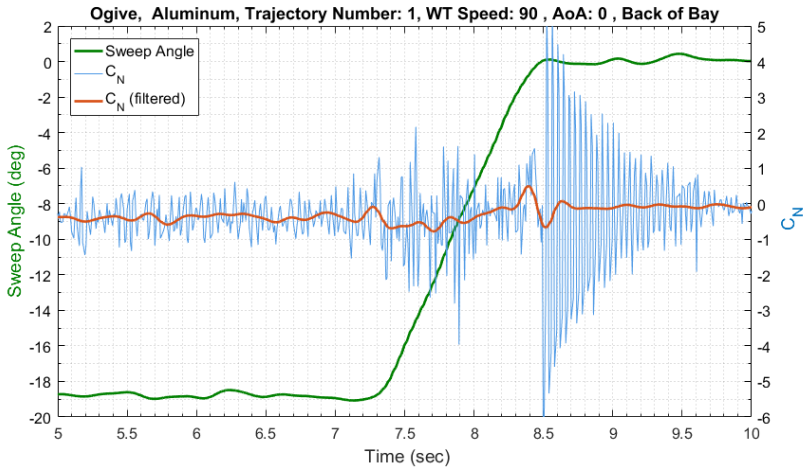
Ogive, Aluminum, Trajectory Number: 1, WT Speed: 90 , AoA: 0 , Back of Bay
Sweep Angle
C_N
C_N (filtered)
Sweep Angle (deg)
C_N
Time (sec)

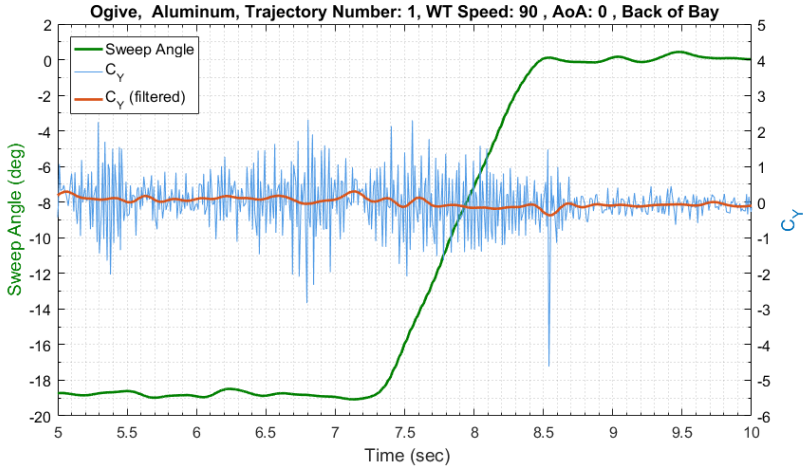
Ogive, Aluminum, Trajectory Number: 1, WT Speed: 90 , AoA: 0 , Back of Bay
Sweep Angle
C_Y
C_Y (filtered)
Sweep Angle (deg)
C_Y
Time (sec)

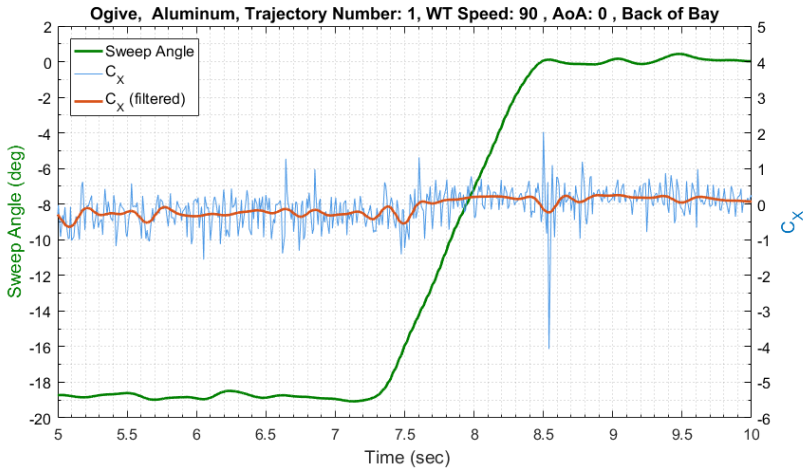
Ogive, Aluminum, Trajectory Number: 1, WT Speed: 90 , AoA: 0 , Back of Bay
Sweep Angle
C_X
C_X (filtered)
Sweep Angle (deg)
C_X
Time (sec)

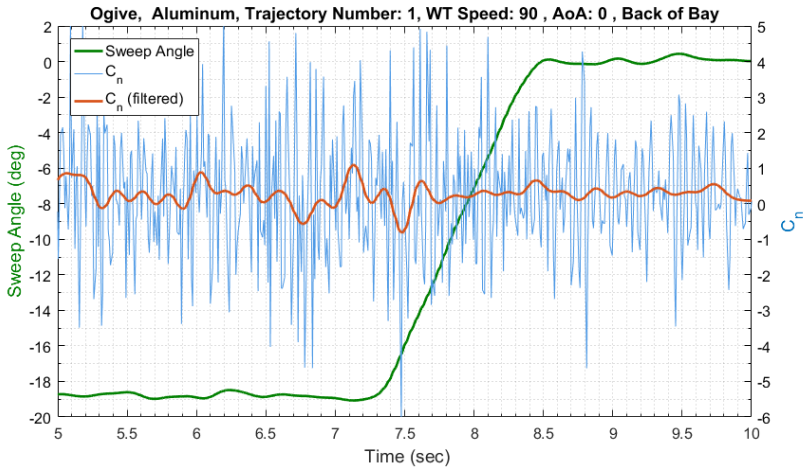
Ogive, Aluminum, Trajectory Number: 1, WT Speed: 90 , AoA: 0 , Back of Bay
Sweep Angle
C_n
C_n (filtered)
Sweep Angle (deg)
C_n
Time (sec)

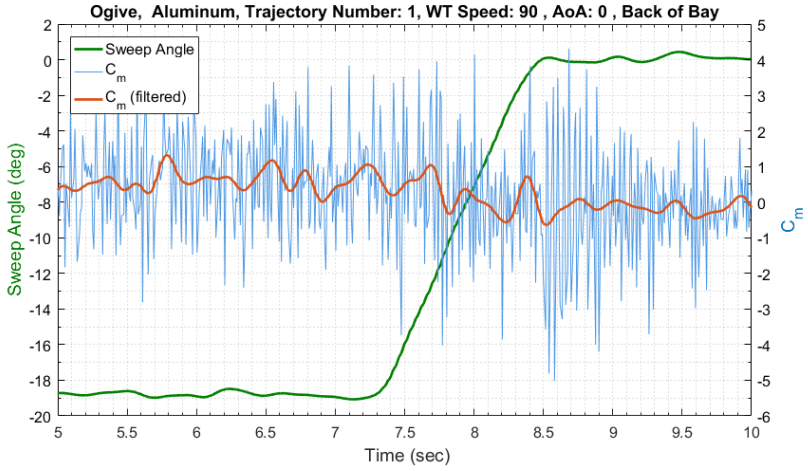
Ogive, Aluminum, Trajectory Number: 1, WT Speed: 90 , AoA: 0 , Back of Bay
Sweep Angle
C_m
C_m (filtered)
Sweep Angle (deg)
C_m
Time (sec)

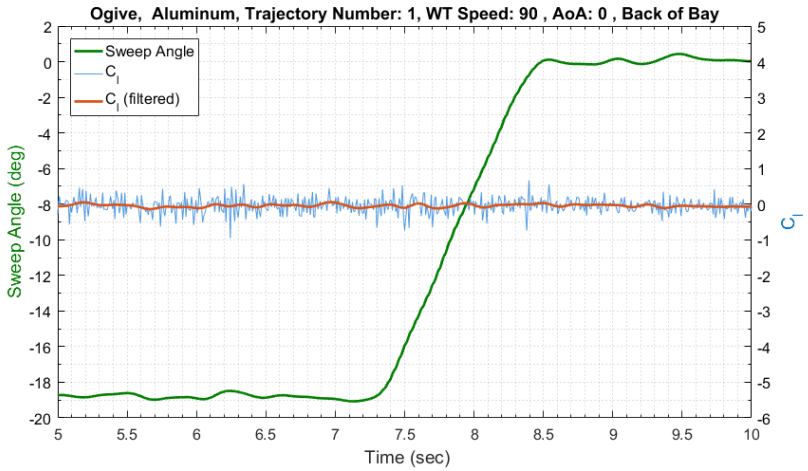
Ogive, Aluminum, Trajectory Number: 1, WT Speed: 90 , AoA: 0 , Back of Bay
Sweep Angle
C_l
C_l (filtered)
Sweep Angle (deg)
C_l
Time (sec)

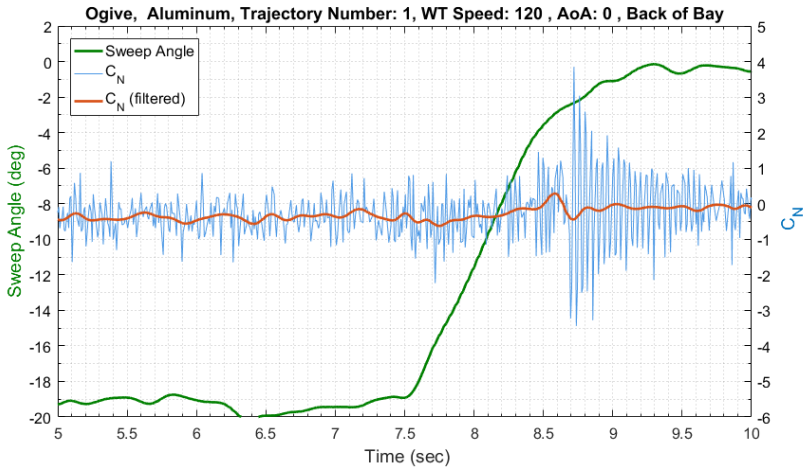
Ogive, Aluminum, Trajectory Number: 1, WT Speed: 120 , AoA: 0 , Back of Bay
Sweep Angle
C_N
C_N (filtered)
Sweep Angle (deg)
C_N
Time (sec)

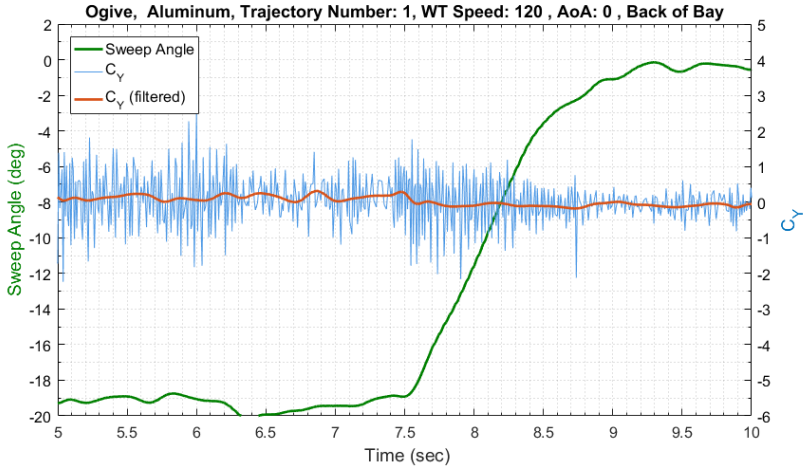
Ogive, Aluminum, Trajectory Number: 1, WT Speed: 120 , AoA: 0 , Back of Bay
Sweep Angle
C_Y
C_Y (filtered)
Sweep Angle (deg)
C_Y
Time (sec)

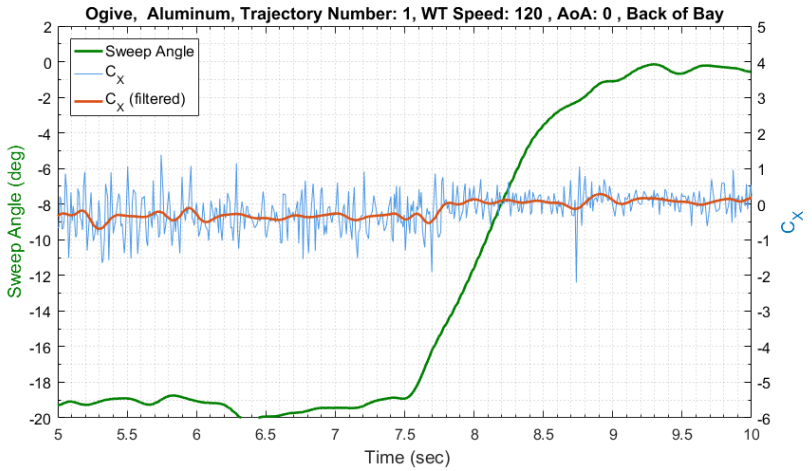
Ogive, Aluminum, Trajectory Number: 1, WT Speed: 120 , AoA: 0 , Back of Bay
Sweep Angle
C_X
C_X (filtered)
Sweep Angle (deg)
C_X
Time (sec)

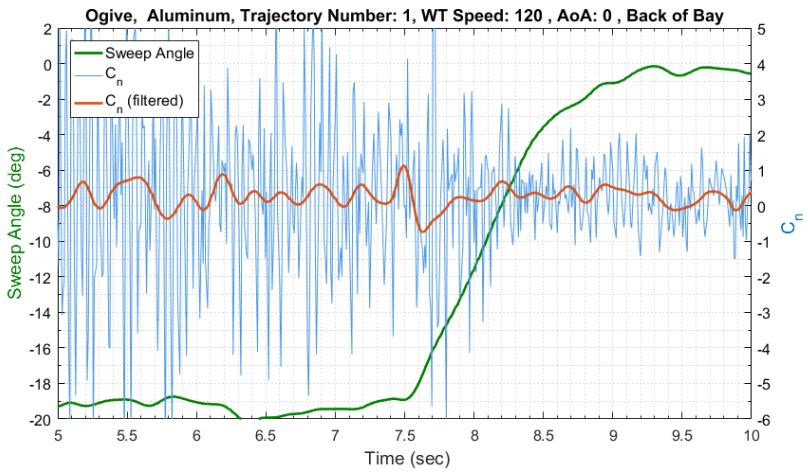
Ogive, Aluminum, Trajectory Number: 1, WT Speed: 120 , AoA: 0 , Back of Bay
Sweep Angle
C_n
C_n (filtered)
Sweep Angle (deg)
C_n
Time (sec)

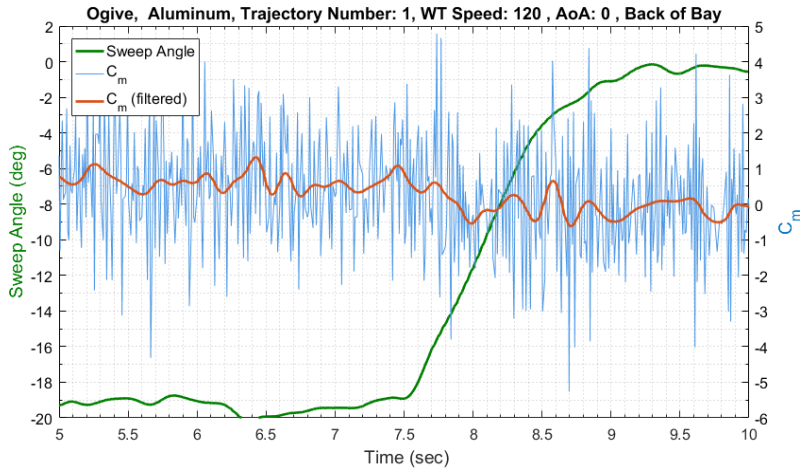
Ogive, Aluminum, Trajectory Number: 1, WT Speed: 120 , AoA: 0 , Back of Bay
Sweep Angle
C_m
C_m (filtered)
Sweep Angle (deg)
C_m
Time (sec)

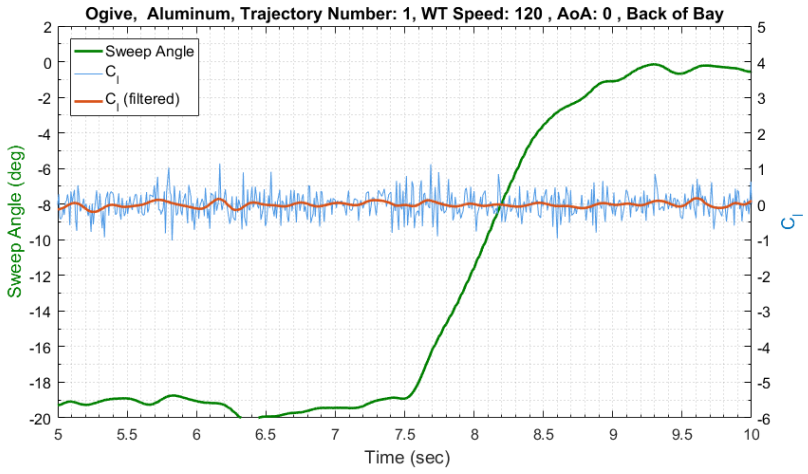
Ogive, Aluminum, Trajectory Number: 1, WT Speed: 120 , AoA: 0 , Back of Bay
Sweep Angle
C_l
C_l (filtered)
Sweep Angle (deg)
C_l
Time (sec)

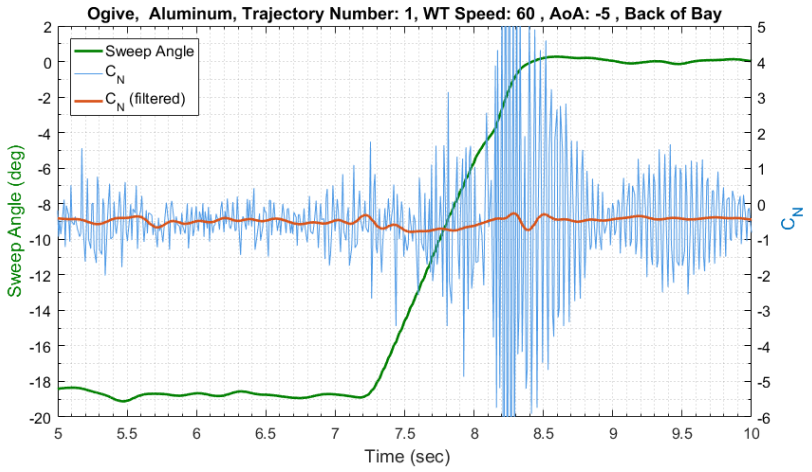
Ogive, Aluminum, Trajectory Number: 1, WT Speed: 60 , AoA: -5 , Back of Bay
Sweep Angle
C_N
C_N (filtered)
Sweep Angle (deg)
C_N
Time (sec)

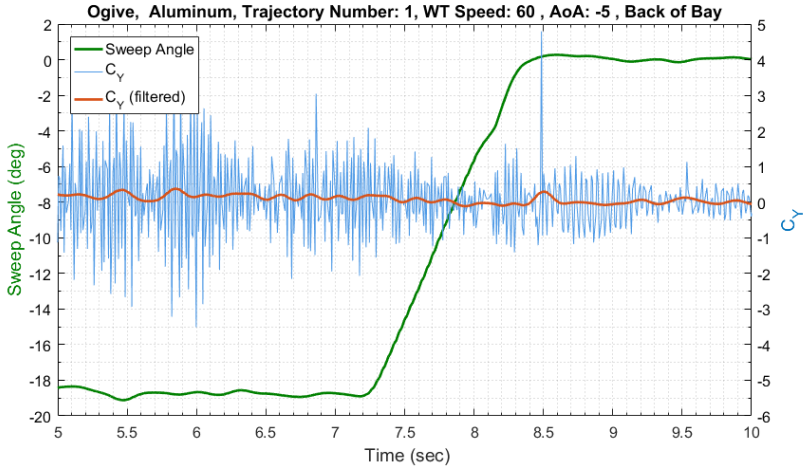
Ogive, Aluminum, Trajectory Number: 1, WT Speed: 60 , AoA: -5 , Back of Bay
Sweep Angle
C_Y
C_Y (filtered)
Sweep Angle (deg)
C_Y
Time (sec)

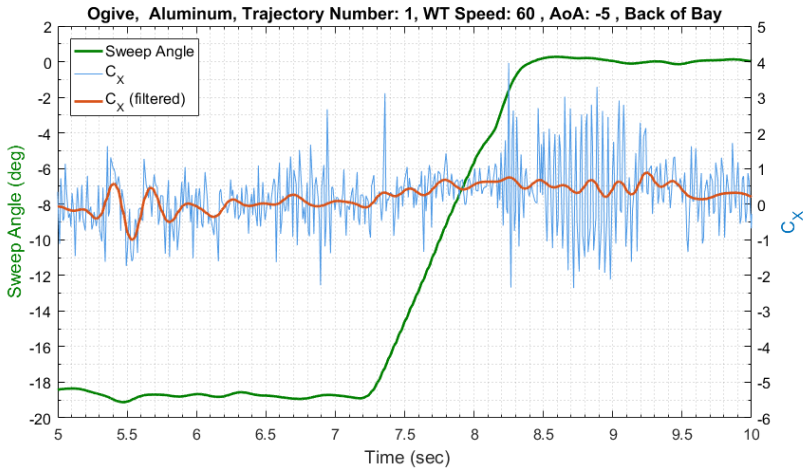
Ogive, Aluminum, Trajectory Number: 1, WT Speed: 60 , AoA: -5 , Back of Bay
Sweep Angle
C_X
C_X (filtered)
Sweep Angle (deg)
C_X
Time (sec)

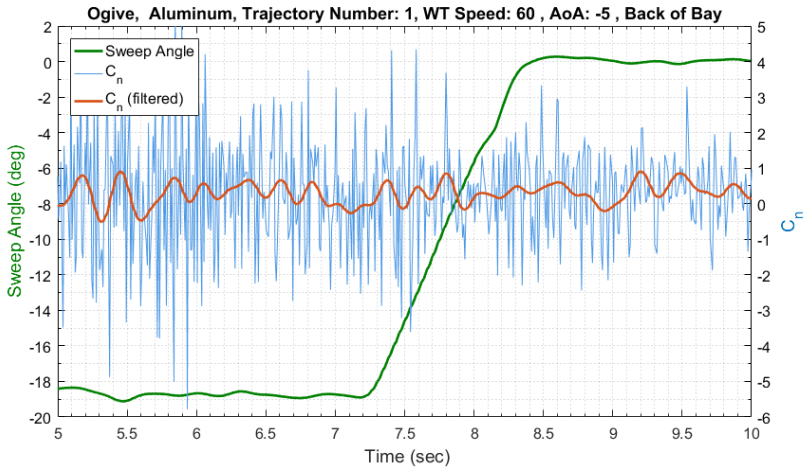
Ogive, Aluminum, Trajectory Number: 1, WT Speed: 60 , AoA: -5 , Back of Bay
Sweep Angle
C_n
C_n (filtered)
Sweep Angle (deg)
C_n
Time (sec)

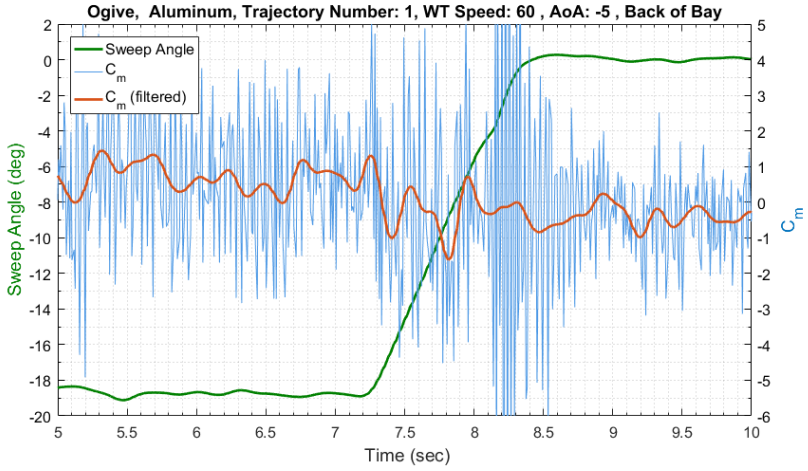
Ogive, Aluminum, Trajectory Number: 1, WT Speed: 60 , AoA: -5 , Back of Bay
Sweep Angle
C_m
C_m (filtered)
Sweep Angle (deg)
C_m
Time (sec)

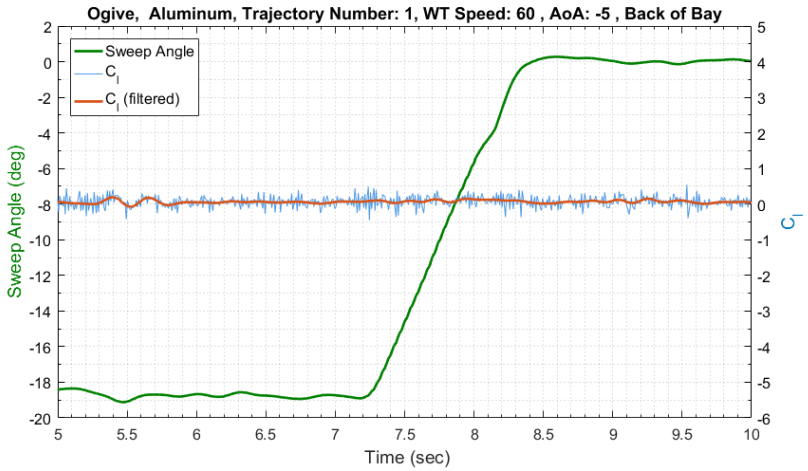
Ogive, Aluminum, Trajectory Number: 1, WT Speed: 60 , AoA: -5 , Back of Bay
Sweep Angle
C_l
C_l (filtered)
Sweep Angle (deg)
C_l
Time (sec)

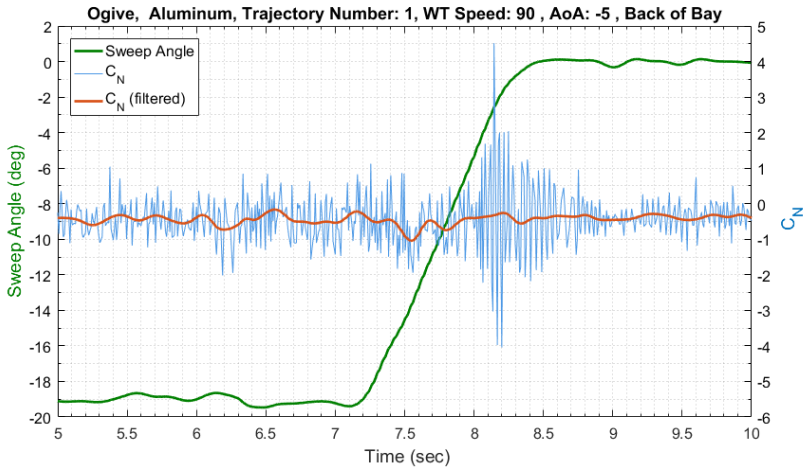
Ogive, Aluminum, Trajectory Number: 1, WT Speed: 90 , AoA: -5 , Back of Bay
Sweep Angle
C_N
C_N (filtered)
Sweep Angle (deg)
C_N
Time (sec)

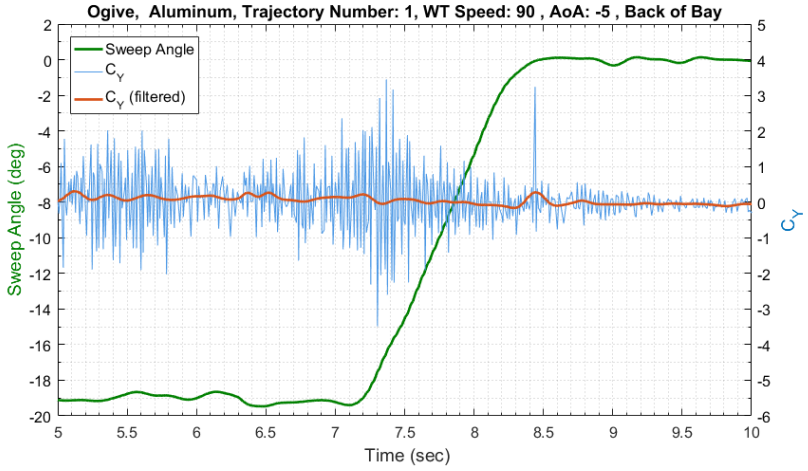
Ogive, Aluminum, Trajectory Number: 1, WT Speed: 90 , AoA: -5 , Back of Bay
Sweep Angle
C_Y
C_Y (filtered)
Sweep Angle (deg)
C_Y
Time (sec)

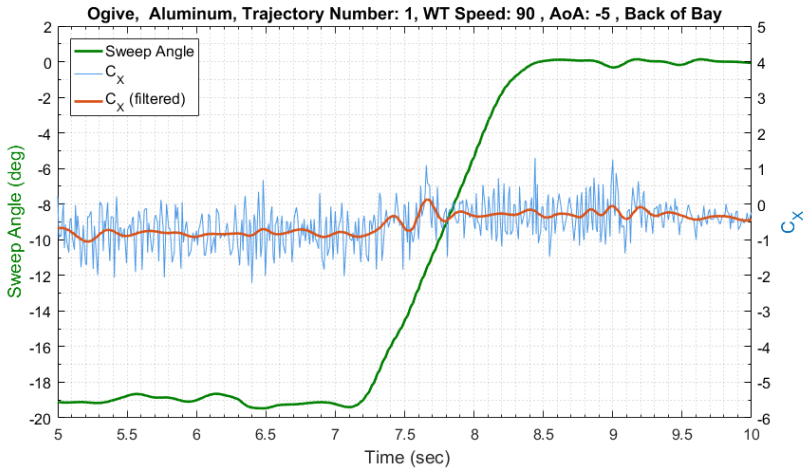
Ogive, Aluminum, Trajectory Number: 1, WT Speed: 90 , AoA: -5 , Back of Bay
Sweep Angle
C_X
C_X (filtered)
Sweep Angle (deg)
C_X
Time (sec)

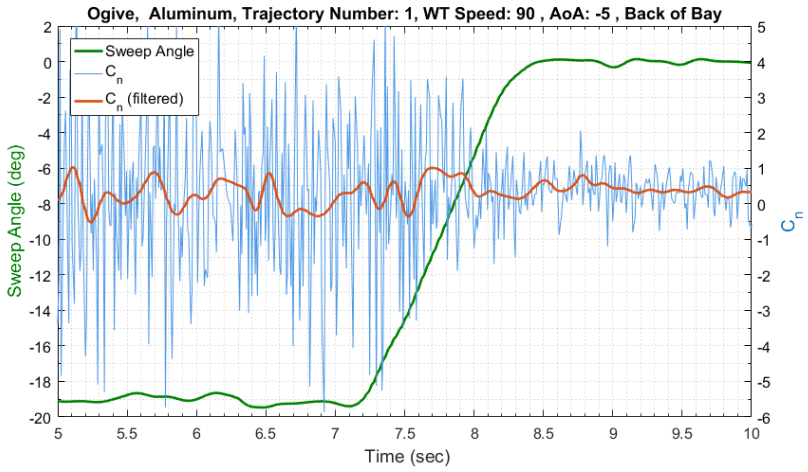
Ogive, Aluminum, Trajectory Number: 1, WT Speed: 90 , AoA: -5 , Back of Bay
Sweep Angle
C_n
C_n (filtered)
Sweep Angle (deg)
C_n
Time (sec)

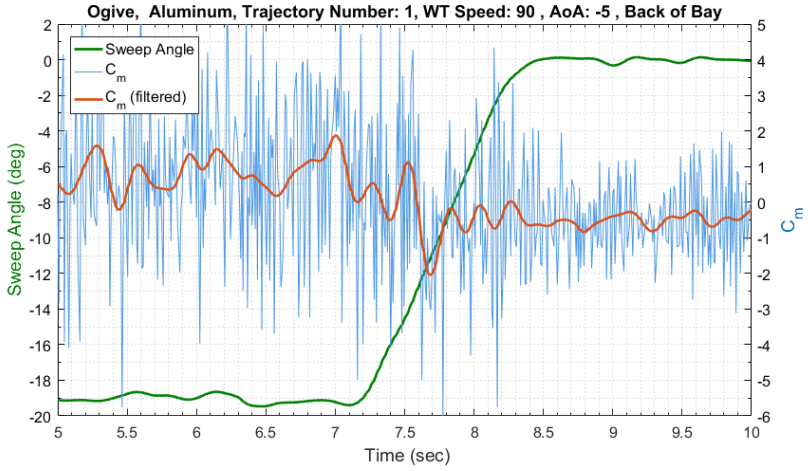
Ogive, Aluminum, Trajectory Number: 1, WT Speed: 90 , AoA: -5 , Back of Bay
Sweep Angle
C_m
C_m (filtered)
Sweep Angle (deg)
C_m
Time (sec)

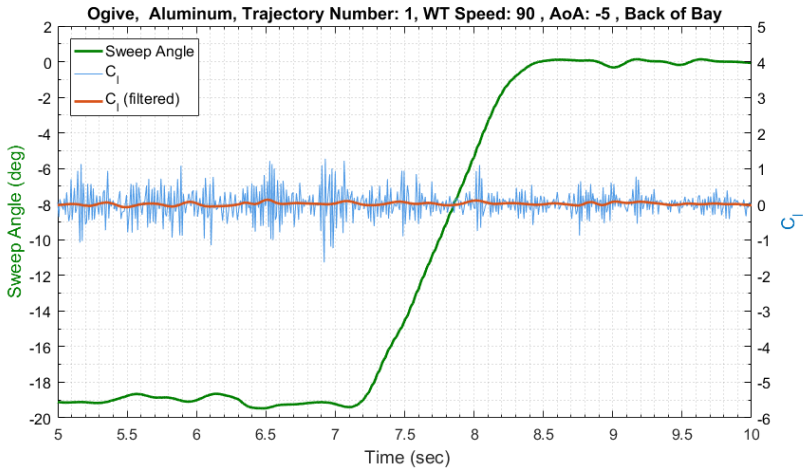
Ogive, Aluminum, Trajectory Number: 1, WT Speed: 90 , AoA: -5 , Back of Bay
Sweep Angle
C_l
C_l (filtered)
Sweep Angle (deg)
C_l
Time (sec)

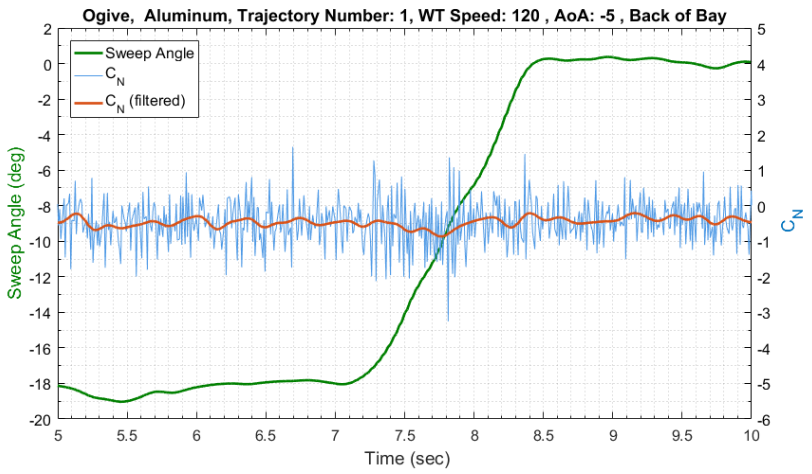
Ogive, Aluminum, Trajectory Number: 1, WT Speed: 120 , AoA: -5 , Back of Bay
Sweep Angle
C_N
C_N (filtered)
Sweep Angle (deg)
C_N
Time (sec)

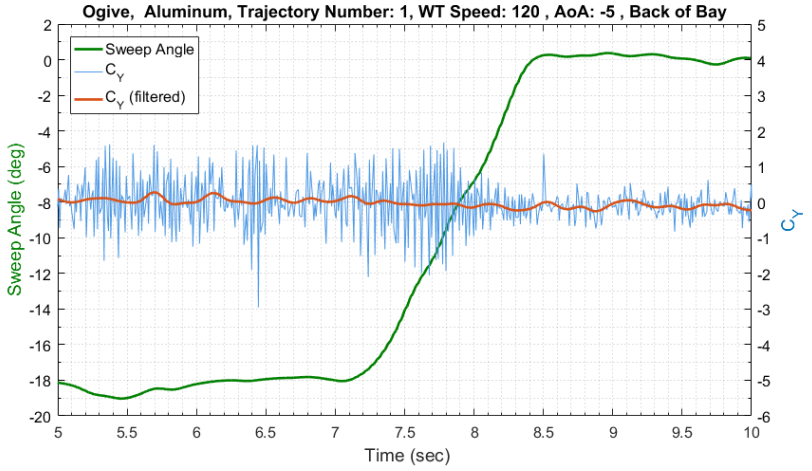
Ogive, Aluminum, Trajectory Number: 1, WT Speed: 120 , AoA: -5 , Back of Bay
Sweep Angle
C_Y
C_Y (filtered)
Sweep Angle (deg)
C_Y
Time (sec)

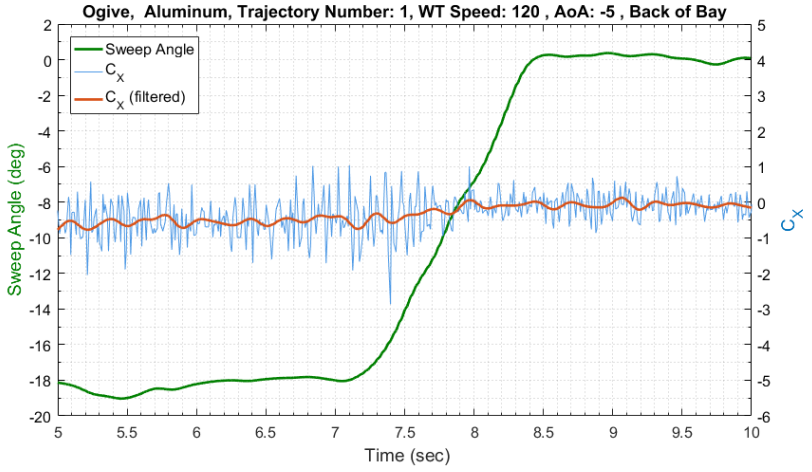
Ogive, Aluminum, Trajectory Number: 1, WT Speed: 120 , AoA: -5 , Back of Bay
Sweep Angle
C_X
C_X (filtered)
Sweep Angle (deg)
C_X
Time (sec)

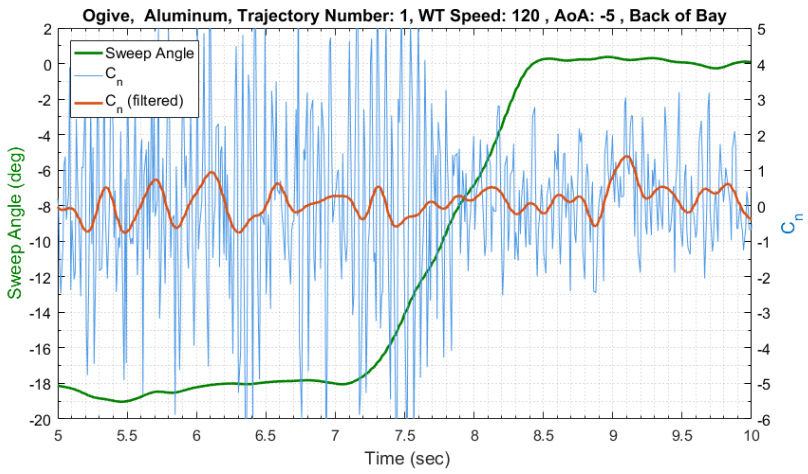
Ogive, Aluminum, Trajectory Number: 1, WT Speed: 120 , AoA: -5 , Back of Bay
Sweep Angle
C_n
C_n (filtered)
Sweep Angle (deg)
C_n
Time (sec)

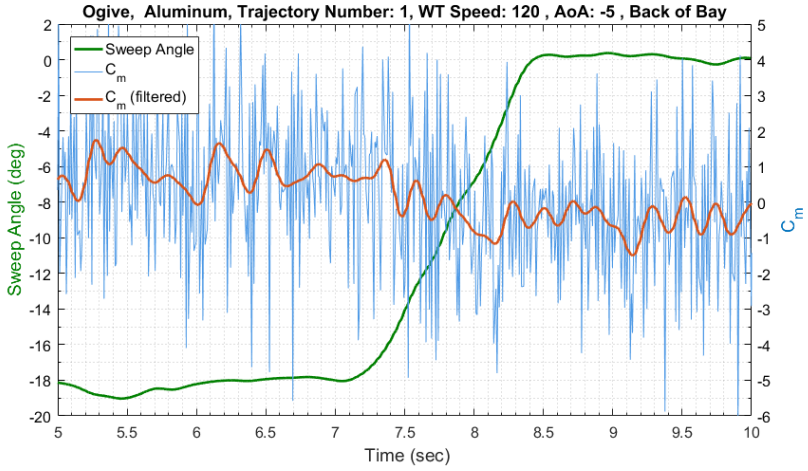
Ogive, Aluminum, Trajectory Number: 1, WT Speed: 120 , AoA: -5 , Back of Bay
Sweep Angle
C_m
C_m (filtered)
Sweep Angle (deg)
C_m
Time (sec)

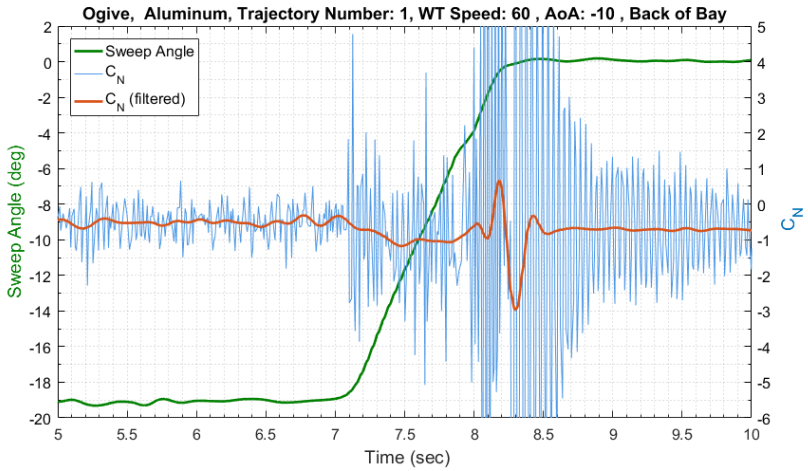
Ogive, Aluminum, Trajectory Number: 1, WT Speed: 60 , AoA: -10 , Back of Bay
Sweep Angle
C_N
C_N (filtered)
Sweep Angle (deg)
C_N
Time (sec)

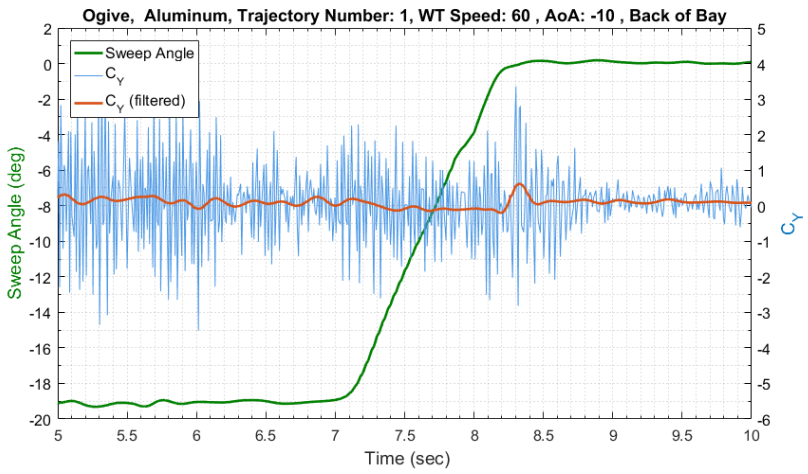
Ogive, Aluminum, Trajectory Number: 1, WT Speed: 60 , AoA: -10 , Back of Bay
Sweep Angle
C_Y
C_Y (filtered)
Sweep Angle (deg)
C_Y
Time (sec)

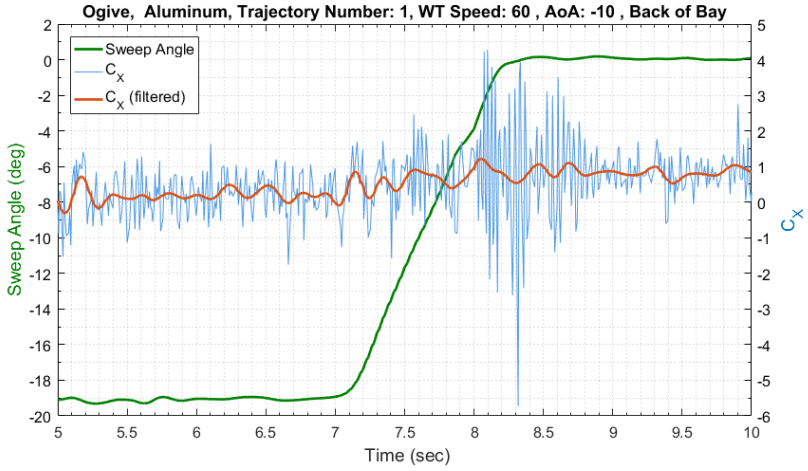
Ogive, Aluminum, Trajectory Number: 1, WT Speed: 60 , AoA: -10 , Back of Bay
Sweep Angle
C_X
C_X (filtered)
Sweep Angle (deg)
C_X
Time (sec)

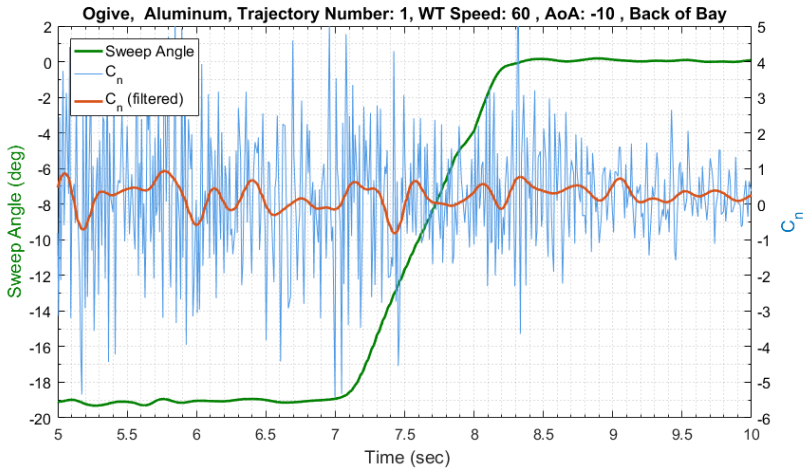
Ogive, Aluminum, Trajectory Number: 1, WT Speed: 60 , AoA: -10 , Back of Bay
Sweep Angle
C_n
C_n (filtered)
Sweep Angle (deg)
C_n
Time (sec)

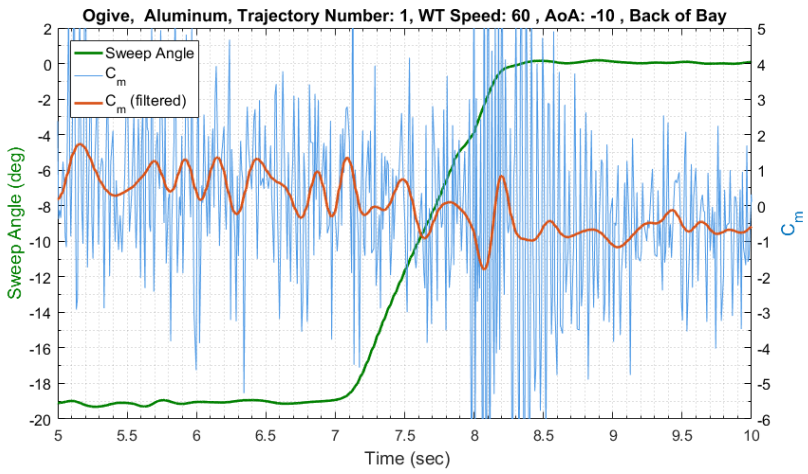
Ogive, Aluminum, Trajectory Number: 1, WT Speed: 60 , AoA: -10 , Back of Bay
Sweep Angle
C_m
C_m (filtered)
Sweep Angle (deg)
C_m
Time (sec)

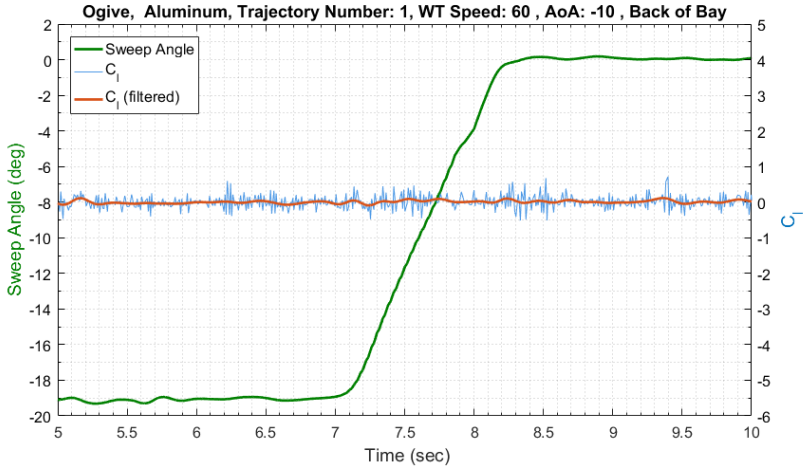
Ogive, Aluminum, Trajectory Number: 1, WT Speed: 60 , AoA: -10 , Back of Bay
Sweep Angle
C_l
C_l (filtered)
Sweep Angle (deg)
C_l
Time (sec)

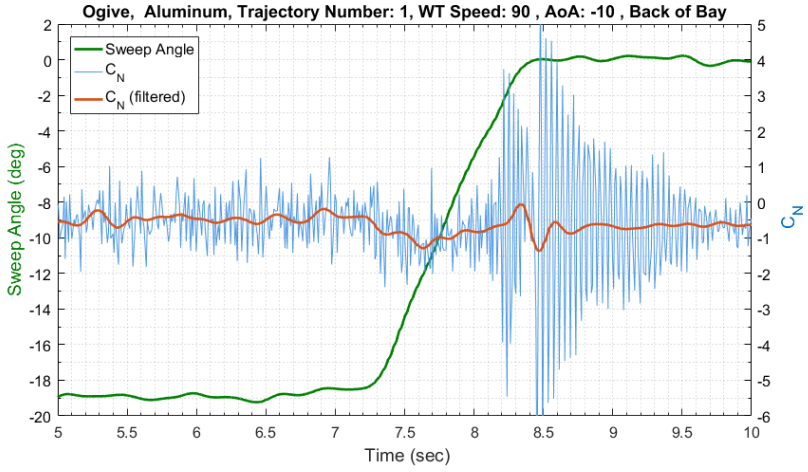
Ogive, Aluminum, Trajectory Number: 1, WT Speed: 90 , AoA: -10 , Back of Bay
Sweep Angle
C_N
C_N (filtered)
Sweep Angle (deg)
C_N
Time (sec)

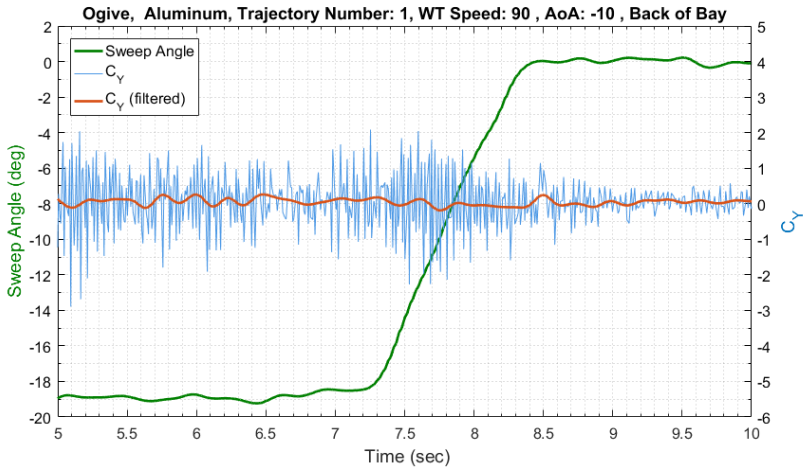
Ogive, Aluminum, Trajectory Number: 1, WT Speed: 90 , AoA: -10 , Back of Bay
Sweep Angle
C_Y
C_Y (filtered)
Sweep Angle (deg)
C_Y
Time (sec)

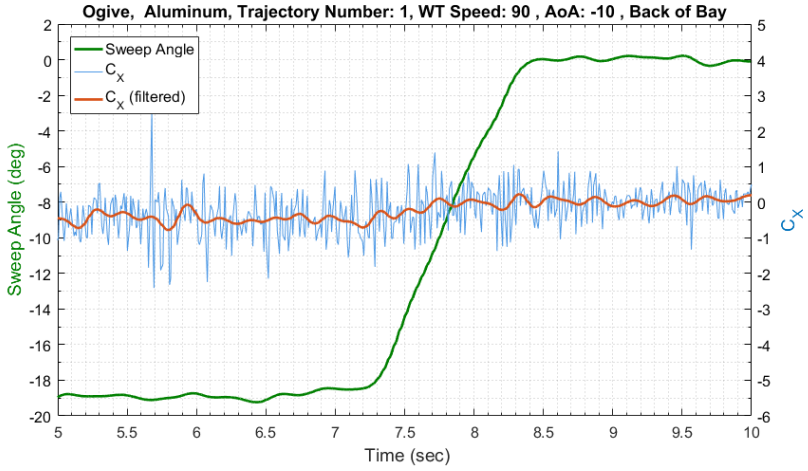
Ogive, Aluminum, Trajectory Number: 1, WT Speed: 90 , AoA: -10 , Back of Bay
Sweep Angle
C_X
C_X (filtered)
Sweep Angle (deg)
C_X
Time (sec)

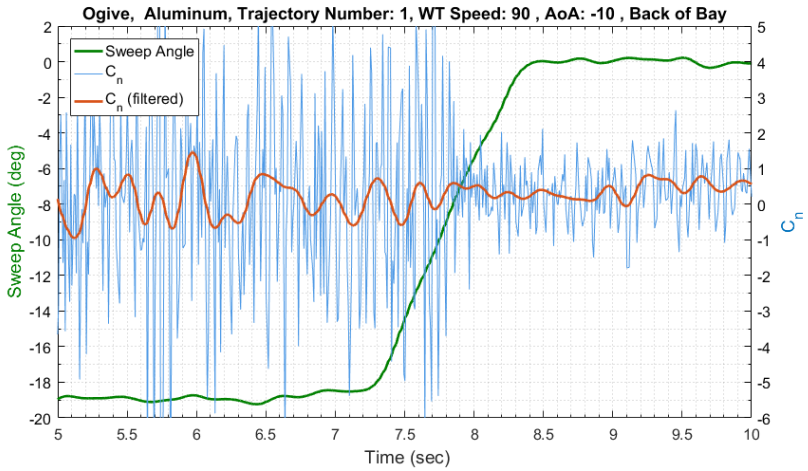
Ogive, Aluminum, Trajectory Number: 1, WT Speed: 90 , AoA: -10 , Back of Bay
Sweep Angle
C_n
C_n (filtered)
Sweep Angle (deg)
C_n
Time (sec)

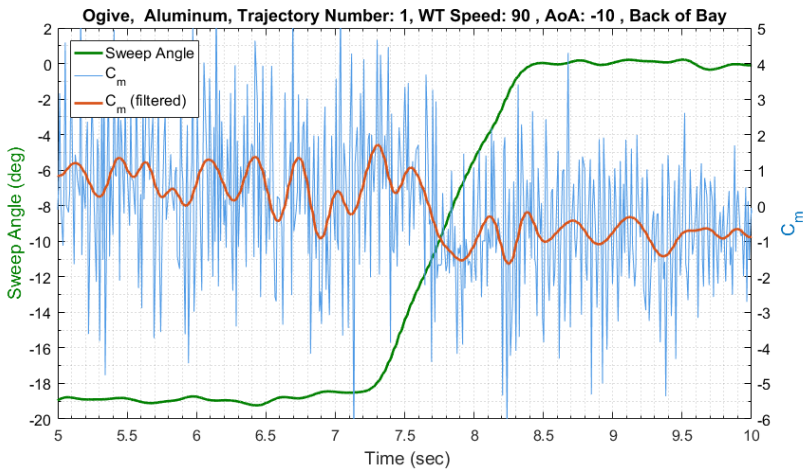
Ogive, Aluminum, Trajectory Number: 1, WT Speed: 90 , AoA: -10 , Back of Bay
Sweep Angle
C_m
C_m (filtered)
Sweep Angle (deg)
C_m
Time (sec)

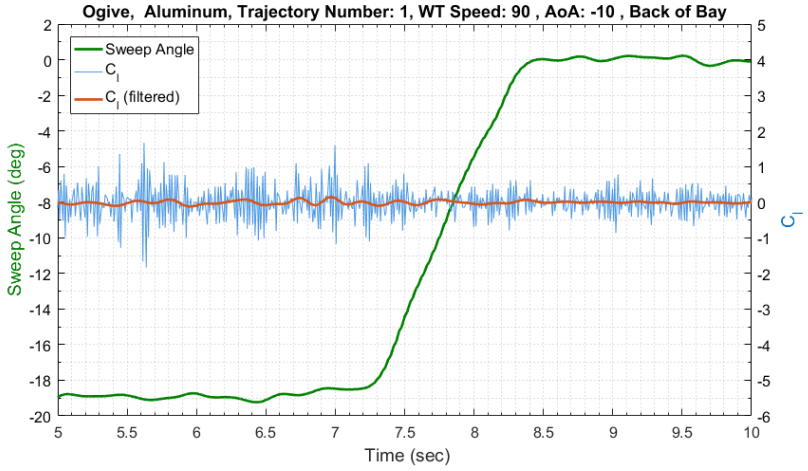
Ogive, Aluminum, Trajectory Number: 1, WT Speed: 90 , AoA: -10 , Back of Bay
Sweep Angle
C_l
C_l (filtered)
Sweep Angle (deg)
C_l
Time (sec)

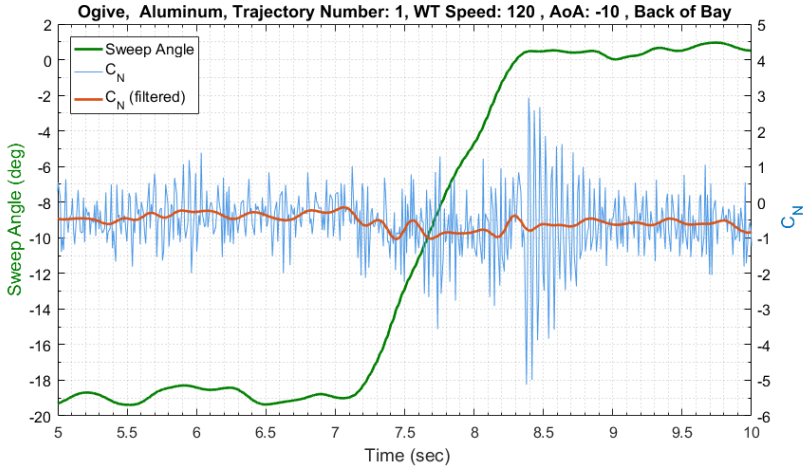
Ogive, Aluminum, Trajectory Number: 1, WT Speed: 120 , AoA: -10 , Back of Bay
Sweep Angle
C_N
C_N (filtered)
Sweep Angle (deg)
C_N
Time (sec)

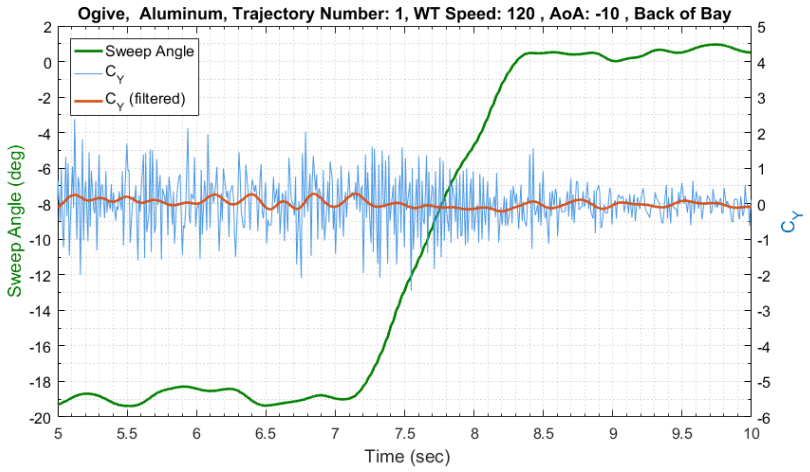
Ogive, Aluminum, Trajectory Number: 1, WT Speed: 120 , AoA: -10 , Back of Bay
Sweep Angle
C_Y
C_Y (filtered)
Sweep Angle (deg)
C_Y
Time (sec)

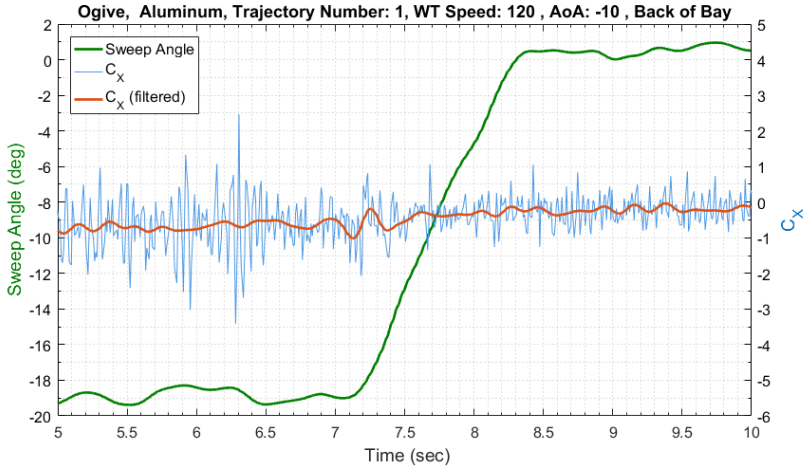
Ogive, Aluminum, Trajectory Number: 1, WT Speed: 120 , AoA: -10 , Back of Bay
Sweep Angle
C_X
C_X (filtered)
Sweep Angle (deg)
C_X
Time (sec)

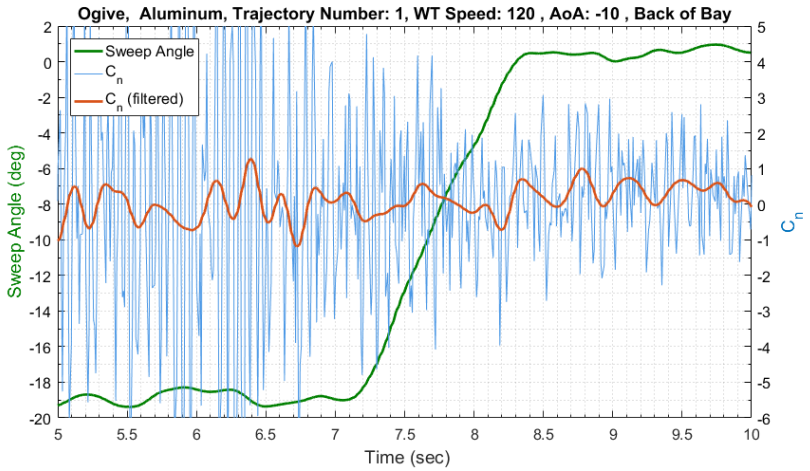
Ogive, Aluminum, Trajectory Number: 1, WT Speed: 120 , AoA: -10 , Back of Bay
Sweep Angle
C_n
C_n (filtered)
Sweep Angle (deg)
C_n
Time (sec)

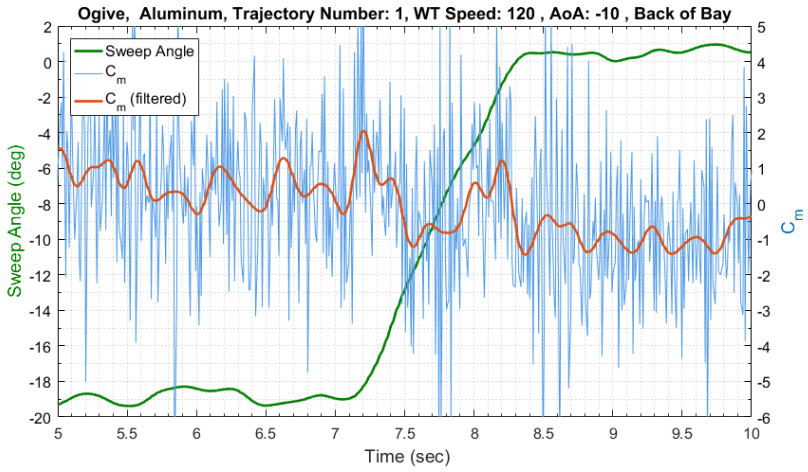
Ogive, Aluminum, Trajectory Number: 1, WT Speed: 120 , AoA: -10 , Back of Bay
Sweep Angle
C_m
C_m (filtered)
Sweep Angle (deg)
C_m
Time (sec)

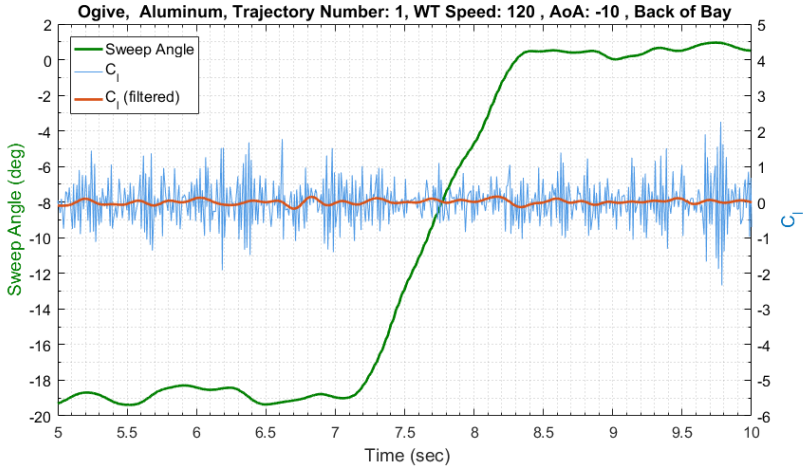
Ogive, Aluminum, Trajectory Number: 1, WT Speed: 120 , AoA: -10 , Back of Bay
Sweep Angle
C_l
C_l (filtered)
Sweep Angle (deg)
C_l
Time (sec)

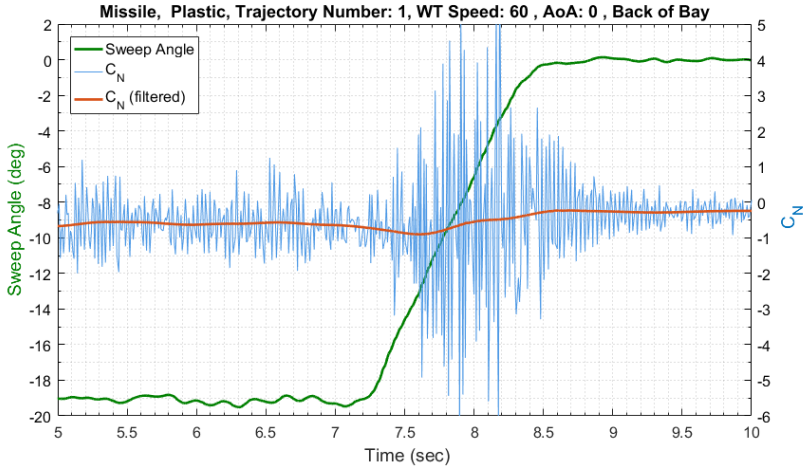
Missile, Plastic, Trajectory Number: 1, WT Speed: 60 , AoA: 0 , Back of Bay
Sweep Angle
C_N
C_N (filtered)
Sweep Angle (deg)
C_N
Time (sec)

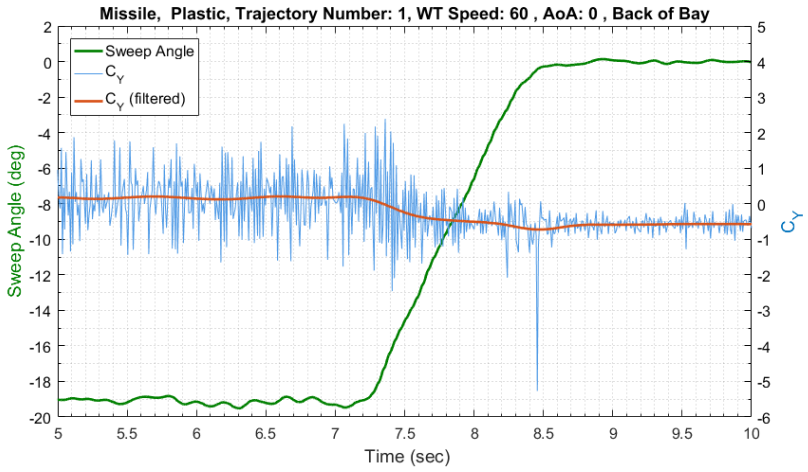
Missile, Plastic, Trajectory Number: 1, WT Speed: 60 , AoA: 0 , Back of Bay
Sweep Angle
C_Y
C_Y (filtered)
Sweep Angle (deg)
C_Y
Time (sec)

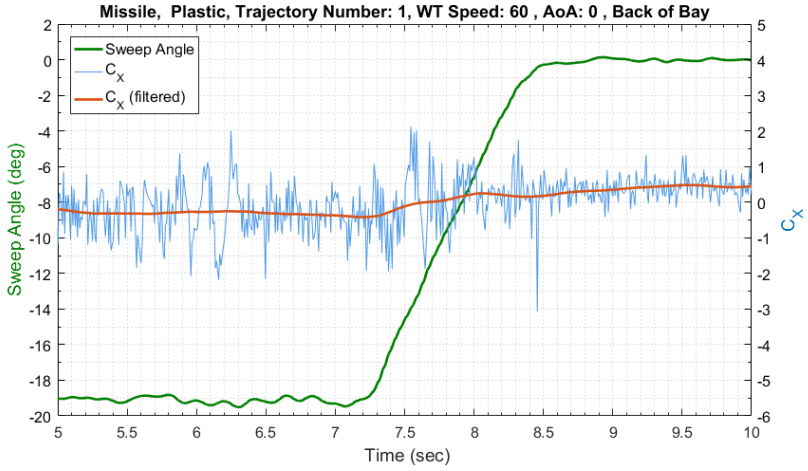
Missile, Plastic, Trajectory Number: 1, WT Speed: 60 , AoA: 0 , Back of Bay
Sweep Angle
C_X
C_X (filtered)
Sweep Angle (deg)
C_X
Time (sec)

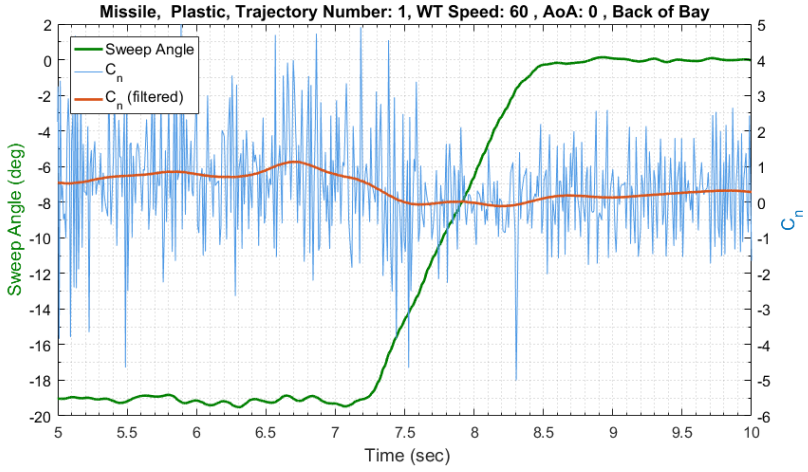
Missile, Plastic, Trajectory Number: 1, WT Speed: 60 , AoA: 0 , Back of Bay
Sweep Angle
C_n
C_n (filtered)
Sweep Angle (deg)
C_n
Time (sec)

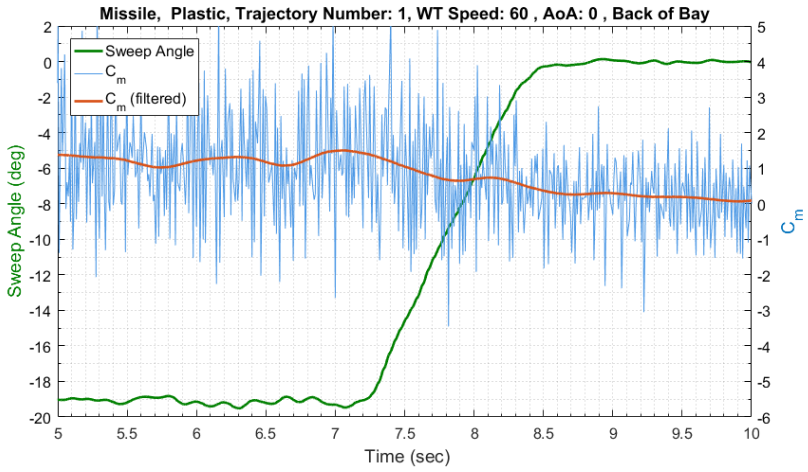
Missile, Plastic, Trajectory Number: 1, WT Speed: 60 , AoA: 0 , Back of Bay
Sweep Angle
C_m
C_m (filtered)
Sweep Angle (deg)
C_m
Time (sec)

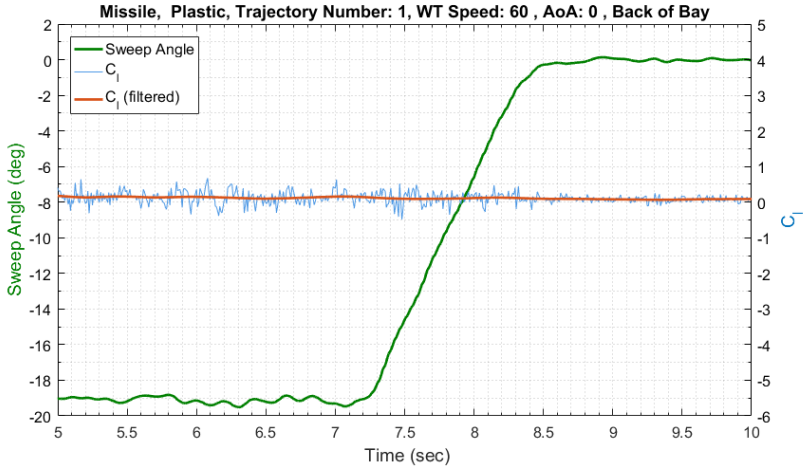
Missile, Plastic, Trajectory Number: 1, WT Speed: 60 , AoA: 0 , Back of Bay
Sweep Angle
C_l
C_l (filtered)
Sweep Angle (deg)
C_l
Time (sec)

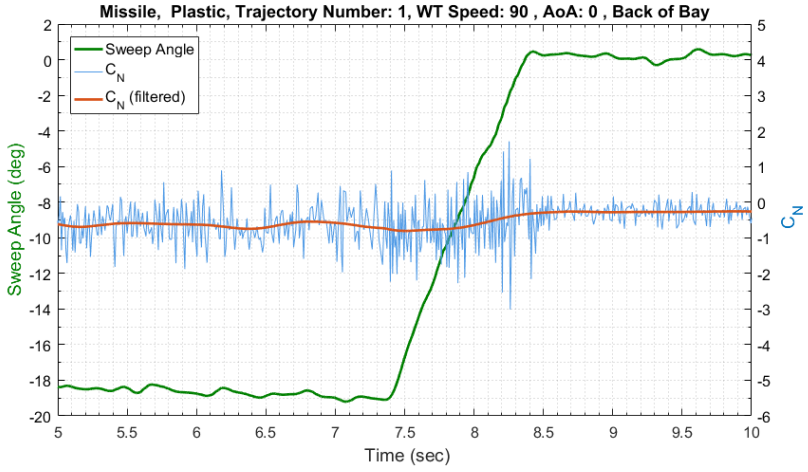
Missile, Plastic, Trajectory Number: 1, WT Speed: 90 , AoA: 0 , Back of Bay
Sweep Angle
C_N
C_N (filtered)
Sweep Angle (deg)
C_N
Time (sec)

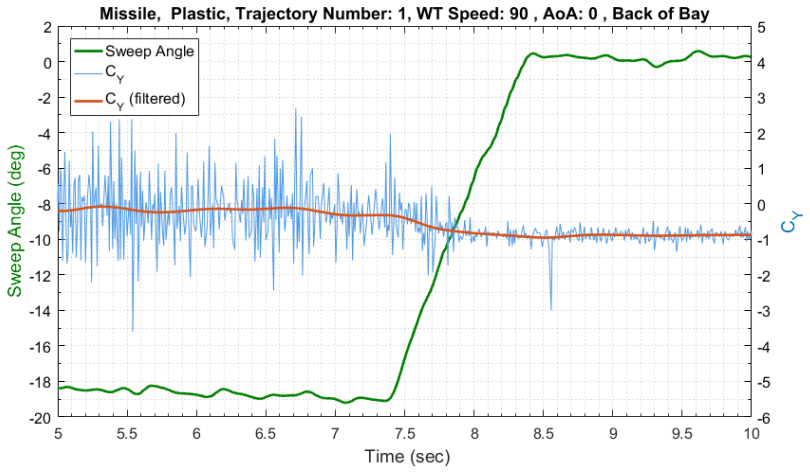
Missile, Plastic, Trajectory Number: 1, WT Speed: 90 , AoA: 0 , Back of Bay
Sweep Angle
C_Y
C_Y (filtered)
Sweep Angle (deg)
C_Y
Time (sec)

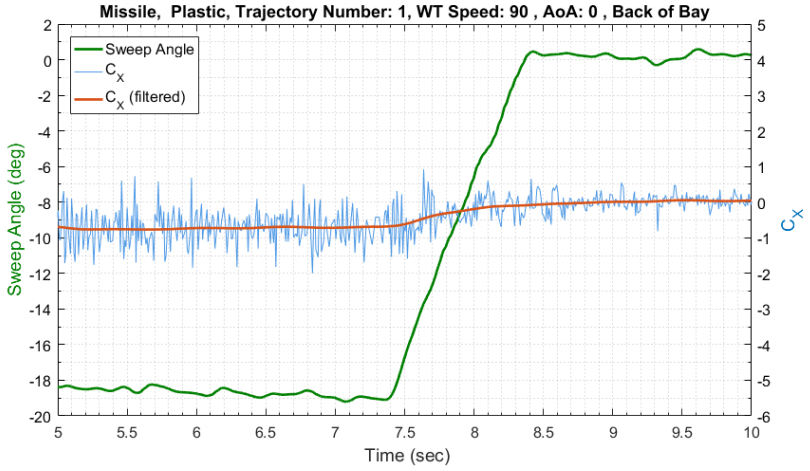
Missile, Plastic, Trajectory Number: 1, WT Speed: 90 , AoA: 0 , Back of Bay
Sweep Angle
C_X
C_X (filtered)
Sweep Angle (deg)
C_X
Time (sec)

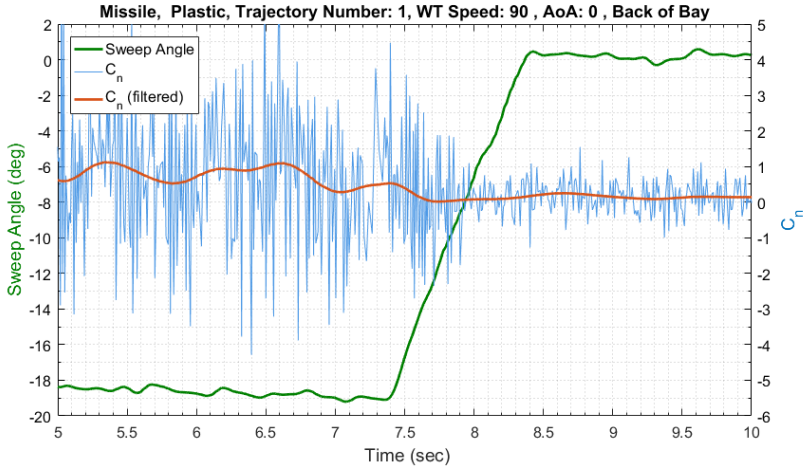
Missile, Plastic, Trajectory Number: 1, WT Speed: 90 , AoA: 0 , Back of Bay
Sweep Angle
C_n
C_n (filtered)
Sweep Angle (deg)
C_n
Time (sec)

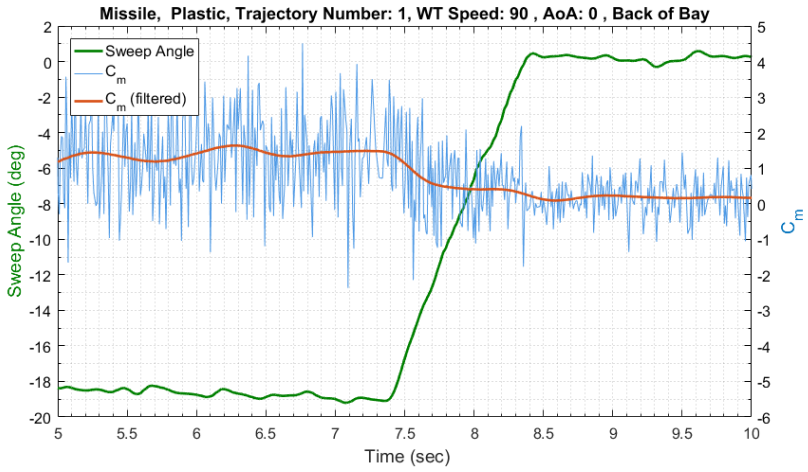
Missile, Plastic, Trajectory Number: 1, WT Speed: 90 , AoA: 0 , Back of Bay
Sweep Angle
C_m
C_m (filtered)
Sweep Angle (deg)
C_m
Time (sec)

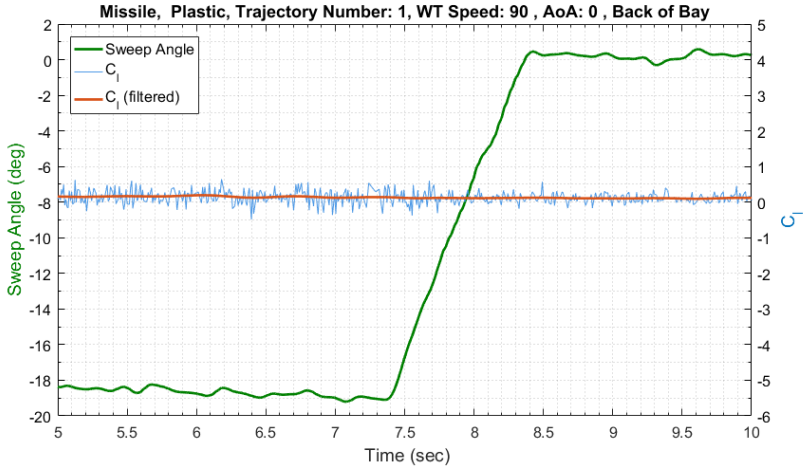
Missile, Plastic, Trajectory Number: 1, WT Speed: 90 , AoA: 0 , Back of Bay
Sweep Angle
C_l
C_l (filtered)
Sweep Angle (deg)
C_l
Time (sec)

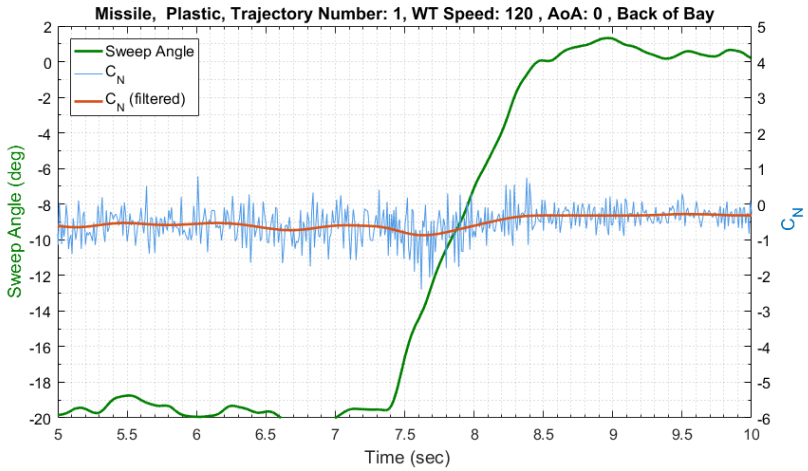
Missile, Plastic, Trajectory Number: 1, WT Speed: 120 , AoA: 0 , Back of Bay
Sweep Angle
C_N
C_N (filtered)
Sweep Angle (deg)
C_N
Time (sec)

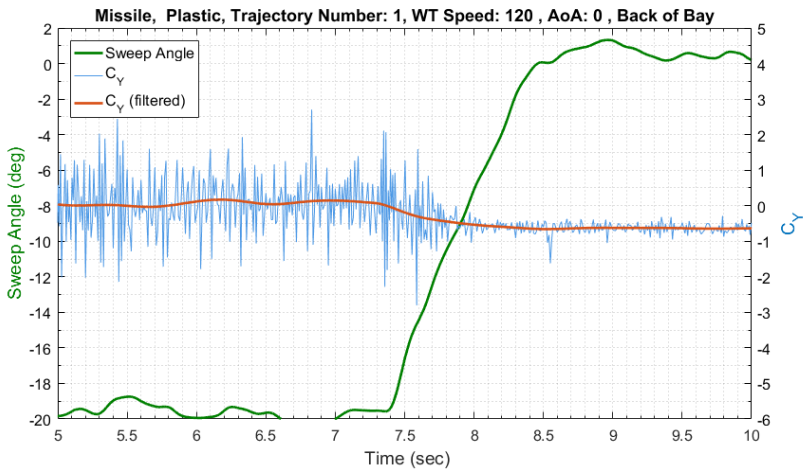
Missile, Plastic, Trajectory Number: 1, WT Speed: 120 , AoA: 0 , Back of Bay
Sweep Angle
C_Y
C_Y (filtered)
Sweep Angle (deg)
C_Y
Time (sec)

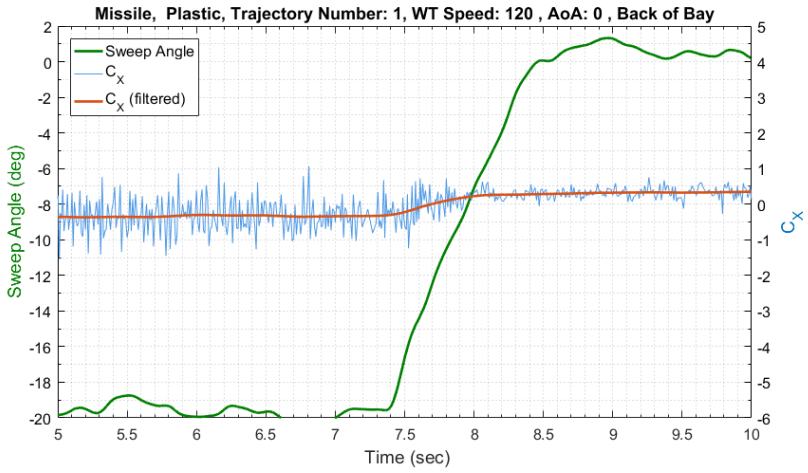
Missile, Plastic, Trajectory Number: 1, WT Speed: 120 , AoA: 0 , Back of Bay
Sweep Angle
C_X
C_X (filtered)
Sweep Angle (deg)
C_X
Time (sec)

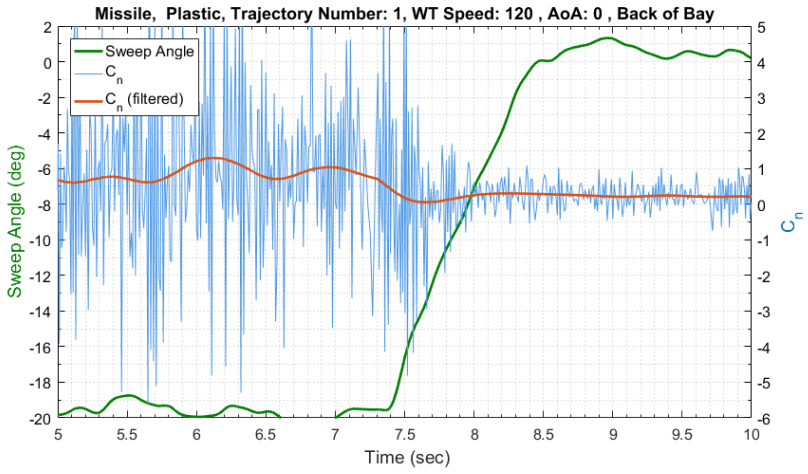
Missile, Plastic, Trajectory Number: 1, WT Speed: 120 , AoA: 0 , Back of Bay
Sweep Angle
C_n
C_n (filtered)
Sweep Angle (deg)
C_n
Time (sec)

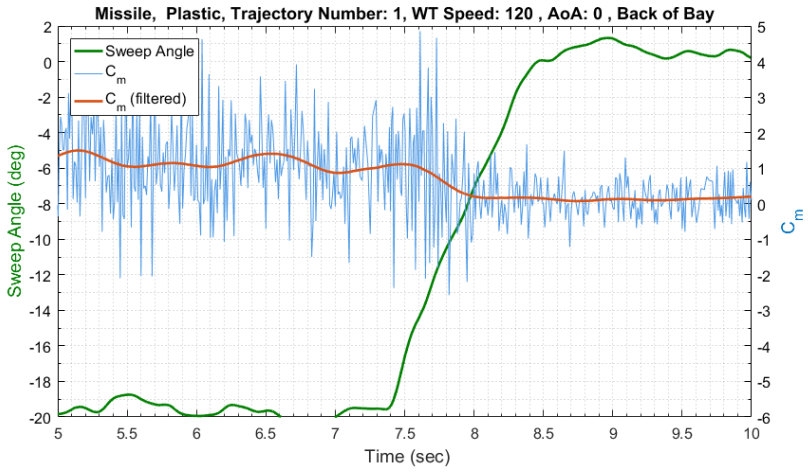
Missile, Plastic, Trajectory Number: 1, WT Speed: 120 , AoA: 0 , Back of Bay
Sweep Angle
C_m
C_m (filtered)
Sweep Angle (deg)
C_m
Time (sec)

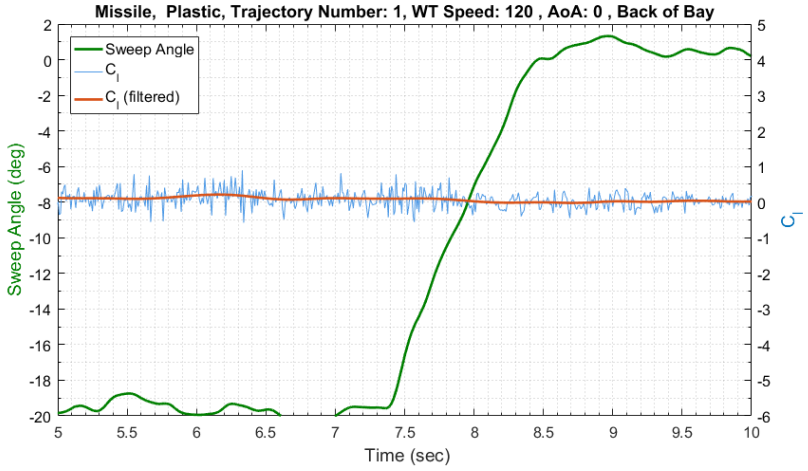
Missile, Plastic, Trajectory Number: 1, WT Speed: 120 , AoA: 0 , Back of Bay
Sweep Angle
C_l
C_l (filtered)
Sweep Angle (deg)
C_l
Time (sec)

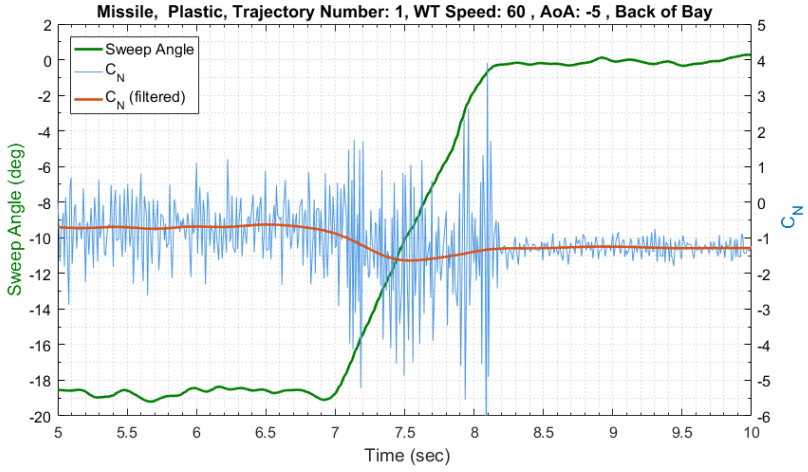
Missile, Plastic, Trajectory Number: 1, WT Speed: 60 , AoA: -5 , Back of Bay
Sweep Angle
C_N
C_N (filtered)
Sweep Angle (deg)
C_N
Time (sec)

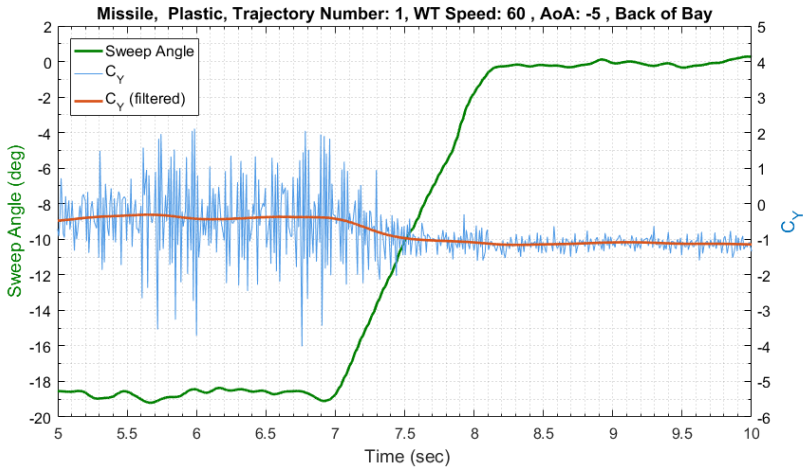
Missile, Plastic, Trajectory Number: 1, WT Speed: 60 , AoA: -5 , Back of Bay
Sweep Angle
C_Y
C_Y (filtered)
Sweep Angle (deg)
C_Y
Time (sec)

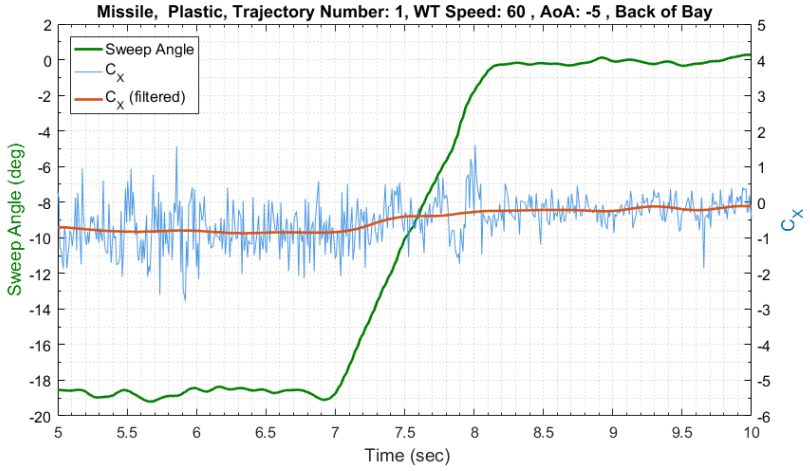
Missile, Plastic, Trajectory Number: 1, WT Speed: 60 , AoA: -5 , Back of Bay
Sweep Angle
C_X
C_X (filtered)
Sweep Angle (deg)
C_X
Time (sec)

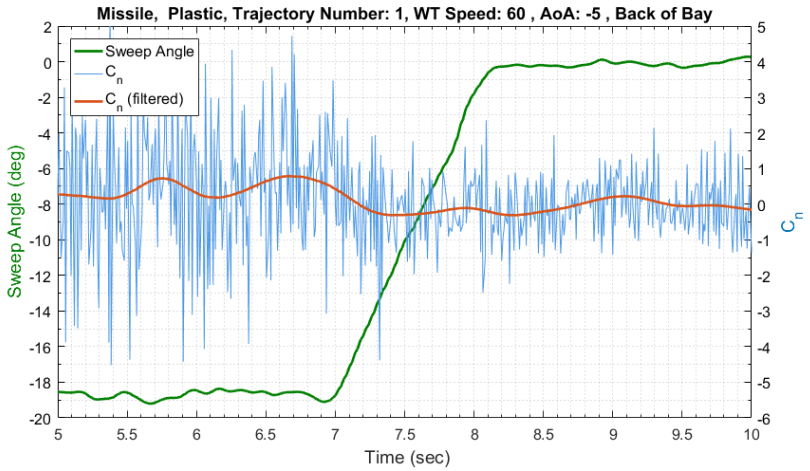
Missile, Plastic, Trajectory Number: 1, WT Speed: 60 , AoA: -5 , Back of Bay
Sweep Angle
C_n
C_n (filtered)
Sweep Angle (deg)
C_n
Time (sec)

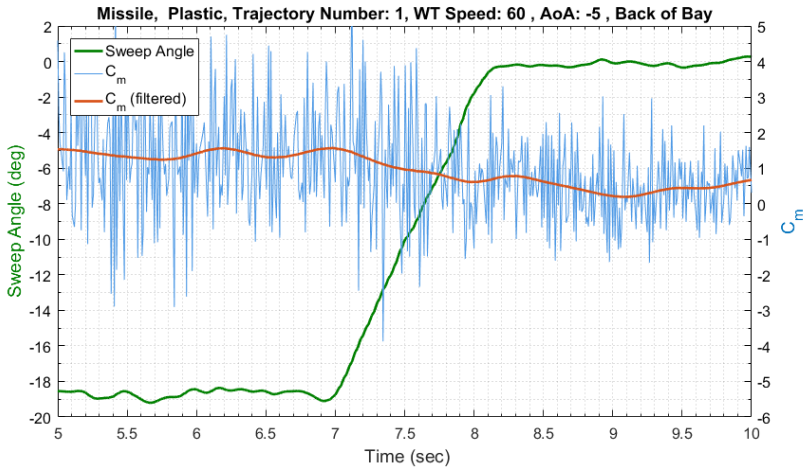
Missile, Plastic, Trajectory Number: 1, WT Speed: 60 , AoA: -5 , Back of Bay
Sweep Angle
C_m
C_m (filtered)
Sweep Angle (deg)
C_m
Time (sec)

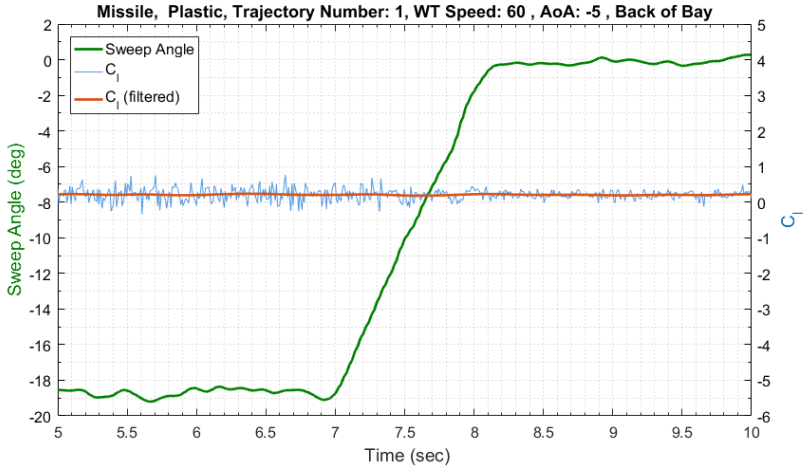
Missile, Plastic, Trajectory Number: 1, WT Speed: 60 , AoA: -5 , Back of Bay
Sweep Angle
C_l
C_l (filtered)
Sweep Angle (deg)
C_l
Time (sec)

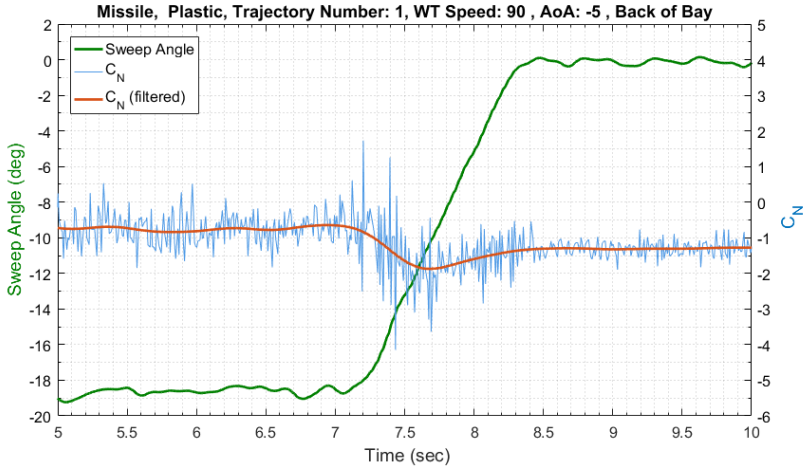
Missile, Plastic, Trajectory Number: 1, WT Speed: 90 , AoA: -5 , Back of Bay
Sweep Angle
C_N
C_N (filtered)
Sweep Angle (deg)
C_N
Time (sec)

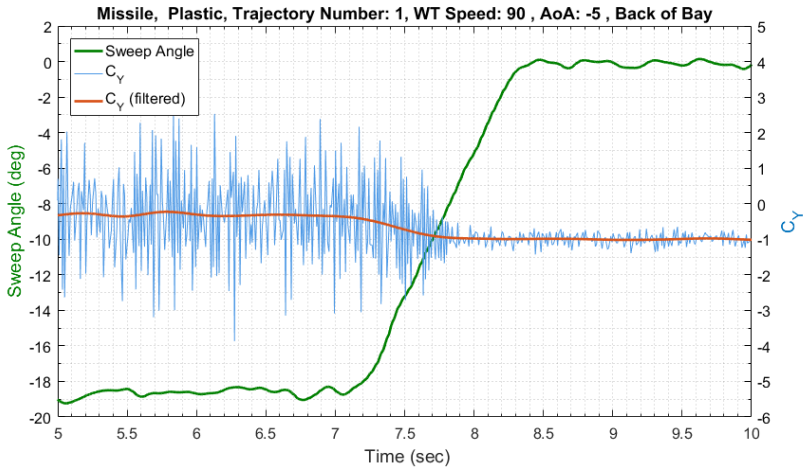
Missile, Plastic, Trajectory Number: 1, WT Speed: 90 , AoA: -5 , Back of Bay
Sweep Angle
C_Y
C_Y (filtered)
Sweep Angle (deg)
C_Y
Time (sec)

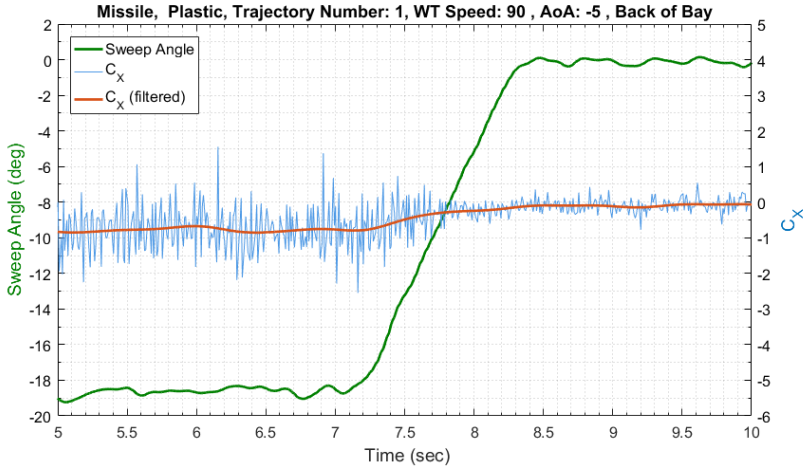
Missile, Plastic, Trajectory Number: 1, WT Speed: 90 , AoA: -5 , Back of Bay
Sweep Angle
C_X
C_X (filtered)
Sweep Angle (deg)
C_X
Time (sec)

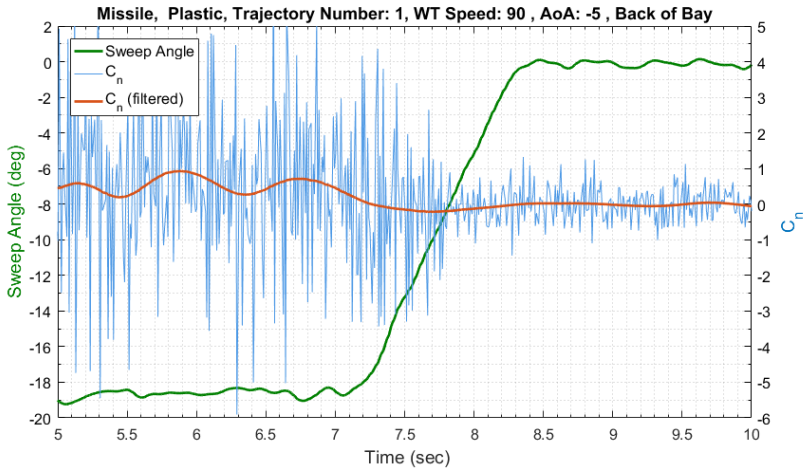
Missile, Plastic, Trajectory Number: 1, WT Speed: 90 , AoA: -5 , Back of Bay
Sweep Angle
C_n
C_n (filtered)
Sweep Angle (deg)
C_n
Time (sec)

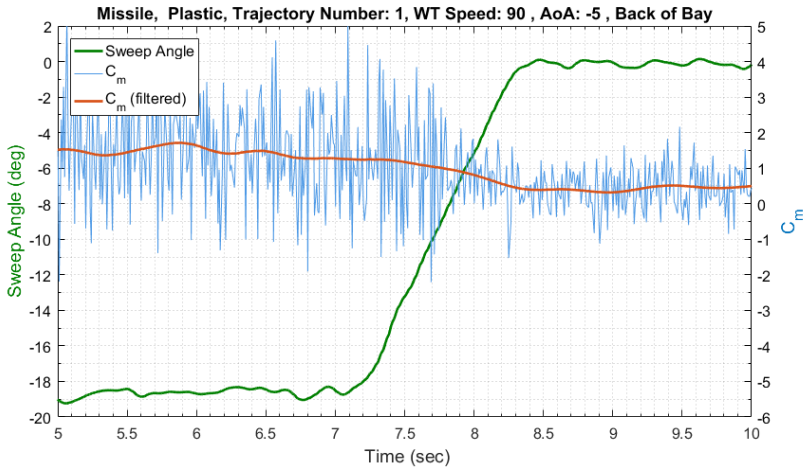
Missile, Plastic, Trajectory Number: 1, WT Speed: 90 , AoA: -5 , Back of Bay
Sweep Angle
C_m
C_m (filtered)
Sweep Angle (deg)
C_m
Time (sec)

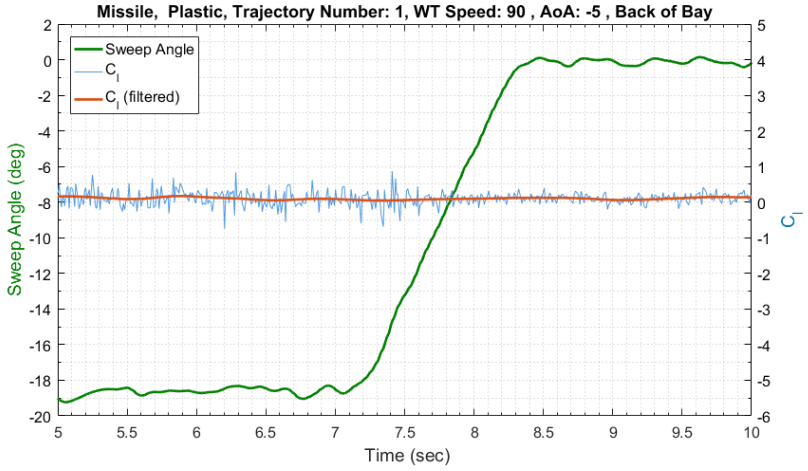
Missile, Plastic, Trajectory Number: 1, WT Speed: 90 , AoA: -5 , Back of Bay
Sweep Angle
C_l
C_l (filtered)
Sweep Angle (deg)
C_l
Time (sec)

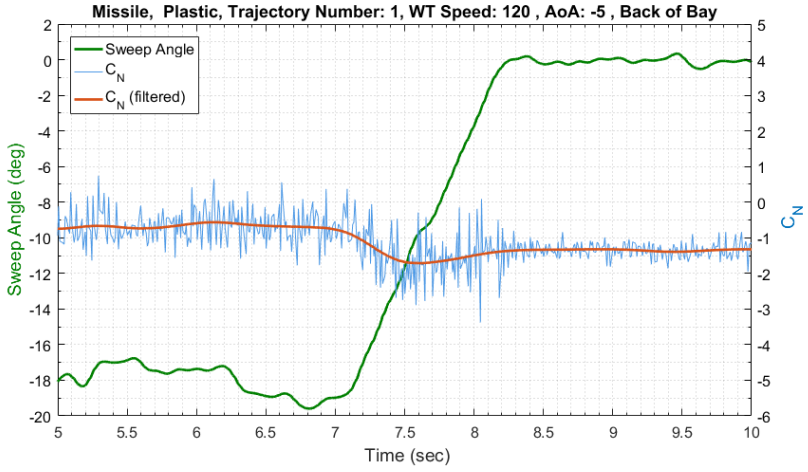
Missile, Plastic, Trajectory Number: 1, WT Speed: 120 , AoA: -5 , Back of Bay
Sweep Angle
C_N
C_N (filtered)
Sweep Angle (deg)
C_N
Time (sec)

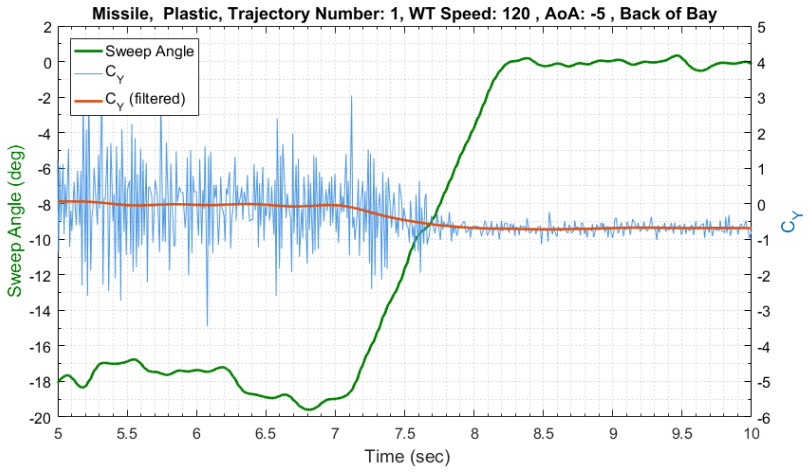
Missile, Plastic, Trajectory Number: 1, WT Speed: 120 , AoA: -5 , Back of Bay
Sweep Angle
C_Y
C_Y (filtered)
Sweep Angle (deg)
C_Y
Time (sec)

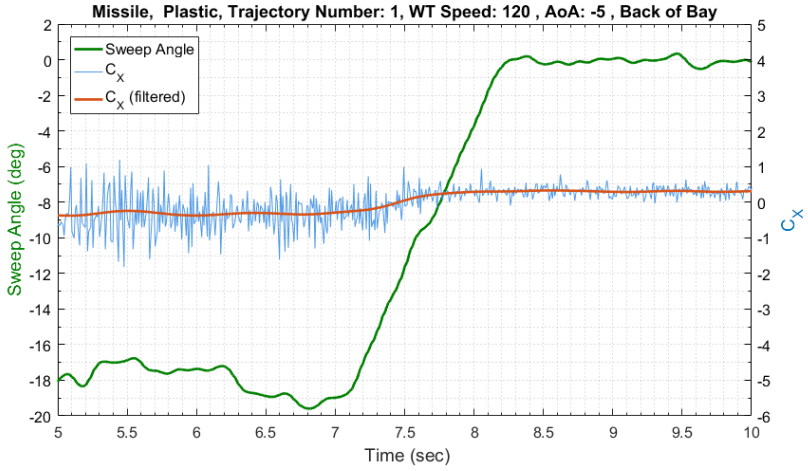
Missile, Plastic, Trajectory Number: 1, WT Speed: 120 , AoA: -5 , Back of Bay
Sweep Angle
C_X
C_X (filtered)
Sweep Angle (deg)
C_X
Time (sec)

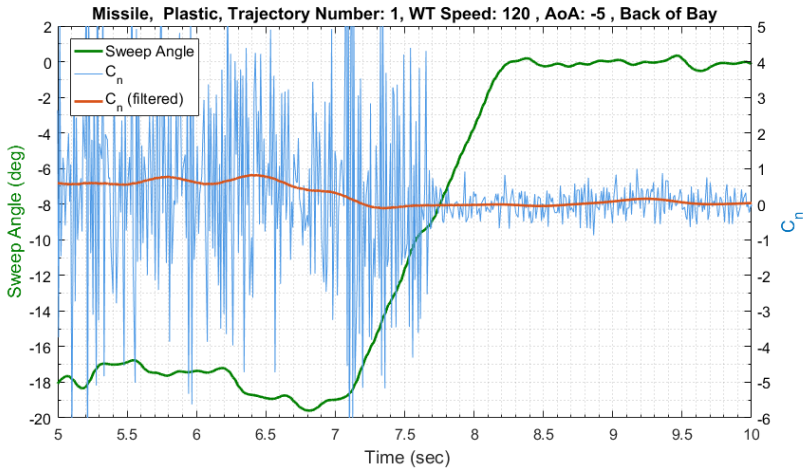
Missile, Plastic, Trajectory Number: 1, WT Speed: 120 , AoA: -5 , Back of Bay
Sweep Angle
C_n
C_n (filtered)
Sweep Angle (deg)
C_n
Time (sec)

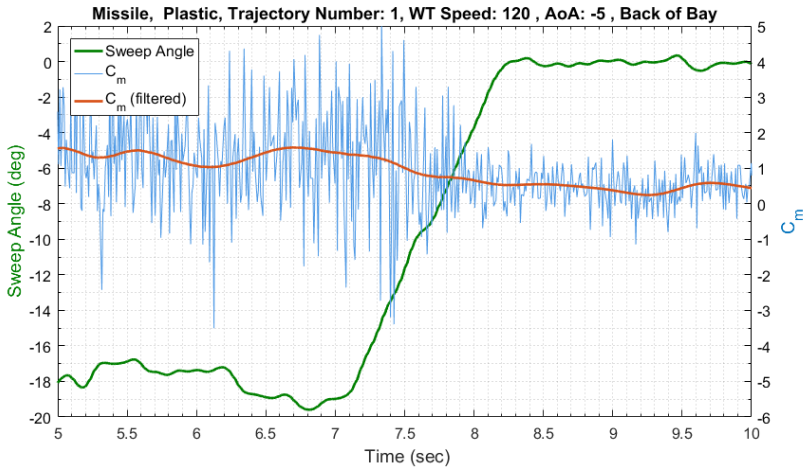
Missile, Plastic, Trajectory Number: 1, WT Speed: 120 , AoA: -5 , Back of Bay
Sweep Angle
C_m
C_m (filtered)
Sweep Angle (deg)
C_m
Time (sec)

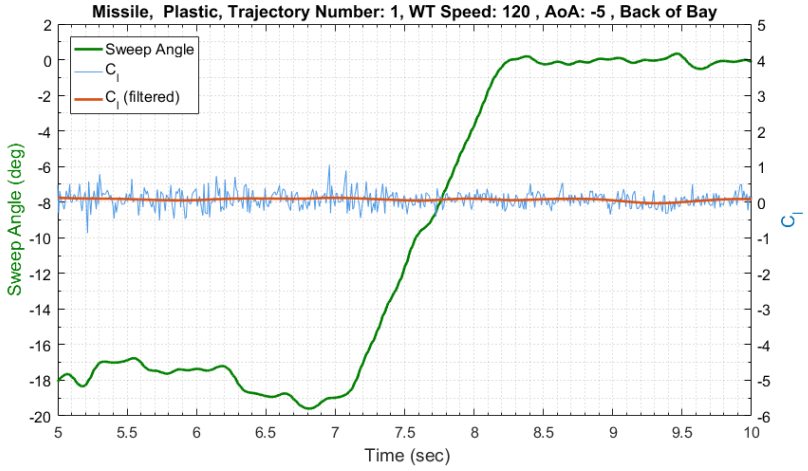
Missile, Plastic, Trajectory Number: 1, WT Speed: 120 , AoA: -5 , Back of Bay
Sweep Angle
C_l
C_l (filtered)
Sweep Angle (deg)
C_l
Time (sec)

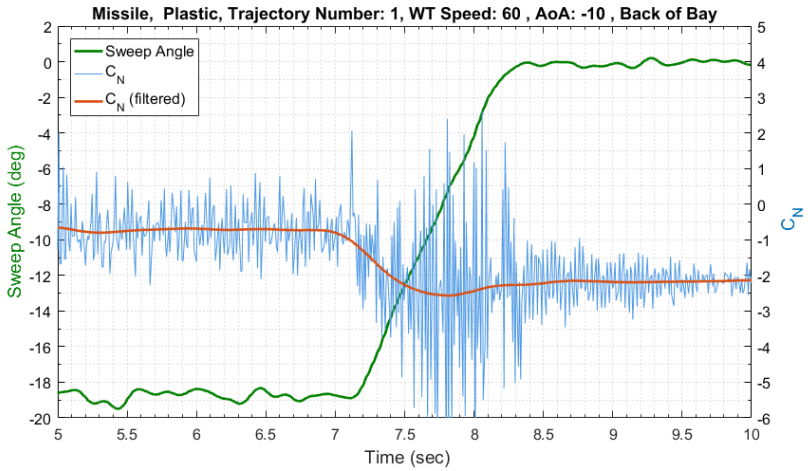
Missile, Plastic, Trajectory Number: 1, WT Speed: 60 , AoA: -10 , Back of Bay
Sweep Angle
C_N
C_N (filtered)
Sweep Angle (deg)
C_N
Time (sec)

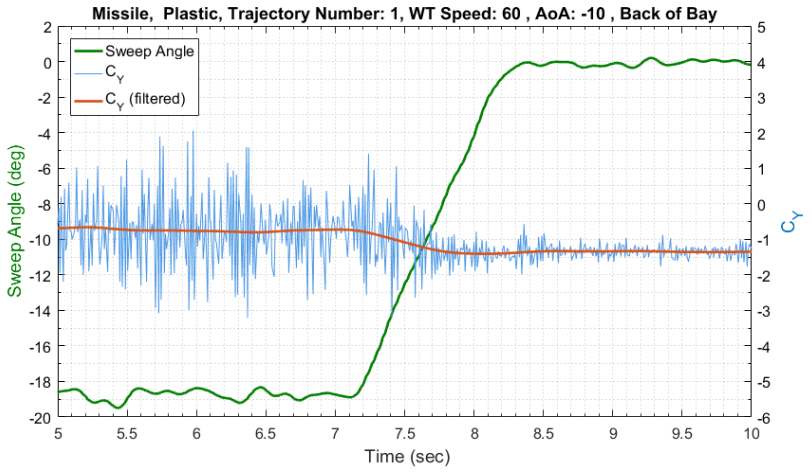
Missile, Plastic, Trajectory Number: 1, WT Speed: 60 , AoA: -10 , Back of Bay
Sweep Angle
C_Y
C_Y (filtered)
Sweep Angle (deg)
C_Y
Time (sec)

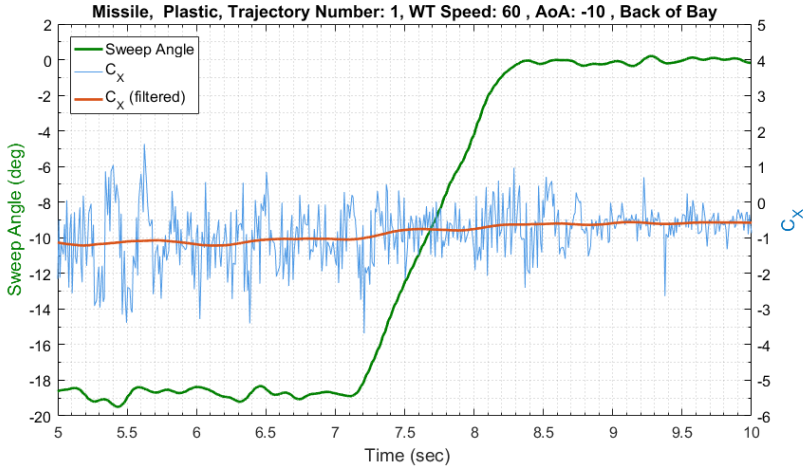
Missile, Plastic, Trajectory Number: 1, WT Speed: 60 , AoA: -10 , Back of Bay
Sweep Angle
C_X
C_X (filtered)
Sweep Angle (deg)
C_X
Time (sec)

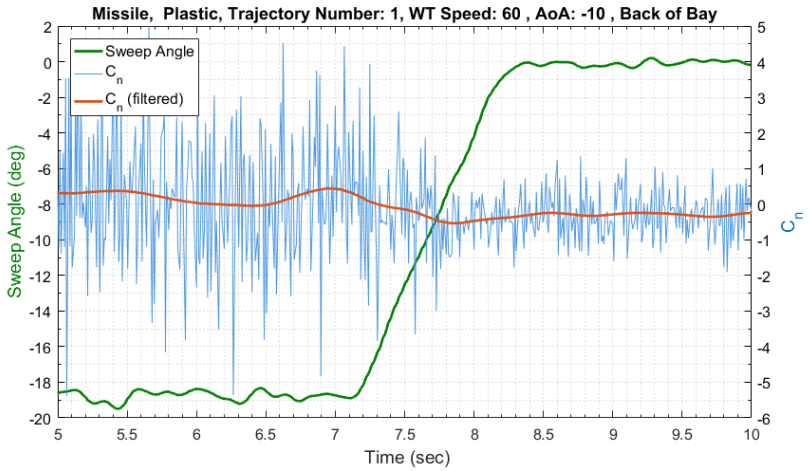
Missile, Plastic, Trajectory Number: 1, WT Speed: 60 , AoA: -10 , Back of Bay
Sweep Angle
C_n
C_n (filtered)
Sweep Angle (deg)
C_n
Time (sec)

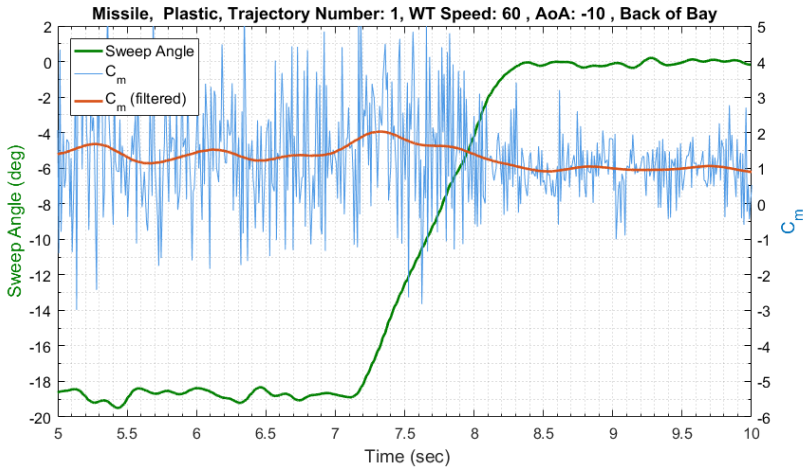
Missile, Plastic, Trajectory Number: 1, WT Speed: 60 , AoA: -10 , Back of Bay
Sweep Angle
C_m
C_m (filtered)
Sweep Angle (deg)
C_m
Time (sec)

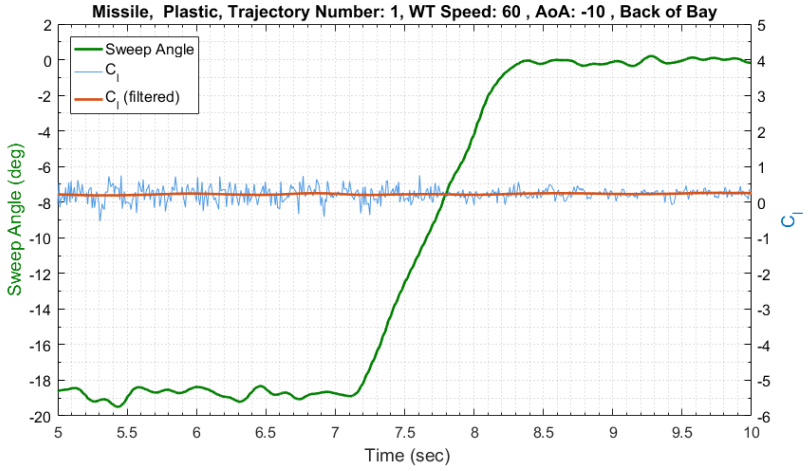
Missile, Plastic, Trajectory Number: 1, WT Speed: 60 , AoA: -10 , Back of Bay
Sweep Angle
C_l
C_l (filtered)
Sweep Angle (deg)
C_l
Time (sec)

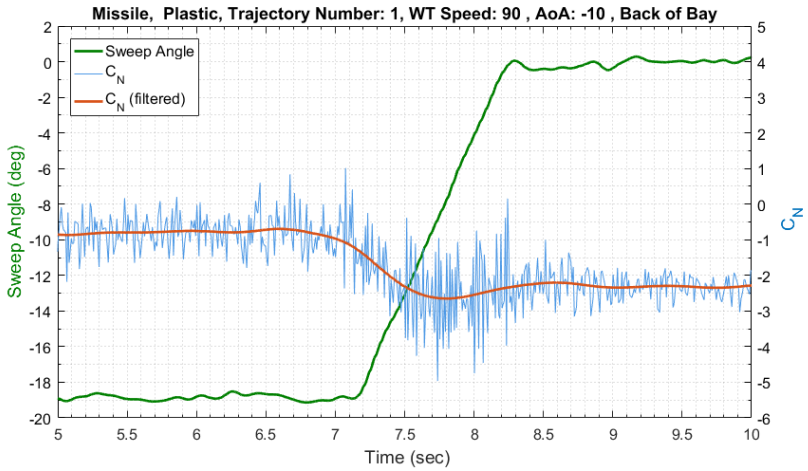
Missile, Plastic, Trajectory Number: 1, WT Speed: 90 , AoA: -10 , Back of Bay
Sweep Angle
C_N
C_N (filtered)
Sweep Angle (deg)
C_N
Time (sec)

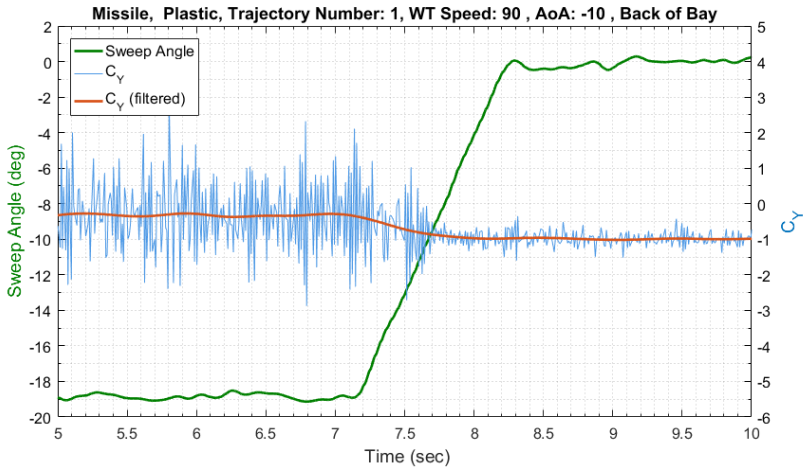
Missile, Plastic, Trajectory Number: 1, WT Speed: 90 , AoA: -10 , Back of Bay
Sweep Angle
C_Y
C_Y (filtered)
Sweep Angle (deg)
C_Y
Time (sec)

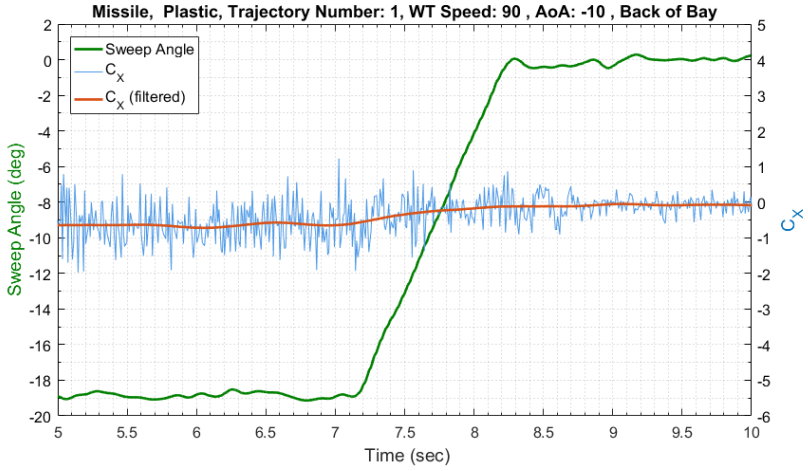
Missile, Plastic, Trajectory Number: 1, WT Speed: 90 , AoA: -10 , Back of Bay
Sweep Angle
C_X
C_X (filtered)
Sweep Angle (deg)
C_X
Time (sec)

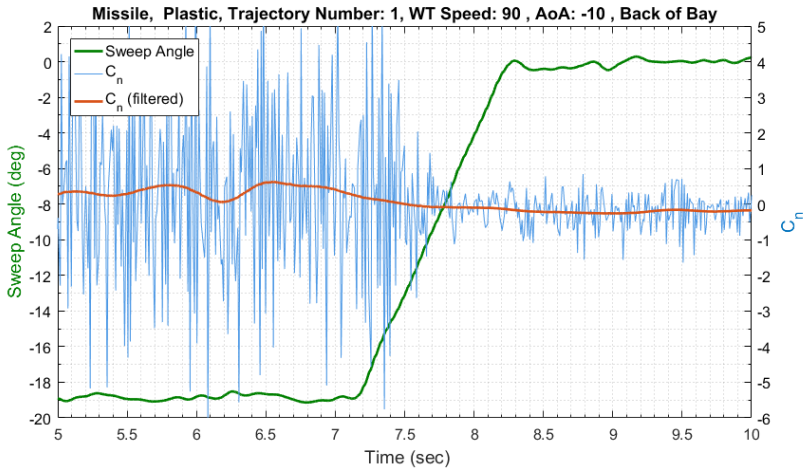
Missile, Plastic, Trajectory Number: 1, WT Speed: 90 , AoA: -10 , Back of Bay
Sweep Angle
C_n
C_n (filtered)
Sweep Angle (deg)
C_n
Time (sec)

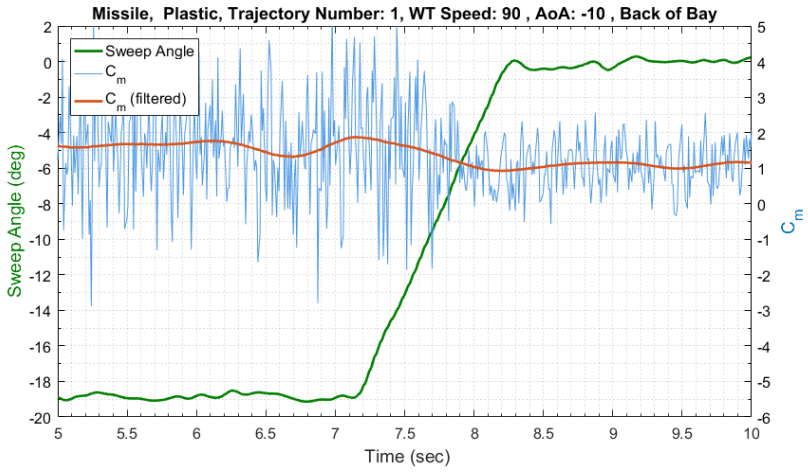
Missile, Plastic, Trajectory Number: 1, WT Speed: 90 , AoA: -10 , Back of Bay
Sweep Angle
C_m
C_m (filtered)
Sweep Angle (deg)
C_m
Time (sec)

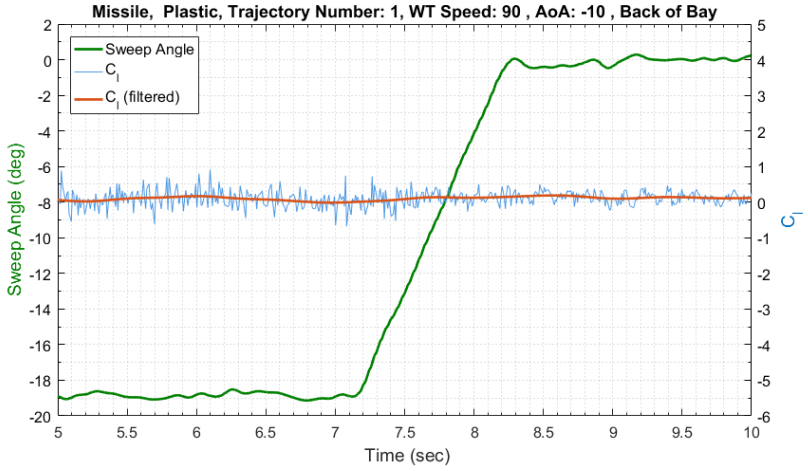
Missile, Plastic, Trajectory Number: 1, WT Speed: 90 , AoA: -10 , Back of Bay
Sweep Angle
C_l
C_l (filtered)
Sweep Angle (deg)
C_l
Time (sec)

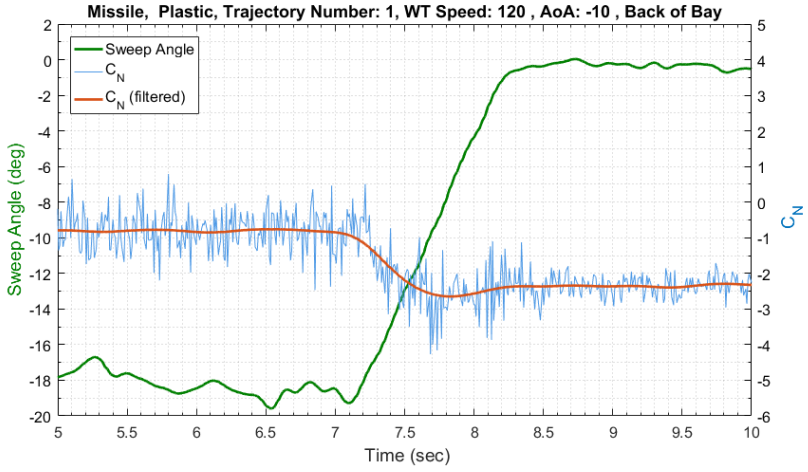
Missile, Plastic, Trajectory Number: 1, WT Speed: 120 , AoA: -10 , Back of Bay
Sweep Angle
C_N
C_N (filtered)
Sweep Angle (deg)
C_N
Time (sec)

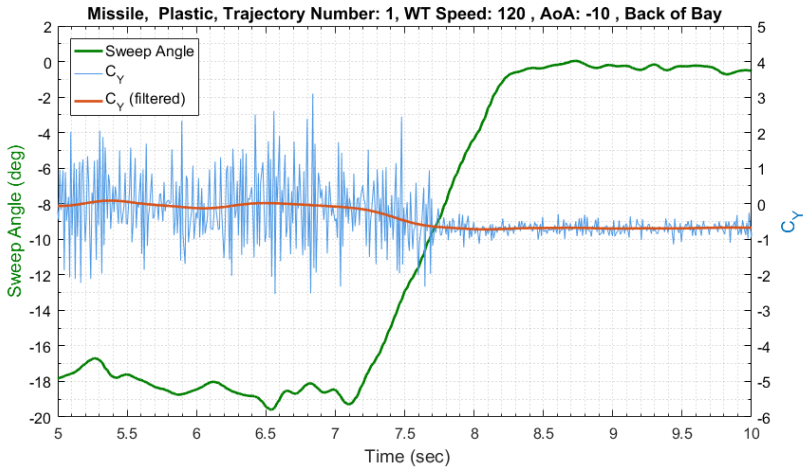
Missile, Plastic, Trajectory Number: 1, WT Speed: 120 , AoA: -10 , Back of Bay
Sweep Angle
C_Y
C_Y (filtered)
Sweep Angle (deg)
C_Y
Time (sec)

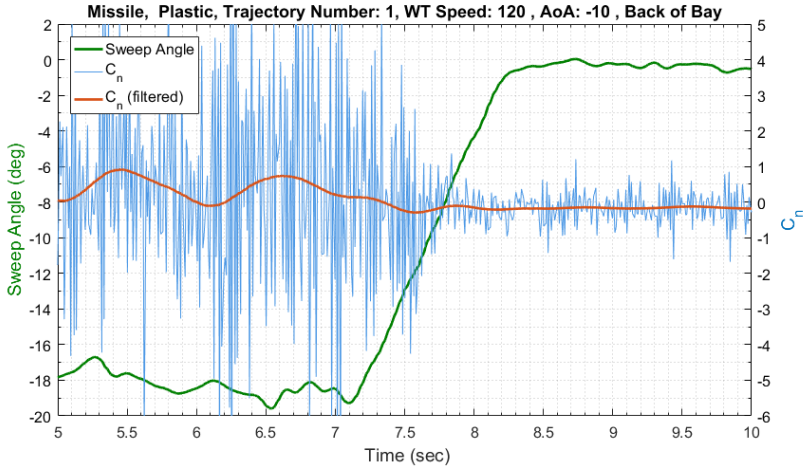
Missile, Plastic, Trajectory Number: 1, WT Speed: 120 , AoA: -10 , Back of Bay
Sweep Angle
C_n
C_n (filtered)
Sweep Angle (deg)
C_n
Time (sec)

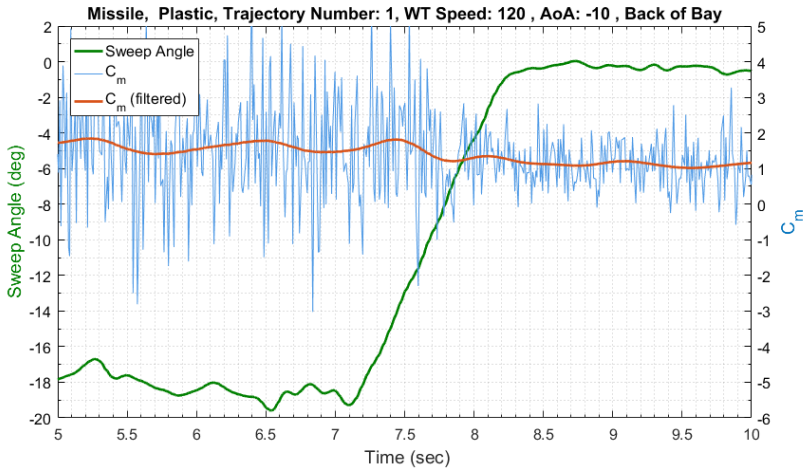
Missile, Plastic, Trajectory Number: 1, WT Speed: 120 , AoA: -10 , Back of Bay
Sweep Angle
C_m
C_m (filtered)
Sweep Angle (deg)
C_m
Time (sec)

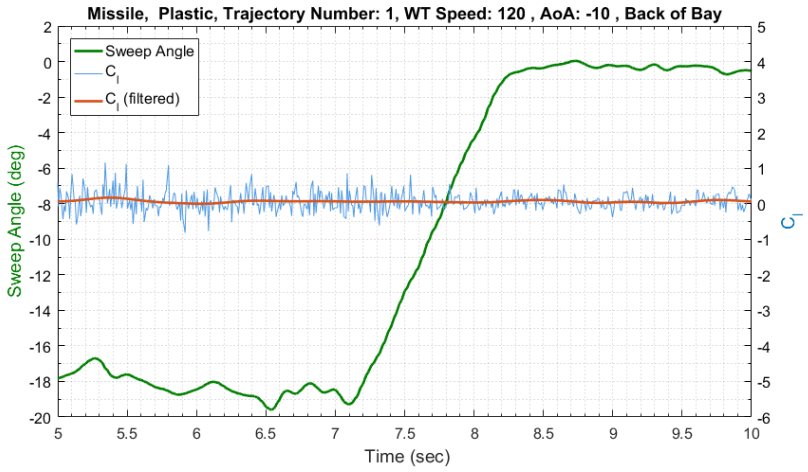
Missile, Plastic, Trajectory Number: 1, WT Speed: 120 , AoA: -10 , Back of Bay
Sweep Angle
C_l
C_l (filtered)
Sweep Angle (deg)
C_l
Time (sec)

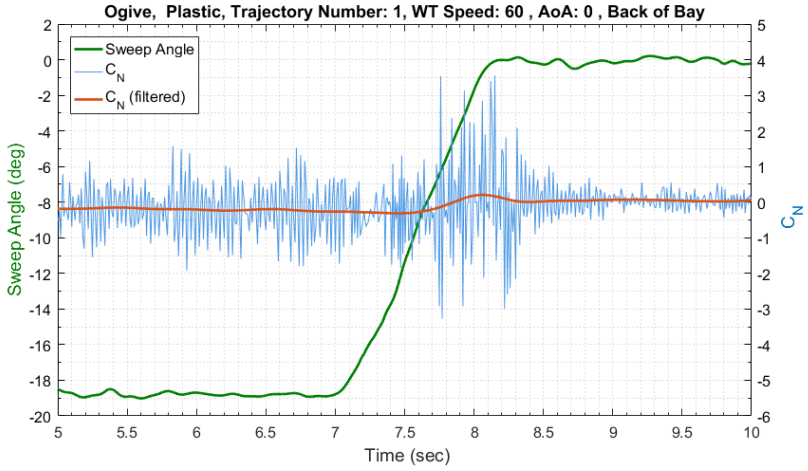
Ogive, Plastic, Trajectory Number: 1, WT Speed: 60 , AoA: 0 , Back of Bay
Sweep Angle
C_N
C_N (filtered)
Sweep Angle (deg)
C_N
Time (sec)

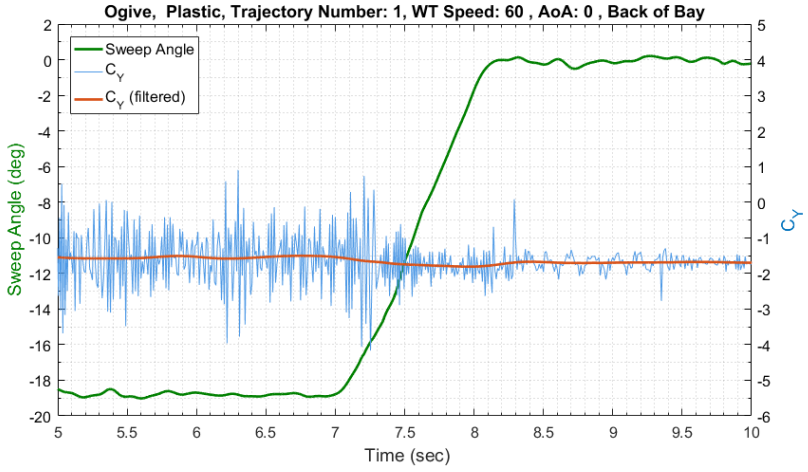
Ogive, Plastic, Trajectory Number: 1, WT Speed: 60 , AoA: 0 , Back of Bay
Sweep Angle
C_Y
C_Y (filtered)
Sweep Angle (deg)
C_Y
Time (sec)

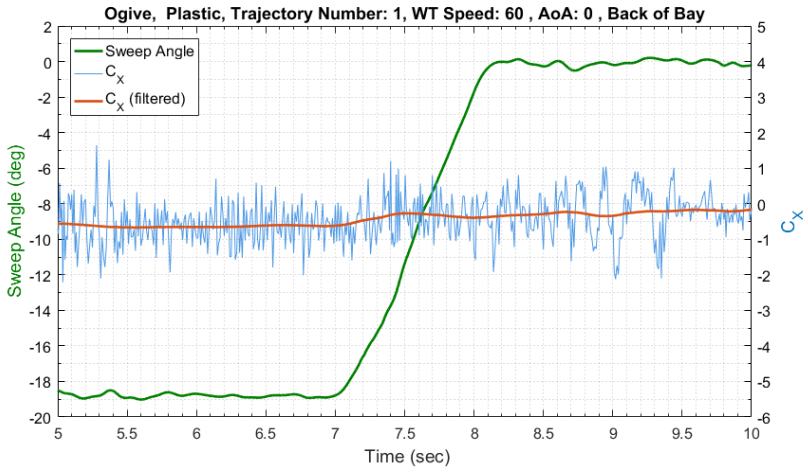
Ogive, Plastic, Trajectory Number: 1, WT Speed: 60 , AoA: 0 , Back of Bay
Sweep Angle
C_X
C_X (filtered)
Sweep Angle (deg)
C_X
Time (sec)

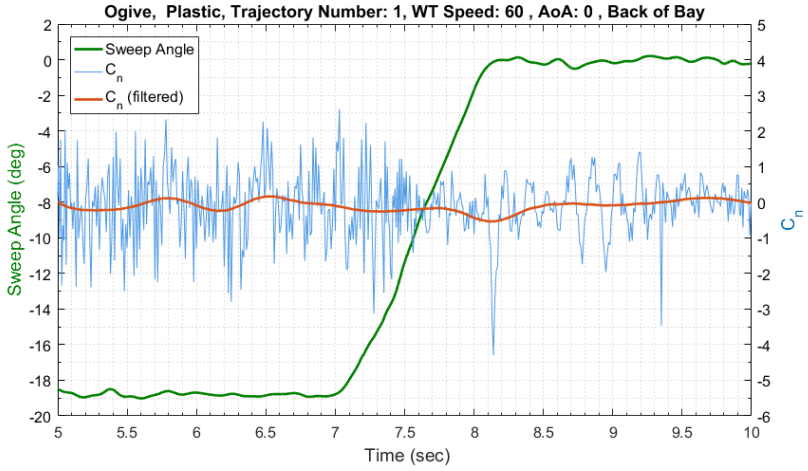
Ogive, Plastic, Trajectory Number: 1, WT Speed: 60 , AoA: 0 , Back of Bay
Sweep Angle
C_n
C_n (filtered)
Sweep Angle (deg)
C_n
Time (sec)

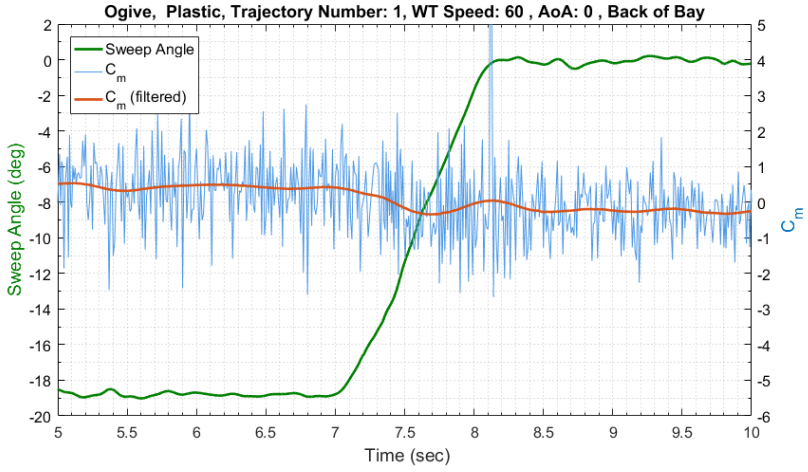
Ogive, Plastic, Trajectory Number: 1, WT Speed: 60 , AoA: 0 , Back of Bay
Sweep Angle
C_m
C_m (filtered)
Sweep Angle (deg)
C_m
Time (sec)

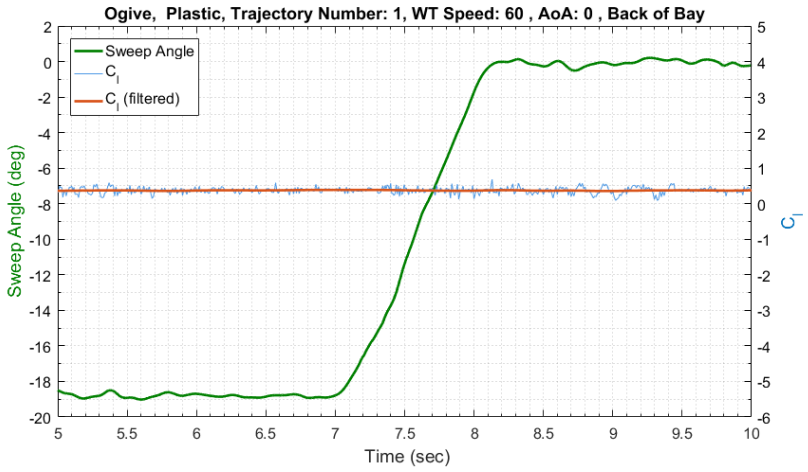
Ogive, Plastic, Trajectory Number: 1, WT Speed: 60 , AoA: 0 , Back of Bay
Sweep Angle
C_l
C_l (filtered)
Sweep Angle (deg)
C_l
Time (sec)

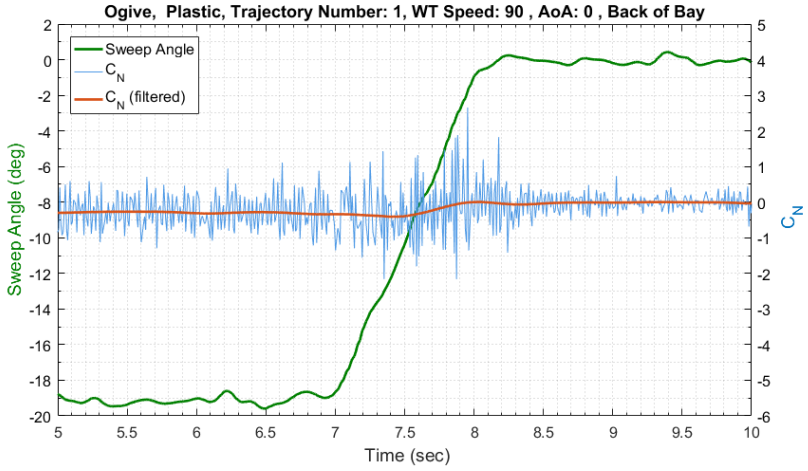
Ogive, Plastic, Trajectory Number: 1, WT Speed: 90 , AoA: 0 , Back of Bay
Sweep Angle
C_N
C_N (filtered)
Sweep Angle (deg)
C_N
Time (sec)

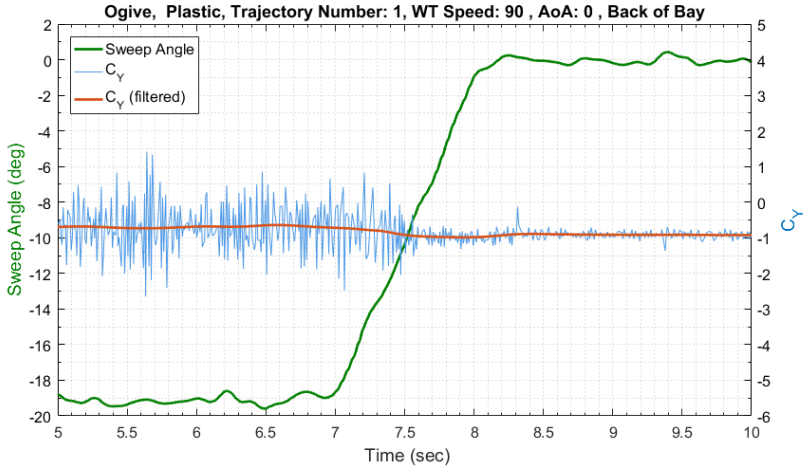
Ogive, Plastic, Trajectory Number: 1, WT Speed: 90 , AoA: 0 , Back of Bay
Sweep Angle
C_Y
C_Y (filtered)
Sweep Angle (deg)
C_Y
Time (sec)

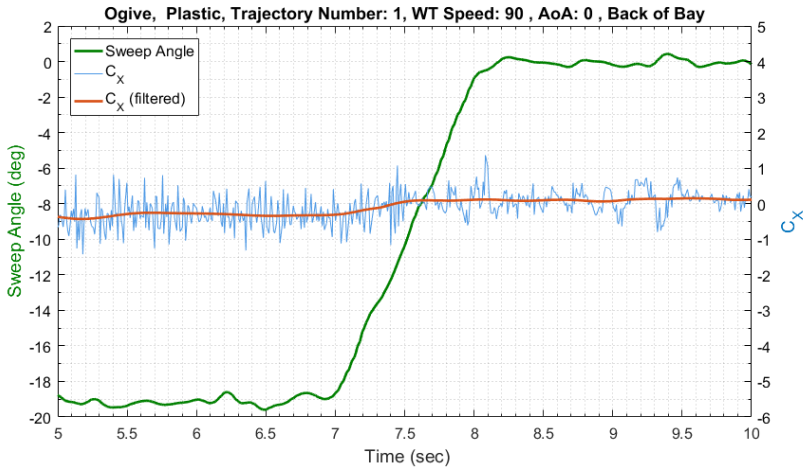
Ogive, Plastic, Trajectory Number: 1, WT Speed: 90 , AoA: 0 , Back of Bay
Sweep Angle
C_X
C_X (filtered)
Sweep Angle (deg)
C_X
Time (sec)

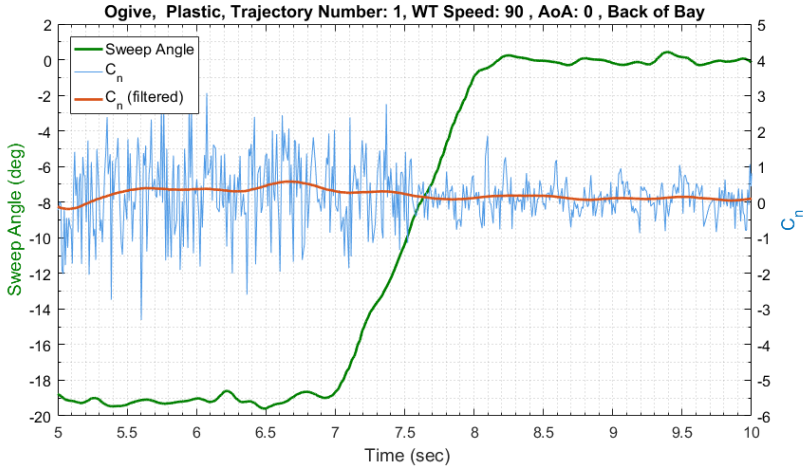
Ogive, Plastic, Trajectory Number: 1, WT Speed: 90 , AoA: 0 , Back of Bay
Sweep Angle
C_n
C_n (filtered)
Sweep Angle (deg)
C_n
Time (sec)

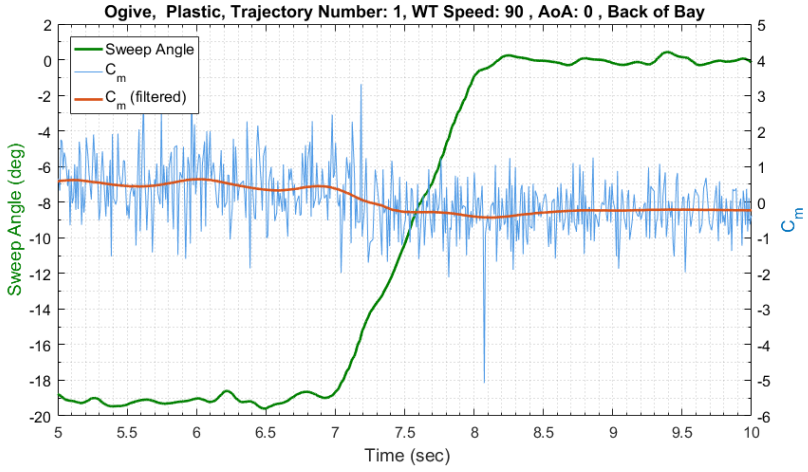
Ogive, Plastic, Trajectory Number: 1, WT Speed: 90 , AoA: 0 , Back of Bay
Sweep Angle
C_m
C_m (filtered)
Sweep Angle (deg)
C_m
Time (sec)

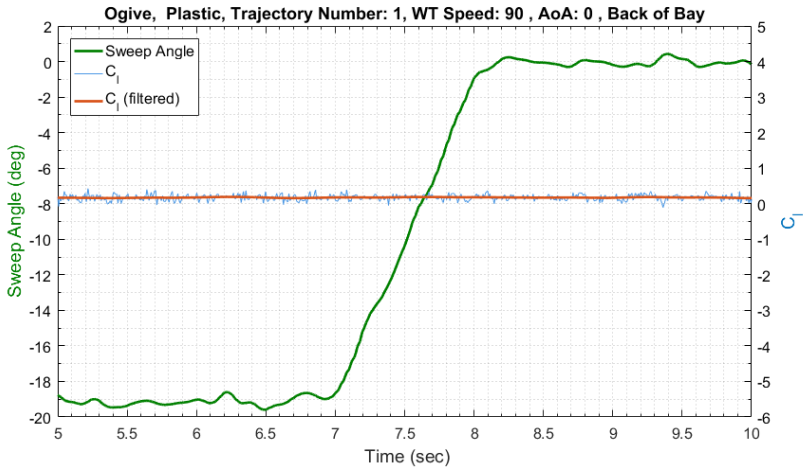
Ogive, Plastic, Trajectory Number: 1, WT Speed: 90 , AoA: 0 , Back of Bay
Sweep Angle
C_l
C_l (filtered)
Sweep Angle (deg)
C_l
Time (sec)

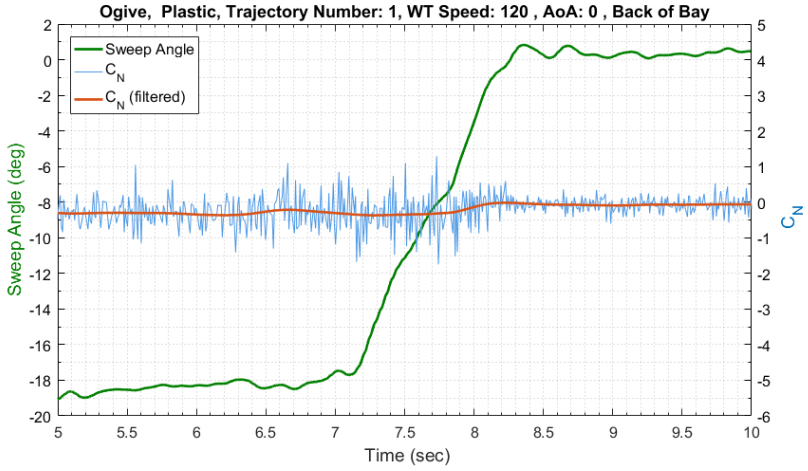
Ogive, Plastic, Trajectory Number: 1, WT Speed: 120 , AoA: 0 , Back of Bay
Sweep Angle
C_N
C_N (filtered)
Sweep Angle (deg)
C_N
Time (sec)

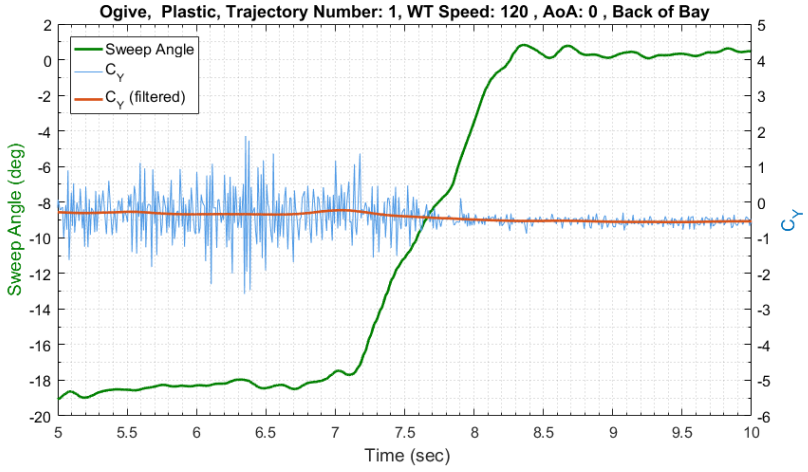
Ogive, Plastic, Trajectory Number: 1, WT Speed: 120 , AoA: 0 , Back of Bay
Sweep Angle
C_Y
C_Y (filtered)
Sweep Angle (deg)
C_Y
Time (sec)

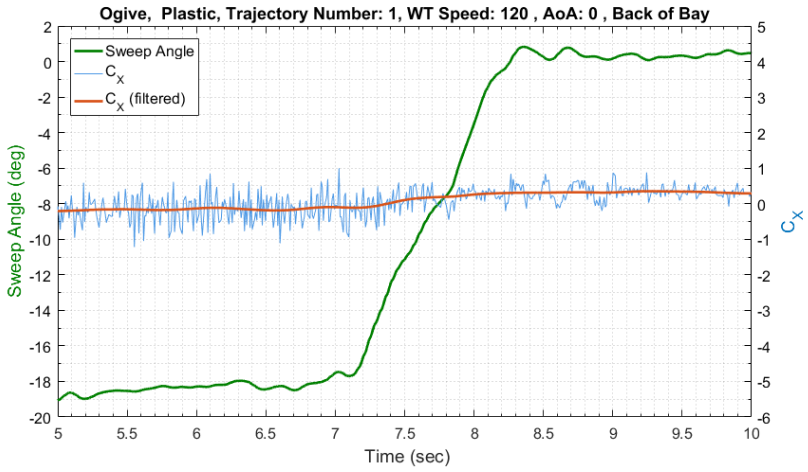
Ogive, Plastic, Trajectory Number: 1, WT Speed: 120 , AoA: 0 , Back of Bay
Sweep Angle
C_X
C_X (filtered)
Sweep Angle (deg)
C_X
Time (sec)

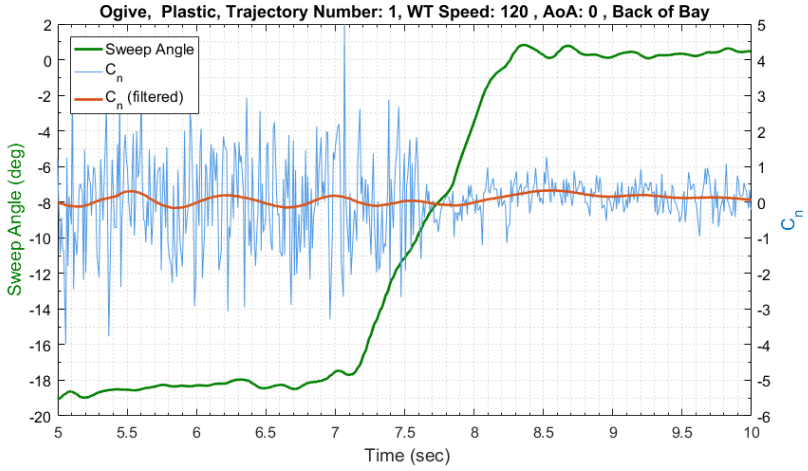
Ogive, Plastic, Trajectory Number: 1, WT Speed: 120 , AoA: 0 , Back of Bay
Sweep Angle
C_n
C_n (filtered)
Sweep Angle (deg)
C_n
Time (sec)

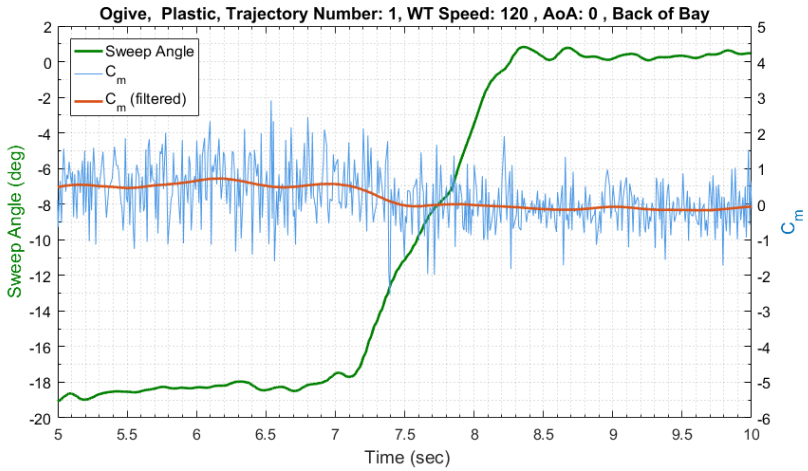
Ogive, Plastic, Trajectory Number: 1, WT Speed: 120 , AoA: 0 , Back of Bay
Sweep Angle
C_m
C_m (filtered)
Sweep Angle (deg)
C_m
Time (sec)

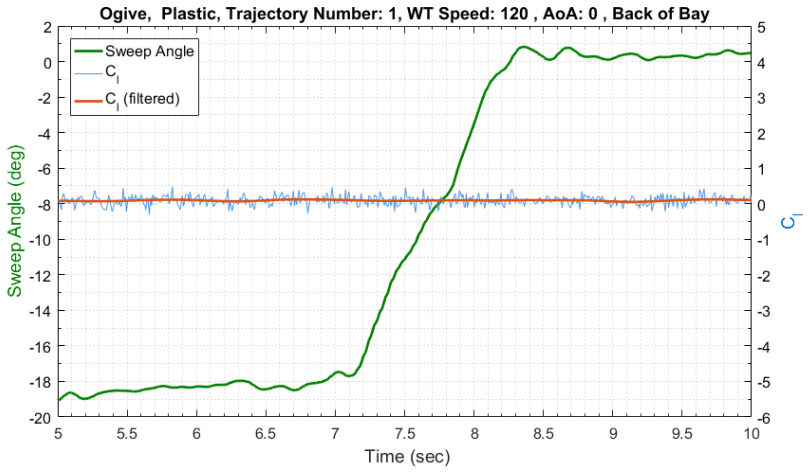
Ogive, Plastic, Trajectory Number: 1, WT Speed: 120 , AoA: 0 , Back of Bay
Sweep Angle
C_l
C_l (filtered)
Sweep Angle (deg)
C_l
Time (sec)

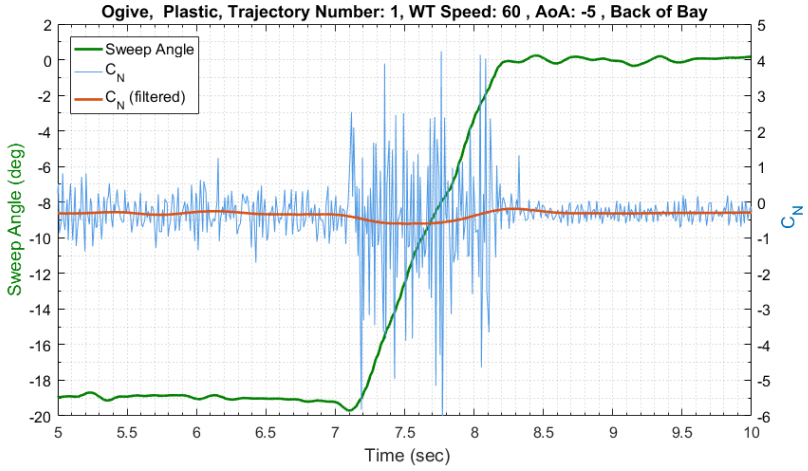
Ogive, Plastic, Trajectory Number: 1, WT Speed: 60 , AoA: -5 , Back of Bay
Sweep Angle
C_N
C_N (filtered)
Sweep Angle (deg)
C_N
Time (sec)

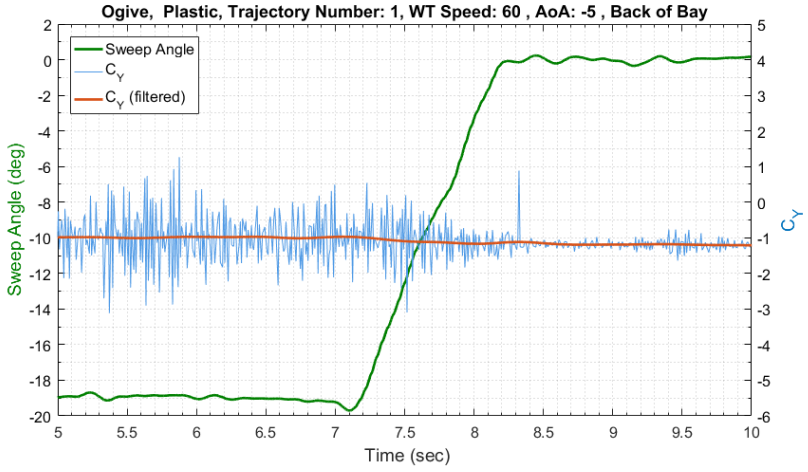
Ogive, Plastic, Trajectory Number: 1, WT Speed: 60 , AoA: -5 , Back of Bay
Sweep Angle
C_Y
C_Y (filtered)
Sweep Angle (deg)
C_Y
Time (sec)

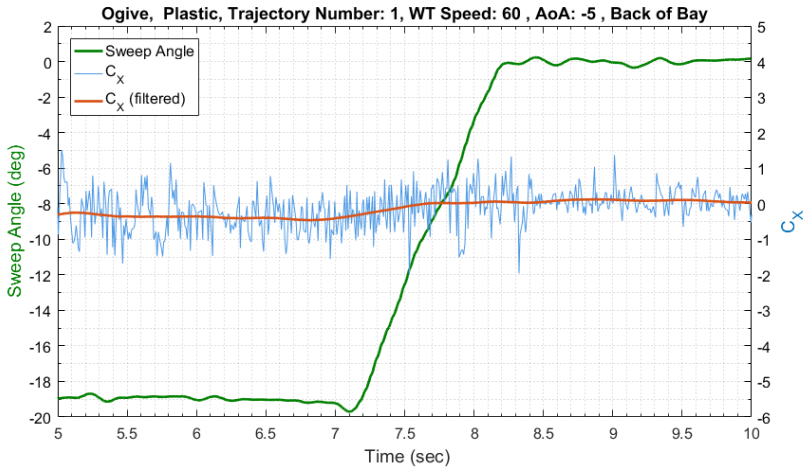
Ogive, Plastic, Trajectory Number: 1, WT Speed: 60 , AoA: -5 , Back of Bay
Sweep Angle
C_X
C_X (filtered)
Sweep Angle (deg)
C_X
Time (sec)

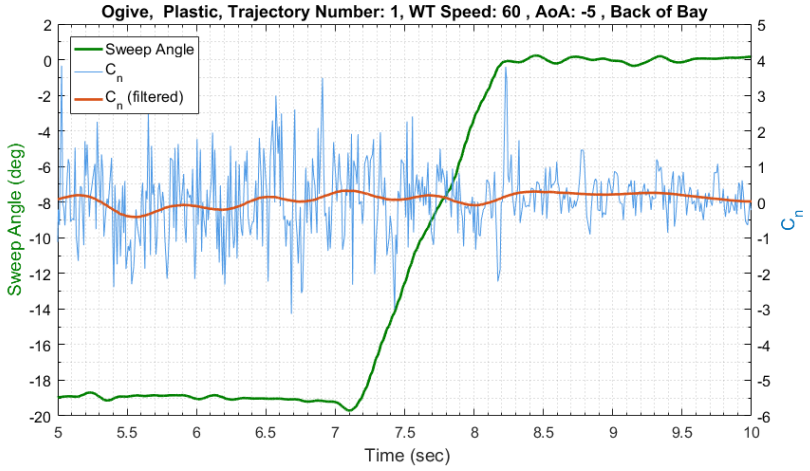
Ogive, Plastic, Trajectory Number: 1, WT Speed: 60 , AoA: -5 , Back of Bay
Sweep Angle
C_n
C_n (filtered)
Sweep Angle (deg)
C_n
Time (sec)

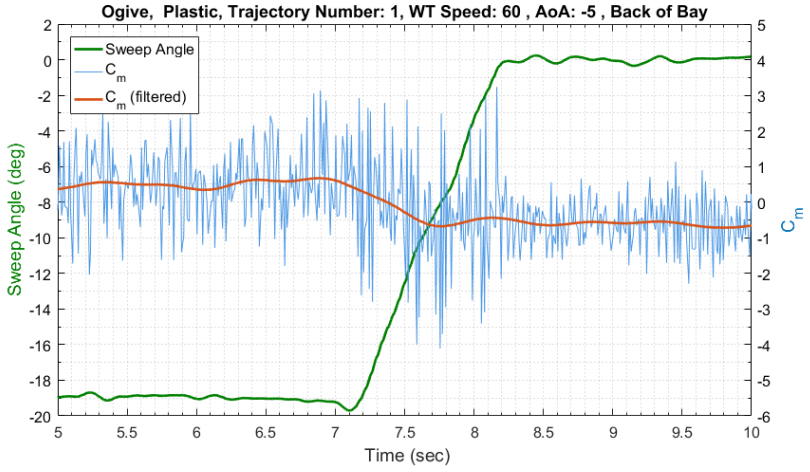
Ogive, Plastic, Trajectory Number: 1, WT Speed: 60 , AoA: -5 , Back of Bay
Sweep Angle
C_m
C_m (filtered)
Sweep Angle (deg)
C_m
Time (sec)

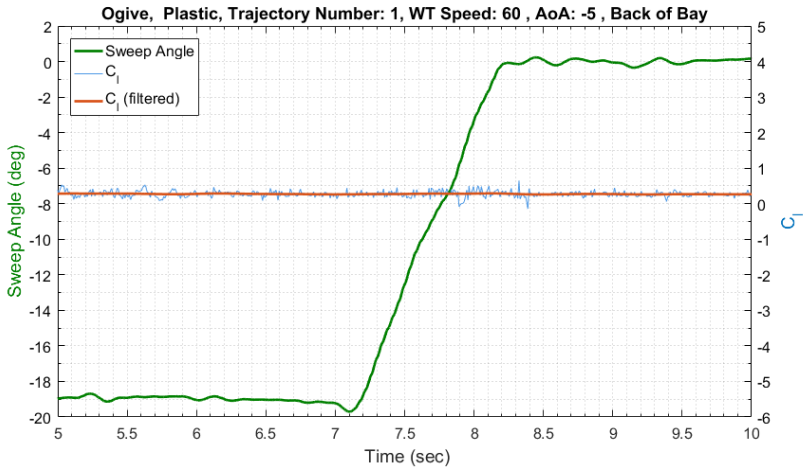
Ogive, Plastic, Trajectory Number: 1, WT Speed: 60 , AoA: -5 , Back of Bay
Sweep Angle
C_l
C_l (filtered)
Sweep Angle (deg)
C_l
Time (sec)

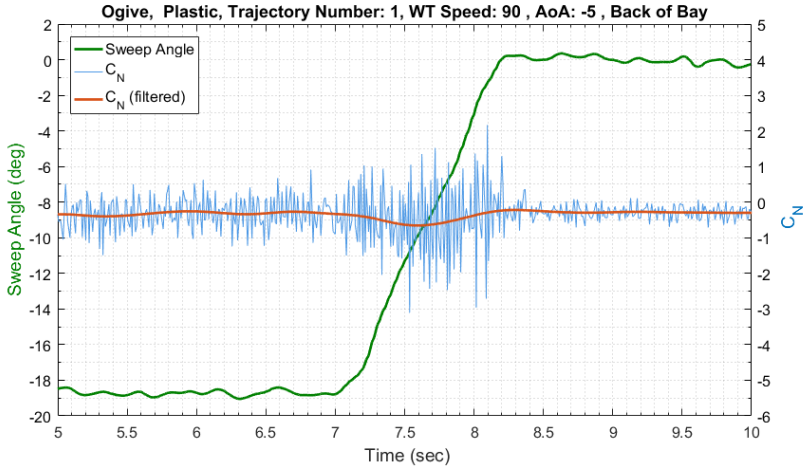
Ogive, Plastic, Trajectory Number: 1, WT Speed: 90 , AoA: -5 , Back of Bay
Sweep Angle
C_N
C_N (filtered)
Sweep Angle (deg)
C_N
Time (sec)

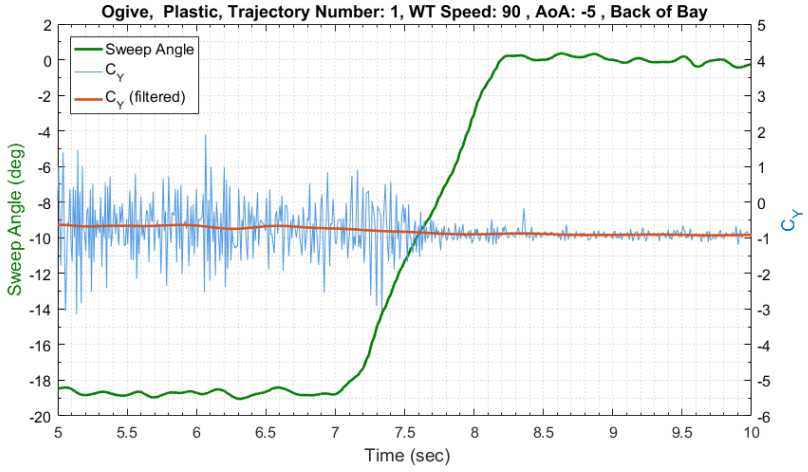
Ogive, Plastic, Trajectory Number: 1, WT Speed: 90 , AoA: -5 , Back of Bay
Sweep Angle
C_Y
C_Y (filtered)
Sweep Angle (deg)
C_Y
Time (sec)

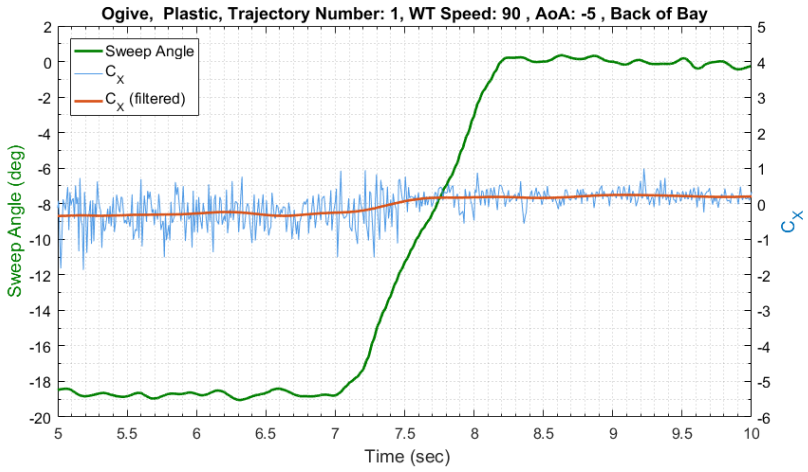
Ogive, Plastic, Trajectory Number: 1, WT Speed: 90 , AoA: -5 , Back of Bay
Sweep Angle
C_X
C_X (filtered)
Sweep Angle (deg)
C_X
Time (sec)

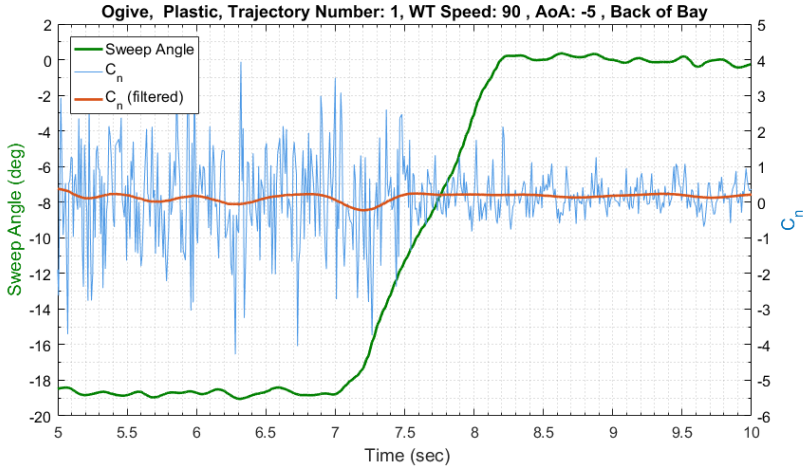
Ogive, Plastic, Trajectory Number: 1, WT Speed: 90 , AoA: -5 , Back of Bay
Sweep Angle
C_n
C_n (filtered)
Sweep Angle (deg)
C_n
Time (sec)

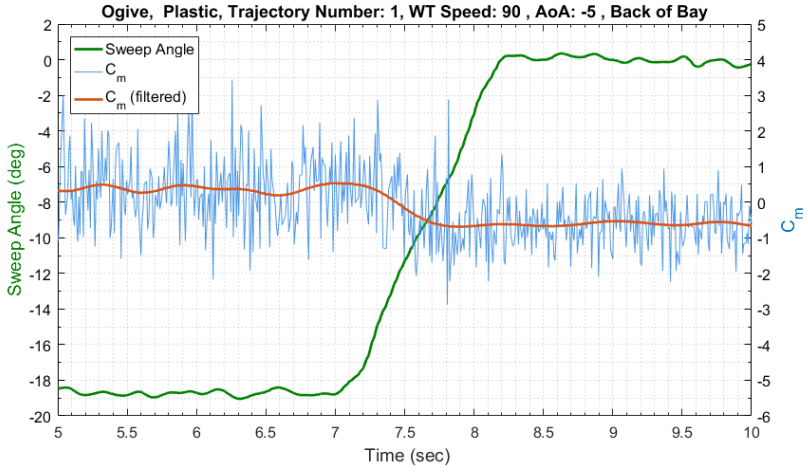
Ogive, Plastic, Trajectory Number: 1, WT Speed: 90 , AoA: -5 , Back of Bay
Sweep Angle
C_m
C_m (filtered)
Sweep Angle (deg)
C_m
Time (sec)

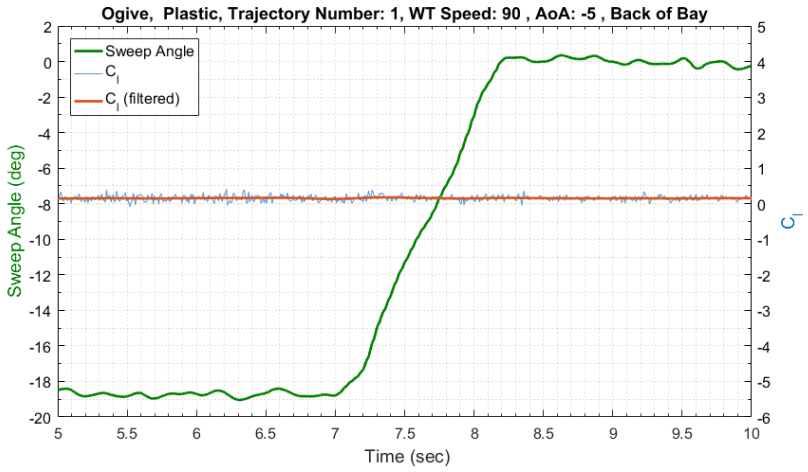
Ogive, Plastic, Trajectory Number: 1, WT Speed: 90 , AoA: -5 , Back of Bay
Sweep Angle
C_l
C_l (filtered)
Sweep Angle (deg)
C_l
Time (sec)

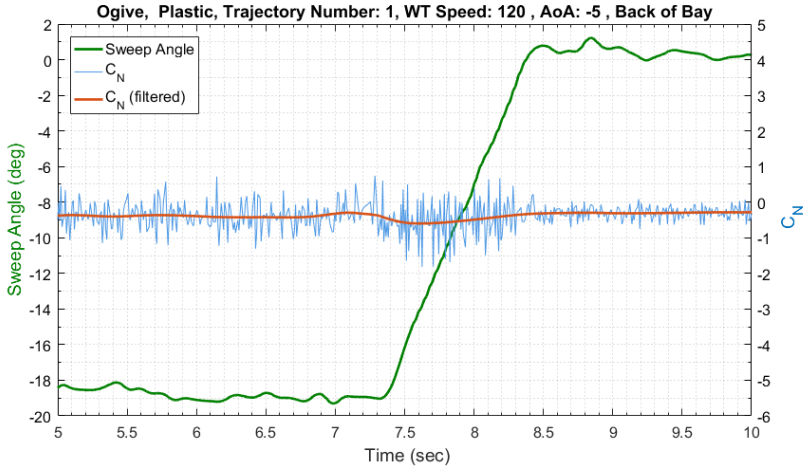
Ogive, Plastic, Trajectory Number: 1, WT Speed: 120 , AoA: -5 , Back of Bay
Sweep Angle
C_N
C_N (filtered)
Sweep Angle (deg)
C_N
Time (sec)

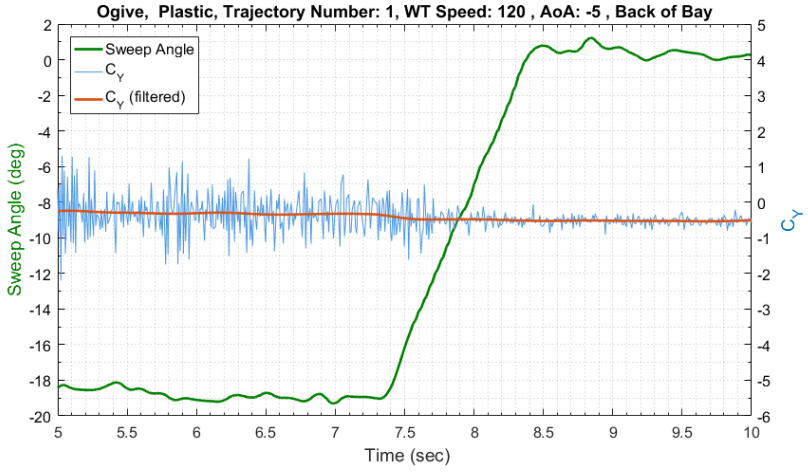
Ogive, Plastic, Trajectory Number: 1, WT Speed: 120 , AoA: -5 , Back of Bay
Sweep Angle
C_Y
C_Y (filtered)
Sweep Angle (deg)
C_Y
Time (sec)

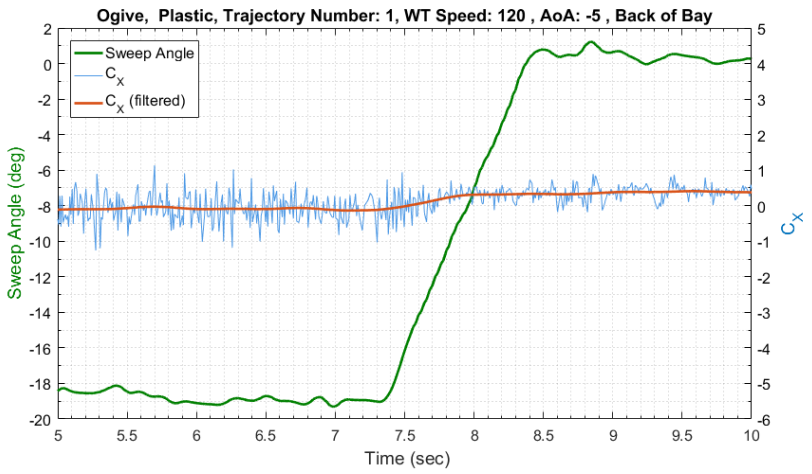
Ogive, Plastic, Trajectory Number: 1, WT Speed: 120 , AoA: -5 , Back of Bay
Sweep Angle
C_X
C_X (filtered)
Sweep Angle (deg)
C_X
Time (sec)

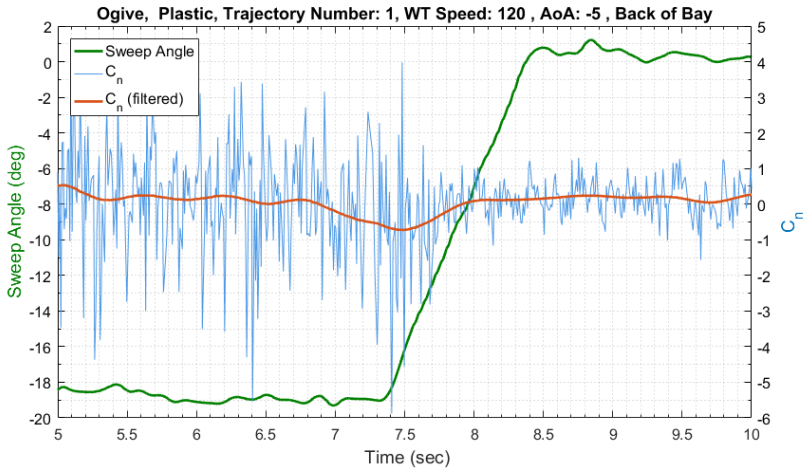
Ogive, Plastic, Trajectory Number: 1, WT Speed: 120 , AoA: -5 , Back of Bay
Sweep Angle
C_n
C_n (filtered)
Sweep Angle (deg)
C_n
Time (sec)

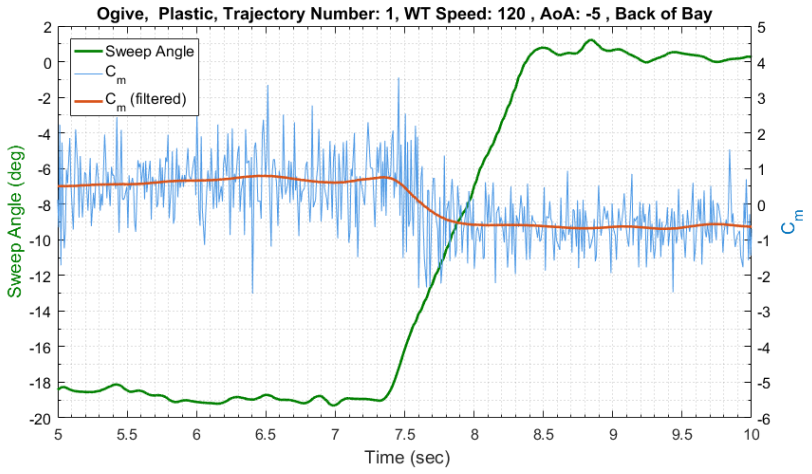
Ogive, Plastic, Trajectory Number: 1, WT Speed: 120 , AoA: -5 , Back of Bay
Sweep Angle
C_m
C_m (filtered)
Sweep Angle (deg)
C_m
Time (sec)

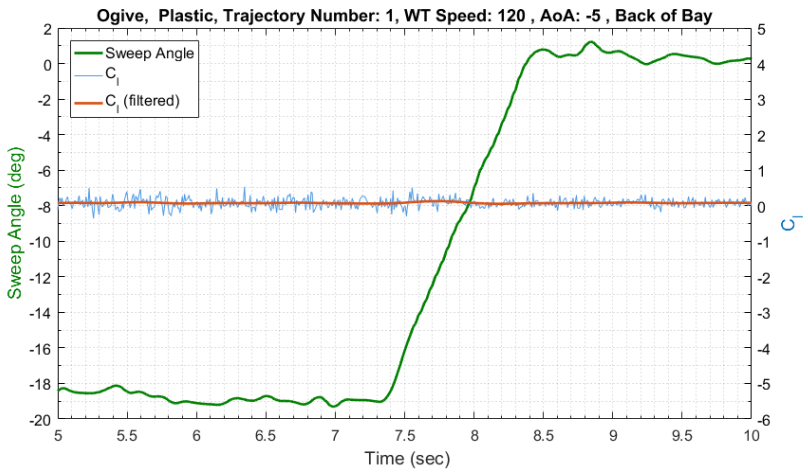
Ogive, Plastic, Trajectory Number: 1, WT Speed: 120 , AoA: -5 , Back of Bay
Sweep Angle
C_l
C_l (filtered)
Sweep Angle (deg)
C_l
Time (sec)

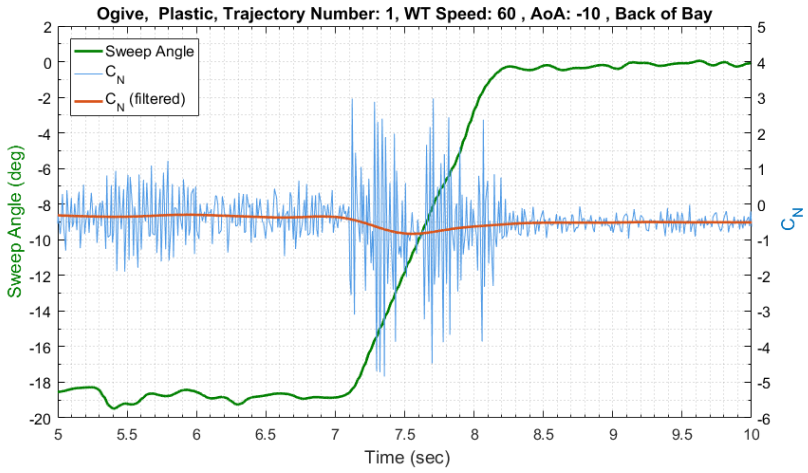
Ogive, Plastic, Trajectory Number: 1, WT Speed: 60 , AoA: -10 , Back of Bay
Sweep Angle
C_N
C_N (filtered)
Sweep Angle (deg)
C_N
Time (sec)

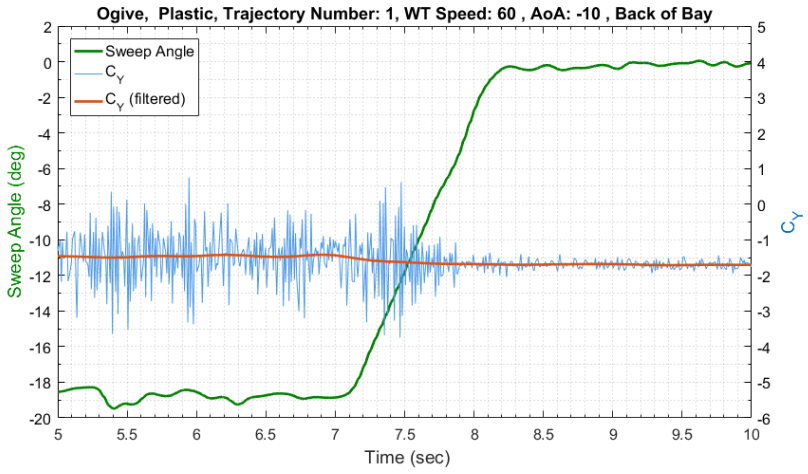
Ogive, Plastic, Trajectory Number: 1, WT Speed: 60 , AoA: -10 , Back of Bay
Sweep Angle
C_Y
C_Y (filtered)
Sweep Angle (deg)
C_Y
Time (sec)

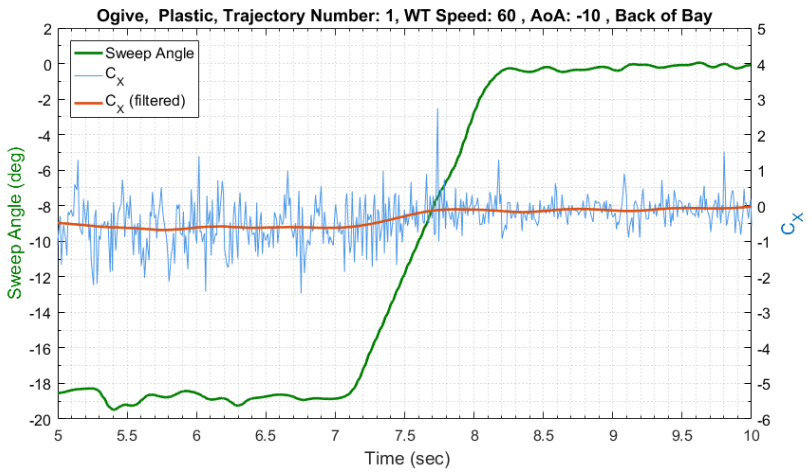
Ogive, Plastic, Trajectory Number: 1, WT Speed: 60 , AoA: -10 , Back of Bay
Sweep Angle
C_X
C_X (filtered)
Sweep Angle (deg)
C_X
Time (sec)

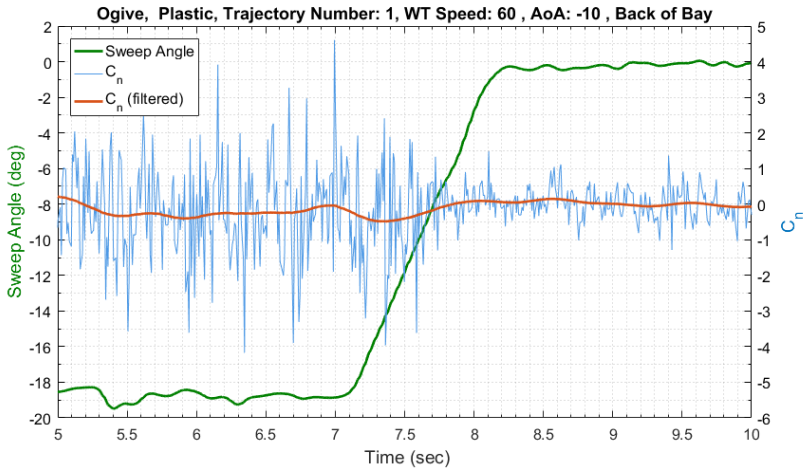
Ogive, Plastic, Trajectory Number: 1, WT Speed: 60 , AoA: -10 , Back of Bay
Sweep Angle
C_n
C_n (filtered)
Sweep Angle (deg)
C_n
Time (sec)

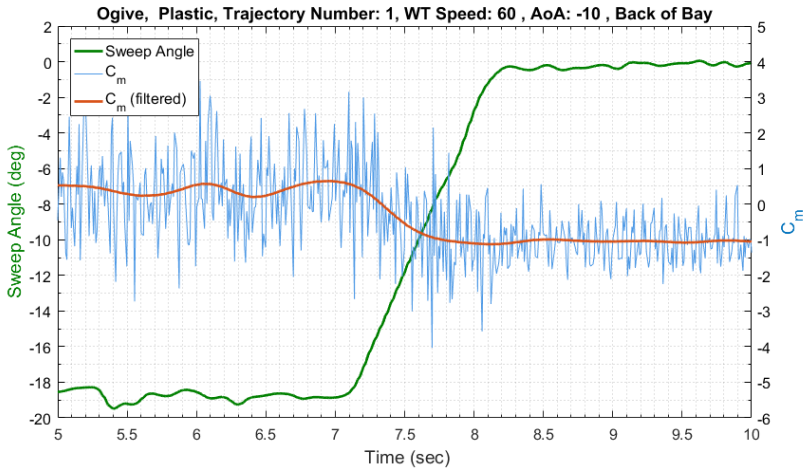
Ogive, Plastic, Trajectory Number: 1, WT Speed: 60 , AoA: -10 , Back of Bay
Sweep Angle
C_m
C_m (filtered)
Sweep Angle (deg)
C_m
Time (sec)

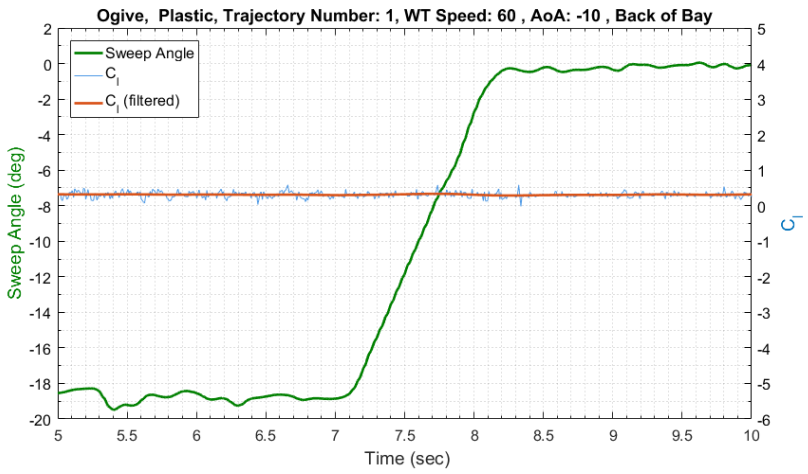
Ogive, Plastic, Trajectory Number: 1, WT Speed: 60 , AoA: -10 , Back of Bay
Sweep Angle
C_l
C_l (filtered)
Sweep Angle (deg)
C_l
Time (sec)

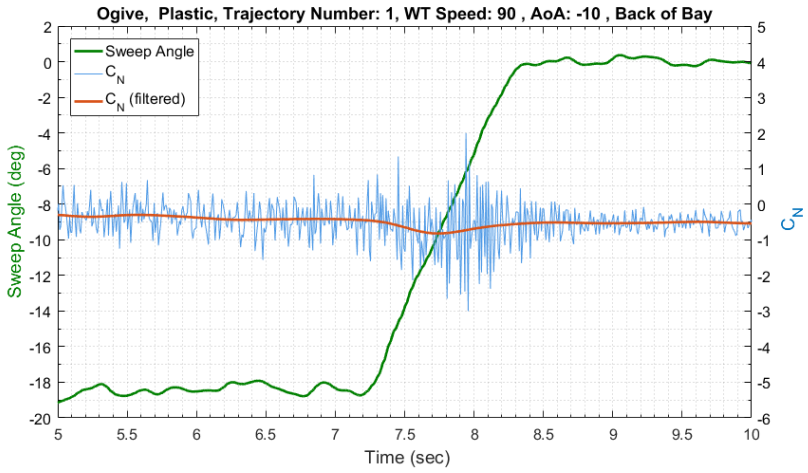
Ogive, Plastic, Trajectory Number: 1, WT Speed: 90 , AoA: -10 , Back of Bay
Sweep Angle
C_N
C_N (filtered)
Sweep Angle (deg)
C_N
Time (sec)

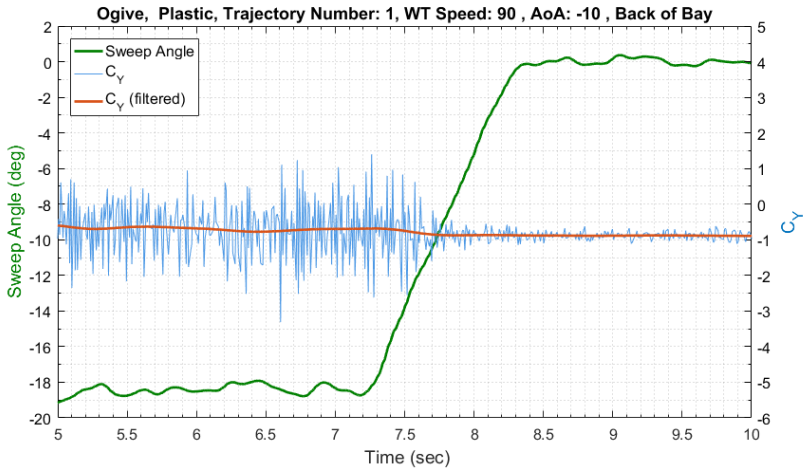
Ogive, Plastic, Trajectory Number: 1, WT Speed: 90 , AoA: -10 , Back of Bay
Sweep Angle
C_Y
C_Y (filtered)
Sweep Angle (deg)
C_Y
Time (sec)

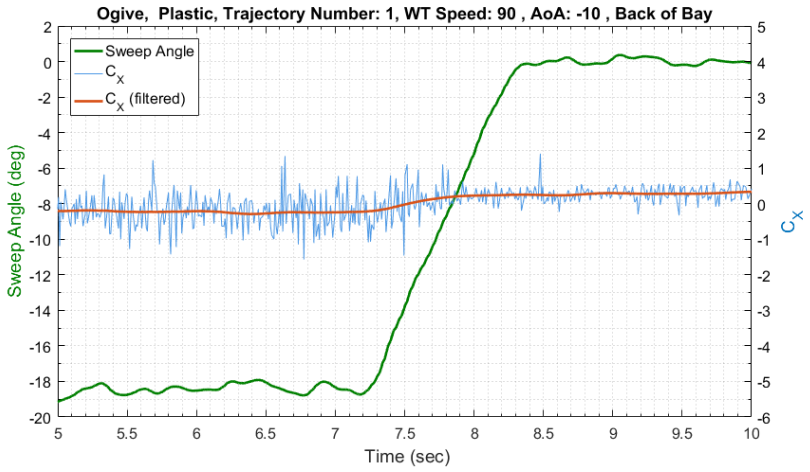
Ogive, Plastic, Trajectory Number: 1, WT Speed: 90 , AoA: -10 , Back of Bay
Sweep Angle
C_X
C_X (filtered)
Sweep Angle (deg)
C_X
Time (sec)

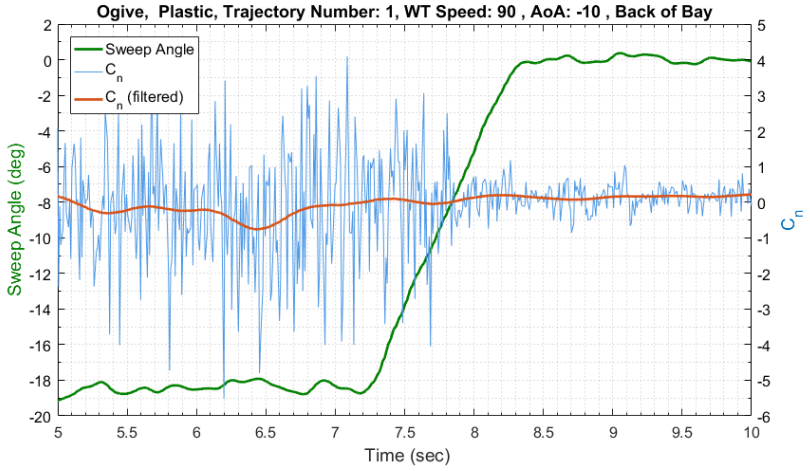
Ogive, Plastic, Trajectory Number: 1, WT Speed: 90 , AoA: -10 , Back of Bay
Sweep Angle
C_n
C_n (filtered)
Sweep Angle (deg)
C_n
Time (sec)

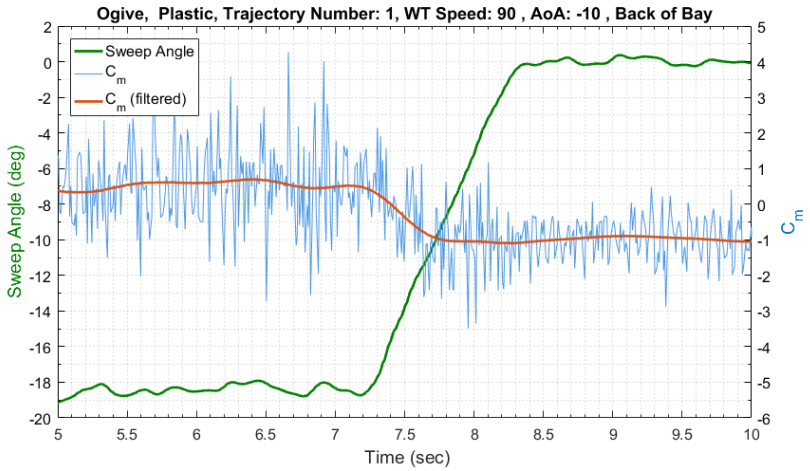
Ogive, Plastic, Trajectory Number: 1, WT Speed: 90 , AoA: -10 , Back of Bay
Sweep Angle
C_m
C_m (filtered)
Sweep Angle (deg)
C_m
Time (sec)

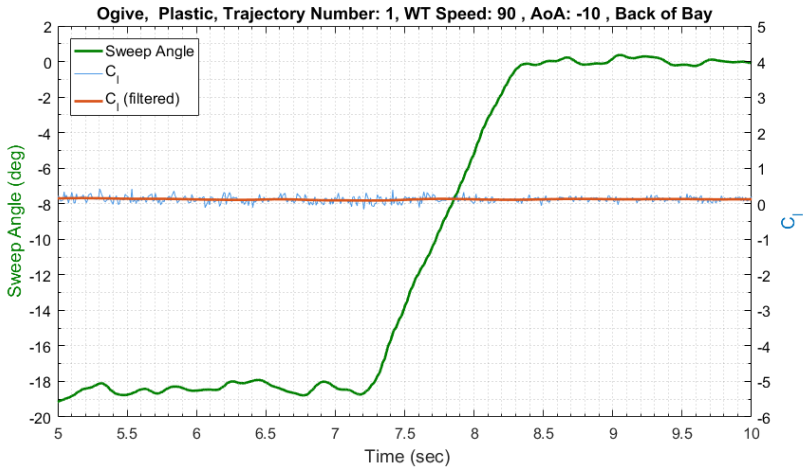
Ogive, Plastic, Trajectory Number: 1, WT Speed: 90 , AoA: -10 , Back of Bay
Sweep Angle
C_l
C_l (filtered)
Sweep Angle (deg)
C_l
Time (sec)

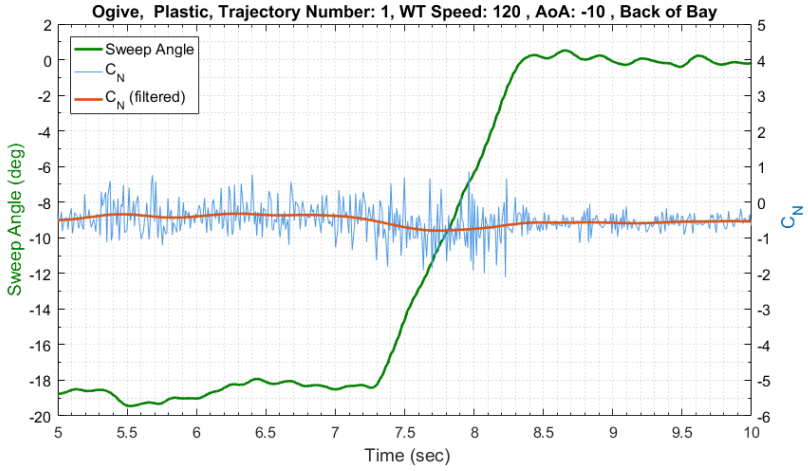
Ogive, Plastic, Trajectory Number: 1, WT Speed: 120 , AoA: -10 , Back of Bay
Sweep Angle
C_N
C_N (filtered)
Sweep Angle (deg)
C_N
Time (sec)

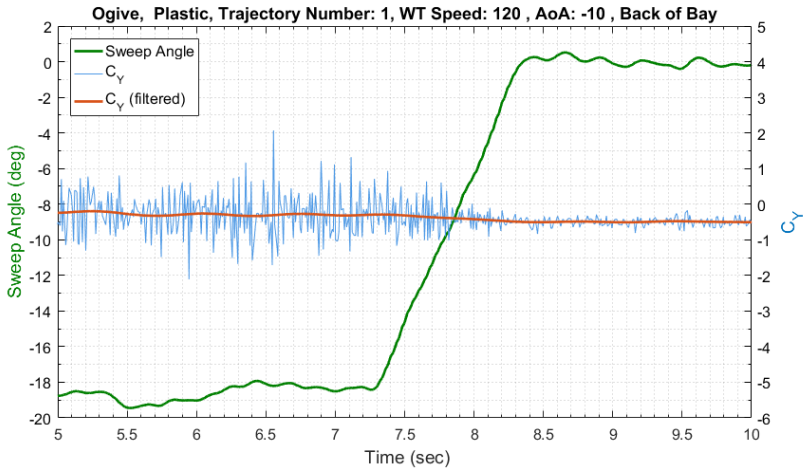
Ogive, Plastic, Trajectory Number: 1, WT Speed: 120 , AoA: -10 , Back of Bay
Sweep Angle
C_Y
C_Y (filtered)
Sweep Angle (deg)
C_Y
Time (sec)

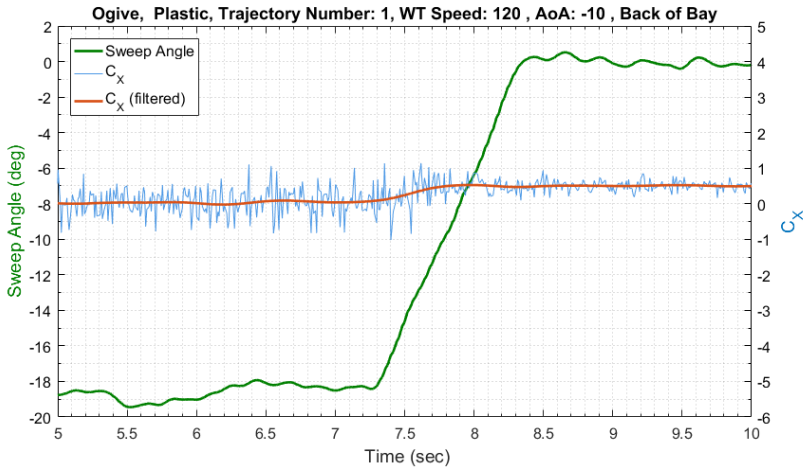
Ogive, Plastic, Trajectory Number: 1, WT Speed: 120 , AoA: -10 , Back of Bay
Sweep Angle
C_X
C_X (filtered)
Sweep Angle (deg)
C_X
Time (sec)

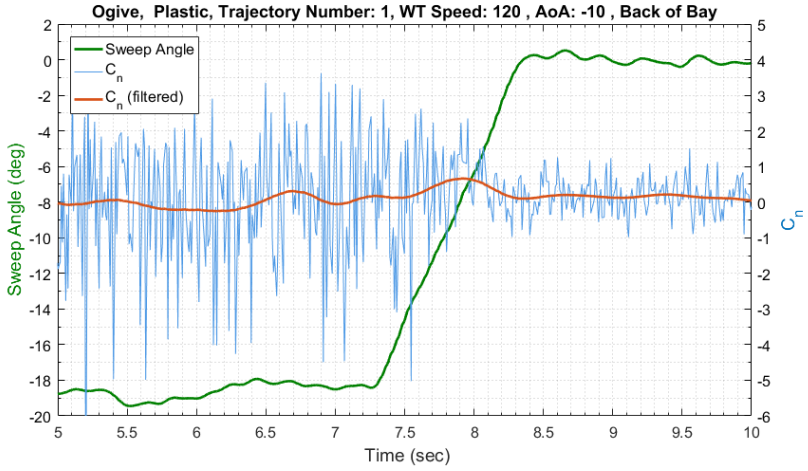
Ogive, Plastic, Trajectory Number: 1, WT Speed: 120 , AoA: -10 , Back of Bay
Sweep Angle
C_n
C_n (filtered)
Sweep Angle (deg)
C_n
Time (sec)

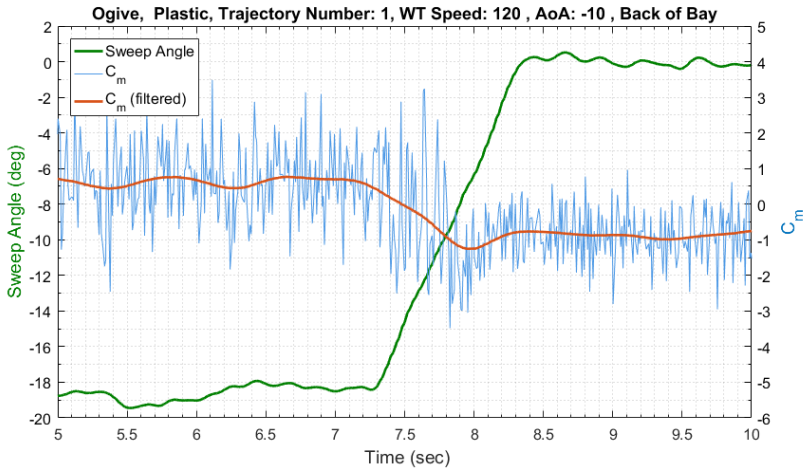
Ogive, Plastic, Trajectory Number: 1, WT Speed: 120 , AoA: -10 , Back of Bay
Sweep Angle
C_m
C_m (filtered)
Sweep Angle (deg)
C_m
Time (sec)

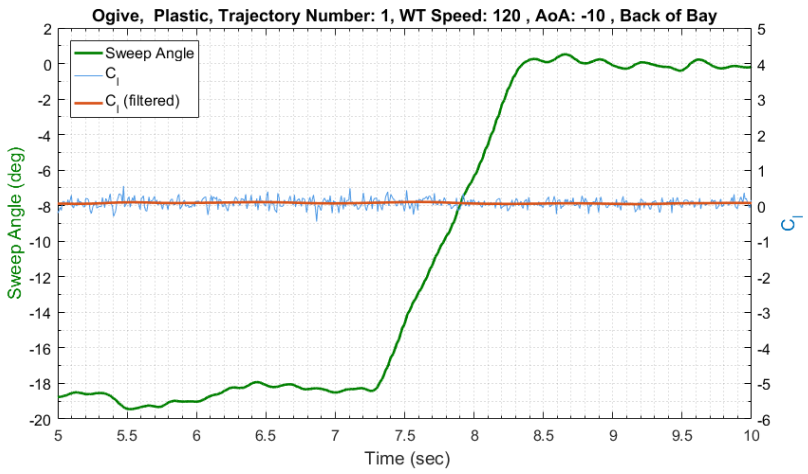
Ogive, Plastic, Trajectory Number: 1, WT Speed: 120 , AoA: -10 , Back of Bay
Sweep Angle
C_l
C_l (filtered)
Sweep Angle (deg)
C_l
Time (sec)

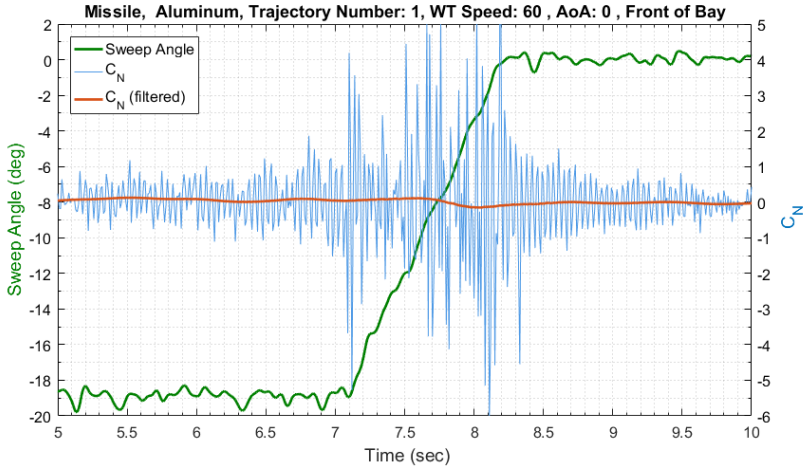
Missile, Aluminum, Trajectory Number: 1, WT Speed: 60 , AoA: 0 , Front of Bay
Sweep Angle
C_N
C_N (filtered)
Sweep Angle (deg)
C_N
Time (sec)

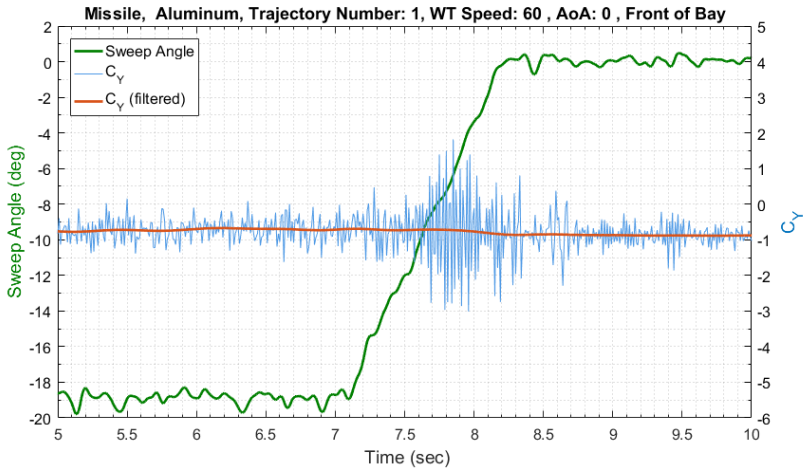
Missile, Aluminum, Trajectory Number: 1, WT Speed: 60 , AoA: 0 , Front of Bay
Sweep Angle
C_Y
C_Y (filtered)
Sweep Angle (deg)
C_Y
Time (sec)

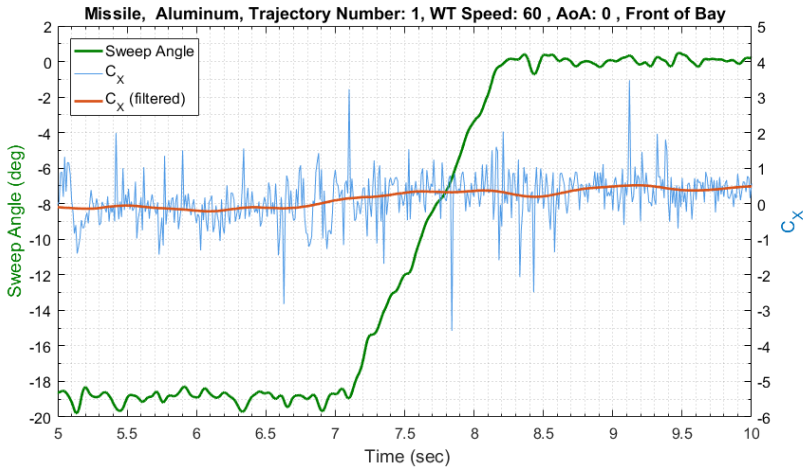
Missile, Aluminum, Trajectory Number: 1, WT Speed: 60 , AoA: 0 , Front of Bay
Sweep Angle
C_X
C_X (filtered)
Sweep Angle (deg)
C_X
Time (sec)

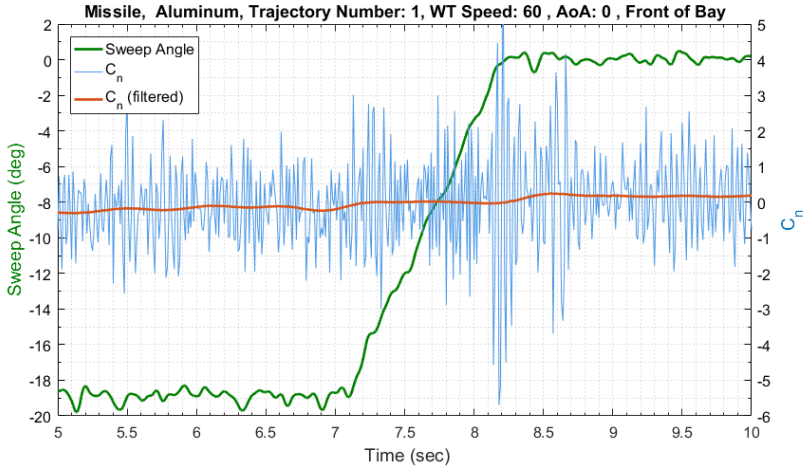
Missile, Aluminum, Trajectory Number: 1, WT Speed: 60 , AoA: 0 , Front of Bay
Sweep Angle
C_n
C_n (filtered)
Sweep Angle (deg)
C_n
Time (sec)

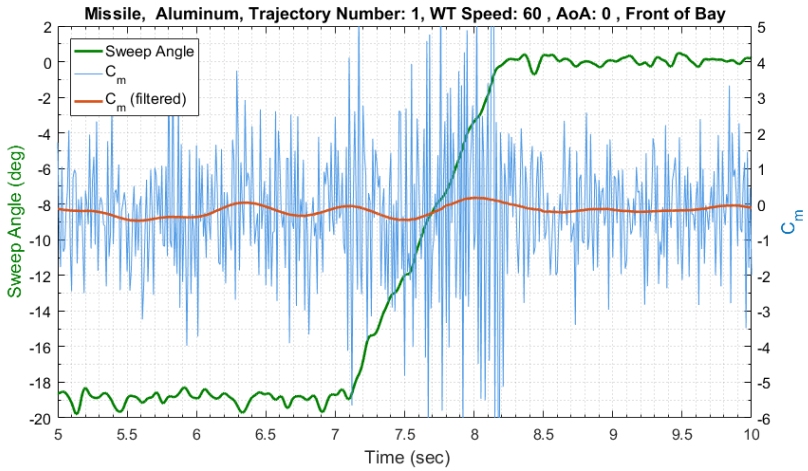
Missile, Aluminum, Trajectory Number: 1, WT Speed: 60 , AoA: 0 , Front of Bay
Sweep Angle
C_m
C_m (filtered)
Sweep Angle (deg)
C_m
Time (sec)

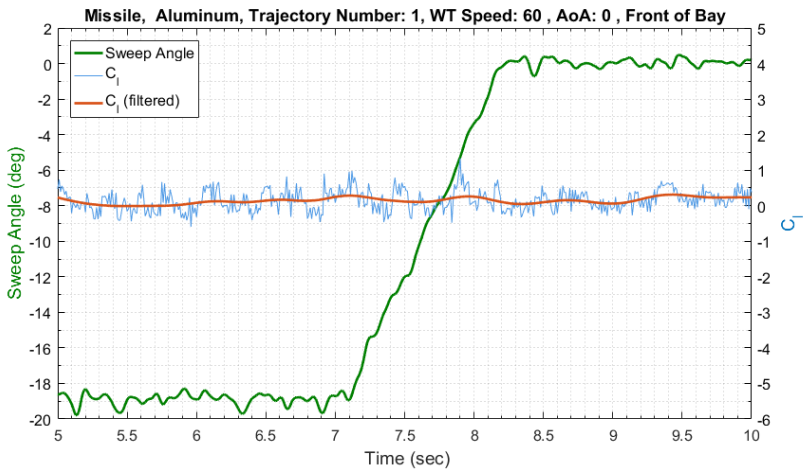
Missile, Aluminum, Trajectory Number: 1, WT Speed: 60 , AoA: 0 , Front of Bay
Sweep Angle
C_l
C_l (filtered)
Sweep Angle (deg)
C_l
Time (sec)

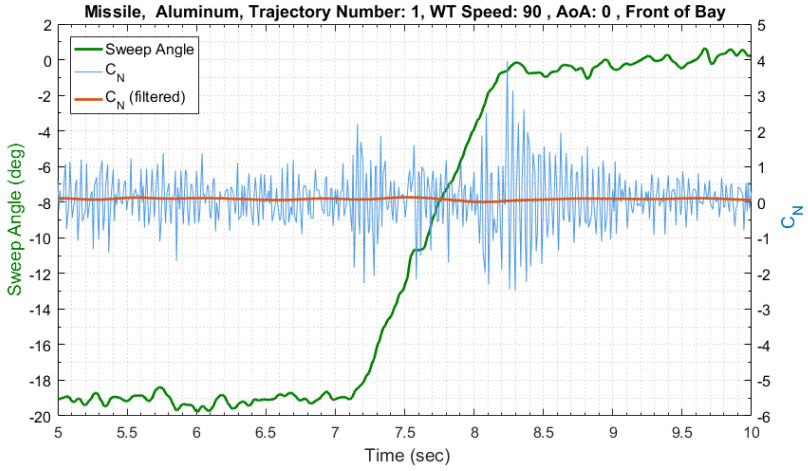
Missile, Aluminum, Trajectory Number: 1, WT Speed: 90 , AoA: 0 , Front of Bay
Sweep Angle
C_N
C_N (filtered)
Sweep Angle (deg)
C_N
Time (sec)

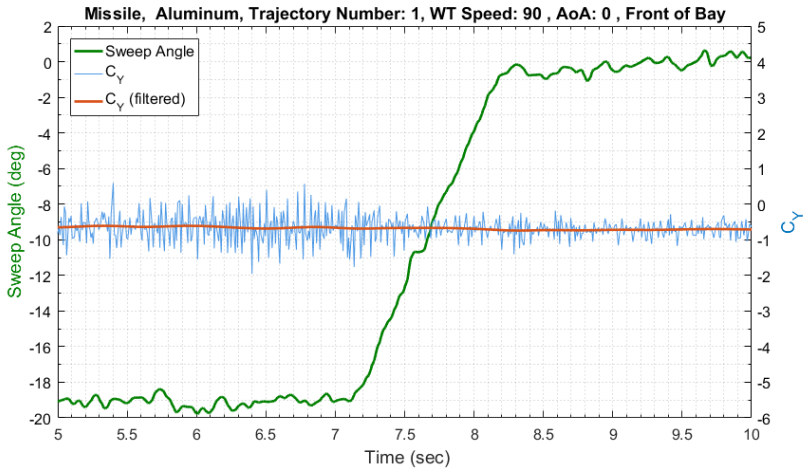
Missile, Aluminum, Trajectory Number: 1, WT Speed: 90 , AoA: 0 , Front of Bay
Sweep Angle
C_Y
C_Y (filtered)
Sweep Angle (deg)
C_Y
Time (sec)

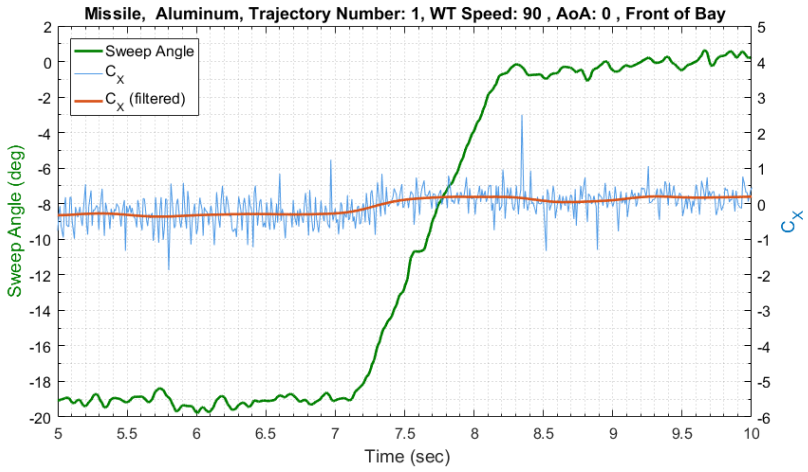
Missile, Aluminum, Trajectory Number: 1, WT Speed: 90 , AoA: 0 , Front of Bay
Sweep Angle
C_X
C_X (filtered)
Sweep Angle (deg)
C_X
Time (sec)

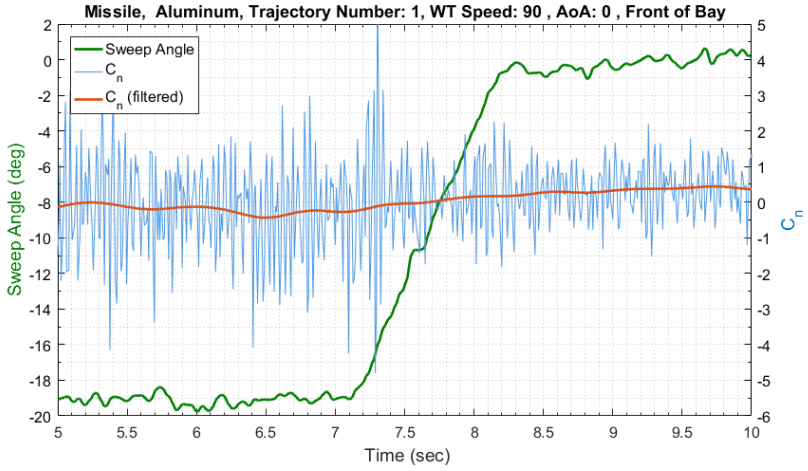
Missile, Aluminum, Trajectory Number: 1, WT Speed: 90 , AoA: 0 , Front of Bay
Sweep Angle
C_n
C_n (filtered)
Sweep Angle (deg)
C_n
Time (sec)

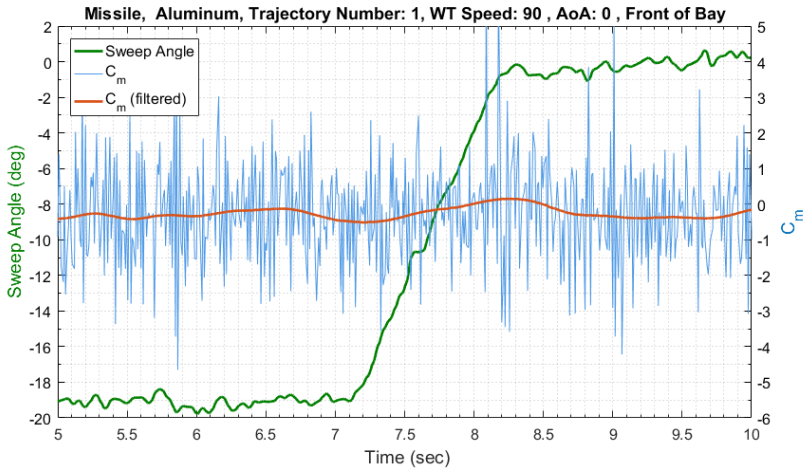
Missile, Aluminum, Trajectory Number: 1, WT Speed: 90 , AoA: 0 , Front of Bay
Sweep Angle
C_m
C_m (filtered)
Sweep Angle (deg)
C_m
Time (sec)

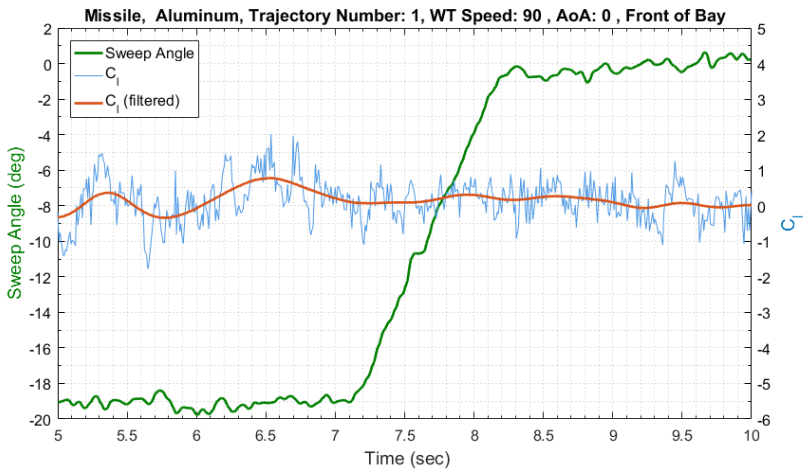
Missile, Aluminum, Trajectory Number: 1, WT Speed: 90 , AoA: 0 , Front of Bay
Sweep Angle
C_l
C_l (filtered)
Sweep Angle (deg)
C_l
Time (sec)

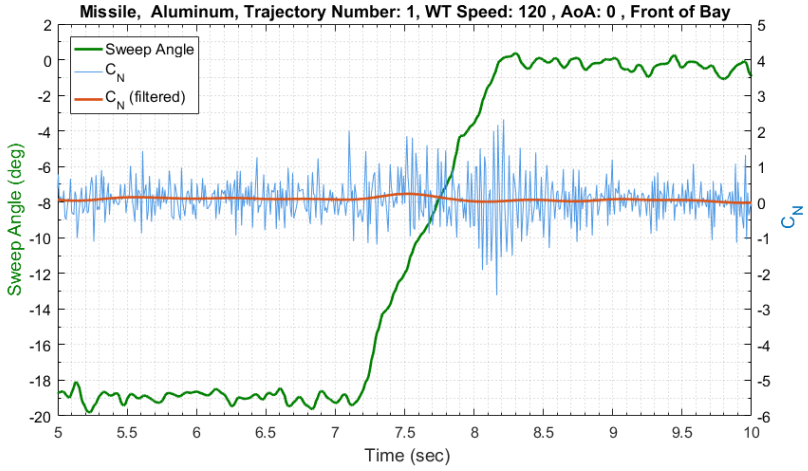
Missile, Aluminum, Trajectory Number: 1, WT Speed: 120 , AoA: 0 , Front of Bay
Sweep Angle
C_N
C_N (filtered)
Sweep Angle (deg)
C_N
Time (sec)

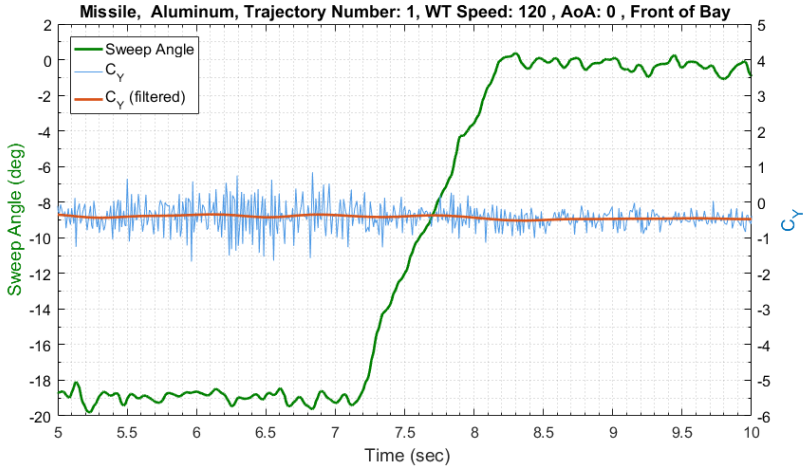
Missile, Aluminum, Trajectory Number: 1, WT Speed: 120 , AoA: 0 , Front of Bay
Sweep Angle
C_Y
C_Y (filtered)
Sweep Angle (deg)
C_Y
Time (sec)

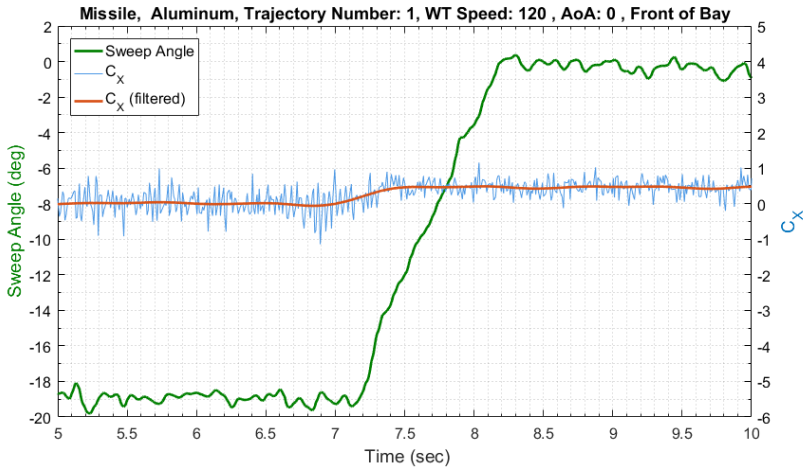
Missile, Aluminum, Trajectory Number: 1, WT Speed: 120 , AoA: 0 , Front of Bay
Sweep Angle
C_X
C_X (filtered)
Sweep Angle (deg)
C_X
Time (sec)

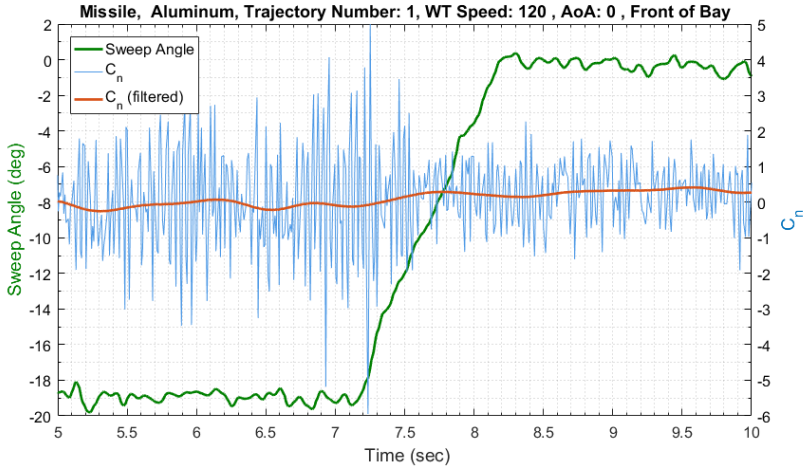
Missile, Aluminum, Trajectory Number: 1, WT Speed: 120 , AoA: 0 , Front of Bay
Sweep Angle
C_n
C_n (filtered)
Sweep Angle (deg)
C_n
Time (sec)

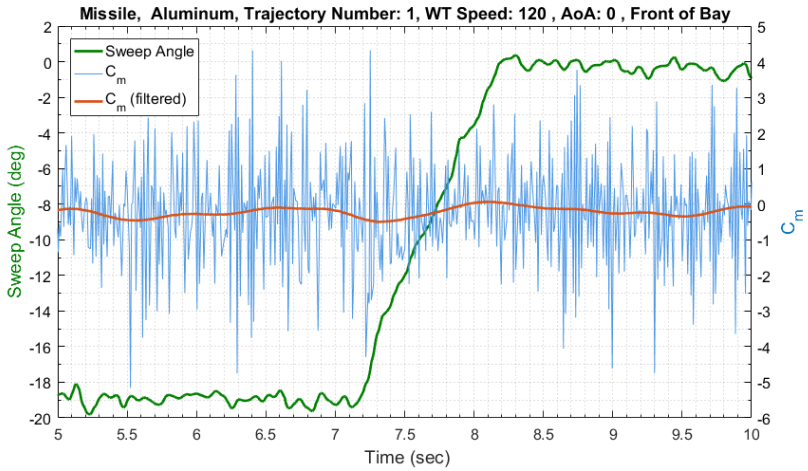
Missile, Aluminum, Trajectory Number: 1, WT Speed: 120 , AoA: 0 , Front of Bay
Sweep Angle
C_m
C_m (filtered)
Sweep Angle (deg)
C_m
Time (sec)

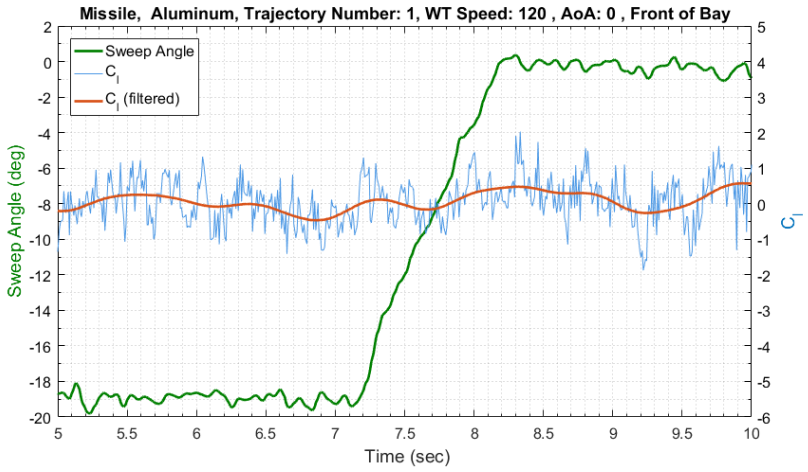
Missile, Aluminum, Trajectory Number: 1, WT Speed: 120 , AoA: 0 , Front of Bay
Sweep Angle
C_l
C_l (filtered)
Sweep Angle (deg)
C_l
Time (sec)

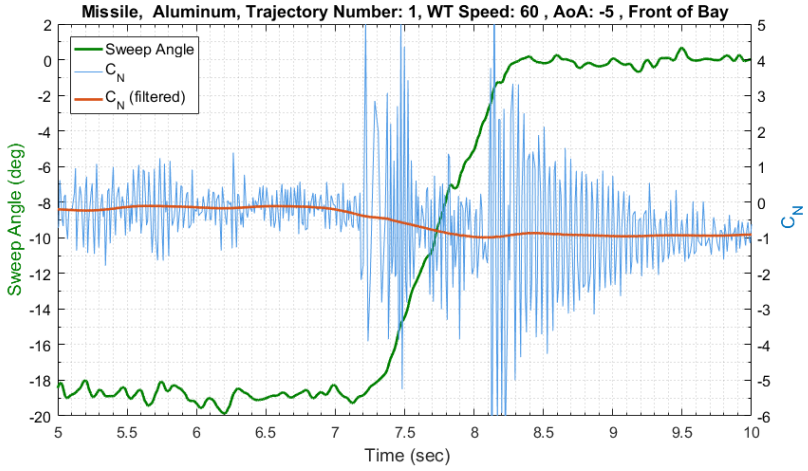
Missile, Aluminum, Trajectory Number: 1, WT Speed: 60 , AoA: -5 , Front of Bay
Sweep Angle
C_N
C_N (filtered)
Sweep Angle (deg)
C_N
Time (sec)

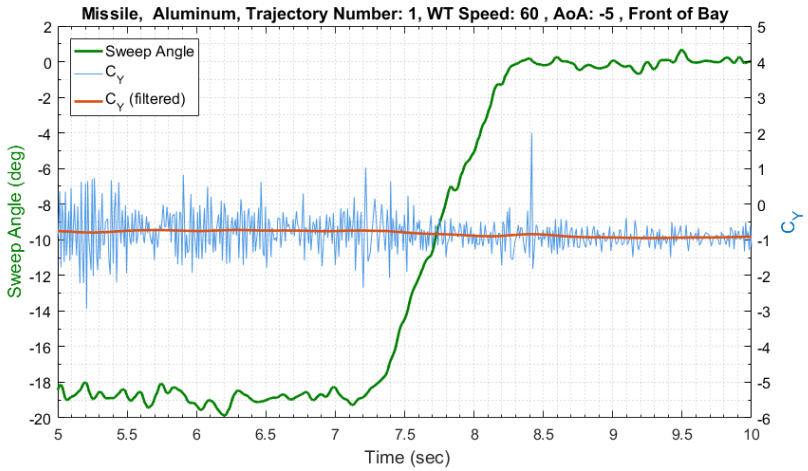
Missile, Aluminum, Trajectory Number: 1, WT Speed: 60 , AoA: -5 , Front of Bay
Sweep Angle
C_Y
C_Y (filtered)
Sweep Angle (deg)
C_Y
Time (sec)

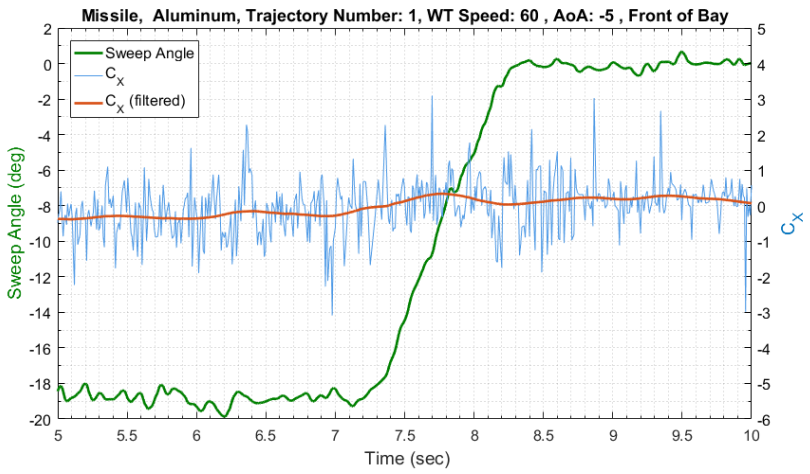
Missile, Aluminum, Trajectory Number: 1, WT Speed: 60 , AoA: -5 , Front of Bay
Sweep Angle
C_X
C_X (filtered)
Sweep Angle (deg)
C_X
Time (sec)

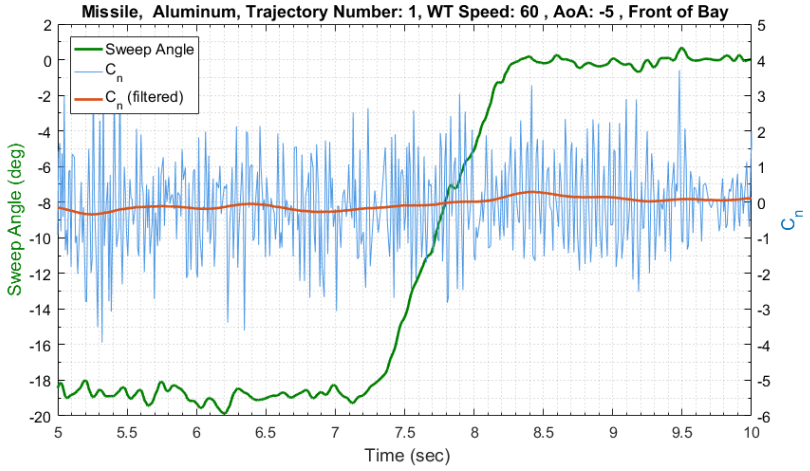
Missile, Aluminum, Trajectory Number: 1, WT Speed: 60 , AoA: -5 , Front of Bay
Sweep Angle
C_n
C_n (filtered)
Sweep Angle (deg)
C_n
Time (sec)

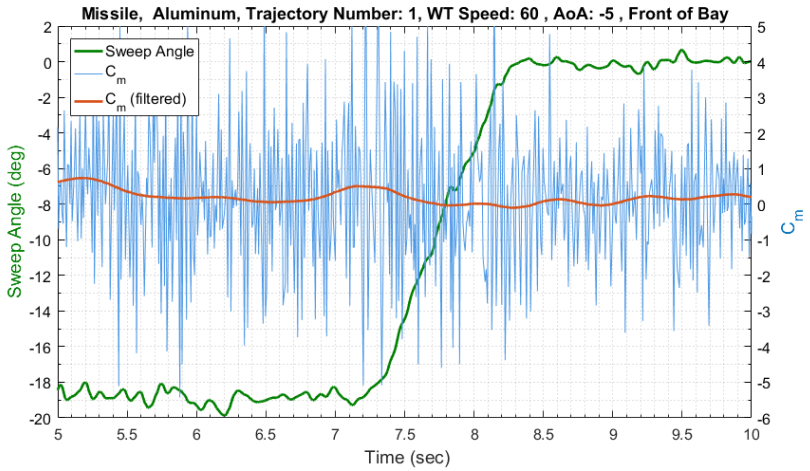
Missile, Aluminum, Trajectory Number: 1, WT Speed: 60 , AoA: -5 , Front of Bay
Sweep Angle
C_m
C_m (filtered)
Sweep Angle (deg)
C_m
Time (sec)

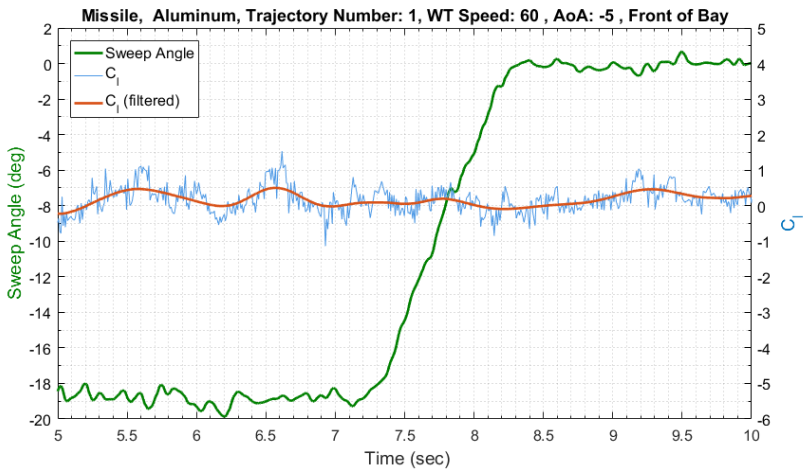
Missile, Aluminum, Trajectory Number: 1, WT Speed: 60 , AoA: -5 , Front of Bay
Sweep Angle
C_l
C_l (filtered)
Sweep Angle (deg)
C_l
Time (sec)

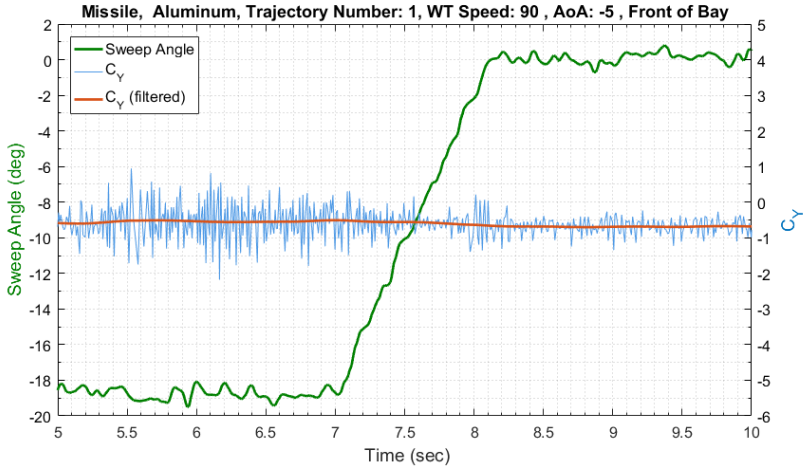
Missile, Aluminum, Trajectory Number: 1, WT Speed: 90 , AoA: -5 , Front of Bay
Sweep Angle
C_Y
C_Y (filtered)
Sweep Angle (deg)
C_Y
Time (sec)

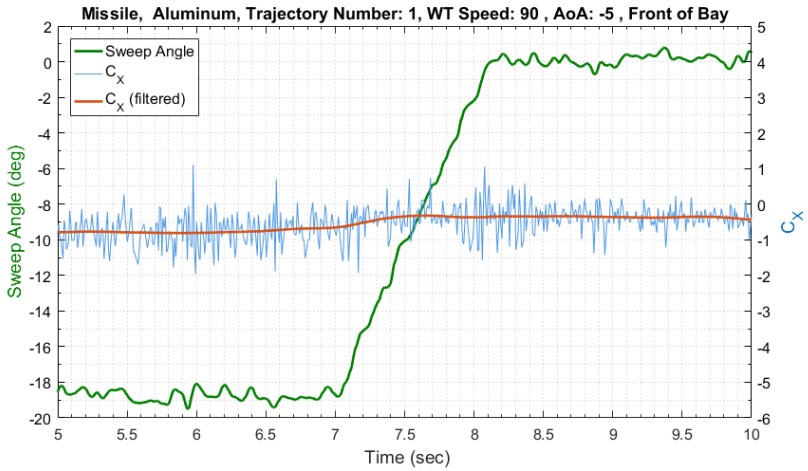
Missile, Aluminum, Trajectory Number: 1, WT Speed: 90 , AoA: -5 , Front of Bay
Sweep Angle
C_X
C_X (filtered)
Sweep Angle (deg)
C_X
Time (sec)

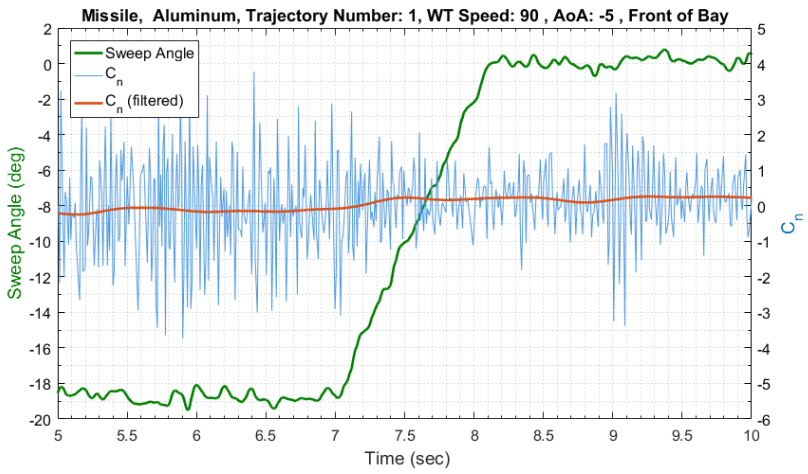
Missile, Aluminum, Trajectory Number: 1, WT Speed: 90 , AoA: -5 , Front of Bay
Sweep Angle
C_n
C_n (filtered)
Sweep Angle (deg)
C_n
Time (sec)

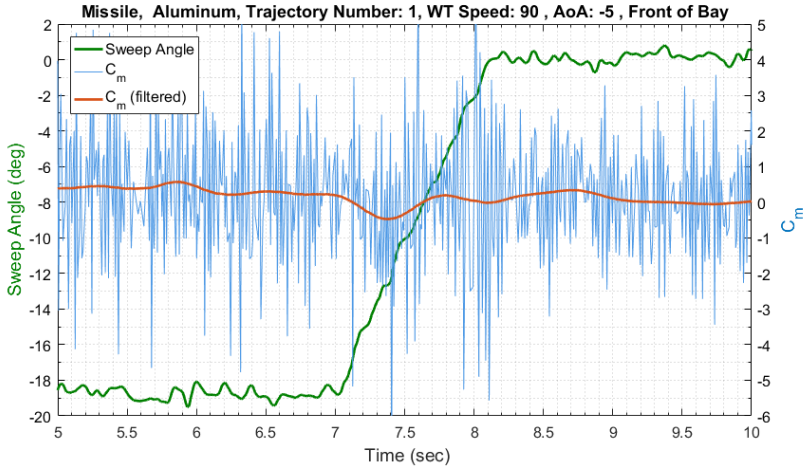
Missile, Aluminum, Trajectory Number: 1, WT Speed: 90 , AoA: -5 , Front of Bay
Sweep Angle
C_m
C_m (filtered)
Sweep Angle (deg)
C_m
Time (sec)

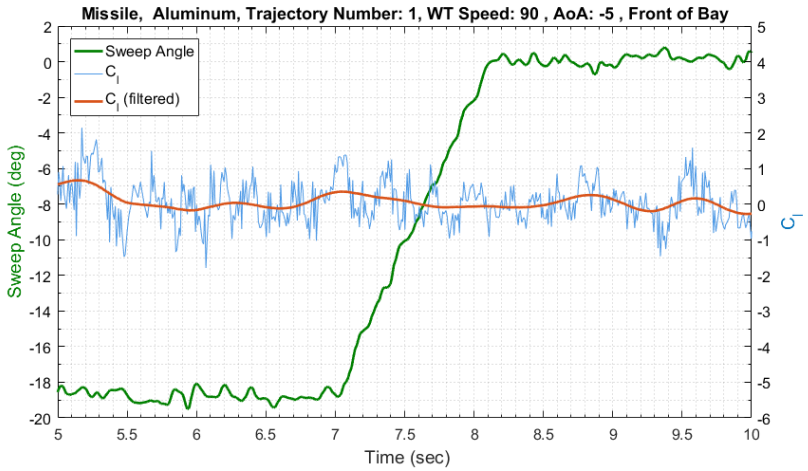
Missile, Aluminum, Trajectory Number: 1, WT Speed: 90 , AoA: -5 , Front of Bay
Sweep Angle
C_l
C_l (filtered)
Sweep Angle (deg)
C_l
Time (sec)

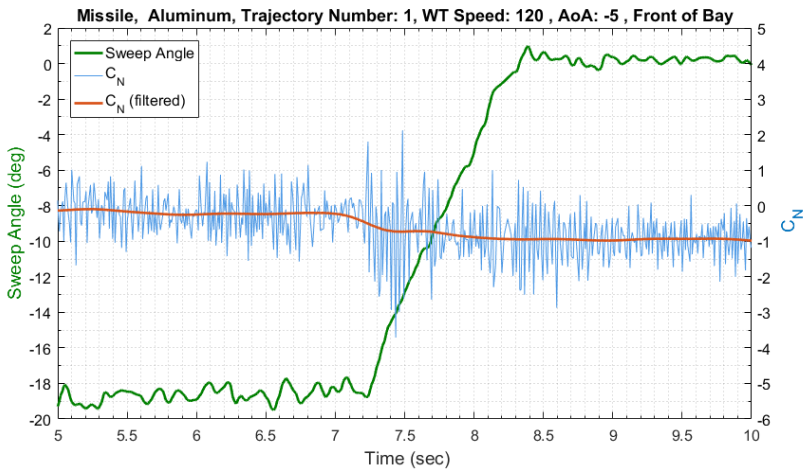
Missile, Aluminum, Trajectory Number: 1, WT Speed: 120 , AoA: -5 , Front of Bay
Sweep Angle
C_N
C_N (filtered)
Sweep Angle (deg)
C_N
Time (sec)

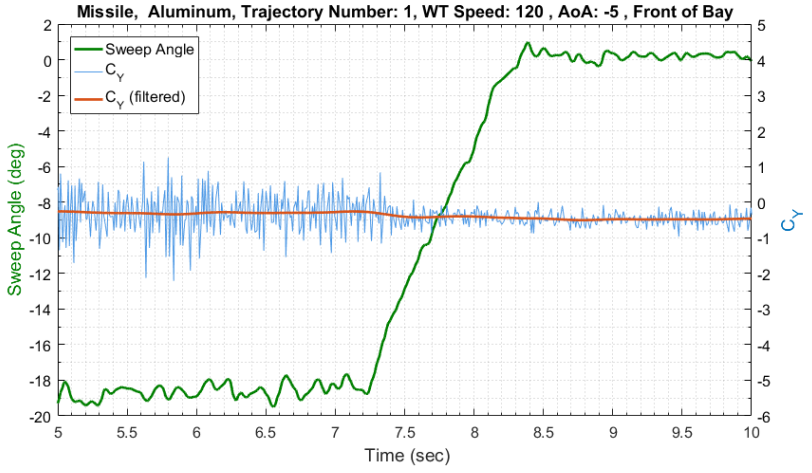
Missile, Aluminum, Trajectory Number: 1, WT Speed: 120 , AoA: -5 , Front of Bay
Sweep Angle
C_Y
C_Y (filtered)
Sweep Angle (deg)
C_Y
Time (sec)

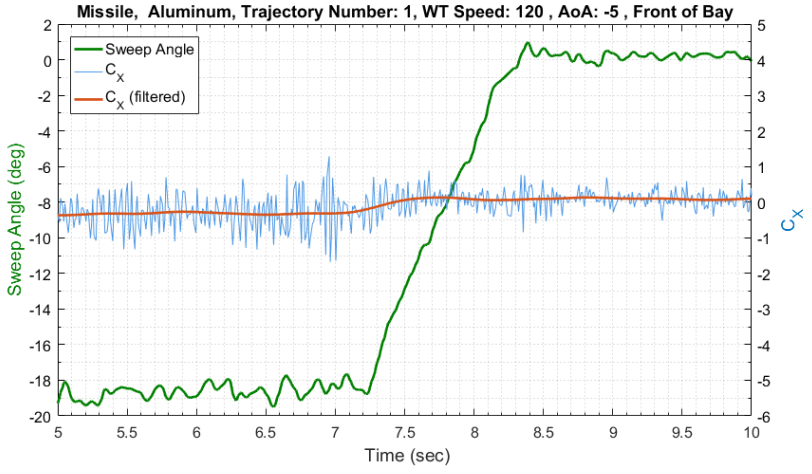
Missile, Aluminum, Trajectory Number: 1, WT Speed: 120 , AoA: -5 , Front of Bay
Sweep Angle
C_X
C_X (filtered)
Sweep Angle (deg)
C_X
Time (sec)

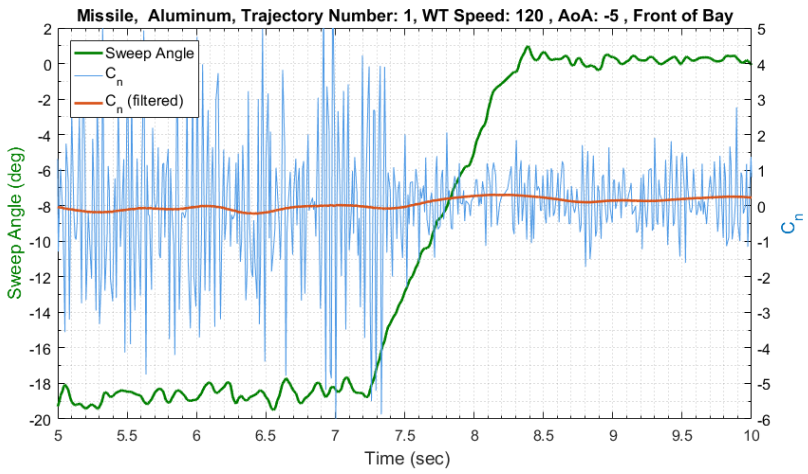
Missile, Aluminum, Trajectory Number: 1, WT Speed: 120 , AoA: -5 , Front of Bay
Sweep Angle
C_n
C_n (filtered)
Sweep Angle (deg)
C_n
Time (sec)

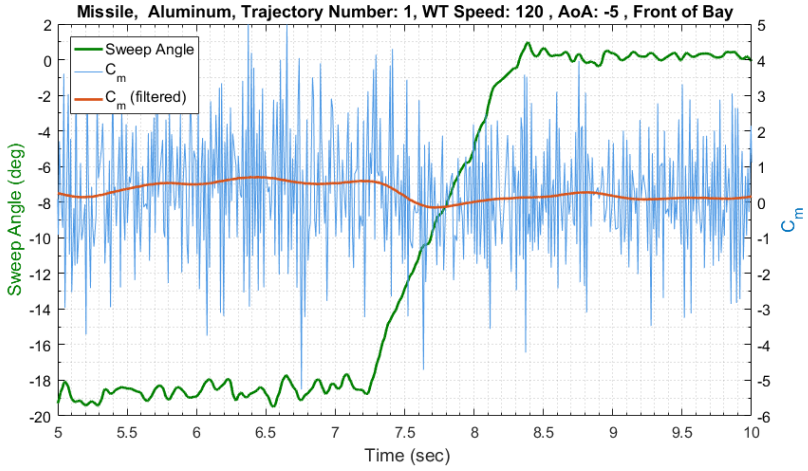
Missile, Aluminum, Trajectory Number: 1, WT Speed: 120 , AoA: -5 , Front of Bay
Sweep Angle
C_m
C_m (filtered)
Sweep Angle (deg)
C_m
Time (sec)

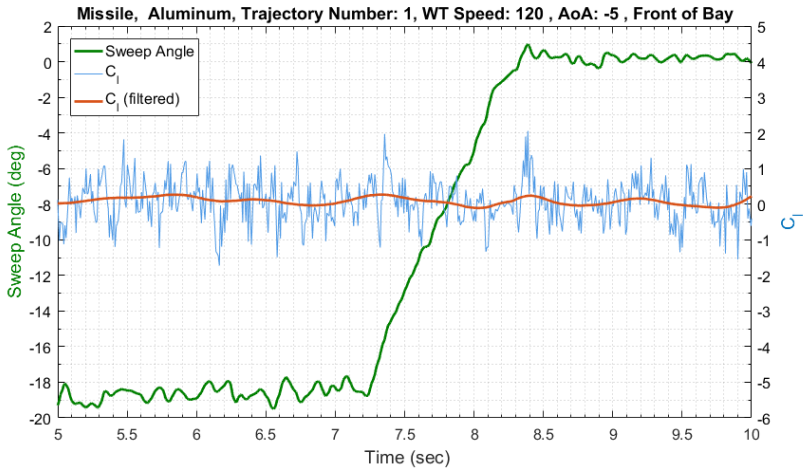
Missile, Aluminum, Trajectory Number: 1, WT Speed: 120 , AoA: -5 , Front of Bay
Sweep Angle
C_l
C_l (filtered)
Sweep Angle (deg)
C_l
Time (sec)

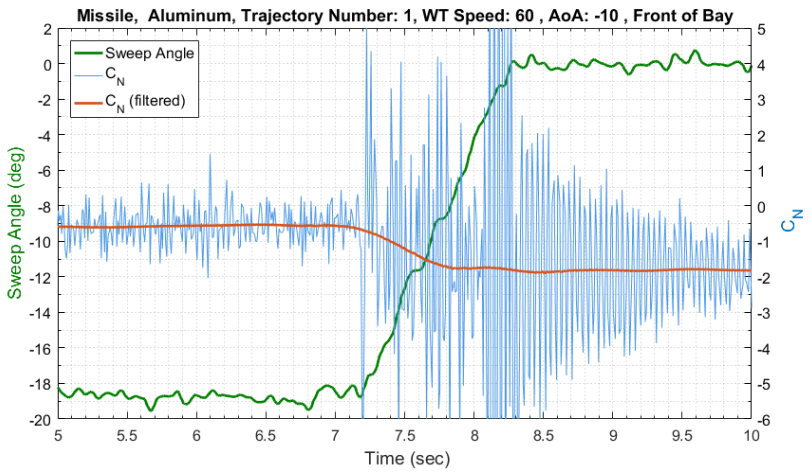
Missile, Aluminum, Trajectory Number: 1, WT Speed: 60 , AoA: -10 , Front of Bay
Sweep Angle
C_N
C_N (filtered)
Sweep Angle (deg)
C_N
Time (sec)

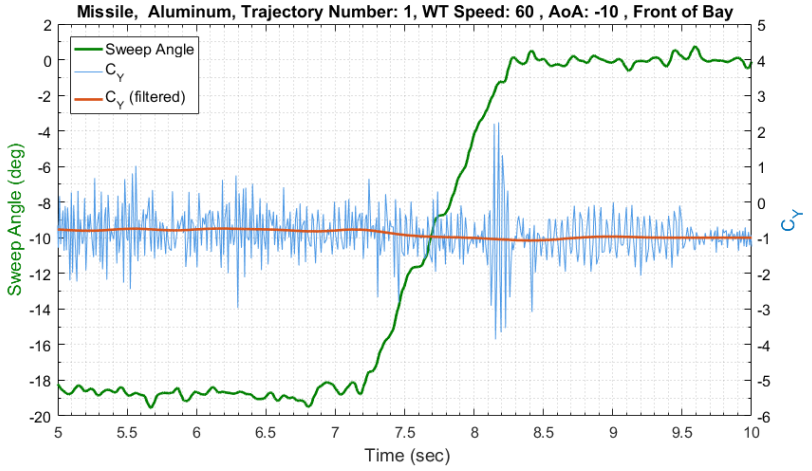
Missile, Aluminum, Trajectory Number: 1, WT Speed: 60 , AoA: -10 , Front of Bay
Sweep Angle
C_Y
C_Y (filtered)
Sweep Angle (deg)
C_Y
Time (sec)

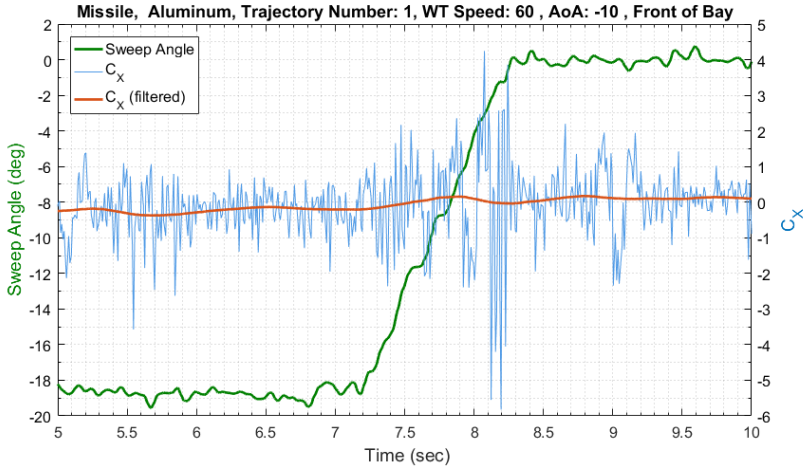
Missile, Aluminum, Trajectory Number: 1, WT Speed: 60 , AoA: -10 , Front of Bay
Sweep Angle
C_X
C_X (filtered)
Sweep Angle (deg)
C_X
Time (sec)

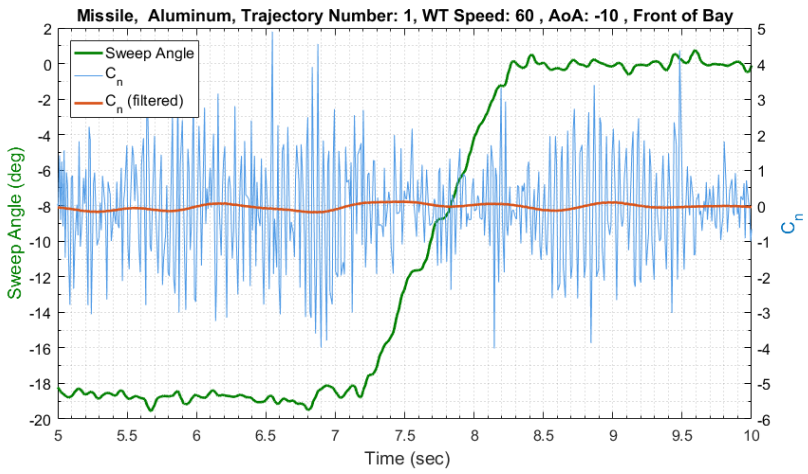
Missile, Aluminum, Trajectory Number: 1, WT Speed: 60 , AoA: -10 , Front of Bay
Sweep Angle
C_n
C_n (filtered)
Sweep Angle (deg)
C_n
Time (sec)

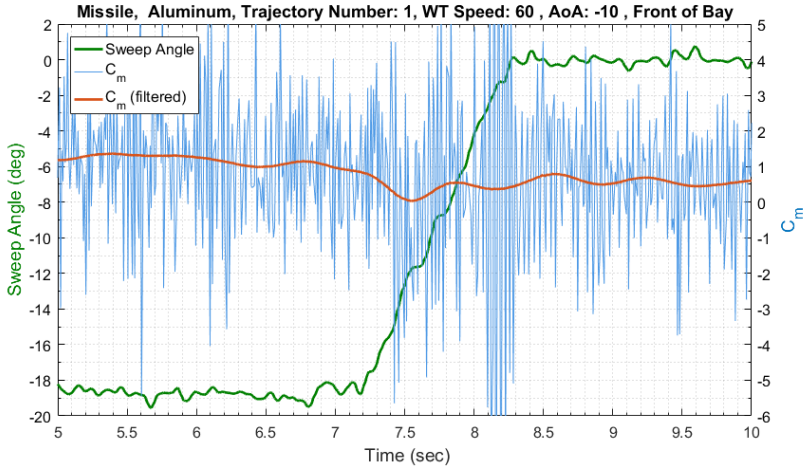
Missile, Aluminum, Trajectory Number: 1, WT Speed: 60 , AoA: -10 , Front of Bay
Sweep Angle
C_m
C_m (filtered)
Sweep Angle (deg)
C_m
Time (sec)

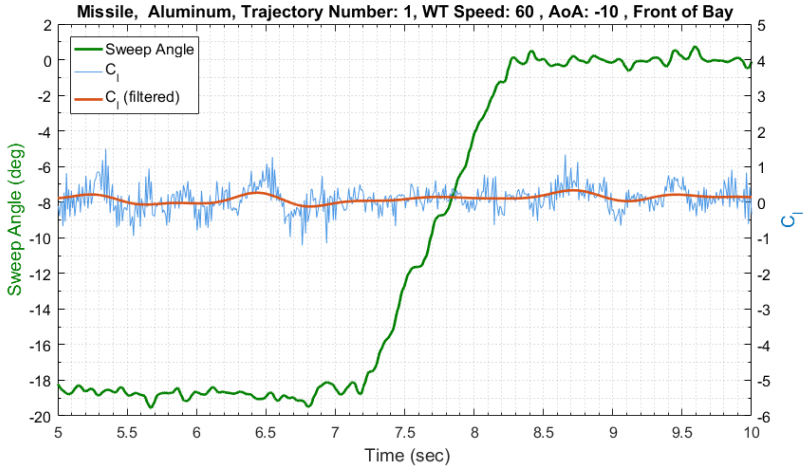
Missile, Aluminum, Trajectory Number: 1, WT Speed: 60 , AoA: -10 , Front of Bay
Sweep Angle
C_l
C_l (filtered)
Sweep Angle (deg)
C_l
Time (sec)

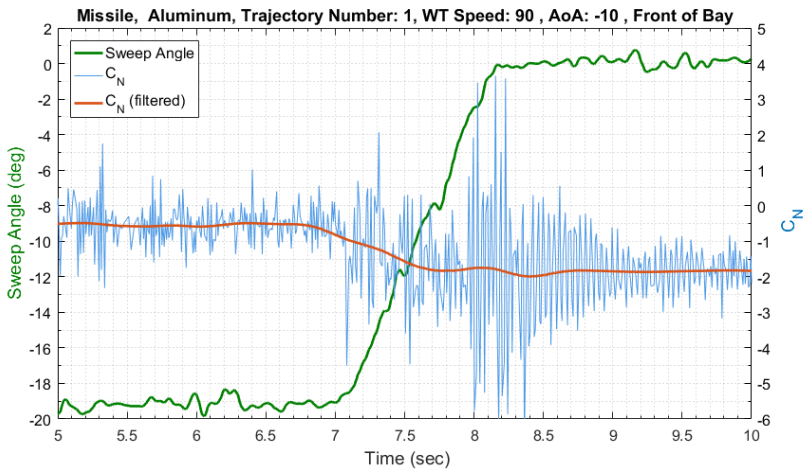
Missile, Aluminum, Trajectory Number: 1, WT Speed: 90 , AoA: -10 , Front of Bay
Sweep Angle
C_N
C_N (filtered)
Sweep Angle (deg)
C_N
Time (sec)

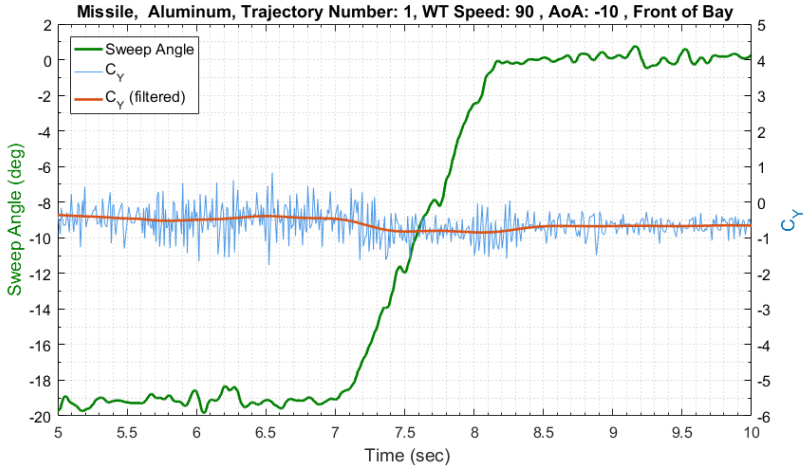
Missile, Aluminum, Trajectory Number: 1, WT Speed: 90 , AoA: -10 , Front of Bay
Sweep Angle
C_Y
C_Y (filtered)
Sweep Angle (deg)
C_Y
Time (sec)

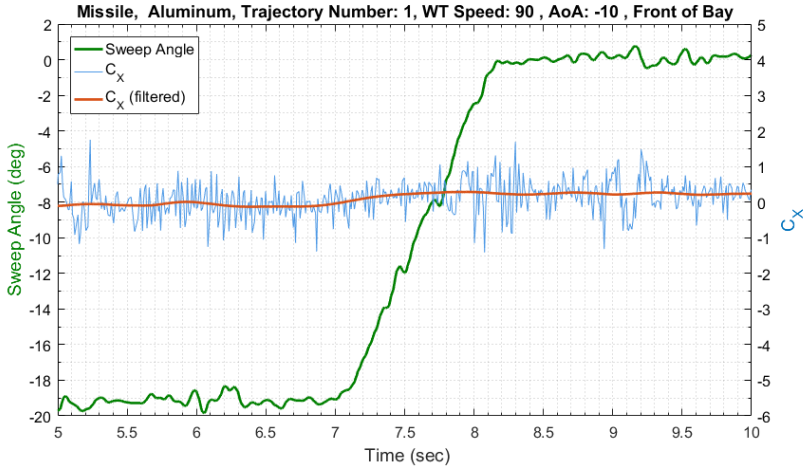
Missile, Aluminum, Trajectory Number: 1, WT Speed: 90 , AoA: -10 , Front of Bay
Sweep Angle
C_X
C_X (filtered)
Sweep Angle (deg)
C_X
Time (sec)

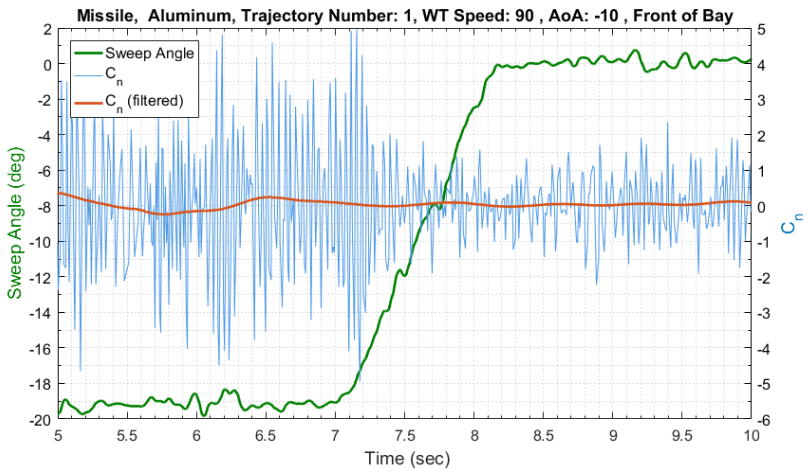
Missile, Aluminum, Trajectory Number: 1, WT Speed: 90 , AoA: -10 , Front of Bay
Sweep Angle
C_n
C_n (filtered)
Sweep Angle (deg)
C_n
Time (sec)

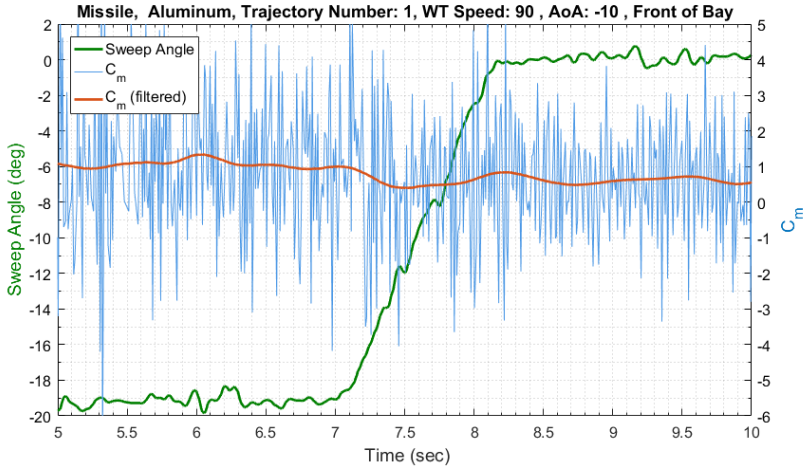
Missile, Aluminum, Trajectory Number: 1, WT Speed: 90 , AoA: -10 , Front of Bay
Sweep Angle
C_m
C_m (filtered)
Sweep Angle (deg)
C_m
Time (sec)

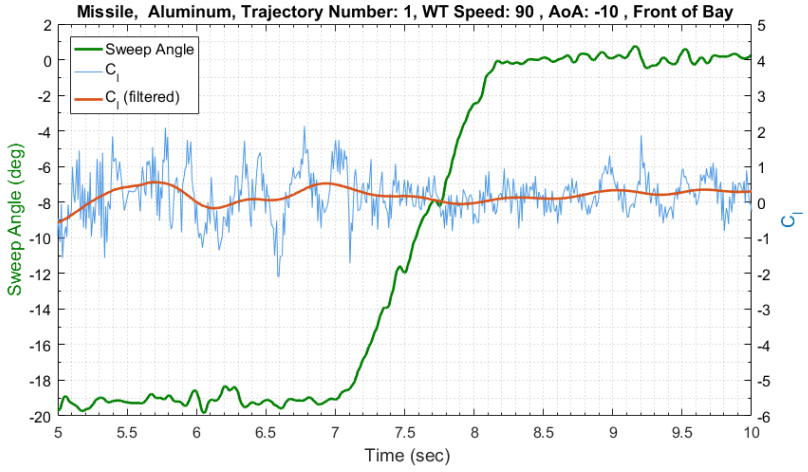
Missile, Aluminum, Trajectory Number: 1, WT Speed: 90 , AoA: -10 , Front of Bay
Sweep Angle
C_l
C_l (filtered)
Sweep Angle (deg)
C_l
Time (sec)

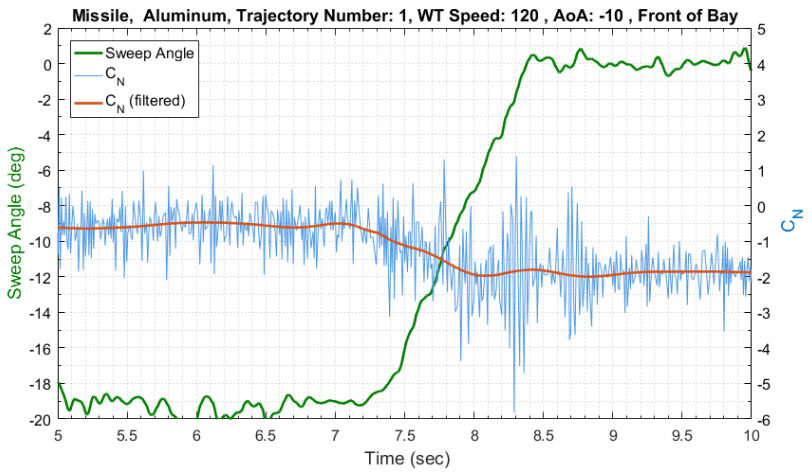
Missile, Aluminum, Trajectory Number: 1, WT Speed: 120 , AoA: -10 , Front of Bay
Sweep Angle
C_N
C_N (filtered)
Sweep Angle (deg)
C_N
Time (sec)

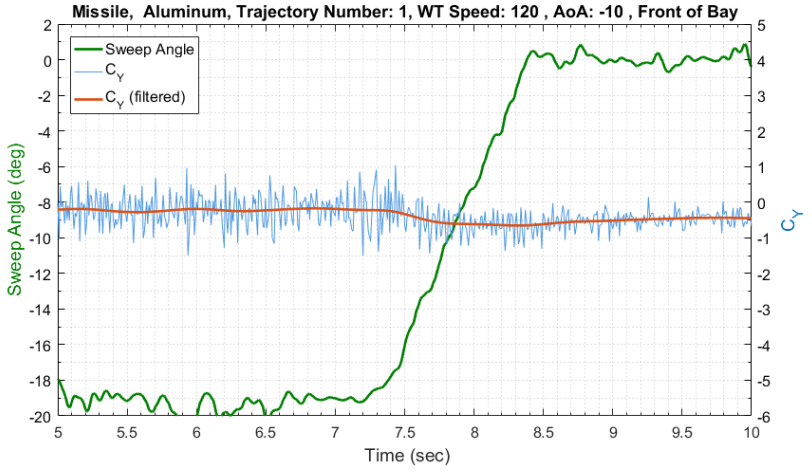
Missile, Aluminum, Trajectory Number: 1, WT Speed: 120 , AoA: -10 , Front of Bay
Sweep Angle
C_Y
C_Y (filtered)
Sweep Angle (deg)
C_Y
Time (sec)

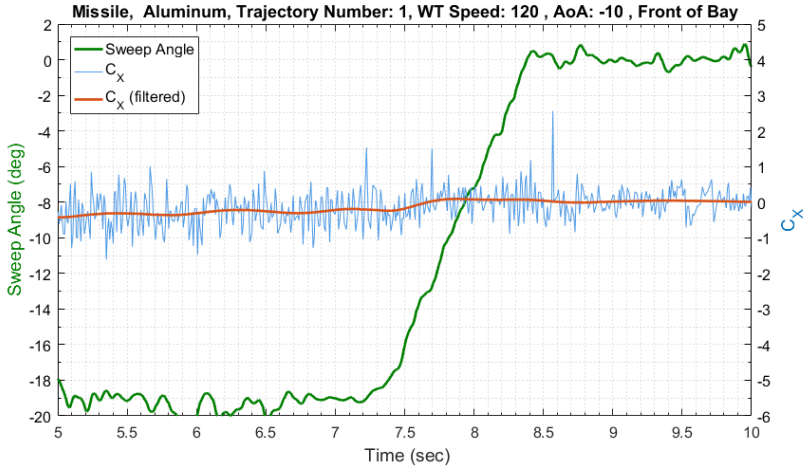
Missile, Aluminum, Trajectory Number: 1, WT Speed: 120 , AoA: -10 , Front of Bay
Sweep Angle
C_X
C_X (filtered)
Sweep Angle (deg)
C_X
Time (sec)

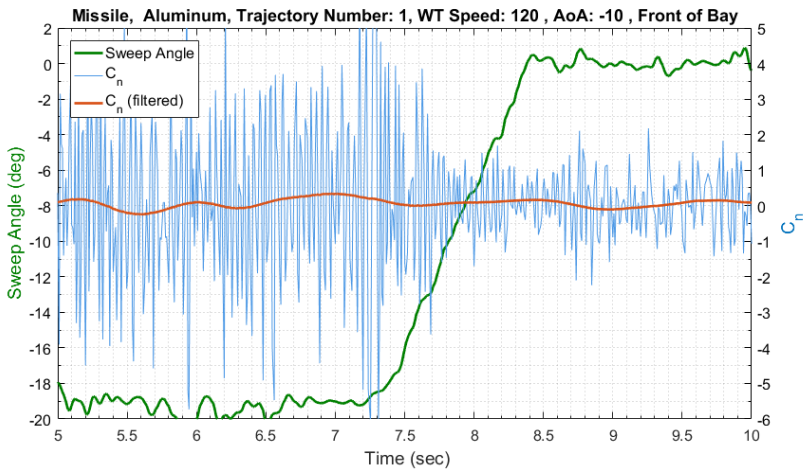
Missile, Aluminum, Trajectory Number: 1, WT Speed: 120 , AoA: -10 , Front of Bay
Sweep Angle
C_n
C_n (filtered)
Sweep Angle (deg)
C_n
Time (sec)

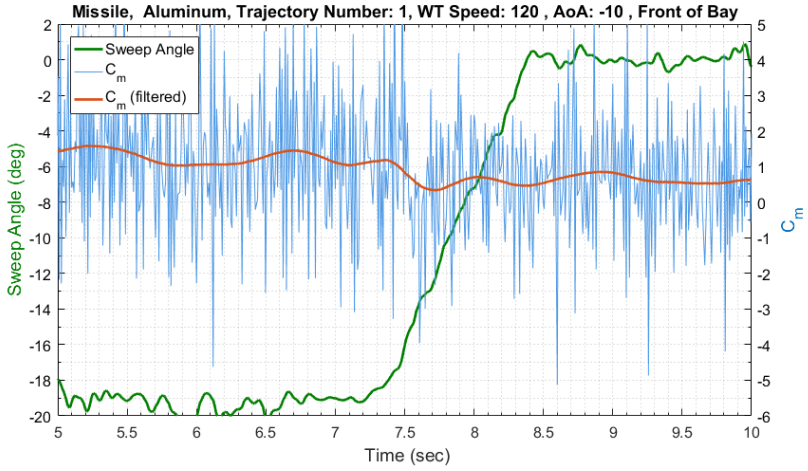
Missile, Aluminum, Trajectory Number: 1, WT Speed: 120 , AoA: -10 , Front of Bay
Sweep Angle
C_m
C_m (filtered)
Sweep Angle (deg)
C_m
Time (sec)

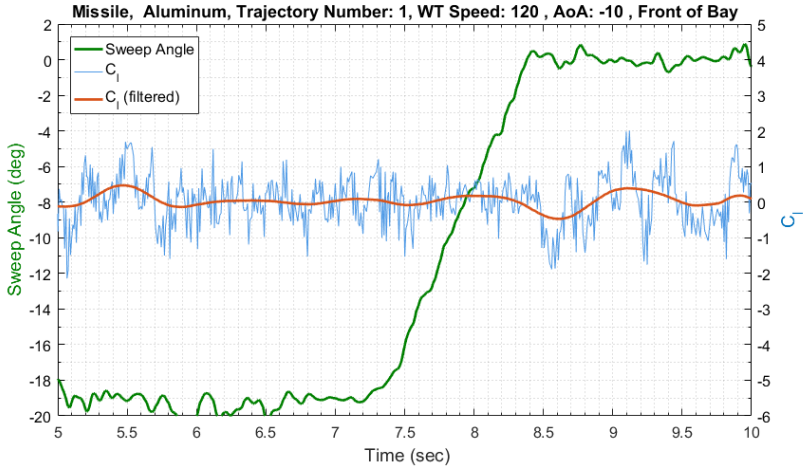
Missile, Aluminum, Trajectory Number: 1, WT Speed: 120 , AoA: -10 , Front of Bay
Sweep Angle
C_l
C_l (filtered)
Sweep Angle (deg)
C_l
Time (sec)

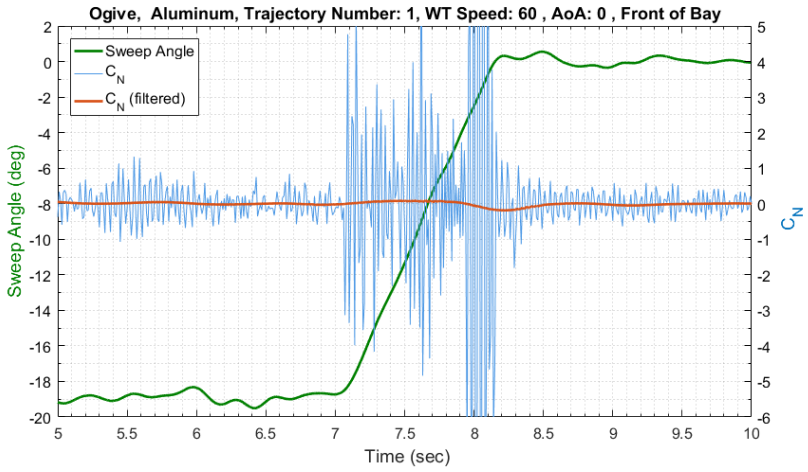
Ogive, Aluminum, Trajectory Number: 1, WT Speed: 60 , AoA: 0 , Front of Bay
Sweep Angle
C_N
C_N (filtered)
Sweep Angle (deg)
C_N
Time (sec)

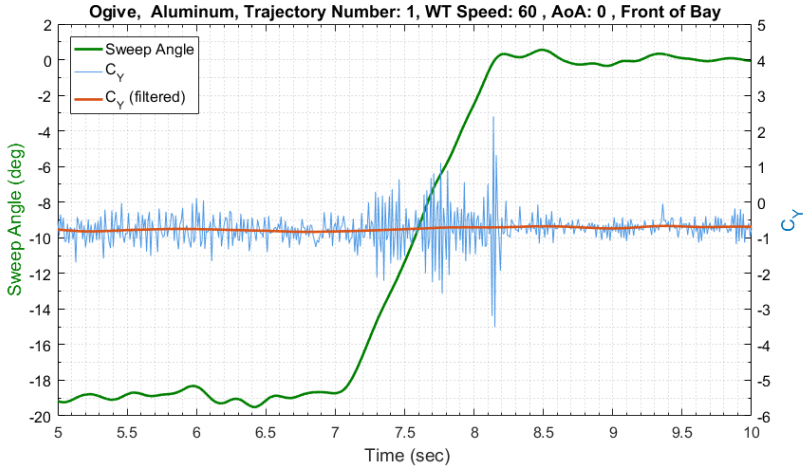
Ogive, Aluminum, Trajectory Number: 1, WT Speed: 60 , AoA: 0 , Front of Bay
Sweep Angle
C_Y
C_Y (filtered)
Sweep Angle (deg)
C_Y
Time (sec)

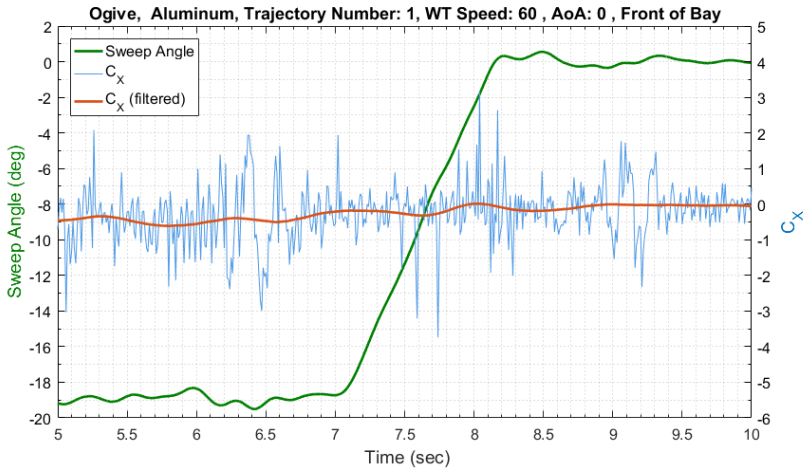
Ogive, Aluminum, Trajectory Number: 1, WT Speed: 60 , AoA: 0 , Front of Bay
Sweep Angle
C_X
C_X (filtered)
Sweep Angle (deg)
C_X
Time (sec)

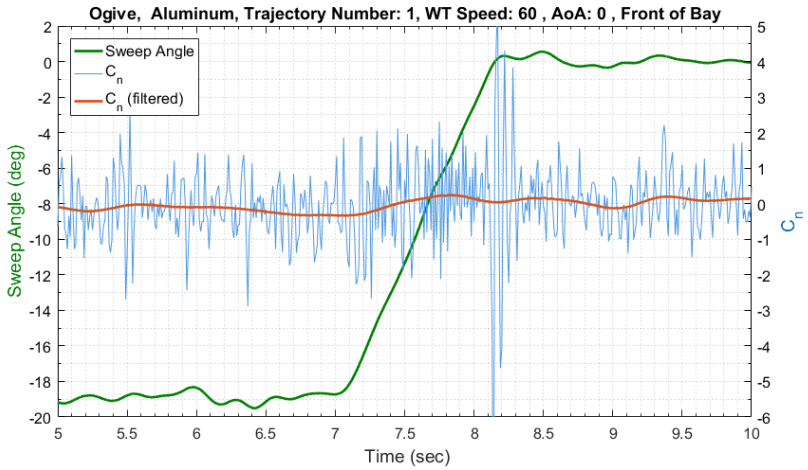
Ogive, Aluminum, Trajectory Number: 1, WT Speed: 60 , AoA: 0 , Front of Bay
Sweep Angle
C_n
C_n (filtered)
Sweep Angle (deg)
C_n
Time (sec)

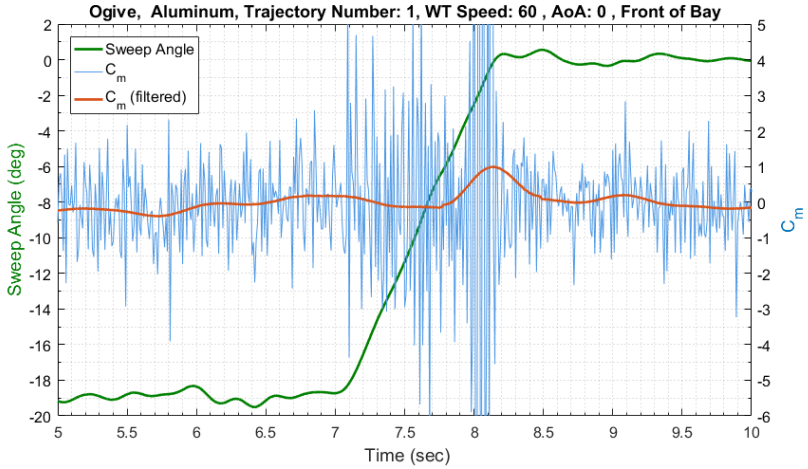
Ogive, Aluminum, Trajectory Number: 1, WT Speed: 60 , AoA: 0 , Front of Bay
Sweep Angle
C_m
C_m (filtered)
Sweep Angle (deg)
C_m
Time (sec)

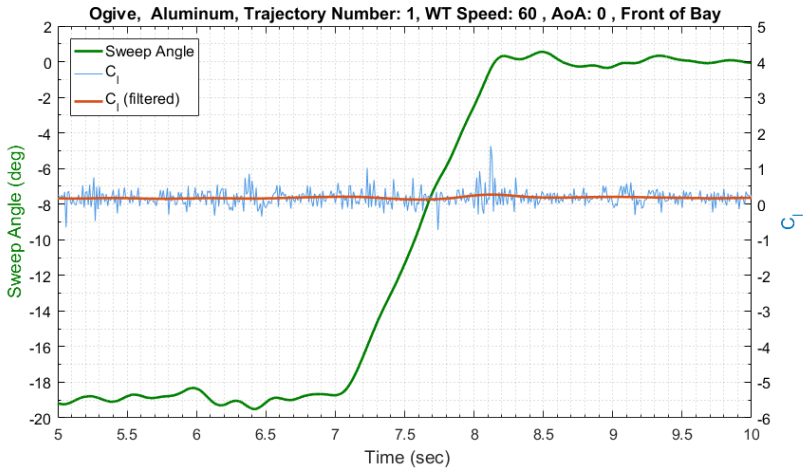
Ogive, Aluminum, Trajectory Number: 1, WT Speed: 60 , AoA: 0 , Front of Bay
Sweep Angle
C_l
C_l (filtered)
Sweep Angle (deg)
C_l
Time (sec)

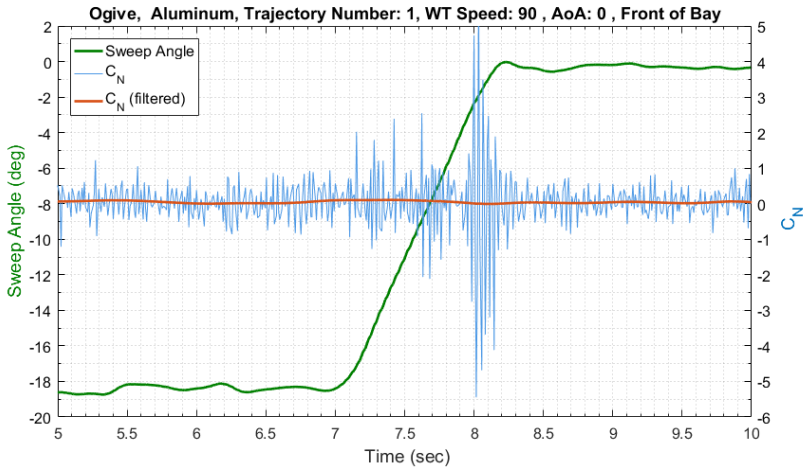
Ogive, Aluminum, Trajectory Number: 1, WT Speed: 90 , AoA: 0 , Front of Bay
Sweep Angle
C_N
C_N (filtered)
Sweep Angle (deg)
C_N
Time (sec)

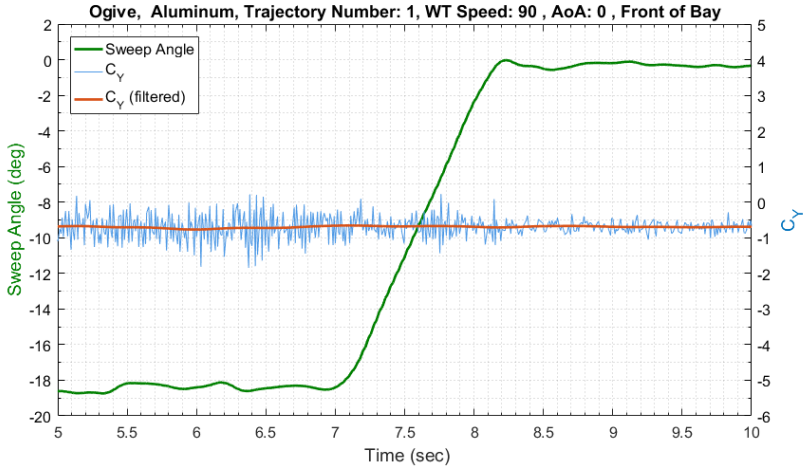
Ogive, Aluminum, Trajectory Number: 1, WT Speed: 90 , AoA: 0 , Front of Bay
Sweep Angle
C_Y
C_Y (filtered)
Sweep Angle (deg)
C_Y
Time (sec)

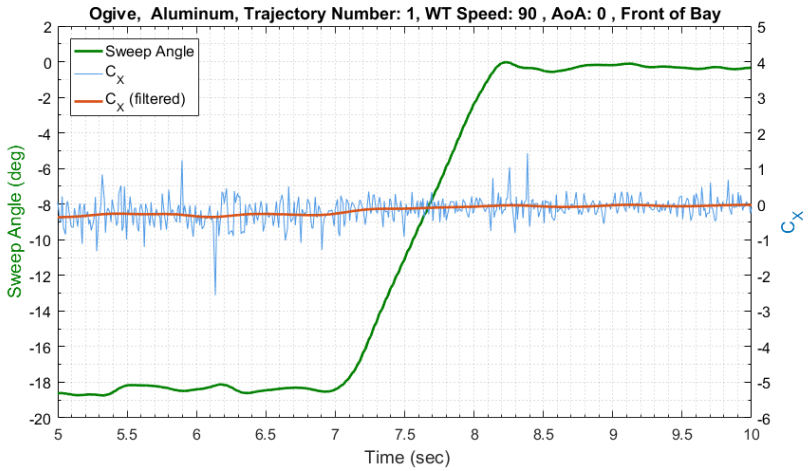
Ogive, Aluminum, Trajectory Number: 1, WT Speed: 90 , AoA: 0 , Front of Bay
Sweep Angle
C_X
C_X (filtered)
Sweep Angle (deg)
C_X
Time (sec)

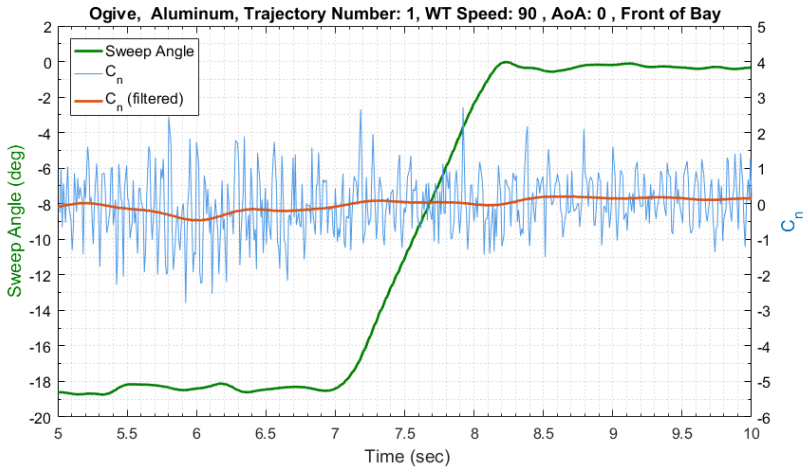
Ogive, Aluminum, Trajectory Number: 1, WT Speed: 90 , AoA: 0 , Front of Bay
Sweep Angle
C_n
C_n (filtered)
Sweep Angle (deg)
C_n
Time (sec)

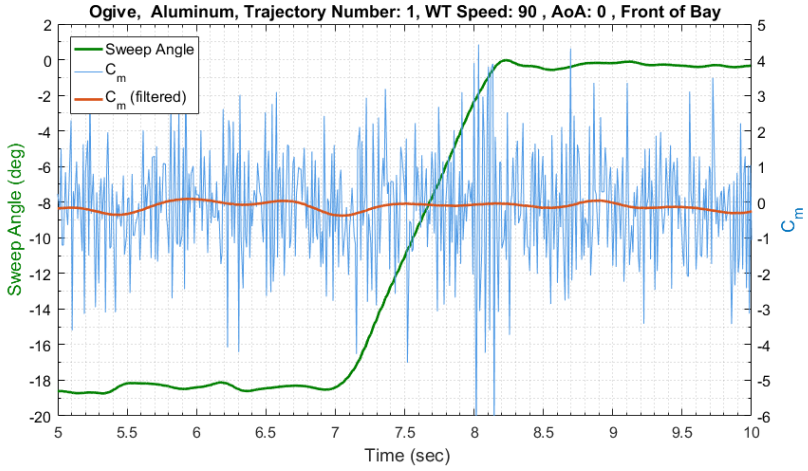
Ogive, Aluminum, Trajectory Number: 1, WT Speed: 90 , AoA: 0 , Front of Bay
Sweep Angle
C_m
C_m (filtered)
Sweep Angle (deg)
C_m
Time (sec)

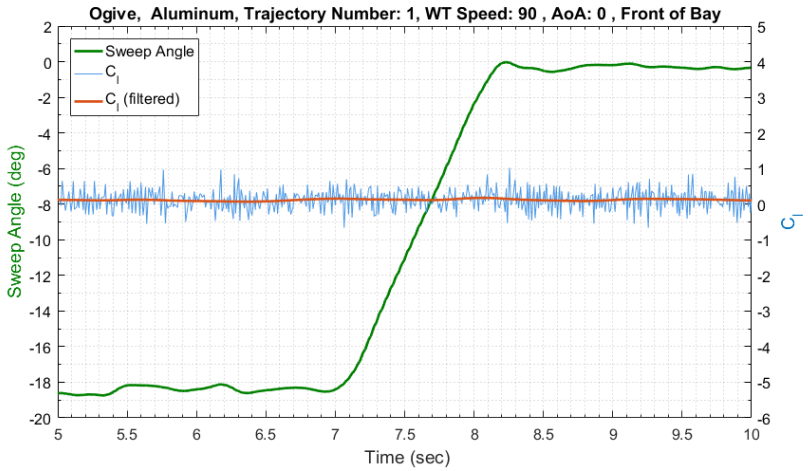
Ogive, Aluminum, Trajectory Number: 1, WT Speed: 90 , AoA: 0 , Front of Bay
Sweep Angle
C_l
C_l (filtered)
Sweep Angle (deg)
C_l
Time (sec)

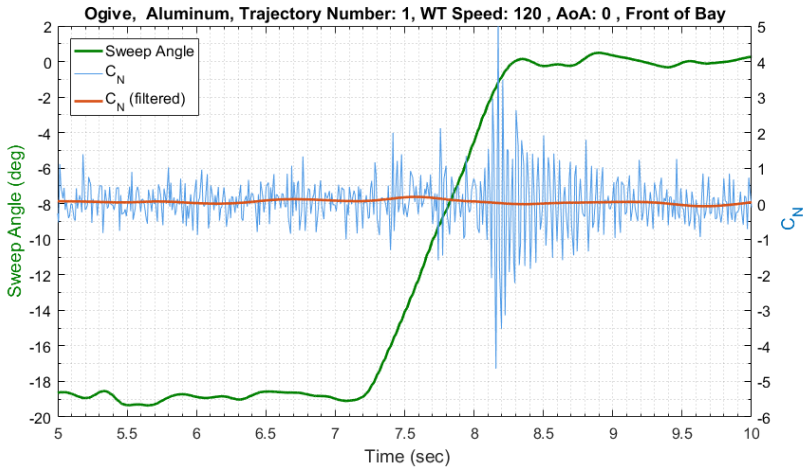
Ogive, Aluminum, Trajectory Number: 1, WT Speed: 120 , AoA: 0 , Front of Bay
Sweep Angle
C_N
C_N (filtered)
Sweep Angle (deg)
C_N
Time (sec)

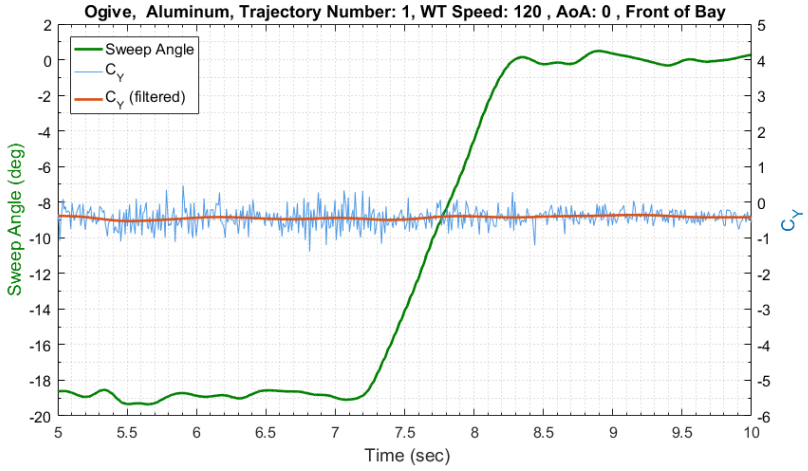
Ogive, Aluminum, Trajectory Number: 1, WT Speed: 120 , AoA: 0 , Front of Bay
Sweep Angle
C_Y
C_Y (filtered)
Sweep Angle (deg)
C_Y
Time (sec)

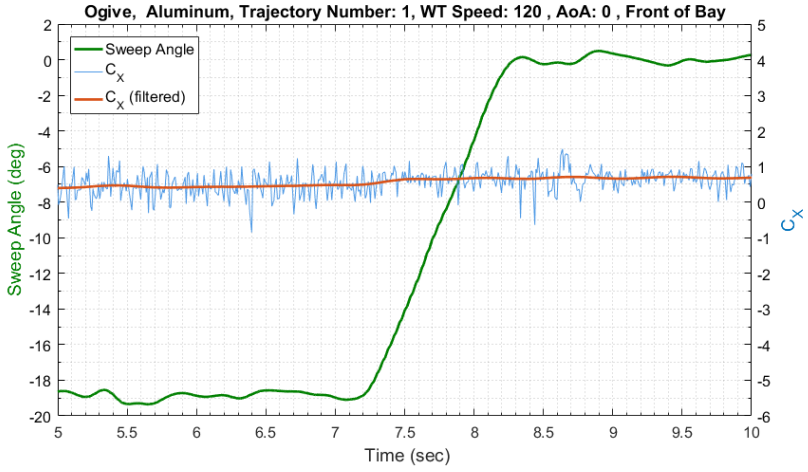
Ogive, Aluminum, Trajectory Number: 1, WT Speed: 120 , AoA: 0 , Front of Bay
Sweep Angle
C_X
C_X (filtered)
Sweep Angle (deg)
C_X
Time (sec)

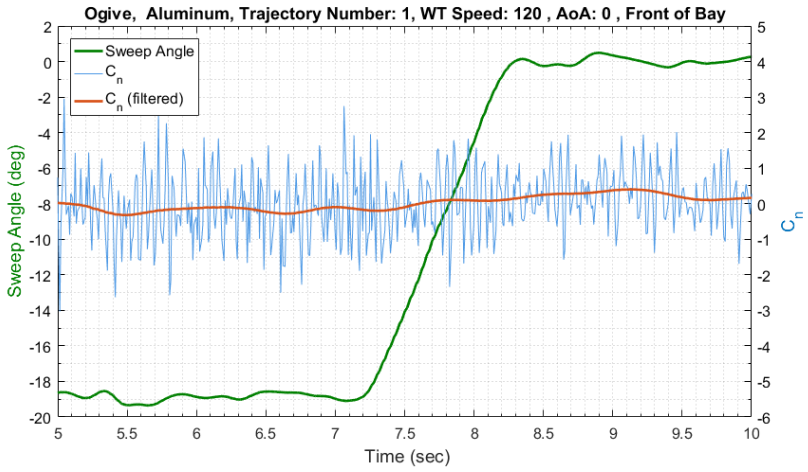
Ogive, Aluminum, Trajectory Number: 1, WT Speed: 120 , AoA: 0 , Front of Bay
Sweep Angle
C_n
C_n (filtered)
Sweep Angle (deg)
C_n
Time (sec)

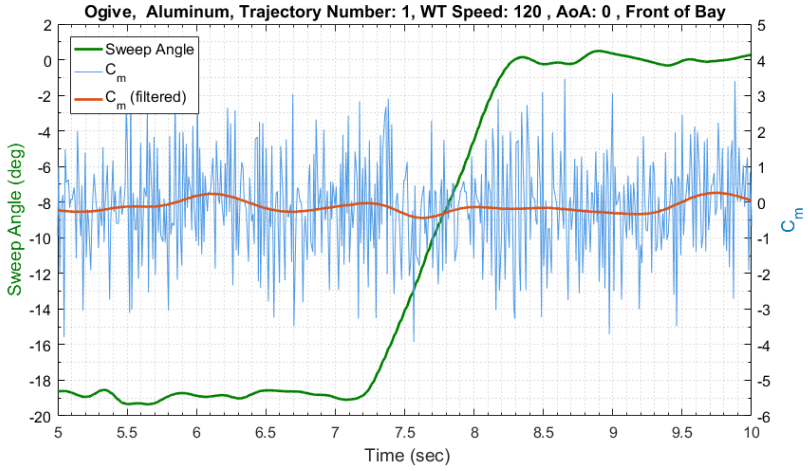
Ogive, Aluminum, Trajectory Number: 1, WT Speed: 120 , AoA: 0 , Front of Bay
Sweep Angle
C_m
C_m (filtered)
Sweep Angle (deg)
C_m
Time (sec)

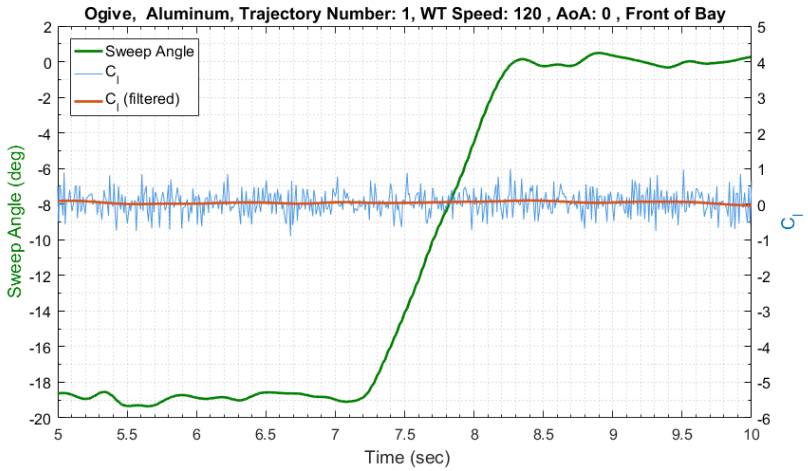
Ogive, Aluminum, Trajectory Number: 1, WT Speed: 120 , AoA: 0 , Front of Bay
Sweep Angle
C_l
C_l (filtered)
Sweep Angle (deg)
C_l
Time (sec)

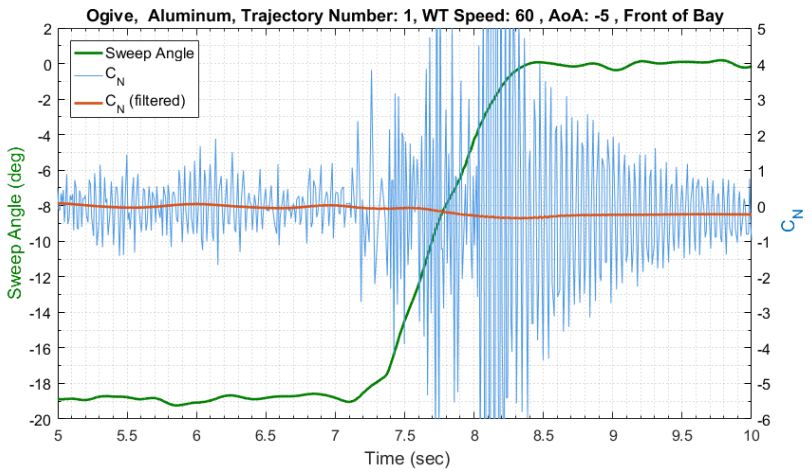
Ogive, Aluminum, Trajectory Number: 1, WT Speed: 60 , AoA: -5 , Front of Bay
Sweep Angle
C_N
C_N (filtered)
Sweep Angle (deg)
C_N
Time (sec)

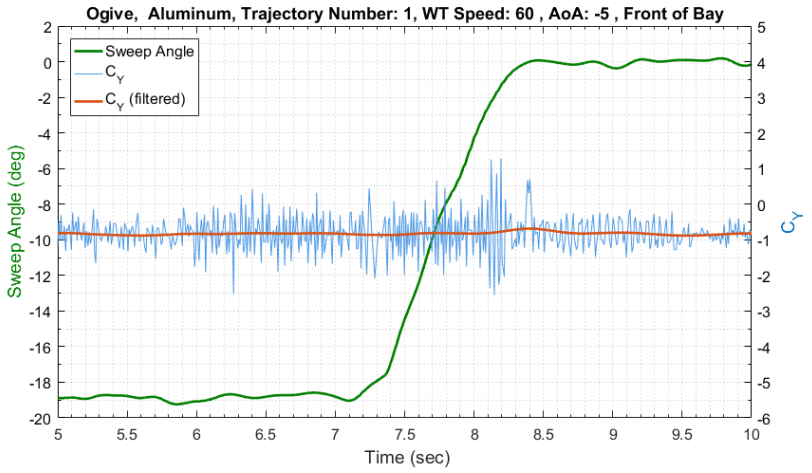
Ogive, Aluminum, Trajectory Number: 1, WT Speed: 60 , AoA: -5 , Front of Bay
Sweep Angle
C_Y
C_Y (filtered)
Sweep Angle (deg)
C_Y
Time (sec)

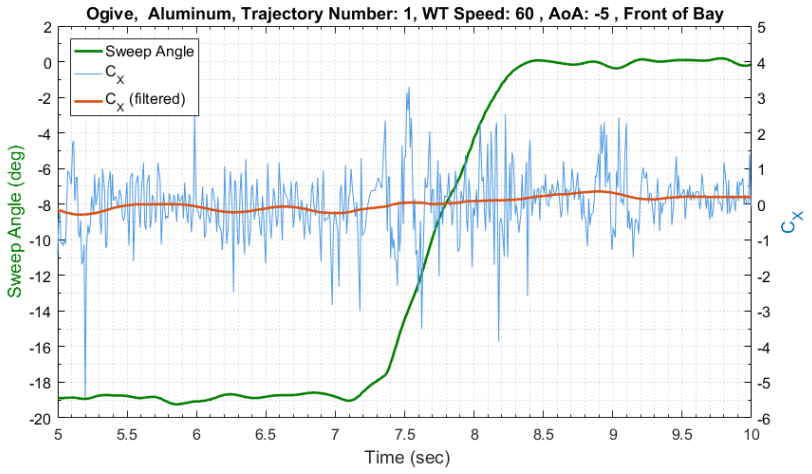
Ogive, Aluminum, Trajectory Number: 1, WT Speed: 60 , AoA: -5 , Front of Bay
Sweep Angle
C_X
C_X (filtered)
Sweep Angle (deg)
C_X
Time (sec)

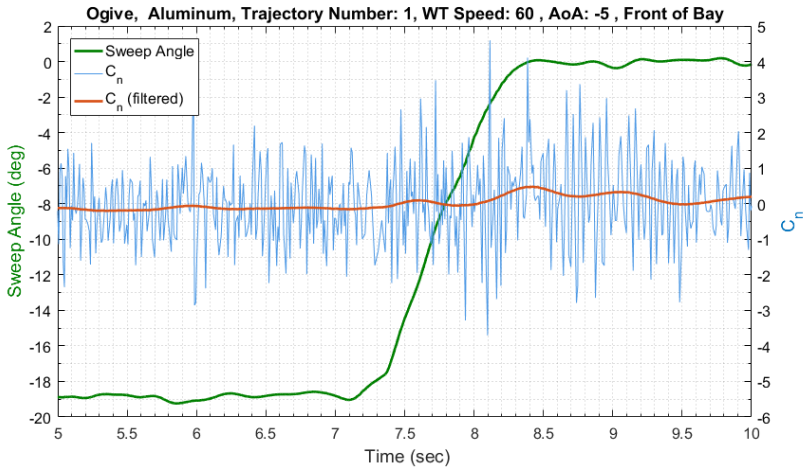
Ogive, Aluminum, Trajectory Number: 1, WT Speed: 60 , AoA: -5 , Front of Bay
Sweep Angle
C_n
C_n (filtered)
Sweep Angle (deg)
C_n
Time (sec)

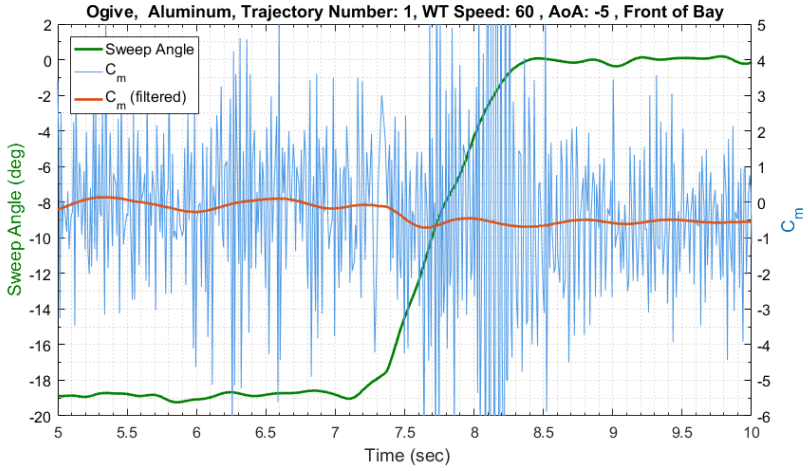
Ogive, Aluminum, Trajectory Number: 1, WT Speed: 60 , AoA: -5 , Front of Bay
Sweep Angle
C_m
C_m (filtered)
Sweep Angle (deg)
C_m
Time (sec)

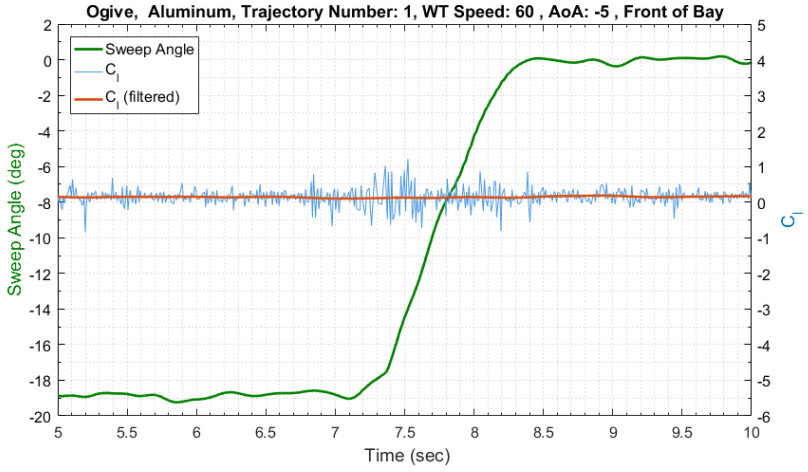
Ogive, Aluminum, Trajectory Number: 1, WT Speed: 60 , AoA: -5 , Front of Bay
Sweep Angle
C_l
C_l (filtered)
Sweep Angle (deg)
C_l
Time (sec)

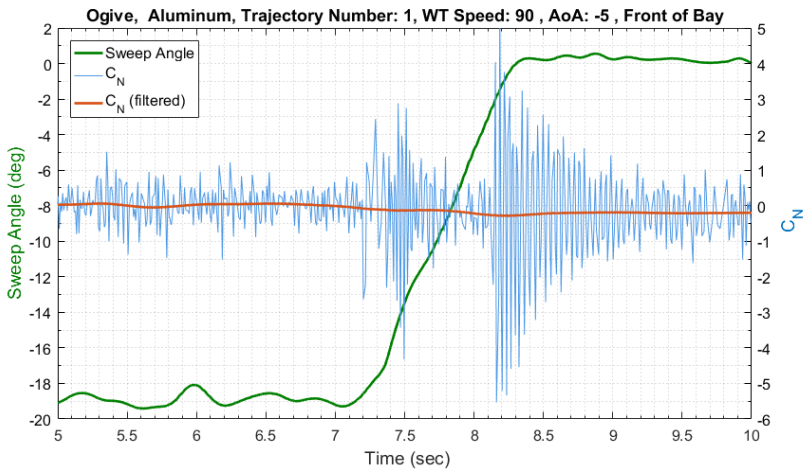
Ogive, Aluminum, Trajectory Number: 1, WT Speed: 90 , AoA: -5 , Front of Bay
Sweep Angle
C_N
C_N (filtered)
Sweep Angle (deg)
C_N
Time (sec)

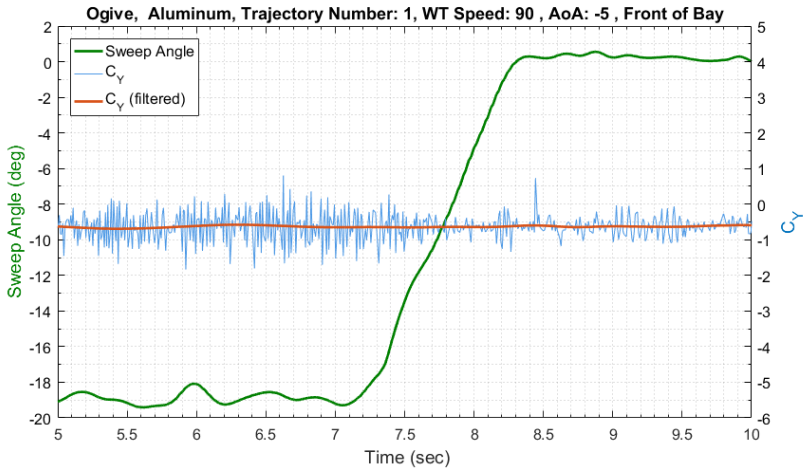
Ogive, Aluminum, Trajectory Number: 1, WT Speed: 90 , AoA: -5 , Front of Bay
Sweep Angle
C_Y
C_Y (filtered)
Sweep Angle (deg)
C_Y
Time (sec)

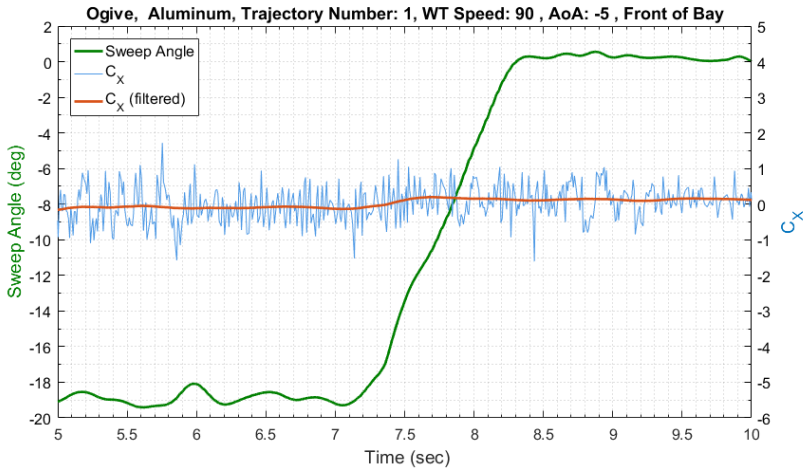
Ogive, Aluminum, Trajectory Number: 1, WT Speed: 90 , AoA: -5 , Front of Bay
Sweep Angle
C_X
C_X (filtered)
Sweep Angle (deg)
C_X
Time (sec)

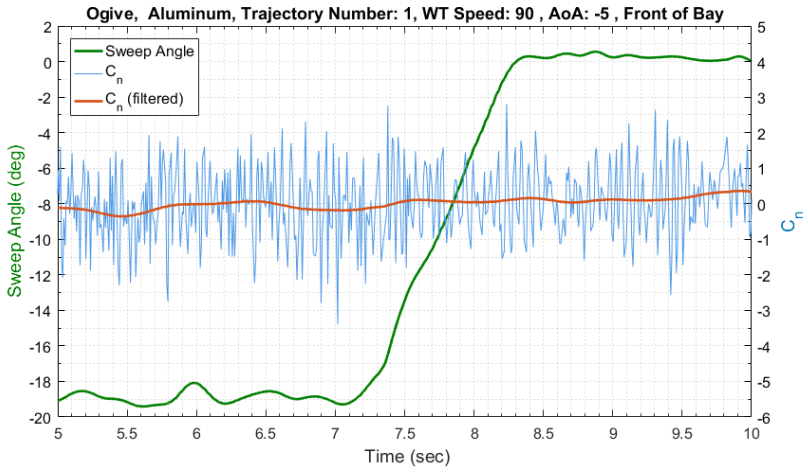
Ogive, Aluminum, Trajectory Number: 1, WT Speed: 90 , AoA: -5 , Front of Bay
Sweep Angle
C_n
C_n (filtered)
Sweep Angle (deg)
C_n
Time (sec)

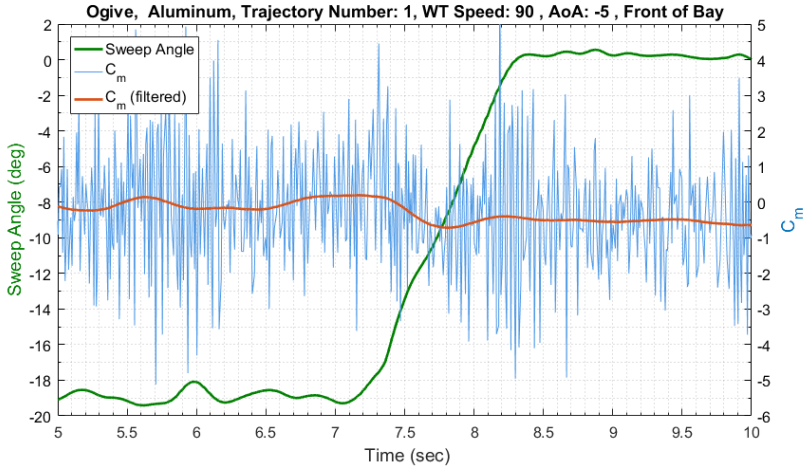
Ogive, Aluminum, Trajectory Number: 1, WT Speed: 90 , AoA: -5 , Front of Bay
Sweep Angle
C_m
C_m (filtered)
Sweep Angle (deg)
C_m
Time (sec)

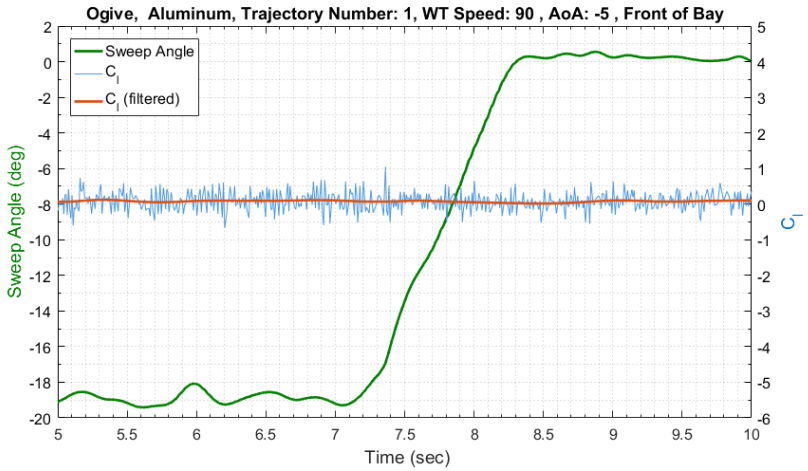
Ogive, Aluminum, Trajectory Number: 1, WT Speed: 90 , AoA: -5 , Front of Bay
Sweep Angle
C_l
C_l (filtered)
Sweep Angle (deg)
C_l
Time (sec)

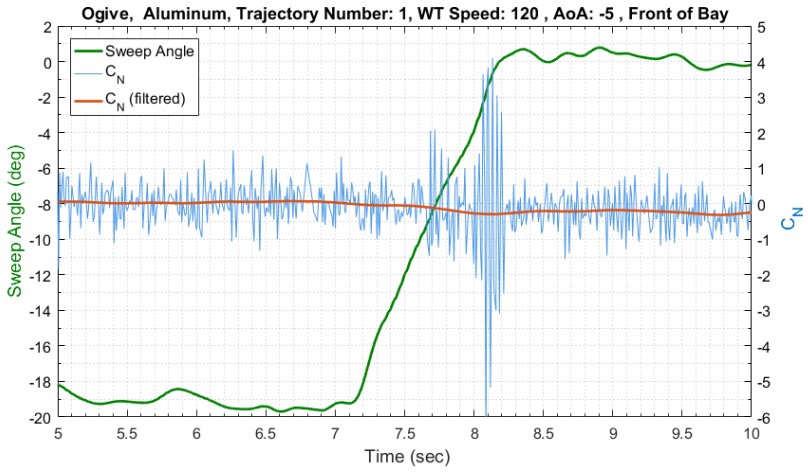
Ogive, Aluminum, Trajectory Number: 1, WT Speed: 120 , AoA: -5 , Front of Bay
Sweep Angle
C_N
C_N (filtered)
Sweep Angle (deg)
C_N
Time (sec)

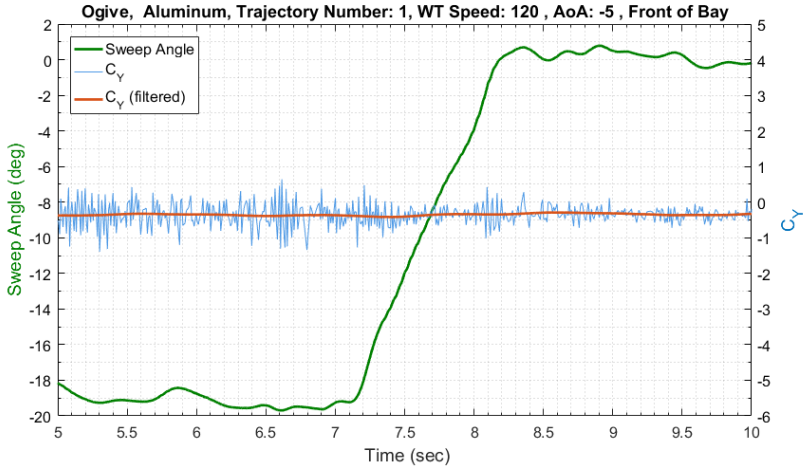
Ogive, Aluminum, Trajectory Number: 1, WT Speed: 120 , AoA: -5 , Front of Bay
Sweep Angle
C_Y
C_Y (filtered)
Sweep Angle (deg)
C_Y
Time (sec)

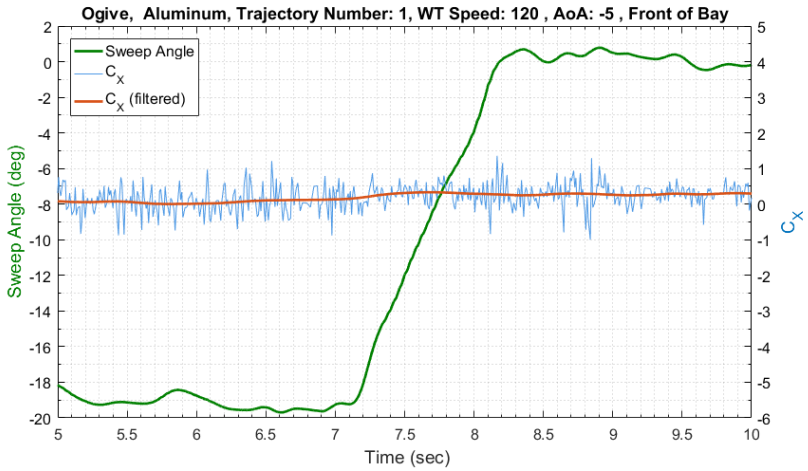
Ogive, Aluminum, Trajectory Number: 1, WT Speed: 120 , AoA: -5 , Front of Bay
Sweep Angle
C_X
C_X (filtered)
Sweep Angle (deg)
C_X
Time (sec)

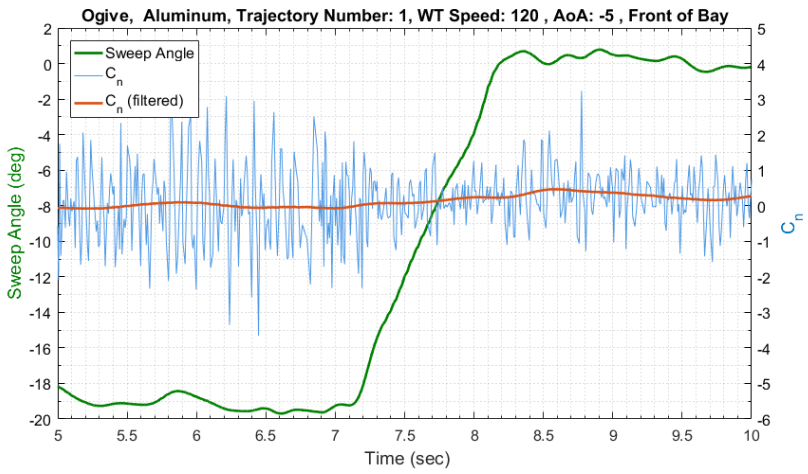
Ogive, Aluminum, Trajectory Number: 1, WT Speed: 120 , AoA: -5 , Front of Bay
Sweep Angle
C_n
C_n (filtered)
Sweep Angle (deg)
C_n
Time (sec)

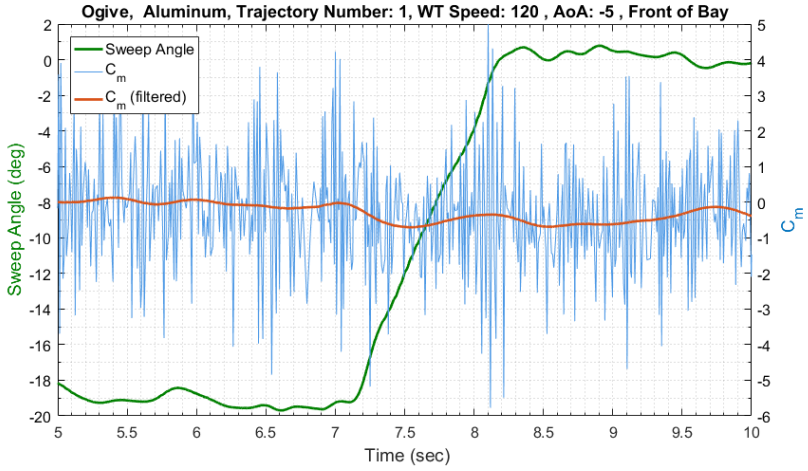
Ogive, Aluminum, Trajectory Number: 1, WT Speed: 120 , AoA: -5 , Front of Bay
Sweep Angle
C_m
C_m (filtered)
Sweep Angle (deg)
C_m
Time (sec)

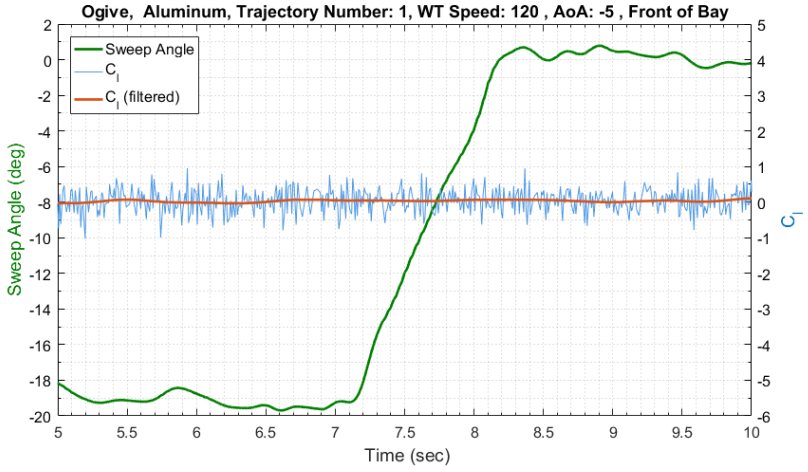
Ogive, Aluminum, Trajectory Number: 1, WT Speed: 120 , AoA: -5 , Front of Bay
Sweep Angle
C_l
C_l (filtered)
Sweep Angle (deg)
C_l
Time (sec)

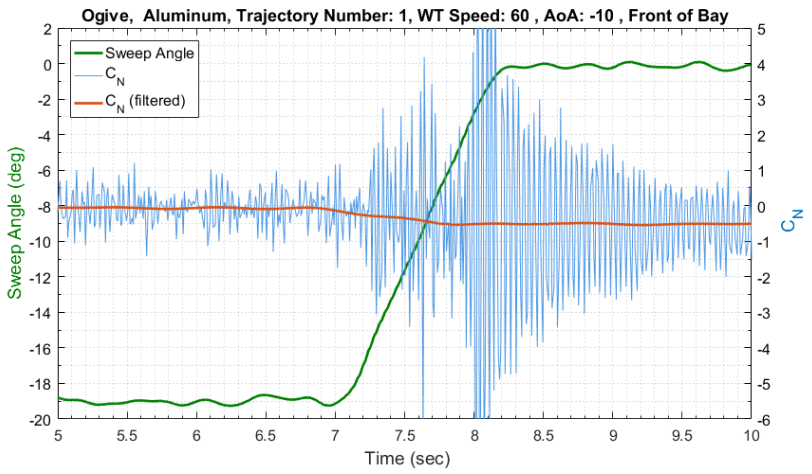
Ogive, Aluminum, Trajectory Number: 1, WT Speed: 60 , AoA: -10 , Front of Bay
Sweep Angle
C_N
C_N (filtered)
Sweep Angle (deg)
C_N
Time (sec)

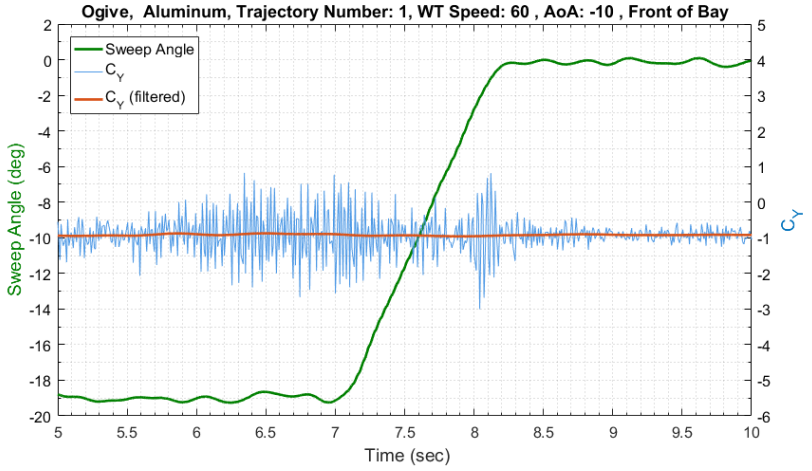
Ogive, Aluminum, Trajectory Number: 1, WT Speed: 60 , AoA: -10 , Front of Bay
Sweep Angle
C_Y
C_Y (filtered)
Sweep Angle (deg)
C_Y
Time (sec)

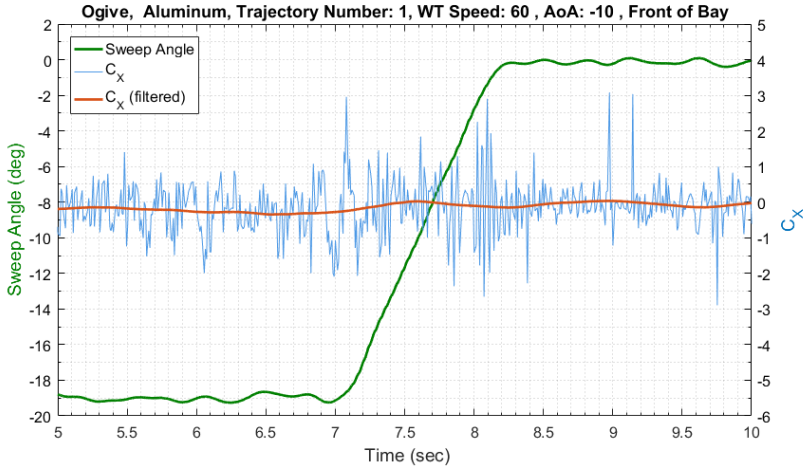
Ogive, Aluminum, Trajectory Number: 1, WT Speed: 60 , AoA: -10 , Front of Bay
Sweep Angle
C_X
C_X (filtered)
Sweep Angle (deg)
C_X
Time (sec)

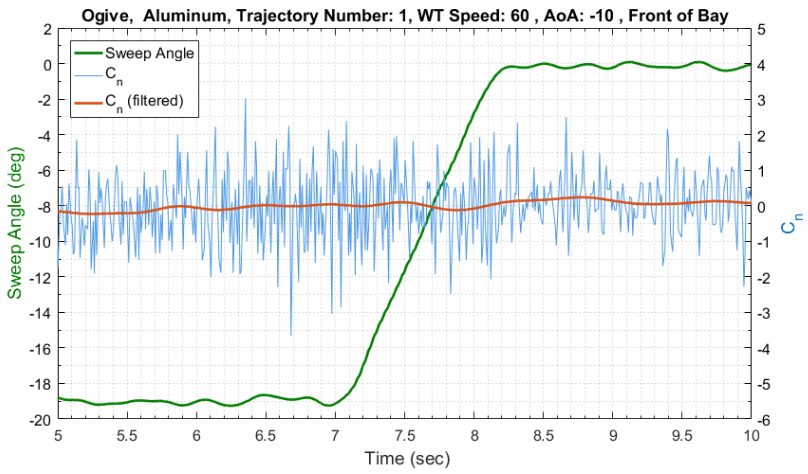
Ogive, Aluminum, Trajectory Number: 1, WT Speed: 60 , AoA: -10 , Front of Bay
Sweep Angle
C_n
C_n (filtered)
Sweep Angle (deg)
C_n
Time (sec)

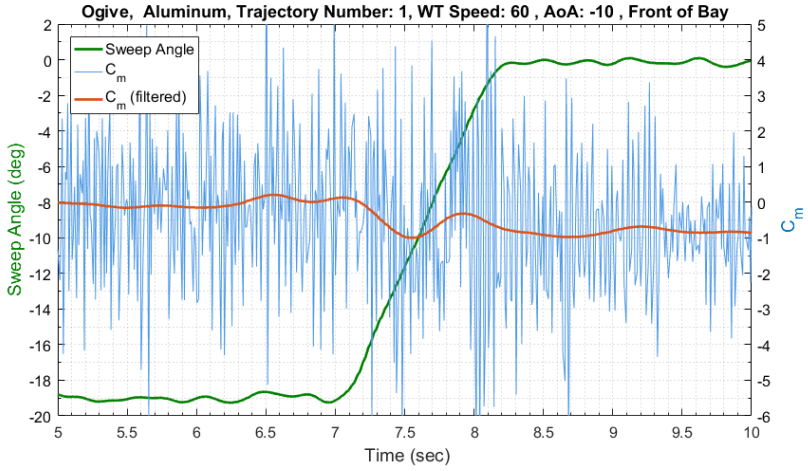
Ogive, Aluminum, Trajectory Number: 1, WT Speed: 60 , AoA: -10 , Front of Bay
Sweep Angle
C_m
C_m (filtered)
Sweep Angle (deg)
C_m
Time (sec)

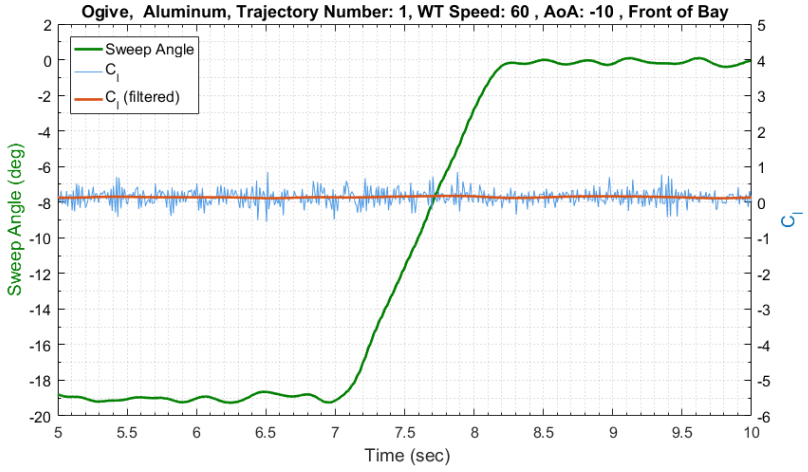
Ogive, Aluminum, Trajectory Number: 1, WT Speed: 60 , AoA: -10 , Front of Bay
Sweep Angle
C_l
C_l (filtered)
Sweep Angle (deg)
C_l
Time (sec)

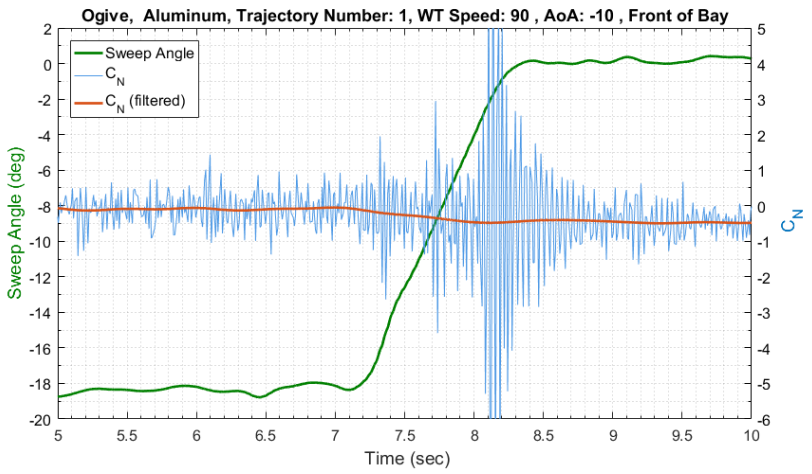
Ogive, Aluminum, Trajectory Number: 1, WT Speed: 90 , AoA: -10 , Front of Bay
Sweep Angle
C_N
C_N (filtered)
Sweep Angle (deg)
C_N
Time (sec)

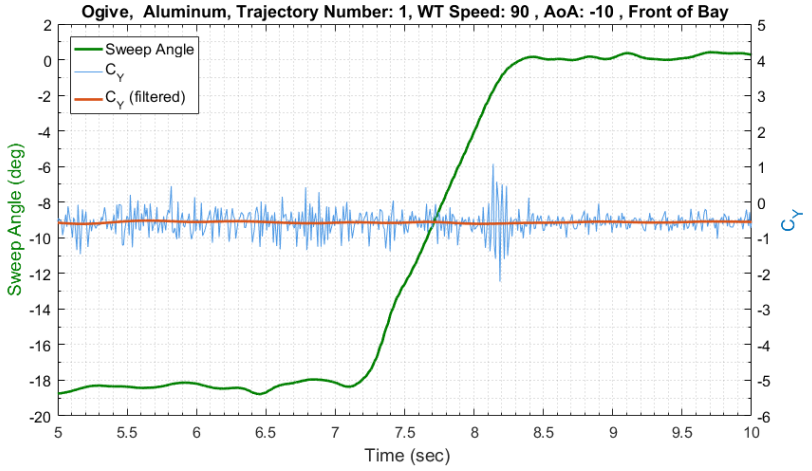
Ogive, Aluminum, Trajectory Number: 1, WT Speed: 90 , AoA: -10 , Front of Bay
Sweep Angle
C_Y
C_Y (filtered)
Sweep Angle (deg)
C_Y
Time (sec)

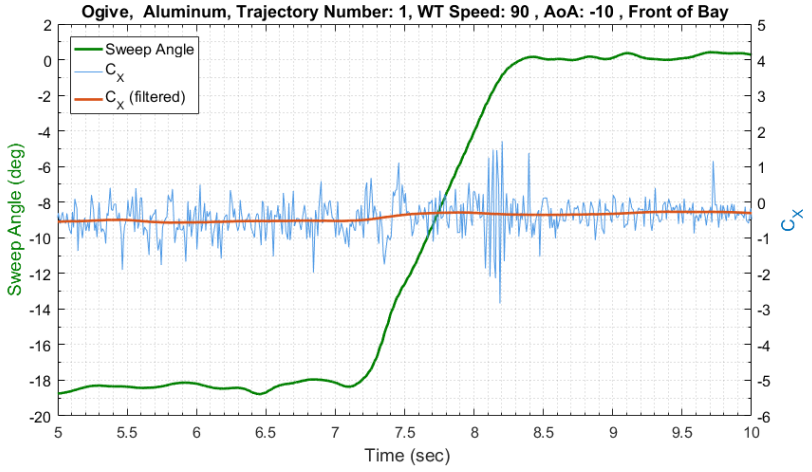
Ogive, Aluminum, Trajectory Number: 1, WT Speed: 90 , AoA: -10 , Front of Bay
Sweep Angle
C_X
C_X (filtered)
Sweep Angle (deg)
C_X
Time (sec)

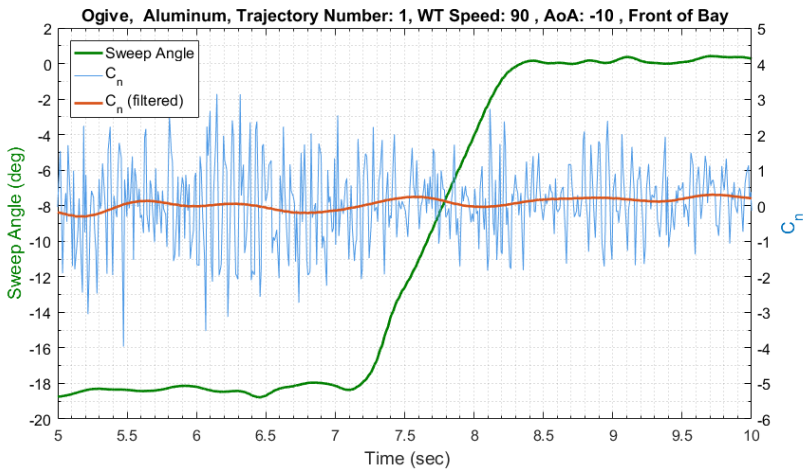
Ogive, Aluminum, Trajectory Number: 1, WT Speed: 90 , AoA: -10 , Front of Bay
Sweep Angle
C_n
C_n (filtered)
Sweep Angle (deg)
C_n
Time (sec)

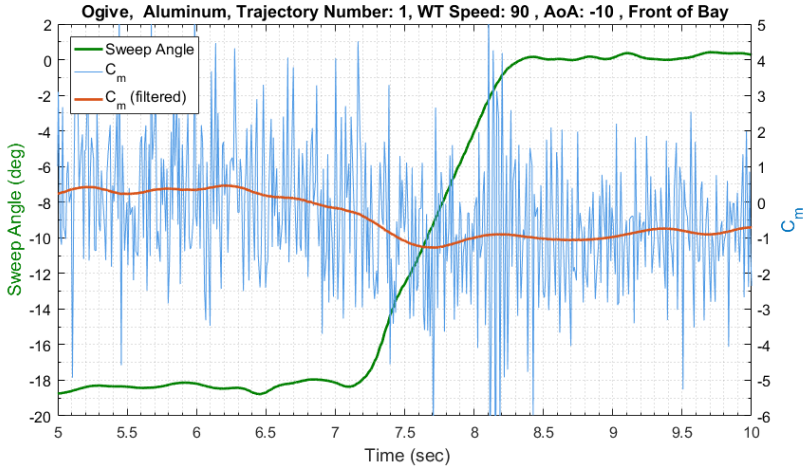
Ogive, Aluminum, Trajectory Number: 1, WT Speed: 90 , AoA: -10 , Front of Bay
Sweep Angle
C_m
C_m (filtered)
Sweep Angle (deg)
C_m
Time (sec)

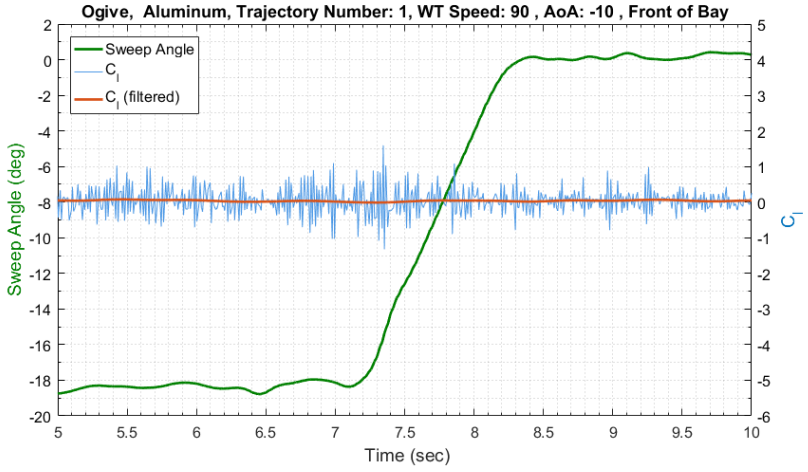
Ogive, Aluminum, Trajectory Number: 1, WT Speed: 90 , AoA: -10 , Front of Bay
Sweep Angle
C_l
C_l (filtered)
Sweep Angle (deg)
C_l
Time (sec)

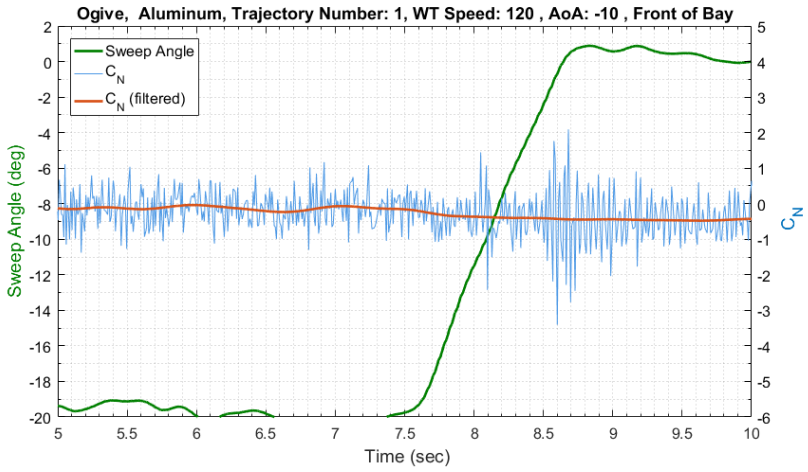
Ogive, Aluminum, Trajectory Number: 1, WT Speed: 120 , AoA: -10 , Front of Bay
Sweep Angle
C_N
C_N (filtered)
Sweep Angle (deg)
C_N
Time (sec)

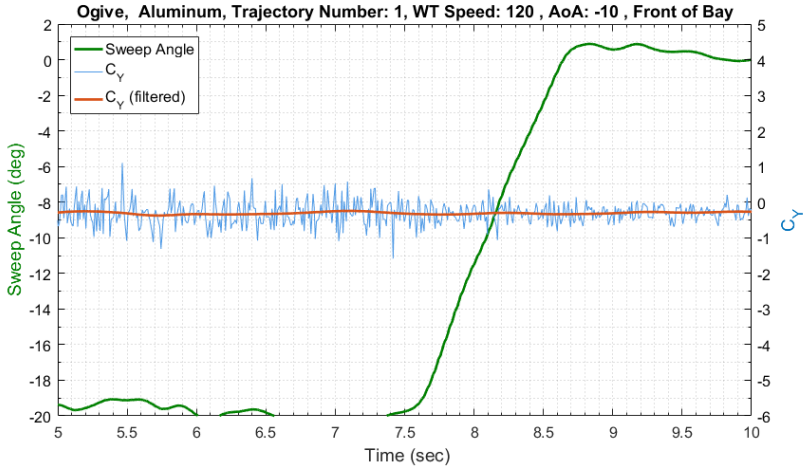
Ogive, Aluminum, Trajectory Number: 1, WT Speed: 120 , AoA: -10 , Front of Bay
Sweep Angle
C_Y
C_Y (filtered)
Sweep Angle (deg)
C_Y
Time (sec)

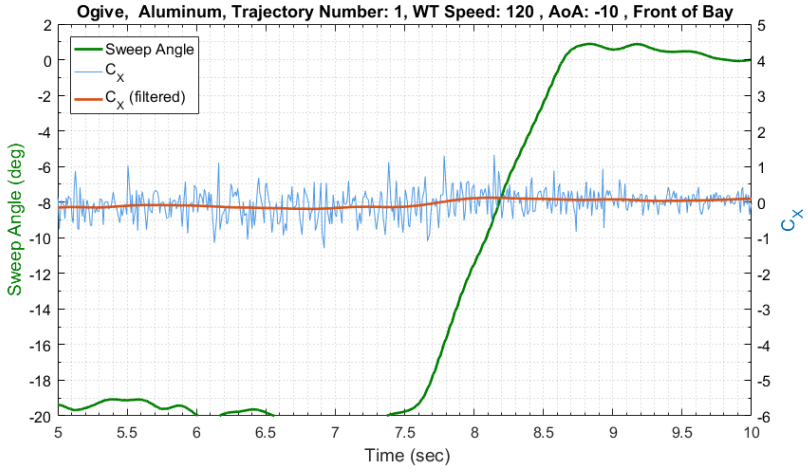
Ogive, Aluminum, Trajectory Number: 1, WT Speed: 120 , AoA: -10 , Front of Bay
Sweep Angle
C_X
C_X (filtered)
Sweep Angle (deg)
C_X
Time (sec)

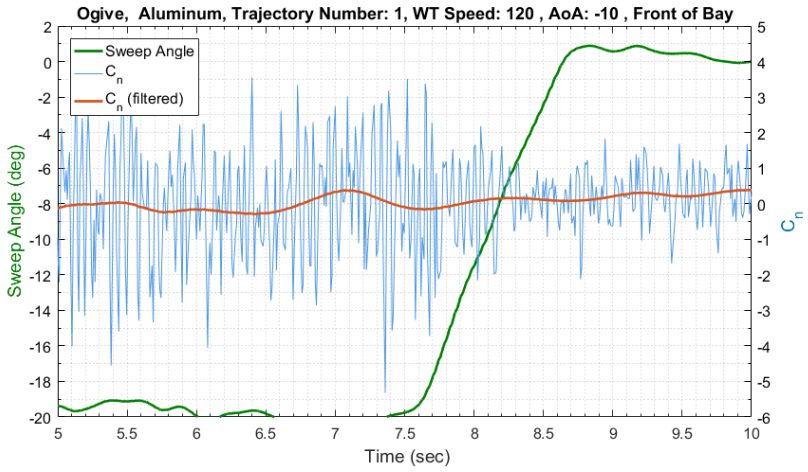
Ogive, Aluminum, Trajectory Number: 1, WT Speed: 120 , AoA: -10 , Front of Bay
Sweep Angle
C_n
C_n (filtered)
Sweep Angle (deg)
C_n
Time (sec)

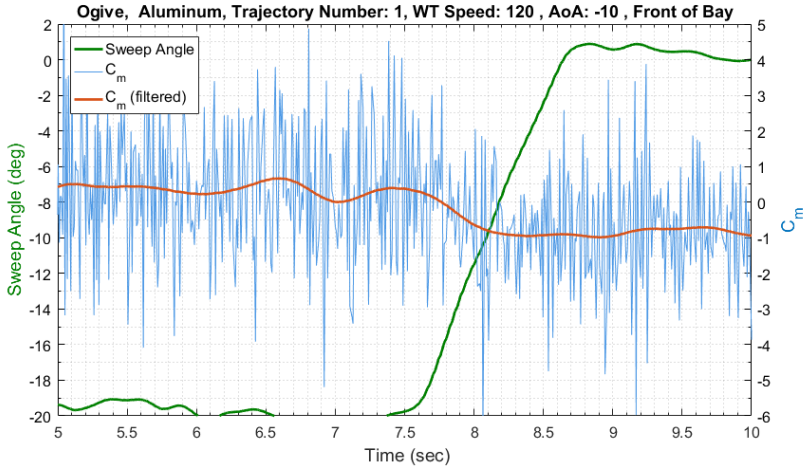
Ogive, Aluminum, Trajectory Number: 1, WT Speed: 120 , AoA: -10 , Front of Bay
Sweep Angle
C_m
C_m (filtered)
Sweep Angle (deg)
C_m
Time (sec)

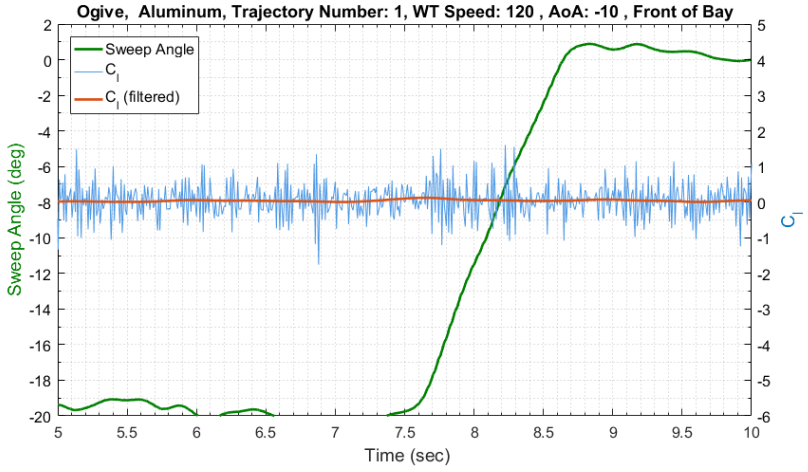
Ogive, Aluminum, Trajectory Number: 1, WT Speed: 120 , AoA: -10 , Front of Bay
Sweep Angle
C_l
C_l (filtered)
Sweep Angle (deg)
C_l
Time (sec)

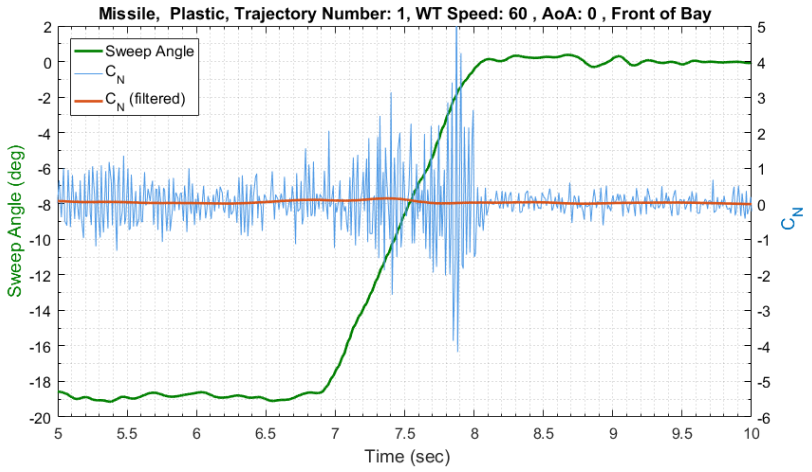
Missile, Plastic, Trajectory Number: 1, WT Speed: 60 , AoA: 0 , Front of Bay
Sweep Angle
C_N
C_N (filtered)
Sweep Angle (deg)
C_N
Time (sec)

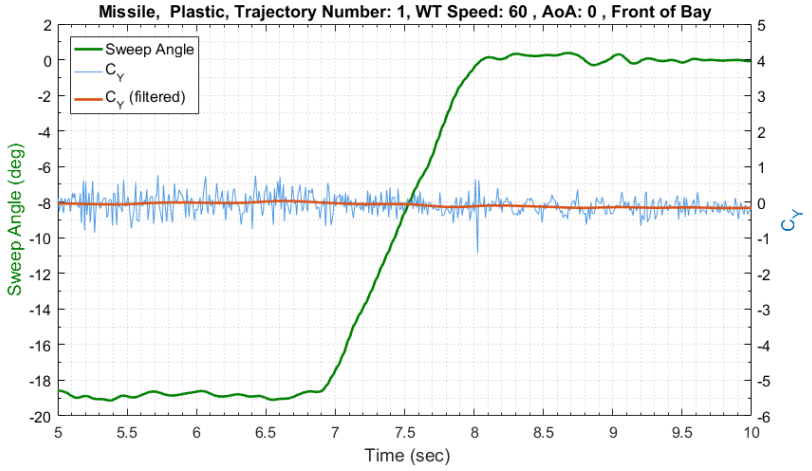
Missile, Plastic, Trajectory Number: 1, WT Speed: 60 , AoA: 0 , Front of Bay
Sweep Angle
C_Y
C_Y (filtered)
Sweep Angle (deg)
C_Y
Time (sec)

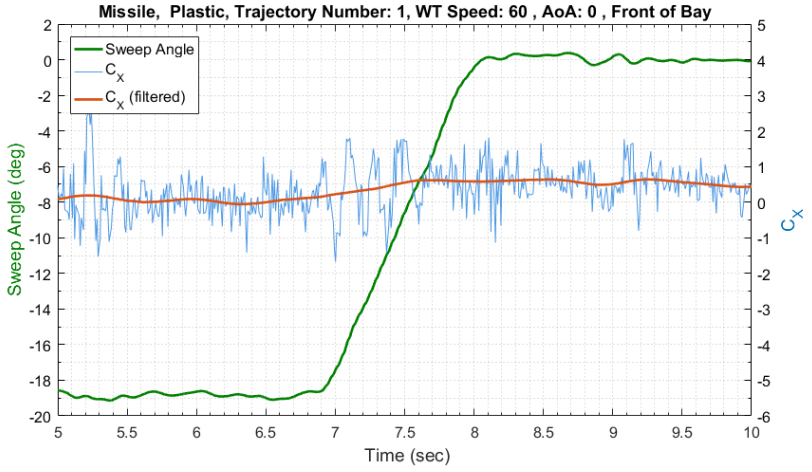
Missile, Plastic, Trajectory Number: 1, WT Speed: 60 , AoA: 0 , Front of Bay
Sweep Angle
C_X
C_X (filtered)
Sweep Angle (deg)
C_X
Time (sec)

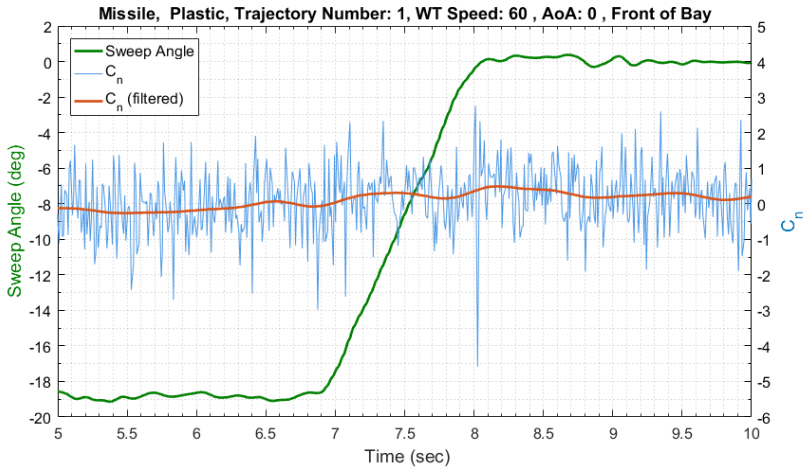
Missile, Plastic, Trajectory Number: 1, WT Speed: 60 , AoA: 0 , Front of Bay
Sweep Angle
C_n
C_n (filtered)
Sweep Angle (deg)
C_n
Time (sec)

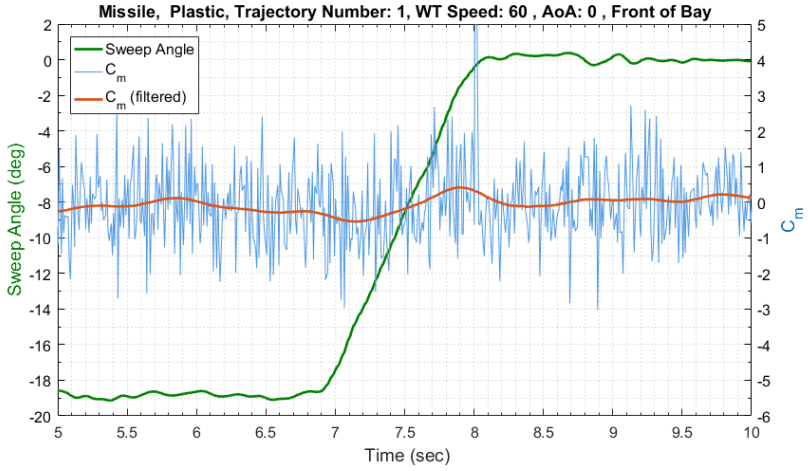
Missile, Plastic, Trajectory Number: 1, WT Speed: 60 , AoA: 0 , Front of Bay
Sweep Angle
C_m
C_m (filtered)
Sweep Angle (deg)
C_m
Time (sec)

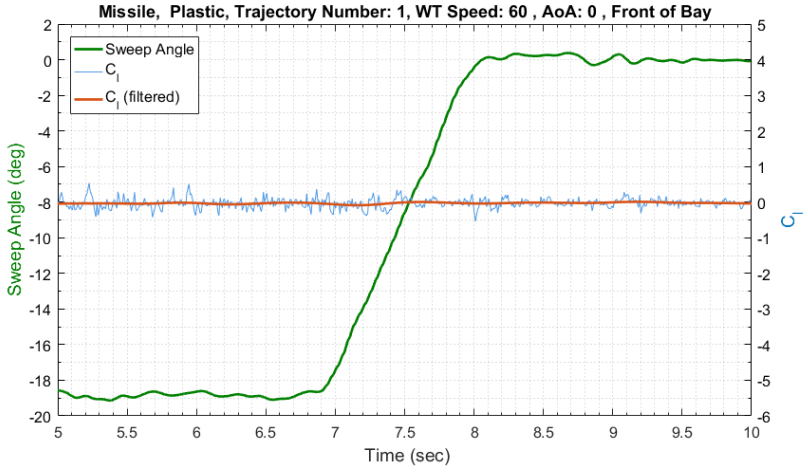
Missile, Plastic, Trajectory Number: 1, WT Speed: 60 , AoA: 0 , Front of Bay
Sweep Angle
C_l
C_l (filtered)
Sweep Angle (deg)
C_l
Time (sec)

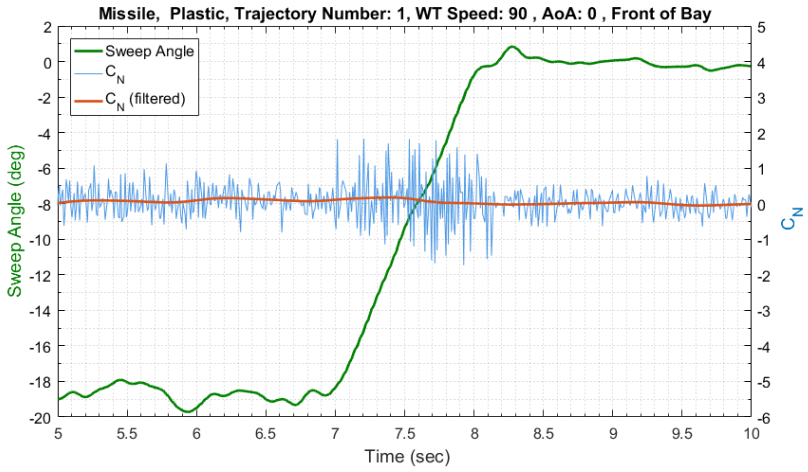
Missile, Plastic, Trajectory Number: 1, WT Speed: 90 , AoA: 0 , Front of Bay
Sweep Angle
C_N
C_N (filtered)
Sweep Angle (deg)
C_N
Time (sec)

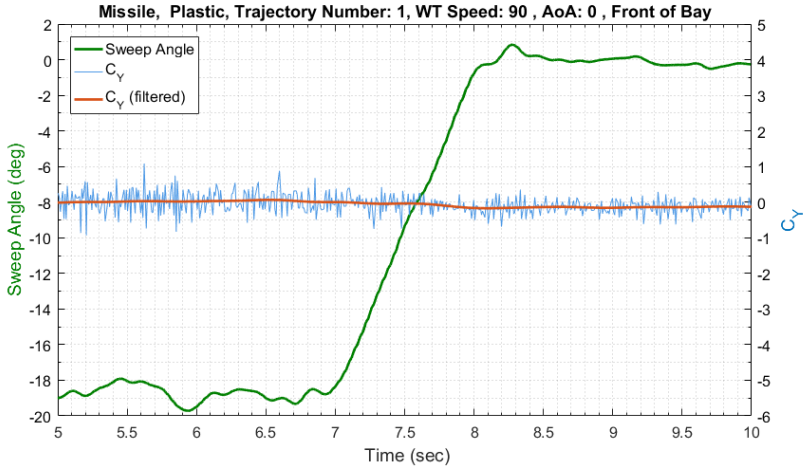
Missile, Plastic, Trajectory Number: 1, WT Speed: 90 , AoA: 0 , Front of Bay
Sweep Angle
C_Y
C_Y (filtered)
Sweep Angle (deg)
C_Y
Time (sec)

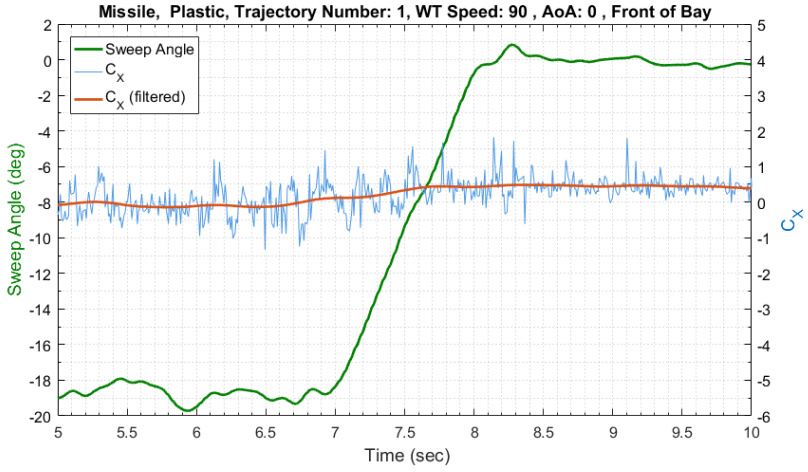
Missile, Plastic, Trajectory Number: 1, WT Speed: 90 , AoA: 0 , Front of Bay
Sweep Angle
C_X
C_X (filtered)
Sweep Angle (deg)
C_X
Time (sec)

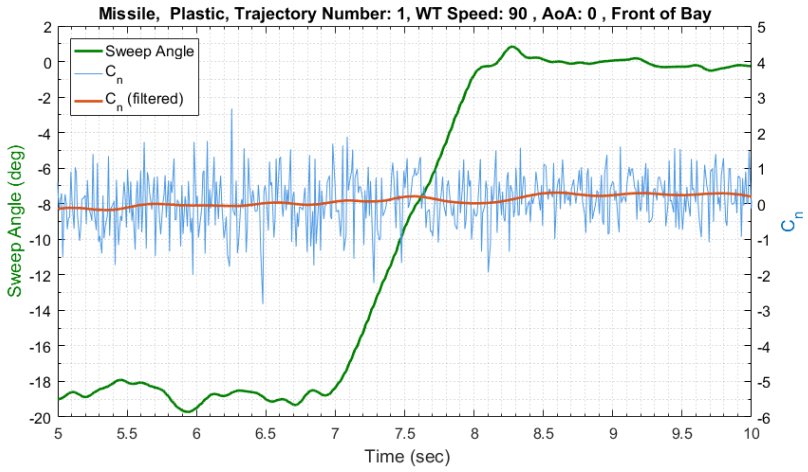
Missile, Plastic, Trajectory Number: 1, WT Speed: 90 , AoA: 0 , Front of Bay
Sweep Angle
C_n
C_n (filtered)
Sweep Angle (deg)
C_n
Time (sec)

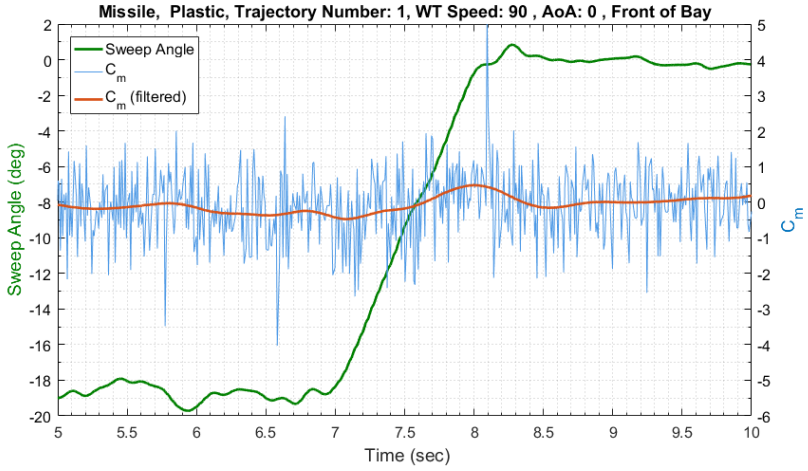
Missile, Plastic, Trajectory Number: 1, WT Speed: 90 , AoA: 0 , Front of Bay
Sweep Angle
C_m
C_m (filtered)
Sweep Angle (deg)
C_m
Time (sec)

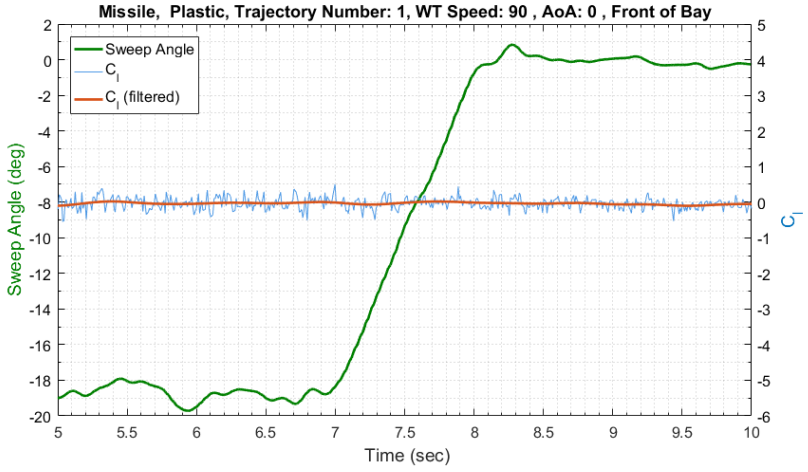
Missile, Plastic, Trajectory Number: 1, WT Speed: 90 , AoA: 0 , Front of Bay
Sweep Angle
C_l
C_l (filtered)
Sweep Angle (deg)
C_l
Time (sec)

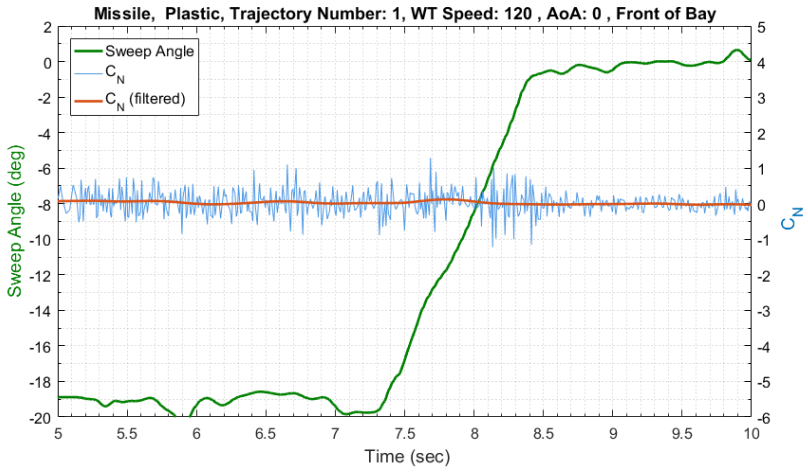
Missile, Plastic, Trajectory Number: 1, WT Speed: 120 , AoA: 0 , Front of Bay
Sweep Angle
C_N
C_N (filtered)
Sweep Angle (deg)
C_N
Time (sec)

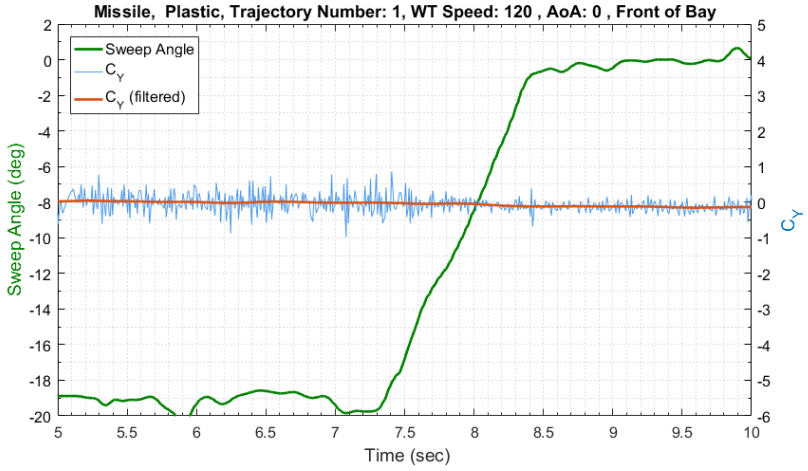
Missile, Plastic, Trajectory Number: 1, WT Speed: 120 , AoA: 0 , Front of Bay
Sweep Angle
C_Y
C_Y (filtered)
Sweep Angle (deg)
C_Y
Time (sec)

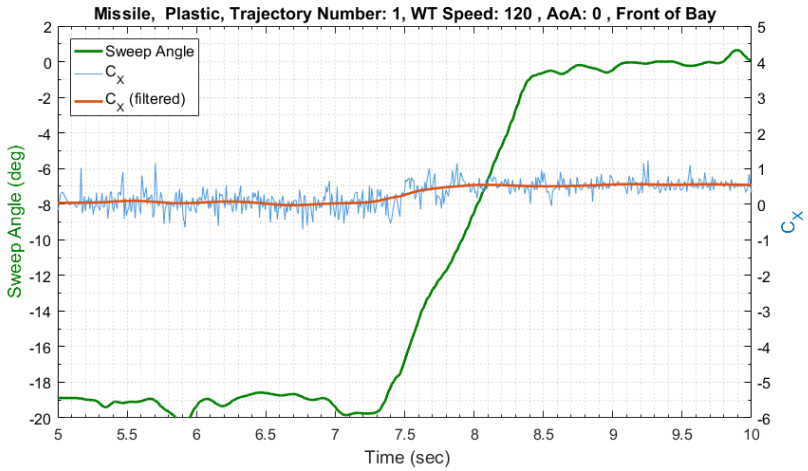
Missile, Plastic, Trajectory Number: 1, WT Speed: 120 , AoA: 0 , Front of Bay
Sweep Angle
C_X
C_X (filtered)
Sweep Angle (deg)
C_X
Time (sec)

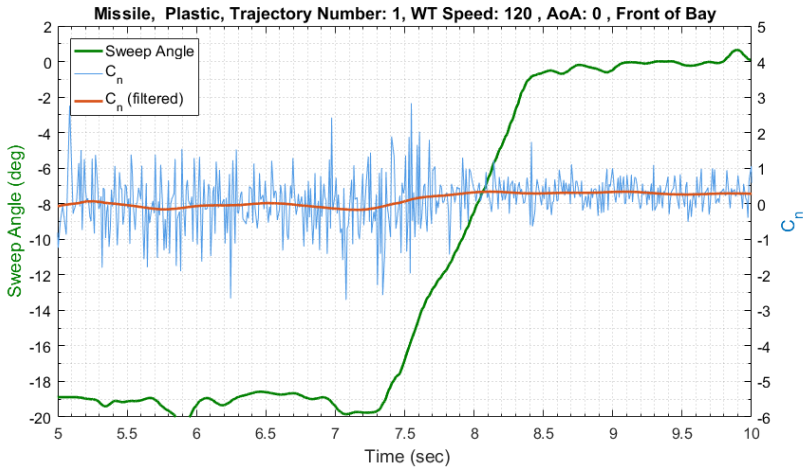
Missile, Plastic, Trajectory Number: 1, WT Speed: 120 , AoA: 0 , Front of Bay
Sweep Angle
C_n
C_n (filtered)
Sweep Angle (deg)
C_n
Time (sec)

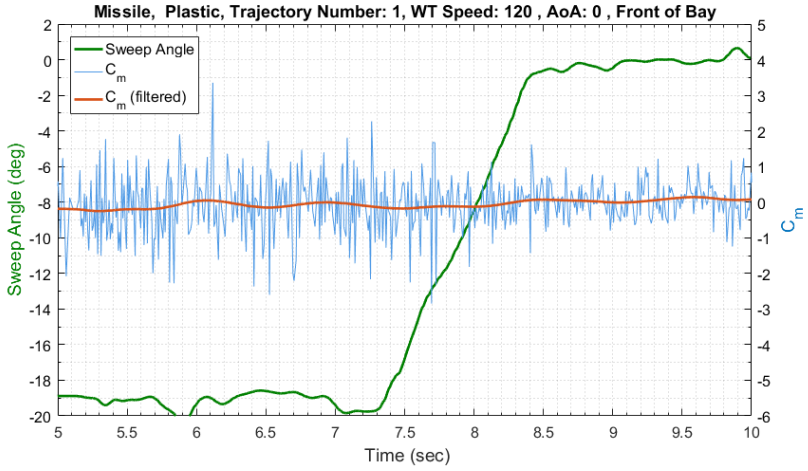
Missile, Plastic, Trajectory Number: 1, WT Speed: 120 , AoA: 0 , Front of Bay
Sweep Angle
C_m
C_m (filtered)
Sweep Angle (deg)
C_m
Time (sec)

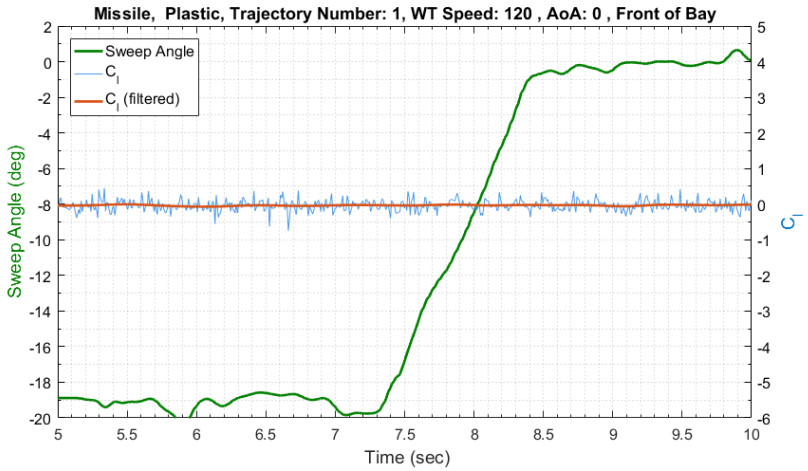
Missile, Plastic, Trajectory Number: 1, WT Speed: 120 , AoA: 0 , Front of Bay
Sweep Angle
C_l
C_l (filtered)
Sweep Angle (deg)
C_l
Time (sec)

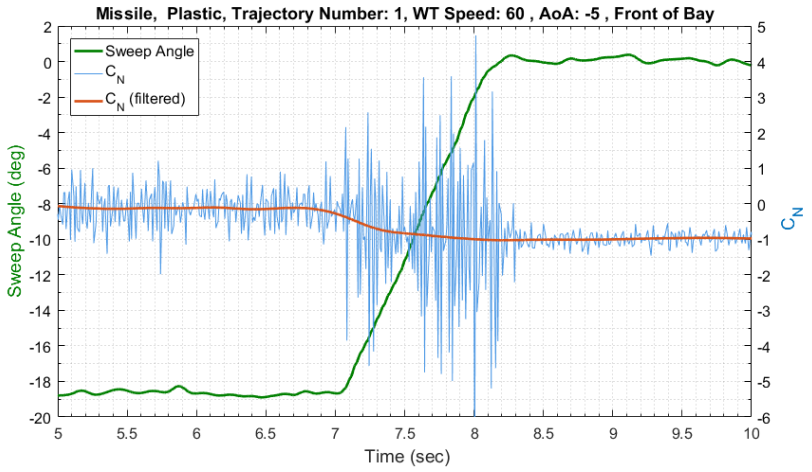
Missile, Plastic, Trajectory Number: 1, WT Speed: 60 , AoA: -5 , Front of Bay
Sweep Angle
C_N
C_N (filtered)
Sweep Angle (deg)
C_N
Time (sec)

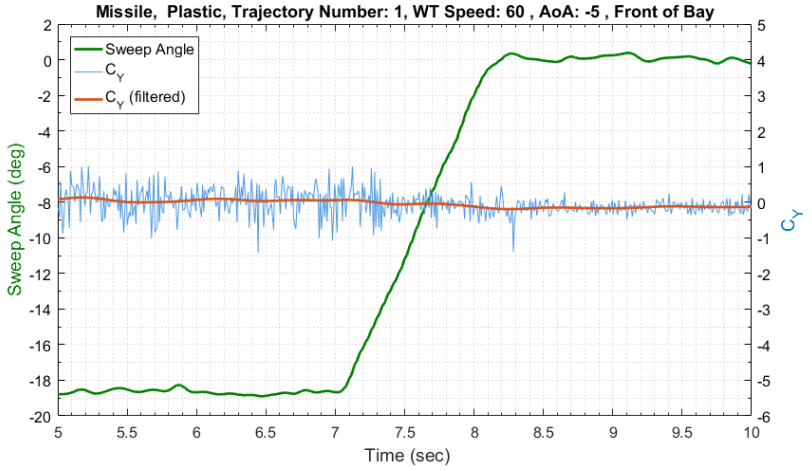
Missile, Plastic, Trajectory Number: 1, WT Speed: 60 , AoA: -5 , Front of Bay
Sweep Angle
C_Y
C_Y (filtered)
Sweep Angle (deg)
C_Y
Time (sec)

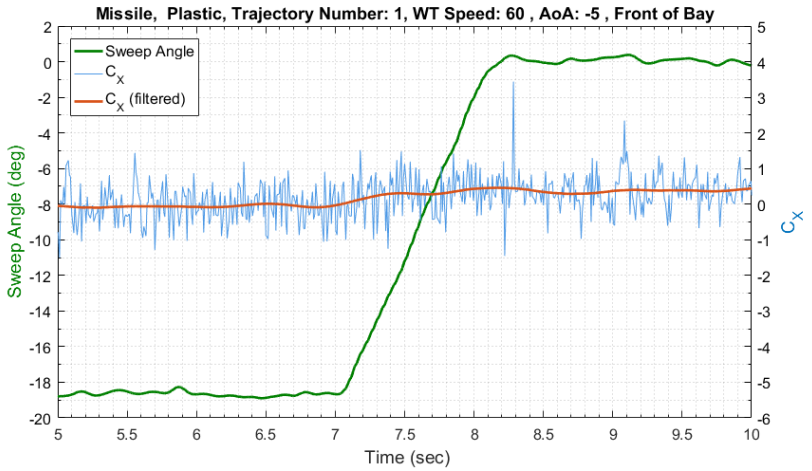
Missile, Plastic, Trajectory Number: 1, WT Speed: 60 , AoA: -5 , Front of Bay
Sweep Angle
C_X
C_X (filtered)
Sweep Angle (deg)
C_X
Time (sec)

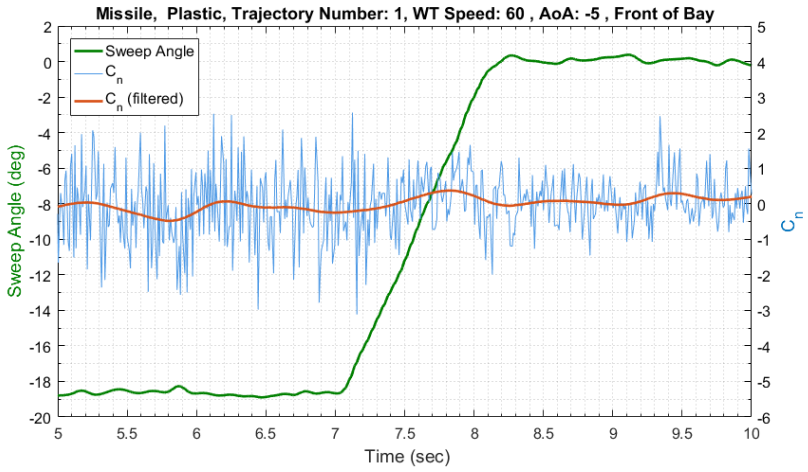
Missile, Plastic, Trajectory Number: 1, WT Speed: 60 , AoA: -5 , Front of Bay
Sweep Angle
C_n
C_n (filtered)
Sweep Angle (deg)
C_n
Time (sec)

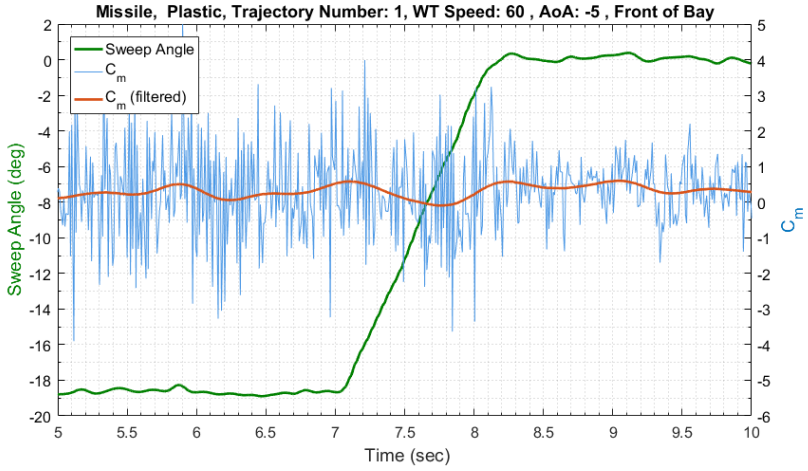
Missile, Plastic, Trajectory Number: 1, WT Speed: 60 , AoA: -5 , Front of Bay
Sweep Angle
C_m
C_m (filtered)
Sweep Angle (deg)
C_m
Time (sec)

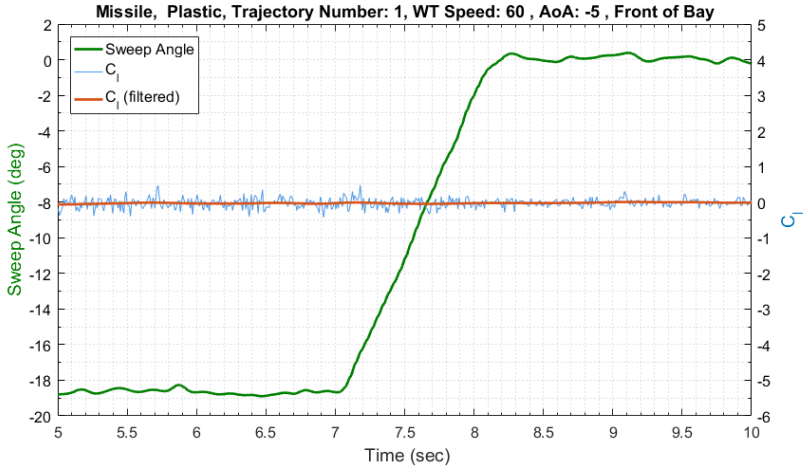
Missile, Plastic, Trajectory Number: 1, WT Speed: 60 , AoA: -5 , Front of Bay
Sweep Angle
C_l
C_l (filtered)
Sweep Angle (deg)
C_l
Time (sec)

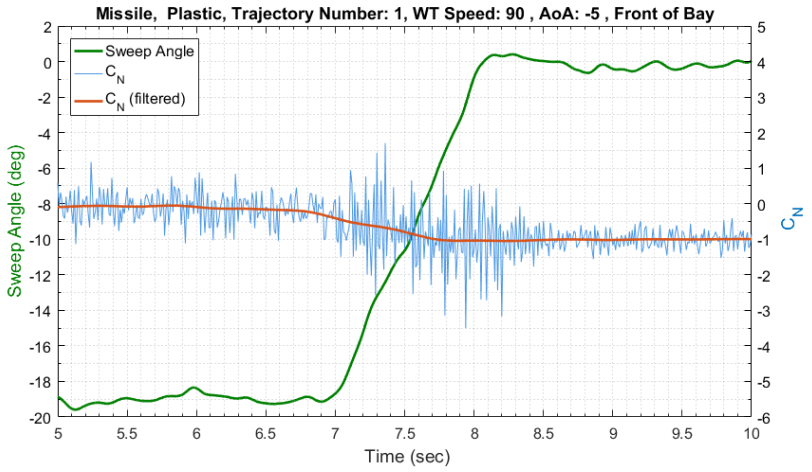
Missile, Plastic, Trajectory Number: 1, WT Speed: 90 , AoA: -5 , Front of Bay
Sweep Angle
C_N
C_N (filtered)
Sweep Angle (deg)
C_N
Time (sec)

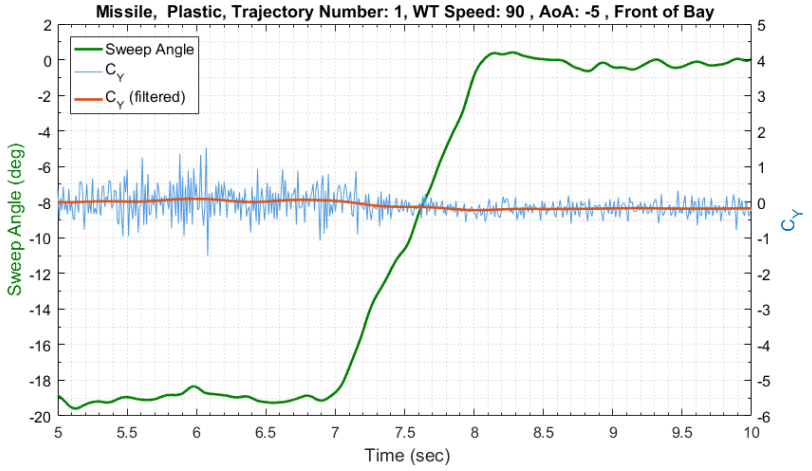
Missile, Plastic, Trajectory Number: 1, WT Speed: 90 , AoA: -5 , Front of Bay
Sweep Angle
C_Y
C_Y (filtered)
Sweep Angle (deg)
C_Y
Time (sec)

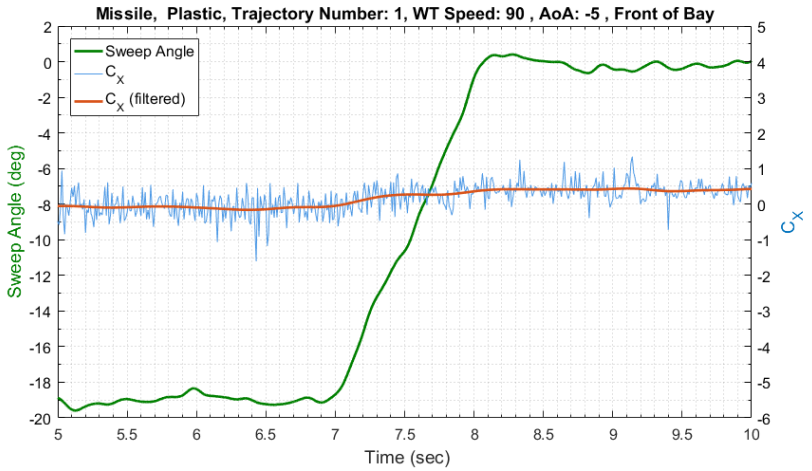
Missile, Plastic, Trajectory Number: 1, WT Speed: 90 , AoA: -5 , Front of Bay
Sweep Angle
C_X
C_X (filtered)
Sweep Angle (deg)
C_X
Time (sec)

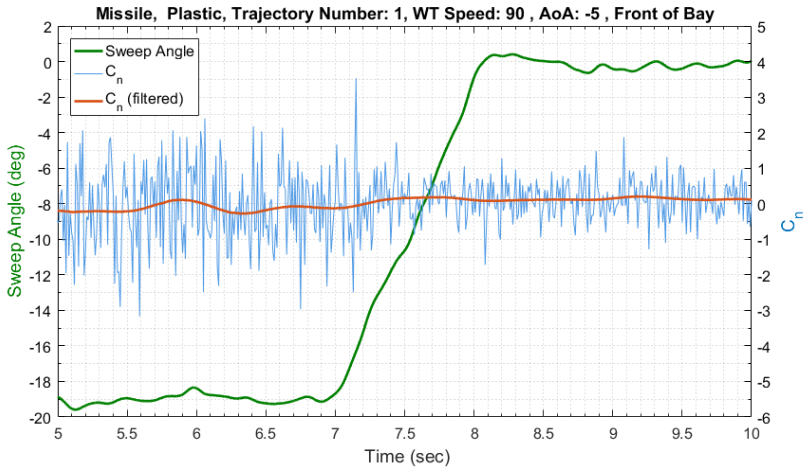
Missile, Plastic, Trajectory Number: 1, WT Speed: 90 , AoA: -5 , Front of Bay
Sweep Angle
C_n
C_n (filtered)
Sweep Angle (deg)
C_n
Time (sec)

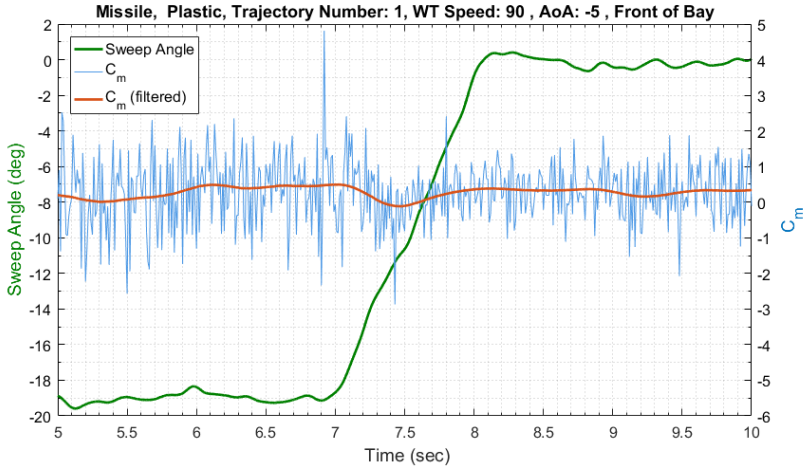
Missile, Plastic, Trajectory Number: 1, WT Speed: 90 , AoA: -5 , Front of Bay
Sweep Angle
C_m
C_m (filtered)
Sweep Angle (deg)
C_m
Time (sec)

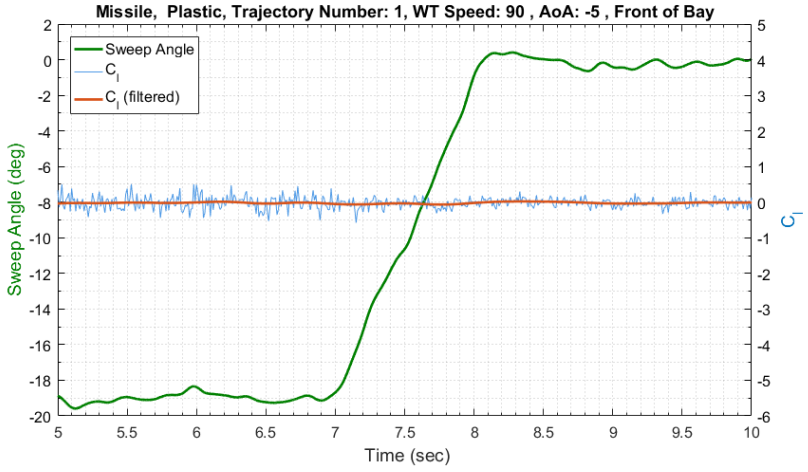
Missile, Plastic, Trajectory Number: 1, WT Speed: 90 , AoA: -5 , Front of Bay
Sweep Angle
C_l
C_l (filtered)
Sweep Angle (deg)
C_l
Time (sec)

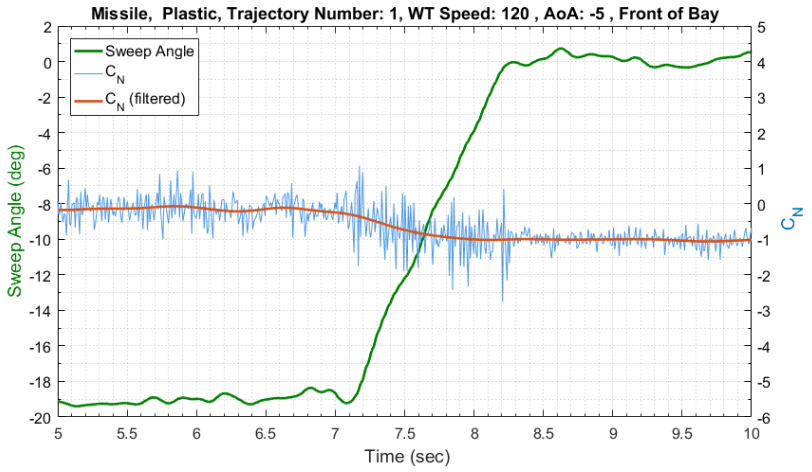
Missile, Plastic, Trajectory Number: 1, WT Speed: 120 , AoA: -5 , Front of Bay
Sweep Angle
C_N
C_N (filtered)
Sweep Angle (deg)
C_N
Time (sec)

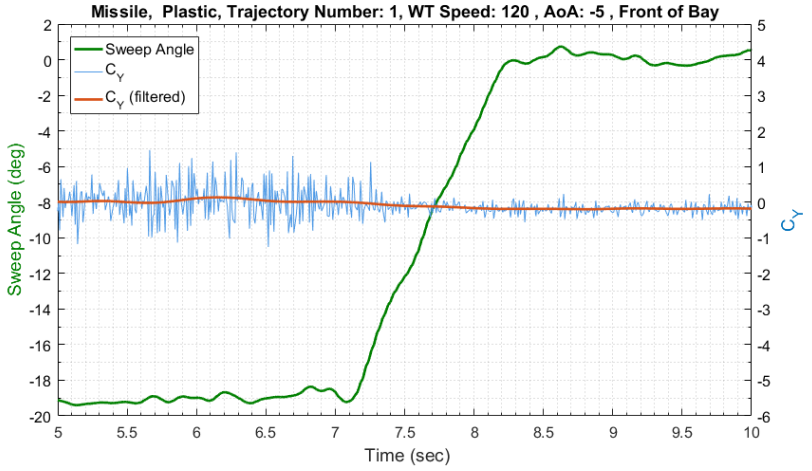
Missile, Plastic, Trajectory Number: 1, WT Speed: 120 , AoA: -5 , Front of Bay
Sweep Angle
C_Y
C_Y (filtered)
Sweep Angle (deg)
C_Y
Time (sec)

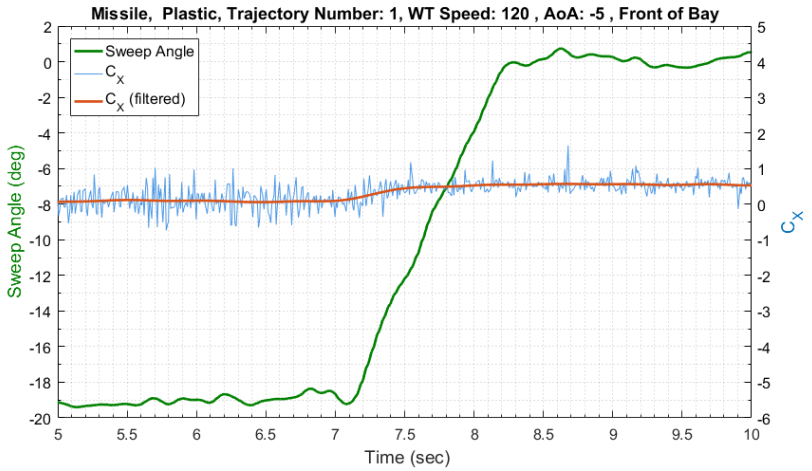
Missile, Plastic, Trajectory Number: 1, WT Speed: 120 , AoA: -5 , Front of Bay
Sweep Angle
C_X
C_X (filtered)
Sweep Angle (deg)
C_X
Time (sec)

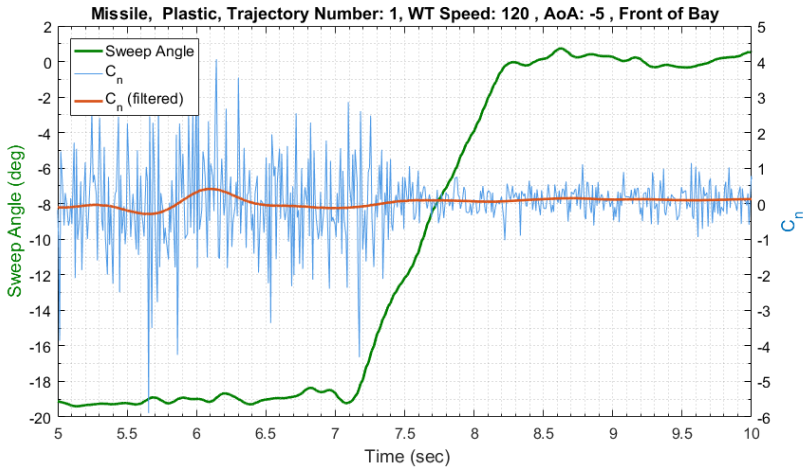
Missile, Plastic, Trajectory Number: 1, WT Speed: 120 , AoA: -5 , Front of Bay
Sweep Angle
C_n
C_n (filtered)
Sweep Angle (deg)
C_n
Time (sec)

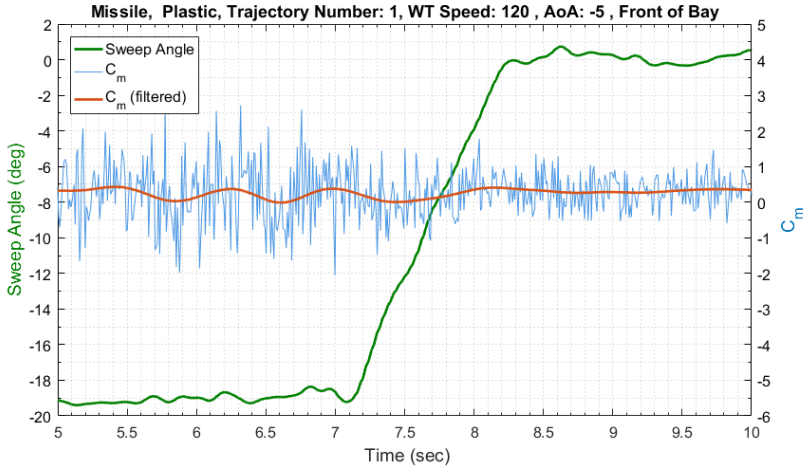
Missile, Plastic, Trajectory Number: 1, WT Speed: 120 , AoA: -5 , Front of Bay
Sweep Angle
C_m
C_m (filtered)
Sweep Angle (deg)
C_m
Time (sec)

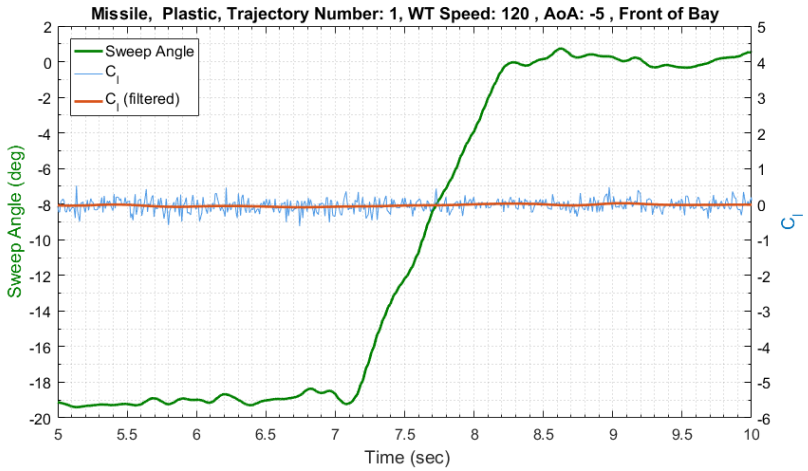
Missile, Plastic, Trajectory Number: 1, WT Speed: 120 , AoA: -5 , Front of Bay
Sweep Angle
C_l
C_l (filtered)
Sweep Angle (deg)
C_l
Time (sec)

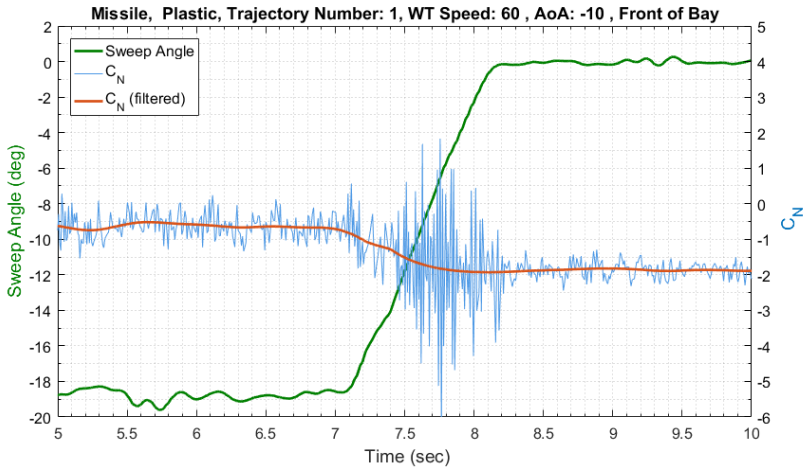
Missile, Plastic, Trajectory Number: 1, WT Speed: 60 , AoA: -10 , Front of Bay
Sweep Angle
C_N
C_N (filtered)
Sweep Angle (deg)
C_N
Time (sec)

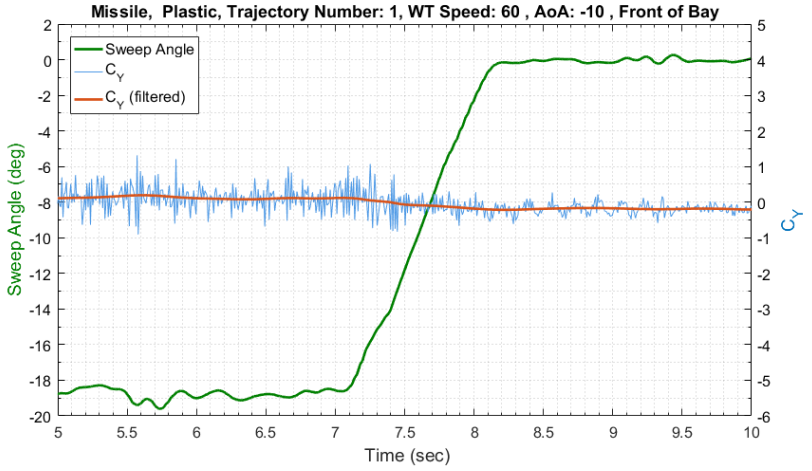
Missile, Plastic, Trajectory Number: 1, WT Speed: 60 , AoA: -10 , Front of Bay
Sweep Angle
C_Y
C_Y (filtered)
Sweep Angle (deg)
C_Y
Time (sec)

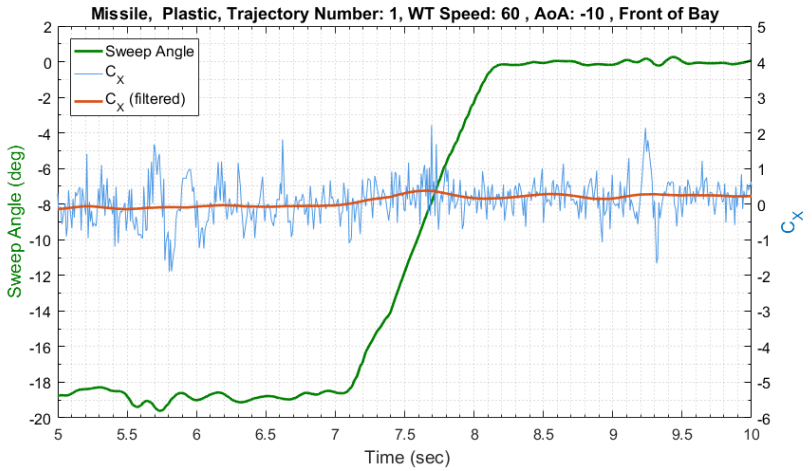
Missile, Plastic, Trajectory Number: 1, WT Speed: 60 , AoA: -10 , Front of Bay
Sweep Angle
C_X
C_X (filtered)
Sweep Angle (deg)
C_X
Time (sec)

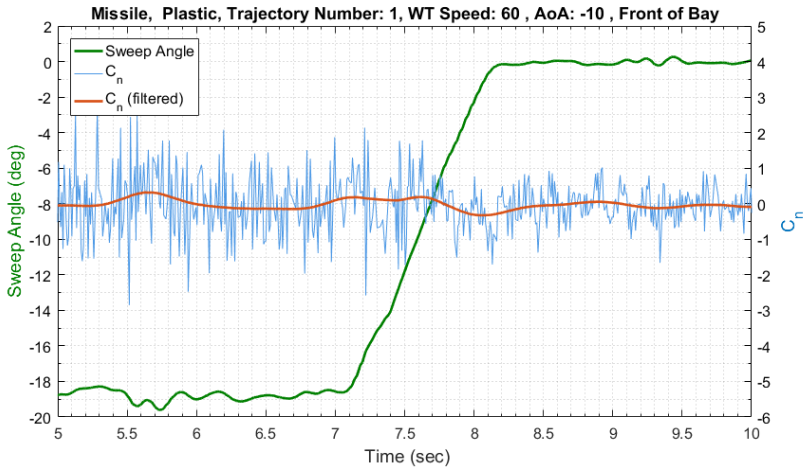
Missile, Plastic, Trajectory Number: 1, WT Speed: 60 , AoA: -10 , Front of Bay
Sweep Angle
C_n
C_n (filtered)
Sweep Angle (deg)
C_n
Time (sec)

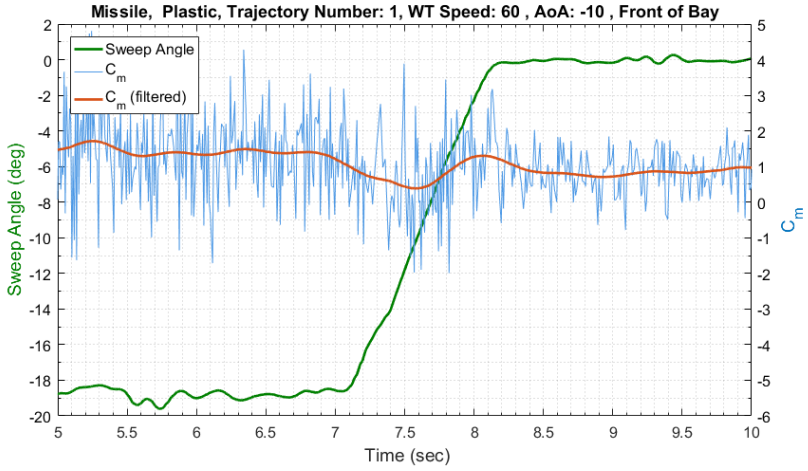
Missile, Plastic, Trajectory Number: 1, WT Speed: 60 , AoA: -10 , Front of Bay
Sweep Angle
C_m
C_m (filtered)
Sweep Angle (deg)
C_m
Time (sec)

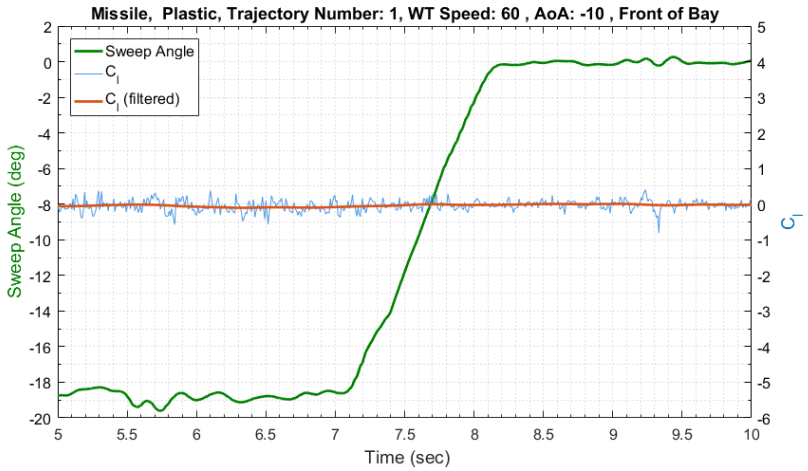
Missile, Plastic, Trajectory Number: 1, WT Speed: 60 , AoA: -10 , Front of Bay
Sweep Angle
C_l
C_l (filtered)
Sweep Angle (deg)
C_l
Time (sec)

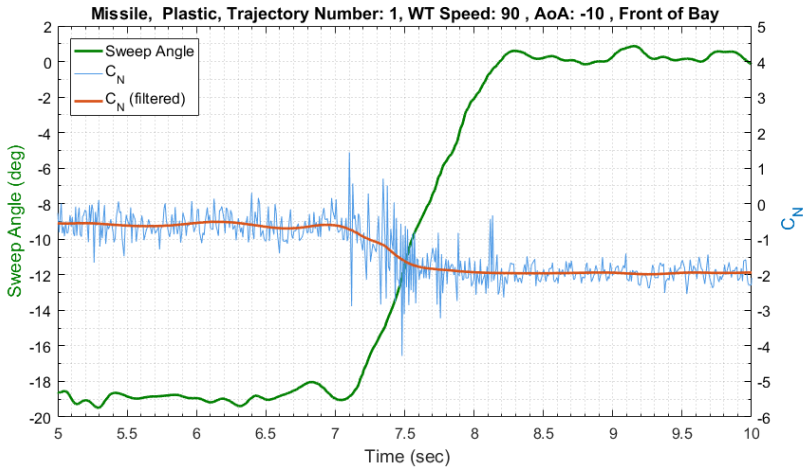
Missile, Plastic, Trajectory Number: 1, WT Speed: 90 , AoA: -10 , Front of Bay
Sweep Angle
C_N
C_N (filtered)
Sweep Angle (deg)
C_N
Time (sec)

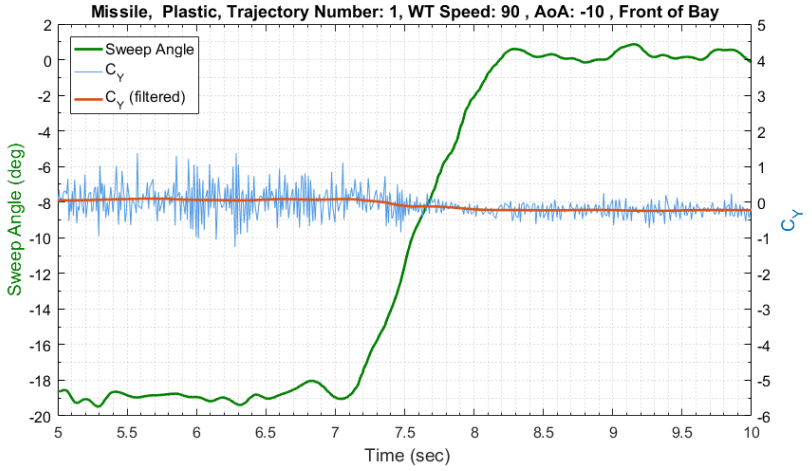
Missile, Plastic, Trajectory Number: 1, WT Speed: 90 , AoA: -10 , Front of Bay
Sweep Angle
C_Y
C_Y (filtered)
Sweep Angle (deg)
C_Y
Time (sec)

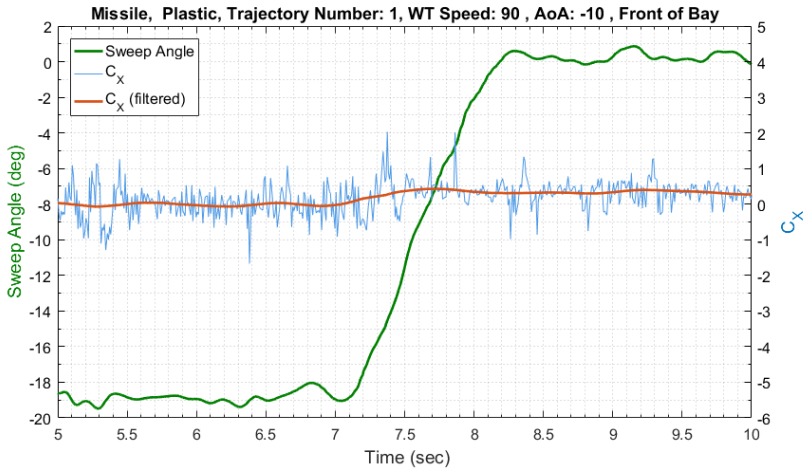
Missile, Plastic, Trajectory Number: 1, WT Speed: 90 , AoA: -10 , Front of Bay
Sweep Angle
C_X
C_X (filtered)
Sweep Angle (deg)
C_X
Time (sec)

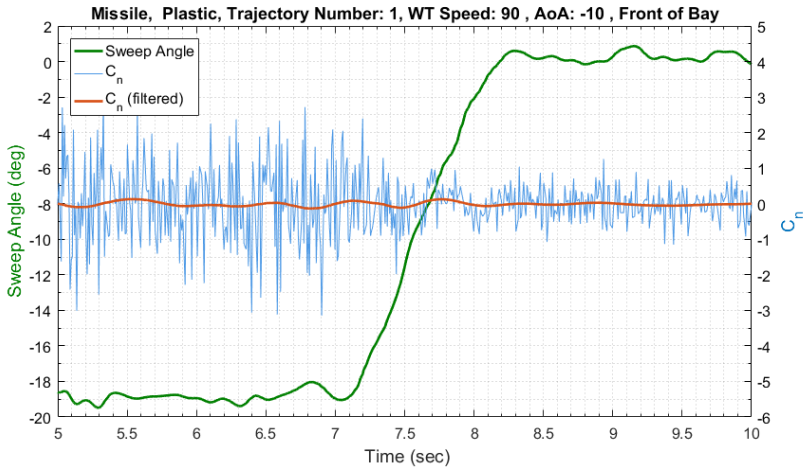
Missile, Plastic, Trajectory Number: 1, WT Speed: 90 , AoA: -10 , Front of Bay
Sweep Angle
C_n
C_n (filtered)
Sweep Angle (deg)
C_n
Time (sec)

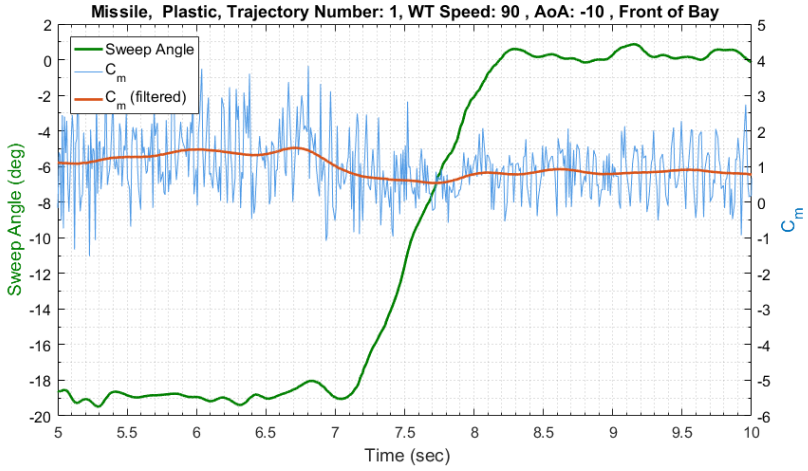
Missile, Plastic, Trajectory Number: 1, WT Speed: 90 , AoA: -10 , Front of Bay
Sweep Angle
C_m
C_m (filtered)
Sweep Angle (deg)
C_m
Time (sec)

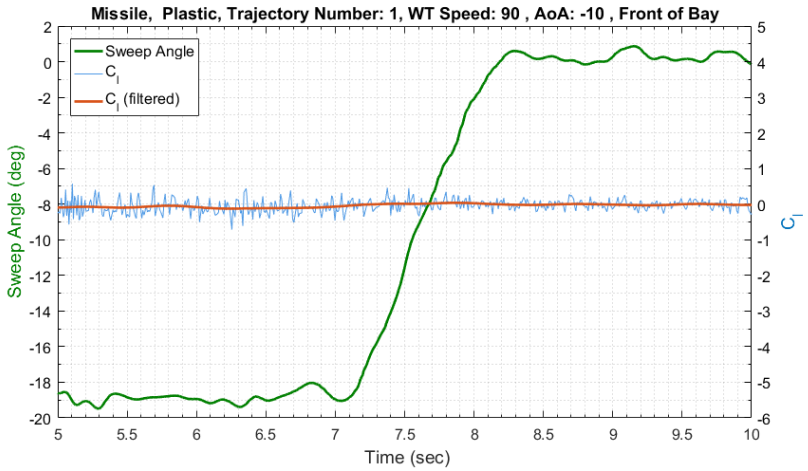
Missile, Plastic, Trajectory Number: 1, WT Speed: 90 , AoA: -10 , Front of Bay
Sweep Angle
C_l
C_l (filtered)
Sweep Angle (deg)
C_l
Time (sec)

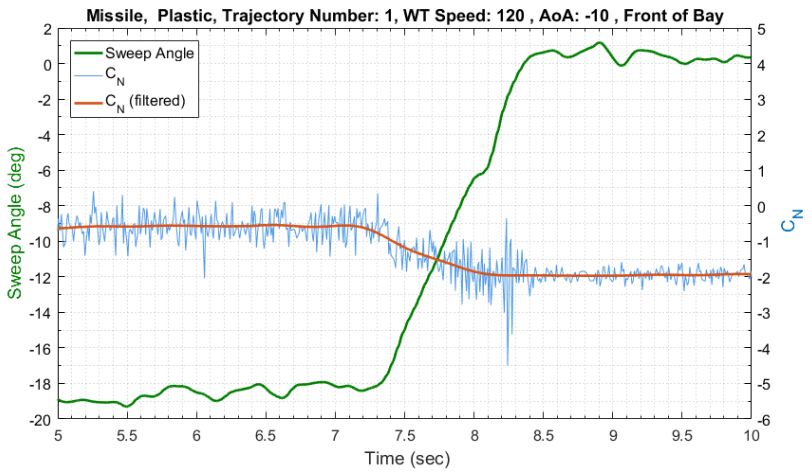
Missile, Plastic, Trajectory Number: 1, WT Speed: 120 , AoA: -10 , Front of Bay
Sweep Angle
C_N
C_N (filtered)
Sweep Angle (deg)
C_N
Time (sec)

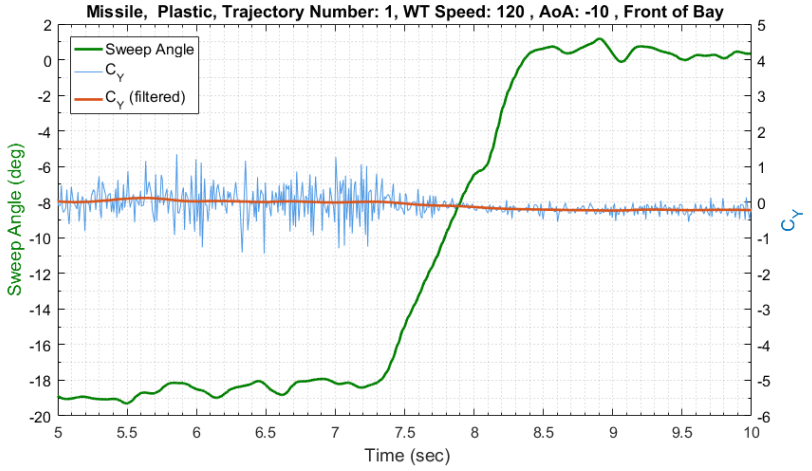
Missile, Plastic, Trajectory Number: 1, WT Speed: 120 , AoA: -10 , Front of Bay
Sweep Angle
C_Y
C_Y (filtered)
Sweep Angle (deg)
C_Y
Time (sec)

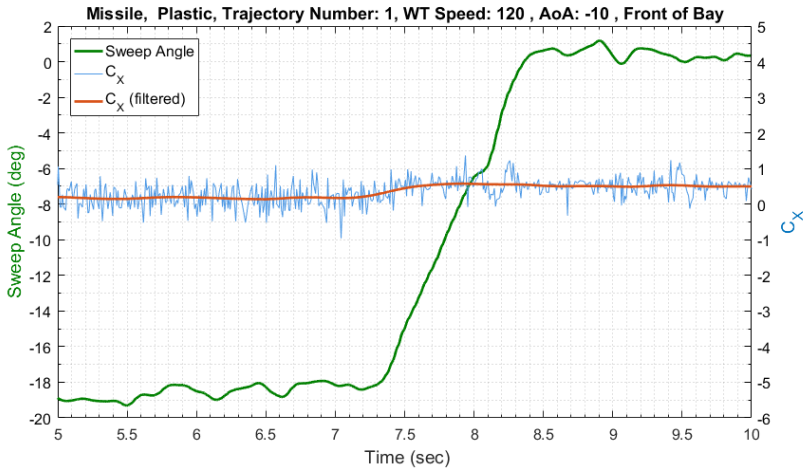
Missile, Plastic, Trajectory Number: 1, WT Speed: 120 , AoA: -10 , Front of Bay
Sweep Angle
C_X
C_X (filtered)
Sweep Angle (deg)
C_X
Time (sec)

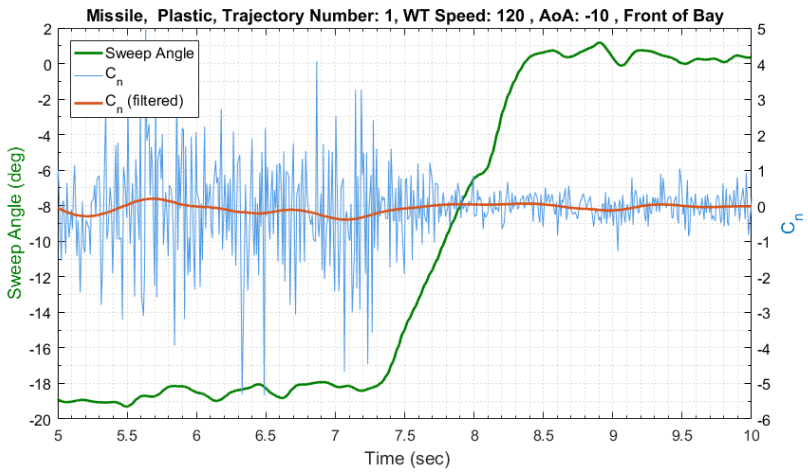
Missile, Plastic, Trajectory Number: 1, WT Speed: 120 , AoA: -10 , Front of Bay
Sweep Angle
C_n
C_n (filtered)
Sweep Angle (deg)
C_n
Time (sec)

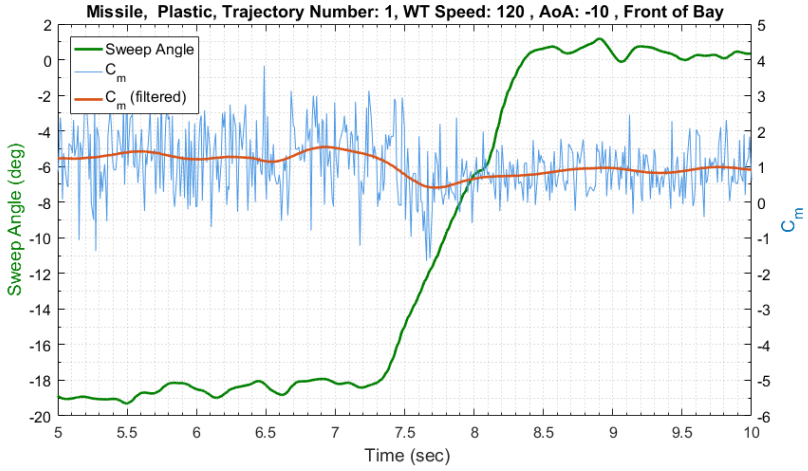
Missile, Plastic, Trajectory Number: 1, WT Speed: 120 , AoA: -10 , Front of Bay
Sweep Angle
C_m
C_m (filtered)
Sweep Angle (deg)
C_m
Time (sec)

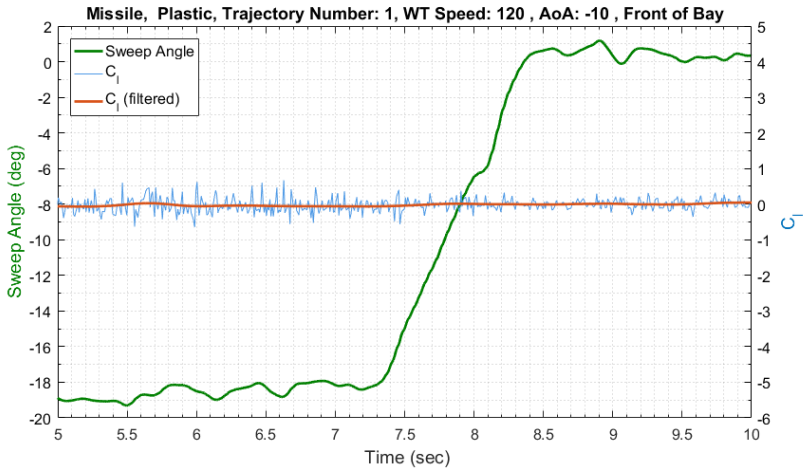
Missile, Plastic, Trajectory Number: 1, WT Speed: 120 , AoA: -10 , Front of Bay
Sweep Angle
C_l
C_l (filtered)
Sweep Angle (deg)
C_l
Time (sec)

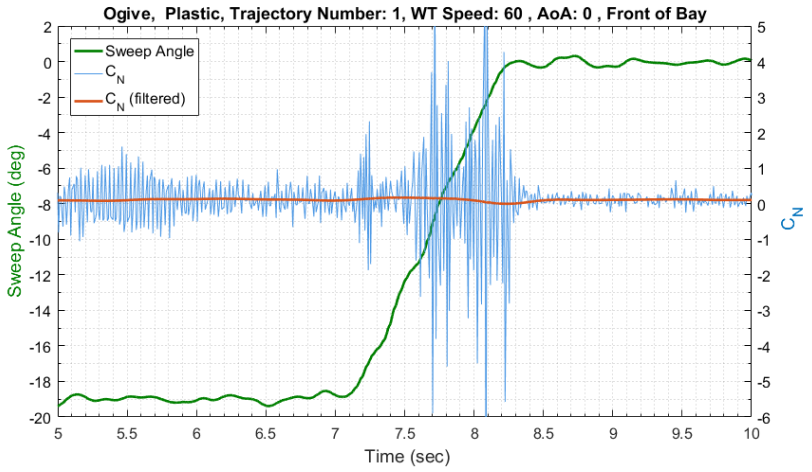
Ogive, Plastic, Trajectory Number: 1, WT Speed: 60 , AoA: 0 , Front of Bay
Sweep Angle
C_N
C_N (filtered)
Sweep Angle (deg)
C_N
Time (sec)

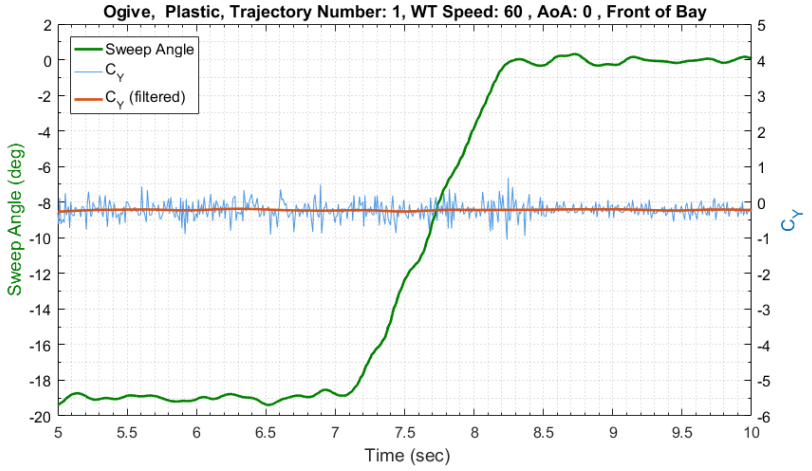
Ogive, Plastic, Trajectory Number: 1, WT Speed: 60 , AoA: 0 , Front of Bay
Sweep Angle
C_Y
C_Y (filtered)
Sweep Angle (deg)
C_Y
Time (sec)

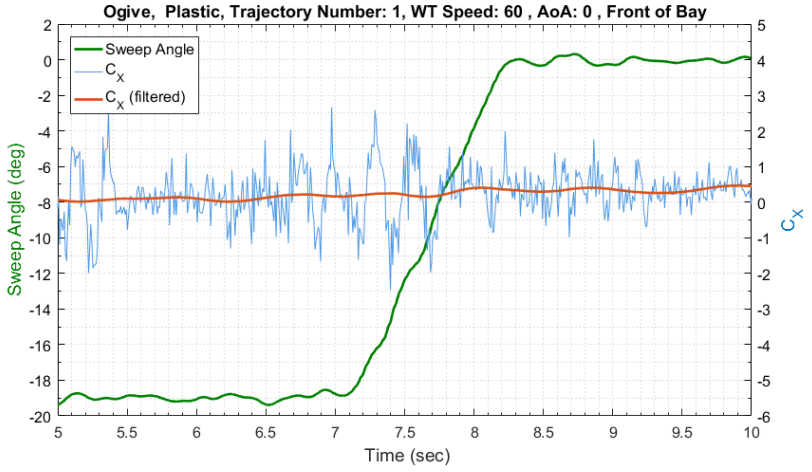
Ogive, Plastic, Trajectory Number: 1, WT Speed: 60 , AoA: 0 , Front of Bay
Sweep Angle
C_X
C_X (filtered)
Sweep Angle (deg)
C_X
Time (sec)

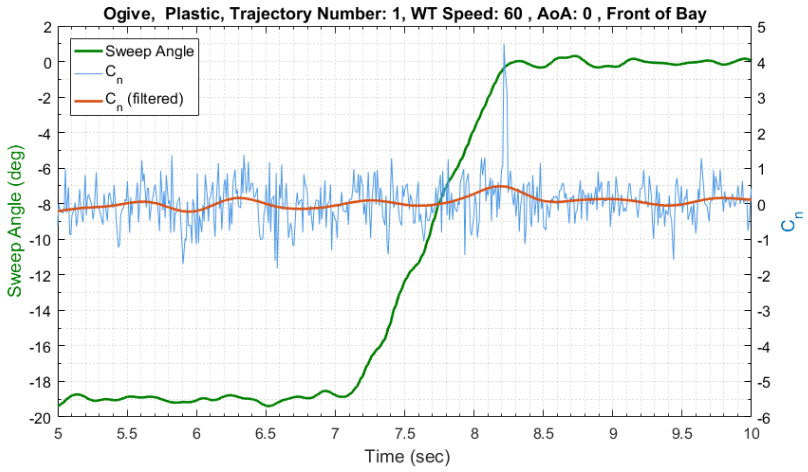
Ogive, Plastic, Trajectory Number: 1, WT Speed: 60 , AoA: 0 , Front of Bay
Sweep Angle
C_n
C_n (filtered)
Sweep Angle (deg)
C_n
Time (sec)

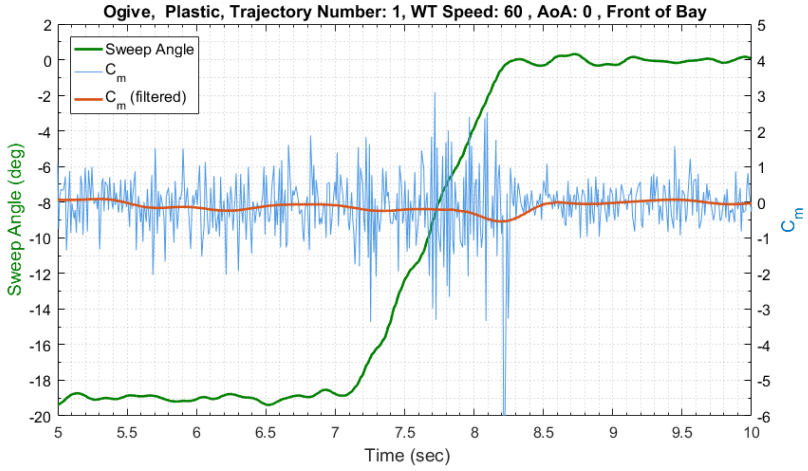
Ogive, Plastic, Trajectory Number: 1, WT Speed: 60 , AoA: 0 , Front of Bay
Sweep Angle
C_m
C_m (filtered)
Sweep Angle (deg)
C_m
Time (sec)

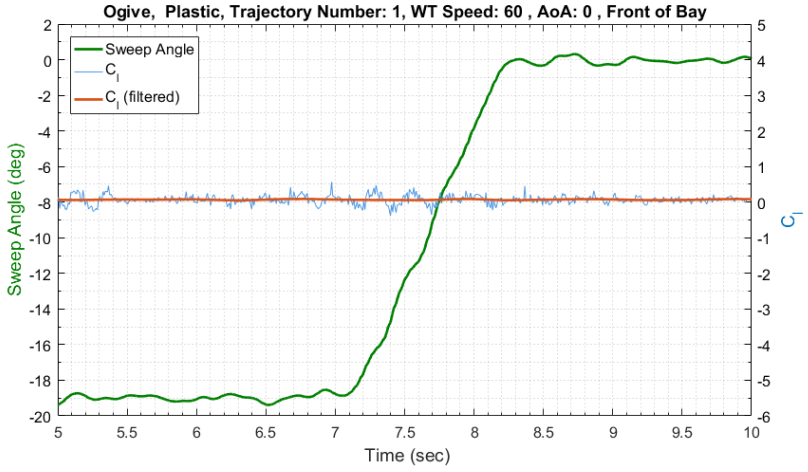
Ogive, Plastic, Trajectory Number: 1, WT Speed: 60 , AoA: 0 , Front of Bay
Sweep Angle
C_l
C_l (filtered)
Sweep Angle (deg)
C_l
Time (sec)

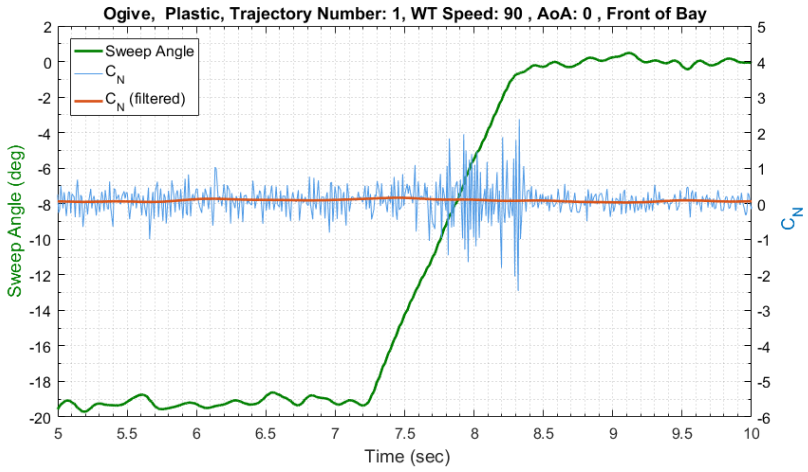
Ogive, Plastic, Trajectory Number: 1, WT Speed: 90 , AoA: 0 , Front of Bay
Sweep Angle
C_N
C_N (filtered)
Sweep Angle (deg)
C_N
Time (sec)

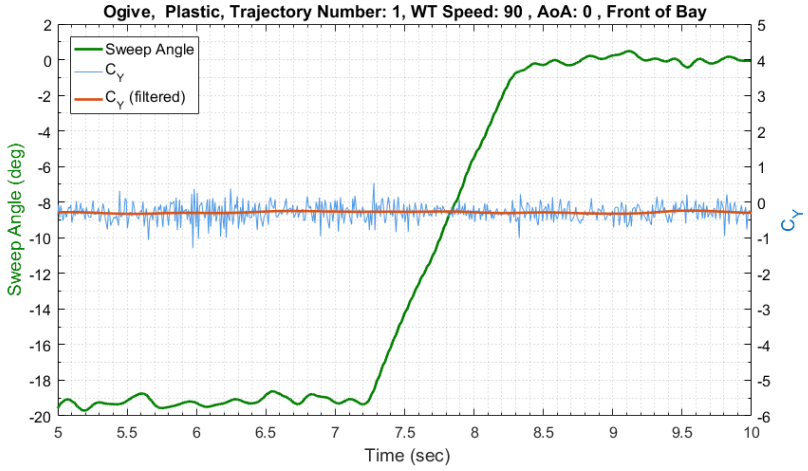
Ogive, Plastic, Trajectory Number: 1, WT Speed: 90 , AoA: 0 , Front of Bay
Sweep Angle
C_Y
C_Y (filtered)
Sweep Angle (deg)
C_Y
Time (sec)

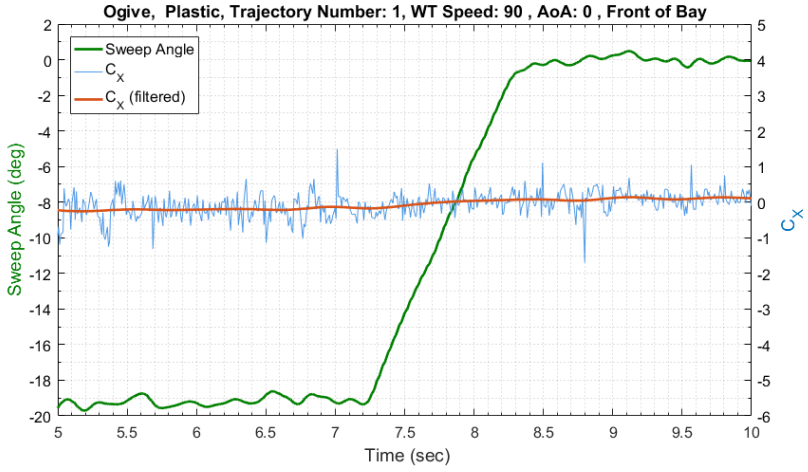
Ogive, Plastic, Trajectory Number: 1, WT Speed: 90 , AoA: 0 , Front of Bay
Sweep Angle
C_X
C_X (filtered)
Sweep Angle (deg)
C_X
Time (sec)

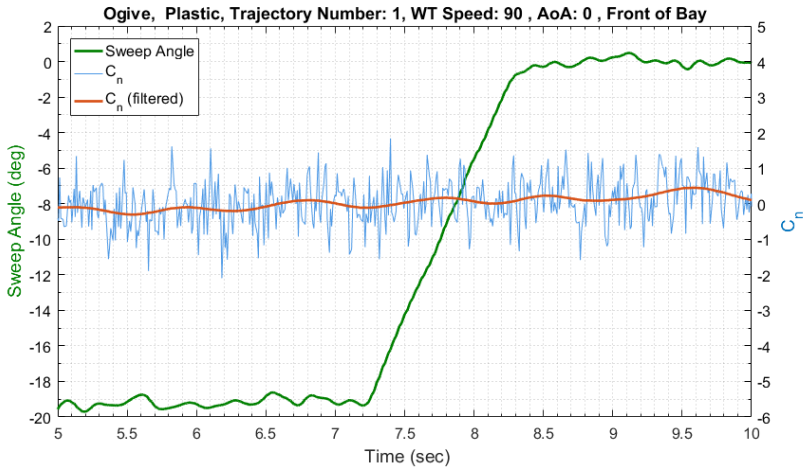
Ogive, Plastic, Trajectory Number: 1, WT Speed: 90 , AoA: 0 , Front of Bay
Sweep Angle
C_n
C_n (filtered)
Sweep Angle (deg)
C_n
Time (sec)

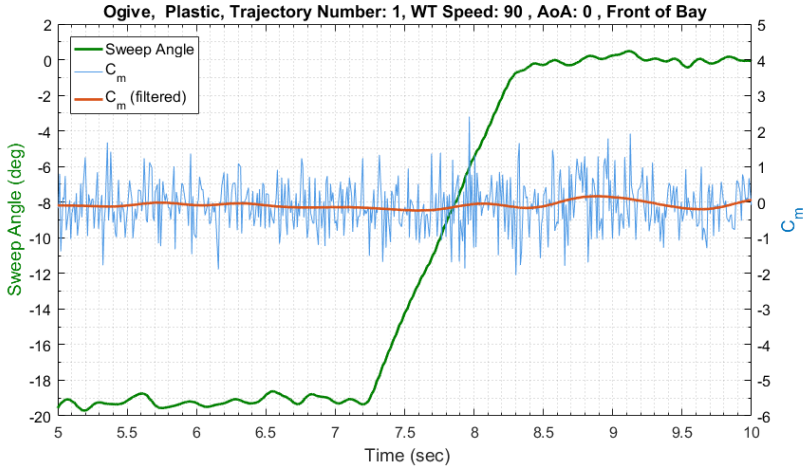
Ogive, Plastic, Trajectory Number: 1, WT Speed: 90 , AoA: 0 , Front of Bay
Sweep Angle
C_m
C_m (filtered)
Sweep Angle (deg)
C_m
Time (sec)

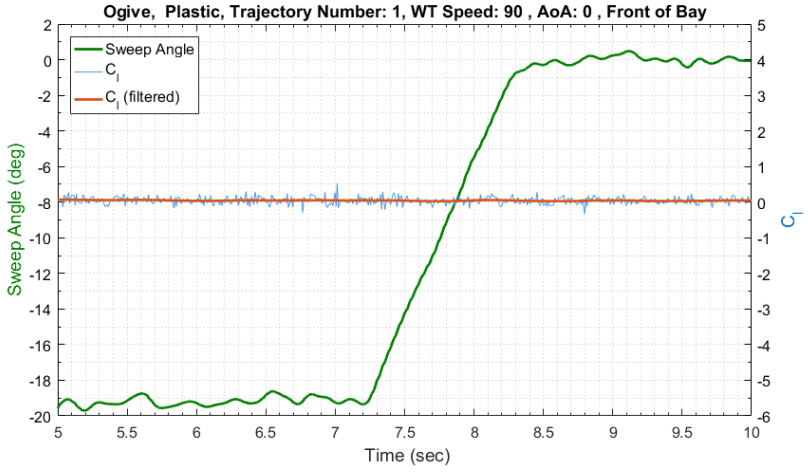
Ogive, Plastic, Trajectory Number: 1, WT Speed: 90 , AoA: 0 , Front of Bay
Sweep Angle
C_l
C_l (filtered)
Sweep Angle (deg)
C_l
Time (sec)

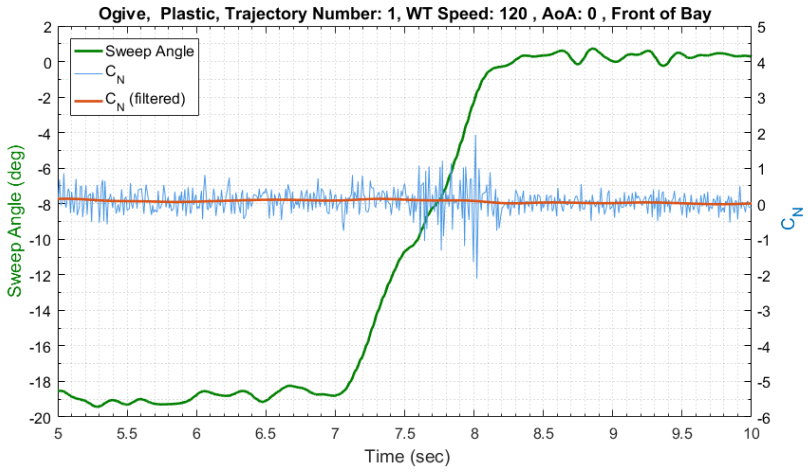
Ogive, Plastic, Trajectory Number: 1, WT Speed: 120 , AoA: 0 , Front of Bay
Sweep Angle
C_N
C_N (filtered)
Sweep Angle (deg)
C_N
Time (sec)

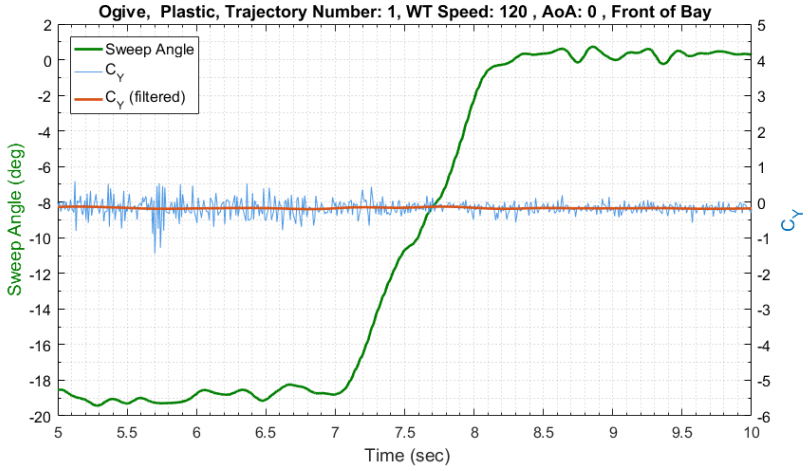
Ogive, Plastic, Trajectory Number: 1, WT Speed: 120 , AoA: 0 , Front of Bay
Sweep Angle
C_Y
C_Y (filtered)
Sweep Angle (deg)
C_Y
Time (sec)

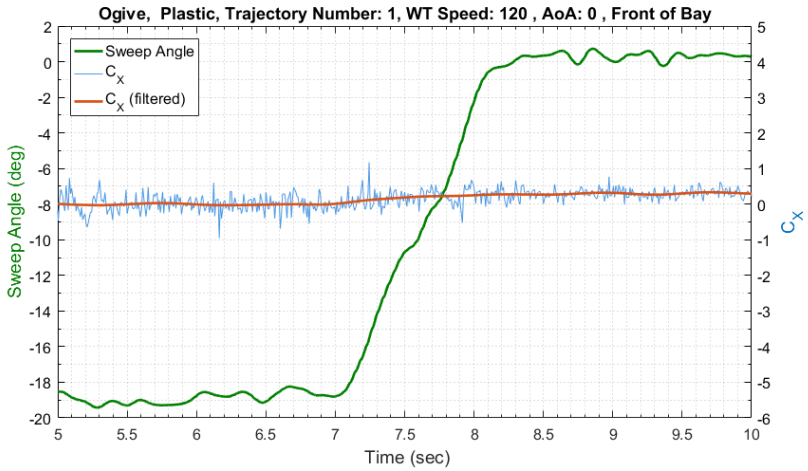
Ogive, Plastic, Trajectory Number: 1, WT Speed: 120 , AoA: 0 , Front of Bay
Sweep Angle
C_X
C_X (filtered)
Sweep Angle (deg)
C_X
Time (sec)

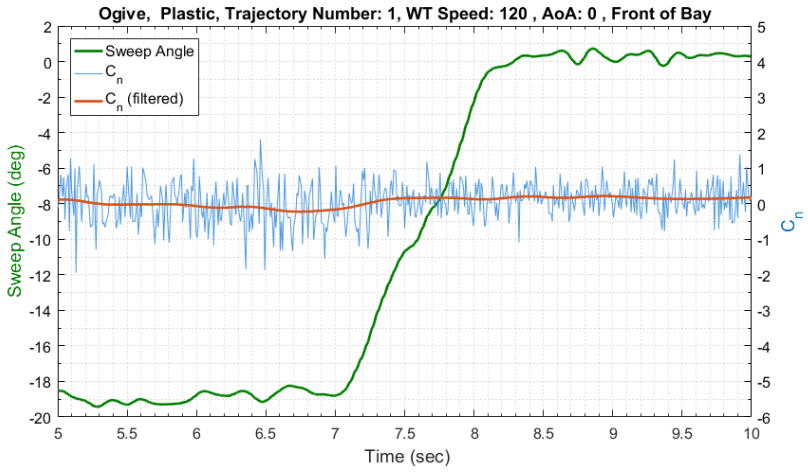
Ogive, Plastic, Trajectory Number: 1, WT Speed: 120 , AoA: 0 , Front of Bay
Sweep Angle
C_n
C_n (filtered)
Sweep Angle (deg)
C_n
Time (sec)

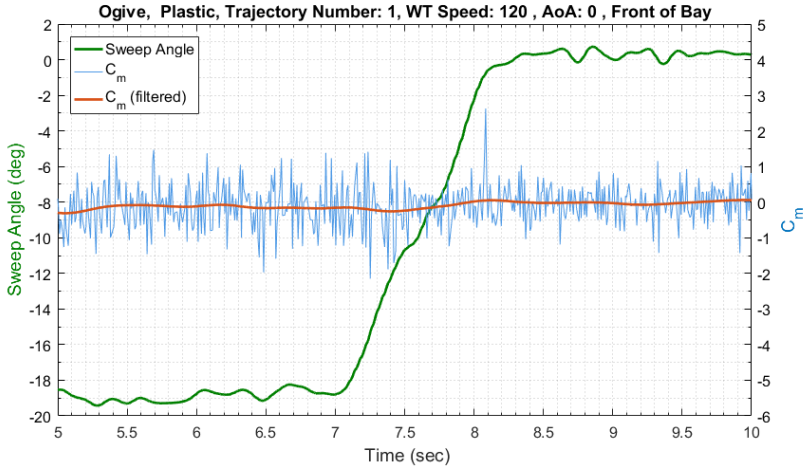
Ogive, Plastic, Trajectory Number: 1, WT Speed: 120 , AoA: 0 , Front of Bay
Sweep Angle
C_m
C_m (filtered)
Sweep Angle (deg)
C_m
Time (sec)

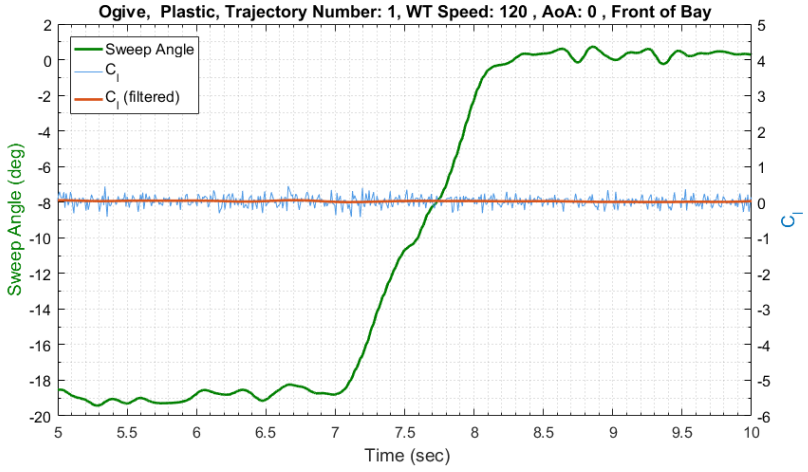
Ogive, Plastic, Trajectory Number: 1, WT Speed: 120 , AoA: 0 , Front of Bay
Sweep Angle
C_l
C_l (filtered)
Sweep Angle (deg)
C_l
Time (sec)

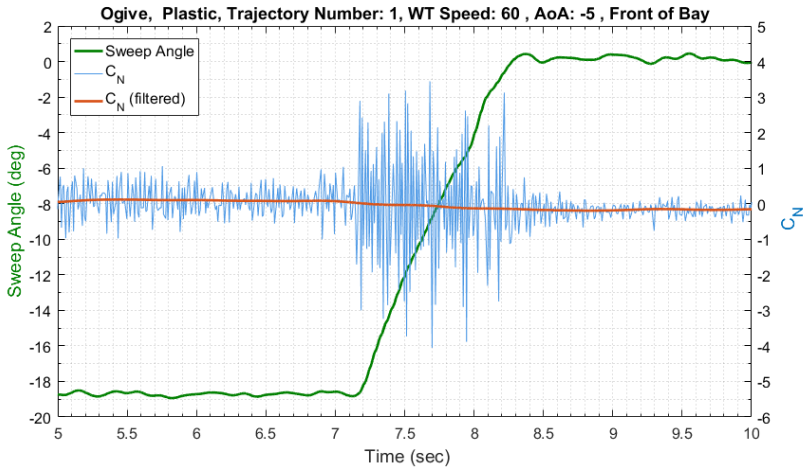
Ogive, Plastic, Trajectory Number: 1, WT Speed: 60 , AoA: -5 , Front of Bay
Sweep Angle
C_N
C_N (filtered)
Sweep Angle (deg)
C_N
Time (sec)

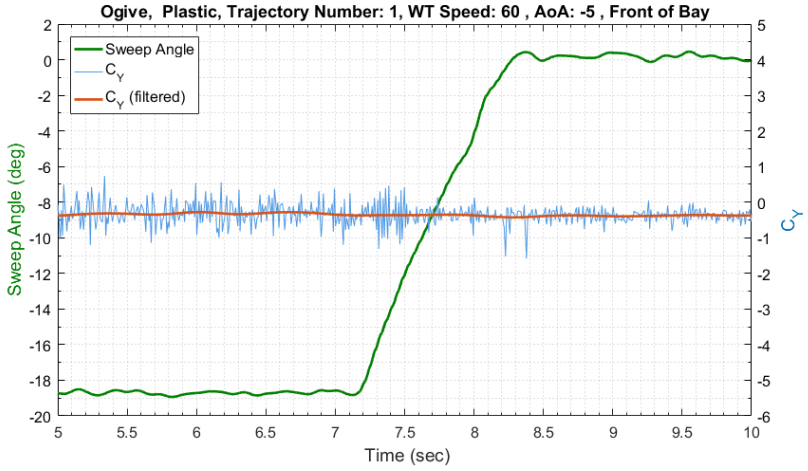
Ogive, Plastic, Trajectory Number: 1, WT Speed: 60 , AoA: -5 , Front of Bay
Sweep Angle
C_Y
C_Y (filtered)
Sweep Angle (deg)
C_Y
Time (sec)

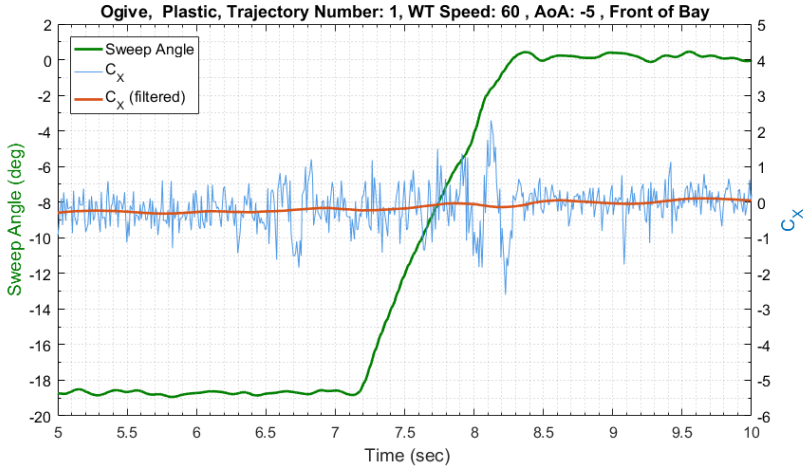
Ogive, Plastic, Trajectory Number: 1, WT Speed: 60 , AoA: -5 , Front of Bay
Sweep Angle
C_X
C_X (filtered)
Sweep Angle (deg)
C_X
Time (sec)

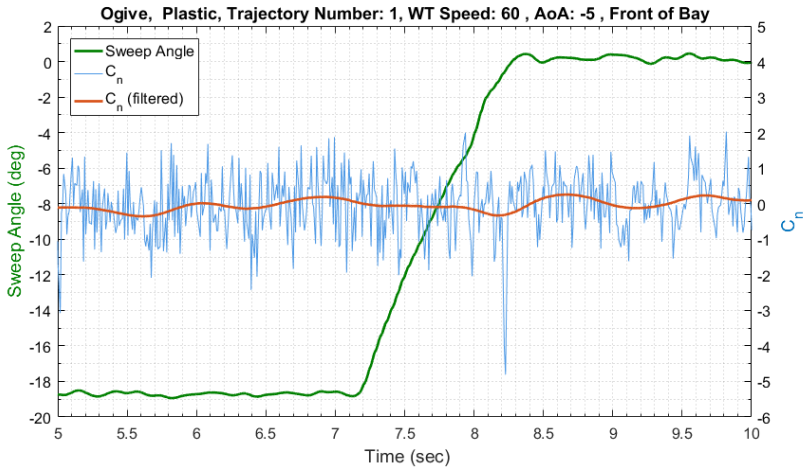
Ogive, Plastic, Trajectory Number: 1, WT Speed: 60 , AoA: -5 , Front of Bay
Sweep Angle
C_n
C_n (filtered)
Sweep Angle (deg)
C_n
Time (sec)

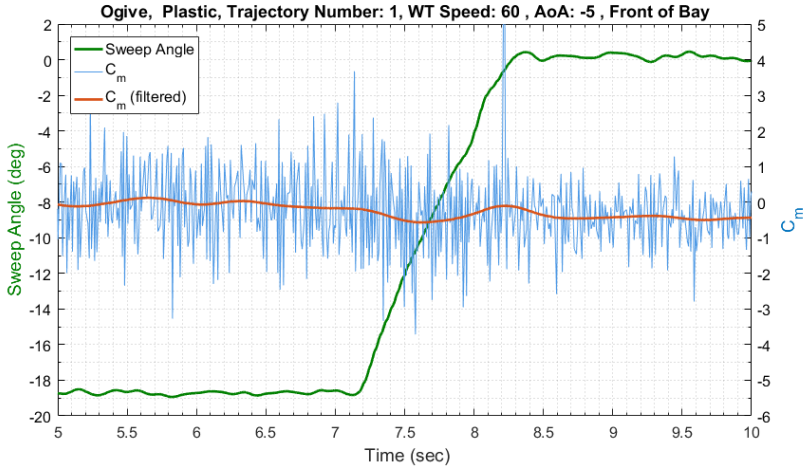
Ogive, Plastic, Trajectory Number: 1, WT Speed: 60 , AoA: -5 , Front of Bay
Sweep Angle
C_m
C_m (filtered)
Sweep Angle (deg)
C_m
Time (sec)

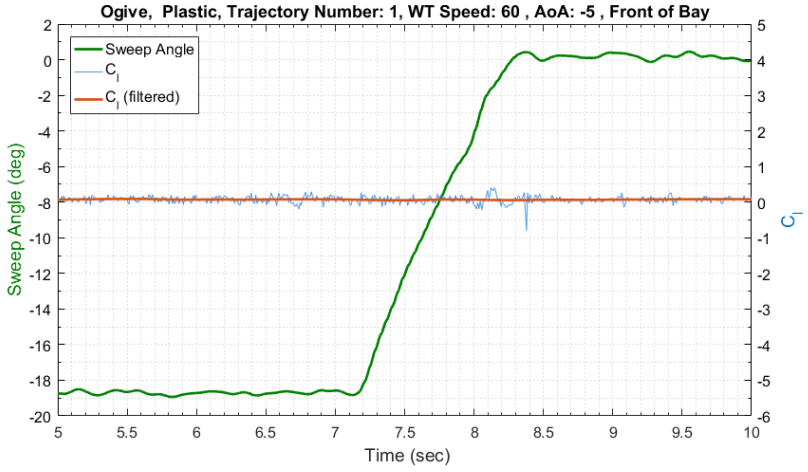
Ogive, Plastic, Trajectory Number: 1, WT Speed: 60 , AoA: -5 , Front of Bay
Sweep Angle
C_l
C_l (filtered)
Sweep Angle (deg)
C_l
Time (sec)

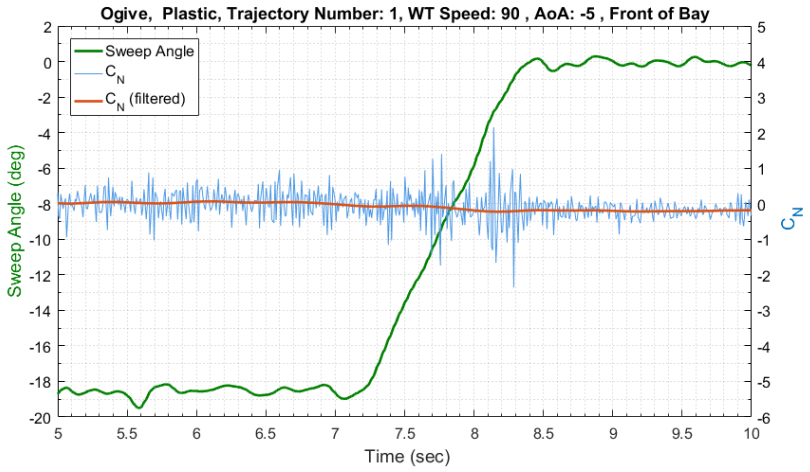
Ogive, Plastic, Trajectory Number: 1, WT Speed: 90 , AoA: -5 , Front of Bay
Sweep Angle
C_N
C_N (filtered)
Sweep Angle (deg)
C_N
Time (sec)

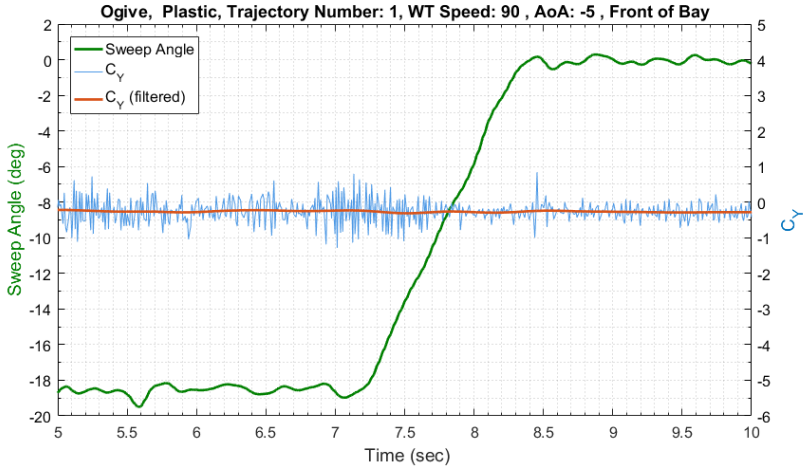
Ogive, Plastic, Trajectory Number: 1, WT Speed: 90 , AoA: -5 , Front of Bay
Sweep Angle
C_Y
C_Y (filtered)
Sweep Angle (deg)
C_Y
Time (sec)

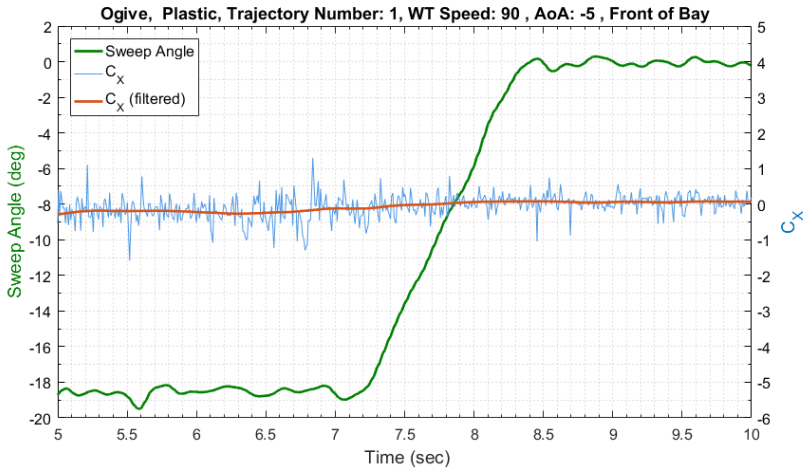
Ogive, Plastic, Trajectory Number: 1, WT Speed: 90 , AoA: -5 , Front of Bay
Sweep Angle
C_X
C_X (filtered)
Sweep Angle (deg)
C_X
Time (sec)

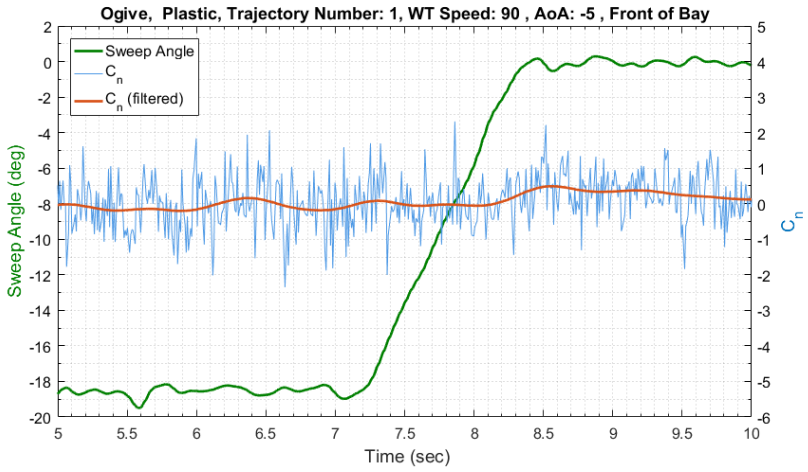
Ogive, Plastic, Trajectory Number: 1, WT Speed: 90 , AoA: -5 , Front of Bay
Sweep Angle
C_n
C_n (filtered)
Sweep Angle (deg)
C_n
Time (sec)

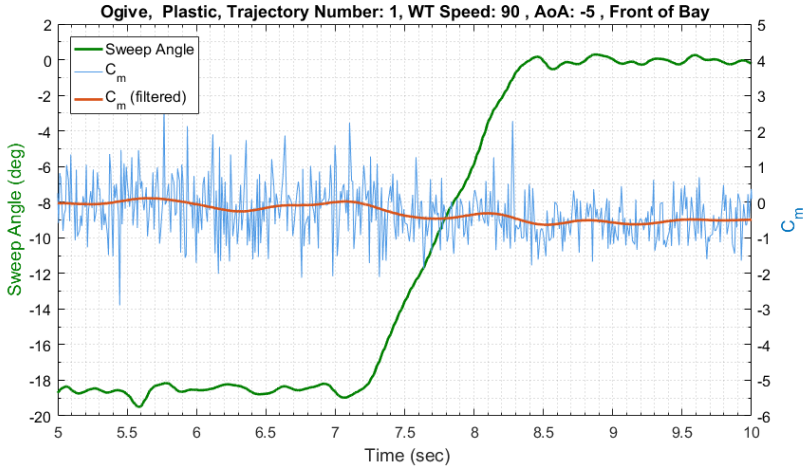
Ogive, Plastic, Trajectory Number: 1, WT Speed: 90 , AoA: -5 , Front of Bay
Sweep Angle
C_m
C_m (filtered)
Sweep Angle (deg)
C_m
Time (sec)

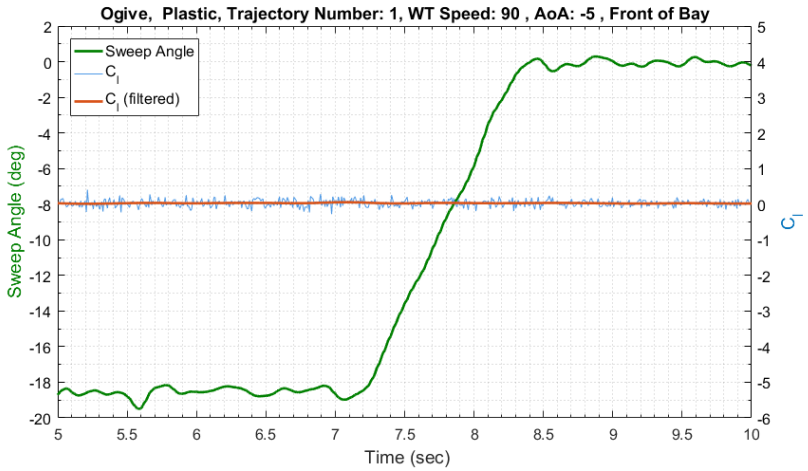
Ogive, Plastic, Trajectory Number: 1, WT Speed: 90 , AoA: -5 , Front of Bay
Sweep Angle
C_l
C_l (filtered)
Sweep Angle (deg)
C_l
Time (sec)

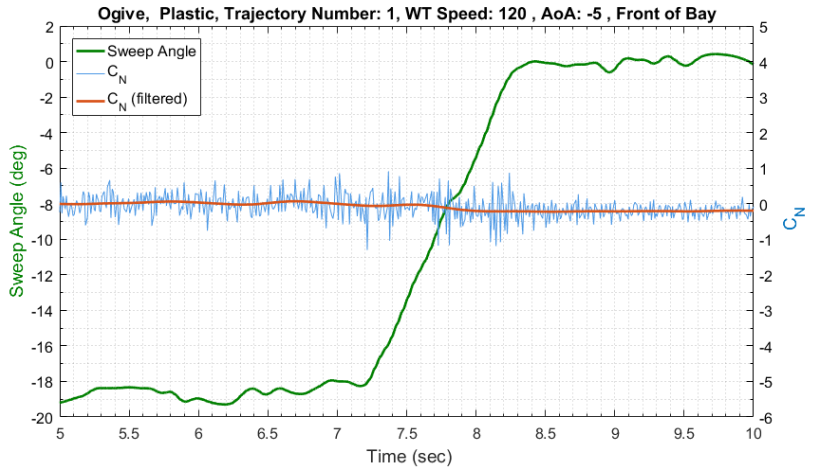
Ogive, Plastic, Trajectory Number: 1, WT Speed: 120 , AoA: -5 , Front of Bay
Sweep Angle
C_N
C_N (filtered)
Sweep Angle (deg)
C_N
Time (sec)

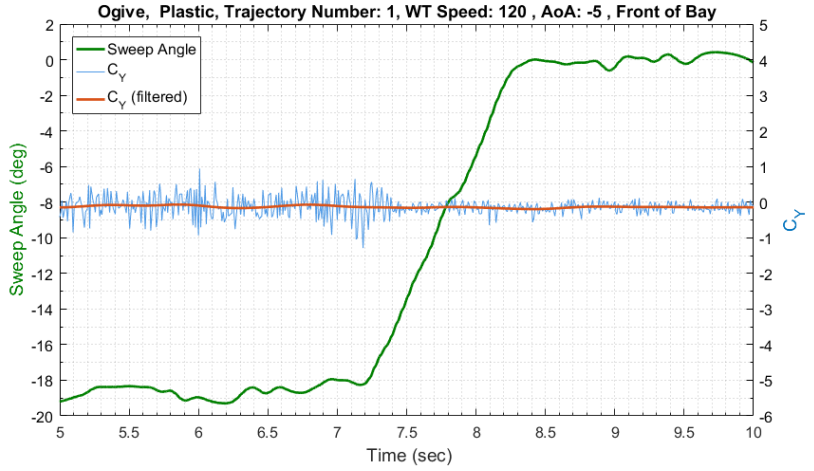
Ogive, Plastic, Trajectory Number: 1, WT Speed: 120 , AoA: -5 , Front of Bay
Sweep Angle
C_Y
C_Y (filtered)
Sweep Angle (deg)
C_Y
Time (sec)

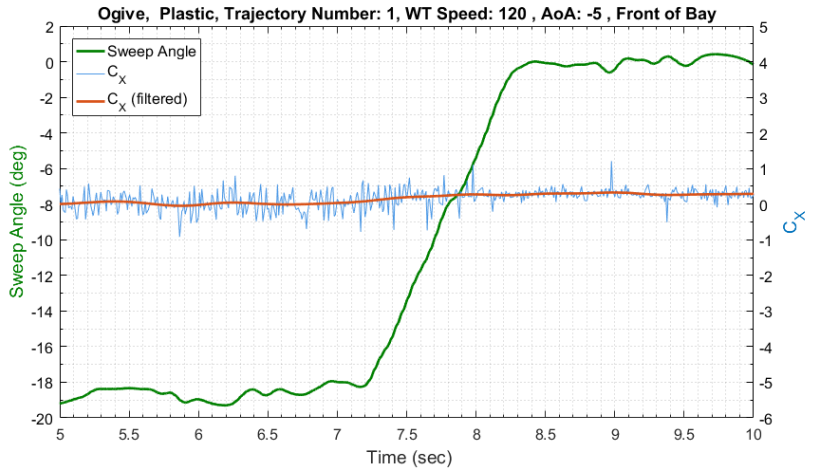
Ogive, Plastic, Trajectory Number: 1, WT Speed: 120 , AoA: -5 , Front of Bay
Sweep Angle
C_X
C_X (filtered)
Sweep Angle (deg)
C_X
Time (sec)

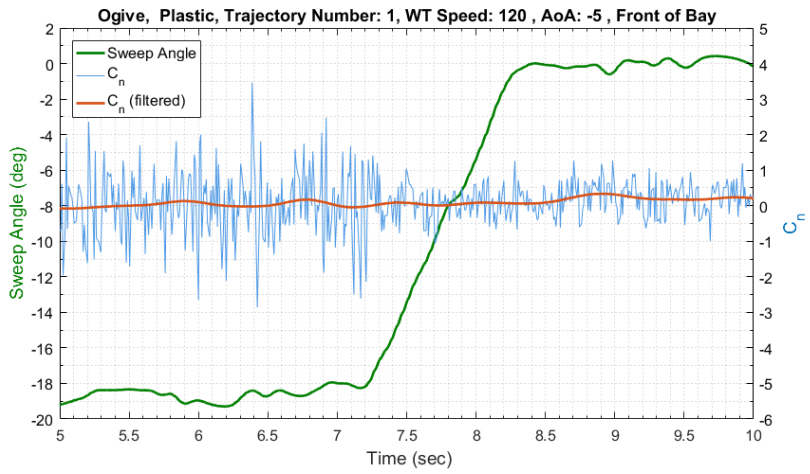
Ogive, Plastic, Trajectory Number: 1, WT Speed: 120 , AoA: -5 , Front of Bay
Sweep Angle
C_n
C_n (filtered)
Sweep Angle (deg)
C_n
Time (sec)

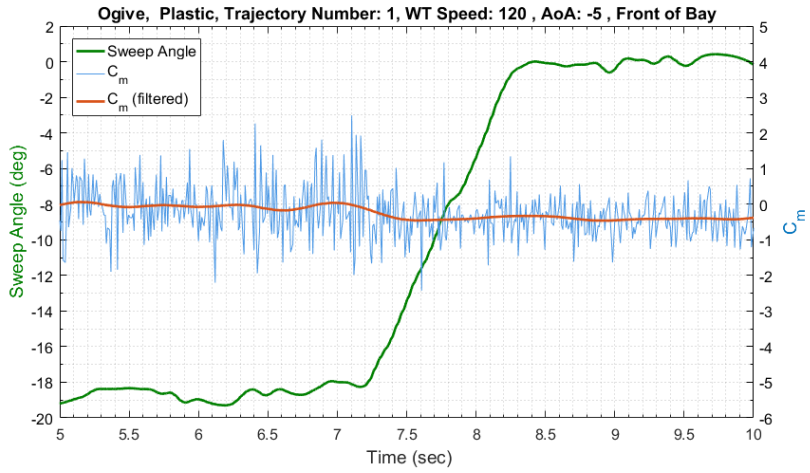
Ogive, Plastic, Trajectory Number: 1, WT Speed: 120 , AoA: -5 , Front of Bay
Sweep Angle
C_m
C_m (filtered)
Sweep Angle (deg)
C_m
Time (sec)

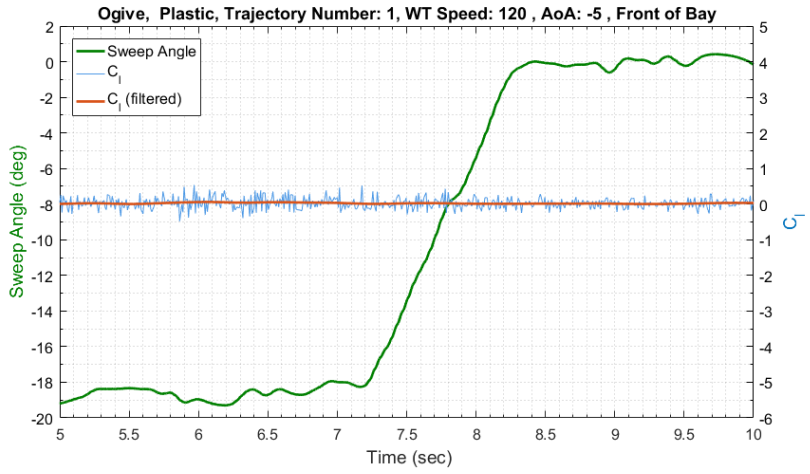
Ogive, Plastic, Trajectory Number: 1, WT Speed: 120 , AoA: -5 , Front of Bay
Sweep Angle
C_l
C_l (filtered)
Sweep Angle (deg)
C_l
Time (sec)

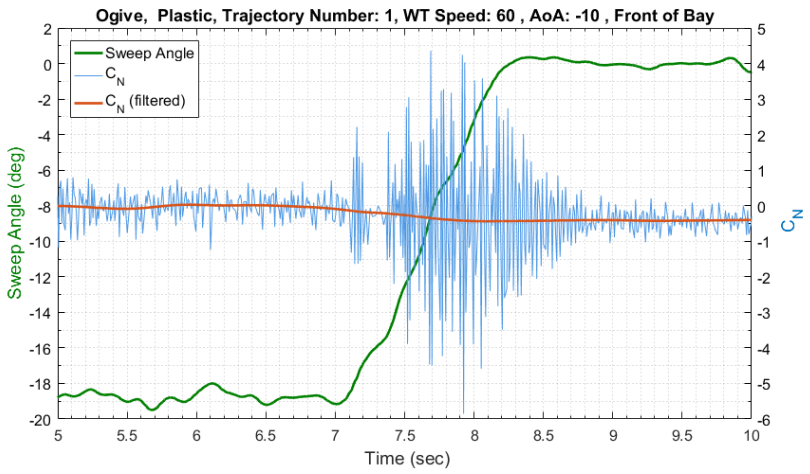
Ogive, Plastic, Trajectory Number: 1, WT Speed: 60 , AoA: -10 , Front of Bay
Sweep Angle
C_N
C_N (filtered)
Sweep Angle (deg)
C_N
Time (sec)

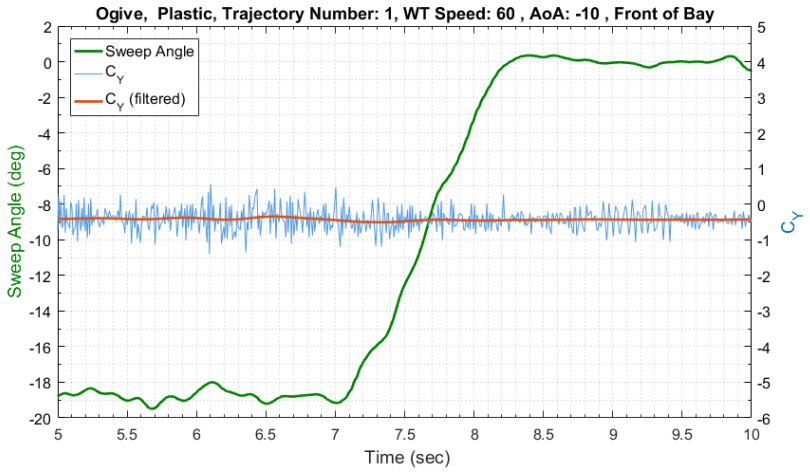
Ogive, Plastic, Trajectory Number: 1, WT Speed: 60 , AoA: -10 , Front of Bay
Sweep Angle
C_Y
C_Y (filtered)
Sweep Angle (deg)
C_Y
Time (sec)

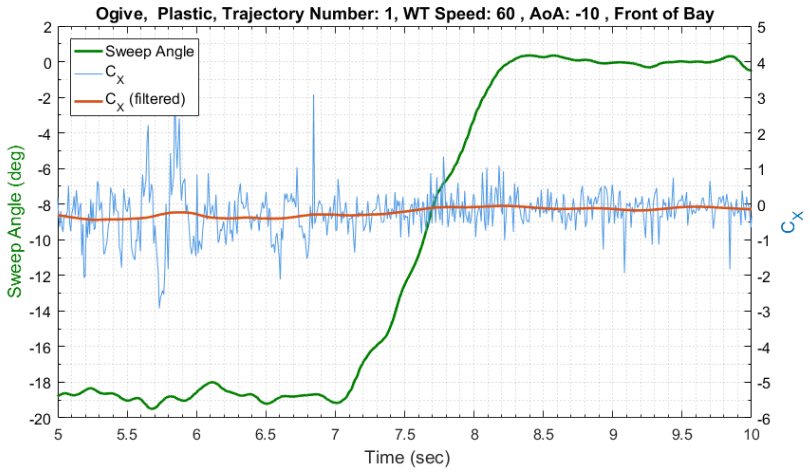
Ogive, Plastic, Trajectory Number: 1, WT Speed: 60 , AoA: -10 , Front of Bay
Sweep Angle
C_X
C_X (filtered)
Sweep Angle (deg)
C_X
Time (sec)

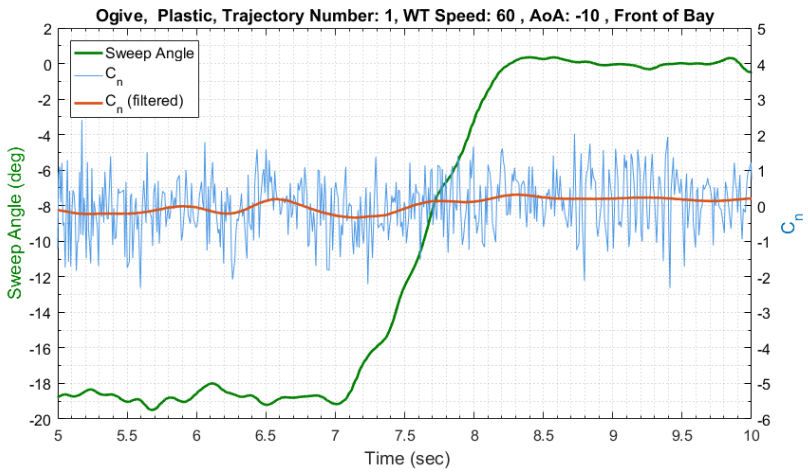
Ogive, Plastic, Trajectory Number: 1, WT Speed: 60 , AoA: -10 , Front of Bay
Sweep Angle
C_n
C_n (filtered)
Sweep Angle (deg)
C_n
Time (sec)

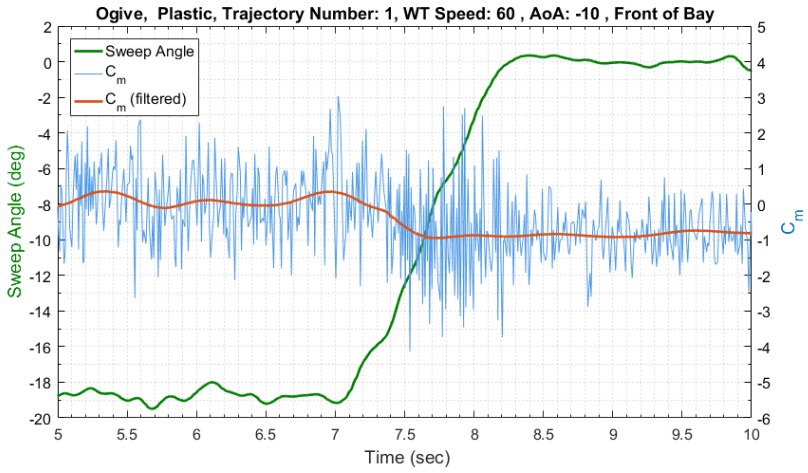
Ogive, Plastic, Trajectory Number: 1, WT Speed: 60 , AoA: -10 , Front of Bay
Sweep Angle
C_m
C_m (filtered)
Sweep Angle (deg)
C_m
Time (sec)

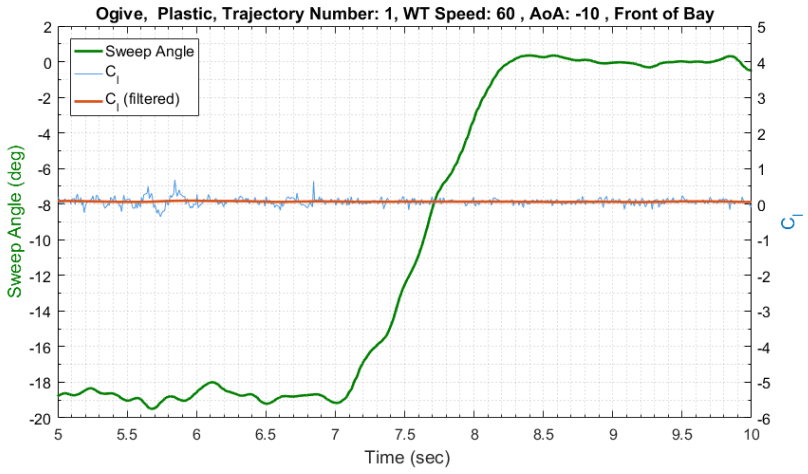
Ogive, Plastic, Trajectory Number: 1, WT Speed: 60 , AoA: -10 , Front of Bay
Sweep Angle
C_l
C_l (filtered)
Sweep Angle (deg)
C_l
Time (sec)

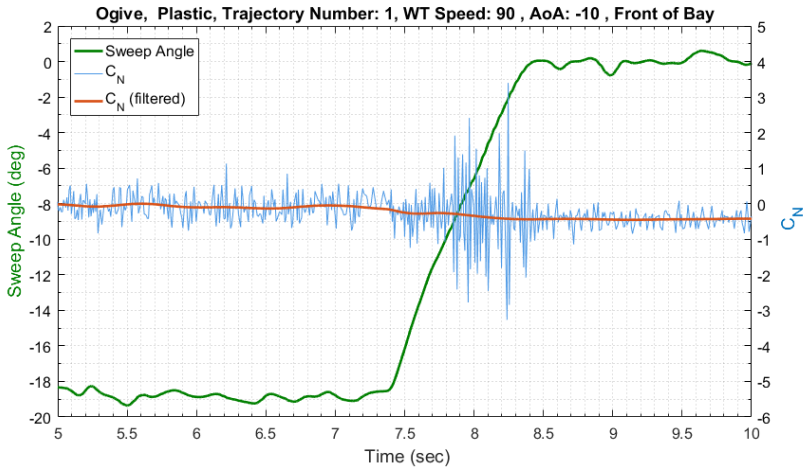
Ogive, Plastic, Trajectory Number: 1, WT Speed: 90 , AoA: -10 , Front of Bay
Sweep Angle
C_N
C_N (filtered)
Sweep Angle (deg)
C_N
Time (sec)

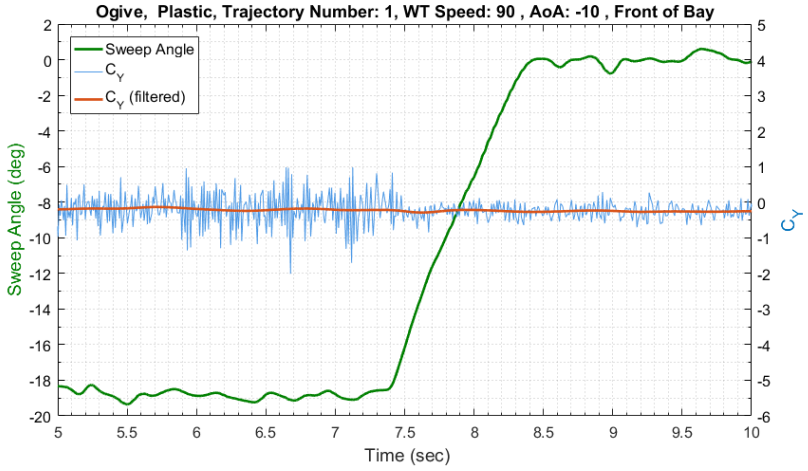
Ogive, Plastic, Trajectory Number: 1, WT Speed: 90 , AoA: -10 , Front of Bay
Sweep Angle
C_Y
C_Y (filtered)
Sweep Angle (deg)
C_Y
Time (sec)

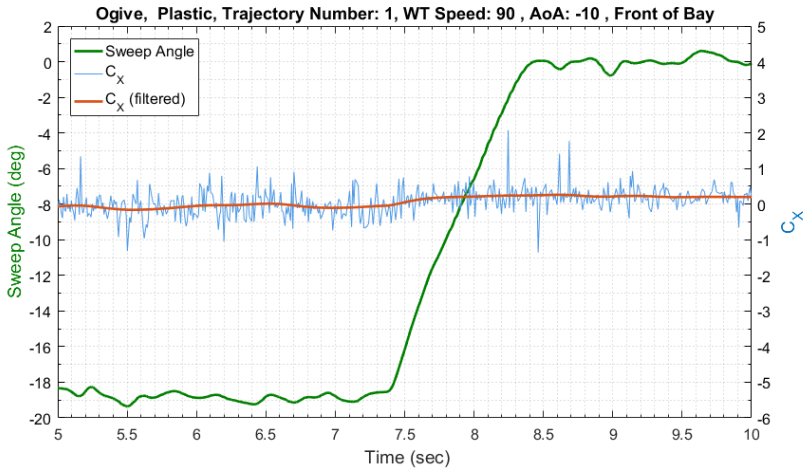
Ogive, Plastic, Trajectory Number: 1, WT Speed: 90 , AoA: -10 , Front of Bay
Sweep Angle
C_X
C_X (filtered)
Sweep Angle (deg)
C_X
Time (sec)

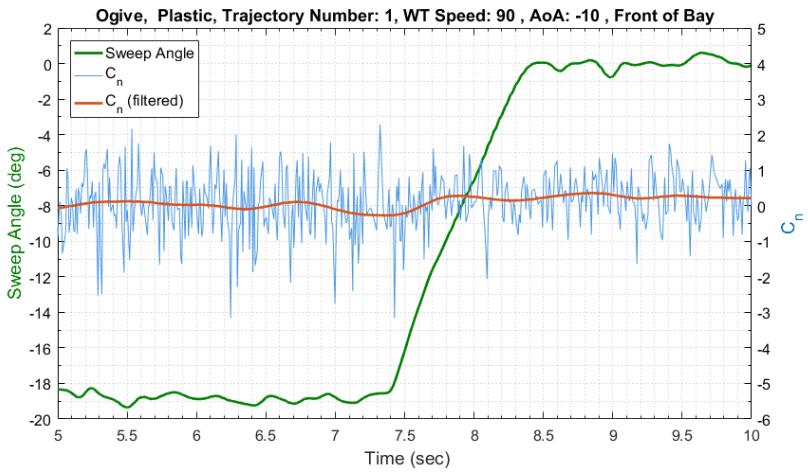
Ogive, Plastic, Trajectory Number: 1, WT Speed: 90 , AoA: -10 , Front of Bay
Sweep Angle
C_n
C_n (filtered)
Sweep Angle (deg)
C_n
Time (sec)

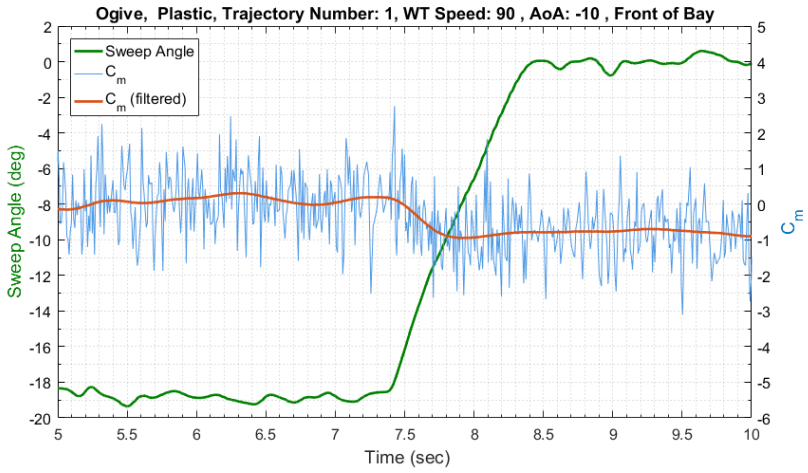
Ogive, Plastic, Trajectory Number: 1, WT Speed: 90 , AoA: -10 , Front of Bay
Sweep Angle
C_m
C_m (filtered)
Sweep Angle (deg)
C_m
Time (sec)

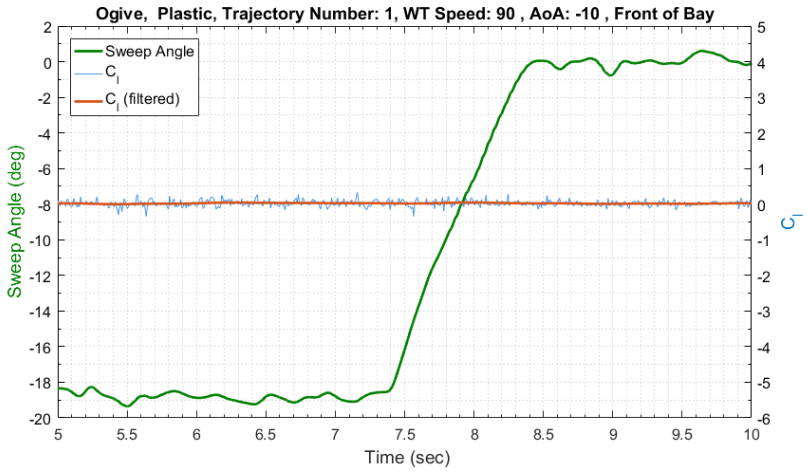
Ogive, Plastic, Trajectory Number: 1, WT Speed: 90 , AoA: -10 , Front of Bay
Sweep Angle
C_l
C_l (filtered)
Sweep Angle (deg)
C_l
Time (sec)

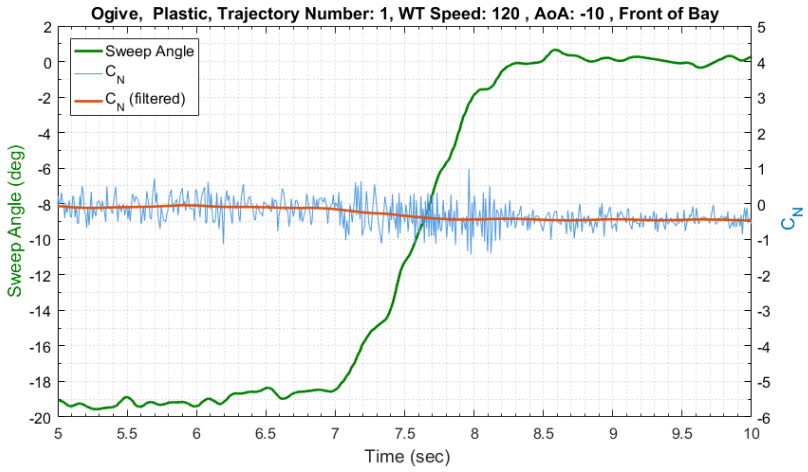
Ogive, Plastic, Trajectory Number: 1, WT Speed: 120 , AoA: -10 , Front of Bay
Sweep Angle
C_N
C_N (filtered)
Sweep Angle (deg)
C_N
Time (sec)

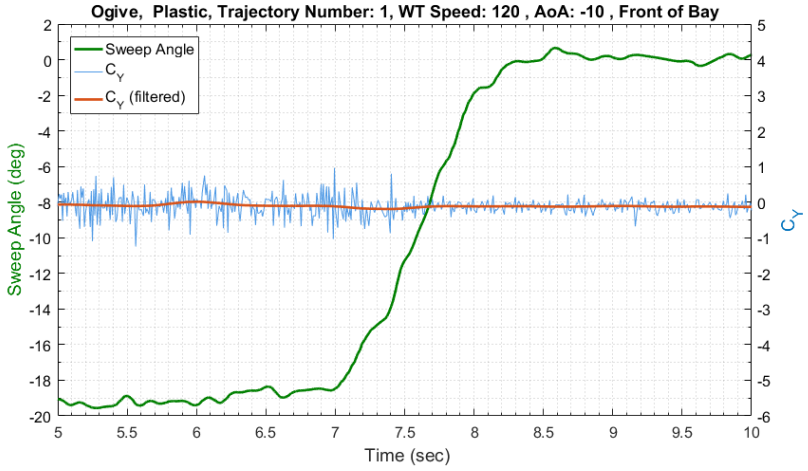
Ogive, Plastic, Trajectory Number: 1, WT Speed: 120 , AoA: -10 , Front of Bay
Sweep Angle
C_Y
C_Y (filtered)
Sweep Angle (deg)
C_Y
Time (sec)

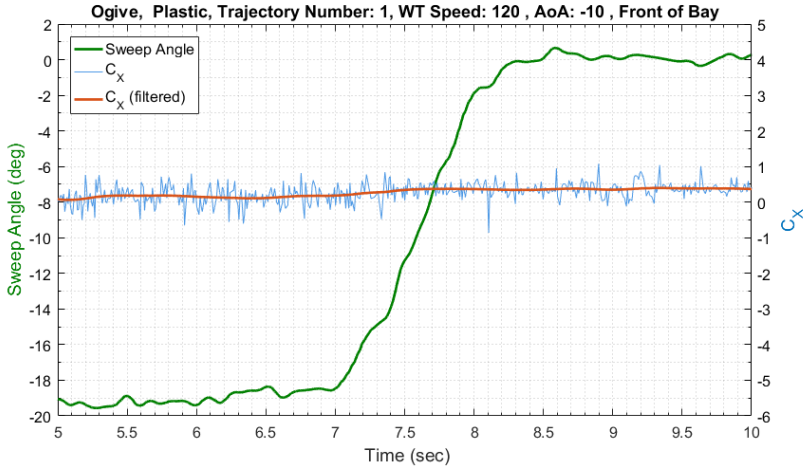
Ogive, Plastic, Trajectory Number: 1, WT Speed: 120 , AoA: -10 , Front of Bay
Sweep Angle
C_X
C_X (filtered)
Sweep Angle (deg)
C_X
Time (sec)

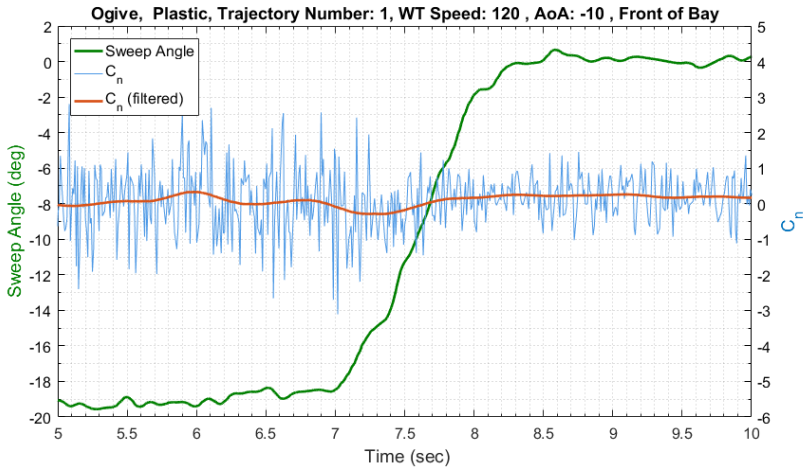
Ogive, Plastic, Trajectory Number: 1, WT Speed: 120 , AoA: -10 , Front of Bay
Sweep Angle
C_n
C_n (filtered)
Sweep Angle (deg)
C_n
Time (sec)

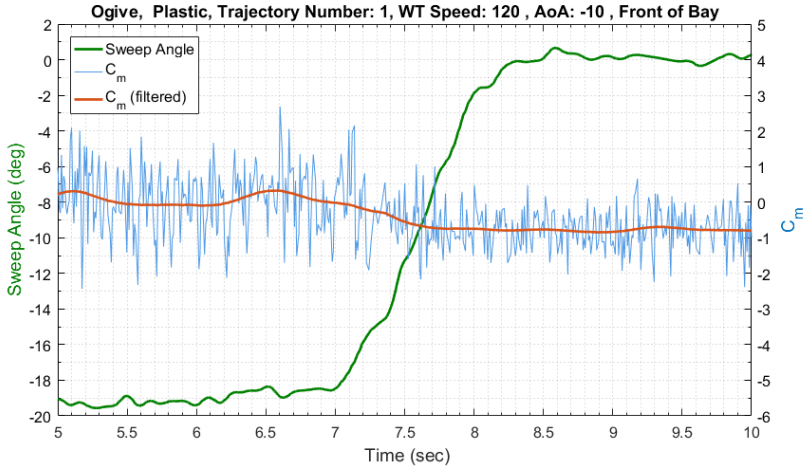
Ogive, Plastic, Trajectory Number: 1, WT Speed: 120 , AoA: -10 , Front of Bay
Sweep Angle
C_m
C_m (filtered)
Sweep Angle (deg)
C_m
Time (sec)

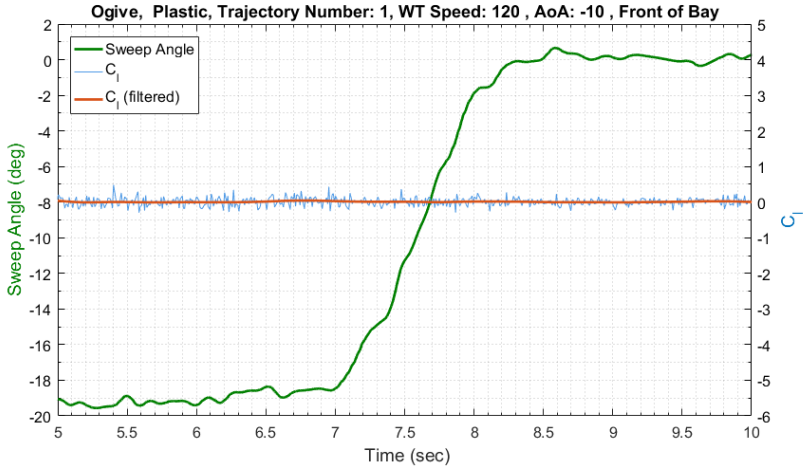
Ogive, Plastic, Trajectory Number: 1, WT Speed: 120 , AoA: -10 , Front of Bay
Sweep Angle
C_l
C_l (filtered)
Sweep Angle (deg)
C_l
Time (sec)

This Page Intentionally Left Blank

Appendix B. LabVIEW and MATLAB Code

MATLAB Code for Voltage to Force, Torque, and Cp conversion: Pages

MATLAB Code for calculating aerodynamic coefficients and plotting: Pages

This Page Intentionally Left Blank

Calibration MATRIX from ATI for the newer Nano25 (FT18962)

```
CalMat = ...
       [  0.15346  -0.01697  -0.01582   2.87077  -0.03571  -2.96696;
         -0.38481  -3.33084   0.09813   1.62079   0.07247   1.72610;
          5.71675   0.04764   5.47653   0.02115   5.63704  -0.18079;
         -0.13441  -1.10252   2.19394   0.53490  -2.12916   0.62782;
          -2.54867  -0.01872   1.20386  -0.96034   1.37114   0.95817;
          -0.05067  -1.04394  -0.13412  -1.01168   0.04208  -1.05521 ];
```

Missile and wind tunnel properties

```
Fahrenheit = 68.4;
Inches_Hg  = 29.6660;
    Bay_Length = 2; % weapon bay length (ft)
    Dia = 1.29/12; % missile Dia converted to ft
    Ref_Area = (pi/4)*Dia^2; % Model refference Area (ft^2)
        P_psi = Inches_Hg*0.49115420057253 ;% Inches Hg converted to psi
        P_psf = P_psi*12^2; % psi converted to psf
        T = Fahrenheit + 459.67;% temp deg F converted to Rankine
        R = 1716;  % (lb*ft)/(slug*R) Imperial Gas constant for Air
    rho = P_psf/(R*T); % density from ideal gas law [slug/ft^3]
```

File names

```
filename_0   = 'bb8_0_Missile_P_0.lvm';
filename_60  = 'bb8_0_Missile_P_60.lvm';
filename_90  = 'bb8_0_Missile_P_90.lvm';
filename_120 = 'bb8_0_Missile_P_120.lvm';
Initial_AoA    =   -0; % 0 -5 -10 % degrees
Model       =     ' Missile, ';
Material    =     ' Plastic, ';
Test_Number =        1;
StorePos    =   ' , Back of Bay ';

Figure_Handle=[Model,Material, 'Trajectory Number: ',num2str(Test_Number), ' , AoA: '
,num2str(Initial_AoA), StorePos ];
    delimiterIn = '\t';
    headerlinesIn = 21;
```

.lvm column handles

```
Time_col = 2;
Fx_col   = 4;
Fy_col   = 5;
Fz_col   = 6;
Tx_col   = 7;
Ty_col   = 8;
Tz_col   = 9;
Vimu_col = 10;
PT1_col  = 11;
PT2_col  = 12;
PT3_col  = 13;
PT4_col  = 14;
```

Test, 0 mph

```
DATA_0 = importdata(filename_0, delimiterIn, headerlinesIn);
Data_0 = DATA_0.data;

    time_0 = Data_0(:,Time_col);
    N_0 = length(time_0); % number of data points

     VFx_0 = Data_0(:,Fx_col);
     VFy_0 = Data_0(:,Fy_col);
     VFz_0 = Data_0(:,Fz_col);

     VTx_0 = Data_0(:,Tx_col);
     VTy_0 = Data_0(:,Ty_col);
     VTz_0 = Data_0(:,Tz_col);

     Vimu_0 = Data_0(:,Vimu_col);

     PT1_0 = Data_0(:,PT1_col);
     PT2_0 = Data_0(:,PT2_col);
     PT3_0 = Data_0(:,PT3_col);
     PT4_0 = Data_0(:,PT4_col);

for i = 1:N_0
    Voltages_0 = [VFx_0(i); VFy_0(i); VFz_0(i); VTx_0(i); VTy_0(i); VTz_0(i)];
    Forces_0(:,i) = CalMat*Voltages_0;
end
```

Tare values: from 0 MPH case

```
Tare_Fx = Forces_0(1,:);
Tare_Fy = Forces_0(2,:);
Tare_Fz = (-1)*Forces_0(3,:); % -1 is for AIAA convention

Tare_Tx = Forces_0(4,:)*(1/12); % converted to ft*lbs
Tare_Ty = Forces_0(5,:)*(1/12); %
Tare_Tz = Forces_0(6,:)*(1/12); %
```

Test, 60 mph

```
DATA_60 = importdata(filename_60, delimiterIn, headerlinesIn);
Data_60 = DATA_60.data;

    time_60 = Data_60(:,Time_col);
    N_60 = length(time_60); % number of data points

     VFx_60 = Data_60(:,Fx_col);
     VFy_60 = Data_60(:,Fy_col);
     VFz_60 = Data_60(:,Fz_col);

     VTx_60 = Data_60(:,Tx_col);
     VTy_60 = Data_60(:,Ty_col);
     VTz_60 = Data_60(:,Tz_col);

     Vimu_60 = Data_60(:,Vimu_col);

     PT1_60 = Data_60(:,PT1_col);
     PT2_60 = Data_60(:,PT2_col);
     PT3_60 = Data_60(:,PT3_col);
     PT4_60 = Data_60(:,PT4_col);

for i = 1:N_60
    Voltages_60 = [VFx_60(i); VFy_60(i); VFz_60(i); VTx_60(i); VTy_60(i); VTz_60(i)];
    Forces_60(:,i) = CalMat*Voltages_60;
end
```

Test, 90 mph

```
DATA_90 = importdata(filename_90, delimiterIn, headerlinesIn);
Data_90 = DATA_90.data;

    time_90 = Data_90(:,Time_col);
    N_90 = length(time_90); % number of data points

     VFx_90 = Data_90(:,Fx_col);
     VFy_90 = Data_90(:,Fy_col);
     VFz_90 = Data_90(:,Fz_col);

     VTx_90 = Data_90(:,Tx_col);
     VTy_90 = Data_90(:,Ty_col);
     VTz_90 = Data_90(:,Tz_col);

     Vimu_90 = Data_90(:,Vimu_col);

     PT1_90 = Data_90(:,PT1_col);
     PT2_90 = Data_90(:,PT2_col);
     PT3_90 = Data_90(:,PT3_col);
     PT4_90 = Data_90(:,PT4_col);

for i = 1:N_90
    Voltages_90 = [VFx_90(i); VFy_90(i); VFz_90(i); VTx_90(i); VTy_90(i); VTz_90(i)];

    Forces_90(:,i) = CalMat*Voltages_90;

end
```

Test, 120 mph

```
DATA_120 = importdata(filename_120, delimiterIn, headerlinesIn);
Data_120 = DATA_120.data;

    time_120 = Data_120(:,Time_col);
    N_120 = length(time_120); % number of data points

     VFx_120 = Data_120(:,Fx_col);
     VFy_120 = Data_120(:,Fy_col);
     VFz_120 = Data_120(:,Fz_col);

     VTx_120 = Data_120(:,Tx_col);
     VTy_120 = Data_120(:,Ty_col);
     VTz_120 = Data_120(:,Tz_col);

     Vimu_120 = Data_120(:,Vimu_col);

     PT1_120 = Data_120(:,PT1_col);
     PT2_120 = Data_120(:,PT2_col);
     PT3_120 = Data_120(:,PT3_col);
     PT4_120 = Data_120(:,PT4_col);

for j = 1:N_120
    Voltages_120 = [VFx_120(j); VFy_120(j); VFz_120(j); VTx_120(j); VTy_120(j);
VTz_120(j)];

    Forces_120(:,j) = CalMat*Voltages_120;

end
```

Plot All Pressure Coefficients, Cp, 1 2 3 4 for all speeds, for Trajectory #1 experiment

```
V_fps = [60 90 120]*(1/60)*(1/60)*(5280/1); % velocity (# MPH) converted to ft/s
q = (1/2)*rho*V_fps.^2; % dynamic pressures
g1 = 2.9883;g2 = 2.9879;g3 = 2.9874;g4 = 3.0041; % gains
% Freestream Pressure from Bernoulli
    P_inf_60_1  = mean(PT1_0)*g1*144 - 0.5*rho*V_fps(1)^2;
        P_inf_60_2  = mean(PT2_0)*g2*144 - 0.5*rho*V_fps(1)^2;
            P_inf_60_3  = mean(PT3_0)*g3*144 - 0.5*rho*V_fps(1)^2;
                P_inf_60_4  = mean(PT4_0)*g4*144 - 0.5*rho*V_fps(1)^2;

    P_inf_90_1  = mean(PT1_0)*g1*144 - 0.5*rho*V_fps(2)^2;
        P_inf_90_2  = mean(PT2_0)*g2*144 - 0.5*rho*V_fps(2)^2;
            P_inf_90_3  = mean(PT3_0)*g3*144 - 0.5*rho*V_fps(2)^2;
                P_inf_90_4  = mean(PT4_0)*g4*144 - 0.5*rho*V_fps(2)^2;

    P_inf_120_1 = mean(PT1_0)*g1*144 - 0.5*rho*V_fps(3)^2;
         P_inf_120_2  = mean(PT2_0)*g2*144 - 0.5*rho*V_fps(3)^2;
            P_inf_120_3  = mean(PT3_0)*g3*144 - 0.5*rho*V_fps(3)^2;
                P_inf_120_4  = mean(PT4_0)*g4*144 - 0.5*rho*V_fps(3)^2;
P1_60 = mean(PT1_60)*g1; P2_60 = mean(PT2_60)*g2; P3_60 = mean(PT3_60)*g3; P4_60 =
mean(PT4_60)*g4;
Cp_60 = ([P1_60 P2_60 P3_60 P4_60]*144- [P_inf_60_1 P_inf_60_2 P_inf_60_3 P_inf_60_4
])/q(1);
P1_90 = mean(PT1_90)*g1; P2_90 = mean(PT2_90)*g2; P3_90 = mean(PT3_90)*g3; P4_90 =
mean(PT4_90)*g4;
Cp_90 = ([P1_90 P2_90 P3_90 P4_90]*144-[P_inf_90_1 P_inf_90_2 P_inf_90_3 P_inf_90_4
])/q(2);
P1_120 = mean(PT1_120)*g1; P2_120 = mean(PT2_120)*g2; P3_120 = mean(PT3_120)*g3; P4_120 =
mean(PT4_120)*g4;
Cp_120 = ([P1_120 P2_120 P3_120 P4_120]*144-[P_inf_120_1 P_inf_120_2 P_inf_120_3
P_inf_120_4 ])/q(3);
PT_Positions = [6.5, 12.5, 18.5, 24]/(Bay_Length*12); % (inch/inch)
figure('Name',Figure_Handle,'NumberTitle','off','units','normalized','outerposition',[0 0
.5 .5])
             plot(PT_Positions, Cp_60, 's','LineWidth',2); hold on
              plot(PT_Positions, Cp_90, 'd','LineWidth',2)
               plot(PT_Positions, Cp_120,'^','LineWidth',2)
               xlim([0 1])
    legend('60','90','120','location','northwest')
    grid minor
    title(Figure_Handle)
    xlabel(('\fontsize{14} Streamwise position x/L'),'interpreter','tex')
    ylabel(('\fontsize{14} Pressure Coeffectient C_p '),'interpreter','tex')

    Mach = [V_fps]/sqrt(1.4*R*T); table(Mach)
    mu = 3.82e-7; % lbf*s/ft^2
    Re = (rho*V_fps*Dia)/mu; table(Re)
```

Calculate Aerodynamic Coefficients and Plot Results

```
Test_Speed  =        90; % CHANGE 90 and _90 to #MPH case with “ctrl+F”
Fx          = Forces_90(1,:);  % corresponds to Nano25 Fx
Fy          = Forces_90(2,:);  % corresponds to Nano25 Fy
Fz     = (-1)*Forces_90(3,:);  % corresponds to Nano25 Fz. (-1) is for AIAA convention
Tx          = Forces_90(4,:)*(1/12); % Corresponds to Nano25 Ty converted to ft*lb
Ty          = Forces_90(5,:)*(1/12); % Corresponds to Nano25 Ty converted to ft*lb.
Tz          = Forces_90(6,:)*(1/12); % Corresponds to Nano25 Ty converted to ft*lb.
Vimu        =   Vimu_90;
time        =   time_90;
PT1         =   Data_90(:,PT1_col);
PT2         =   Data_90(:,PT2_col);
PT3         =   Data_90(:,PT3_col);
PT4         =   Data_90(:,PT4_col);

Test_Number =        1; % Trajectory #1
Model       =     ' Missile, ';
Material    =     ' Plastic, ';
StorePos    =     ' , Back of Bay ';
Figure_Handle=[Model,Material, 'Trajectory Number: ',num2str(Test_Number),', WT Speed: ',
num2str(Test_Speed), ' , AoA: ' ,num2str(Initial_AoA), StorePos ];

% % Get indices for the tare
% Match by aligning initial peaks

figure('Name',Figure_Handle,'NumberTitle','on','units','normalized','outerposition',[0 .5
.5 .5])
    legend_str_index = [ num2str(Test_Speed), ' MPH'];
    subplot(2,1,1); hold on; title('F_x signals');ylabel('from this plot.')
    plot(Tare_Fx); hold on; plot(Fx); % Tare_Fx is from "Grab_"
    legend('0 MPH',legend_str_index); grid minor
    subplot(2,1,2); hold on; title('F_y signals');ylabel('Get your Index...')
    plot(Tare_Fy);plot(Fy);xlabel('data points')
    legend('0 MPH',legend_str_index); grid minor
```

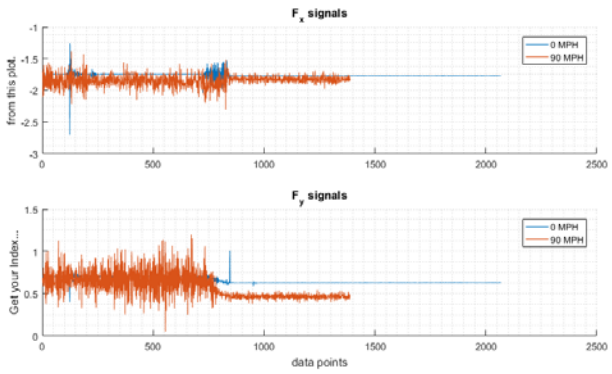

Declare the indices

```
switch Initial_AoA; % cases switch by the Initial AoA
    case 0 % 0 AoA case
        index_0 =   124;
                                  if   Test_Speed == 60
index_MPH = 125;%_____________________________________/
                                     elseif Test_Speed == 90
index_MPH = 134;%_____________________________________________/
                                  elseif Test_Speed == 120
index_MPH = 134;%_____________________________________/
                                   end
    case -5
        index_0 =   128;
                                   if   Test_Speed == 60
index_MPH = 102;%_____________________________________/
                                     elseif Test_Speed == 90
index_MPH = 121;%_____________________________________________/
                                  elseif Test_Speed == 120
index_MPH = 112;%_____________________________________/
                                   end
    case -10
        index_0 =   112;
                                   if   Test_Speed == 60
index_MPH = 119;%_____________________________________/
                                     elseif Test_Speed == 90
index_MPH = 114;%_____________________________________________/
                                  elseif Test_Speed == 120
index_MPH = 132;%_____________________________________/125
                                   end
end

    time_diff =  abs( time_0(index_0)-time(index_MPH) );
    race = time_0(index_0)-time(index_MPH); % determines lead vs lag race
            if race > 0
                a = -1;
            else
                a = 1;
            end
```

Always make sure the TARE run goes the LONGEST when acquiring data!!!
Cut the tail-end off of the 0 MPH data.

```
o_MPH_end = length(Fx(index_MPH:end))+length(Tare_Fx(1:index_0-1));%1542;
% % % Align the data sets

% % % Fx Tare
    Tare_Fx_align = Tare_Fx(index_0:o_MPH_end); % Tare data, 0 mph
    Fx_align = Fx(index_MPH:end); % Normal Force data, # mph

% % % Fy Tare
    Tare_Fy_align = Tare_Fy(index_0:o_MPH_end); % Tare data, 0 mph
    Fy_align = Fy(index_MPH:end); % Normal Force data, # mph

% % % Fz Tare
    Tare_Fz_align = Tare_Fz(index_0:o_MPH_end); % Tare data, 0 mph
    Fz_align = Fz(index_MPH:end); % Moment data, # mph

% % % Tx Tare
    Tare_Tx_align = Tare_Tx(index_0:o_MPH_end); % Tare data, 0 mph
    Tx_align = Tx(index_MPH:end); % Moment data, # mph

% % % Ty Tare
    Tare_Ty_align = Tare_Ty(index_0:o_MPH_end); % Tare data, 0 mph
    Ty_align = Ty(index_MPH:end); % Moment data, # mph

% % % Tz Tare
    Tare_Tz_align = Tare_Tz(index_0:o_MPH_end); % Tare data, 0 mph
    Tz_align = Tz(index_MPH:end); % Moment data, # mph

    TARED_Fx = (Fx_align) - (Tare_Fx_align);  %
    TARED_Fy = (Fy_align) - (Tare_Fy_align);  %
    TARED_Fz = (Fz_align) - (Tare_Fz_align);  %
    TARED_Tx = (Tx_align) - (Tare_Tx_align);  %
    TARED_Ty = (Ty_align) - (Tare_Ty_align);  %
    TARED_Tz = (Tz_align) - (Tare_Tz_align);  %

% % % Check that the FORCE data lines-up well

figure('Name',Figure_Handle,'NumberTitle','off','units','normalized','outerposition',[.5
0 .5 1])
     legend_str_index = [ num2str(Test_Speed), ' MPH'];
     subplot(3,1,1); hold on; title('Tared: F_x');ylabel('...from this plot.')
     plot( Tare_Fx_align ); hold on; plot( Fx_align );
     plot(TARED_Fx)
     legend('0 MPH',legend_str_index,'Tared Data'); grid minor
     subplot(3,1,2); hold on; title('Tared: F_y');ylabel('...Tare alignment...')
     plot(Tare_Fy_align);plot(Fy_align );
     plot(TARED_Fy)
     legend('0 MPH',legend_str_index, 'Tared Data'); grid minor
     subplot(3,1,3); hold on; title('Tared: F_z');ylabel('Check for good...')
     plot(Tare_Fz_align);plot(Fz_align );xlabel('data points')
```

```
      plot(TARED_Fz)
      legend('0 MPH',legend_str_index, 'Tared Data'); grid minor

% % % Check that the TORQUE data lines-up well

figure('Name',Figure_Handle,'NumberTitle','off','units','normalized','outerposition',[.5
0 .5 1])
      legend_str_index = [ num2str(Test_Speed), ' MPH'];
      subplot(3,1,1); hold on; title('Tared: T_x');ylabel('...from this plot.')
      plot( Tare_Tx_align ); hold on; plot( Tx_align );
      plot(TARED_Tx)
      legend('0 MPH',legend_str_index,'Tared Data'); grid minor
      subplot(3,1,2); hold on; title('Tared: T_y');ylabel('...Tare alignment...')
      plot(Tare_Ty_align);plot(Ty_align );
      plot(TARED_Ty)
      legend('0 MPH',legend_str_index, 'Tared Data'); grid minor
      subplot(3,1,3); hold on; title('Tared: T_z');ylabel('Check for good...')
      plot(Tare_Tz_align);plot(Tz_align );xlabel('data points')
      plot(TARED_Tz)
      legend('0 MPH',legend_str_index, 'Tared Data'); grid minor

% % % Check that the IMU data lines-up well
      figure('Name',Figure_Handle,'NumberTitle','off')
      legend_str_index = [ num2str(Test_Speed), ' MPH'];
      plot(Vimu_0(index_0:o_MPH_end)); hold on;
      plot(Vimu(index_MPH:end))
      plot(Vimu_0(index_0:o_MPH_end)-Vimu(index_MPH:end))
      title('IMU Line-Up');
      xlabel(' Data Point Index ');
      ylabel('IMU Voltage Data. Check for good alignment')
      legend('0 MPH',legend_str_index,'Subtracted Data','location','southeast');grid minor
```

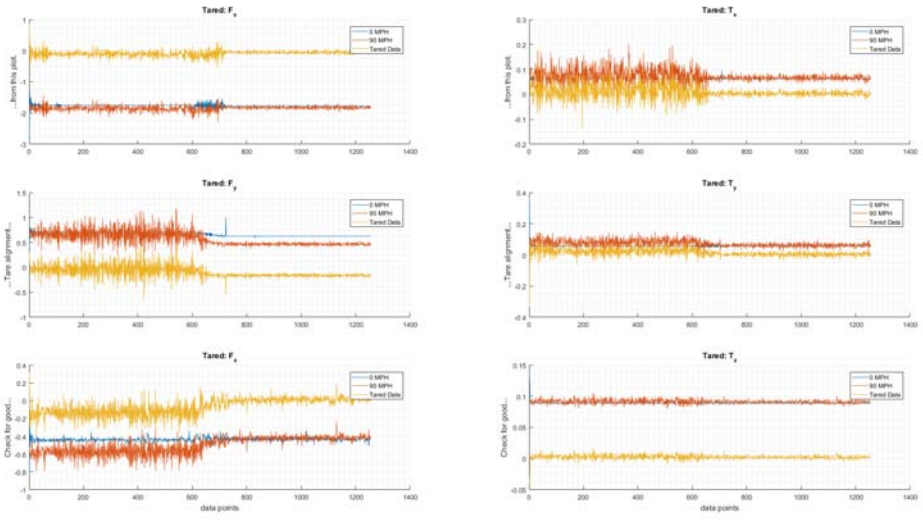

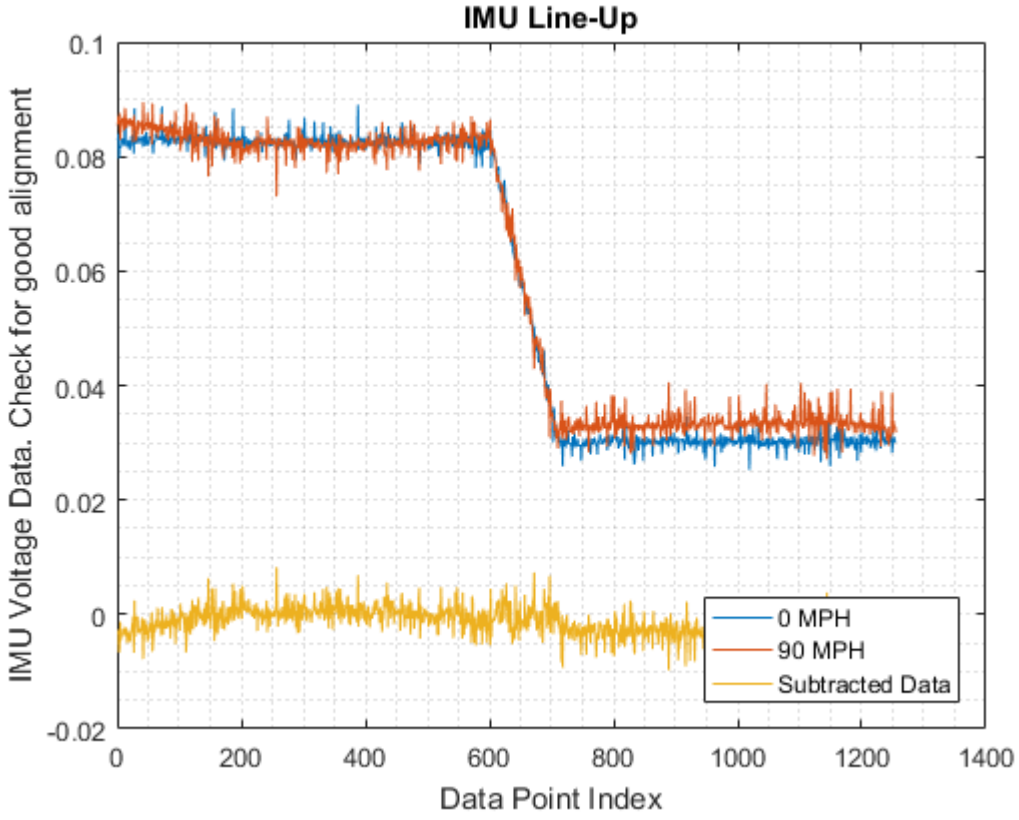
IMU Line-Up
IMU Voltage Data. Check for good alignment
Data Point Index
0.1
0.08
0.06
0.04
0.02
0
-0.02
0
200
400
600
800
1000
1200
1400
0 MPH
90 MPH
Subtracted Data

Convert Voltage for the IMU to Sweep Angles [deg]

```
    Vimu_start_avg = mean(Vimu(1:500)); % 1:500 is the initial state
    Vimu_end_avg = mean(Vimu(1000:end)); % 1000:end is the steady state
    SweepAngle = (Vimu-Vimu_start_avg)*(-19)/(Vimu_start_avg-Vimu_end_avg)-19;
    SweepAngle = (SweepAngle(index_MPH:end))';
        Fs_imu = 100;         % sample rate in Hz
        cof_imu = 0.1;        % cufoff frequency in Hz
        order_imu = 20;       % -th Order of lowpas filter
        Noisy_SweepAngle = SweepAngle';      % noisy data
        Fnorm_imu = cof_imu/(Fs_imu/2);      % Normalized frequency
        df_imu =
designfilt('lowpassfir','FilterOrder',order_imu,'CutoffFrequency',Fnorm_imu);
Delay_imu = mean(grpdelay(df_imu)); % filter delay in samples
filtered_imu = filter(df_imu,[Noisy_SweepAngle; zeros(Delay_imu,1)]); % Append Delay
FILTERED_SweepAngle = filtered_imu(Delay_imu+1:end); % Shift data to compensate for delay
```

Calculate Coefficients

```
    V = Test_Speed*(1/60)*(1/60)*(5280/1); % velocity (# MPH) converted to ft/s
    q = (1/2)*rho*V^2; % dynamic pressure

    CN = ( TARED_Fx )/( q*Ref_Area );  % Normal force coeff
    CY = ( TARED_Fy )/( q*Ref_Area );  % Side force coeff
    CX = ( TARED_Fz )/( q*Ref_Area );  % Axial force coeff

    Cn = (TARED_Tx)/(q*Ref_Area*Dia);  % Yaw moment coeff
    Cm = (TARED_Ty)/(q*Ref_Area*Dia);  % Pitch moment coeff
    Cl = (TARED_Tz)/(q*Ref_Area*Dia);  % Roll moment coeff
```

Filter Coefficient Data Sets

```
    Fs = 100;     % sample rate in Hz
cof = 0.1;        % cufoff frequency in Hz
order = 20;       % 20-th Order of lowpas filter
    CN = CN';      % noisy data
    CY = CY';
    CX = CX';
        Cn = Cn';
        Cm = Cm';
        Cl = Cl';
    % Design a 20-th order lowpass FIR filter with cutoff frequency of "cof" Hz.
    Fnorm = cof/(Fs/2);           % Normalized frequency
    df = designfilt('lowpassfir','FilterOrder',order,'CutoffFrequency',Fnorm);
    Delay = mean(grpdelay(df)); % filter delay in samples

    filtered_CN = filter(df,[CN; zeros(Delay,1)]); % Append Delay zeros to the input data
    filtered_CN = filtered_CN(Delay+1:end);        % Shift data to compensate for delay
        filtered_CY = filter(df,[CY; zeros(Delay,1)]);
        filtered_CY = filtered_CY(Delay+1:end);
            filtered_CX = filter(df,[CX; zeros(Delay,1)]);
            filtered_CX = filtered_CX(Delay+1:end);

    filtered_Cn = filter(df,[Cn; zeros(Delay,1)]);
    filtered_Cn = filtered_Cn(Delay+1:end);
        filtered_Cm = filter(df,[Cm; zeros(Delay,1)]);
        filtered_Cm = filtered_Cm(Delay+1:end);
            filtered_Cl = filter(df,[Cl; zeros(Delay,1)]);
            filtered_Cl = filtered_Cl(Delay+1:end);
```

Plot Normal Force Coefficient, C_N

```
figure('Name',Figure_Handle,'NumberTitle','off','units','normalized','outerposition',[0 0
.5 .5])
    [ax,k1,k2] = plotyy( time(index_MPH:end),FILTERED_SweepAngle, time(index_MPH:end),CN
);
    hold on
    line(time(index_MPH:end),filtered_CN,'parent',ax(2),'LineWidth',2)
    k1.Color = [0 .5 0]; k1.LineWidth = 2;
    k2.Color = [0.3 0.6 .9]; k2.LineWidth = 0.1;
    grid minor
    legend({'Sweep Angle','C_N', 'C_N (filtered)'},'FontSize',12, 'location',
'northwest')
    xlabel(('\fontsize{14} Time (sec)'),'interpreter','tex')
    ylabel(ax(1),('\fontsize{14} {\color[rgb]{0 .5 0}Sweep Angle (deg)}
'),'interpreter','tex')
        set(ax(1),'YColor','k')
    ylabel(ax(2),('\fontsize{14} {\color[rgb]{0 0.4470 0.7410} C_N}
'),'interpreter','tex')
        set(ax(2),'YColor','k','FontSize',12)
    set(gca,'XMinorTick','on','YMinorTick','on','FontSize',12)

        title((Figure_Handle),'interpreter','tex')
        YTICK_left = -20:2:2;
       set(ax(1), 'YLim', [min(YTICK_left) max(YTICK_left)] , 'YTick' , YTICK_left );
            YTICK_right = -6:1:5;
       set(ax(2), 'YLim', [min(YTICK_right) max(YTICK_right)] , 'YTick' , YTICK_right);

                set(ax(1), 'XLim', [2 13]);
                set(ax(2), 'XLim', [2 13]);
```

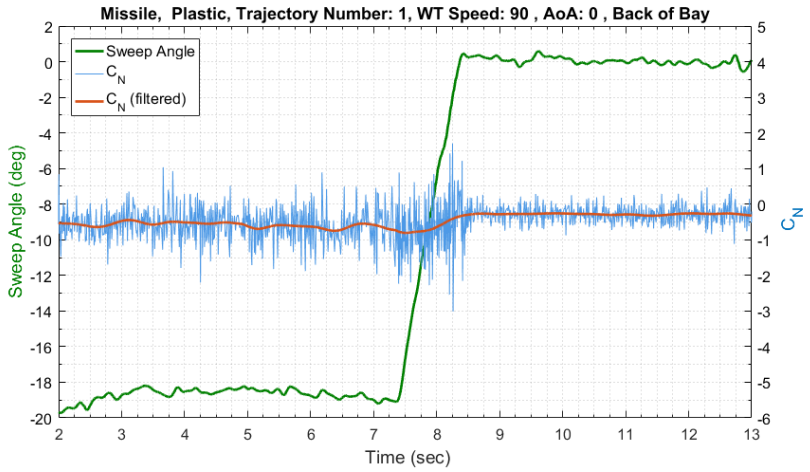

Plot Side Force Coefficient, C_Y

```
figure('Name',Figure_Handle,'NumberTitle','off','units','normalized','outerposition',[0 0
.5 .5])
[ax,k1,k2] = plotyy(  time(index_MPH:end),FILTERED_SweepAngle, time(index_MPH:end),CY  );
    hold on
    line(time(index_MPH:end),filtered_CY,'parent',ax(2),'LineWidth',2)
    k1.Color = [0 .5 0]; k1.LineWidth = 2;
    k2.Color = [0.3 0.6 .9]; k2.LineWidth = 0.1;
    grid minor
    legend({'Sweep Angle','C_Y', 'C_Y (filtered)'},'FontSize',12, 'location',
'northwest')
    xlabel(('\fontsize{14} Time (sec)'),'interpreter','tex')
ylabel(ax(1),('\fontsize{14} {\color[rgb]{0 .5 0}Sweep Angle (deg)}
'),'interpreter','tex')
    set(ax(1),'YColor','k')
    ylabel(ax(2),('\fontsize{14} {\color[rgb]{0 0.4470 0.7410}C_Y}
'),'interpreter','tex')
    set(ax(2),'YColor','k','FontSize',12)
    set(gca,'XMinorTick','on','YMinorTick','on','FontSize',12)

        title((Figure_Handle),'interpreter','tex')
        YTICK_left = -20:2:2;
       set(ax(1), 'YLim', [min(YTICK_left) max(YTICK_left)] , 'YTick' , YTICK_left );
            YTICK_right = -6:1:5;
       set(ax(2), 'YLim', [min(YTICK_right) max(YTICK_right)] , 'YTick' , YTICK_right);

            set(ax(1), 'XLim', [2 13]);
                 set(ax(2), 'XLim', [2 13]);
```

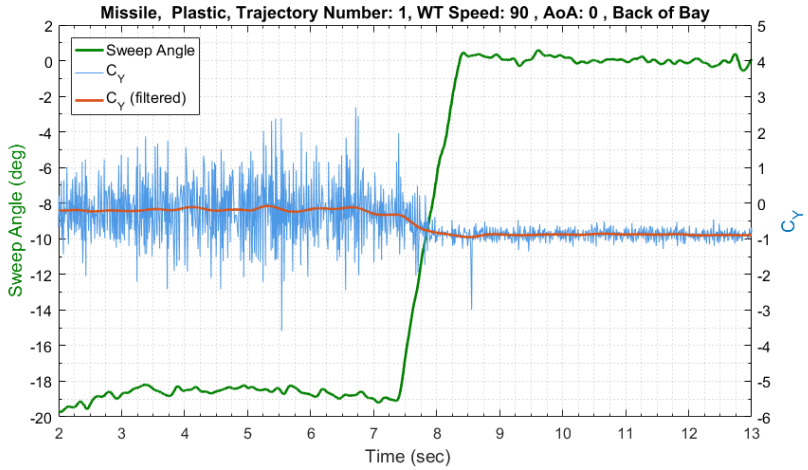

Plot Axial Force Coefficient, C_X

```
figure('Name',Figure_Handle,'NumberTitle','off','units','normalized','outerposition',[0 0
.5 .5])
[ax,k1,k2] = plotyy(  time(index_MPH:end),FILTERED_SweepAngle, time(index_MPH:end),CX  );
    hold on
    line(time(index_MPH:end),filtered_CX,'parent',ax(2),'LineWidth',2)
    k1.Color = [0 .5 0]; k1.LineWidth = 2;
    k2.Color = [0.3 0.6 .9]; k2.LineWidth = 0.1;
    grid minor
    legend({'Sweep Angle','C_X', 'C_X (filtered)'},'FontSize',12, 'location',
'northwest')
    xlabel(('\fontsize{14} Time (sec)'),'interpreter','tex')
    ylabel(ax(1),('\fontsize{14} {\color[rgb]{0 .5 0}Sweep Angle (deg)}
'),'interpreter','tex')
    set(ax(1),'YColor','k')
    ylabel(ax(2),('\fontsize{14} {\color[rgb]{0 0.4470 0.7410}C_X}
'),'interpreter','tex')
    set(ax(2),'YColor','k','FontSize',12)
    set(gca,'XMinorTick','on','YMinorTick','on','FontSize',12)

        title((Figure_Handle),'interpreter','tex')
        YTICK_left = -20:2:2;
        set(ax(1), 'YLim', [min(YTICK_left) max(YTICK_left)] , 'YTick' , YTICK_left );
            YTICK_right = -6:1:5;
       set(ax(2), 'YLim', [min(YTICK_right) max(YTICK_right)] , 'YTick' , YTICK_right);


            set(ax(1), 'XLim', [2 13]);
                 set(ax(2), 'XLim', [2 13]);
```

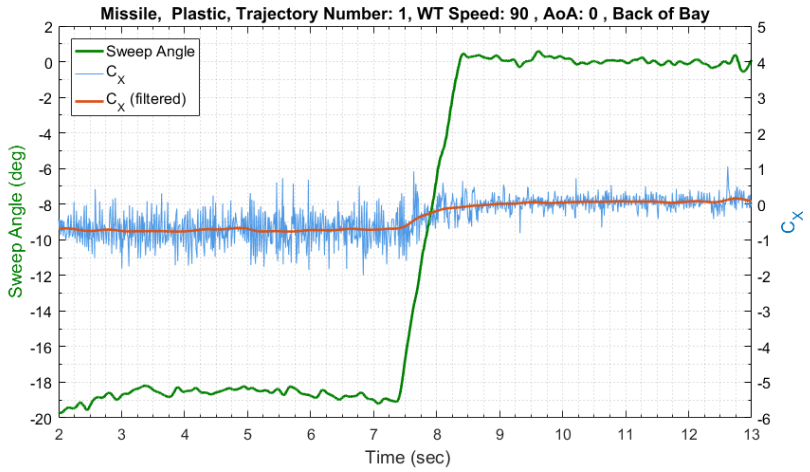

Plot Yaw Moment Coeffcient, C_n (about Xb-axis)

```
figure('Name',Figure_Handle,'NumberTitle','off','units','normalized','outerposition',[0 0
.5 .5])
[ax,k1,k2] = plotyy(  time(index_MPH:end),FILTERED_SweepAngle, time(index_MPH:end),Cn  );
    hold on
    line(time(index_MPH:end),filtered_Cn,'parent',ax(2),'LineWidth',2)
    k1.Color = [0 .5 0]; k1.LineWidth = 2;
    k2.Color = [0.3 0.6 .9]; k2.LineWidth = 0.1;
    grid minor
    legend({'Sweep Angle','C_n', 'C_n (filtered)'},'FontSize',12, 'location',
'northwest')
    xlabel(('\fontsize{14} Time (sec)'),'interpreter','tex')
    ylabel(ax(1),('\fontsize{14} {\color[rgb]{0 .5 0}Sweep Angle (deg)}
'),'interpreter','tex')
    set(ax(1),'YColor','k')
    ylabel(ax(2),('\fontsize{14} {\color[rgb]{0 0.4470 0.7410}C_n}
'),'interpreter','tex')
    set(ax(2),'YColor','k','FontSize',12)
    set(gca,'XMinorTick','on','YMinorTick','on','FontSize',12)

        title((Figure_Handle),'interpreter','tex')
        YTICK_left = -20:2:2;
        set(ax(1), 'YLim', [min(YTICK_left) max(YTICK_left)] , 'YTick' , YTICK_left );
            YTICK_right = -6:1:5;
       set(ax(2), 'YLim', [min(YTICK_right) max(YTICK_right)] , 'YTick' , YTICK_right);


            set(ax(1), 'XLim', [2 13]);
                 set(ax(2), 'XLim', [2 13]);
```

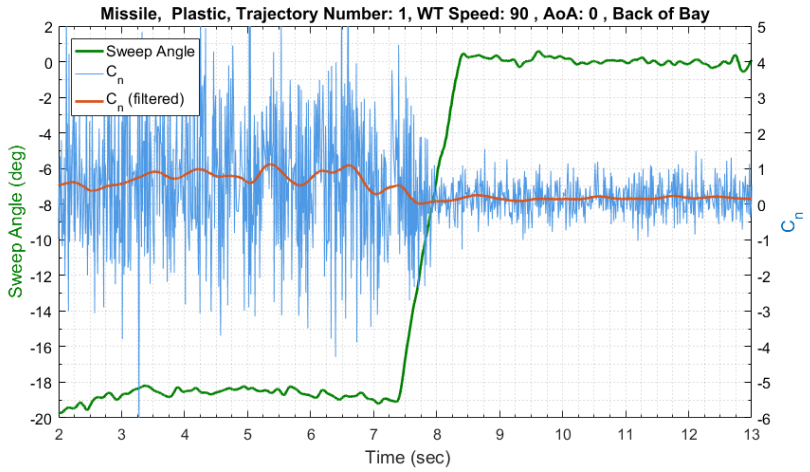

Plot Pitch Moment Coefficient, C_m (about Yb-axis)

```
figure('Name',Figure_Handle,'NumberTitle','off','units','normalized','outerposition',[0 0
.5 .5])
[ax,k1,k2] = plotyy(  time(index_MPH:end),FILTERED_SweepAngle, time(index_MPH:end),Cm  );
    hold on
    line(time(index_MPH:end),filtered_Cm,'parent',ax(2),'LineWidth',2)
    k1.Color = [0 .5 0]; k1.LineWidth = 2;
    k2.Color = [0.3 0.6 .9]; k2.LineWidth = 0.1;
    grid minor
    legend({'Sweep Angle','C_m', 'C_m (filtered)'},'FontSize',12, 'location',
'northwest')
    xlabel(('\fontsize{14} Time (sec)'),'interpreter','tex')
    ylabel(ax(1),('\fontsize{14} {\color[rgb]{0 .5 0}Sweep Angle (deg)}
'),'interpreter','tex')
    set(ax(1),'YColor','k')
    ylabel(ax(2),('\fontsize{14} {\color[rgb]{0 0.4470 0.7410}C_m}
'),'interpreter','tex')
    set(ax(2),'YColor','k','FontSize',12)
    set(gca,'XMinorTick','on','YMinorTick','on','FontSize',12)

        title((Figure_Handle),'interpreter','tex')
        YTICK_left = -20:2:2;
        set(ax(1), 'YLim', [min(YTICK_left) max(YTICK_left)] , 'YTick' , YTICK_left );
            YTICK_right = -6:1:5;
      set(ax(2), 'YLim', [min(YTICK_right) max(YTICK_right)] , 'YTick' , YTICK_right);


            set(ax(1), 'XLim', [2 13]);
                 set(ax(2), 'XLim', [2 13]);
```

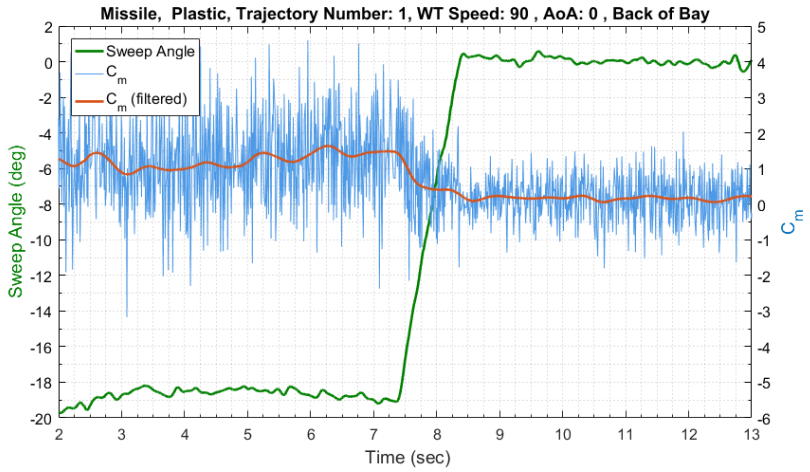

Plot Roll Moment Coefficient, C_l (about Zb-axis)

```
figure('Name',Figure_Handle,'NumberTitle','off','units','normalized','outerposition',[0 0
.5 .5])
[ax,k1,k2] = plotyy(  time(index_MPH:end),FILTERED_SweepAngle, time(index_MPH:end),Cl  );
    hold on
    line(time(index_MPH:end),filtered_Cl,'parent',ax(2),'LineWidth',2)
    k1.Color = [0 .5 0]; k1.LineWidth = 2;
    k2.Color = [0.3 0.6 .9]; k2.LineWidth = 0.1;
    grid minor
    legend({'Sweep Angle','C_l', 'C_l (filtered)'},'FontSize',12, 'location',
'northwest')
    xlabel(('\fontsize{14} Time (sec)'),'interpreter','tex')
    ylabel(ax(1),('\fontsize{14} {\color[rgb]{0 .5 0}Sweep Angle (deg)}
'),'interpreter','tex')
    set(ax(1),'YColor','k')
    ylabel(ax(2),('\fontsize{14} {\color[rgb]{0 0.4470 0.7410}C_l}
'),'interpreter','tex')
    set(ax(2),'YColor','k','FontSize',12)
    set(gca,'XMinorTick','on','YMinorTick','on','FontSize',12)

        title((Figure_Handle),'interpreter','tex')
        YTICK_left = -20:2:2;
        set(ax(1), 'YLim', [min(YTICK_left) max(YTICK_left)] , 'YTick' , YTICK_left );
            YTICK_right = -6:1:5;
      set(ax(2), 'YLim', [min(YTICK_right) max(YTICK_right)] , 'YTick' , YTICK_right);

            set(ax(1), 'XLim', [2 13]);
                 set(ax(2), 'XLim', [2 13]);
```

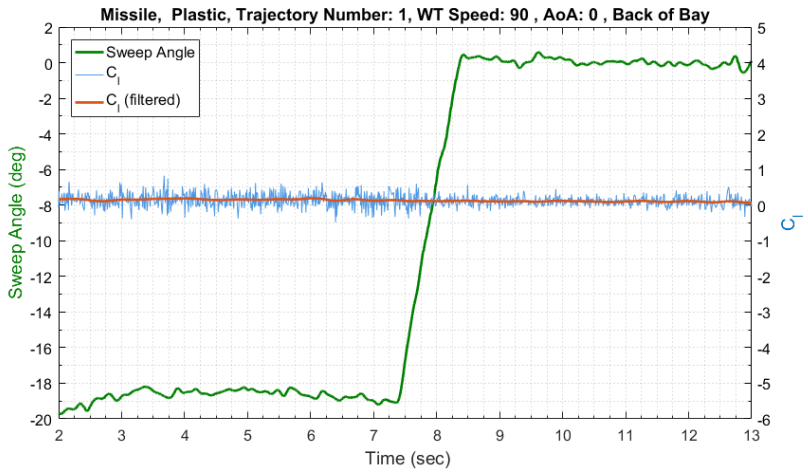

Plot the Coefficients: C_N and C_m vs Sweep Angle

```
figure('Name',Figure_Handle,'NumberTitle','off','units','normalized','outerposition',[0 0
.5 .5])
    plot(SweepAngle,CN,'*' ); hold on
    grid minor
     title((Figure_Handle),'interpreter','tex')
     xlabel(('\fontsize{14} Sweep Angle (deg)'),'interpreter','tex')
     ylabel(('\fontsize{14} C_N'),'interpreter','tex')
     ylim([-10 10])
     xlim([-20 1])
plot([-19 -19],[10 -10],'r','LineWidth',2)
plot([0 0],[10 -10],'r','LineWidth',2)
% get(gca) % to pull up the menu items.
set(gca, 'XTick', [-20:1:1] , 'XTickLabelRotation' , 45)% , 'XTick' , Xtick );
LegendHandle = legend('Unfiltered C$_N$','Start: -19$^\circ$','End: 0$^\circ$');
set(LegendHandle,'interpreter','latex','fontsize',12,'location','southeast')


% Plot Pitch Moment Coeff, C_m vs PitchAngle

figure('Name',Figure_Handle,'NumberTitle','off','units','normalized','outerposition',[0 0
.5 .5])
    plot(SweepAngle,Cm,'g*' ); hold on
    grid minor
     title((Figure_Handle),'interpreter','tex')
     xlabel(('\fontsize{14} Sweep Angle (deg)'),'interpreter','tex')
     ylabel(('\fontsize{14} C_m'),'interpreter','tex')
     ylim([-10 10])
     xlim([-20 1])
plot([-19 -19],[10 -10],'r','LineWidth',2)
plot([0 0],[10 -10],'r','LineWidth',2)
% get(gca) % to pull up the menu items.
set(gca, 'XTick', [-20:1:1] , 'XTickLabelRotation' , 45)% , 'XTick' , Xtick );
LegendHandle = legend('Unfiltered C$_m$','Start: -19$^\circ$','End: 0$^\circ$');
set(LegendHandle,'interpreter','latex','fontsize',12,'location','northeast')
```

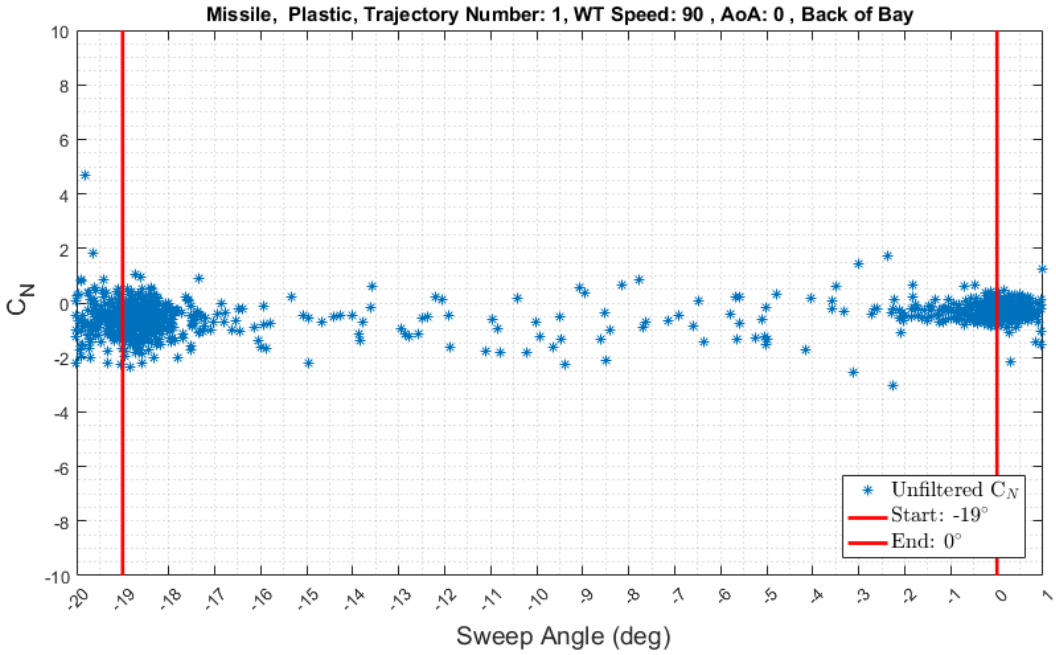
Missile, Plastic, Trajectory Number: 1, WT Speed: 90 , AoA: 0 , Back of Bay
C_N
Sweep Angle (deg)
Unfiltered C_N
Start: -19°
End: 0°

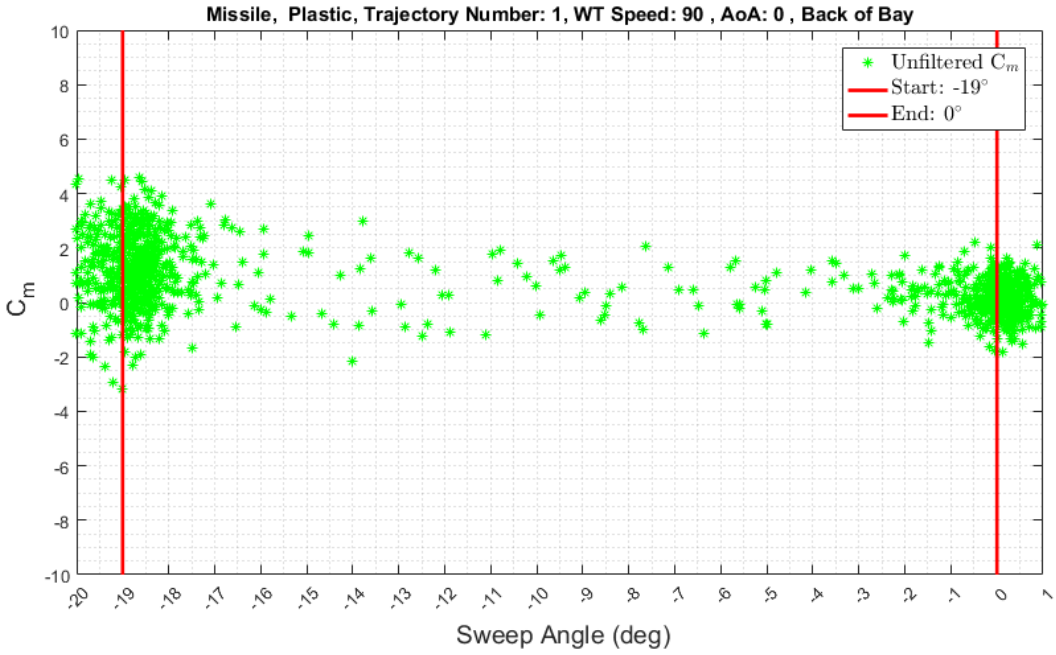
Missile, Plastic, Trajectory Number: 1, WT Speed: 90 , AoA: 0 , Back of Bay
C_m
Sweep Angle (deg)
Unfiltered C_m
Start: -19°
End: 0°

This Page Intentionally Left Blank

Appendix C. Drawings of Models

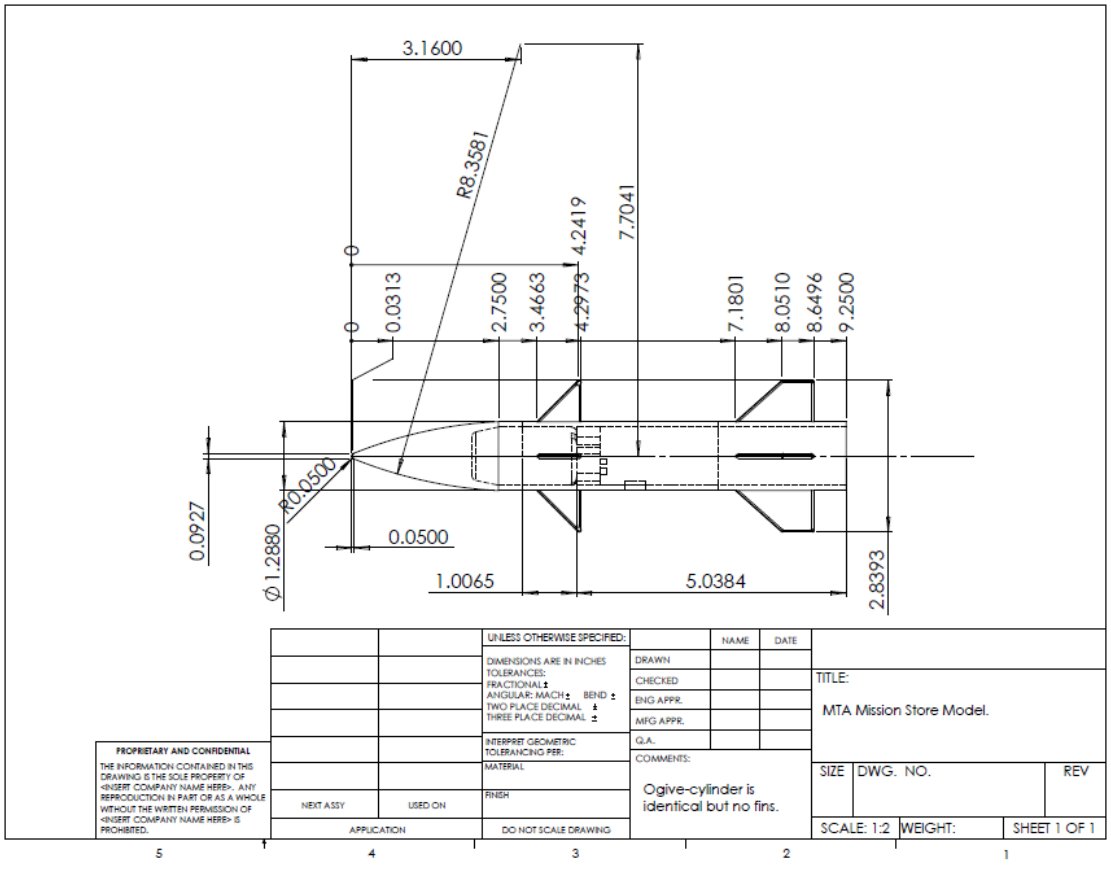

Bibliography

[1] M. Purdon, C. Hetreed, and M. Hudson, "F-35 Pre-Flight Store Separation Analyses: Innovative Techniques for Affordability," *47th AIAA Aerosp. Sci. Meet.*, no. Paper 2009-0102, pp. 1–15, 2009.

[2] K. S. Keen, C. H. Morgret, T. F. Langham, and W. B. Baker, "Trajectory Simulations Should Match Flight Tests and Other Lessons Learned in 30 Years of Store-Separation Analysis," *New Horizons*, no. January, pp. 1–38, 2009.

[3] A. Cenko and P. River, "Unsteady Weapon Bay Aerodynamics - Urban Legend or Flight Clearance Nightmare," no. January, pp. 1–13, 2008.

[4] J. C. Lancaster, "Characterization of a Robotic Manipulation for Dynamic Wind Tunnel Applications," 2015.

[5] J. B. A. Sellers, "Force and Moment Measuremsnts Applicable to a Flexible Weapons System," 2016.

[6] Z. Probst, M. F. Reeder, R. Johnson, and J. Grove, "Flight Test Experiments on Cavity Flow in a SUU-41 Pod," *AIAA Flight Test. Conf.*, no. June, pp. 1–16, 2016.

[7] R. A. Johnson, M. J. Stanek, and J. E. Grove, "Store Separation Trajectory Deviations Due to Unsteady Weapons Bay Aerodynamics," in *46th AIAA Aerospace Sciences Meeting and Exhibit*, 2008, no. January, pp. 1–15.

[8] P. Rowe and J. Lancaster, "Motion Test Apparatus (MTA) Manipulator User Manual," 2014.

[9] J. Wright, "A Compilation of Aerodynamic Nomenclature and Axes Systems," *Nav. Ordnance Lab.*, 1962.

[10] J. B. Barlow, W. H. Rae, and A. Pope, *Low-Speed Wind Tunnel Testing*. Wiley, New York, 1999.

[11] N. C. Prewitt, D. M. Belk, and R. C. Maple, "Multiple-Body Trajectory Calculations Using the Beggar Code," *J. Aircr.*, vol. 36, no. 5, pp. 802–808, 1999.

[12] J. Babcock and R. Maple, "Free-Flight Store Simulation Using Beggar," *24th Appl. Aerodyn. Conf.*, no. June, 2006.

[13] T. J. Flora, M. F. Reeder, A. Lofthouse, and N. Kraft, “Dynamic Store Release of Ice Models from a Cavity into Mach 2.9 Flow,” *J. Aircr.*, vol. 51, no. 6, pp. 1927–1941, 2014.

[14] B. L. Stevens and F. L. Lewis, *Aircraft Control and Simulation*. 2003.

[15] J. Pattinson, M. H. Lowenberg, and M. G. Goman, “Multi-Degree-of-Freedom Wind-Tunnel Maneuver Rig for Dynamic Simulation and Aerodynamic Model Identification,” *J. Aircr.*, vol. 50, no. 2, pp. 551–566, 2013.

[16] A. Bergmann, A. Huebner, and T. Loeser, “Experimental and numerical research on the aerodynamics of unsteady moving aircraft,” *Progress in Aerospace Sciences*, vol. 44, no. 2. pp. 121–137, 2008.

[17] B. Binkley and A. Vanderwyst, “Application of Statistical Techniques to Analyze and Model Trajectory Envelopes for Subscale Store Separation Testing,” *30th AIAA Appl. Aerodyn. Conf.*, no. June, 2012.

[18] J. Jordan, A. Denny, J. Jordan, and A. Denny, “Approximation methods for computational trajectory predictions of a store released from a bay,” *15th Appl. Aerodyn. Conf.*, 1997.

[19] D. Greenwell and M. Goman, “Wind Tunnel Simulation of Combat Aircraft Manoeuvres,” *Aiaa*. 1998.

[20] J. Pattinson, M. H. Lowenberg, and M. Goman, “A multi-degree-of-freedom rig for the wind tunnel determination of dynamic data.,” *AIAA Atmos. Flight Mech. Conf.*, no. August, 2009.

[21] R. Randall, L. Wilson, and S. Shkarayev, “Flow Interactions around a Rapidly-Pitching MAV Wing,” in *50th AIAA Aerospace Sciences Meeting*, 2012, no. January, pp. 1–18.

[22] J. R. Chambers, “Modeling Flight: The Role of Dynamically Scaled Free-Flight Models in Support of NASA’s Aerospace Programs,” *Nasa Sp 2009-575*, p. 202, 2009.

[23] D. E. Hahne, T. R. Wendel, and J. R. Boland, “Wind-Tunnel Free-Flight Investigation of a Supersonic Persistence Fighter,” 1993.

[24] K. Hufnagel and G. Schewe, “Springer Handbook of Experimental Fluid Mechanics - Force and Moment Measurement.,” Springer, Berlin, 2007.

[25] Ö. H. Ünalmis, N. T. Clemens, and D. S. Dolling, “Cavity Oscillation Mechanisms in High-Speed Flows,” 2004.

[26] L. P. Erm, “Development and Use of a Dynamic-Testing Capability for the DSTO Water Tunnel,” *Def. Sci. Technol. Organ.*, 2006.

[27] AIAA, *Guide: Nomenclature and Axis Systems for Aerodynamic Wind Tunnel Testing*. 2012.

[28] O. Wysocki and E. Schülein, “Experimental Investigations on the Phantom Yaw Effect on a Maneuvering Slender Body,” *J. Spacecr. Rockets*, vol. 52, no. 1, pp. 264–274, 2015.

[29] L. SMITH and R. H. NUNN, “Aerodynamic Characteristics of an Axisymmetric Body Undergoing a Uniform Pitching Motion,” *J. Spacecr.*, vol. 13, no. 1, 1976.

[30] Z. Probst, “Design and Flight Test of A Weapons-Cavity Acoustics And Store Separation Test Bed,” *Thesis*, 2016.

[31] R. L. Spinetti and B. A. Jolly, “Time-Accurate Numerical Simulation of GBU-38s Separating from the B-1B Aircraft with Various Ejector Forces , Store Properties , and Load-out Configurations - IHAAA Store Separation Cavity (SSC) Project -,” no. January, p. 32542, 2008.

This Page Intentionally Left Blank

REPORT DOCUMENTATION PAGE

Form Approved
OMB No. 074-0188

1. REPORT DATE *(DD-MM-YYYY)*	2. REPORT TYPE	3. DATES COVERED *(From – To)*
22-02-2017	Master's Thesis	March 2015 – March 2017

TITLE AND SUBTITLE

INVESTIGATION OF DYNAMIC STORE SEPARATION OUT OF A WEAPONS BAY CAVITY UTILIZING A LOW SPEED WIND TUNNEL

5a. CONTRACT NUMBER

5b. GRANT NUMBER

5c. PROGRAM ELEMENT NUMBER

6. AUTHOR(S)

Bower, Andrew D., Civilian, USAF

5d. PROJECT NUMBER

5e. TASK NUMBER

5f. WORK UNIT NUMBER

7. PERFORMING ORGANIZATION NAMES(S) AND ADDRESS(S)
Air Force Institute of Technology
Graduate School of Engineering and Management (AFIT/ENY)
2950 Hobson Way, Building 640
WPAFB OH 45433-8865

8. PERFORMING ORGANIZATION REPORT NUMBER

AFIT-ENY-MS-15-M-244

9. SPONSORING/MONITORING AGENCY NAME(S) AND ADDRESS(ES)
AGENCY (spelled out)
ADDRESS
PHONE and EMAIL
ATTN: POC
(no sponsor enter: Intentionally left blank)

10. SPONSOR/MONITOR'S ACRONYM(S)

AFRL/RHIQ (example)

11. SPONSOR/MONITOR'S REPORT NUMBER(S)

12. DISTRIBUTION/AVAILABILITY STATEMENT
DISTRUBTION STATEMENT A. APPROVED FOR PUBLIC RELEASE; DISTRIBUTION UNLIMITED.

13. SUPPLEMENTARY NOTES
This material is declared a work of the U.S. Government and is not subject to copyright protection in the United States.

14. ABSTRACT
Characterizing store trajectories as they separate from a weapons bay cavity is relevant to the Air Force mission. The flow around a weapons bay is unsteady. The unsteady flow can cause a mission store separation trajectory to be unpredictable, and such is the case for what some have termed a pitch bifurcation. Traditional wind tunnel testing is incapable of detecting a bifurcation because traditional wind tunnel testing records time-averaged data. In this study, an experimental testing system was developed in order to support the time-accurate characterization of dynamic store separation events. A Motion Test Apparatus integrated with a low-speed wind tunnel maneuvers a model within the wind tunnel test section along a prescribed trajectory. A dedicated data acquisition system, along with sensors, record time-accurate force-and-moment measurements as well as model attitude. Two mission store geometries fabricated of two different materials were studied as they performed store separation trajectories from a weapons bay cavity. The mission store models separated, alternatively, from forward and aft positions from the weapons bay. Data confirmed that variability in pitch moment experienced by the models was higher for store separation from the aft position. Force-and-moment data also suggests a bifurcation was present for certain test cases.

15. SUBJECT TERMS
Mission store separation. Weapons bay cavity. Ogive-cylinder. Missile. Wind tunnel. Trajectory.

16. SECURITY CLASSIFICATION OF:			17. LIMITATION OF ABSTRACT	18. NUMBER OF PAGES	19a. NAME OF RESPONSIBLE PERSON
a. REPORT	b. ABSTRACT	c. THIS PAGE			Mark F. Reeder, AFIT/ENY
U	U	U	UU	19	19b. TELEPHONE NUMBER *(Include area code)* (937) 255-6565, ext 4530 (mark.reeder@afit.edu)

Standard Form 298 (Rev. 8-98)
Prescribed by ANSI Std. Z39-18